J. W. Evans
EP24

NATIONAL AERONAUTICS AND SPACE ADMINISTRATION
MARSHALL SPACE FLIGHT CENTER, ALABAMA

DUAL-THROAT THRUSTER THERMAL MODEL
CONTRACT NAS 8-34136

FINAL REPORT
AUGUST 1986

BY:

R. L. EWEN, C. J. O'BRIEN, AND L. W. MATTHEWS

AEROJET TECHSYSTEMS COMPANY
SACRAMENTO, CALIFORNIA 95813

REPORT 34136F
AUGUST 1986

NATIONAL AERONAUTICS AND SPACE ADMINISTRATION

DUAL-THROAT THRUSTER THERMAL MODEL

FINAL REPORT

BY

R. L. EWEN, C. J. O'BRIEN AND L. W. MATTHEWS

AEROJET TECHSYSTEMS COMPANY

PREPARED FOR

NATIONAL AERONAUTICS AND SPACE ADMINISTRATION

NASA-MARSHALL FLIGHT CENTER

CONTRACT NAS 8-34136

RPT/BB0216

1. Report No.	2. Government Accession No.	3. Recipient's Catalog No.
34136F		

4. Title and Subtitle	5. Report Date
Dual Throat Thruster Thermal Model, Final Report	June 1986
	6. Performing Organization Code

7. Author(s)	8. Performing Organization Report No.
R. L. Ewen, C. J. O'Brien, and L. W. Matthews	
	10. Work Unit No.

9. Performing Organization Name and Address	11. Contract or Grant No.
Aerojet TechSystems Company **Post Office Box 13222** **Sacramento, California 95813**	**NAS 8-** 34136
	13. Type of Report and Period Covered
12. Sponsoring Agency Name and Address	**Contractor Report, Final**
National Aeronautics and Space Administration **Washington, D.C. 20546**	14. Sponsoring Agency Code

15. Supplementary Notes

Project Manager; F. W. Braam, Propulsion Division
NASA-Marshall Space Flight Center
Marshall Space Flight Center, Alabama 35812

16. Abstract The dual-throat engine is one of the dual nozzle engine concepts that have been studied for advanced space transportation applications. It provides a thrust change and an in-flight area ratio change through the use of two concentric combustors with two throats arranged in series.

Test results are presented for a dual throat thruster burning gaseous oxygen and hydrogen at primary (inner) chamber pressures from 380 to 680 psia. Heat flux profiles were obtained from calorimetric cooling channels in the inner nozzle, outer or secondary chamber and the tip of the inner nozzle. Data were obtained for two nozzle spacings over a chamber pressure ratio (secondary/primary) range of 0.45 to 0.83 with both chambers firing (Mode I). Fluxes near the end of the inner nozzle were significantly higher than in Mode II when only the inner chamber was fired, due to the flow separation and recirculation caused by the back pressure imposed by the secondary chamber. As the pressure ratio increased, these heat fluxes increased and the region of high heat flux relative to Mode II extended farther upstream. The use of a gaseous hydrogen bleed flow in the secondary chamber to control heat fluxes in the primary plume attachment region was investigated in Mode II testing.

A thermal model of a dual throat thruster was developed and upgraded using the experimental data.

17. Key Words (Suggested by Author(s))	18. Distribution Statement
Dual Throat Heat Transfer Dual Throat Calorimeter Chamber GO_2/GH_2 Rocket Chamber Testing Dual Nozzle Rocket Engine	**Unclassified - Unlimited**

19. Security Classif. (of this report)	20. Security Classif. (of this page)	21. No. of Pages	22. Price*
Unclassified	**Unclassified**		

TABLE OF CONTENTS

TABLE OF CONTENTS (cont.)

TABLE OF CONTENTS (cont.)

LIST OF TABLES

LIST OF TABLES (cont.)

LIST OF FIGURES

LIST OF FIGURES (cont.)

LIST OF FIGURES (cont.)

LIST OF FIGURES (cont.)

I. FOREWORD

The work described herein was performed at the Aerojet TechSystems (ATC) Company under NASA Contract NAS 8-34136 with Mr. F. W. Braam, NASA-Marshall Space Flight Center, as Project Manager. The ALRC Program managers were Mr. R. W. Michel and Mr. D. C. Rousar, and the Project Engineers were Mr. C. J. O'Brien and Dr. R. L. Ewen. Dr. Ewen was responsible for thermal design, test, and analysis activities. Mr. O'Brien was responsible for all other technical aspects of the program.

The technical period of performance for the study was from June 1981 to May 1986.

The following ATC personnel contributed significantly to the success of this program.

B. J. Anderson	Thruster Design
H. H. Mueggenburg	Thruster Design Manager
A. H. Galvan	Thruster Design Layout
J. E. Stammer	Thruster Design Project Manager
L. W. Matthews	Thruster Fabrication/Assembly
N. A. Hayes	Thruster Fabrication Manager
S. E. Colucci	Design Analysis Support
S. Buccela	Thermal Model Computer Program
E. J. Arreguin	Thermal Data Analysis
K. Gustafsen	Primary Chamber Assembly
C. M. Cotter	Coolant Circuit Hydraulic Analysis
J. I. Ito	Injector Design Analysis
G. M. Meagher	Aerodynamic Design Analysis
R. A. Hewitt	Coolant Circuit Calibration/Model
R. A. Winter	Injector Assembly
M. L. Drutt	Test Engineer
C. R. Crossman	Test Program Manager
P. D. Hill	Test Area Manager
D. E. Robertson	Test Instrumentation Manager
A. R. Keller	Orifice Flow Calibration
R. E. Walker	Hydraulic Analysis Manager
H. C. Howard	Test Data Computer Summary
W. E. Baker	Test Data Computer Analysis
F. E. Whalen	Test Technician
T. M. Hubbard	Test Technician

I. SUMMARY

The unique configuration of the dual throat thrust chamber posed several questions regarding its cooling. NASA-NSFC initiated the dual throat thruster thermal model program to ascertain the answers to the questions.

The major objectives of the program were to (1) develop an analytical model of the thrust chamber, (2) design, fabricate, and test hardware to determine the heat flux profiles, and (3) update the model as necessary to reflect the experimental data.

A thermal model of the dual throat chamber was developed based on previous cold flow and analytical studies. At the same time, a very sophisticated calorimeter chamber was designed, fabricated, and tested over a broad range of conditions.

The test results for a dual throat thruster burning gaseous oxygen and hydrogen at primary (inner) chamber pressures from 380 to 680 psia are reviewed in detail in this document. Heat flux profiles were obtained from calorimetric cooling channels in the inner nozzle, outer or secondary chamber and the tip of the inner nozzle. Data was obtained for two nozzle spacings over a chamber pressure ratio (secondary/primary) range of 0.45 to 0.83 with both chambers firing (Mode I). Fluxes near the end of the inner nozzle were significantly higher than in Mode II when only the inner chamber was fired, due to the flow separation and recirculation caused by the back pressure imposed by the secondary chamber. As the pressure ratio increased, these heat fluxes increased and the region of high heat flux relative to Mode II extended farther upstream. The use of a gaseous hydrogen bleed flow in the secondary chamber to control heat fluxes in the primary plume attachment region was investigated in Mode II testing. A bleed flow of less than two percent of the primary chamber flow was required.

The basic conclusions from the program are as follows:

- Heat fluxes during conventional operation of the primary nozzle (Mode II) are consistent with data from other applications. Use of an enthalpy-based model, rather than the product of temperature difference and a frozen specific heat, is required to predict the effect of mixture ratio.

- During Mode I operation the primary throat is choked, but the primary nozzle is unable to flow full against the high back pressure imposed by the secondary chamber. Large increases in heat flux relative to Mode II observed near the end of the primary nozzle are consistent with a twin vortex recirculation pattern in the separated region, which includes the wake region downstream of the end of the primary chamber. As the secondary chamber pressure increases, the region of increased heat flux extends farther upstream and the perturbation at the end of the nozzle increases.

- Unsymmetrical heating of the tip of the primary chamber is caused by the flow separation in the primary nozzle and the resultant recirculation pattern noted above.

- Secondary chamber heat fluxes during Mode I operation can be predicted with the secondary flow stream tube model used herein and correlation coefficients consistent with other applications. High heat fluxes observed near the swirl coaxial element injector are consistent with previous experience. Rapid decreases and increases with axial distance of correlation coefficients in the secondary nozzle are probably caused by oblique shock waves created by the flow separation in the primary nozzle.

I, Summary (cont.)

- Heat fluxes in the secondary throat region during Mode II operation are easily limited to values well below Mode I fluxes using small bleed flow rates, e.g., two percent of the primary flow for the geometry tested. Therefore, primary plume attachment is not a thermal design issue.

- Although the analytical model of Mode II can predict secondary nozzle heat fluxes under limited test conditions, it does not exhibit the correct sensitivity to bleed flow rate. Additional model development is required to account for velocity components normal to the wall. A Nash factor of 0.2 in the aerodynamic model results in very good prediction of the recirculation region pressure and its sensitivity to bleed flow rate.

- The fabrication of the dual throat calorimetric hardware established the feasibility of the assembly of dual thrust chambers by conventional means. The problems associated with the calorimetric hardware was unique. The basic steps in assembly, however, would be similar for a regeneratively cooled dual thrust chamber. The problems encountered during assembly indicated alternate procedures that will be beneficial for future builds of dual throat chambers.

II. INTRODUCTION

A. BACKGROUND

The dual-throat engine is one of the major engine system design candidates that has been studied for advanced space transportation applications. The engine provides a thrust change and an in-flight area ratio change through the use of two concentric combustors with two throats in series. As shown in Figure 1 both the primary (inner) and the secondary (outer) combustors are fired simultaneously (parallel burn) in Mode I (sea level) operation. The characteristics of Mode I operation are high mass flow (high thrust) and low area ratio.. In Mode II, only the primary (inner) çomubstor operates. The exhaust plume fom the inner chamber expands through a low area ratio nozzle and attaches at the secondary (outer) nozzle throat surface. The plume shape and point of attachment to the secondary nozzle are controlled by a small bleed flow in the secondary chamber. Operation of the primary (inner) combustor alone allows the effective area ratio to be established by the exit of the secondary combustor. The resulting large-area-ratio, lower-thrust unit is typical of an upper stage engine. This dual-thrust, dual-area-ratio feature of the engine provides a vehicle with an optimized thrust trajectory for ascent-type missions--high thrust at sea level and low thrust, higher performance at altitude.

The dual-throat thruster can provide dual-mode operation as well by using different propellant combinations in each combustor (e.g., LOX/LH_2 in the primary and LOX/RP-1 in the secondary chamber). That is, the engine can change from high-density propellants in the early flight stages to lower-density, higher-performance propellants in the later stages of the flight. Potential applications for dual-throat engines range from the space shuttle and its derivatives to single-stage-to-orbit (SSTO) vehicles. A typical preliminary design layout of a dual throat engine burning both LH2 and a high density fuel (HDF) such as RP-1 is shown in Figure 2 (Reference 1). An artist's sketch of this engine with cutaway showing the dual throat arrangement is shown in Figure 3. A closeup of the dual throat arrangement from Figure 3 is given in Figure 4 to show the relative positioning of the manifolds, injectors, and chambers, and to identify the regions where thermal investigation was deemed necessary.

B. PURPOSE AND SCOPE

The purpose of the program is to develop a thermal model of a dual-throat thruster and to acquire experimental data to upgrade the model. The results of the program will allow detailed thermal design of dual-throat thrusters to identify both cooling feasibility and pressure drops. Such data are needed for power balance analyses which must accompany engine designs for particular applications.

C. APPROACH

To accomplish the program objectives, the following specific tasks were conducted according to the schedule of Figure 4a.

(1) Develop a detailed dual-throat thruster thermal model for use in identifying thruster cooling requirements (Figure 5).

(2) Use the thermal model to examine four different systems, operating at different thrust ratios and different chamber pressure ratios (Figure 6).

(3) Design, fabricate, and test subscale hardware to obtain data for selected areas identified in Task 2 as having an insufficient data base (Figure 7). The three areas that were identified as needing experimental heat flux data were: (a) the primary nozzle during Mode I operation with the high back pressure imposed by the secondary chamber, (b) the wake region at the tip of the primary nozzle in Mode I and (c) the plume attachment region in Mode II near the secondary chamber throat (see Figure 4).

(4) Analyze and correlate the test data, and upgrade the thermal model (Figure 8).

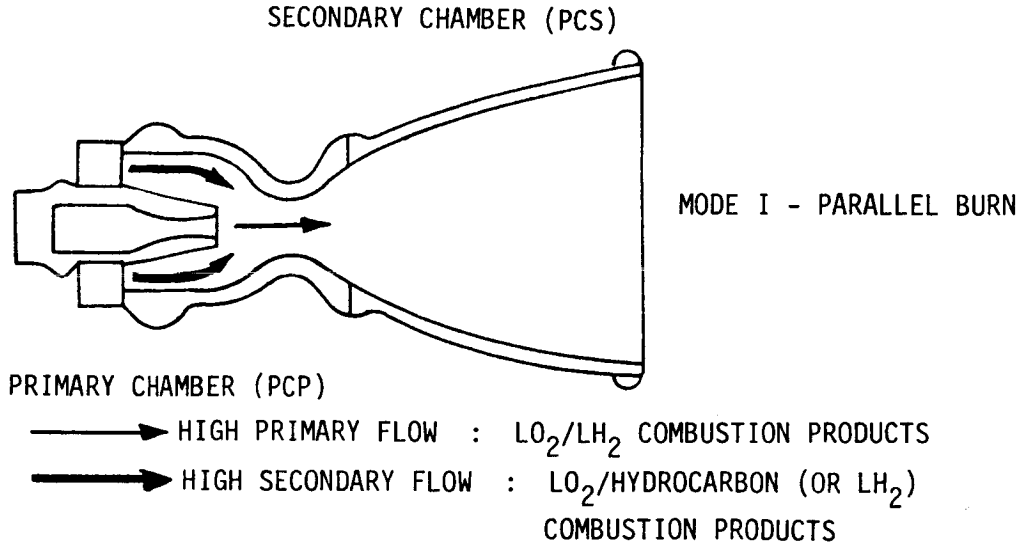

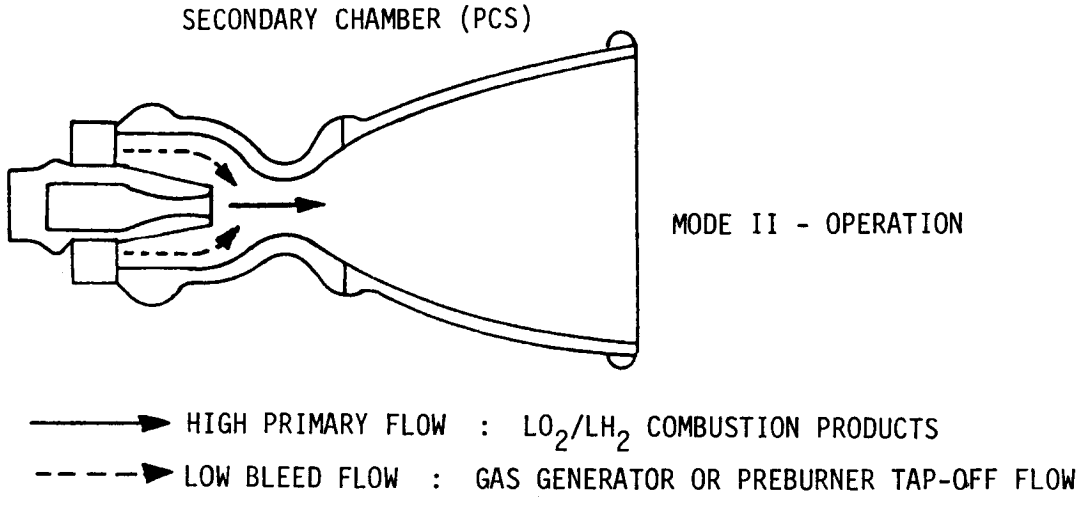

Figure 1. Dual-Throat Engine Configurations and Nomenclature

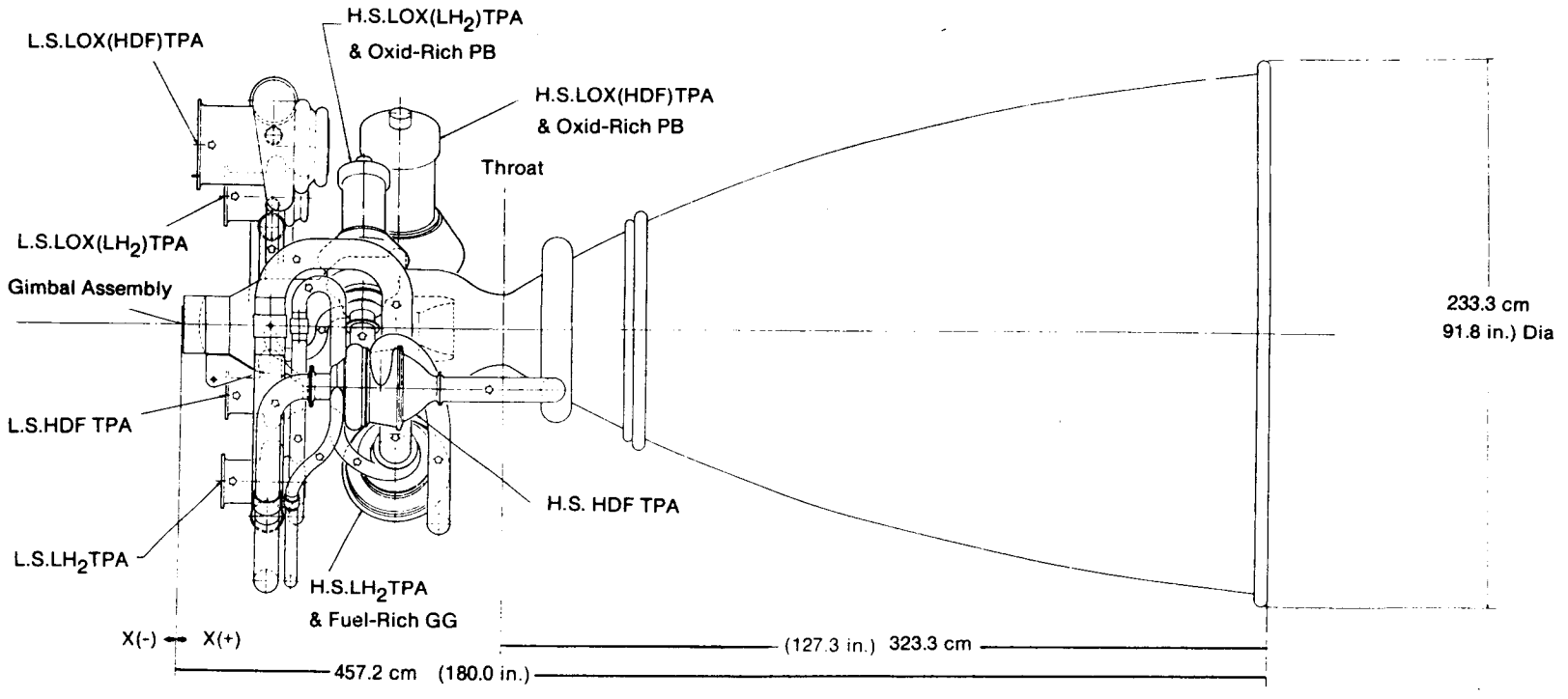

Figure 2 . Dual-Throat Engine

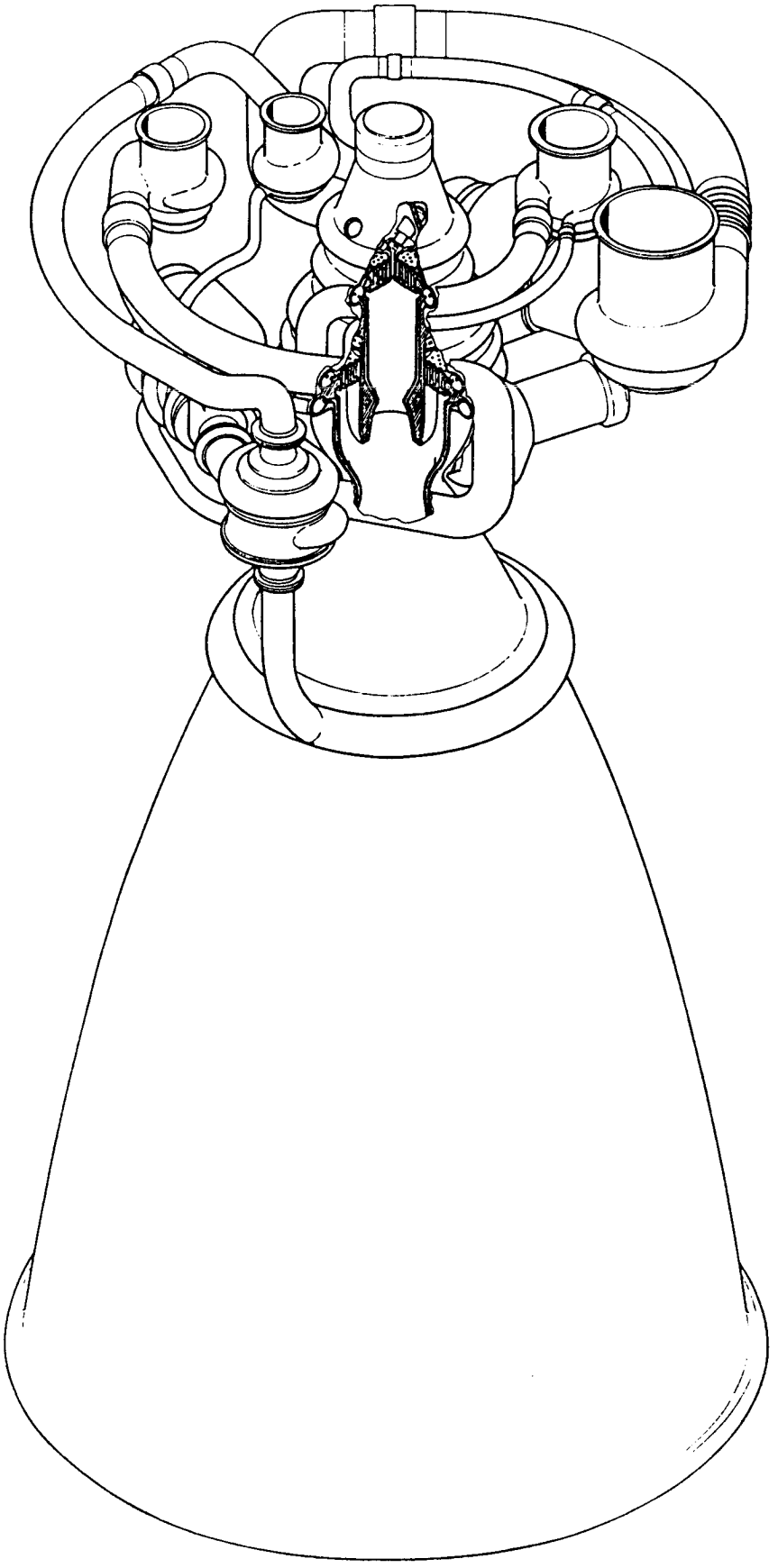

Figure 3. Dual-Throat Engine Projection/Cutaway

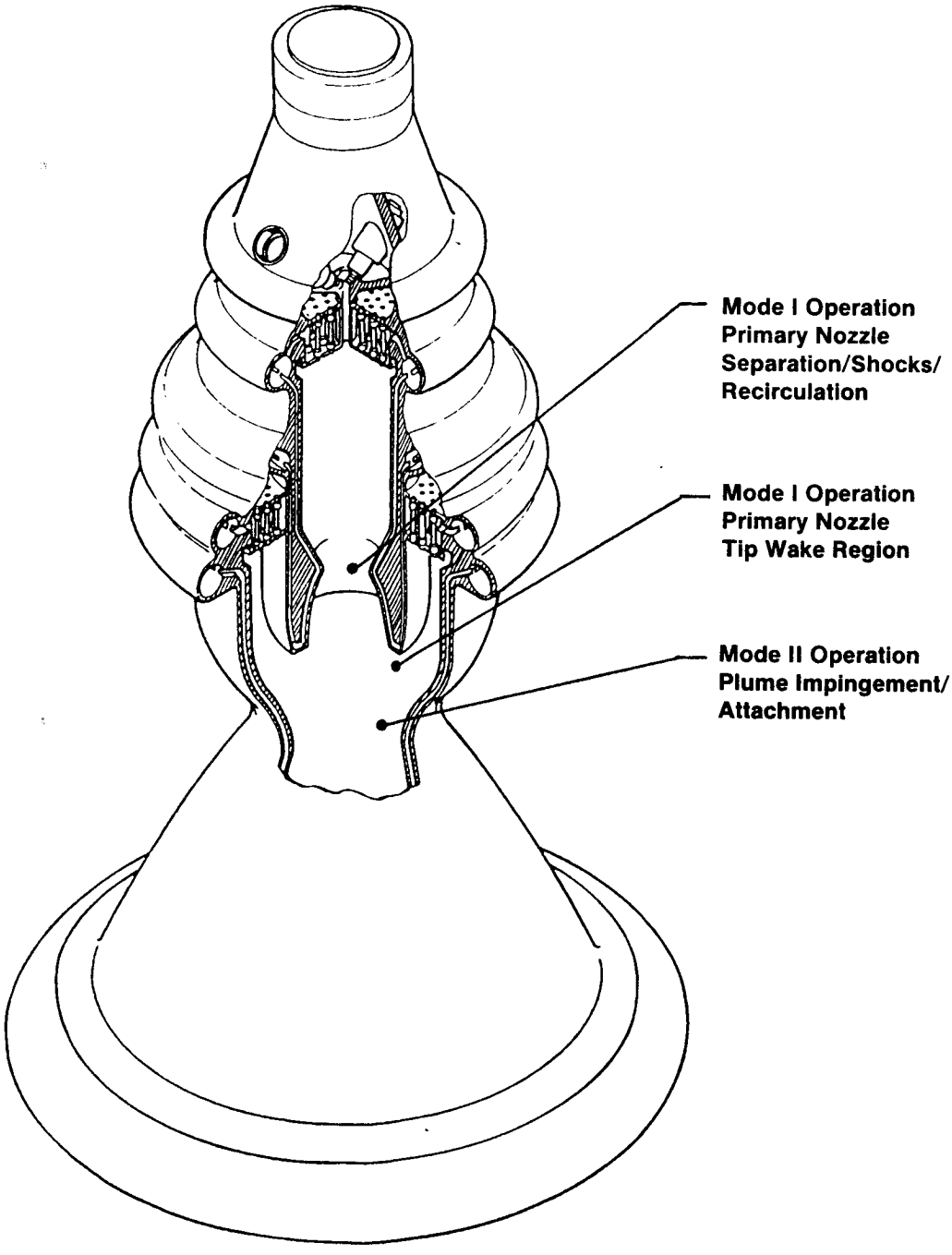

Figure 4. Dual-Throat Chamber Cutaway and Regions Investigatred

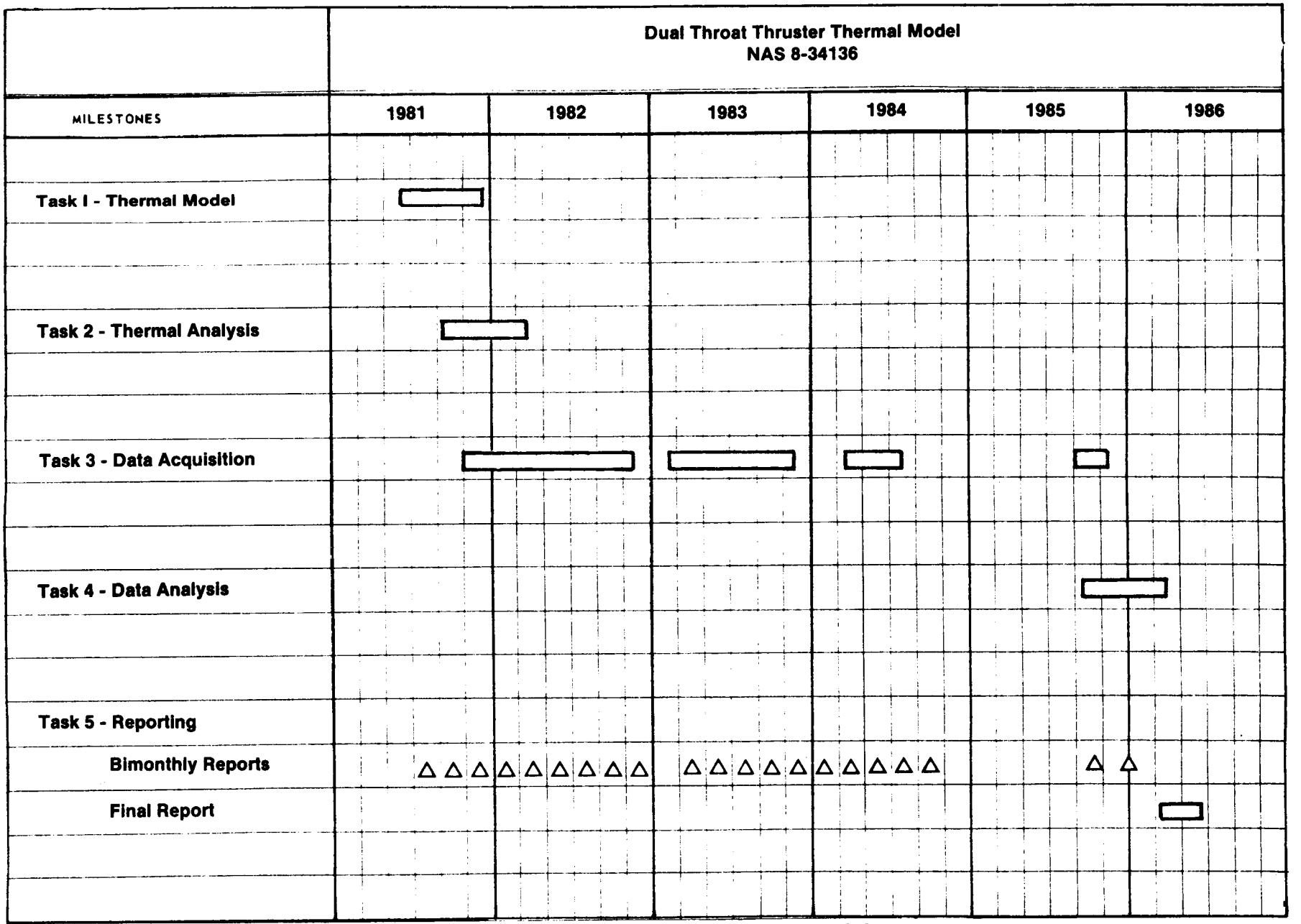

Figure 4a. Dual Throat Program Schedule

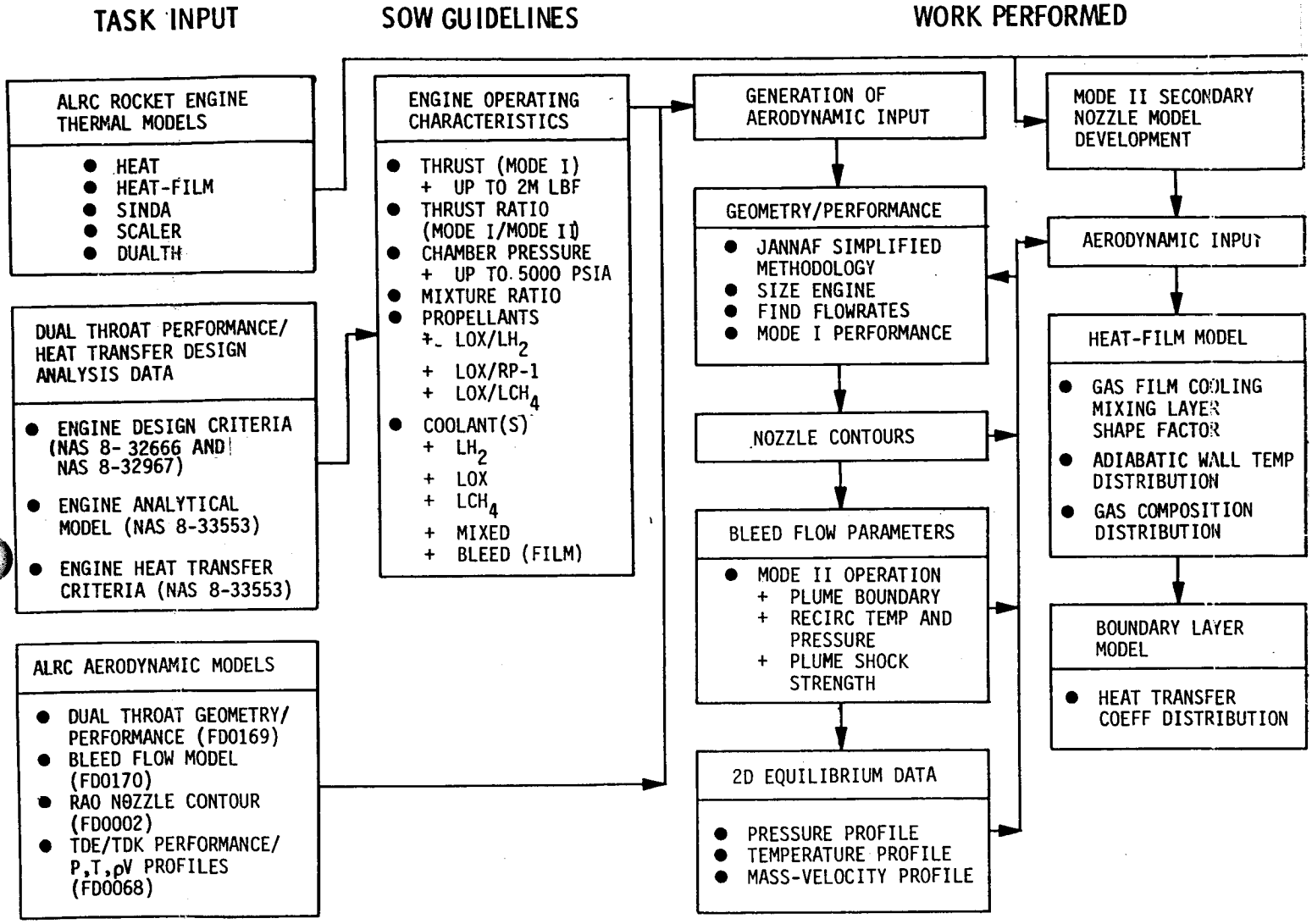

FOLDOUT FRAME

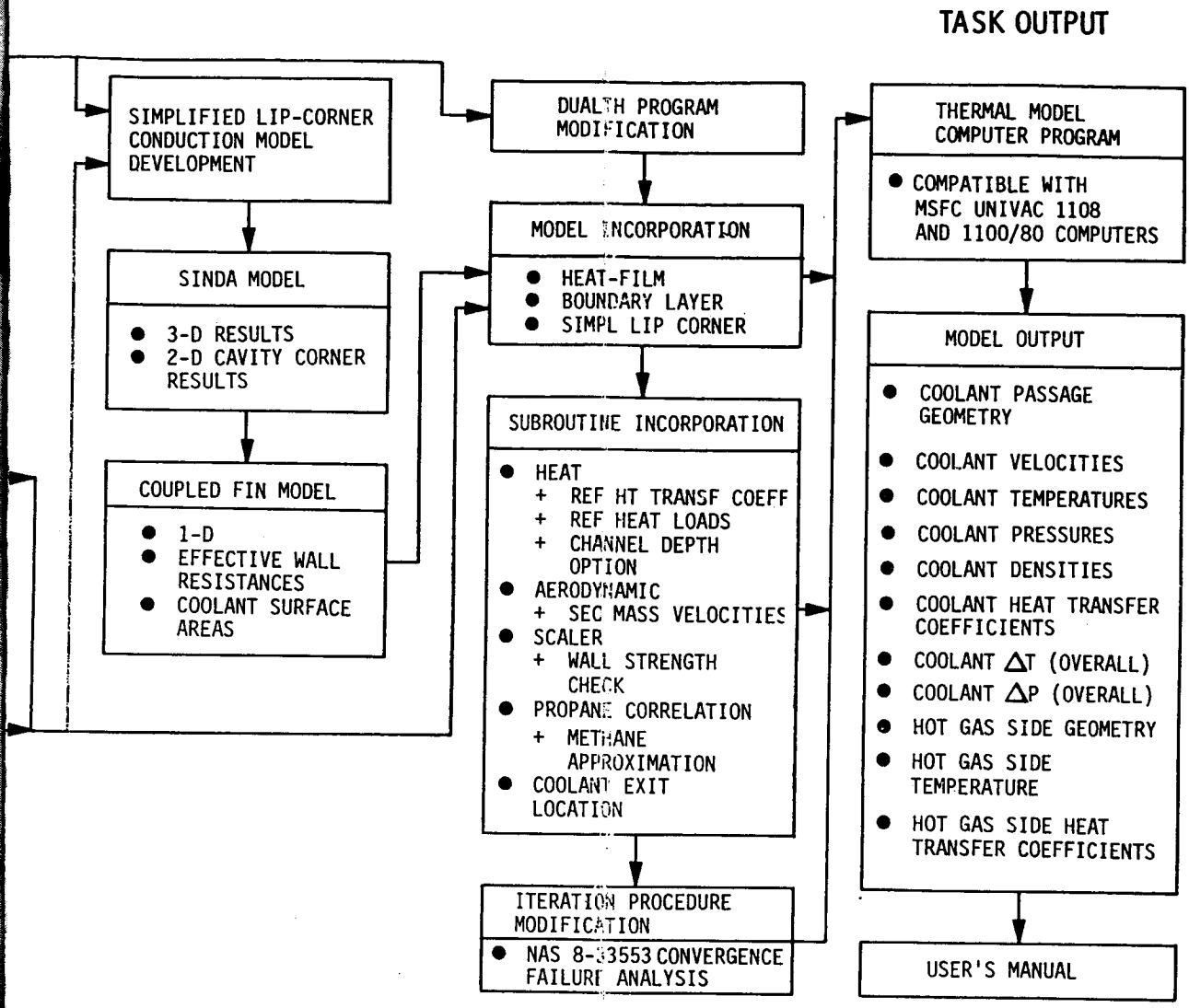

2 FOLDOUT FRAME

Figure 5. The Thermal Model Results from the Use of Existing Models and Dual-Throat Experience, Thermal Model Elements, and Aerodynamic Models

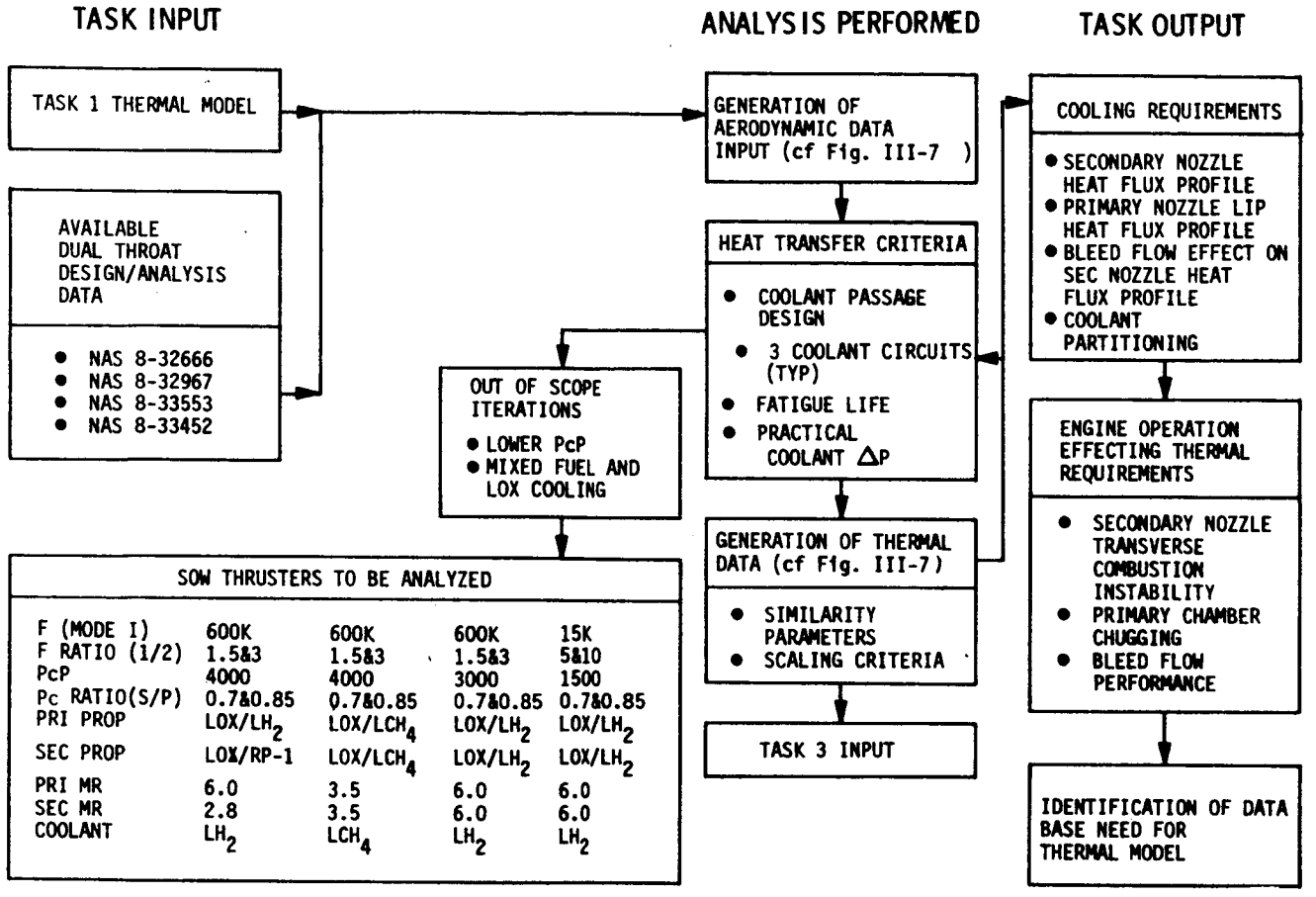

Figure 6 . The Task 2 Analysis of Dual-Throat Thrusters Starts with the Generation of Aerodynamic Data

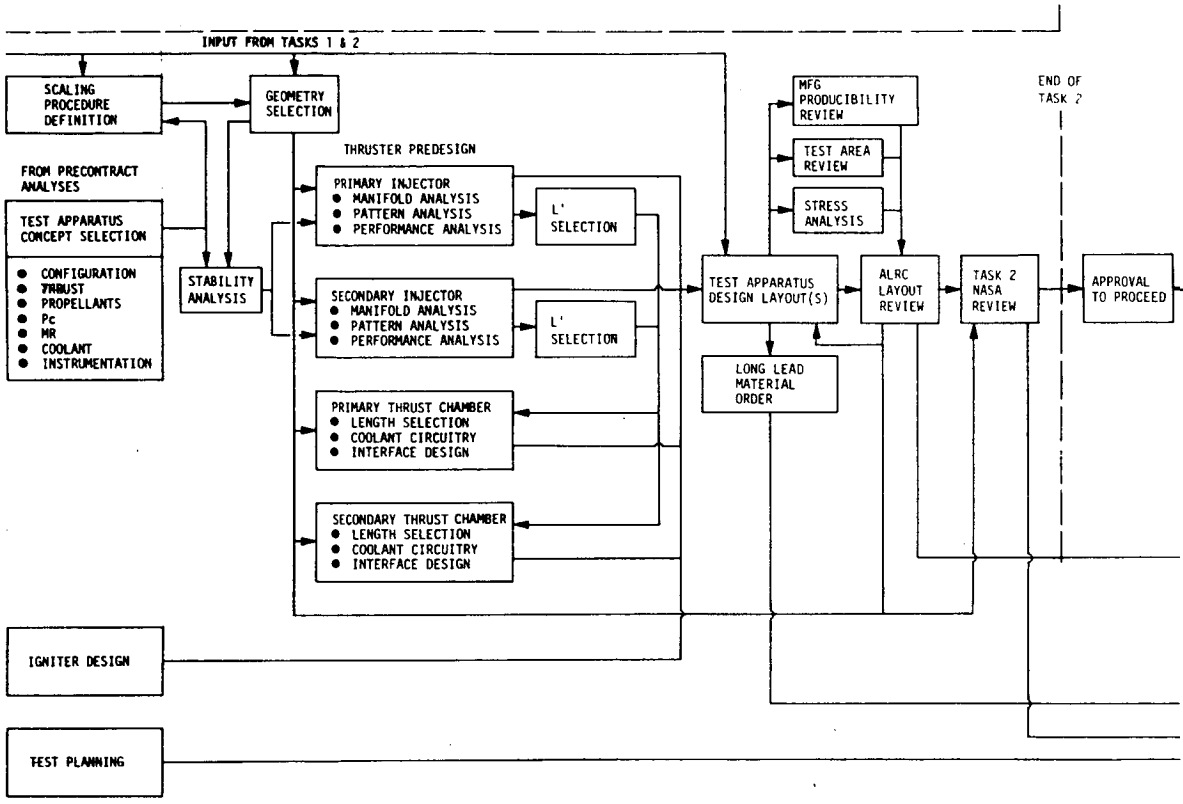

FOLDOUT FRAME

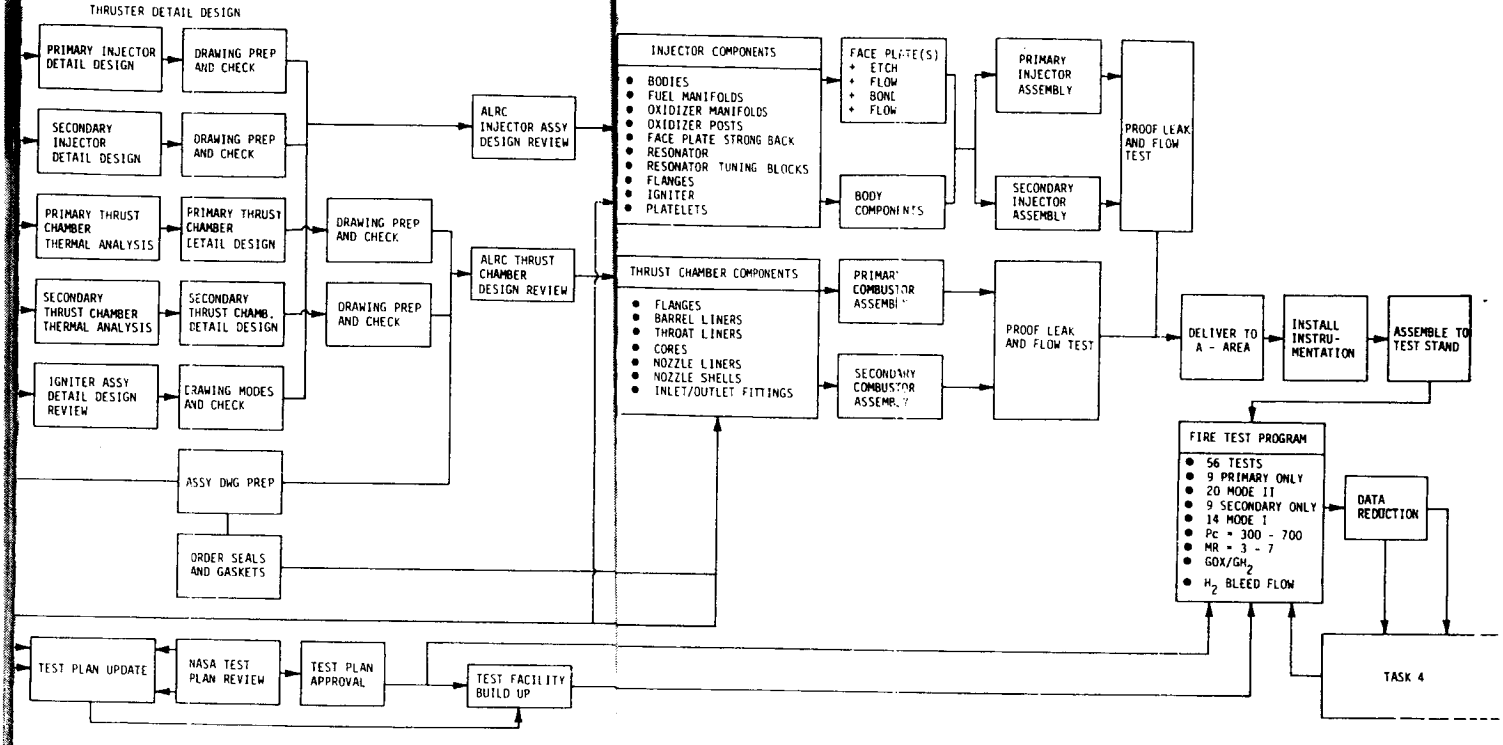

Figure 7. Task 3 - Data Acquisition Logic Chart

FOLDOUT FRAME

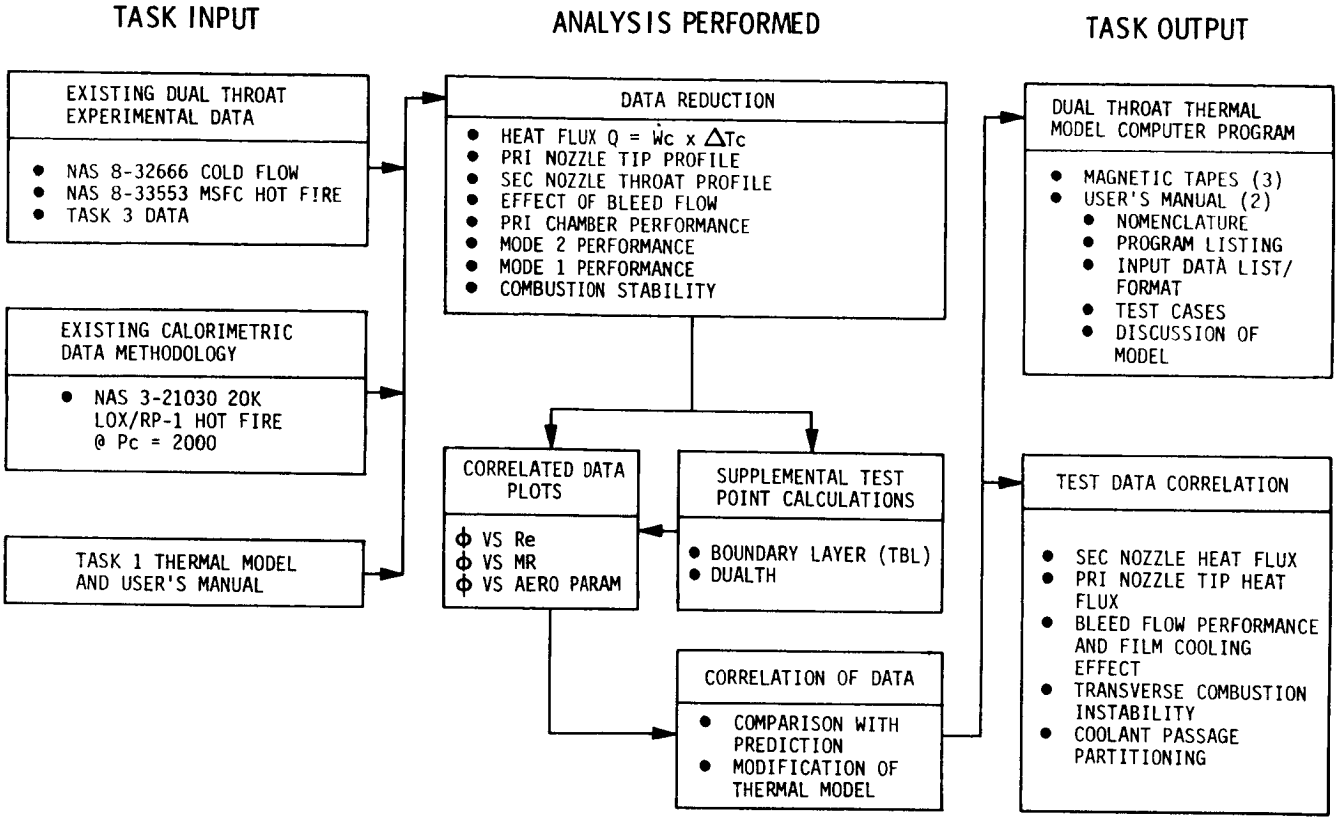

Figure 8 . Task 4 - Data Analysis, Program Activities

III. THERMAL MODEL (TASK I)

A. OBJECTIVE

The purpose of this task is to develop a detailed thermal model of the dual-throat thruster to be used to describe its cooling requirements.

The model output will describe the thruster coolant circuits and operating characteristics such as coolant passage geometry, coolant velocities, temperatures, pressure, density, coolant heat transfer coefficients and overall temperature and pressure change. The output shall also describe the corresponding hot gas side characteristics and chamber material properties including hot wall temperature and heat transfer coefficients.

B. APPROACH

The general approach to developing the thermal model is outlined in Figure 5. Thermal model development consisted of three efforts: development of a simplified model of the primary chamber lip region to replace 2-D and 3-D SINDA models; development of a gas-side boundary condition model for the secondary contour during Mode II operation with bleed flow; and consolidation of all dual throat model components, except TDE and the aerodynamic bleed flow model, into a single thermal analysis computer program.

Special studies of the lip region were conducted previously, Reference 2, using a 3-D SINDA model with a square coolant channel corner. A 2-D model with channel curvature but without lands between channels was also available from acoustic cavity corner design studies. The purpose of the present lip region effort was to develop a simplified analytical model with channel curvature which simulates the SINDA network models. Pressure drop and coolant bulk temperature rise calculations in the lip studies of Reference R2 were performed by hand. Therefore, it was necessary to include these calculations as well as the simplified wall analysis model in the overall thermal analysis computer program.

III, B, Approach (cont.)

Previous thermal analyses of the dual throat concept have not considered the effects of bleed flow in Mode II. The original study, Reference 1, considered only Mode I, since that is the mode which would normally define the cooling system. The next study, Reference 2, also considered Mode II operation but without bleed flow. As a result, a thermal model of the secondary with bleed flow was required. Such a model should include the recirculation region and the film cooling effects of the bleed flow downstream of the primary plume attachment point. The latter has been developed herein by extending the shear layer analysis of the aerodynamic bleed flow model, Reference 2, in the form of a wall mixing layer adapted from the ATC gas film cooling model of Reference 3. The emphasis in the present model is on nominal bleed flow rates which result in the primary exhaust plume creating very weak oblique shocks when attaching to the secondary nozzle.

Previous thermal analyses required a number of computer programs, including a boundary layer program to determine the Mode II heat transfer coefficients downstream of the primary plume attachment point as well as separate programs for the selection of channel depths and the anlaysis of specified depth profiles. Therefore, a primary objective of Task I of the present contract was to consolidate the various parts of the regenerative-cooling analyses into a single program and include the above lip region and Mode II bleed flow models. This was accomplished by modifying a version of the SCALER regenerative-cooling program for conventional chambers, which already included the gas film cooling model. A brief discussion of the resultant program is included herein; a detailed user's manual is provided in Reference 4.

C. RESULTS

1. Lip Region Model

A simplified lip region thermal model has been developed using the coupled fin approach shown in Figure 9 along with corrections for land width. The model is symetrical except for different gas-side heat transfer coefficients, with the end-wall (wake region) value being specified as a fraction of the side-wall coefficient. A uniform coolant heat transfer coefficient is applied, except for the curvature effect on fins 1A and 2A, with the wall temperature dependence based on the average of TWLC and TWL2 (see Figure 9).

Fins 1 and 1A are solved for an effective heat transfer coefficient h_{e1} at the interface with fin 3. An identical solution for fins 2 and 2A, but using the wake region h_g, yields h_{e2}. Fin 3 is oriented with its end points at the side wall and the interface with fin 2A; thus h_{e2} is used as a boundary condition while h_{e1} appears in the fin differential equation. Internal resistances included in the fin equations are shown in Figure 9 and are used to calculate surface temperatures such as TWGC, TWLC and TWL2 from the fin solution temperatures.

The length of fins 1A and 2A and their internal resistance on the coolant side are related to the channel radius of curvature R_c. As noted on Figure 9, the length plus the additional wall thickness relative to fins 1 and 2 is equal to the radius of curvature. The total thickness t_{WA} of fins 1A and 2A is based on the correlation of Figure 10 developed by simulating 2-D SINDA model results. This correlation relates t_{WA} to R_c and the thickness t_w of fins 1 and 2; t_w is the actual wall thickness adjacent to the channel curve.

Comparisons of model predictions for cases with no channel curvature with results from the 3-D SINDA model of Reference 2 defined corrections to the two corner temperature predictions to account for land width variations. There corrections are shown in Figure 11: the model predicts the gas-side corner temperature with no correction for a land width of about 0.050 in. Two alternate approaches could be developed using the fin model of Figure 12 to account for the land perturbation. In one case the channel centerline would be insulated and a land correction defined relative to the one-dimensional solution with no land. In the other case the solution for the heat transfer at the channel centerline for an assumed centerline temperature would be used to create transverse heat source terms in the fin equations associated with the model of Figure 9. These alternate approaches have the advantage of accounting for the effect of channel depth on the land fin effectiveness.

The lip region pressure drop includes a turn loss based on the higher velocity head, calculated using a specified k-factor, plus a friction term based on the length $t_{lip} - 2\ t_w$.

2. Mode II Secondary Model

A gas-side boundary condition model for the secondary chamber during Mode II operation has been developed for the region downstream of the primary plume attachment point. As shown schematically in Figure 13, the model represents a continuation of the shear layer from the aerodynamic bleed flow model in the form of a mixing layer with a wall boundary layer submerged within it. The flow in the shear layer outside the "d" streamline forms the initial flow in the mixing layer, which accounts for the film cooling effect of the bleed flow on the adiabatic wall temperature. The mixing layer model was developed from the ATC entrainment film cooling model, Reference 3, and predicts axial profiles of the mixture ratio at the wall and the adiabatic wall temperature. An integral energy equation model of the thermal boundary layer was added to define heat transfer coefficients. Details of these models are given in Appendix A.

Two-dimensional, finite-difference boundary layer analyses were run for the baseline design of Reference 2 using the NASA-Langley computer program described in References 5 and 6 with initial profiles from the shear layer model. These analyses provided the detailed mixing layer and wall heat transfer characteristics which the engineering models developed in this task must represent. Two such analyses were made: adiabatic wall and cooled wall. Adiabatic wall cases were run for two values of the reference Reynolds number to approximate the range of primary chamber pressures of interest in Task II.

3. Consolidated Computer Program Development

A regenerative-cooling computer program with dual throat geometry features was available from the design studies of Reference 2; this program has been developed from an early version of the SCALER program for conventional chambers. However, subsequent development of SCALER, including addition of the gas film cooling model of Reference 3, had created a program which was easier to use, was a much more powerful design tool and included the framework for the new Mode II mixing layer model. Therefore, it was decided to use the latest SCALER program as the starting point for the new consolidated dual throat thermal analysis program. The major modifications required were:

(1) Incorporating the dual throat geometry features from the previous program used in Reference 2,

(2) Adding the special wall analysis at the primary chamber exit lip corners,

(3) Generalizing the film cooling model as defined in Appendix A to account for the initial mixing of bleed and primary flows which occurs in the shear layer of the aerodynmic bleed flow model,

(4) Adding the simplified heat transfer model defined in Appendix A for the recirculation region,

(5) Adding the boundary layer model downstream of the primary plume attachment point, and

(6) Incorporating an analysis option for specified channel depth profiles.

Additional changes provided for greater flexibility in defining the starting and termination points for cooling circuit segments and for expanded diagnostic output after convergence failures.

Features included in the program as a result of its derivation from the latest SCALER include the following:

(1) Channel layouts may be specified or calculated internally based on constraints on channel aspect ratio, coolant mass velocity or friction pressure gradient,

(2) A wall strength check, with the wall thickness increased as needed,

(3) Axial increment subdivision in the event of convergence failure.

A detailed user's manual for the thermal analysis program is included in Reference 4.

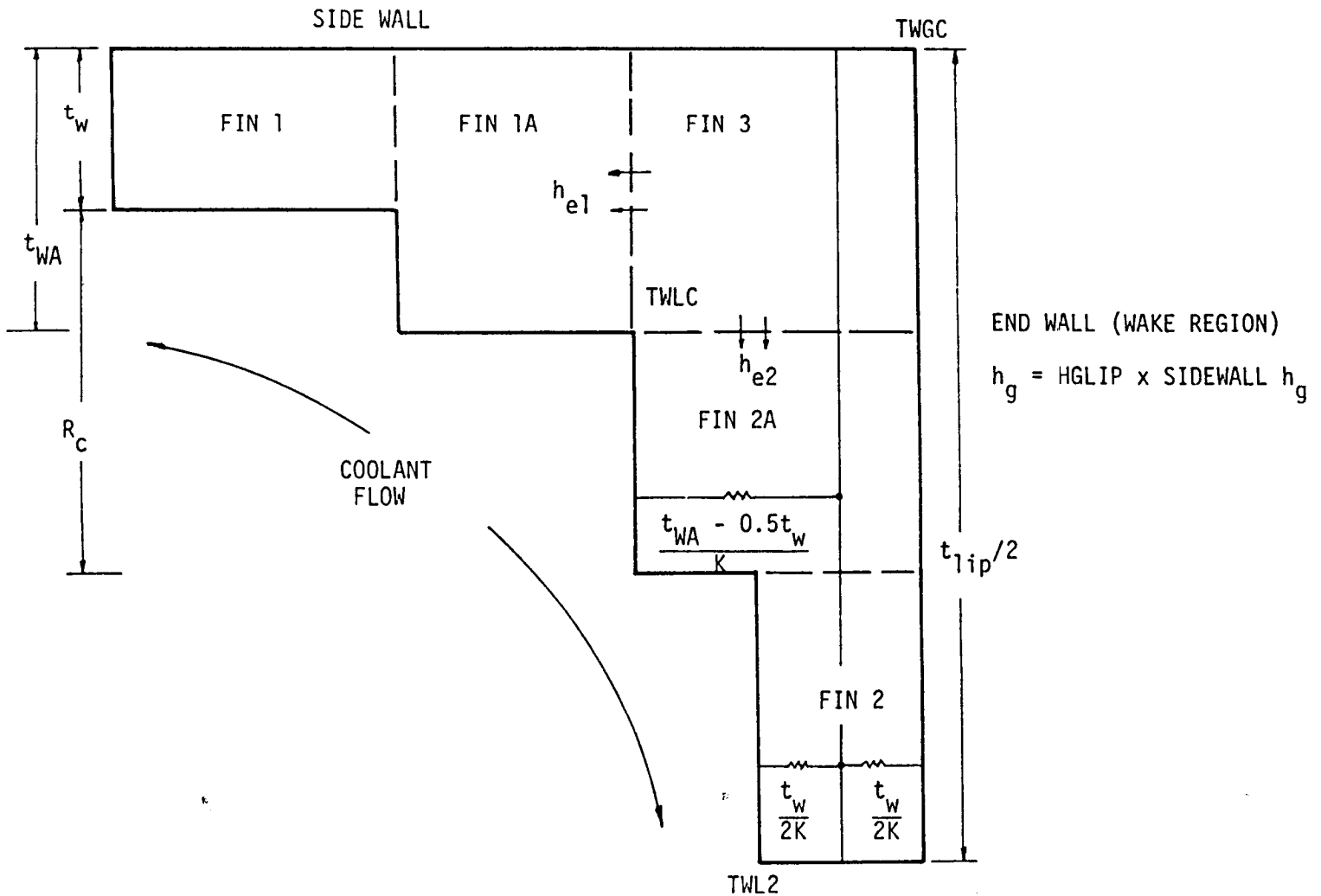

Figure 9. LIP Corner Model

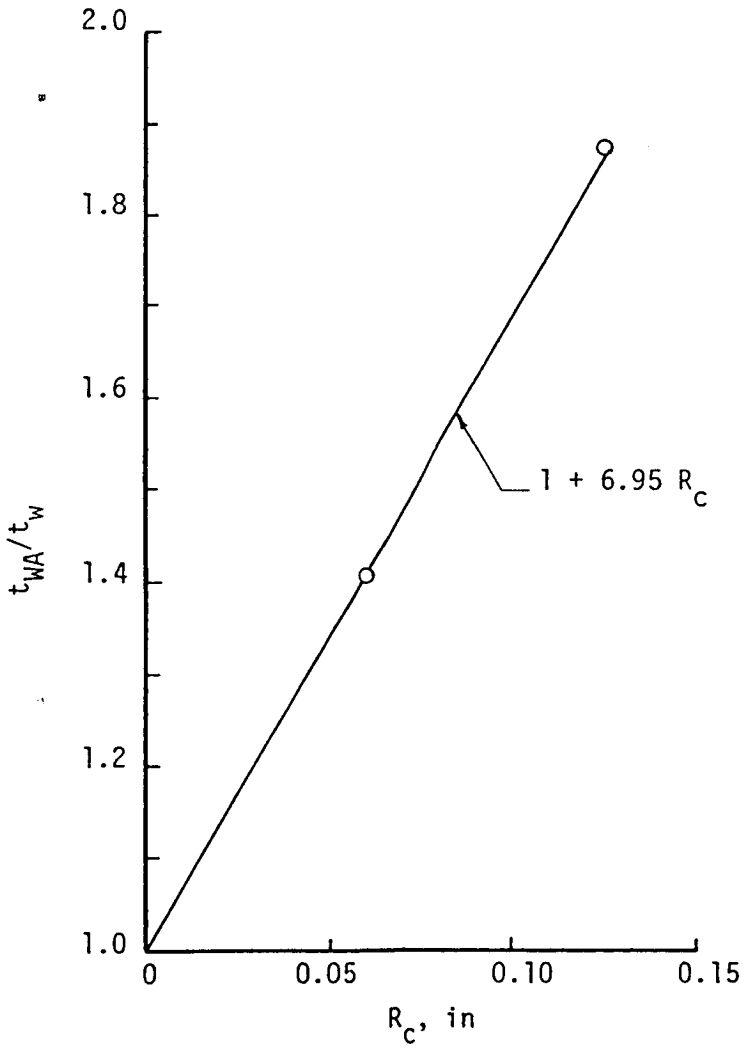

Figure 10. Thickness Correlation for FINS 1A and 2A of the LIP Corner Model

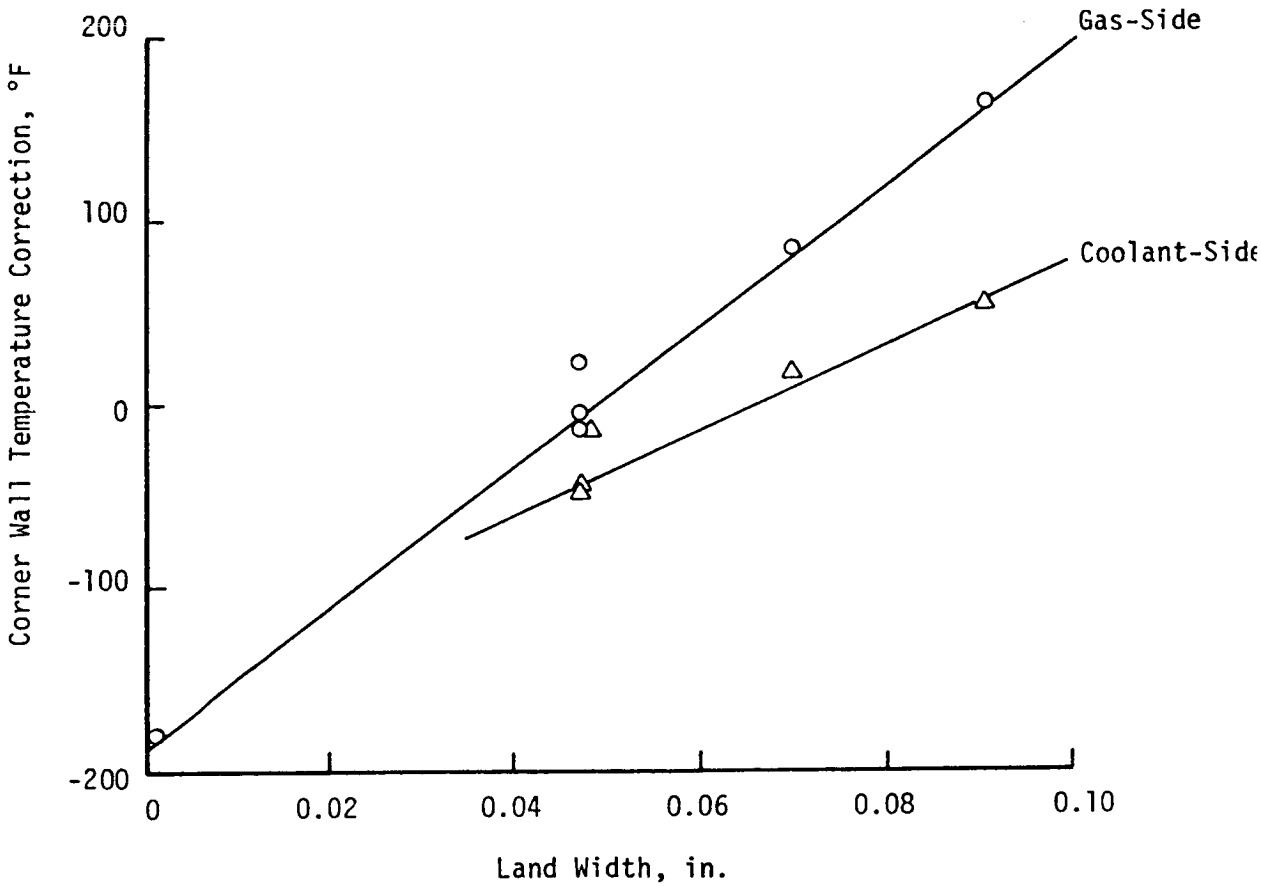

Figure 11. LIP Model Corner Temperature Corrections to Account for Land Perturbations

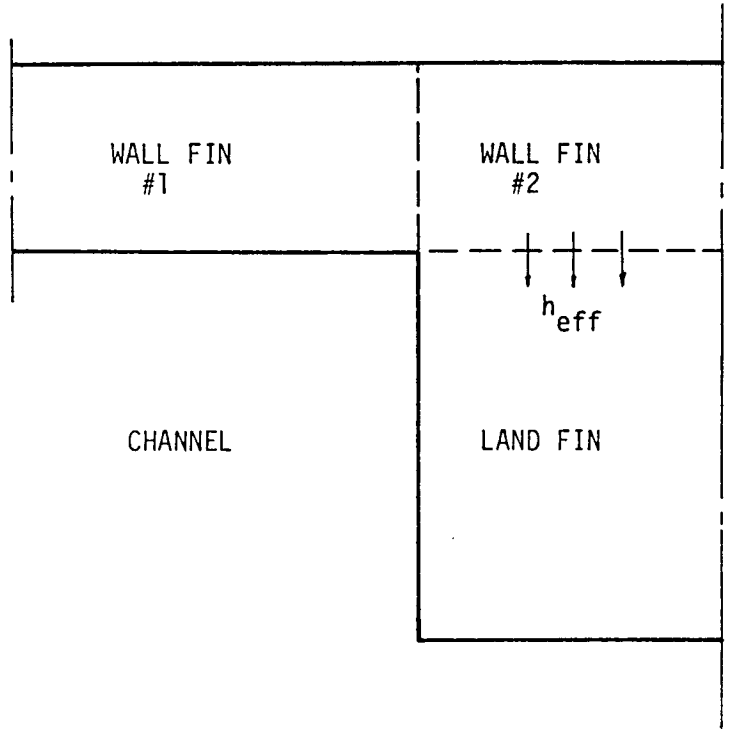

Figure 12. Potential Transverse FIN Model to Account for Land Perturbations in the LIP Corner Model

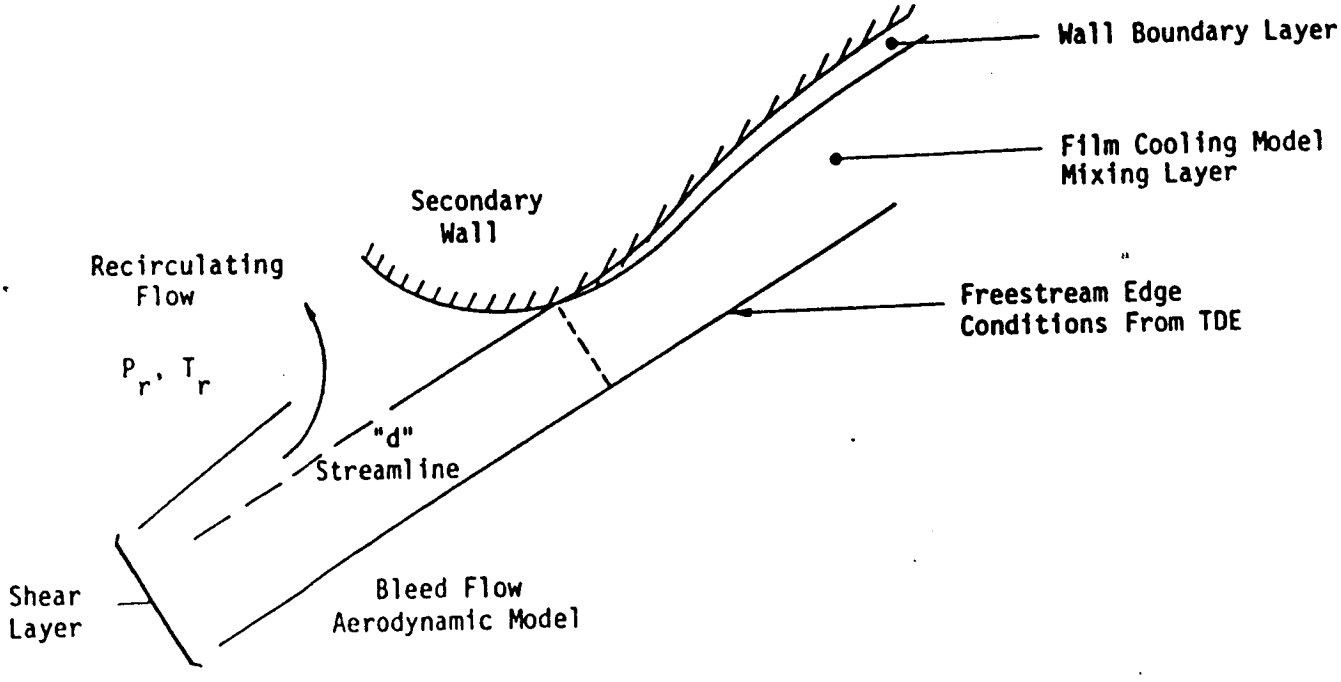

Figure 13. Mode II Thermal Model is a Continuation of the Aerodynamic Bleed Flow Model Shear Layer

IV. DATA ACQUISITION

A. OBJECTIVES

The objective of this task was to design, fabricate, and test experimental dual throat hardware to provide the data base for tuning the thermal model. Because full scale hardware was beyond the scope of the program, an additional objective was to provide the scaling rationale that justified the selected low thrust and reduced chamber pressure test conditions.

B. APPROACH

The approach for this task is summarized in Figure 7. The approach includes the following subtasks:

(1) Test Apparatus concept selection.
(2) Scaling procedure selection.
(3) Geometry definition.
(4) Thruster design (preliminary and detail).
(5) Test hardware manufacture.
(6) Test planning/test stand preparation.
(7) Hardware assembly and installation.
(8) Hardware/Test stand flow calibration.
(9) Hot fire test program.
(10) Data reduction.

C. RESULTS

1. Test Apparatus Concept Selection

The axisymmetric bipropellant dual-throat thruster assembly, shown in Figures 14 and 15, was selected after detailed examination of several candidate concepts. These alternates included larger-scale calorimeter chambers and non-axisymmetric (2-D) thrusters. Both bipropellant gas

generation and the use of hot gas (e.g., heated N2) were considered. H2-cooled, water-cooled, and uncooled combustion chambers were examined. The larger scale chambers were rejected for cost considerations. Uncertainties in the interpretation of aerodynamic and thermal data from 2-D chambers led to their rejection.

The study concluded that the configuration shown in Figure 14 offered the best flexibility, lowest costs and the minimum risk since all of its components are based upon successful results with previously tested hardware. The design readily allowed for changes in chamber-to-chamber length.

The selected apparatus utilized a gaseous oxygen/gaseous hydrogen injector to avoid the exponential delta P that results from liquid propellant injection. Ignition of the primary chamber was accomplished with a hydrogen/oxygen torch igniter. The secondary chamber was back-lighted by hot primary gases.

The injector geometry included resonator cavities for dynamic stability and tuning blocks to modify the cavity size as required. No modification of the cavities were needed during the test series.

Circular calorimetric coolant passage geometry was utilized to obtain heat flux data versus axial station. The coolant passage design was selected to allow sufficient coolant temperature rise during the tests. The coolant flow rate was modified in any circuit by changing its orifice size. Because conduction between axial passages could obscure temperature data, the passages were through a low conductivity material core.

2. Scaling Procedure Selection

Similarity parameters conventionally utilized for heat transfer scaling were applied to predict the range of scaling allowed by the test

parameters. For example, the turbulent boundary layer conditions in the primary chamber nozzle dictated the lower limit in chamber pressure that would provide scalable test data. Experimental data indicate a freestream Reynolds number of about 600,000 to be the lower limit of the turbulent regime, which corresponds to a film Reynolds number of 1.3×10^6. These criteria were converted to a thrust-chamber pressure (F X PC) product at a given mixture ratio and expansion area ratio. (See Figure 17).

The similarity criteria indicated the need for a large chamber pressure variation in order to maximize the Reynolds number variation for scaling. It was also necessary to operate the test hardware over a wide range of mixture ratio in order to obtain a large gas property (gamma, etc.) range to simulate dual fuel gas properties.

3. Geometry Definition

The design point operating characteristics of the dual throat thruster are given in Table I. The nominal sea level thrust for mode I is 5000 LBF, with the secondary stream tube contributing 70% of the thrust. The vacuum thrust ratio (F1/F2) is just under 3:1. Mode II testing was conducted at sea level conditions at a thrust level of 1500 lbf.

The dimensions of the test unit were established from aerodynamic (aerodynamic model), thermal (thermal model), and fabrication (mechanical design) considerations. The test unit geometry is shown in the schematic of Figure 16.

a. Design Point Selection

Relative sizing of the two chambers was based on providing 70 percent of the Mode I thrust from the secondary at a pressure ratio (secondary/primary) of 0.7. Primary throat diameter selection was based on provid-

TABLE I

BASELINE DESIGN FOR SIZING TEST HARDWARE

* * * Dual Throat Engine Performance Model * * *

	Mode 1 - Parallel				Mode 2 (Conventional Nozzle)
	Primary Chamber Stream Tube		Secondary Chamber Mass Averaged		
Propellants	O2/H2		O2/H2		O2/H2
Thrust (Sea Level), LBF	1512.7		3487.3	TOTAL = 5000.0	
Thrust (Vacuum), LBF	1613.3		3719.3	TOTAL = 5332.6	2013.1
Per Cent Thrust	30.3		69.7		
PC, PSIA	349.9	EFFECTIVE	350.0		500.0
O/F	7.0		7.0		7.0
Gamma	1.197		1.198		1.197
Nozzle Exit Pressure, PSIA	40.00		40.000		
Nozzle Area Ratio	2.08		2.08	2.08	9.77
ODE ISP (Sea Level), Sec	310.9		310.9	310.9	
ODE ISP (Vacuum), Sec	330.5		330.5	330.5	403.3
Divergence Efficiency	.9842		.9842		.9990
Kinetics Efficiency	.9767		.9796		.9854
Energy Release Efficiency	.9900		.9900		.9900
Boundary Layer Loss, Sec			1.3		1.8
Delivered ISP (Sea Level), Sec	294.9		294.6	294.7	
Delivered ISP (Vacuum), Sec	314.5		314.1	314.3	392.4
ISP Efficiency (Sea Level)	.9486		.9475	.9478	
ISP Efficiency (Vacuum)	.9516		.9506	.9509	.9731
C-Star, Ft/Sec	7232.5		7232.6		7263.0
Fuel Flow Rate, LBM/Sec	.6		1.5		.6
Oxidizer Flow Rate, LBM/Sec	4.5		10.4		4.5
Total Flow Rate, LBM/Sec	5.1		11.8	17.0	5.1
Throat Radius, In.	1.02		1.56	1.86	.86
Throat Area, IN2	3.30		7.60	10.90	2.32
Per Cent Bell				100.0	127.9
X/RT				1.6	10.2
Nozzle Length, In.				3.1	8.7

Mode 1 to Mode 2 Thrust Split = 2.649
Primary Nozzle Area Ratio = 2.615
Secondary Nozzle Convergence Length = 3.673
Secondary Contraction Ratio = 3.346

RPT/BB0216-T

ing a maximum primary chamber pressure range in order to provide for extrapolation of the resultant test data to prototype Reynolds numbers. This selection was constrained by the following factors, which are illustrated in Figure 17 for water-cooled OFHC walls with O_2/H_2 propellants:

(1) Maintaining turbulent flow in the throat region of the primary chamber, which requires a film Reynolds number (based on diameter) of 1.3×10^6 or higher.

(2) Providing 6 sec test durations with existing water tank capacity.

(3) Limiting the primary chamber pressure to provide adequate cooling with the available tank pressure of 3300 psia and minimizing extrapolation of the data base for the proposed injector design.

(4) Providing adequate heat flux measurement resolution without resorting to very small channel widths (minimum hardware size limit).

These considerations resulted in selection of a maximum primary chamber pressure of 850 psia and a thruster size which would produce 8500 lbf thrust at that pressure. All design studies assumed a mixture ratio of 5.0, which results in the maximum heat flux, and were limited to the nominal nozzle spacing of 2.5 in. At the design pressure ratio and nozzle spacing, operation at a primary Pc of 1000 psia is possible at mixture ratios below 3.0 in order to maximize the Reynolds number.

4. Thruster Design (Preliminary and Detail)

The design and analytic processes required to complete the design of the dual-throat thruster hardware included a variety of activities

which had considerable interaction. The activities are necessarily doubled because of the dual-throat thruster with its coaxial injector-chamber arrangement. Preliminary design activities allowed the development of an analytically supported design layout of the test thruster. Detailed thermal design of the thruster followed to finalize the coolant circuitry details.

a. Primary Injector Design

The primary injector design was based on prior Aerojet experience obtained on three different O2/H2 injector programs (References 7-9). The GO_2/GH_2 injector design was selected because of: (1) the gas-gas system's broader range of operating conditions, (2) the elimination of time-consuming chill-down operations between tests, and (3) the improved stability characteristics for off-design conditions.

Details of the primary injector design are given in Appendix E. Primary injector fuel platelet and oxidizer platelet assemblies are given in Appendix E. The injector utilizes swirl co-axial elements similar to those used in Reference 7.

The faceplate of the primary injector was electron-beam welded to the injector body at its periphery and near its center. Resonator cavities located at the periphery of the injector were milled into the injector bodies. Cavity inserts (not needed during testing) could be attached by bolting to the ceiling of the cavities to allow the resonators to be tuned.

The fuel inlet torus surrounding each injector resonator was designed for constant flow velocity. Fuel distribution holes were spaced circumferentially midway between the outer row of coaxial elements. The fuel manifolds were bounded by the faceplate and injector body.

The oxidizer manifold of the primary combustor was located on the backside of the injector surrounding the torch igniter port.

The oxidizer tubes were recessed approximately one tube diameter into the faceplate and were held concentric within the fuel discharge orifice by tabs integral with the faceplate. The oxidizer tubes were brazed into the injector body. Gaseous oxygen entered the oxidizer tubes tangentially to form a hollow cone spray as it ejected from the tube into the surrounding GH2. The tangential oxidizer flow was established by means of flow passages located in a stack of photoetched and bonded steel platelets which were located immediatley upstream of the tube inlets. The oxidizer manifold of the primary injector was created by electron-beam welding the outside diameter of the closure plate to the injector body and by brazing the central portion of the closure plate which contains the igniter chamber.

The fuel manifold was machined from the face side of the injector body. The fuel entered the manifold from equally spaced radial drilled bleed holes which match the number of injection elements in the outer most row. The primary injector was joined to the combustor by 12 bolts which passed through the primary chamber flange into the secondary injector oxidizer cover plate.

b. Secondary Injector Design

The secondary injector utilized co-axial elements similar to the primary injector. The secondary injector design details are shown in Figures in Appendix E and the injector fuel and oxidizer platelet assembly details are given in Appendix E.

The design details, manufacture, and assembly of the secondary injector were similar to those given for the primary injector. Back lighting of the secondary combustor from the primary combustor eliminated the need for a separate secondary ignitor.

c. Thrust Chamber Design

The thrust chamber design process proved to be very complicated. There were double the usual injector-chamber interfaces and there were interfaces between the chambers themselves. The most complicated design involved the coolant circuits of the primary chamber. Because the primary chamber was cantilevered inside the secondary chamber, coolant circuits had to be fed axially down the chamber barrel.

Both the primary and secondary combustion chambers were water-cooled and featured calorimetric circuits over their convergent-divergent nozzles. The circuits of the secondary combustor nozzle were arrayed on the internal diameter, while the wall of the primary combustor had coolant passages on both internal and outside diameters. The overall arrangement of the two chambers is shown in Figure 14.

Three types of water-cooling circuits were utilized in the chamber designs as illustrated in Figure 18. Type A were circumferential circuits for the local heat flux measurement in which a number of segments flow in series. Bulk temperatures were measured at the crossovers between segments, each of which consisted of 1 to 3 channels in parallel. A bulk temperature rise of at least 50 degrees fahrenheit was desired for each segment to assure heat load measurement accuracy. These circuits were located in three regions as shown in Figure 18: (1) primary chamber from just upstream of the throat to the end of the nozzle, (2) primary chamber exit lip, and (3) secondary chamber from the mode 2 impingment location farthest upstream to a point downstream of the throat.

Type B were circumferential circuits in which a larger number of channels flow in parallel. These circuits cooled the remainder of the secondary chamber (outer wall) and provided a gross heat load measurement over a relatively large axial section.

IV, C, Results (cont.)

Type C were axial circuits in which multiple channels flowed in parallel. These circuits cooled the remainder of the primary nozzle and most of the outer wall of the primary chamber (inner wall of the secondary chamber).

(1) Primary Chamber

The coolant circuitry for the primary chamber is given in Figure 19. The circuitry was designed for finer flux resolution in the areas of thermal interest. These are the internal diameter and tip of the primary nozzle and are numbered for easy reference in Figure 20.

The channels in the tip (or lip) region of the primary nozzle were at each corner and in the center of the downstream (wake region) surface. In addition, small channels were provided just upstream on both the primary and secondary surfaces to obtain side wall heat fluxes for use in partitioning the corner channel heat loads into side wall and wake wall components. Each bulk temperature rise segment in the primary nozzle and lip was a separate circuit.

The cross section of circuit no. 2 in the primary chamber is shown in Figure 21. Cross sections of circuits no. 2 and 3 in Figure 22 illustrate the inlet and outlet feed channel to the circuits.

The surfaces which were exposed to the combustion processes were made from OFHC copper. The water passages were mostly circumferential, providing axial flux distribution data and allowing fabrication by turning rather than milling operations.

Detail drawings of the primary chamber assembly are given in Appendix E. Drawings for the primary chamber lip platelet section are given in Appendix E. A discussion of these components and their assembly will be given in the section on test hardware manufacture.

IV, C, Results (cont.)

Thermal analyses of the primary chamber axial channels (which cooled the inner and outer surfaces) and the size required for the feed holes for the calorimeter channels dictated a chamber wall thickness of 0.78 in. The wall cross-section data are given in Table II.

Hydraulic analysis of the water cooling circuits of the primary chamber indicated a chamber pressure limit of about 850 psia using the channel geometry values shown in Table III and the assumption that the cooling circuits would be orificed to maintain a minimum static pressure of 1000 psia. Results of the hydraulic pressure drop analysis are summarized in Table IV for eight of the twelve primary chamber calorimeter circuits and the axial coolant circuit. The analysis (1) the defined maximum pressure drop (Delta P) expected (i.e., the maximum supply pressure required for testing), (2) determined the areas of minimum and maximum static pressure in the cooling channels for subcooling and strength conditions, and (3) determined the areas of potential flow separation considered undesirable for heat transfer.

As a result of the analysis, it was recommended that the inlets to the EDM channels be chamferred to avoid flow discontinuities.

A thermal analysis was performed to finalize the primary chamber channel dimensions and the coolant flowrates. The thermal design considerations are summarized in Table V. The number of cooling circuits and temperature measurements, and the maximum coolant flow for each component of the dual-throat system are summarized in Table VI.

Thermal design data for the primary chamber axial circuit are given in Table VII. The thermal data for the primary chamber channels are given in Tables III and VIII. The wall strength margins of the primary chamber are presented in Table IX.

TABLE II

PRIMARY CHAMBER WALL CROSS-SECTION

Inner wall (Cu)	.055 in.			
Inner channel	.170			
Steel wall	.050			
Calorimeter feed holes	.250			
Steel wall	.050		.100	
Outer channel	.125	feed channels	.075	coolant channels
Outer wall (Cu)	.080			
Wall thickness	.780 in.			

TABLE III

PRIMARY CHAMBER CALORIMETER CIRCUIT GEOMETRY/THERMAL DATA

Circuit	Channel Width	Land Width	Channel Depth (Avg)	Flow Lb/Sec	ΔT_b °F
1	0.0625 ± 0.003	0.078	0.047 ± 0.005	1.13	50
	0.0625 ± 0.003	0.078			50
2	0.0625 ± 0.003	0.078	0.046	0.55	50
3	0.0625 ± 0.003	0.078	0.048	1.13	50
	0.0625 ± 0.003	0.088			50
4	0.0625 ± 0.003	0.098	0.055	1.26	50
	0.0625 ± 0.003	0.108			50
5	0.0625 ± 0.003	0.118	0.060	1.35	50
	0.0625 ± 0.003	0.118			50
6	0.0625 ± 0.003	0.118	0.065	1.35	50
	0.0625 ± 0.003	0.128			50
7	0.0625 ± 0.003	0.130	0.070	1.34	50
	0.0625 ± 0.003	0.120			50
8	0.080		0.053 ± 0.003	0.58	54
		0.080			
9	0.040		0.077	0.63	61
		0.098			
10	0.040		0.077	0.30	89
		0.098			
11	0.040		0.077	0.59	73
		0.080			
12	0.080		0.053	0.45	82
		0.120			

TABLE IV

SUMMARY OF HYDRAULICS ANALYSIS RESULTS

Circuit Analyzed	Range of Maximum Inlet Pressure Required	Maximum Static Pressure in Heated Channel (Range)	Comments
13, Axial	2580/2410	2400/2230	Overall ΔP not a problem. Difficulty lies in minimum/maximum static pressure relationship. Potential flow separation at exit of EDM channel into primary barrel.
9, Inner Corner Lip	3010/2960	2536/1820	Analyzed by using two sets of channel entrance assumptions. Worst channel for overall ΔP. Possibility of a problem with maximum static pressure. Design change has decreased risk of flow separation at channel entrance. Cored flow could be a problem.
2, Throat Channel	2550/2255	2107/1295	Analyzed by using two sets of channel entrance assumptions. Overall ΔP not a problem. Maximum static pressure not a problem. Cored flow could be a problem.
Primary Chamber			
1	2558	2076/1585	Analyzed by using only the Crane channel entrance loss assumptions. No apparent problems with either overall ΔP or maximum static pressure. Possibility of cored flow in the channels.
3	2441	2067/1605	
4	2453	1997/1585	
5	2361	1949/1555	
6	2180	1812/1456	
7	2129	1703/1404	

TABLE V

THERMAL DESIGN CONSIDERATIONS

1. Design Points

   Pc = 850/595 O/F = 5

   Pc = 1000/700 O/F = 2

2. Bulk Temperature Rise $\geq$ 50°F in Calorimeter Circuits

3. Burnout Safety Factor $\geq$ 2.01

   = 1.25 (Correlation data scatter)

   x 1.15 (Operating point and dimensional tolerances, except channel dimensions)

   x 1.40 (h_g uncertainty allowance)

4. Wall Temperature $\leq$ 900°F (750°F in barrels)

5. Wall Strength

$$\frac{w + 0.003}{t_w - 0.005} \leq \left(\frac{2 F_{ty}}{P_{ch}} \right)^{0.5}$$

   F_{ty} for coarse grain OFHC

6. Coolant Static Pressure $\geq$ 1000 psia

TABLE VI

DUAL-THROAT COOLING SYSTEM SUMMARY

	No. Circuits	No. ΔT_b Measurements	Maximum Coolant Flow, lb/sec
Primary-Axial	1	1	26.66
Primary-Calorimeter	12	12	10.66
Secondary Chamber	13	18	36.49
Secondary Spacers	2	2	7.82
Total	28	33	81.63*

*Maximum flow testing will probably be with a single spacer,

$\therefore$ Maximum flow = 77.72 lb/sec

TABLE VII

PRIMARY CHAMBER AXIAL CIRCUIT DESIGN SUMMARY

	Inside		Outside	
	Barrel	EDM	Barrel	EDM
No. of Channels	36	36	72	72
Wall Thickness, in.	0.055	0.050	0.080	0.075
Channel Width, in.	0.09375	0.077	0.125	0.100 Dia
Land Width, in.	0.189	0.101	0.072	0.051
Channel Depth, in.	0.170	0.134	0.081	-
Minimum Velocity, ft/sec	101	155	78	99
Wall Temperature, °F	705	915	769	722
ΔT_b, °F	24	11	17	11
Heat Flux, Btu/in.^{2}-sec				
Gas-Side	16.2	32.2	12.4	17.0
Coolant-Side	18.1	32.0	17.6	14.7
BOSF*	2.23	2.05	2.04	2.95

Coolant Flow: 26.7 lb/sec

* Burnout Safety Factor

TABLE VIII

PRIMARY CHAMBER CHANNEL DESIGN SUMMARY

Channel	Heat Flux, Btu/in.^{2}-sec		Wall Temperature, °F	Minimum Velocity, ft/sec	BOSF *
	Gas-Side	Coolant-Side			
EDM Annulus	28.9	32.3	928	155	2.01
1A	32.3	37.6	882	192	1.99
1B, 2, 3A	34.5	36.7	886	191	2.02
4B	32.5	36.4	897	187	1.99
5A	31.1	35.8	892	184	2.00
6A	28.5	33.5	861	171	1.99
7A	26.0	31.3	825	158	1.99
8	24.5	27.7	767	151	2.13
9	22.0	42.6	913	230	2.01
10	18.5	19.4	658	108	2.06
11	18.4	38.9	832	213	2.02
12	17.5	22.0	780	118	2.01
EDM Transition	17.0	16.4	731	78	2.04
Primary Exit	8.0	13.4	772	101	2.98

* Burnout Safety Factor

TABLE IX

PRIMARY CHAMBER WALL STRENGTH MARGINS

	Coolant Pressures, psia	
	Allowable	Predicted
Axial		
Outer Barrel	2780	2353
Outer EDM	2500	2278
Inner EDM	2390	1721
Inner Barrel	2280	1066
Calorimeter		
8, 12	2570*	
9	2600	2228/2536
10	2730	
11	2640	

*Based on minimum wall section

(2) Secondary Chamber

The coolant circuitry for the secondary chamber is shown in Figure 23 and the relative position of primary to secondary circuits is shown in Figure 23A. The flowrates, coolant temperature rise, and channel depths for the secondary chamber are given in Table X. Th coolant channel and wall thickness criteria from the thermal and structures analysis are given in Table XI.

The supply pressures required for each circuit of the secondary chamber are listed in Table XII. The minimum static pressure assumed for the calorimeter channels is 1000 psia, based on subcooling criteria. The supply pressures were calculated at the inlet to a six inch long feed tube into the chamber.

Secondary chamber assembly drawings are shown in Appendix E. A drawing of the L' spacer is depicted in Appendix E.

5. Test Hardware Manufacture

To accomplish the goals of the program it was necessary to build both an operating dual thrust chamber and a data gathering instrument into the same unit. The two functions compounded the already complex design and the fabricability of the thrust chamber assemblies (Reference 10). The driving design factors, the major problems encountered, and the repairs that resulted in a deliverable test thruster are summarized in this section.

The cutaway drawing that illustrates the general arrangement of the bolt-together assembly of the dual throat thruster is shown in Figure 14. The manufacturing process consisted of precision machining and state-of-the-art brazing. There were five major assemblies in the order of decreasing complexity: primary chamber, secondary chamber, primary injector, secondary injector, and L' rings.

TABLE X

SECONDARY CHAMBER CIRCUITS

Channels In Parallel	Circuit	Coolant Flow, lb/sec	ΔT_b, °F	Smaller Channel Depth, in.
Spacer		3.91	75	0.150
1-3	1A	5.75	55	0.155
4-6	1B		50	0.195
7-9	2B	5.09	50	0.200
10-12	2A		50	0.190
13-14	3B	2.41	50	0.095
15-16	3A		52	0.105
17-18	4	2.66	50	0.090
19-20	5	2.64	50	0.083
21-22	6	2.43	50	0.077
23-24	7	2.26	50	0.081
25-26	8	2.18	50	0.083
27-28	9	2.15	50	0.080
29-30	10	2.05	50	0.090
31-32	11	2.15	50	0.090
33-34	12A	2.43	53	0.121
35-36	12B		50	0.106
37-38	13B	2.29	50	0.112
39-40	13A		56	0.092

TABLE XI

SECONDARY CHAMBER GEOMETRY

Channels	Wall Thickness, in.	Channel Width, in.	Land Width, in.
			0.180 Maximum
1-5	0.075	0.125	0.180
			0.170
6	0.075	0.125	-
			0.150
7-12	0.060	0.094	0.150
			0.070
13-32	0.060	0.094	0.070
			0.133
33-40	0.060	0.094	0.133
			0.153
			0.200 Maximum
Spacer	0.075	0.125 (2)	0.350
			0.200 Maximum

TABLE XII

REQUIRED SUPPLY PRESSURES FOR SECONDARY CHAMBER CIRCUITS

Circuit	Supply Pressure (Psia)
1	2785
2	2720
3	2560
4	2130
5	2180
6	2500
7	2100
8	2010
9	1950
10	1770
11	1870
12	2930
13	2340

IV, C, Results (cont.)

The chamber designs, with their complex passages and details of assembly, did not offer many joining alternatives. Electron beam welding (EBW) was utilized for the circular butt welds very effectively. The long cylindrical and inaccessible internal joints could only be brazed. Because of the nature of the designs, it was necessary to go through several sequential braze cycles in order to build up the assemblies. Nickel-gold braze alloys of varying composition were selected to allow decreasing brazing temperatures during subsequent subassemblies.

a. Primary Chamber (Drawing 1194055)

The primary combustion chamber (see Appendix E) was a complex bimetallic brazed assembly that was internally cooled. It was designed to gather calorimetric data. Both the inner and outer copper surfaces were contoured. The inside has a typical converging/diverging configuration and the external surface was complimentary to the contour of the secondary chamber. The internal configuration included longitudinal slots and deep drilled holes that were the supply passages for the water cooling and the calormetric circuits. These circuits provided for gathering data from the throat area to the nozzle tip via circumferential grooves in the inner liner and a brazed-on copper photoetched platelet bonded nozzle tip.

Because of the uniformity required for accurate data gathering, the precise fitup required for brazing, and the exact clocking required for line-up of the passages during the heat shrink assemblies, the unit became a precise instrument. Figures 24, 25, 26 illustrate the assembly process.

(1) Liner Ring -9 Assembly

The inner liner consisted of the OFHC copper core with CRES 304L split rings brazed into the calorimetric circuit grooves in the throat and nozzle. Only half of the taper bottom grooves, shown in Figure 63, were machined at a time and their respective split rings brazed into place.

This procedure rigidified the part so the cycle could be repeated for the other half of the grooves and rings. Figure 27 also shows the 36 feed slots or channels that were formed in the inner liner by the EDM process.

(2) Liner Core -19 Assembly

The liner core assembly consisted of the copper outer liner and the two CRES 304L core (forward and aft) members. Figures 28 and 29 show the components prior to assembly, and Figure 30 is a sketch of the assembly sequence.

The forward and aft cores acted as internal stiffening members to the two copper liners. The most difficult operation was the drilling of the 24 .25-in. dia. by 6-in. deep calorimeter feed holes with a true position tolerance of .005 dia. over their entire lengths. The holes were gun drilled and the tolerances were met.

The radial slots in the forward core (see Figures 28 and 29) were to feed the aft core slots, which in turn were to feed the calorimetric grooves of the inner liner. Because of the precise clocking required during heat shrink assembly, the special tool shown in Figure 30 was utilized.

(3) Liner Ring/Liner Core -29 Assembly

This assembly match machined the -9 liner ring assembly and the -19 liner core assembly and brazed them together. Figure 31 shows the assembly and the sequence of using a long guide pin to orient the inner liner. This brazing operation represented the third braze cycle the unit had experienced.

(4) Liner Platelet -39 Assembly

A copper platelet stack (Figure 32) with photoetched cooling circuits for the primary nozzle lip was diffusion bonded and prepared

for assembly to the unit shown in Figure 33. Figure 34 shows the unit after assembly and Figure 35 is a schematic sketch of the assembly.

Upon completion of this assembly, the unit had been through 6 cycles of brazing temperatures. A proof test was performed on the unit at this point to check the integrity of the brazes. The outer liner failed indicating that the braze had been degraded or that the liner had never been satisfactorily brazed. A portion of the outer liner was machined off and a flanged copper sleeve was brazed to the unit for repair (Fig. 37).

(5) Final Machine -49 Assembly

The inside and outside diameter contours of the primary chamber were tracer turned and 48 feed tubes were brazed to the unit as shown in Figure 36. The chamber was traced from both ends to machine the internal configuration. The outside diameter taper was changed from 20 to 23 degrees in order to add length to the copper to copper repair joint line of the sleeve and cylinder. Figure 37 shows the final configuration and the deviation. The final unit had experienced 10 brazing cycles.

(6) Final Proof and Leak Test

When the primary chamber assembly was subjected to a proof pressure check at 1200 psig small leaks were found at the flange repair joint and at the inner liner forward cone joint. It was decided not to risk any more braze cycles with the unit, especially since the wall thickness was now at its minimum (.078-in.) and would contribute very little to the structural strength during brazing. The leaks were closed by peening to allow completion of the 1200 psig test.

A cursory gaseous nitrogen leak check on the unit indicated cross talk between the calorimeter circuits. Water calibration tests showed that circuits 5 and 6 (Figure 20) had an excessive internal

leak. A review of the drawing dimensions showed that circuit 6 had a .022-in. built-in gap if all dimensions were nominal, as shown in Figure 38. No such gap was designed into circuit 5 so it was assumed that there was a continuous gap between the two CRES core sections. It was believed that the internal leakage would cause some problems in interpreting the test data, but that the leakage could be accounted for. This assumption proved to be correct.

b. Secondary Chamber (Drawing 1194060)

The secondary (or outer) chamber was a 40 groove copper chamber brazed into a CRES 304 outer liner with 26 inlet/outlet tubes and several instrumentation ports. Figure 39 is a sketch of the completed unit.

A minimum of four brazing cycles were required to assemble the chamber. As with the primary chamber, the internal diameter contour was tracer turned in the final machining operation.

(1) Core

With 40 grooves in the core, many of the lands were only .038-in. thick and could be easily distorted. Therefore, they were machined in 3 cycles to maintain maximum body strength. The three machining and brazing cycles shown in Figure 40 were as follows: (1) machine approximately one half of the grooves and braze the appropriate split rings as shown in Figure 41, (2) machine all but the grooves at the ends of the inserts and braze the appropriate split rings, (3) machine the slots and grooves for the inserts and braze the inserts.

The core was final match machined on the outside diameter for insertion into the outer liner. Photographs of the core before and after machining are given in Figures 42 and 43.

(2) Outer Liner

The outer liner was roughed out, finish turned on the outside diameter, and then semi-finished on the inside diameter from a CRES 304L billet. The tubing sockets and instrumentation ports were milled at location and the shaped recesses in the ID were EDM'd to design. The liner and tubes were brazed at a temperature that also served to anneal the part. The ID was then machined to join with the core.

(3) Assembly and Final Machining

The liner was heated to 500 degrees F and the core was frozen to -320 degrees F in liquid nitrogen for assembly. The part was brazed at 1800 degrees F. The I.D. of the chamber was contoured in a tracer lathe from both ends. Because of one deep groove mistakenly machined into the hardware, the contour was made to the lowest possible dimension. Therefore, the forward, aft, and throat diameters are .010-in. less than the nominal dimension. The finished secondary chamber is shown in Figure 44.

(4) Proof Test and Leak Check

The secondary chamber passed a proof pressure test with 1200 psig gaseous nitrogen. Water flow of the circuits indicated a small amount of cross-talk in the throat circuits.

c. Primary Injector (Drawing 1194044)

The primary injector was a coaxial type design with 42 .312-in. dia oxidizer swirler tubes passing through the fuel manifold and platelet stack. An oxidizer platelet stack was also used to induce swirling in the oxidizer tubes. The injector had 12 pocket tuneable acoustical cavities surrounding the face plate. Figures 45-47 present sketches and photographs of the assembly.

Copper brazing was used to join the body, swirler tubes, and the fuel face stack. The oxidizer and fuel covers were E.B. welded in place and the fuel inlet tube was tig weld assembled.

Because of the similarity of the primary and secondary injector platelet stacks the art work was made so that both stacks would be photoetched and diffusion bonded as a single stack. A photograph of the machined oxidizer stacks are given in Figure 48. After the stack was match machined to the strongback dimensions, the stack was bonded to the strongback.

Final machining consisted of finishing the face side and machining the igniter port. A backflush cleaning was performed and the part was sent to the test area for assembly.

d. Secondary Injector (Drawing 1194060)

The secondary injector was coaxial and similar to the primary injector except for the annual shape. It had 126 brazed swirler tubes, swirler platelet stack, and fuel face plate similar to the primary injector. The same brazing techniques were used as with the primary.

Photographs of the secondary injector in various stages of assembly are given in Figures 49-53.

e. L' Spacer Ring (Drawing 1194058)

There were two L' rings made to allow adjustment of the primary to secondary nozzle spacing. The assembly consisted of a CRES 304L outer ring and a grooved copper inner ring. Photographs of the brazed rings are given in Figure 54.

6. Test Planning/Test Stand Preparation

The test plan was generated to evaluate the critical areas associated with the unique configuration of the dual-throat system. Cold flow testing (Reference 11) had shown a plume attachment shock (Figure 55) in the secondary chamber nozzle area during Mode II (primary chamber only firing). The heat transfer associated with this shock and the effect of bleed flow on the thermal conditions had to be determined. The test series to generate the required mode 2 data is described in Figure 56 and in Table XIII.

The mode 2 test series involved the following: (1) a bleed flow survey with gaseous hydrogen, (2) a mixture ratio survey to provide a wide reynolds number range, (3) a pressure survey to generate a heat flux range, and (4) a nozzle spacing survey to determine the aerothermodynamic effects that were geometry-related.

Two areas of concern during mode 1 firing were the heat transfer at the primary chamber nozzle lip and the heat transfer associated with the shocks in the primary nozzle. The test series to provide the mode 1 data is described in Figure 57 and in Table XIV. Like the mode 2 tests, the mode 1 test series involved test variations in mixture ratio, chamber pressure, and nozzle spacing. In addition, the effect of the secondary-to-primary chamber pressure ratio on the thermal conditions were to be evaluated.

Test stand J1A in the Aerojet J-area was selected for hot fire testing of the dual throat hardware. The J1A test stand flow diagram is depicted in Figure 58. The gaseous oxygen and gaseous hydrogen piping layout for the stand are shown in the figure. The water supply circuits and the anticipated manifold pressures are indicated in Figure 59. Instrumentation for the test program is described in Figure 60.

TABLE XIII

DUAL-THROAT THRUSTER THERMAL MODEL PRELIMINARY TEST PLAN *

Series / Mode	Test No.	Pc_p (psia)	MR_p/MR_s (-)	L_e (in.)	$\dot{w}_p$ (lb/sec)	$\dot{w}_s$ (lb/sec)	$\dot{w}_{op}$ (lb/sec)	$\dot{w}_{fp}$ (lb/sec)	$\dot{w}_{os}$ (lb/sec)	$\dot{w}_{fs}$ (lb/sec)	$\dot{w}_{H_2O}$ (lb/sec)	$\dot{w}_{H_2OS}$ (lb/sec)	P_{wp} (psia)	P_{ws} (psia)	Pc_s (psia)	Duration (sec)	Remarks
	1															0.5	Igniter checkout with primary chamber
SERIES 1/ MODE 2	2	500	3/-	Nom.	4.50	0.27	3.38	1.13	0	0.27	21.00	8.21	1800	<1180	-	0.5	Checkout test - GH_2 secondary bleed flow
	3	850	5/-	(i.e., 2.50 in.)	8.00	0.60	6.67	1.33		0.60	37.20	12.93	3100	TBD	64	6.0	Bleed flow survey - high GH_2 flow
	4					0.48				0.48					57		Bleed flow survey - nominal GH_2 flow
	5					0.30				0.20					48		Bleed flow survey - low GH_2 flow
	6					0.10				0.10					15+		Bleed flow survey - adverse GH_2 flow
	7	500	2/0.9		4.52	0.27	3.01	1.51	0.128	0.142	15.80	8.21	1560	TBD	36	0.5	Checkout test - high-temperature bleed flow
	8	500	7/0.9		5.08	0.10	4.45	0.64	0.090	0.100	22.30	8.21	1880	1180	15+	6.0	Heat transfer calibration - adverse bleed
	9	850	5/0.9		8.00	1.00	6.67	1.33	0.474	0.526	37.20	12.93	3100	TBD	64		High-temprature bleed flow survey - high bleed flow
	10					0.48			0.227	0.253					57		High-temperature bleed flow survey - nominal bleed flow
	11					0.30			0.142	0.158					48		High-temperature bleed flow survey - low bleed flow
	12					0.10			0.047	0.053					15+		High-temperature bleed flow survey - adverse bleed flow
	13	850	7/0.9		8.56	1.00	7.49	1.07	0.474	0.526	35.20	12.93	2800	1300	64		High-temprature bleed flow survey - high bleed flow
	14					0.51			0.242	0.268					57		High-temprature bleed flow survey - nominal bleed flow
	15					0.30			0.142	0.158					48		High-temprature bleed flow survey - low bleed flow
	16	850	3/0.9		7.67	1.00	5.75	1.92	0.474	0.526	32.10	12.93	2570	TBD	64		High-temperature bleed flow survey - high bleed flow
	17					0.46			0.218	0.242					57		High-temperature bleed flow survey - nominal bleed flow
	18					0.30			0.142	0.158					48		High-temperature bleed flow survey - low bleed flow
	19	500	7/0.9		5.08	1.00	4.45	0.64	0.474	0.526	22.5	8.21	1880	1180	36		High-temperature bleed flow survey - high bleed flow
	20					0.30			0.142	0.158					36		High-temperature bleed flow survey - nominal bleed flow
	21					0.20			0.095	0.105					36		High-temperature bleed flow survey - low bleed flow
	22	700	3/0.9		6.30	0.38	4.72	1.58	0.180	0.200	27.4	10.88	2180	TBD	50		Blow-off flow; unequal primary/secondary MR
	23	700	7/0.9		7.09	0.42	6.20	.89	0.199	0.221	29.8	10.88	2370	1250	50		Blow-off bleed flow; unequal primary/secondary MR
	24	1000	2/0.9		9.06	0.54	6.04	3.02	0.256	0.284	27.5	14.87	2260	TBD	60		Blow-off bleed flow; extend R_e range
	25	850	5/0.9	Large	8.00	1.00	6.67	1.33	0.474	0.526	37.20	14.27	3100	TBD	64		L_e variation, High-temperature bleed flow survey
	26					0.48			0.227	0.253					57		L_e variation, high-temperature bleed flow survey
	27					0.30			0.142	0.158					48		L_e variation, high-temperature bleed flow survey
	28	850	5/0.9	Small	8.00	1.00	6.67	1.33	0.474	0.526	37.20	11.70	3100	TBD	64		L_e variation, high-temperature bleed flow survey
	29					0.48			0.227	0.253					57		L_e variation, high-temperature bleed flow survey
	30					0.30			0.142	0.158					48		L_e variation, high-temperature bleed flow survey
	31	TBD															Contingency

* These are planned tests. For actual tests, see Table XVIII, p. 63.

TABLE XIV

DUAL-THROAT THRUSTER THERMAL MODEL PRELIMINARY TEST PLAN *

Series Mode	Test No.	Pc_p (psia)	MR_p/MR_s (-)	L_e (in.)	$\dot{w}_p$ (lb/sec)	$\dot{w}_s$ (lb/sec)	$\dot{w}_{op}$ (lb/sec)	$\dot{w}_{fp}$ (lb/sec)	$\dot{w}_{os}$ (lb/sec)	$\dot{w}_{fs}$ (lb/sec)	$\dot{w}_{H_2O}$ (lb/sec)	$\dot{w}_{H_2O_s}$ (lb/sec)	$P_{\dot{w}p}$ (psia)	$P\dot{w}_s$ (psia)	Pc_s (psia)	Duration (sec)	Remarks
	1	500	7/7	Nominal	5.08	9.4	4.45	0.64	8.23	1.18	22.3	18.0	1880	1470	250	0.5	Ignition and calibration run
SERIES 2/ MODE 1	2	500	7/7			9.4			8.23	1.18		18.0	1880	1470	250	6.0	Heat transfer calibration - overcooled
	3					13.2			11.35	1.65		21.2		1750	350		Secondary/primary pressure survey
	4					15.0			13.13	1.88		23.8		1900	400		Secondary/primary pressure survey
	5					16.8			14.70	2.10		26.1		2070	450		Secondary/primary pressure survey
	6	700	7/7		7.09	13.2	6.20	0.89	11.55	1.65	29.7	21.2	2370	1750	350		Heat transfer calibration and pc_s/pc_p survey
	7					18.3			16.01	2.29		28.0		2210	490		Heat transfer calibration and pc_s/pc_p survey
	8					20.9			18.29	2.61		31.5		2550	560		Heat transfer calibration and pc_s/pc_p survey
	9					23.5			20.56	2.94		34.8		3150	630		Heat transfer calibration and pc_s/pc_p survey
	10	700	3/3		6.28	11.6	4.71	1.57	8.70	2.90	29.7	20.0	2180	1680	350		Heat transfer calibration and pc_s/pc_p survey
	11					16.3			12.23	4.08		26.1		2080	490		Heat transfer calibration and pc_s/pc_p survey
	12					18.7			14.03	4.68		29.2		2340	560		Heat transfer calibration and pc_s/pc_p survey
	13					20.9			15.68	5.23		32.3		2680	630		Heat transfer calibration and pc_s/pc_p survey
	14	1000	2/2		9.05	16.7	6.03	3.02	11.13	5.57	27.5	20.0	2260	1680	500		Heat transfer calibration and pc_s/pc_p survey
	15					20.0			13.33	6.67		23.3		1920	600		Heat transfer calibration and pc_s/pc_p survey
	16					24.8			16.53	8.27		28.1		2590	750		Heat transfer calibration and pc_s/pc_p survey
	17					30.0			20.00	10.00		32.8		3350	900		Heat transfer calibration and pc_s/pc_p survey
	18	700	3/7		6.28	18.30	4.71	1.57	16.01	2.29	27.4	28.0	2180	2210	490		Unequal primary/secondary MR
	19	700	7/3		7.09	16.30	6.20	0.89	12.23	4.08	29.7	26.1	2370	2080	490		Unequal primary/secondary MR
	20	410	3/3	Small	3.68	6.75	2.76	0.92	5.06	1.69	18.1	13.5	1680	1350	205		Effect of pc_s/pc_p with small L_e
	21					8.25			6.19	2.06		15.5		1440	250		Effect of pc_s/pc_p with small L_e
	22					10.03			7.52	2.51		18.2		1580	310		Effect of pc_s/pc_p with small L_e
	23					12.25			9.19	3.06		20.8		1730	370		Effect of pc_s/pc_p with small L_e
	24	TBD	TBD	TBD	TBD	TBD	TBD	TBD	TBD	TBD	TBD	TBD	TBD	TBD	TBD		Contingency tests to complete L_e and pc_s/pc_p ratio survey
	25	TBD												TBD	TBD		Contingency tests to complete L_e and pc_s/pc_p ratio survey

* These are planned tests. For actual tests, see Table XVIII, p. 63.

7. Hardware Assembly and Installation

The assembled dual throat thruster was installed on the J1A test stand corresponding to the diagrams of Figures 59 and 60. The locations of the many water circuits and instrumentation ports for the thruster are given in Figure 61. Only the locations in the circumferential plane are shown. The water inlet and outlet circuits for the primary system are all basically in the same axial plane. The figure defines the location for the circuits given in Table XV.

Two views of the installed hardware are given in Figures 62 and 63. The hardware is seen with the pressure-check end plate mounted to the secondary nozzle exit. Water feed and exit lines to the axial coolant channels and the calorimeter channels are not connected in the figure. The inlet and outlet manifolds for the water coolant calorimeter channels are shown in Figure 63 as upright manifolds at each side of the pciture. The inlet and outlet manifolds for the axial circuits of the primary chamber are the horizontal manifolds near the ground on both side of Figure 63. Flex lines on the inlet manifold (right side of Figure 63) are shown connected to the manifold, but pulled out of the picture for clarity.

8. Hardware/Test Stand Flow Calibration

Three views of the dual throat hardware on the J1A test stand are shown in Figures 64, 65, and 66 prior to hot firing. The water coolant lines are connected (see Figure 62 for comparison). Each outlet line was equipped with an orifice, a pressure transducer and a thermocouple. Five of the outlet lines were equipped with flowmeters.

a. Igniter Checkout Testing

The GOX/GH_2 was checked out with both cold flow and ignition tests. There was a 65 msec lag from the GOX valve signal to GOX manifold pressure (POJI) rise, and a corresponding 45 msec lag to GH2 manifold

TABLE XV

INSTRUMENTATION NOMENCLATURE

Chamber Pressure	Pc-p	Pc-s
Oxidizer Manifold Pressure	Poj-p	Poj-s
Fuel Manifold Pressure	Pfj-p	Pfj-s
Chamber Pressure (high frequency)	K-1	K-5
	K-2	K-6
	K-3	
Water Circuits	1 thru 13	1 thru 13
Temperature		T-1, T-2, T-3
		T-12, T-13

pressure (PFJI) rise. An igniter GOX lead of 150 msec was utilized during ignition. Upstream pressures in the GOX and GH_2 circuits were set at 1000 psia and 1500 psia, respectively, for an igniter chamber pressure of 400 psia.

The igniter proved to be very reliable for primary chamber ignition over all mixture ratios tested.

b. Injector Checkout Testing

The primary and secondary injectors were cold flowed with GOX and with Helium (GH2 circuit only). The injector flow equation and the KW of the flow circuits are given in Table XVI.

c. Water Coolant Circuit Calibration

Calibration tests were conducted to measure the flow coefficients of the calorimeter and axial coolant circuits at rated flow rates. Because of the interchannel leakage in the primary chamber circuits and in some of the secondary chamber circuits, flowmeters were placed in both inlet and outlet lines as shown in Figure 67.

The calibration data are summarized in Table XVII. The pressures PWY-XX for each circuit are those upstream of the measuring orifice shown in Figure 67. The flowrates, FWY-XX, the orifice diameters, DWY-XX, and the pressure drop across the orifice, Δ PWY-XX, were used to calculate the CDWY-XX values shown. The variation in flow coefficients (CD) can be attributed to the differences in configurations and line sizes, to slight variations in the actual orifice diameters, and to normal variations in the pressure and flow rate measurements. Because each circuit is calibrated, the absolute value of the coefficients is not necessary in obtaining accurate flow rates from the pressure drop across the orifice circuit.

The water inlet pressure to the unit in the tests was 1571 psig and the outlet pressure was 572 psig. The inlet and outlet manifold

TABLE XVI

CALCULATED Kw VALUES FOR EACH INJECTOR AND PROPELLANT

Injector	Propellant	Kw
Primary	GH_2	.404
Primary	GOX	.548
Secondary	GH_2	.927
Secondary	GOX	1.534

KW Equations

$$W_{O2} = 2.16 \frac{Kw\ P1}{\sqrt{T}} \sqrt{\left(\frac{P_2}{P_1}\right)^{1.429} - \left(\frac{P_2}{P_1}\right)^{1.714}}$$

$$W_{H2} = 0.54 \frac{Kw\ P1}{\sqrt{T}} \sqrt{\left(\frac{P_2}{P_1}\right)^{1.429} - \left(\frac{P_2}{P_1}\right)^{1.714}}$$

where P_1 = upstream gas pressure

P_2 = downstream gas pressure

TABLE XVII

WATER COOLANT CIRCUIT CALIBRATION DATA

CIRCUIT Y-XX	Pressure PWY-XX (psig)	Flow Rate FWY-XX (lb/sec)	Orifice Diameter DWY-XX (in.)	Orifice Pressure Drop ΔPWY-XX (psi)	Orifice Flow Coefficient C_DWY-XX --
P-1	741	1.525	.179	169	.883
P-2	801	.770	.122	228	.825
P-3	776	1.205	.156	204	.836
P-4	812	1.422	.179	240	.691
P-5	816	2.260	.215	244	.755
P-6	777	2.484	.230	205	.791
P-7	810	1.374	.161	238	.829
P-8	746	.961	.138	174	.923
P-9	783	.636	.115	211	.798
P-10	733	.729	.122	161	.931
P-11	732	.869	.138	160	.870
P-12	718	.714	.131	146	.830
P-13	764	24.16(22.11)	.725	192	.80 (.732)
S-1	1570	.492	.075	998	.668
S-2	1566	.492	.075	994	.669
S-3	1364	.999	.106	792	.762
S-4	818	1.421	.179	246	.682
S-5	1285	1.543	.131	713	.812
S-6	1323	1.134	.110	751	.825
S-7	1316	1.137	.110	744	.831
S-8	1318	1.011	.110	746	.738
S-9	1283	1.254	.115	711	.858
S-10	1412	1.076	.106	840	.797
S-11	1514	.683	.081	942	.818
S-12	1503	.517	.084	931	.579
S-13	1470	.598	.075	898	.856
L1	1551	.695	.081	979	.817
UNIT	1571	52.16(50.11)	--	999	--

Inlet and Outlet Manifold Flow Rates (See Figure 67 for definitions)

FWIM = 51.05 lb/sec
FWOM = 51.03 lb/sec
$C_{DWY-XX} = .2412\ \dot{w}/(DWY-XX)^2\ \sqrt{\Delta PWY-XX}$
Where ΔPWY-XX = (PWY-XX) - PWOM $\dot{w}$ = coolant water flow rate

flow rate measurements (FWIM and FWOM) are in good agreement as shown in Table XVII. The sum of the individual circuit flow rates amounts to 52.16 and 50.11 LBM/SEC depending upon whether the axial primary circuit P13 is computed from a flow calibration C_p or by difference from the total inlet flow and a sum of the individual circuits. The average of the two P13 values when added to the sum of the other circuits gives exceptional agreement with the measured inlet and outlet total flows.

Several approaches were considered for caibrating the coolant channels for flow measurement and control purposes. The method that had proved successful on a previous study (Reference 12) was the preferred approach. That experimental setup provided for redundancy in a number of key measurements. Each chamber cooling circuit KW was determined, calibrated discharge orifices were utilized in each circuit, and flow meters were used in five of the coolant circuits to obtain triple redundancy. This methodology, adapted for the dual throat system, is depicted in Figure 67.

Special water flow tests of the primary coolant circuits (plugging outlets of individual and/or combined circuits, and reverse flowing the circuits with or without plugged circuits) allowed the accumlation of leak KW's for each circuit and allowed the formulation of a computer model of the primary coolant system. This model is diagrammed in Figure 68. Confidence in this model depended upon a uniform outlet pressure in the primary circuits. Therefore, the orifices in the primary circuit were sized to give as close to a uniform outlet pressure as possible.

As hot fire testing proceeded and orifice changes were made, additional water circuit calibrations were made. These served to ensure the gathering of consistent data. Because of the internal leakage in the calorimeter circuits, considerable effort was required to reduce and interpret the thermal data. Careful examination of these data indicated that the cold flow calibration data needed to be corrected for hot flow conditions. The types of corrections and the methodology are described later in this report in Section V.

9. Hot Fire Test Program

A total of 43 combustion tests were conducted with the dual throat hardware. A historical first was accomplished on 19 December 1983 when both primary and secondary chambers of a cooled dual throat system were successfully fired. Thirteen tests were conducted before a major water leak occurred. The remainder of the tests were conducted after the hardware was repaired. The detailed test data are presented in Appendix B of this report. This section presents a summary of the hot fire data.

The hot fire test data are summarized in Tables XVIII and XIX.

The valve sequencing, ignition and start and shutdown transients are depicted in the oscillograph traces of Figure 69a and 69b. The nomenclature used on the oscillographs are defined in Table XV11A. Figure 69A shows a typical mode 2 (Primary Only) Test. The scheduled test duration (Test 105) was 0.5 second to checkout the system. The igniter spark was on for 0.285 second after fire switch one (FS1). The primary chamber pressure began to rise at FS1 + 0.24 second and reached steady state pressure at FS1 + 0.3 second.

Figure 69B shows a typical Mode 1 (both chambers firing) test. The duration of this test (Test 115) was 1.2 seconds. The primary chamber was ignited as in previous tests. The secondary chamber ignition took place approximately 0.2 second after primary chamber steady state pressure was reached. Ignition was accomplished using the primary chamber exhaust for ignition of the secondary chamber gaseous oxygen and hydrogen. This "back lighting" technique is possible with GOX and GH_2, but may provide too great a pressure rise for ignition of propellants (E.G., Liquids) where larger volume changes occur on combustion.

An analysis of the high frequency data for Test 115 showed a 130 psi pressure spike on primary chamber ignition. The Kistler transducer

TABLE XVIIA

DUAL THROAT THRUSTER OSCILLOGRAPH NOMENCLATURE

SYMBOL	PARAMETER
FS	Fireswitch (1: Start,; 2: Shutdown)
LPTCOV	Thrust chamber GOX Valve Position
LPTCFV	Thrust Chamber GH_2 Valve Position
LOFCV	Facility GOX Valve Position
LFFCV	Facility GH_2 Valve Position
SPARK	Igniter Spark
IGNOV	Igniter GOX Valve
IGNFV	Igniter GH_2 Valve
IGNOPV	Igniter GOX Purge Valve
IGNFPV	Igniter GH_2 Purge Valve
PTCOVPV	Thrust Chamber GOX Valve Purge Pressure
PTCFVPV	Thrust Chamber GH_2 Valve Purge Pressure
STCOPV	Thrust Chamber GOX Purge Valve Command
STCFPV	Thrust Chamber GH_2 Purge Valve Command
POLI (POIL)	GOX Facility Line Pressure
PFLT (PFIL)	GH_2 Facility Line Pressure
PPC	Primary Chamber Pressure
PSC	Secondary Chamber Pressure
POIJ	Igniter GOX Pressure
PFIJ	Igniter GH_2 Pressure
FA	Thrust
POPJ	Primary Injector GOX Pressure
PFPJ	Primary Injector GH_2 Pressure
POSJ	Secondary Injector GOX Pressure
PFSJ	Secondary Injector GH_2 Pressure

TABLE XVIII

DUAL THROAT THRUSTER TEST SUMMARY*

Test No.	Duration (sec)	PCP (psia)	PSC (psia)	MRP	MRS	PWIM (psig)	FWIM (lb/s)	Thrust (lb)	wOP lb/s	wFP lb/s	wOS lb/s	wFS lb/s	Remarks
-105	0.5	527	26	3.00	-	1576	51.05	1577	3.40	1.13	-	-	Initial Hot Fire Checkout
-106	6.0	549	26	3.13	-	1566	50.38	1720	3.68	1.18	-	-	Steady State with GH_2 Bleed
-107	0.5	534	30	2.04	-	1559	50.46	1730	3.26	1.60	-	-	Sec. Ignition Not Accomplished
-108	1.5	529	27	1.96	-	1565	50.51	1716	3.09	1.58	-	-	Sec. Ignition Not Accomplished
-109	6.0	543	29	3.14	-	1565	50.41	1673	3.63	1.16	-	-	Sec. Ignition Not Accomplished
-110	0.4	620	36	5.57	-	1551	50.22	2032	4.87	0.87	-	-	PCP Kill @ 600/Fuel Bleed Only
-111	6.0	528	37	7.11	-	1389	40.49	1750	4.60	0.65	-	0.16	Re-Orificed Sec. Circ. N_2-Purge on Ox. Inj.
-112	6.0	524	35	7.11	-	1372	40.83	1701	4.56	0.64	-	0.15	Reduced GH_2 Bleed
-113	6.0	532	33	7.09	-	1382	40.14	1706	4.56	0.64	-	0.09	Reduced GH_2 Bleed
-114	5.0	536	31	7.10	-	1389	40.41	1688	4.58	0.65	-	0	Reduced GH_2 Bleed/TS-7 Kill (WT>80^{0}F
-115	1.2	463	345	6.53	6.16	1911	64.65	5304	3.93	0.60	9.66	1.57	First Mode I Test/TP-7 Kill (WT>43^{0}F)
-116	6.0	515	245	7.91	7.80	1346	65.78	3983	4.67	0.59	7.46	0.96	Leak (Spray) at Circuit 9 Inside Prim. Nozzle
-117	6.0	559	267	7.18	7.09	1341	65.72	4357	4.88	0.68	7.80	1.10	Leak @ 9 o'clock in Prim. Chamb. Cavi

* Test Data Details Appear in Appendix B

Le = 2.5-in. in all tests

TABLE XVIII (cont.)

DUAL THROAT THRUSTER TEST SUMMARY *

Test No.	Duration (sec)	PPC (psia)	PSC (psia)	MRP	MRS	PWIM (psig)	FWIM (lb/s)	Thrust (lb)	wOP lb/s	wFP lb/s	wOS lb/s	wFS lb/s	PSC PPC	Remarks
-118	0.2	65	27	-	-	1275	63.87	290	-	-	-	-	-	Facility valve control and sequencing problems
-119	0.9	440	44	-	-	1269	63.79	1576	-	-	-	-	-	Facility valve control and sequencing problems
-120	0.9	435	283	6.21	6.27	1298	64.70	4177	3.71	.60	8.40	1.34	0.65	Facility valve control and sequencing problems
-121	2.4	520	339	8.04	8.17	1302	64.87	5070	4.98	.62	11.34	1.39	0.65	Facility valve control and sequencing problems
-122	0.9	429	276	-	-	1494	69.48	3856	-	-	-	-	0.64	Facility valve control and sequencing problems
-123	0.7	406	255	-	-	1486	69.49	3790	-	-	-	-	0.63	Facility valve control and sequencing problems
-124	0.9	408	266	-	-	1496	69.56	3812	-	-	-	-	0.65	Facility valve control and sequencing problems
-125	4.6+	487	316	6.74	6.85	1488	68.81	4738	4.25	.63	9.68	1.41	0.65	Facility valve control and sequencing problems
-126	6.0	495	322	6.92	7.03	1474	68.46	4808	4.36	.63	9.94	1.41	0.65	Fine leak in Pc nozzle platelet at 1:00, 6:30 and 7:00. SC leak at O-ring.
-127	6.0	492	364	6.92	6.95	1475	68.61	5302	4.34	.63	11.31	1.63	0.74	
-128	1.1	482	398	7.30	7.74	1493	69.99	5839	4.39	.60	12.98	1.68	0.83	TP-5 Shutdown
-129	1.6	489	402	7.09	7.56	1813	76.74	5794	4.33	.61	12.84	1.70	0.83	TP-5 Shutdown

* Le = 2.5-in. in all tests

TABLE XVIII (cont.)

Test No.	Duration (sec)	PPC (psia)	PSC (psia)	MRP	MRS	PWIM (psig)	FWIM (lb/s)	Thrust (lb)	wOP lb/s	wFP lb/s	wOS lb/s	wFS lb/s	PSC PPC	Remarks*
-130	6.0	490	327	3.02	6.96	1481	69.13	4851	3.45	1.14	9.94	1.43	0.67	Satisfactory test
-131	6.0	501	298	6.91	2.94	1482	69.38	4576	4.42	.64	7.00	2.38	0.60	Satisfactory test
-132	6.0	414	277	3.0	2.95	1231	63.17	4067	2.89	.96	6.65	2.25	0.67	Satisfactory test
-133	-	-	-	-		(2130)	(50.1)	-	-	-	-	-	-	Fuel pilot valve failed to open
-134	7	457	31	6.8	-	2120	54.06	1483	-	-	-	-	-	Wrong venturi C_D. Orifice loose. Low Pcp.
-135	7	664	45	6.0	-	2126	54.06	2266	5.33	0.88	0	.27	-	Water Coolant System back pressure orifice loose.
-136	7	683	44	6.8	-	2113	56.97	2314	6.05	0.89	0	(.18)	-	Back pressure orifice broke loose completely.
-137	7	677	40	6.8	-	2111	50.67	2222	5.97	0.87	0	(.103)	-	DWOM - 0.912, New orifice
-138	7	676	36	6.8	-	2123	50.83	2177	5.97	0.87	0	0	-	Satisfactory test
-139	7	676	42	6.8	-	2132	51.02	2240	5.96	0.88	0	(.17)	-	Satisfactory test
-140	7	663	32	3.0	-	2132	51.15	2115	4.71	1.59	0	(.094)	-	Satisfactory test
-141	7	675	34	3.0	-	2122	51.08	2177	4.81	1.61	0	(.164)	-	Satisfactory test
-142	7	674	29	3.1	-	2106	51.04	2106	4.83	1.58	0	0	-	Satisfactory test
-143	6	662	416	3.0	2.8	2174	85.28	6265	4.78	1.58	9.91	3.51	0.63	Deluge water leak on shutdown - L' Section
-144	6	399	179	2.8	3.0	1475	67.67	2820	2.85	1.02	4.13	1.37	0.45	Satisfactory test Le = 1.5 in.
-145	6	397	288	2.8	3.0	1469	67.52	3905	2.82	1.02	7.12	2.38	0.73	Satisfactory test Le = 1.5 in.
-146	6	395	326	2.8	2.8	1469	67.51	4267	2.81	1.01	7.41	2.62	0.83	Satisfactory test Le = 1.5 in.
-147	6	381	315	3.4	3.4	1479	67.73	4084	2.83	0.85	7.47	2.20	0.83	Satisfactory test Le = 1.5 in.
-148	6	648	437	3.1	3.2	2204	84.93	6623	4.78	1.53	11.20	3.50	0.67	Satisfactory test Le = 1.5 in.

* Le = 2.5-in. unless noted

TABLE XIX

DUAL THROAT THRUSTER PERFORMANCE SUMMARY

Test No.	PCP	MRP	WP	C^*_p	C^*_{Theo}	η^*_{cp}	PCS	MRS	WS	C^*_s	C^*_{Theo}	η^*_{cs}	F	$I_s{}^*$	$I_{s_{Theo}}$ e=0(II) e=2(I)	η_{I_s}
-105	515	3.0	4.53	8499	8300	1.02	26	-	-	-	-	-	1577	348	364	0.96
-106	547	3.1	4.86	8414	8295	1.01	26	-	-	-	-	-	1697	349	370	0.94
-107	534	2.0	4.86	8214	8270	0.99	30	-	-	-	-	-	1730	356	360	0.99
-108	529	2.0	4.67	8468	8270	1.02	27	-	-	-	-	-	1716	367	360	1.02
-109	543	3.1	4.79	8475	8295	1.02	29	-	-	-	-	-	1673	349	370	0.94
-110	540	5.6	5.74	7033	7730	0.91	36	-	-	-	-	-	2032	354	360	0.98
-111	528	7.1	5.25	7518	7350	1.02	37.5	-	0.18	-	-	-	1750	333.3	346	0.96
-112	524	7.1	5.21	7519	7350	1.02	35.0	-	0.12	-	-	-	1701	326.7	346	0.94
-113	532	7.1	5.20	7648	7350	1.04	32.7	-	0.09	-	-	-	1706	327.8	346	0.95
-114	536	7.1	5.22	7676	7350	1.04	30.7	-	0.04	-	-	-	1688	323.2	346	0.93
-115	463	6.5	4.53	7641	7495	1.02	345	6.2	11.23	7655	7450	1.03	4900	311	328	0.95
-116	515	7.9	5.27	7305	7105	1.03	245	7.8	8.42	258	7100	0.88	3983	291	295	0.99
-117	559	7.2	5.56	7516	7310	1.03	267	7.1	8.89	6461	7300	0.89	4357	301.5	307	0.98

* I_s not degraded for GH_2 bleed flow in mode 2 tests.

TABLE XIX (cont.)

Test No.	PCP	MRP	WP	C^*_p	C^*_{Theo}	η^*_{cp}	PCS	MRS	WS	C^*_s	C^*_{Theo}	η^*_{cs}	F	I_s*	Is_{Theo} e=10(II)	Is_{Theo} e=2(I)	η_{Is}
-137	677	6.8	6.85	7388	7430	.99	39.7	-	0.10	-	-	-	2222	324.4	364	-	0.89
-138	676	6.8	6.84	7388	7430	.99	35.6	-	0	-	-	-	2177	318.3	364	-	0.87
-139	676	6.8	6.84	7388	7430	.99	42.2	-	0.17	-	-	-	2240	327.7	364	-	0.90
-140	663	3.0	6.30	7867	8300	.95	31.9	-	0.09	-	-	-	2115	335.5	382	-	0.88
-141	675	3.0	6.42	7860	8300	.95	34.5	-	0.16	-	-	-	2177	339.0	383	-	0.89
-142	674	3.1	6.41	7861	8290	.95	28.6	-	0	-	-	-	2106	328.3	383	-	0.86
-125	487	6.7	4.87	7476	7435	1.01	316.	6.9	11.09	6924	7345	.94	4738	296.8	-	315	0.94
-126	495	6.9	4.99	7416	7380	1.00	322	7.0	11.35	6891	7320	.94	4808	294.2	-	314	0.94
-127	492	6.9	4.96	7415	7380	1.00	364	7.0	12.93	7115	7330	.97	5302	296.2	-	317	0.93
-129	489	7.1	4.94	7400	7320	1.01	402	7.6	14.54	7216	7165	1.01	5794	297.4	-	315	0.94
-130	490	3.0	4.60	7963	8300	.96	327	7.0	11.37	7160	7320	.98	4851	303.8	-	331	0.92
-131	501	6.9	5.06	7402	7385	1.00	298	2.9	9.39	7212	8310	.87	4576	316.8	-	341	0.93
-132	414	3.0	3.85	8039	8300	.97	277	3.0	8.91	7591	8300	.91	4067	318.7	-	350	0.91
-144	399	2.8	3.87	7708	8310	.93	179	3.0	5.50	6680	8300	.80	2820	300.9	-	333	0.90
-145	397	2.8	3.83	7749	8310	.93	288	3.0	9.50	7555	8300	.91	3905	292.8	-	350	0.84
-146	395	2.8	3.82	7730	8310	.93	326	2.8	10.04	8225	8310	.99	4267	308.0	-	353	0.87
-147	381	3.3	3.68	7740	8270	.94	315	3.4	9.67	8251	8255	1.0	4084	306.1	-	350	0.87
-148	648	3.1	6.31	7677	8290	.93	437	3.2	14.70	7273	8280	.88	6623	315.3	-	358	0.88

* I_s not degraded for GH_2 bleed flow in mode 2 tests.

trace settled out 120 milliseconds after the spike occured. A pressure spike of 600 psi was seen at secondary chamber ignition, with a corresponding spike of 60 psi sensed by the primary chamber Kistler transducer. The secondary chamber Kistler transducer trace settled out after about 90 milliseconds. The duration of the spike on secondary ignition was about 10 milliseconds (major spike followed by 2 lesser spikes).

Although not a contract requirement, thrust was measured on each test using the existing thrust stand. The thrust data allowed the computation of thruster performance (specific impulse), and thus a quantitative measurement of the perofrmance differences as variables were changed throughout the test series. Because the stand was not calibrated for these tests, the thrust values should not be used to estimate dual throat engine performance.

The calculated values of specific impulse and characteristic velocity are included in Table XIX. It should be noted that the calculated specific impulse values for Mode 2 tests do not include the amount of GH_2 bleed flow. An operational dual throat engine would use the gas generator-turbine exhaust as bleed flow rather than gaseous hydrogen. The lower performance reflected with GH_2 bleed was, therefore, not shown in the table.

10. Data Reduction

a. Coolant Flow Rates

Coolant flow rates were calculated from the outlet orifice discharge coefficients given in Tables XX to XXII. These coefficients were obtained from special cold flow tests and the limited use of flow meters in individual circuts during the hot fire tests. Note that many of the secondary chamber orifices are cavitating, as indicated by the specification of C_C rather than C_D. The flow rate for cavitating orifices is a function of

TABLE XX

PRIMARY ORIFICE CALIBRATION

Circuit	Orifice Diameter in.	C_D
1	.166	.817
2	.122	.893
3	.156	.836
4	.179	.691
5	.215	.747
6	.230	.791
7	.161	.829
8	.129	.742
9	.115	.831
9A	.243	.856
10	.111	.780
11	.125	.790
12	.117	.781
13	.697	.845

$$W = 4.147\ C_D\ D^2\ (PWPO\text{-}X - PWOM)^{0.5}$$

TABLE XXI

SECONDARY MODE II ORIFICE CALIBRATION

Circuit	Orifice Diameter in.	C_C	C_D
1	.035	.734	
2	.035	.766	
3	.035	.769	
4	.055		.907
5	.046	.642	Tests 111-114
		.595	Tests 137-142
6	.060	.661	
7	.064	.578	
8	.055	.678	
9	.052	.654	
10	.043	.686	
11	.040	.674	
12	.043	.620	
13	.040	.590	
L-1*	.035	.772	

$W = 4.147\ C_C\ D^2\ (PWSO\text{-}X \text{ or } PWL\text{-}1)^{0.5}$

$W = 4.147\ C_D\ D^2\ (PWSO\text{-}4 - PWOM)^{0.5}$

* Assume PWL-1 = PWIM for Tests 137-142

TABLE XXII

WATER FLOW ORIFICE COEFFICIENTS

Circuit	Orifice Diameter in	C_C (Cavitating)	C_D
1	.188	.656	
2	.177	.590	
3	.150	.624	
4	.210		.840
5	.180		.837
6	.162		.993
7	.162		.876
8	.156		.701
9	.167		.794
10	.150	.708	
11	.124	.625	
12	.180		.677
13	.150		.835
L-1	.166	.608	

$W = 4.147\ C_C\ D^2\ (PWSO\text{-}X \text{ or } PWL\text{-}1)^{0.5}$

$W = 4.147\ C_D\ D^2\ (PWSO\text{-}X - PWOM)^{0.5}$

inlet pressure and not a function of pressure drop across the orifice as it is for non-cavitating orifices. Of the Mode II secondary orifices, only S4 is not cavitating, this results from the use of an orifice upstream of the chamber in S4 to limit the pressure in the channels. Note that the orifice in P9 was changed after Test 127; the second orifice is designated as P9A. PWL-1 was not measured on Tests 137-142. Since the cooling circuit pressure drop in the spacer is very small, PWL-1 was assumed to be equal to the inlet manifold pressure PWIM.

b. Heat Load

(1) Mode II

Calculation of the coolant bulk temperature rise in each circuit accounted for (1) frictional heating of the coolant due to its high velocity in the cooling channels, (2) potential bias between inlet and outlet thermocouples and (3) small changes in inlet temperature during the test. Thus

$$\Delta T_c = T_{out} - T_{out_o} - Tin + Tin_o$$

in which

T_{in} = inlet manifold temperature over a steady-state summary period near the end of the firing

T_{out} = outlet temperature or crossover manifold temperature between segments for the same period

T_{in_o}, T_{out_o} = temperatures at the above locations just prior to firing.

Heat loads are the product of the coolant flow rate and ΔT_c since the deviation of the water specific heat from unity was negligible. Heat loads in the

second segment of secondary circuits 1, 2, 12 and 13 were obtained by subtracting the heat load of the first segment from the total heat load. The crossover manifold thermocouple in cirucit S3 was inoperative throughout the test program, so two heat loads could not be obtained.

Heating of the end wall of circuit P9 at the inner corner of the primary nozzle tip was assumed to be negligible in Mode II, so the sidewall area was used to calculate the reported heat flux from the measured heat load.

Data reduction printouts for Mode II are given in Table XXIII, and the resulting heat flux profiles are shown in Figures B-1 to B-10 in Appendix B.

(2) Mode I

The heat load calculation methodology for Mode II is also applicable for the secondary chamber in Mode I. However, data reduction for the primary chamber in Mode I utilized the analytical model of the internal leakage, Appendix C. This leakage is most likely to occur between the axial circuit and each calorimeter circuit after the former has cooled the outer surface of the chamber. Therefore, a model is required to account for the preheating of the leakage flow which dilutes the outlet flow of each calorimeter circuit. Leakage resistances were defined by matching cold flow data from special tests designed to isolate the leakage by capping either the inlets or outlets of the calorimeter circuits. Measured and predicted circuit resistances for these tests agreed within 10 percent.

Resultant ratios of the calorimeter circuit internal flow to the outlet flow are given in Table XXIV.

Calculation of the primary chamber calorimetric heat loads for Mode I tests were based on the following equation:

TABLE XXIII

TEST NO. 2381-BU1-0C-111
DSNAME DTHIS
TEST MODE II

DUAL THROAT CALORIMETER CHAMBER
COOLANT CIRCUIT HEATFLUX PROGRAM

J0678
DATE 08-06-85
TIME 09.10.10

DATA PERIOD FS1 + 5.51 SECS. TO FS1 + 6.01 SECS.

CIRCUIT NUMBER	CIRCUIT SURFACE AREA SQ.IN	CIRCUIT KW	COOLANT FLOW LB/SEC FLOW METER	COOLANT FLOW LB/SEC ORIFICE	DELTA TEMP DEG F	HEAT LOAD BTU/SEC	HEAT FLUX BTU/SQ.IN.SEC
PRIMARY							
1	1.675	.0934		1.5140	30.05	45.495	27.161
2	.762	.0551		.8566	23.59	20.206	26.517
3	1.613	.0844		1.2900	27.17	35.048	21.729
4	1.921	.0918		1.5072	24.35	36.698	19.103
5	2.226	.1432		2.3795	17.83	42.429	19.061
6	2.468	.1735		2.6346	13.87	36.532	14.802
7	2.736	.0891		1.4575	30.96	45.126	16.493
8	1.351	.0512		.8543	20.77	17.743	13.133
9	.998	.0456		.7080	15.94	11.284	11.307
10	1.491	.0399		.6772	6.82	4.616	3.096
11	3.242	.0512		.8604	6.15	5.292	2.229
12	2.262	.0443		.6943	2.98	2.066	.913
13	1.000	1.7024		20.841	30.24	811.65	811.648
SECONDARY							
SPACER	23.06	.0039		.1453	.88	.127	.006
1A	23.17	.0037		.1381	.83	.115	.005
1B	20.50	.0037		.1381	1.23	.055	.003
2B	16.75	.0039		.1454	2.27		
2A	14.34	.0039		.1454	2.60	.378	.026
3	11.74	.0039		.1451	8.58	1.245	.106
4	5.193	.0114		.2509	8.06	2.023	.390
5	4.532	.0056	.2068	.2083	17.60	3.664	.809
6	4.034	.0099	.3647	.3659	28.79	10.535	2.611
7	3.839	.0098	.3606	.3620	37.81	13.689	3.566
8	3.908	.0085	.3125	.3145	39.61	12.458	3.188
9	4.146	.0073		.2708	41.68	11.287	2.722
10	4.337	.0055		.1967	48.03	9.447	2.178
11	4.969	.0045		.1682	58.02	9.760	1.964
12A	6.597	.0048		.1784	65.79	11.738	1.779
12B	6.956	.0048		.1764	121.9	10.005	1.438
13B	7.317	.0039		.1448	145.9	7.535	1.030
13A	9.140	.0039		.1448	93.87	13.592	1.487
			TOTAL 45.9161			TOTAL 1251.79	
			FMWI TOTAL 40.4893			TOTAL 980.486	

PROPELLANT SYSTEM ANALYSIS

PCP	528.498	PSIA	PCS	37.454	PSIA	FA	1753.259 LBS
WOP	4.002278	LB/SEC	WOS		LB/SEC	FB	1743.659 LBS
WFP	.947357	LB/SEC	WFS		LB/SEC	FSL	1749.558 LBS
WTP	5.249615	LB/SEC	WTS		LB/SEC	WTOT	5.249615 LB/SEC
MRP	7.109551		MRS			ISPSL	333.270 SEC.

TEST NO. 2381-B01-0C-112
DSNAME DTHIS
TEST MODE II

DUAL THROAT CALORIMETER CHAMBER
COOLANT CIRCUIT HEATFLUX PROGRAM

J0878
DATE 08-06-85
TIME 08.15.31

DATA PERIOD FSI + 5.51 SECS. TO FSI + 6.01 SECS.

CIRCUIT NUMBER	CIRCUIT SURFACE AREA SQ.IN	CIRCUIT KW	COOLANT FLOW LB/SEC FLOW METER	COOLANT FLOW LB/SEC ORIFICE	DELTA TEMP DEG F	HEAT LOAD BTU/SEC	HEAT FLUX BTU/SQ.IN.SEC
PRIMARY							
1	1.675	.0934		1.4958	30.56	45.715	27.293
2	.762	.0551		.8566	23.32	19.979	26.220
3	1.613	.0844		1.2748	27.12	34.569	21.432
4	1.921	.0918		1.4937	24.08	35.971	18.725
5	2.220	.1432		2.3712	17.60	41.740	18.751
6	2.460	.1735		2.6135	13.81	36.096	14.626
7	2.736	.0891		1.4499	30.62	44.591	16.225
8	1.351	.0512		.8534	20.28	17.304	12.808
9	.998	.0456		.7040	15.59	10.972	10.994
10	1.491	.0399		.6751	6.56	4.430	2.971
11	3.242	.0512		.8518	5.97	5.086	2.173
12	2.262	.0443		.6895	2.77	1.910	.845
13	1.000	1.7024		26.739	30.21	807.87	807.875
SECONDARY							
SPACER	23.00	.0039		.1443	.96	.139	.006
1A	23.17	.0037		.1372	1.01	.139	.006
1B	20.50	.0037		.1372	1.31	.040	.002
2B	10.75	.0039		.1444	3.04		
2A	14.34	.0039		.1444	3.20	.462	.032
3	11.74	.0039		.1439	11.60	1.668	.142
4	5.193	.0114		.2519	10.24	2.580	.497
5	4.532	.0056	.2204	.2069	20.07	4.151	.916
6	4.034	.0099	.3622	.3636	31.27	11.373	2.819
7	5.839	.0098	.3650	.3597	40.29	14.492	5.775
8	5.908	.0085	.3106	.3124	40.99	12.805	5.277
9	4.146	.0073		.2689	42.11	11.322	2.751
10	4.337	.0055		.1954	47.81	9.340	2.154
11	4.969	.0045		.1673	57.64	9.644	1.941
12A	6.597	.0048		.1772	65.67	11.639	1.764
12B	6.956	.0048		.1772	121.4	9.879	1.420
13B	7.517	.0039		.1439	145.9	7.244	.990
13A	9.140	.0039		.1439	95.49	13.737	1.503
			TOTAL 45.0879			TOTAL 1220.67	
			FMWI TOTAL 40.8307			TOTAL 974.205	

PROPELLANT SYSTEM ANALYSIS

PCP	524.396	PSIA	PCS	34.973	PSIA	FA	1694.450 LBS
WOP	4.203702	LB/SEC	WOS		LB/SEC	FR	1707.136 LBS
WFP	.041804	LB/SEC	WFS		LB/SEC	FSL	1700.784 LBS
WTP	5.205565	LB/SEC	WTS		LB/SEC	WTOT	5.205565 LB/SEC
MRP	7.110850		MRS			ISPSL	326.724 SEC.

TABLE XXIII (cont.)

TEST NO. 2361-R01-0C-113 DUAL THROAT CALORIMETER CHAMBER J0878
DSNAME DTHIS COOLANT CIRCUIT HEATFLUX PROGRAM DATE 08-06-85
TEST MODE II TIME 07.52.26

DATA PERIOD FSI + 5.51 SECS. TO FSI + 6.01 SECS.

CIRCUIT NUMBER	CIRCUIT SURFACE AREA SQ.IN	CIRCUIT KW	COOLANT FLOW LB/SEC FLOW METER	COOLANT FLOW LB/SEC ORIFICE	DELTA TEMP DEG F	HEAT LOAD BTU/SEC	HEAT FLUX BTU/SQ.IN.SEC
PRIMARY							
1	1.675	.0934		1.4989	51.82	47.093	28.473
2	.762	.0551		.8543	24.19	20.660	27.121
3	1.613	.0844		1.2720	28.00	35.629	22.088
4	1.921	.0918		1.4907	24.26	36.171	18.829
5	2.220	.1432		2.3621	18.04	42.623	19.148
6	2.468	.1735		2.6058	14.15	36.873	14.941
7	2.736	.0891		1.4408	31.31	45.300	16.557
8	1.351	.0512		.8531	20.74	17.694	13.097
9	.998	.0456		.7031	16.06	11.293	11.316
10	1.491	.0399		.0746	6.84	4.611	3.093
11	3.242	.0512		.8534	6.98	5.956	2.569
12	2.262	.0443		.6889	3.09	2.126	.940
13	1.000	1.7024		20.601	31.17	829.03	829.029
SECONDARY							
SPACER	23.06	.0039		.1438	.65	.095	.004
1A	23.17	.0037		.1307	1.28	.176	.008
1B	20.50	.0037		.1307	3.05	.241	.012
2B	16.75	.0039		.1459	11.16		
2A	14.34	.0039		.1459	11.27	1.622	.113
3	11.74	.0039		.1457	29.20	4.195	.357
4	5.193	.0114		.2497	21.12	5.274	1.016
5	4.532	.0056	.2030	.2001	36.34	7.491	1.653
6	4.034	.0099	.3608	.3623	52.34	18.964	4.701
7	3.839	.0098	.3568	.3585	61.79	22.144	5.768
8	3.908	.0085	.3096	.3113	56.69	17.647	4.516
9	4.140	.0073		.2679	53.45	14.317	3.455
10	4.337	.0053		.1947	58.56	11.400	2.629
11	4.969	.0045		.1602	70.09	11.647	2.344
12A	6.597	.0048		.1706	79.48	14.038	2.128
12B	6.956	.0048		.1706	144.8	11.538	1.659
13B	7.317	.0039		.1453	169.1	8.591	1.174
13A	9.140	.0039		.1453	109.1	15.640	1.711

TOTAL 45.5097 TOTAL 1300.67

FMWI TOTAL 40.1047 TOTAL 967.472

PROPELLANT SYSTEM ANALYSIS

PCP	551.948 PSIA	PCS	32.653 PSIA	FA	1070.685 LBS
WOP	4.560750 LB/SEC	WOS	LB/SEC	FB	1735.104 LBS
WFP	.343551 LB/SEC	WFS	LB/SEC	FSL	1705.925 LBS
WTP	5.204307 LB/SEC	WTS	LB/SEC	WTOT	5.204307 LB/SEC
MRP	7.086859	MRS		ISPSL	327.791 SEC.

TEST NO. 2581-801-0C-114 DUAL THROAT CALORIMETER CHAMBER J0878
OSNAME DTHIS COOLANT CIRCUIT HEATFLUX PROGRAM DATE 08-06-85
TEST MODE II TIME 07.41.06

DATA PERIOD FS1 + 4.64 SECS. TO FS1 + 5.14 SECS.

CIRCUIT NUMBER	CIRCUIT SURFACE AREA SQ.IN	CIRCUIT KW	COOLANT FLOW LB/SEC FLOW METER	COOLANT FLOW LB/SEC ORIFICE	DELTA TEMP DEG F	HEAT LOAD BTU/SEC	HEAT FLUX BTU/SQ.IN.SEC
PRIMARY							
1	1.675	.0954		1.5185	30.96	47.007	28.064
2	.762	.0551		.8611	23.88	20.561	26.983
3	1.613	.0844		1.2825	28.31	36.308	22.509
4	1.921	.0918		1.6011	25.17	40.300	20.979
5	2.220	.1432		2.3900	18.21	43.521	19.551
6	2.468	.1735		2.6382	14.17	37.396	15.152
7	2.736	.0891		1.4676	31.03	45.539	16.644
8	1.351	.0512		.8634	20.79	17.948	13.285
9	.998	.0456		.7071	16.26	11.499	11.522
10	1.491	.0399		.6806	7.41	5.045	3.384
11	3.242	.0512		.8591	7.36	6.325	2.627
12	2.262	.0443		.7011	3.66	2.564	1.134
13	1.000	1.7024		20.905	31.15	837.96	637.960
SECUNDARY							
SPACER	23.00	.0039		.1452	1.12	.162	.007
1A	23.17	.0037		.1380	5.13	.708	.031
1B	20.50	.0037		.1380	9.98	.669	.033
2B	16.75	.0039		.1453	22.03	.092	.005
2A	14.34	.0039		.1455	21.40	3.108	.217
3	11.74	.0039		.1449	48.63	7.048	.600
4	5.193	.0114		.2503	30.50	7.632	1.470
5	4.532	.0056	.2051	.2081	53.86	11.206	2.473
6	4.034	.0099	.3644	.3656	77.23	28.232	6.999
7	3.839	.0098	.3606	.3616	85.22	30.816	8.027
8	3.908	.0085	.3126	.3142	69.66	21.885	5.600
9	4.146	.0075		.2705	62.47	16.897	4.075
10	4.337	.0053		.1966	66.74	13.120	3.025
11	4.969	.0045		.1678	76.56	12.846	2.585
12A	6.597	.0048		.1782	86.74	15.460	2.344
12B	6.956	.0048		.1782	153.0	11.803	1.697
13B	7.317	.0039		.1447	177.0	9.389	1.283
13A	9.140	.0039		.1447	112.1	10.216	1.774
			TOTAL 46.1117			TOTAL 1359.26	
			FMWI TOTAL 40.4088			TOTAL 917.792	

PROPELLANT SYSTEM ANALYSIS

PCP	535.679 PSIA	PCS	30.081 PSIA	FA	1659.311 LBS
WOP	4.578600 LB/SEC	WOS	LB/SEC	FB	1717.670 LBS
WFP	.045149 LB/SEC	WFS	LB/SEC	FSL	1686.491 LBS
WTP	5.223749 LB/SEC	WTS	LB/SEC	WTOT	5.223749 LB/SEC
MRP	7.096961	MRS		ISPSL	325.233 SEC.

TEST NO. 2381-801-0C-137 DUAL THROAT CALORIMETER CHAMBER J0878
DSNAME DTHIS COOLANT CIRCUIT HEATFLUX PROGRAM DATE 08-06-85
TEST MODE II TIME 08.41.09

DATA PERIOD FS1 + 6.51 SECS. TO FS1 + 7.01 SECS.

CIRCUIT NUMBER	CIRCUIT SURFACE AREA SQ.IN	CIRCUIT KW	COOLANT FLOW LB/SEC FLOW METER	COOLANT FLOW LB/SEC ORIFICE	DELTA TEMP DEG F	HEAT LOAD BTU/SEC	HEAT FLUX BTU/SQ.IN.SEC
PRIMARY							
1	1.675	.0934		1.9188	33.17	63.055	38.003
2	.762	.0551		1.0228	20.46	20.930	27.468
3	1.613	.0844		1.5488	24.11	37.342	23.151
4	1.921	.0918		1.8287	21.39	39.110	20.359
5	2.226	.1432		3.0322	16.28	49.363	22.176
6	2.468	.1735		3.3222	11.84	39.341	15.940
7	2.736	.0891		1.5162	25.14	38.115	13.931
8	1.351	.0512		1.0815	18.13	19.603	14.510
9A	.998	.2096		1.3113	10.73	14.074	14.102
10	1.491	.0399		.8303	6.14	5.099	3.420
11	3.242	.0512		1.0854	5.95	6.458	2.713
12	2.262	.0443		.0211	3.09	2.540	1.123
13	1.000	1.7024		32.130	29.48	947.04	947.040
SECONDARY							
SPACER	23.06	.0039		.1788	4.52	.808	.035
1A	23.17	.0037		.1691	5.94	1.004	.043
1B	20.50	.0037		.1691	12.04	1.032	.050
2B	16.75	.0039		.1785	12.90	1.126	.067
2A	14.34	.0039		.1785	6.59	1.176	.082
3	11.74	.0039		.1774	14.09	2.499	.213
4	5.193	.0114		.2860	11.21	3.207	.618
5	4.532	.0052	.2398	.2370	21.12	5.006	1.104
6	4.034	.0099	.4476	.4501	30.93	13.923	3.451
7	3.839	.0098	.4429	.4435	39.80	17.050	4.597
8	3.908	.0085	.3838	.3849	38.69	14.895	3.812
9	4.146	.0073		.3317	40.16	13.321	3.213
10	4.337	.0053		.2413	42.36	10.220	2.356
11	4.969	.0045		.2052	50.52	10.367	2.086
12A	6.597	.0048		.2169	73.49	15.938	2.416
12B	6.956	.0048		.2169	115.1	9.025	1.297
13B	7.317	.0039		.1774	128.7	8.426	1.152
13A	9.140	.0039		.1774	81.24	14.415	1.577
			TOTAL 55.8691			TOTAL 1426.71	
			FMWI TOTAL 50.6671			TOTAL 1185.12	

PROPELLANT SYSTEM ANALYSIS

PCP	676.671	PSIA	PCS	39.728	PSIA	FA	2221.149 LBS
WOP	5.973454	LB/SEC	WOS		LB/SEC	FB	2215.677 LBS
WFP	.874057	LB/SEC	WFS		LB/SEC	FSL	2221.512 LBS
WTP	6.847511	LB/SEC	WTS		LB/SEC	WTOT	6.847511 LB/SEC
MRP	6.834167		MRS			ISPSL	324.426 SEC.

TEST NO. 2381-B01-0C-138 DUAL THROAT CALORIMETER CHAMBER J0878
OSNAME OTHIS COOLANT CIRCUIT HEATFLUX PROGRAM DATE 08-06-85
TEST MODE 11 TIME 08.52.38

DATA PERIOD FS1 + 6.52 SECS. TO FS1 + 7.02 SECS.

CIRCUIT NUMBER	CIRCUIT SURFACE AREA SQ.IN	CIRCUIT KW	COOLANT FLOW LB/SEC FLOW METER	COOLANT FLOW LB/SEC ORIFICE	DELTA TEMP DEG F	HEAT LOAD BTU/SEC	HEAT FLUX BTU/SQ.IN.SEC
PRIMARY							
1	1.675	.0934		1.9419	32.24	62.612	37.380
2	.762	.0551		1.0248	21.09	21.613	28.363
3	1.613	.0844		1.5553	23.34	36.305	22.508
4	1.921	.0918		1.8396	20.70	38.077	19.822
5	2.220	.1432		3.0569	16.32	49.878	22.407
6	2.468	.1735		3.3395	11.88	39.661	16.070
7	2.736	.0891		1.5225	24.15	36.763	13.437
8	1.351	.0512		1.0859	18.01	19.558	14.476
9A	.998	.2096		1.3426	12.21	16.394	16.427
10	1.491	.0399		.8414	7.24	6.088	4.083
11	3.242	.0512		1.0970	7.83	8.589	3.168
12	2.262	.0443		.8300	5.40	4.479	1.980
13	1.000	1.7024		32.488	29.96	973.27	973.274
SECONDARY							
SPACER	23.06	.0039		.1793	27.00	4.841	.210
1A	23.17	.0037		.1695	40.52	6.870	.297
1B	20.50	.0037		.1695	60.74	3.428	.167
2B	16.75	.0039		.1789	60.49	3.790	.226
2A	14.34	.0039		.1789	39.31	7.034	.490
3	11.74	.0039		.1775	53.84	9.559	.814
4	5.193	.0114		.2801	25.95	7.424	1.430
5	4.532	.0052	.2405	.2378	33.15	7.883	1.739
6	4.034	.0099	.4497	.4515	40.41	18.249	4.524
7	3.839	.0098	.4448	.4450	48.04	21.379	5.569
8	3.908	.0085	.3849	.3863	43.87	16.949	4.337
9	4.146	.0073		.3329	42.17	14.041	3.387
10	4.337	.0053		.2422	42.67	10.336	2.383
11	4.969	.0045		.2060	50.12	10.325	2.078
12A	6.597	.0048		.2178	70.91	15.440	2.340
12B	6.956	.0048		.2178	100.3	7.703	1.107
13B	7.317	.0039		.1782	118.0	7.176	.981
13A	9.140	.0039		.1782	77.72	13.851	1.515
			TOTAL	56.3988		TOTAL 1499.57	
			FMWI TOTAL	50.8301		TOTAL 1034.37	

PROPELLANT SYSTEM ANALYSIS

PCP	676.217	PSIA	PCS	35.612	PSIA	FA	2186.704 LBS
WOP	5.967050	LB/SEC	WOS		LB/SEC	FB	2171.330 LBS
WFP	.872991	LB/SEC	WFS		LB/SEC	FSL	2171.017 LBS
WTP	6.840041	LB/SEC	WTS		LB/SEC	WTOT	6.840041 LB/SEC
MRP	6.835178		MRS			ISPSL	316.275 SEC.

TABLE XXIII (cont.)

TEST NO. 2381-RU1-0C-139 DUAL THROAT CALORIMETER CHAMBER J0878
DBNAME DTHIS COOLANT CIRCUIT HEATFLUX PROGRAM DATE 08-06-85
TEST MODE II TIME 09.03.59

DATA PERIOD FS1 + 6.52 SECS. TO FS1 + 7.02 SECS.

CIRCUIT NUMBER	CIRCUIT SURFACE AREA SQ.IN	CIRCUIT KW	COOLANT FLOW LB/SEC FLOW METER	COOLANT FLOW LB/SEC ORIFICE	DELTA TEMP DEG F	HEAT LOAD BTU/SEC	HEAT FLUX BTU/SQ.IN.SEC
PRIMARY							
1	1.675	.0934		1.9450	33.52	65.204	38.928
2	.762	.0551		1.0312	20.56	21.206	27.829
3	1.613	.0844		1.5549	24.04	37.383	23.176
4	1.921	.0918		1.8449	20.87	38.509	20.046
5	2.226	.1432		3.0585	16.21	49.580	22.273
6	2.468	.1735		3.3436	12.20	40.801	16.532
7	2.736	.0891		1.5224	25.01	38.081	13.919
8	1.351	.0512		1.0853	17.77	19.286	14.275
9A	.998	.2096		1.3424	11.24	15.094	15.124
10	1.491	.0399		.8401	5.78	4.854	3.256
11	5.242	.0512		1.0895	6.04	6.581	2.746
12	2.262	.0443		.8254	3.20	2.637	1.166
13	1.000	1.7024		32.683	29.75	972.38	972.383
SECONDARY							
SPACER	23.06	.0039					
1A	23.17	.0037					
1B	20.50	.0037			.50		
2B	16.75	.0039		.1794	2.60	.062	.004
2A	14.34	.0039		.1794	2.25	.404	.028
3	11.74	.0039		.1782	4.14	.738	.063
4	5.193	.0114		.3073	4.19	1.286	.248
5	4.532	.0052	.2333	.2383	11.61	2.767	.610
6	4.034	.0099	.4411	.4514	19.80	8.935	2.215
7	3.839	.0098	.4455	.4458	26.39	11.765	3.065
8	3.908	.0085	.3864	.3858	28.99	11.184	2.862
9	4.146	.0073		.3342	30.09	10.055	2.425
10	4.337	.0053		.2424	30.77	7.460	1.720
11	4.969	.0045		.2066	41.85	8.647	1.740
12A	6.597	.0048		.2180	61.98	13.515	2.049
12B	6.956	.0048		.2160	96.55	7.537	1.084
13B	7.317	.0039		.1784	111.1	6.960	.951
13A	9.140	.0039		.1784	72.13	12.871	1.408
			TOTAL 56.1079			TOTAL 1415.79	
			FMWI TOTAL 51.0169			TOTAL 1147.73	

PROPELLANT SYSTEM ANALYSIS

PCP	676.040	PSIA	PCS	42.213	PSIA	FA	2246.359 LBS
WOP	5.960368	LB/SEC	WOS		LB/SEC	FB	2234.149 LBS
WFP	.875904	LB/SEC	WFS		LB/SEC	FSL	2240.244 LBS
WTP	6.836271	LB/SEC	WTS		LB/SEC	WTOT	6.836271 LB/SEC
MRP	6.804619		MRS			ISPSL	327.700 SEC.

TEST NO. 2381-B01-0C-140 DUAL THROAT CALORIMETER CHAMBER J0878
DSNAME DTHIS COOLANT CIRCUIT HEATFLUX PROGRAM DATE 08-06-85
TEST MODE II TIME 09.18.37

DATA PERIOD FSI + 6.52 SECS. TO FSI + 7.02 SECS.

CIRCUIT NUMBER	CIRCUIT SURFACE AREA SQ.IN	CIRCUIT KW	COOLANT FLOW LB/SEC FLOW METER	COOLANT FLOW LB/SEC ORIFICE	DELTA TEMP DEG F	HEAT LOAD BTU/SEC	HEAT FLUX BTU/SQ.IN.SEC
PRIMARY							
1	1.675	.0934		1.9334	24.65	47.658	28.453
2	.762	.0551		1.0354	14.74	15.263	20.030
3	1.613	.0844		1.5565	17.52	27.269	16.906
4	1.921	.0918		1.8488	14.84	27.431	14.279
5	2.226	.1432		3.0620	11.81	36.160	16.245
6	2.468	.1735		3.3479	8.64	28.939	11.726
7	2.736	.0891		1.5217	18.11	27.555	10.071
8	1.351	.0512		1.0911	12.51	13.645	10.100
9A	.998	.2096		1.3464	7.88	10.609	10.630
10	1.491	.0399		.8444	4.62	3.904	2.618
11	3.242	.0512		1.0917	4.49	4.901	1.761
12	2.262	.0443		.8275	3.23	2.673	1.182
13	1.000	1.7024		32.701	24.85	812.72	812.720
SECONDARY							
SPACER	23.06	.0039		.1797	2.96	.533	.023
1A	23.17	.0037		.1700	4.39	.747	.032
1B	20.50	.0037		.1700	7.08	.457	.022
2B	16.75	.0039		.1794	7.33	.669	.040
2A	14.34	.0039		.1794	3.61	.647	.045
3	11.74	.0039		.1782	5.86	1.044	.089
4	5.193	.0114		.3000	4.59	1.378	.265
5	4.532	.0052	.2378	.2382	13.68	3.259	.719
6	4.034	.0099	.4484	.4493	19.12	8.590	2.129
7	3.839	.0098	.4457	.4459	24.30	10.838	2.823
8	3.908	.0085	.3862	.3859	24.18	9.330	2.387
9	4.146	.0073		.3337	25.60	8.542	2.060
10	4.337	.0053		.2425	24.37	5.910	1.363
11	4.969	.0045		.2064	30.91	6.378	1.284
12A	6.597	.0048		.2183	44.11	9.630	1.460
12B	6.956	.0048		.2183	69.35	5.511	.792
13B	7.317	.0039		.1787	80.67	5.272	.721
13A	9.140	.0039		.1787	51.16	9.143	1.000
			TOTAL 56.6600			TOTAL 1146.60	
			FMWI TOTAL 51.1510			TOTAL 924.206	

PROPELLANT SYSTEM ANALYSIS

PCP	602.791	PSIA	PCS	31.924	PSIA	FA	2120.360 LBS
WOP	4.710042	LB/SEC	WOS		LB/SEC	FB	2109.639 LBS
WFP	1.594607	LB/SEC	WFS		LB/SEC	FSL	2115.000 LBS
WTP	6.304648	LB/SEC	WTS		LB/SEC	WTOT	6.304648 LB/SEC
MRP	2.953732		MRS			ISPSL	335.467 SEC.

C-2

TABLE XXIII (cont.)

TEST NO. 2381-B01-0C-141
DSNAME DTHIS
TEST MODE II

DUAL THROAT CALORIMETER CHAMBER
COOLANT CIRCUIT HEATFLUX PROGRAM

J0878
DATE 04-06-85
TIME 09.26.01

DATA PERIOD FS1 + 6.55 SECS. TO FS1 + 7.05 SECS.

CIRCUIT NUMBER	CIRCUIT SURFACE AREA SQ.IN	CIRCUIT KW	COOLANT FLOW LB/SEC FLOW METER	COOLANT FLOW LB/SEC ORIFICE	DELTA TEMP DEG F	HEAT LOAD BTU/SEC	HEAT FLUX BTU/SQ.IN.SEC
PRIMARY							
1	1.675	.0934		1.9301	24.83	47.923	28.611
2	.762	.0551		1.0333	14.61	15.097	19.812
3	1.613	.0844		1.5544	17.00	26.423	16.381
4	1.921	.0918		1.8439	14.83	27.346	14.235
5	2.226	.1432		3.0525	11.47	35.000	15.723
6	2.468	.1735		3.3361	8.59	28.671	11.617
7	2.736	.0891		1.5206	17.89	27.203	9.943
8	1.351	.0512		1.0864	12.52	13.604	10.070
9A	.998	.2096		1.3234	7.86	10.397	10.418
10	1.491	.0399		.8395	4.10	3.442	2.309
11	3.242	.0512		1.0896	4.23	4.613	1.948
12	2.262	.0443		.8293	2.16	1.789	.791
13	1.000	1.7024		32.457	24.54	796.34	796.341
SECONDARY							
SPACER	23.06	.0039					
1A	23.17	.0037					
1B	20.50	.0037			1.72		
2B	16.75	.0039			2.01		
2A	14.34	.0039					
3	11.74	.0039		.1779	.84	.150	.013
4	5.193	.0114		.2954	2.13	.028	.121
5	4.532	.0052	.2376	.2375	8.05	1.911	.422
6	4.034	.0099	.4468	.4477	13.45	6.023	1.493
7	3.839	.0098	.4440	.4446	18.70	8.313	2.166
8	3.908	.0085	.3853	.3847	20.18	7.766	1.987
9	4.146	.0073		.3328	21.06	7.009	1.690
10	4.337	.0053					
11	4.969	.0045		.2058	26.38	5.430	1.093
12A	6.597	.0048		.2177	40.89	8.902	1.349
12B	6.956	.0048		.2177	61.65	4.520	.650
13B	7.317	.0039		.1782	70.68	4.569	.624
13A	9.140	.0039		.1782	45.04	8.025	.878
			TOTAL 55.2145			TOTAL 1101.09	
			FMWI TOTAL 51.0749			TOTAL 917.472	

PROPELLANT SYSTEM ANALYSIS

PCP	674.803	PSIA	PCS	34.465	PSIA	FA	2182.642 LBS
WOP	4.814409	LB/SEC	WOS		LB/SEC	FR	2171.133 LBS
WFP	1.006364	LB/SEC	WFS		LB/SEC	FSL	2176.888 LBS
WTP	6.420774	LB/SEC	WTS		LB/SEC	WTOT	6.420774 LB/SEC
MRP	2.997084		MRS			ISPSL	339.036 SEC.

TEST NO. 2381-B01-0C-142 DUAL THROAT CALORIMETER CHAMBER J0878
DSNAME DTHIS COOLANT CIRCUIT HEATFLUX PROGRAM DATE 08-06-85
TEST MODE II TIME 09.32.55

DATA PERIOD FS1 + 6.52 SECS. TO FS1 + 7.02 SECS.

CIRCUIT NUMBER	CIRCUIT SURFACE AREA SQ.IN	CIRCUIT KW	COOLANT FLOW LB/SEC FLOW METER	COOLANT FLOW LB/SEC ORIFICE	DELTA TEMP DEG F	HEAT LOAD BTU/SEC	HEAT FLUX BTU/SQ.IN.SEC
PRIMARY							
1	1.675	.0934		1.9251	24.69	47.480	28.346
2	.762	.0551		1.0284	15.26	15.694	20.596
3	1.613	.0844		1.5477	17.08	26.433	16.388
4	1.921	.0918		1.8368	15.02	27.590	14.362
5	2.226	.1432		3.0411	11.97	36.393	16.349
6	2.468	.1735		3.3256	8.85	29.429	11.924
7	2.736	.0891		1.5222	17.93	27.297	9.977
8	1.351	.0512		1.0839	13.02	14.110	10.444
9A	.998	.2096		1.3212	8.62	11.391	11.414
10	1.491	.0399		.8400	5.39	4.527	3.036
11	5.242	.0512		1.0870	5.81	6.316	2.315
12	2.262	.0443		.8305	4.01	3.329	1.472
13	1.000	1.7024		32.294	25.33	817.94	817.943
SECONDARY							
SPACER	23.06	.0039		.1785	19.60	3.498	.152
1A	23.17	.0037		.1688	28.50	4.812	.208
1B	20.50	.0037		.1688	44.29	2.665	.130
2B	16.75	.0039		.1782	43.89	2.995	.179
2A	14.34	.0039		.1782	27.08	4.825	.336
3	11.74	.0039		.1773	37.44	6.638	.565
4	5.193	.0114		.2946	18.57	5.472	1.054
5	4.532	.0052	.2365	.2366	24.38	5.768	1.273
6	4.034	.0099	.4449	.4456	29.53	13.158	3.262
7	3.839	.0098	.4432	.4429	39.25	17.384	4.528
8	3.908	.0085	.3844	.3833	36.42	13.959	3.572
9	4.146	.0073		.3315	33.11	10.978	2.648
10	4.337	.0053					
11	4.969	.0045		.2050	40.61	8.324	1.675
12A	0.597	.0048		.2169	56.83	12.324	1.868
12B	0.956	.0048		.2169	87.36	6.620	.952
13B	7.317	.0039		.1775	98.45	6.237	.852
13A	9.140	.0039		.1775	63.30	11.233	1.229
			TOTAL 55.8590			TOTAL 1204.82	
			FMWI TOTAL 51.0448			TOTAL 998.912	

PROPELLANT SYSTEM ANALYSIS

PCP	674.071 PSIA	PCS	28.553 PSIA	FA	2111.045 LBS
WOP	4.630115 LB/SEC	WOS	LB/SEC	FB	2100.152 LBS
WFP	1.582837 LB/SEC	WFS	LB/SEC	FSL	2105.598 LBS
WTP	6.412952 LB/SEC	WTS	LB/SEC	WTOT	6.412952 LB/SEC
MRP	3.051555	MRS		ISPSL	328.335 SEC.

TABLE XXIV

COLD-FLOW LEAKAGE MODEL FLOW FACTORS

Primary Circuit No. (i)	$W_{channel}/W_{outlet}$ f_i
1	.790
2	.716
3	.918
4	.743
5	.471
6	.437
7	.867
8	.686
9	.704
10	.600
11	.640
12	.578

IV, C, Results (cont.)

$$Q_i = W_i \left[\Delta T_i - (1 - f_i)\left(\Delta T_x - \frac{Q_{X2}}{W_x}\right)\right]$$

in which

Q_i = calorimetric heat load

W_i = calorimeter circuit measured outlet flow rate

ΔT_i = calorimeter circuit bulk temperature rise

f_i = leakage model flow factor, Table XXIV

ΔT_x = axial circuit bulk temperature rise

w_x = axial circuit flow rate (P13)

Q_{X2} = axial circuit heat load for Mode II operation at the same primary chamber P_c and mixture ratio

This analysis assumes the heating of the outer part of the axial circuit is negligible in Mode II, and that the heat load on the inner part is the same for both modes. A review of the data indicates the primary throat was sonic in all Mode I tests, which justifies the latter assumption since the axial circuit is upstream of the primary throat.

Heat fluxes reported for circuits P9 and P11 at the corners of the primary nozzle tip are estimates for the end wall obtained by subtracting an approximate side wall heat load from the measured total heat load. Side wall heat loads were obtained by analytically correcting upstream heat fluxes from circuits P8 and P12 for freestream mass velocity changes. Thus

$$Q_{end} = Q_{total} - g\,\Phi_i\,A_{side}$$

circuit	g	i	A_{side}, $in.^2$
9	0.961	8	0.998
11	1.038	12	1.511

IV, C, Results (cont.)

Data reduction printouts for Mode I are given in Table XXV, and the resulting heat flux profiles are shown in B-11 to B-24 in Appendix B.

TABLE XXV

TEST NO. 2381-RU1-0C-110 DUAL THROAT CALORIMETER CHAMBER J0878
DSNAME DTHIS COOLANT CIRCUIT HEATFLUX PROGRAM DATE 12-06-85
TEST MODE 1 PRIMARY COLDFLOW LEAKAGE MODEL TIME 09.54.05

DATA PERIOD FS1 + 5.52 SECS. TO FS1 + 6.02 SECS.

CIRCUIT NUMBER	CIRCUIT SURFACE AREA SQ.IN	CIRCUIT KW	COOLANT FLOW LB/SEC FLOW METER	COOLANT FLOW LB/SEC ORIFICE	DELTA TEMP DEG F	HEAT LOAD BTU/SEC	HEAT FLUX BTU/SQ.IN.SEC
PRIMARY							
1	1.675	.0934		1.5312	51.25	42.058	25.107
2	.762	.0551		.6900	20.63	14.296	25.363
3	1.613	.0844		1.3009	25.84	31.989	19.685
4	1.921	.0918		1.5485	23.24	28.855	15.021
5	2.220	.1432		2.4868	25.55	39.868	17.910
6	2.466	.1735		2.7200	21.26	51.287	12.272
7	2.736	.0891		1.5013	27.23	37.283	13.627
8	1.351	.0516		.8875	30.71	24.019	17.777
9	2.378	.0456		.7404	55.10	35.418	15.309
10	1.491	.0399		.7073	37.61	21.511	14.327
11	5.202	.0512		.8937	32.12	22.922	5.760
12	2.262	.0443		.7200	33.51	13.080	5.782
13	1.900	1.7024		27.055	44.66	1208.3	1208.32
SECONDARY							
SPACER	23.06	.0695		2.3698	110.1	260.98	11.313
1A	23.17	.0902		3.1010	55.57	172.37	7.439
1B	29.50	.0902		3.1010	91.98	112.91	5.503
2B	10.75	.0706		2.5300	84.92	113.93	8.402
2A	14.34	.0706		2.5300	40.01	101.50	7.078
3	11.74	.0582		1.7105	50.35	96.593	8.212
4	5.193	.1556		2.1507	21.78	46.857	9.019
5	4.532	.1125	2.2947	2.3342	17.39	40.602	8.959
6	4.034	.1041	1.9729	1.9836	17.16	34.045	8.440
7	5.439	.0953	1.8517	1.8909	17.75	33.524	6.163
8	3.906	.0707	1.6394	1.6519	18.39	30.377	7.774
9	4.146	.0910		1.8190	18.73	34.065	8.216
10	4.337	.0661		1.9909	19.51	38.843	8.956
11	4.969	.0399		1.3499	28.70	38.489	7.746
12A	3.597	.0910	1.8238	1.8226	29.10	53.030	14.738
12B	6.350	.0919		1.8262	57.90	52.022	7.595
13B	7.317	.0779		1.5869	60.65	58.194	7.952
13A	9.143	.0779		1.5869	42.79	67.896	7.424

TOTAL 80.5277 TOTAL 2920.80

PRI TOTAL 65.7864 TOTAL 2669.50

PROPELLANT SYSTEM ANALYSIS

PCP	515.324 PSIA	PCS	245.263 PSIA	FA	3985.864 LBS
WOP	4.274518 LB/SEC	WOS	1.469465 LB/SEC	FR	3986.047 LBS
WFP	.991512 LB/SEC	WFS	.956505 LB/SEC	FSI	3986.930 LBS
WTP	5.265830 LB/SEC	WTS	8.420971 LB/SEC	WTOT	13.686801 LB/SEC
MRP	7.905352	MRS	7.803847	ISPSL	291.007 SEC.

TEST [illegible] 2301-P01-01-117 DUAL THROAT CALORIMETER CHAMBER J087A
DSNAME [illegible] COOLANT CIRCUIT HEATFLUX PROGRAM DATE 12-09-85
TEST MODE 1 PRIMARY CULDFLOW LEAKAGE MODEL TIME 09.21.06

DATA PERIOD FSI + 3.51 SECS. TO FSI + 6.01 SECS.

CIRCUIT NUMBER	CIRCUIT SURFACE AREA SQ.IN	CIRCUIT K/W	COOLANT FLOW LB/SEC FLOW METER	COOLANT FLOW LB/SEC ORIFICE	DELTA TEMP DEG F	HEAT LOAD BTU/SEC	HEAT FLUX BTU/SQ.IN.SEC
PRIMARY							
1	1.075	.0934		1.5291	35.85	48.995	29.251
2	.784	.0551		.8955	29.00	21.411	25.099
3	1.015	.0484		1.3600	28.55	35.184	21.813
4	1.921	.0918		1.5486	25.03	31.534	10.416
5	2.220	.1032		2.4910	27.49	44.566	20.021
6	2.468	.1735		2.7219	22.41	33.231	13.485
7	1.730	.0841		1.4988	28.77	39.499	10.437
8	1.361	.0512		.8890	33.83	25.009	18.511
9	2.378	.0435		.7424	54.40	30.457	15.553
10	1.491	.0399		.7092	59.25	22.675	15.207
11	3.282	.0512		.8927	34.25	24.746	8.532
12	2.282	.0445		.7185	45.35	19.881	8.749
13	1.000	1.7024		26.940	48.41	1304.9	1301.90
SECONDARY							
SPACER	25.00	.0095		2.3745	110.2	275.81	11.961
1A	23.17	.0982		3.0991	60.64	187.91	8.110
1B	20.60	.0982		3.0991	101.0	120.36	5.164
2B	10.75	.0706		2.5350	94.91	127.10	7.592
2A	14.34	.0700		2.5550	44.75	113.45	7.910
3	11.74	.0582		1.7095	62.49	106.83	9.101
4	5.195	.1530		2.1480	24.45	52.514	10.112
5	4.532	.1125	2.2925	2.3331	19.50	45.659	10.070
6	4.034	.1081	1.9728	1.9857	20.85	41.559	10.253
7	5.439	.0955	1.0540	1.8955	22.65	42.681	11.170
8	5.908	.0707	1.0595	1.0528	24.33	40.244	10.298
9	4.145	.0918		1.8178	22.67	41.200	9.937
10	4.337	.0651		1.9887	22.65	45.047	10.387
11	3.969	.0339		1.5399	32.89	44.067	8.868
12A	3.597	.0710	1.8247	1.8210	32.82	59.594	9.933
12B	3.955	.0910		1.8210	24.97	35.927	6.471
13B	7.317	.0779		1.5879	74.36	41.993	5.739
13A	7.140	.0779		1.5879	47.91	70.077	9.814
			TOTAL	80.2029	TOTAL	3214.97	
			FMWI TOTAL	85.7150	TOTAL	2886.97	

PROPELLANT SYSTEM ANALYSIS

PCP	520.529 PSIA	PCS	257.002 PSIA	FA	4545.357 LBS
WOP	.378015 LB/SEC	WOS	7.795075 LB/SEC	FR	4560.820 LBS
WFP	.378015 LB/SEC	WFS	1.099178 LB/SEC	FSL	4357.192 LBS
WTP	5.557627 LB/SEC	WTS	8.894253 LB/SEC	WTOT	14.45200 LB/SEC
MRP	7.177534	MRS	7.091731	ISPSL	301.486 SEC.

TEST NO. 2381-801-0C-125 DUAL THROAT CALORIMETER CHAMBER J0878
DSNAME DTHIS COOLANT CIRCUIT HEATFLUX PROGRAM DATE 12-09-85
TEST MODE I PRIMARY COLDFLOW LEAKAGE MODEL TIME 07.55.20

DATA PERIOD FS1 + 4.19 SECS. TO FS1 + 4.69 SECS.

CIRCUIT NUMBER	CIRCUIT SURFACE AREA SQ.IN	CIRCUIT KW	COOLANT FLOW LB/SEC FLOW METER	COOLANT FLOW LB/SEC ORIFICE	DELTA TEMP DEG F	HEAT LOAD BTU/SEC	HEAT FLUX BTU/SQ.IN.SEC
PRIMARY							
1	1.675	.0934		1.0473	31.98	40.858	27.975
2	.762	.0551		.9161	22.50	16.236	21.307
3	1.613	.0844		1.3032	24.21	29.751	18.445
4	1.921	.0918		1.5774	19.58	24.963	12.526
5	2.226	.1432		2.6102	24.59	40.964	18.403
6	2.468	.1735		2.8451	22.37	36.720	14.878
7	2.736	.0891		1.2604	34.76	40.989	14.981
8	1.351	.0512		.6959	38.46	29.864	21.957
9	2.378	.0456		.7650	55.51	38.659	12.754
10	1.491	.0399	.7266	.7238	41.40	25.092	16.829
11	3.242	.0512	.9316	.9283	34.50	26.405	8.180
12	2.262	.0443	.7211	.7222	39.46	22.855	10.015
13	1.000	1.7024		27.855	43.70	1217.3	1217.29
SECONDARY							
SPACER	23.06	.0695		2.5037	133.7	334.72	14.515
1A	23.17	.0962		3.2351	68.95	223.07	9.627
1B	20.50	.0962		3.2351	111.0	135.89	6.629
2B	16.75	.0766		2.5713	93.47	122.50	7.313
2A	14.34	.0700		2.5713	45.83	117.83	8.217
3	11.74	.0582		1.7806	72.12	128.41	10.940
4	5.193	.1536		2.2064	29.33	64.714	12.462
5	4.532	.1125	2.3576	2.4486	25.81	63.274	13.962
6	4.034	.1041		2.0494	30.29	62.071	15.387
7	3.839	.0953		2.2517	32.87	74.010	19.278
8	3.908	.0707		1.7056	27.41	46.756	11.964
9	4.146	.0918		1.8894	25.15	47.515	11.460
10	4.337	.0601		2.0911	24.23	50.660	11.681
11	4.969	.0399		1.3996	33.56	46.972	9.453
12A	6.507	.0910	1.9061	1.8785	36.96	69.431	10.525
12B	6.956	.0910		1.8785	53.44	49.545	7.123
13B	7.317	.0779		1.6337	73.49	42.534	5.821
13A	9.140	.0779		1.6337	47.42	77.473	8.476
			TOTAL 83.0114		TOTAL 3352.78		
			FMWI TOTAL 68.8092		TOTAL 3073.68		

PROPELLANT SYSTEM ANALYSIS

PCP	436.780 PSIA	PCS	316.083 PSIA	FA	4740.092 LBS
WOP	4.245504 LB/SEC	WOS	9.678871 LB/SEC	FB	4729.354 LBS
WFP	.029449 LB/SEC	WFS	1.412497 LB/SEC	FSL	4735.027 LBS
WTP	4.274953 LB/SEC	WTS	11.09137 LB/SEC	WTOT	15.96633 LB/SEC
MRP	6.744795	MRS	6.852313	ISPSL	299.751 SEC.

TEST NO. 2381-R01-0C-12b DUAL THROAT CALORIMETER CHAMBER J0878
DSNAME DTHIS COOLANT CIRCUIT HEATFLUX PROGRAM DATE 12-09-85
TEST MODE 1 PRIMARY COLDFLOW LEAKAGE MODEL TIME 08.01.31

DATA PERIOD FSI + 5.52 SECS. TO FSI + 6.02 SECS.

CIRCUIT NUMBER	CIRCUIT SURFACE AREA SQ.IN	CIRCUIT KW	COOLANT FLOW LB/SEC FLOW METER	COOLANT FLOW LB/SEC ORIFICE	DELTA TEMP DEG F	HEAT LOAD BTU/SEC	HEAT FLUX BTU/SQ.IN.SEC
PRIMARY							
1	1.675	.0934		1.6469	30.53	51.715	30.875
2	.762	.0551		.9141	26.60	20.449	26.836
3	1.513	.0844		1.2885	23.97	29.316	19.175
4	1.921	.0918		1.5740	18.69	23.402	12.182
5	2.220	.1432		2.6025	23.67	41.099	18.463
6	2.468	.1735		2.8357	23.00	41.441	16.791
7	2.736	.0891		1.2709	35.47	42.563	15.557
8	1.351	.0512		.8955	37.80	29.588	21.901
9	2.378	.0456		.7651	57.88	40.913	14.427
10	1.491	.0399	.7240	.7230	40.44	24.936	16.724
11	3.242	.0512	.9332	.9290	36.53	28.954	8.778
12	2.262	.0415	.7160	.7101	40.87	24.836	10.980
13	1.900	1.7024		27.694	42.05	1164.7	1164.05
SECONDARY							
SPACER	23.00	.0695		2.4955	140.0	349.26	15.146
1A	23.17	.0962		3.2210	71.29	229.61	9.910
1B	20.50	.0962		3.2210	114.6	369.41	6.801
2B	16.75	.0766		2.5596	100.9	128.10	7.649
2A	14.34	.0766		2.5596	50.82	130.09	9.072
3	11.74	.0582		1.7722	76.11	134.88	11.491
4	5.193	.1556		2.1983	27.70	61.015	11.749
5	4.532	.1125	2.5469	2.4392	30.18	73.622	16.245
6	4.034	.1061		2.0426	33.98	69.409	17.206
7	3.839	.0953		2.2318	29.79	66.492	17.320
8	3.908	.0707		1.6977	22.64	38.437	9.836
9	4.106	.0918		1.8809	28.97	54.486	13.142
10	4.337	.0661		2.0822	28.15	58.620	13.516
11	4.969	.0599		1.3927	34.20	47.634	9.586
12A	6.597	.0910	1.8974	1.8726	41.05	76.875	11.653
12B	6.956	.0910		1.8726	65.79	46.321	6.659
13B	7.317	.0779		1.6266	76.68	42.824	5.853
13A	9.180	.0779		1.6266	50.35	81.903	8.961
			TOTAL 82.0074		TOTAL 3592.85		
			FNWI TOTAL 68.4500		TOTAL 3187.11		

PROPELLANT SYSTEM ANALYSIS

PCP	475.351 PSIA	PCS	321.529 PSIA	FA	4619.360 LBS
WOP	4.559855 LB/SEC	WOS	9.936939 LB/SEC	FB	4790.702 LBS
WFP	.029922 LB/SEC	WFS	1.413883 LB/SEC	FSL	4807.712 LBS
WTP	4.989750 LB/SEC	WTS	11.350882 LB/SEC	WTOT	16.340656 LB/SEC
MRP	6.721225	MRS	7.028117	TSPSL	294.219 SEC.

TABLE XXV (cont.)

TEST NO. 2501-R01-0C-127 DUAL THROAT CALORIMETER CHAMBER JOB78
DSNAME DTHIS COOLANT CIRCUIT HEATFLUX PROGRAM DATE 12-09-85
TEST MODE 1 PRIMARY COLDFLOW LEAKAGE MODEL TIME 08.10.46

DATA PERIOD FSI + 5.51 SECS. TO FSI + 6.01 SECS.

CIRCUIT NUMBER	CIRCUIT SURFACE AREA SQ.IN	CIRCUIT KW	COOLANT FLOW LB/SEC FLOW METER	COOLANT FLOW LB/SEC ORIFICE	DELTA TEMP DEG F	HEAT LOAD BTU/SEC	HEAT FLUX BTU/SQ.IN.SEC
PRIMARY							
1	1.675	.0934		1.0000	31.74	45.598	27.223
2	.762	.0551		.9099	24.95	17.852	23.428
3	1.613	.0844		1.2700	24.23	28.974	17.963
4	1.921	.0918		1.5704	20.27	24.351	12.676
5	2.220	.1432		2.6046	29.23	59.288	22.591
6	2.468	.1735		2.8355	20.20	41.352	17.971
7	2.736	.0691		1.2705	40.63	38.452	17.709
8	1.351	.0512		.6919	45.94	33.935	25.117
9	2.378	.0456		.7608	61.83	42.816	15.571
10	1.491	.0399	.7269	.7247	47.51	28.996	19.447
11	3.242	.0512	.9267	.9212	40.06	30.080	7.775
12	2.262	.0443	.7239	.7234	42.25	24.839	10.981
13	1.000	1.7024		27.695	45.78	1267.8	1267.82
SECONDARY							
SPACER	23.06	.0695		2.4997	102.9	557.33	15.499
1A	23.17	.0962		3.2207	74.73	241.14	10.408
1B	20.50	.0962		3.2207	123.6	157.53	7.684
2B	16.75	.0760		2.5622	113.5	147.42	8.425
2A	14.34	.0760		2.5622	55.85	143.09	9.979
3	11.74	.0582		1.7740	85.13	151.07	12.871
4	5.193	.1530		2.2019	34.34	75.622	14.562
5	4.532	.1125	2.3491	2.4410	31.30	70.572	15.698
6	4.034	.1031		2.0412	35.30	72.061	17.863
7	3.839	.0953		2.2362	35.25	78.819	20.531
8	3.908	.0707		1.0994	27.28	45.356	11.602
9	4.146	.0918		1.8781	26.98	50.678	12.223
10	4.337	.0661		2.0850	26.17	54.594	12.591
11	4.969	.0399		1.3935	35.00	48.851	9.831
12A	8.597	.0910	1.8989	1.8702	39.74	74.554	11.301
12B	8.956	.0910		1.8702	67.64	52.349	7.526
13B	7.317	.0779		1.2304	81.22	43.539	5.950
13A	9.140	.0779		1.6304	54.51	88.871	9.723
		TOTAL 82.0721				TOTAL 3819.77	
		FMWI TOTAL 68.0008				TOTAL 3559.50	

PROPELLANT SYSTEM ANALYSIS

PCP	492.262 PSIA	PCS	363.770 PSIA	FA	5313.492 LBS
WOP	4.358275 LB/SEC	WOS	11.307765 LB/SEC	FB	5290.127 LBS
WFP	.026015 LB/SEC	WFS	1.620150 LB/SEC	FSL	5301.765 LBS
WTP	4.964890 LB/SEC	WTS	12.933840 LB/SEC	WTOT	17.898869 LB/SEC
MRP	6.923347	MRS	6.955033	ISPSL	296.210 SEC.

TEST NO. 2381-801-0C-129 DUAL THROAT CALORIMETER CHAMBER J0878
DSNAME DTHIS COOLANT CIRCUIT HEATFLUX PROGRAM DATE 12-11-85
TEST MODE I PRIMARY COLDFLOW LEAKAGE MODEL TIME 10.12.10

DATA PERIOD FS1 + 1.61 SECS. TO FS1 + 1.65 SECS.

CIRCUIT NUMBER	CIRCUIT SURFACE AREA SQ.IN	CIRCUIT KW	COOLANT FLOW LB/SEC FLOW METER	COOLANT FLOW LB/SEC ORIFICE	DELTA TEMP DEG F	HEAT LOAD BTU/SEC	HEAT FLUX BTU/SQ.IN.SEC
PRIMARY							
1	1.675	.0934		1.8211	28.64	46.654	27.853
2	.762	.0551		.9539	24.39	19.374	25.426
3	1.613	.0844		1.4456	22.70	31.110	19.287
4	1.921	.0918		1.7586	19.40	27.622	14.379
5	2.226	.1432		2.8933	29.12	62.244	27.962
6	2.468	.1735		3.1546	25.66	55.414	22.453
7	2.736	.0891		1.4218	35.91	48.343	17.669
8	1.351	.0512		.9892	37.24	32.373	23.962
9A	2.378	.2096		1.1333	45.74	47.015	17.416
10	1.491	.0399	.8015	.8028	42.79	29.739	19.946
11	3.242	.0512	1.0451	1.0424	36.48	32.634	7.839
12	2.262	.0443	.8009	.8005	40.41	27.495	12.155
13	1.000	1.7024		30.561	38.49	1176.4	1176.37
SECONDARY							
SPACER	23.06	.0695		2.9282	128.6	376.48	16.326
1A	23.17	.0962		3.5821	66.75	239.10	10.319
1B	20.50	.0962		3.5821	111.8	161.44	7.875
2B	16.75	.0766		2.8467	106.0	150.14	8.963
2A	14.34	.0766		2.8467	53.28	151.68	10.577
3	11.74	.0582		1.9712	82.44	162.50	13.844
4	5.193	.1536		2.4383	34.79	84.823	16.334
5	4.532	.1125	2.6090	2.6978	30.00	80.942	17.860
6	4.034	.1081		2.2652	33.62	76.157	18.879
7	3.839	.0953		2.4806	34.79	86.302	22.480
8	3.908	.0707		1.8737	27.71	51.920	13.286
9	4.146	.0918		2.0771	24.43	50.743	12.239
10	4.337	.0661		2.3159	23.33	54.020	12.456
11	4.969	.0399		1.5470	32.45	50.197	10.102
12A	6.597	.0910	2.1030	2.0690	35.15	72.729	11.025
12B	6.956	.0910		2.0690	57.41	46.055	6.621
13B	7.317	.0779		1.7949	73.02	43.413	5.933
13A	9.140	.0779		1.7949	48.84	87.652	9.590
			TOTAL	91.9587		TOTAL 3662.68	
			FMWI TOTAL	76.7389		TOTAL 929.869	

PROPELLANT SYSTEM ANALYSIS

PCP	488.869 PSIA	PCS	401.757 PSIA	FA	5806.622 LBS
WOP	4.326728 LB/SEC	WOS	12.84422 LB/SEC	FB	5781.793 LBS
WFP	.609953 LB/SEC	WFS	1.698763 LB/SEC	FSL	5794.207 LBS
WTP	4.936681 LB/SEC	WTS	14.54298 LB/SEC	WTOT	19.47966 LB/SEC
MRP	7.093540	MRS	7.560922	ISPSL	297.449 SEC.

TABLE XXV (cont.)

TEST NO. 2541-B01-0C-130 DUAL THROAT CALORIMETER CHAMBER JOB/R
OSNAME DTHTS COOLANT CIRCUIT HEATFLUX PROGRAM DATE 12-09-85
TEST MODE 1 PRIMARY COLDFLOW LEAKAGE MODEL TIME 08.16.11

DATA PERIOD FSI + 5.53 SECS. TO FSI + 6.03 SECS.

CIRCUIT NUMBER	CIRCUIT SURFACE AREA SQ.IN	CIRCUIT KW	COOLANT FLOW LB/SEC FLOW METER	COOLANT FLOW LB/SEC ORIFICE	DELTA TEMP DEG F	HEAT LOAD BTU/SEC	HEAT FLUX BTU/SQ.IN.SEC
PRIMARY							
1	1.675	.0934		1.6037	27.75	39.869	23.805
2	.762	.0551		.8499	21.68	14.411	18.913
3	1.613	.0844		1.3126	19.89	24.521	15.078
4	1.921	.0918		1.5869	14.62	19.422	3.549
5	2.226	.1452		2.6201	23.58	38.745	17.406
6	2.468	.1735		2.8601	21.62	35.067	14.209
7	2.736	.0891		1.3005	29.22	35.118	12.836
8	1.351	.0512		.9311	32.35	25.258	18.696
9A	2.378	.2096		1.0033	40.26	35.453	12.697
10	1.491	.0399	.7308	.7206	37.54	22.504	15.094
11	5.242	.0512	.9419	.9395	34.02	26.344	5.747
12	2.262	.0443	.7219	.7217	49.75	25.046	11.453
13	1.000	1.7024		27.854	39.53	1101.0	1101.96
SECONDARY							
SPACER	23.00	.0695		2.6475	129.7	343.26	14.886
1A	23.17	.0962		3.2402	69.80	226.16	9.761
1B	20.50	.0962		3.2402	112.7	169.12	8.252
2B	16.75	.0760		2.5731	102.2	120.49	7.671
2A	14.34	.0760		2.5731	52.27	134.50	9.380
3	11.74	.0582		1.7851	79.75	142.42	12.133
4	5.193	.1556		2.2140	55.18	75.478	14.149
5	4.532	.1125	2.3547	2.4480	30.87	75.580	16.677
6	4.034	.1081		2.0453	33.93	69.404	17.205
7	3.839	.0953		2.2436	33.68	75.548	19.679
8	3.908	.0767		1.7035	26.51	44.820	11.469
9	4.140	.0918		1.8816	27.14	51.076	12.319
10	4.337	.0601		2.0929	26.46	55.381	12.769
11	4.969	.0399		1.3991	33.90	47.434	9.546
12A	6.597	.0910	1.9021	1.8658	38.39	72.401	10.975
12B	6.956	.0910		1.8658	43.09	40.581	5.837
13B	7.317	.0779		1.6272	72.45	41.154	5.624
13A	9.140	.0779		1.6272	47.16	70.743	8.396
			TOTAL 63.4651		TOTAL 3201.07		
			FHWT TOTAL 69.1355		TOTAL 3305.18		

PROPELLANT SYSTEM ANALYSIS

PCP	470.158 PSIA	PCS	327.293 PSIA	FA	4862.174 LBS
WOP	5.453044 LB/SEC	WOS	9.940064 LB/SEC	FB	4840.115 LBS
WFP	1.143533 LB/SEC	WFS	1.428520 LB/SEC	FSL	4851.140 LBS
WTP	4.596578 LB/SEC	WTS	11.36919 LB/SEC	WTOT	15.96577 LB/SEC
MRP	3.019627	MRS	6.958680	ISPSL	303.847 SEC.

TEST NO. 2361-801-0C-151 DUAL THROAT CALORIMETER CHAMBER JOB73
DSNAME DIMIS COOLANT CIRCUIT HEATFLUX PROGRAM DATE 12-09-85
TEST MODE I PRIMARY COLDFLOW LEAKAGE MODEL TIME 08.21.50

DATA PERIOD FS1 + 5.52 SECS. TO FS1 + 6.02 SECS.

CIRCUIT NUMBER	CIRCUIT SURFACE AREA SQ.IN	CIRCUIT KW	COOLANT FLOW LB/SEC FLOW METER	COOLANT FLOW LB/SEC ORIFICE	DELTA TEMP DEG F	HEAT LOAD BTU/SEC	HEAT FLUX BTU/SQ.IN.SEC
PRIMARY							
1	1.675	.0934		1.0449	34.69	51.588	30.880
2	.762	.0551		.8492	25.74	18.600	24.410
3	1.613	.0844		1.3070	24.96	31.172	19.325
4	1.921	.0910		1.5648	20.20	26.514	13.802
5	2.926	.1432		2.6131	23.15	41.832	14.292
6	2.468	.1735		2.8540	18.76	31.843	12.902
7	2.736	.0891		1.3076	28.15	34.533	12.549
8	1.351	.0512		.9169	30.33	23.920	17.706
8A	2.378	.2096	1.1189	1.1199	37.91	37.973	15.211
10	1.491	.0399	.7262	.7207	32.53	19.713	13.221
11	5.242	.0516	.9416	.9396	28.92	22.607	5.038
12	2.262	.0443		.7181	31.50	18.529	8.191
13	1.000	1.7024		27.736	40.91	1134.7	1134.66
SECONDARY							
SPACER	23.66	.0695		2.6540	102.3	271.67	11.781
1A	23.17	.0902		3.2383	52.77	170.88	7.375
1B	20.59	.0952		3.2383	85.66	106.50	5.195
2B	10.75	.0706		2.5706	81.41	101.40	6.054
2A	14.34	.0705		2.5706	41.97	107.88	7.523
3	11.74	.0582		1.7842	64.20	114.55	9.759
4	5.193	.1536		2.2146	26.04	57.670	11.105
5	4.532	.1125	2.3556	2.4401	25.97	63.531	14.018
6	4.034	.1081		2.0403	28.10	57.339	14.214
7	3.839	.0953		2.2417	26.17	58.661	15.280
8	5.908	.0707		1.7014	19.93	35.910	6.077
9	4.140	.0918		1.8701	20.83	39.086	9.427
10	4.337	.0661		2.0920	19.81	41.443	9.556
11	4.969	.0519		1.3979	24.98	34.922	7.028
12A	9.597	.0910	1.9028	1.8866	29.21	55.110	6.354
12B	9.956	.0910		1.8856	47.22	33.970	4.864
13B	7.317	.0779		1.6231	54.74	30.051	4.189
13A	9.140	.0779		1.6231	35.85	58.194	5.367
			TOTAL 83.4050		TOTAL 2930.46		
			FMWJ TOTAL 69.3780		TOTAL 2725.91		

PROPELLANT SYSTEM ANALYSIS

PCP	511.471 PSIA	PCS	298.242 PSIA	FA	4583.545 LBS
WOP	4.418725 LB/SEC	WOS	7.003113 LB/SEC	FB	4567.805 LBS
WFP	.039122 LB/SEC	WFS	2.384573 LB/SEC	FSL	4575.671 LBS
WTP	5.057845 LB/SEC	WTS	9.387686 LB/SEC	WTOT	14.44555 LB/SEC
MRP	6.213744	MRS	2.936843	ISPSL	316.754 SEC.

TABLE XXV (cont.)

TEST NO. 2561-R01-0C-132 DUAL THROAT CALORIMETER CHAMBER 1087A
DSNAME DTHIS COOLANT CIRCUIT HEATFLUX PROGRAM DATE 12-09-85
TEST MODE 1 PRIMARY COLDFLOW LEAKAGE MODEL TIME 08.26.20

DATA PERIOD FSI + 5.51 SECS. TO FSI + 6.01 SECS.

CIRCUIT NUMBER	CIRCUIT SURFACE AREA SQ.IN	CIRCUIT KW	COOLANT FLOW LB/SEC FLOW METER	COOLANT FLOW LB/SEC ORIFICE	DELTA TEMP DEG F	HEAT LOAD BTU/SEC	HEAT FLUX BTU/SQ.IN.SEC
PRIMARY							
1	1.675	.0934		1.5129	24.41	52.510	19.[illegible]
2	.762	.0551		.7738	19.16	11.706	15.[illegible]
3	1.613	.0844		1.1899	17.29	19.210	11.91[illegible]
4	1.921	.0918		1.4393	13.60	14.429	7.511
5	2.226	.1432		2.3854	20.25	30.717	13.799
6	2.468	.1735		2.5944	17.97	26.268	11.[illegible]
7	2.736	.0891		1.1774	25.88	24.284	10.338
8	1.351	.0512		.8478	28.23	20.223	14.969
9A	2.378	.2096	1.0030	.9836	34.48	29.863	11.257
10	1.491	.0399	.6557	.6651	31.79	17.435	11.[illegible]
11	3.242	.0512	.8503	.8444	27.57	19.048	4.882
12	2.262	.0445		.6499	30.93	16.282	7.198
13	1.000	1.7024		25.154	36.03	906.19	9[illegible].186
SECONDARY							
SPACER	23.06	.0695		2.4103	108.[illegible]	261.09	11.348
1A	23.17	.0962		2.9489	54.77	161.52	6.971
1B	29.50	.0962		2.9489	89.06	161.10	4.952
2B	16.75	.0700		2.3411	84.04	95.452	5.[illegible]
2A	14.34	.0700		2.3411	43.27	101.30	7.[illegible]
3	11.74	.0582		1.6225	65.82	100.79	9.[illegible]
4	5.193	.1530		2.0170	26.89	54.236	10.[illegible]
5	4.532	.1125	2.1476	2.2221	27.85	61.886	13.655
6	4.034	.1081		1.8518	28.26	52.337	12.974
7	3.839	.0953		2.0420	26.56	54.237	14.128
8	3.908	.0707		1.5476	20.60	31.874	8.156
9	4.146	.0618		1.7071	20.34	34.724	8.375
10	4.337	.0661		1.9026	20.05	38.150	8.796
11	4.969	.0399		1.2729	23.21	29.539	5.945
12A	6.597	.0910	1.7319	1.7184	28.72	49.359	7.482
12B	2.956	.0910		1.7184	45.47	28.770	4.136
13B	7.317	.0779		1.4759	52.14	27.949	3.820
13A	9.140	.0779		1.4759	33.21	49.008	5.362
			TOTAL 75.7883		TOTAL 2512.15		
			FMM1 TOTAL 63.1747		TOTAL 2367.05		

PROPELLANT SYSTEM ANALYSIS

PCP	414.221 PSIA	PCS	276.769 PSIA	FA	4075.712 LBS
WOP	2.[illegible]89829 LB/SEC	WOS	0.052303 LB/SEC	FR	4057.510 LBS
WFP	.963848 LB/SEC	WFS	2.253344 LB/SEC	FSI	4060.013 LBS
WTP	3.853076 LB/SEC	WTS	8.905647 LB/SEC	WTOT	12.75932 LB/SEC
MRP	2.998221	MRS	2.952102	ISPSL	318.717 SEC.

TEST NO. 2381-801-0C-144 DUAL THROAT CALORIMETER CHAMBER J0878
DSNAME OTHIS COOLANT CIRCUIT HEATFLUX PROGRAM DATE 12-09-85
TEST MODE 1 PRIMARY COLDFLOW LEAKAGE MODEL TIME 08.32.11

DATA PERIOD FSI + 5.51 SECS. TO FSI + 6.01 SECS.

CIRCUIT NUMBER	CIRCUIT SURFACE AREA SQ.IN	CIRCUIT KW	COOLANT FLOW LB/SEC FLOW METER	COOLANT FLOW LB/SEC ORIFICE	DELTA TEMP DEG F	HEAT LOAD BTU/SEC	HEAT FLUX BTU/SQ.IN.SEC
PRIMARY							
1	1.675	.0934		1.0902	20.30	31.221	18.639
2	.762	.0551		.9039	14.28	10.595	13.904
3	1.013	.0844		1.3521	14.01	17.940	11.122
4	1.921	.0918		1.0174	10.57	13.362	6.956
5	2.220	.1432		2.0638	15.01	27.312	12.270
6	2.468	.1735		2.9068	11.87	19.781	8.015
7	2.736	.0891		1.3232	13.45	15.212	5.925
8	1.351	.0512		.9455	15.40	11.691	8.802
9A	2.578	.2096	1.1359	1.1353	19.21	18.789	7.498
10	1.491	.0399	.7524	.7519	18.98	11.191	7.506
11	3.242	.0512	.9541	.9546	19.31	15.338	2.193
12	2.262	.0443		.7406	20.58	10.871	7.458
13	1.000	1.7024		28.180	27.52	775.64	775.638
SECONDARY							
SPACER	23.00	.0695		2.0650	3.67	9.775	.424
1A	23.17	.0902		3.2312	53.50	172.88	7.461
1B	20.50	.0902		3.2312	73.58	64.860	3.164
2B	10.75	.0700		2.5051	60.98	70.420	4.204
2A	14.34	.0700		2.5051	53.53	86.008	5.998
3	11.74	.0582		1.8017	54.05	97.387	8.297
4	5.193	.1536		2.2058	21.21	46.779	9.008
5	4.532	.1125	2.3719	2.4519	18.36	45.021	9.934
6	4.034	.1081		2.0911	18.00	37.650	9.328
7	3.839	.0953		2.2575	16.41	37.046	9.650
8	3.908	.0707		1.7067	12.60	21.509	5.504
9	4.140	.0918		1.9171	13.95	26.745	6.461
10	4.337	.0801		2.0509	13.27	27.220	6.276
11	4.969	.0399		1.3960	16.36	22.842	4.597
12A	6.597	.0910	1.9038	1.9270	19.24	37.084	5.621
12B	6.950	.0910		1.9270	31.95	24.485	3.520
13B	7.317	.0779		1.6604	34.67	20.568	2.810
13A	9.140	.0779		1.6604	22.27	30.978	4.046

TOTAL 84.4888 TOTAL 1871.40

FNWI TOTAL 67.6758 TOTAL 1730.91

PROPELLANT SYSTEM ANALYSIS

PCP	379.354 PSIA	PCS	178.986 PSIA	FA	2825.642 LBS
WOP	2.451681 LB/SEC	WOS	4.129547 LB/SEC	FB	2814.152 LBS
WFP	1.017771 LB/SEC	WFS	1.371733 LB/SEC	FSL	2819.847 LBS
WTP	3.469452 LB/SEC	WTS	5.501281 LB/SEC	WTOT	9.370733 LB/SEC
MRP	2.[illegible]	MRS	3.010459	ISPSL	300.926 SEC.

TABLE XXV (cont.)

TEST NO. 2361-R01-0C-145
DSNAME DTHIS
TEST MODE I

DUAL THROAT CALORIMETER CHAMBER
COOLANT CIRCUIT HEATFLUX PROGRAM
PRIMARY COLDFLOW LEAKAGE MODEL

DATE 12-09-85
TIME 08.57.45

DATA PERIOD FSI + 5.53 SECS. TO FSI + 6.03 SECS.

CIRCUIT NUMBER	CIRCUIT SURFACE AREA SQ.IN	CIRCUIT KW	COOLANT FLOW LB/SEC FLOW METER	COOLANT FLOW LB/SEC ORIFICE	DELTA TEMP DEG F	HEAT LOAD BTU/SEC	HEAT FLUX BTU/SQ.IN.SEC
PRIMARY							
1	1.675	.0934		1.0926	23.96	35.813	21.381
2	.762	.0551		.9044	20.79	15.365	20.164
3	1.613	.0844		1.3507	16.05	20.195	12.520
4	1.921	.0918		1.0120	11.89	13.032	7.096
5	2.226	.1432		2.0626	18.61	30.717	13.799
6	2.468	.1735		2.9029	10.56	20.227	11.967
7	2.736	.0991		1.5114	16.98	14.936	7.288
8	1.351	.0512		.9435	20.72	15.566	11.537
9A	2.378	.2096	1.1377	1.1201	29.92	29.081	15.055
10	1.491	.0399	.7519	.7506	26.39	15.796	10.594
11	2.242	.0512	.9513	.9532	29.66	23.081	5.002
12	2.262	.0443		.7406	39.61	25.101	11.123
13	1.000	1.7024		28.045	31.77	891.11	891.114
SECONDARY							
SPACER	23.06	.0695		2.6588	11.88	31.584	1.370
1A	23.17	.0962		3.2265	72.72	234.62	10.126
1B	20.50	.0962		3.2265	102.2	95.058	4.637
2B	10.75	.0766		2.5627	93.20	104.91	9.760
2A	14.34	.0766		2.5627	52.61	134.82	9.402
3	11.74	.0582		1.7997	78.99	142.16	12.111
4	5.193	.1536		2.1979	30.84	67.795	13.055
5	4.532	.1125	2.3692	2.4489	29.56	72.402	15.976
6	4.034	.1081		2.1093	27.79	58.568	14.469
7	5.839	.0955		2.2553	21.90	49.399	12.[illegible]
8	5.908	.0707		1.7055	15.40	26.266	3.721
9	4.140	.0918		1.9156	21.27	40.747	9.828
10	4.337	.0661		2.0491	20.49	41.977	9.679
11	4.969	.0399		1.3941	21.65	30.184	6.074
12A	6.597	.0910	1.9011	1.9061	27.44	52.315	7.929
12B	9.956	.0910		1.9061	43.63	29.719	2.272
13B	7.317	.0779		1.6569	45.87	24.295	3.320
13A	9.140	.0779		1.6569	31.21	51.711	5.658
			TOTAL 84.2200		TOTAL 2449.73		
			FMWI TOTAL 67.5226		TOTAL 2322.61		

PROPELLANT SYSTEM ANALYSIS

PCP	396.852 PSIA	PCS	287.830 PSIA	FA	5916.780 LBS
WOP	2.316631 LB/SEC	WOS	7.120542 LB/SEC	FR	5890.879 LBS
WFP	1.018172 LB/SEC	WFS	2.382840 LB/SEC	FSL	5904.830 LBS
WTP	3.334803 LB/SEC	WTS	9.503387 LB/SEC	WTOT	13.33819 LB/SEC
MRP	2.700302	MRS	2.988250	ISPSL	292.756 SEC.

TEST NO. 2301-R01-0C-106 DUAL TERMAT CALORIMETER CHAMBER J087H
DSNAME DTHIS COOLANT CIRCUIT HEATFLUX PROGRAM DATE 12-09-85
TEST MODE I PRIMARY COLDFLOW LEAKAGE MODEL TIME 09.30.15

DATA PERIOD FSI + 5.51 SECS. TO FSI + 6.01 SECS.

CIRCUIT NUMBER	CIRCUIT SURFACE AREA SQ.IN	CIRCUIT KW	COOLANT FLOW LB/SEC FLOW METER	COOLANT FLOW LB/SEC ORIFICE	DELTA TEMP DEG F	HEAT LOAD BTU/SEC	HEAT FLUX BTU/SQ.IN.SEC
PRIMARY							
1	1.675	.0954		1.6931	22.73	33.523	20.014
2	.762	.0551		.9081	18.65	13.308	17.464
3	1.613	.0844		1.5481	15.60	19.483	12.079
4	1.921	.0918		1.0121	10.09	10.479	5.455
5	2.220	.1432		2.0689	18.16	28.758	12.919
6	2.468	.1735		2.0999	15.98	23.545	9.540
7	2.736	.0891		1.3199	18.09	21.423	7.830
8	1.351	.0512		.9414	21.81	16.407	12.144
8A	2.378	.2096	1.1539	1.1188	29.26	28.110	11.929
10	1.491	.0399	.7551	.7526	27.84	16.748	11.233
11	3.242	.0512	.9505	.9514	31.03	24.737	5.469
12	2.262	.0413		.7377	42.51	27.017	11.944
13	1.000	1.7024		28.020	32.35	906.70	906.702
SECONDARY							
SPACER	23.06	.0695		2.6578	8.91	23.674	1.027
1A	23.17	.0902		3.2306	203.7	659.40	28.459
1B	20.50	.0902		3.2306	111.8		
2B	10.75	.0706		2.5634	102.0	118.18	7.056
2A	10.34	.0700		2.5634	55.92	143.36	9.907
3	11.74	.0582		1.8001	85.98	154.77	13.185
4	5.193	.1536		2.1964	34.27	75.273	14.495
5	4.532	.1125	2.3702	2.4485	29.81	72.981	16.104
6	4.034	.1061		2.0730	27.85	57.733	14.312
7	5.839	.0953		2.2562	24.37	54.986	14.323
8	5.908	.0737		1.7064	15.70	26.786	6.854
9	4.140	.0918		1.9153	20.37	39.019	9.411
10	4.337	.0661		2.0480	19.25	39.421	9.090
11	4.969	.0399		1.3937	22.83	31.820	6.404
12A	5.597	.0910	1.9089	1.9226	26.99	51.897	7.867
12B	9.956	.0910		1.9226	44.38	33.419	4.804
13B	7.317	.0779		1.6567	48.82	27.662	3.781
13A	9.140	.0779		1.6567	32.12	53.221	5.823
			TOTAL 84.2305			TOTAL 2530.42	
			FMWI TOTAL 87.5083			TOTAL 2324.42	

PROPELLANT SYSTEM ANALYSIS

PCP	495.013 PSIA	PCS	525.667 PSIA	FA	4278.288 LBS
WOP	2.805721 LB/SEC	WOS	7.413460 LB/SEC	FB	4250.100 LBS
WFP	1.009688 LB/SEC	WFS	2.624184 LB/SEC	FSI	4267.226 LBS
WTP	3.815408 LB/SEC	WTS	10.037644 LB/SEC	WTOT	13.85395 LB/SEC
MRP	2.778800	MRS	2.825053	ISPSL	308.055 SEC.

TEST NO. 2381-R01-CC-147
DSNAME DTHIS
TEST MODE I

DUAL THROAT CALORIMETER CHAMBER JOB/R
COOLANT CIRCUIT HEATFLUX PROGRAM DATE 12-09-85
PRIMARY COLDFLOW LEAKAGE MODEL TIME 09.37.25

DATA PERIOD FSI + 5.51 SECS. TO FSI + 6.01 SECS.

CIRCUIT NUMBER	CIRCUIT SURFACE AREA SQ.IN	CIRCUIT KW	COOLANT FLOW LB/SEC FLOW METER	COOLANT FLOW LB/SEC ORIFICE	DELTA TEMP DEG F	HEAT LOAD BTU/SEC	HEAT FLUX BTU/SQ.IN.SEC
PRIMARY							
1	1.675	.0934		1.7019	21.21	31.391	18.741
2	.762	.0551		.9089	19.01	13.075	14.209
3	1.613	.0844		1.3564	14.38	18.040	11.184
4	1.921	.0918		1.6164	11.77	13.548	7.052
5	2.226	.1432		2.6693	18.19	29.963	13.461
6	2.466	.1735		2.9087	15.81	24.431	9.899
7	2.736	.0891		1.3296	17.61	21.090	7.708
8	1.351	.0512		.9364	23.29	17.938	13.278
9A	2.378	.2096	1.1706	1.1498	31.06	31.227	13.400
10	1.491	.0399	.7521	.7525	29.45	18.198	12.205
11	3.242	.0512	.9560	.9558	31.39	25.468	3.992
12	2.262	.0443		.7417	41.64	26.765	11.832
13	1.000	1.7024		28.145	32.49	914.41	914.414
SECONDARY							
SPACER	23.06	.0695		2.0664	7.25	19.334	.838
1A	23.17	.0962					
1B	20.50	.0962			113.6		
2B	10.75	.0766		2.5726	103.9	122.41	7.308
2A	14.34	.0766		2.5726	56.34	144.94	10.107
3	11.74	.0582		1.8065	88.05	159.05	13.550
4	5.193	.1536		2.2029	33.16	73.044	14.066
5	4.532	.1125	2.3776	2.4560	29.39	72.177	15.926
6	4.034	.1081		2.0796	27.46	57.105	14.156
7	5.839	.0953		2.2630	23.85	53.983	11.962
8	5.908	.0707		1.7127	18.46	31.615	5.090
9	4.146	.0918		1.9211	19.61	37.665	9.085
10	4.337	.0661		2.0557	18.66	38.352	8.843
11	4.969	.0399		1.3982	21.59	30.184	6.074
12A	8.597	.0910	1.9165	1.9244	26.60	51.190	7.760
12B	8.956	.0910		1.9244	45.21	35.622	5.150
13B	7.317	.0779		1.6649	49.22	29.080	5.974
13A	9.140	.0779		1.6649	31.76	52.871	5.785
		TOTAL 78.0582				TOTAL 2195.17	
		FMWI TOTAL 67.7283				TOTAL 2540.31	

PROPELLANT SYSTEM ANALYSIS

PCP	360.784 PSIA	PCS	314.931 PSIA	FA	4094.105 LBS
WOP	2.829247 LB/SEC	WOS	7.466965 LB/SEC	FR	4074.502 LBS
WFP	.947157 LB/SEC	WFS	2.198952 LB/SEC	FSL	4084.302 LBS
WTP	3.976383 LB/SEC	WTS	9.665918 LB/SEC	WTOT	13.34230 LB/SEC
MRP	5.339774	MRS	3.395693	ISPSL	306.117 SEC.

TEST NO. 2361-R01-0C-148 DUAL THROAT CALORIMETER CHAMBER J0878
DSNAME DTHIS COOLANT CIRCUIT HEATFLUX PROGRAM DATE 12-09-85
TEST MODE I PRIMARY COLDFLOW LEAKAGE MODEL TIME 09.43.40

DATA PERIOD FS1 + 5.51 SECS. TO FS1 + 6.01 SECS.

CIRCUIT NUMBER	CIRCUIT SURFACE AREA SQ.IN	CIRCUIT KW	COOLANT FLOW LB/SEC FLOW METER	COOLANT FLOW LB/SEC ORIFICE	DELTA TEMP DEG F	HEAT LOAD BTU/SEC	HEAT FLUX BTU/SQ.IN.SEC
PRIMARY							
1	1.675	.0934		2.0535	24.12	44.140	26.352
2	.762	.0551		1.1043	15.09	12.745	16.725
3	1.613	.0844		1.8367	17.13	26.354	16.339
4	1.921	.0918		1.9685	13.09	19.456	10.128
5	2.226	.1432		3.2415	20.28	44.299	19.901
6	2.468	.1735		3.5330	17.75	37.863	15.342
7	2.736	.0891		1.8258	24.14	50.548	13.358
8	1.351	.0512		1.1586	26.29	25.915	19.182
9A	2.378	.2096	1.4569	1.5163	29.59	39.253	15.112
10	1.491	.0399	.9060	.9149	29.91	22.789	15.285
11	3.242	.0512	1.1675	1.1691	27.31	26.669	8.403
12	2.262	.0413		.8915	30.49	22.478	9.957
13	1.009	1.7024		34.375	36.00	1239.4	1239.41
SECONDARY							
SPACER	23.00	.0695		3.2349	105.6	341.75	14.820
1A	23.17	.0962		3.9575	40.38	159.82	6.898
1B	20.50	.0962		3.9575	97.00	224.07	10.930
2B	16.75	.0766		3.1387	89.91	140.25	8.373
2A	14.34	.0766		3.1387	45.22	141.94	9.898
3	11.74	.0582		2.2077	68.78	151.85	12.937
4	5.193	.1536		2.6547	28.99	76.953	14.819
5	4.532	.1125	2.8851	2.9415	26.63	78.331	17.284
6	4.034	.1081		2.4647	28.34	69.848	17.315
7	3.839	.0953		2.7136	28.80	78.140	20.354
8	3.908	.0707		2.0583	23.33	46.025	12.289
9	4.146	.0918		2.2997	20.24	46.552	11.228
10	4.337	.0661		2.5153	18.49	46.509	10.724
11	4.969	.0399		1.7053	26.32	44.880	9.032
12A	6.597	.0910	2.2856	2.3259	27.09	63.007	9.551
12B	6.956	.0910		2.3259	49.72	52.639	7.567
13B	7.317	.0779		1.9968	55.59	39.872	5.449
13A	9.140	.0779		1.9988	35.64	71.236	7.794
			TOTAL 102.826		TOTAL 3473.59		
			FMWI TOTAL 84.9344		TOTAL 3279.31		

PROPELLANT SYSTEM ANALYSIS

PCP	698.251 PSIA	PCS	437.426 PSIA	FA	6630.265 LBS
WOP	4.781075 LB/SEC	WOS	11.19616 LB/SEC	FR	6610.446 LBS
WFP	1.359192 LB/SEC	WFS	3.499598 LB/SEC	FSL	6623.359 LBS
WTP	6.311268 LB/SEC	WTS	14.69555 LB/SEC	WTOT	21.00682 LB/SEC
MRP	3.124493	MRS	3.199451	ISPSL	315.296 SEC.

ORIGINAL PAGE IS
OF POOR QUALITY

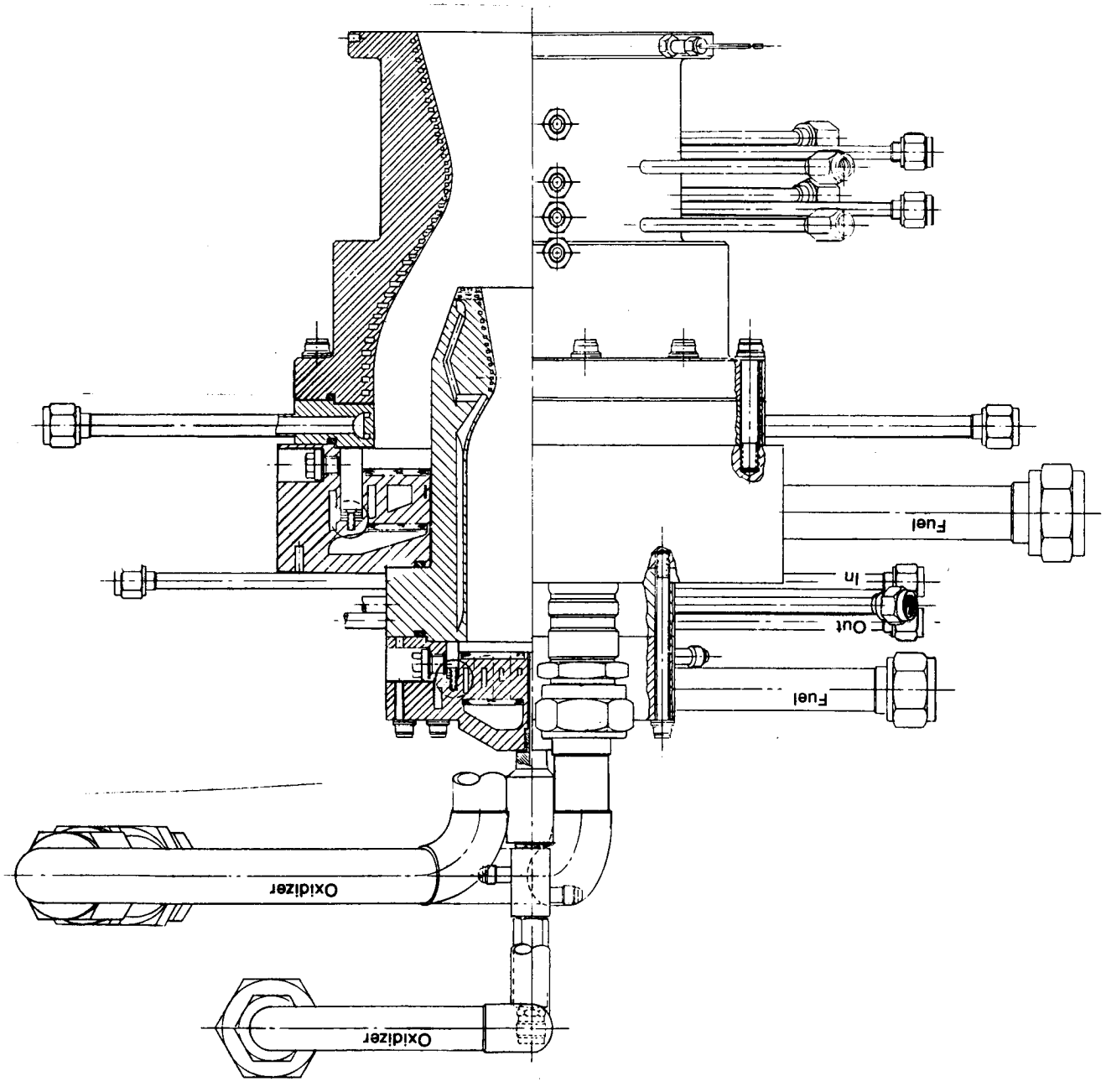

Figure 14 . Dual Throat Thruster Assembly

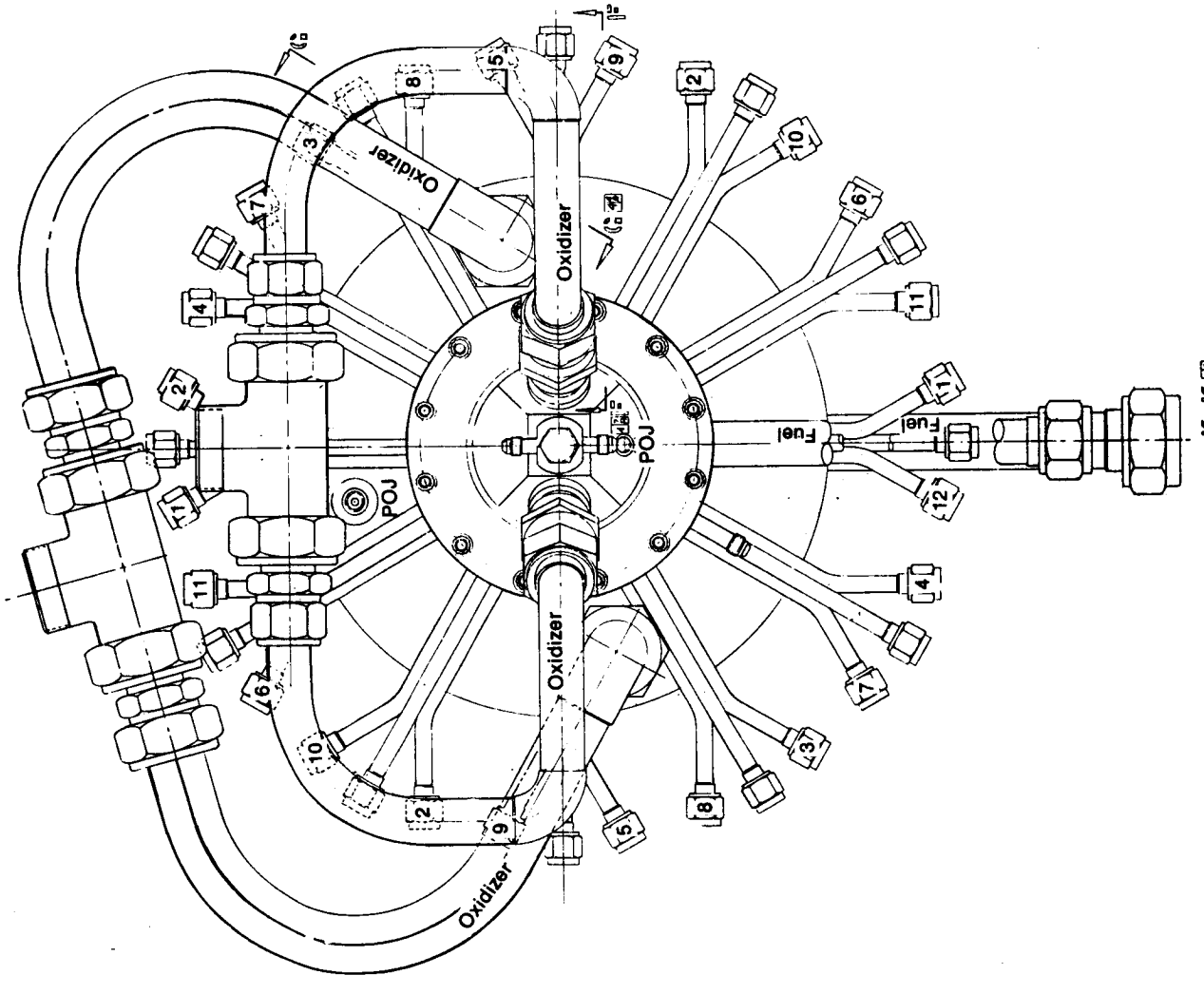

Figure 15. Dual Throat Thruster Assembly

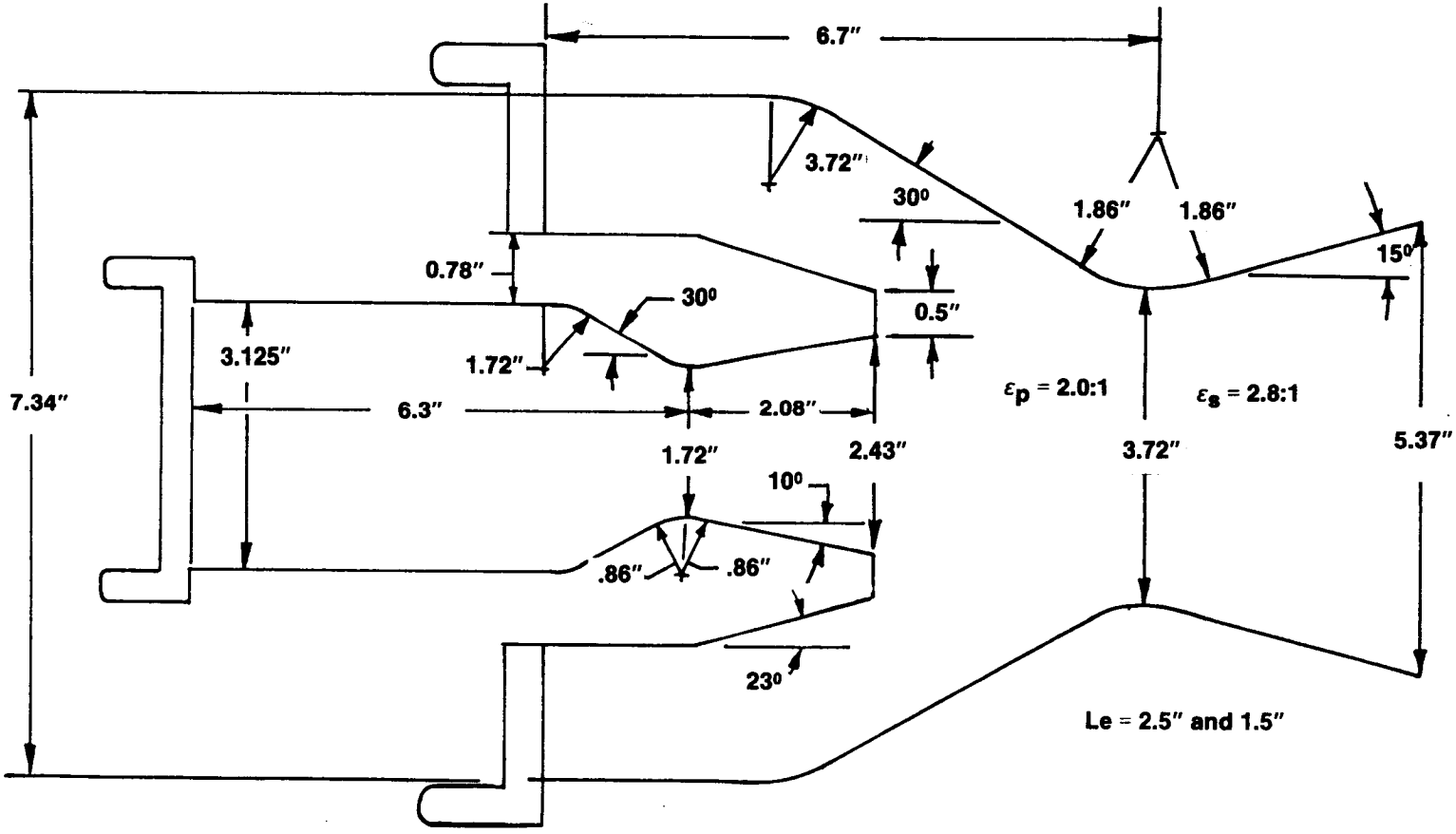

Figure 16. Dual-Throat Thruster Test Unit Geometry

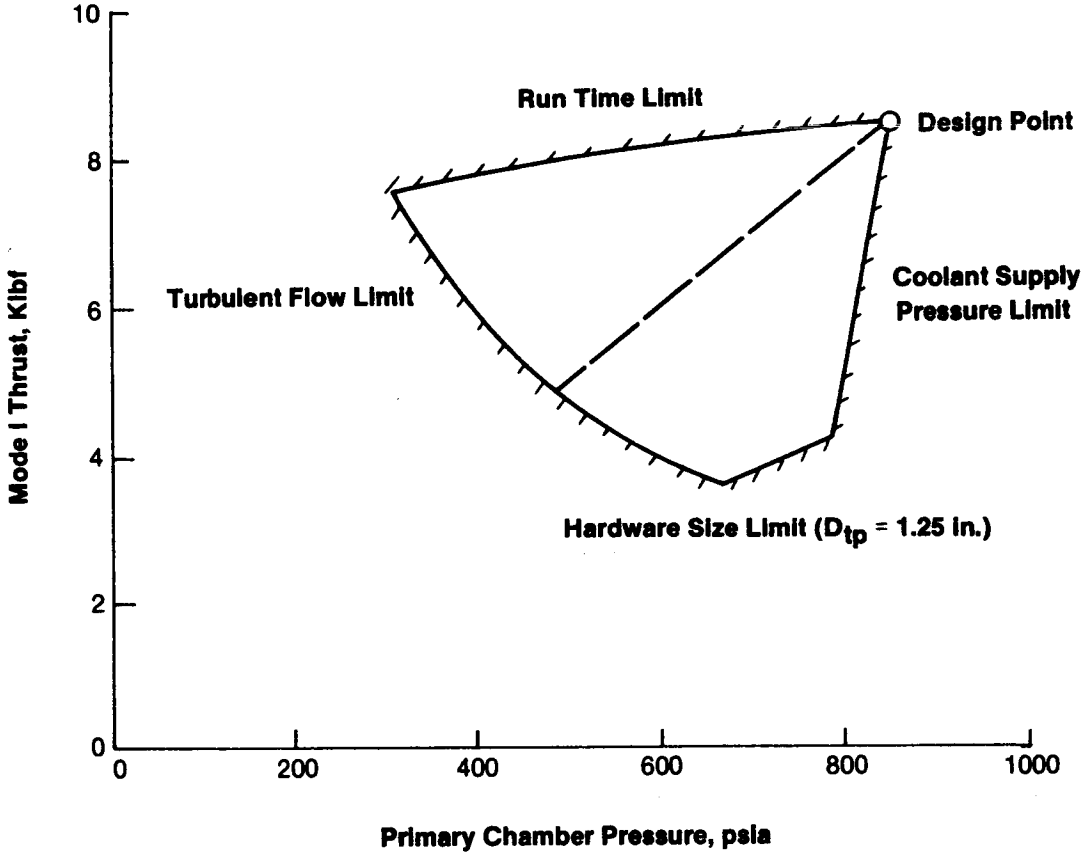

Figure 17. Design Point Selection

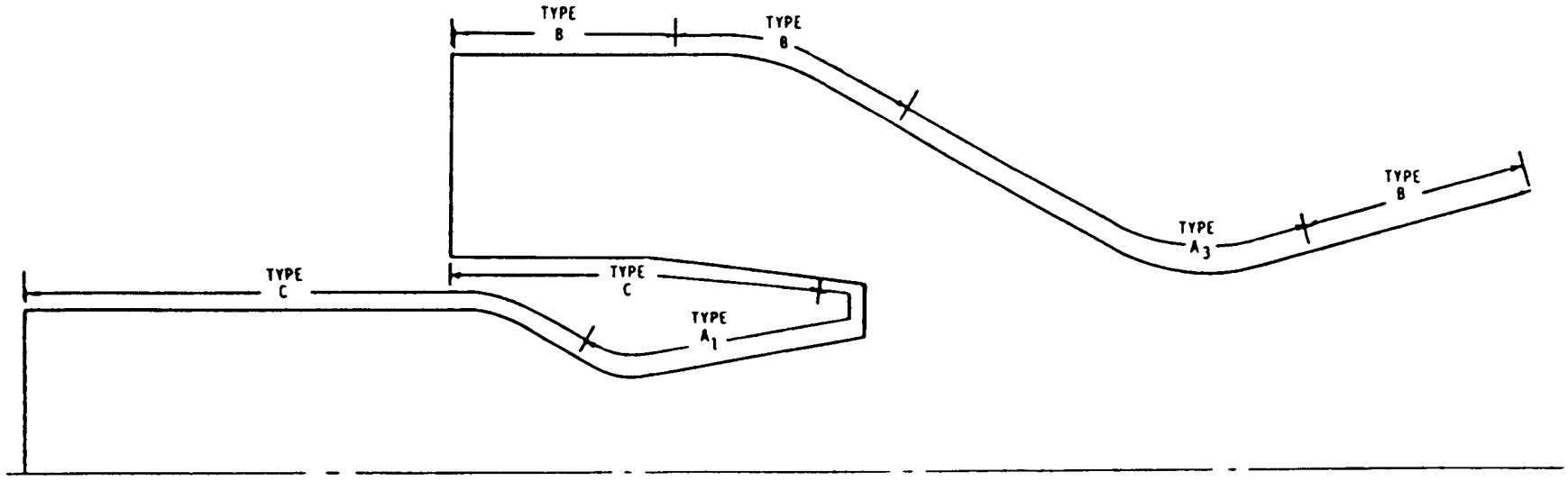

TYPE A CALORIMETER CIRCUITS

A_1 ONE BULK TEMPERATURE RISE MEASUREMENT PER FLOW CIRCUIT

A_3 THREE BULK TEMPERATURE RISE MEASUREMENTS IN SERIES PER FLOW CIRCUIT

TYPE B CIRCUMFERENTIAL COOLING CIRCUITS

TYPE C AXIAL COOLING CIRCUITS

Figure 18. The Dual-Throat Calorimetric Thruster Cooling Circuit Configuration Matches Channel Design to Resolution Desired

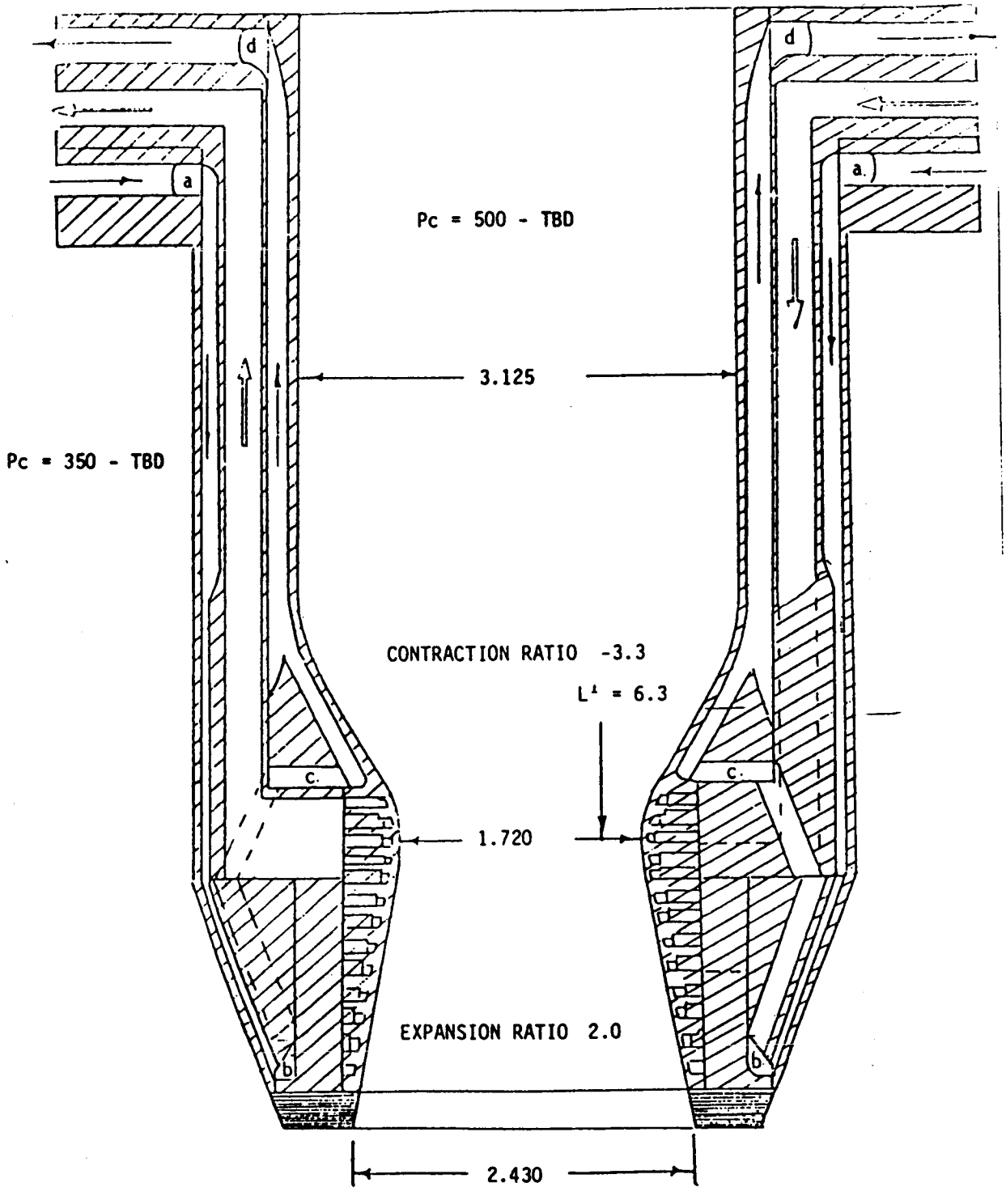

Figure 19. Primary Chamber Coolant Circuitry

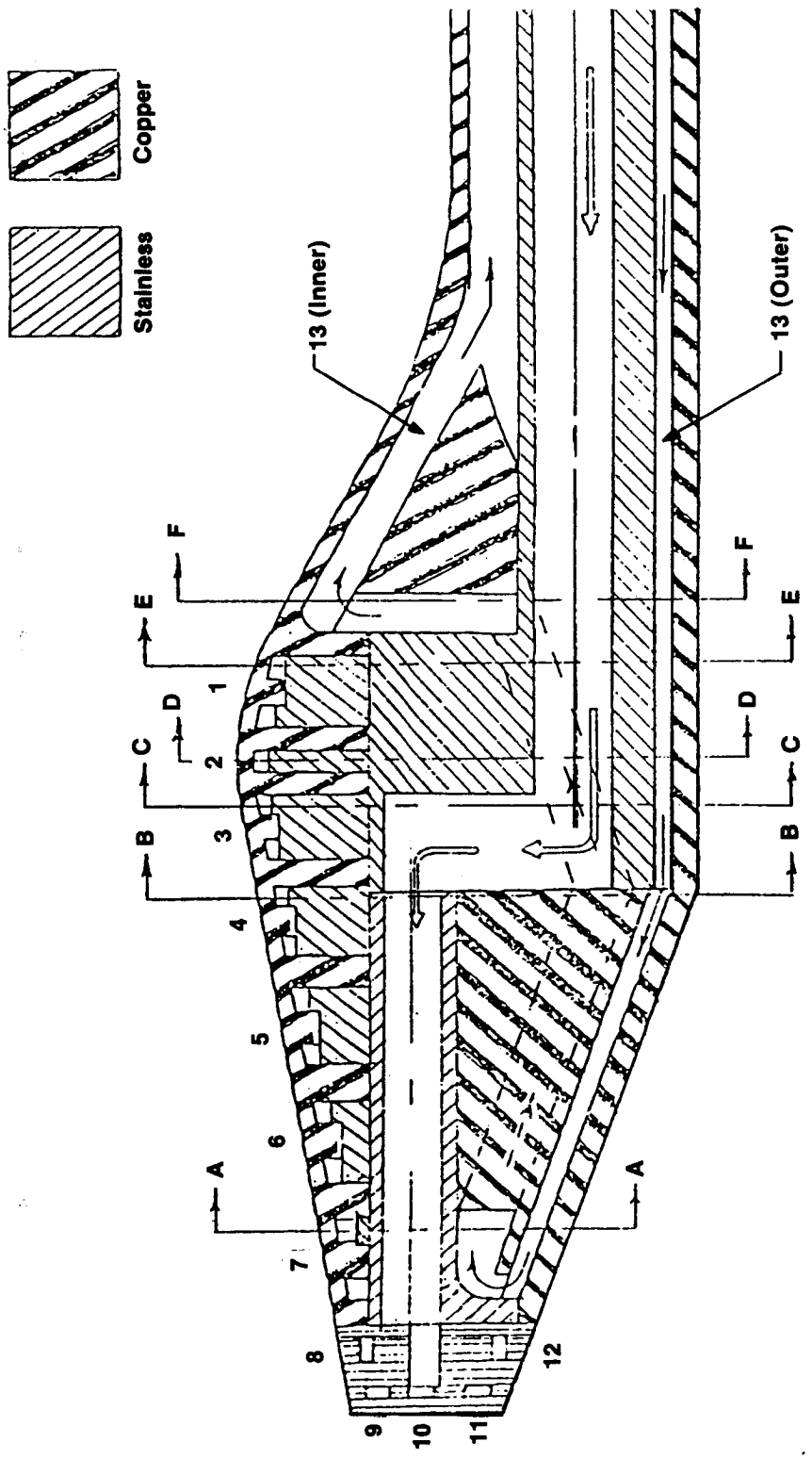

Figure 20. Numbered Primary Chamber Circuits

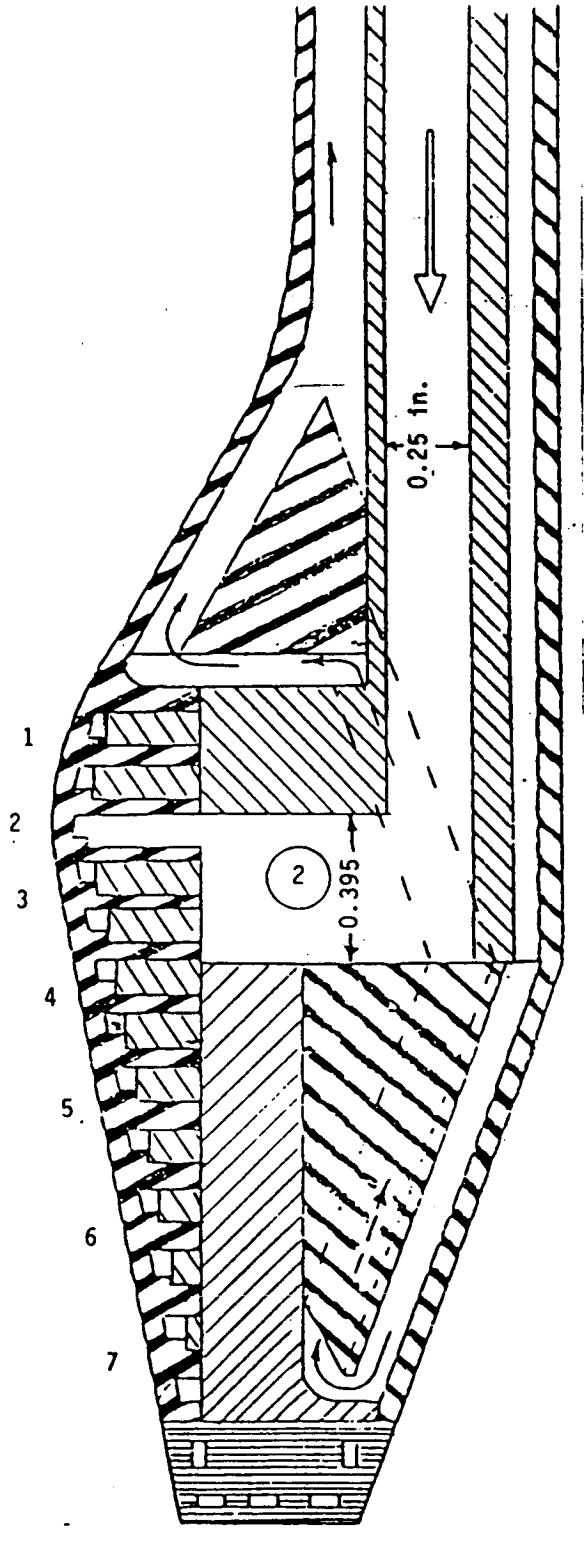

Figure 21. Cross Section of Circuit No. 2

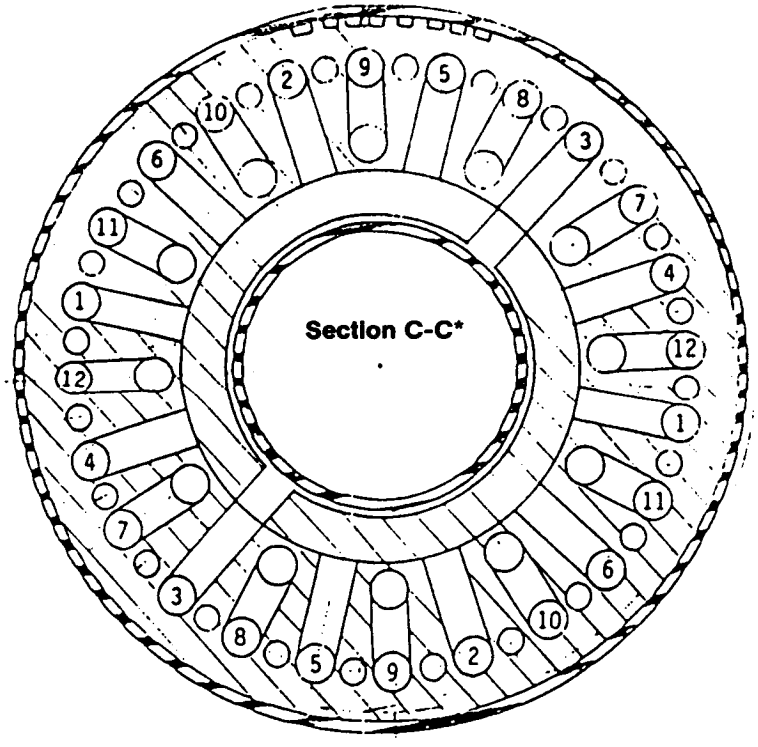

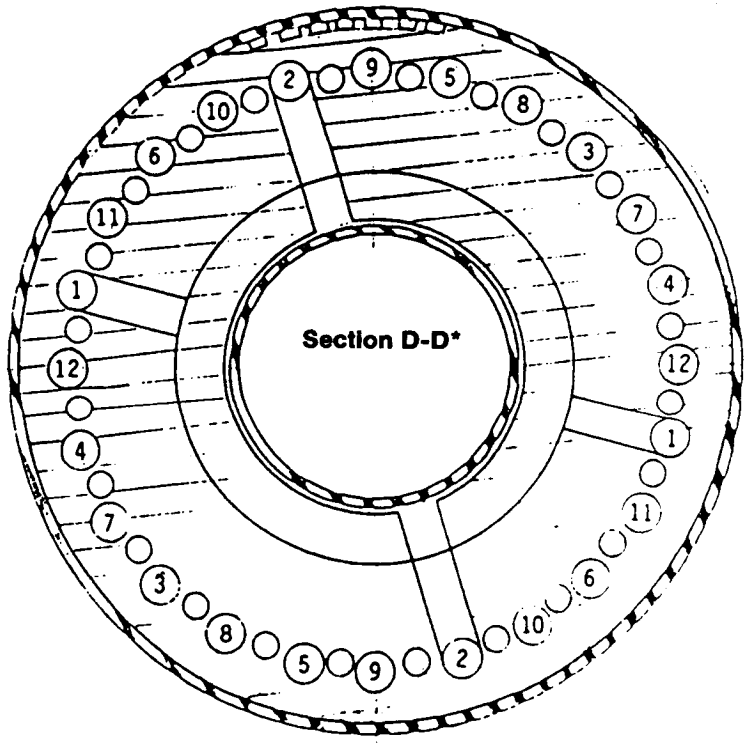

* See Fig. 20

Figure 22. Cross Sections of Circuits No. 2 and No. 3 Showing Inlet and Outlet Feed Channels

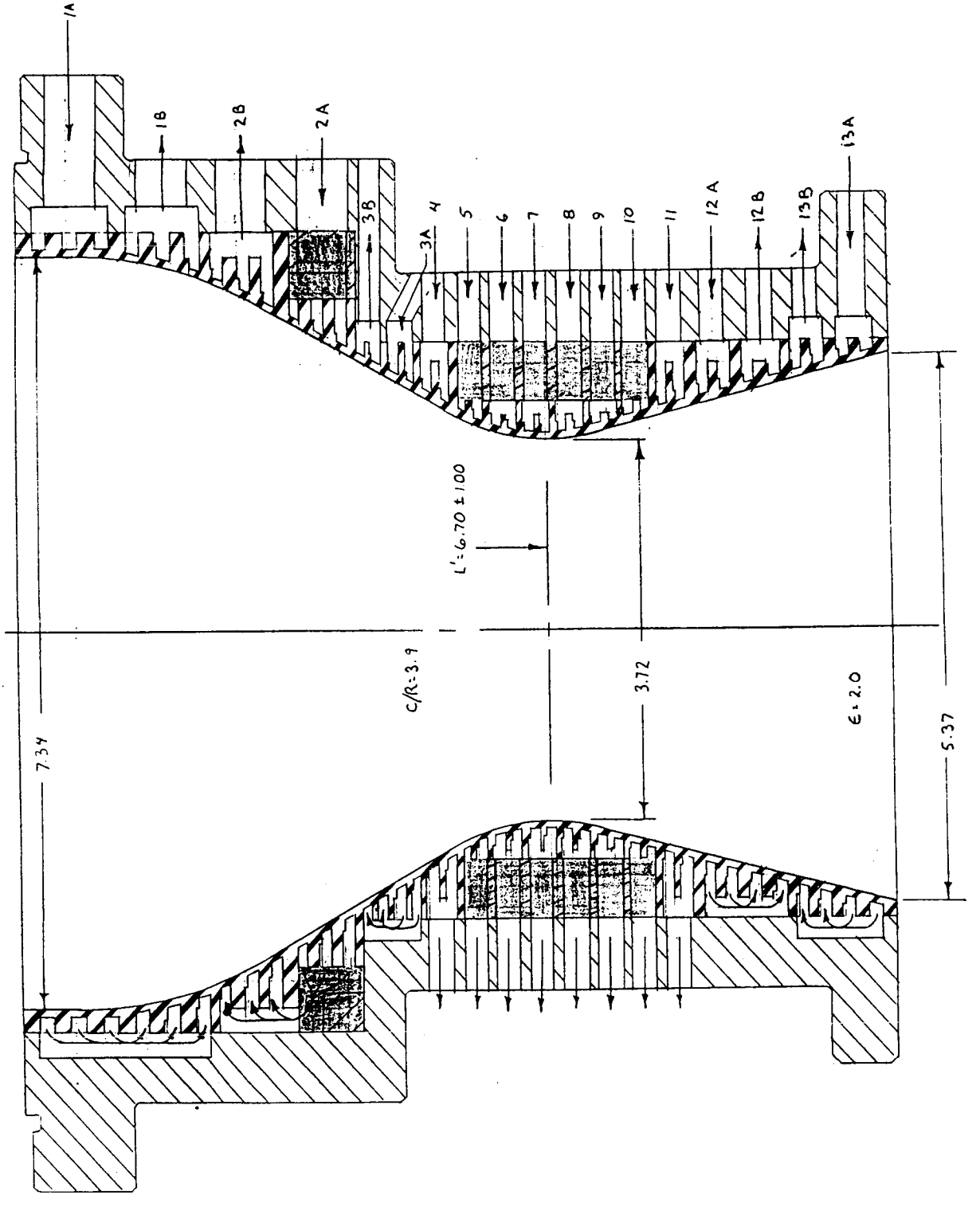

Figure 23. Secondary Chamber Coolant Circuitry

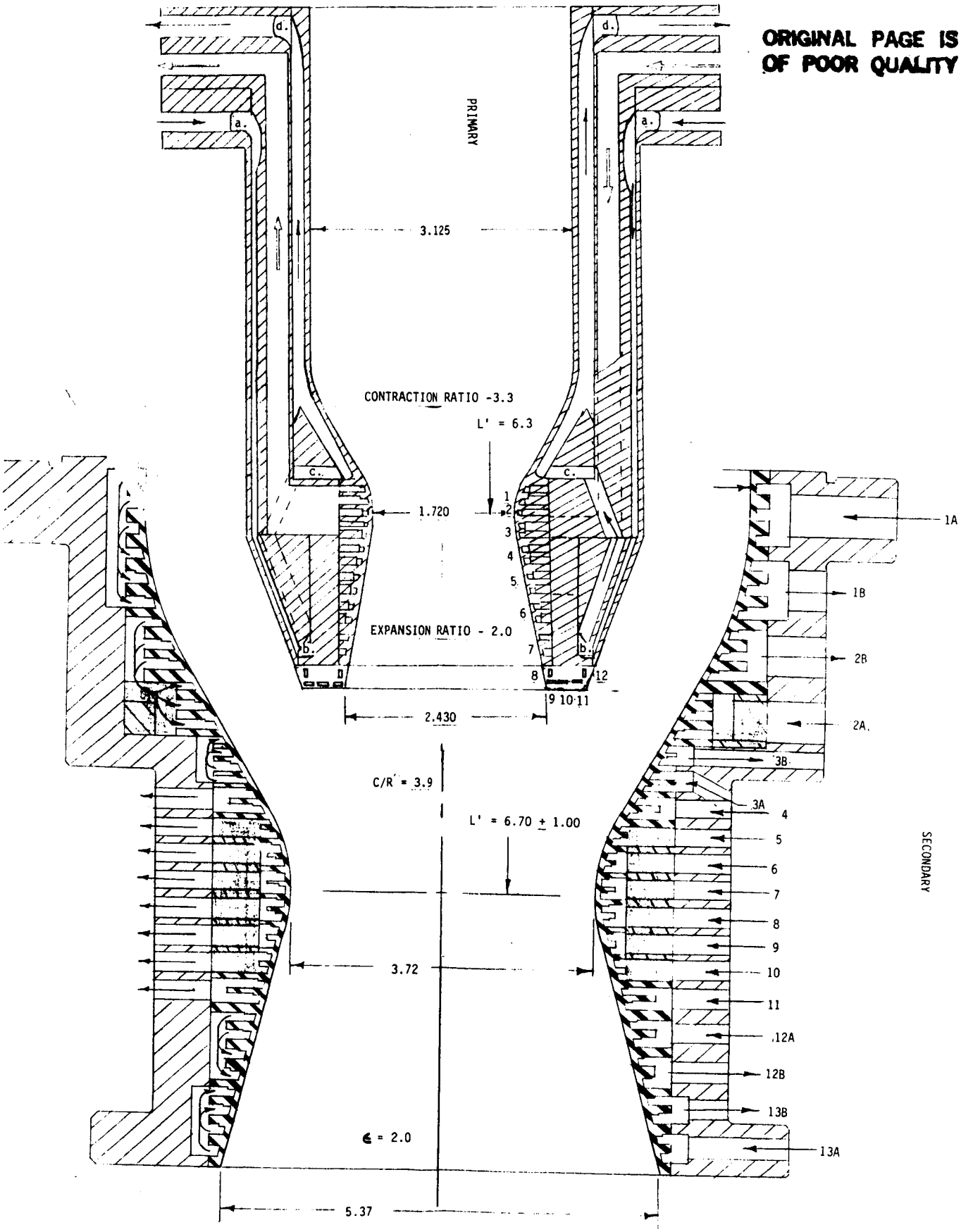

Figure 23A. Relative Positions of Calorimeter Circuits in Test Hardware

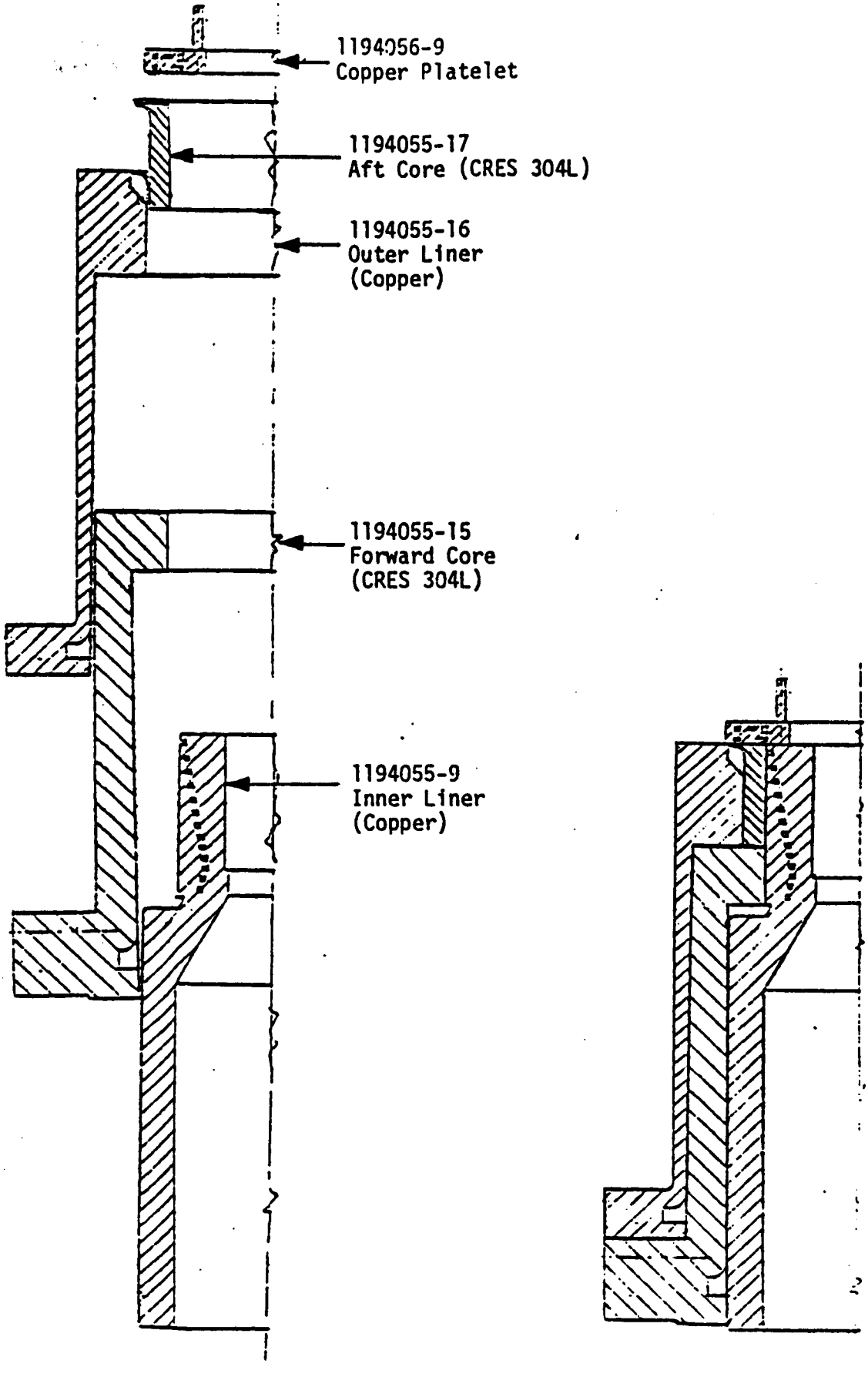

Figure 24. Primary Chamber Projected View and Assembly

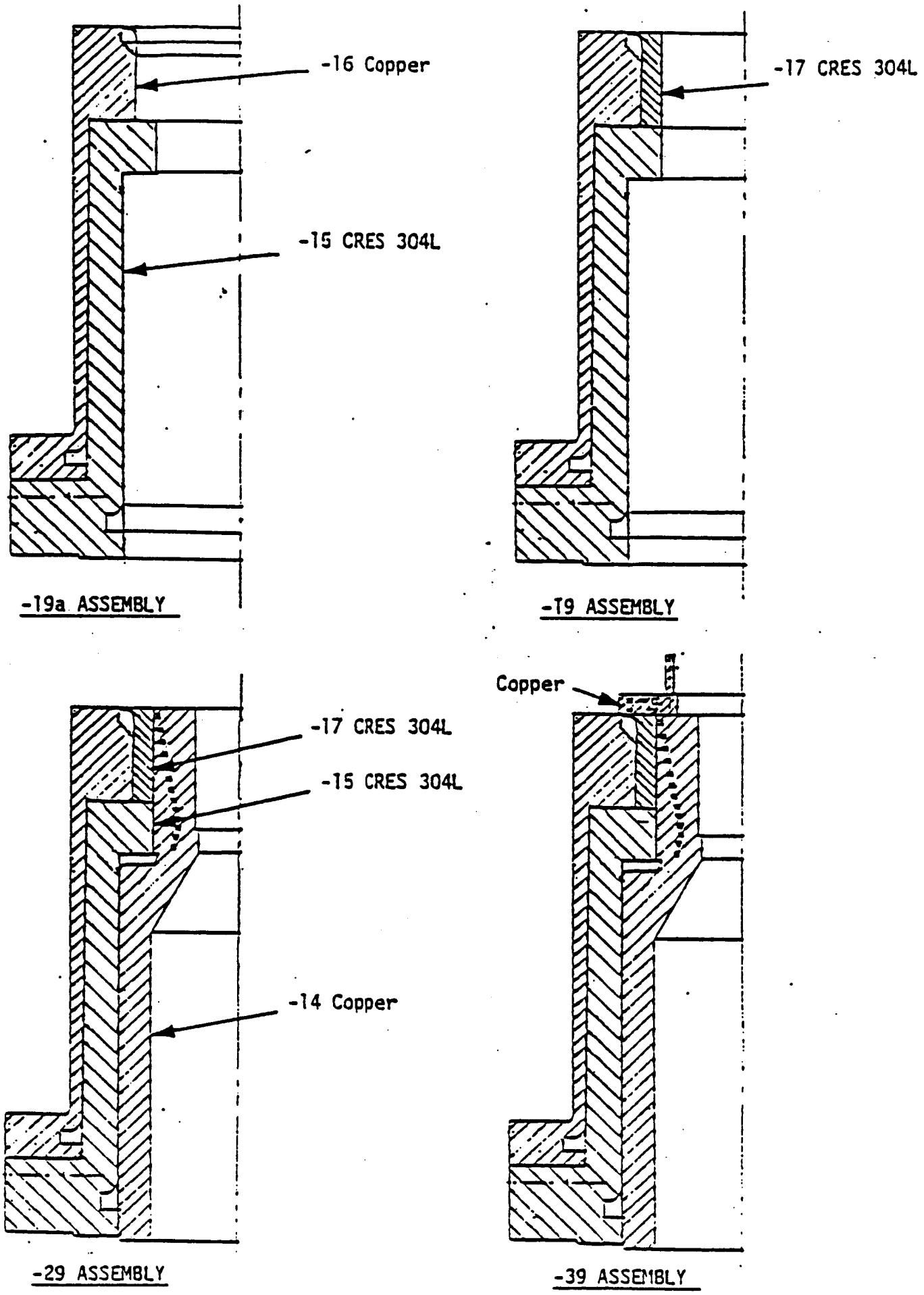

Figure 25. Primary Chamber Assembly Sequence

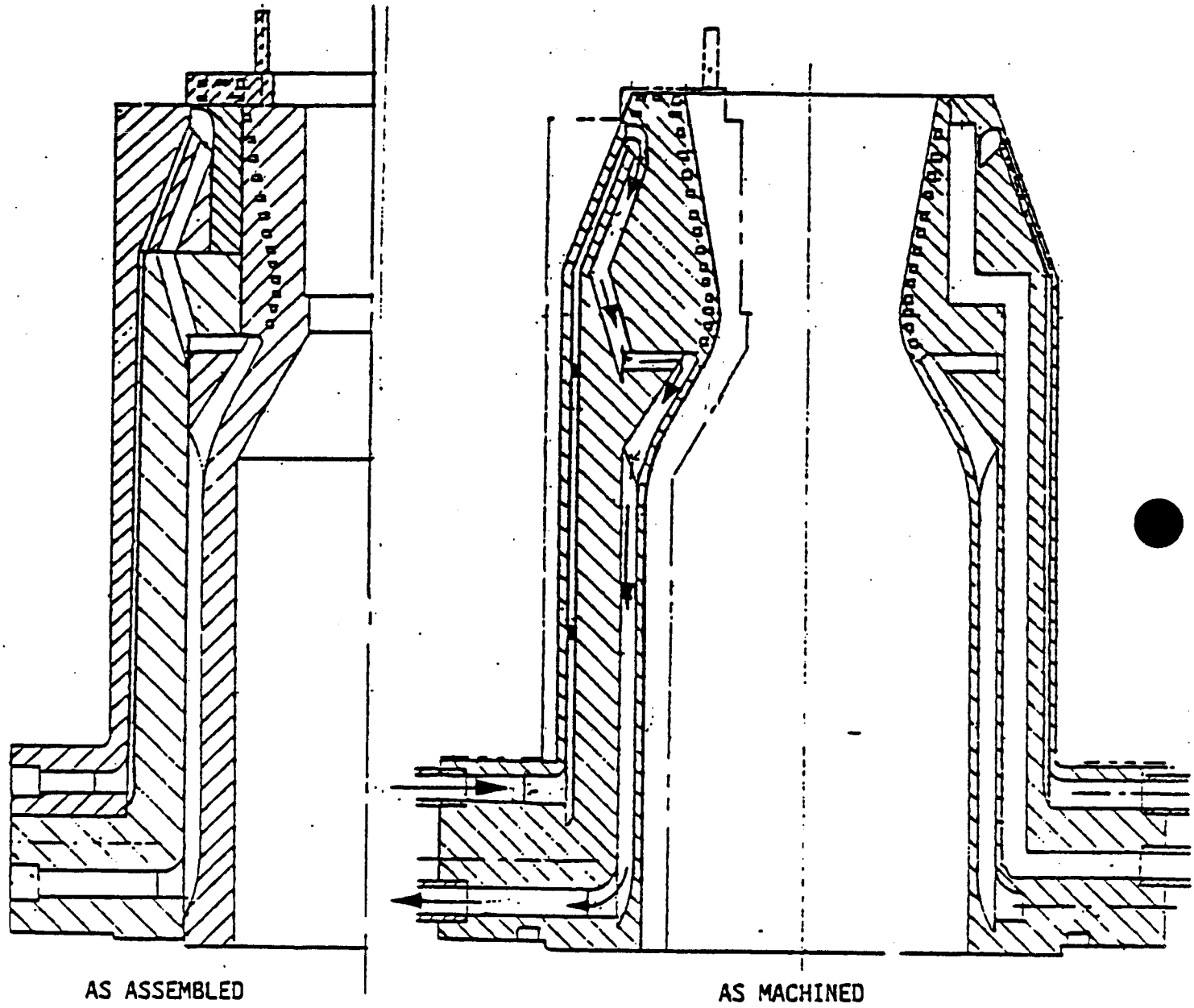

Figure 26. Primary Chamber Showing Cooling and Calorimetric Circuits

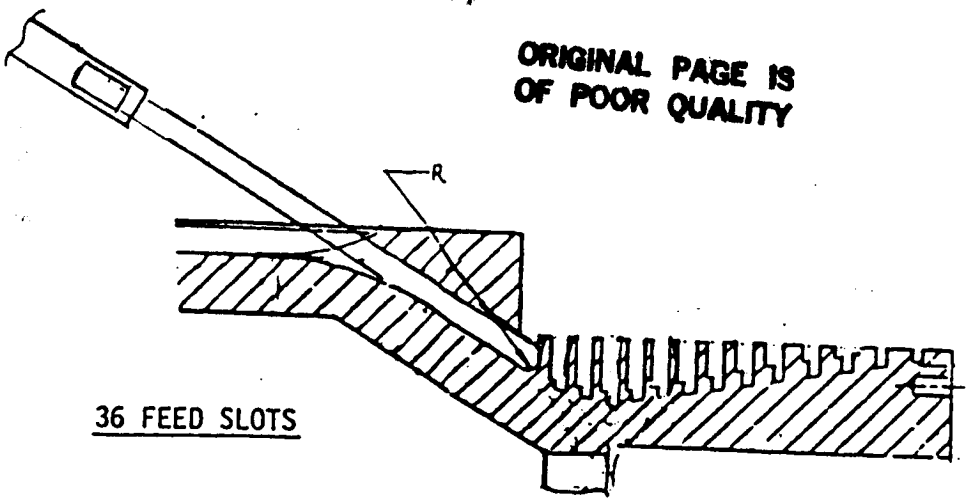

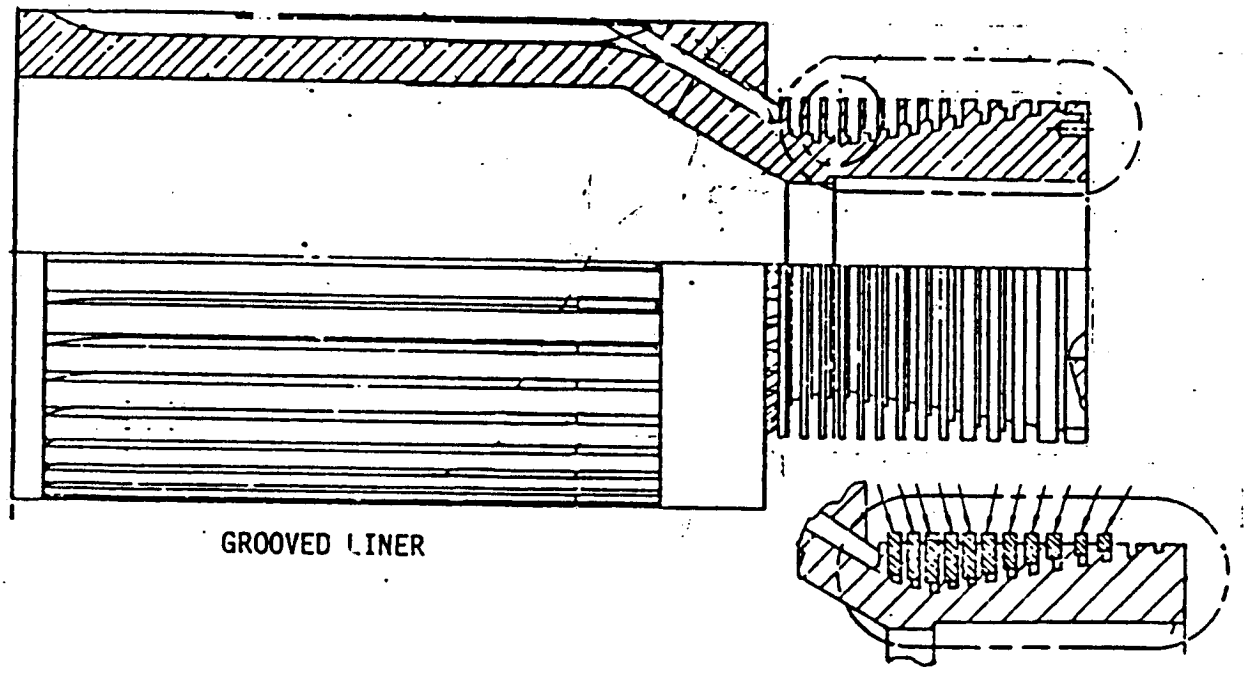

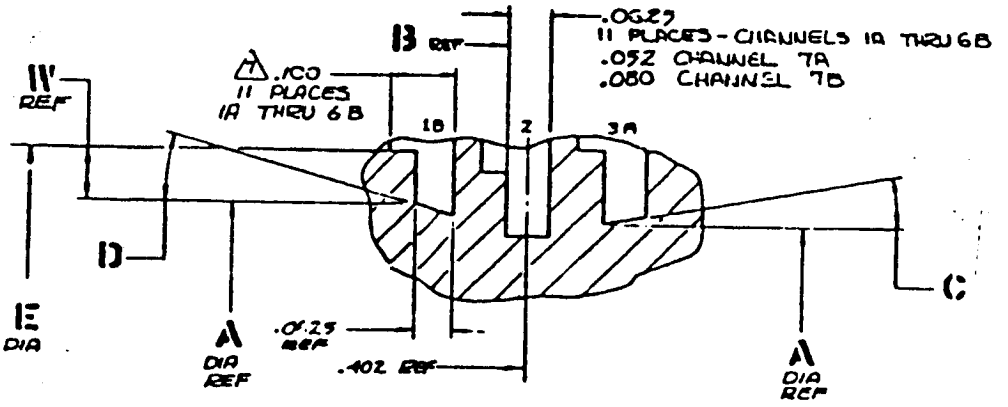

Figure 27. Primary Chamber Inner Liner, Copper

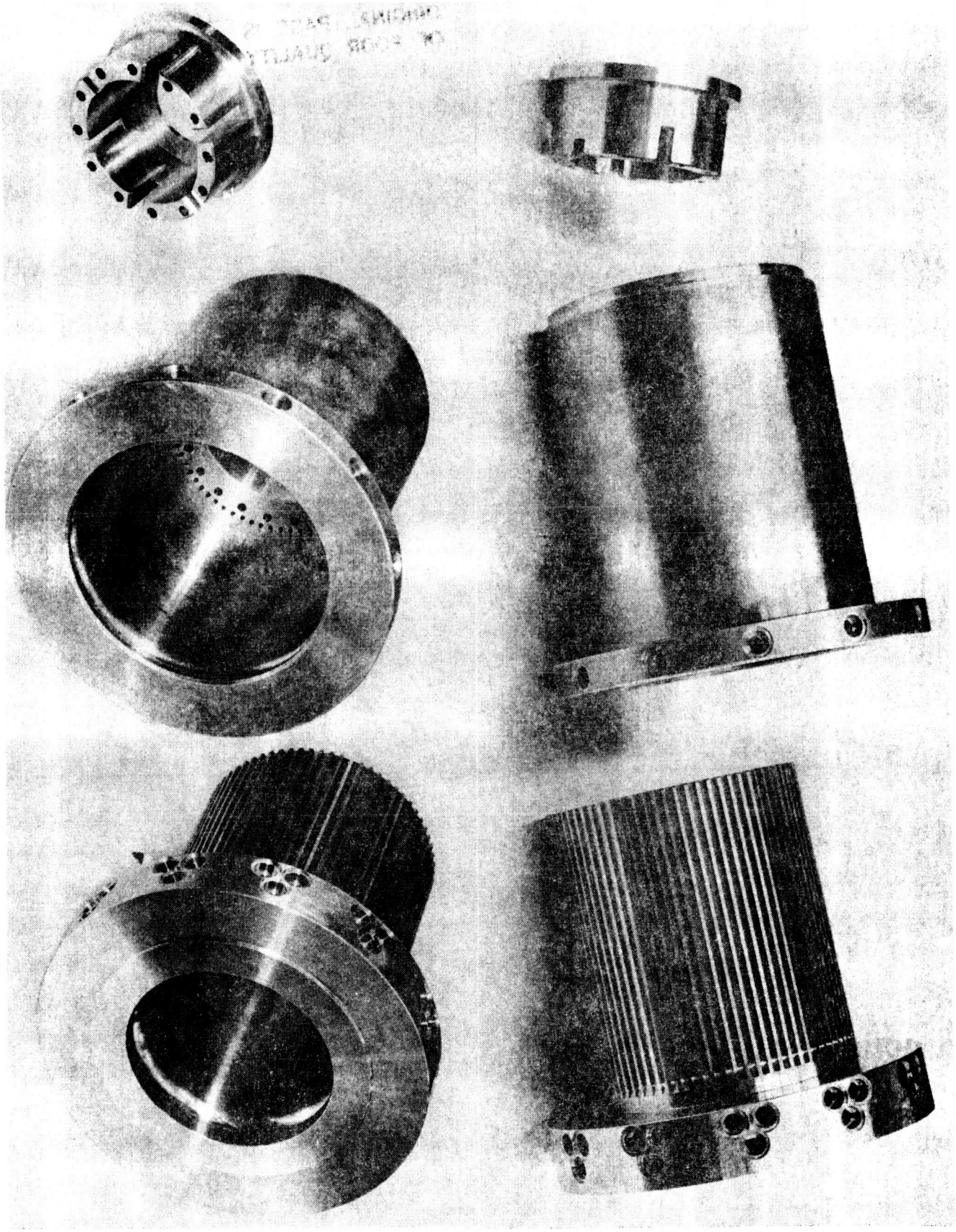

Figure 28. Primary Chamber -19 Assembly Components

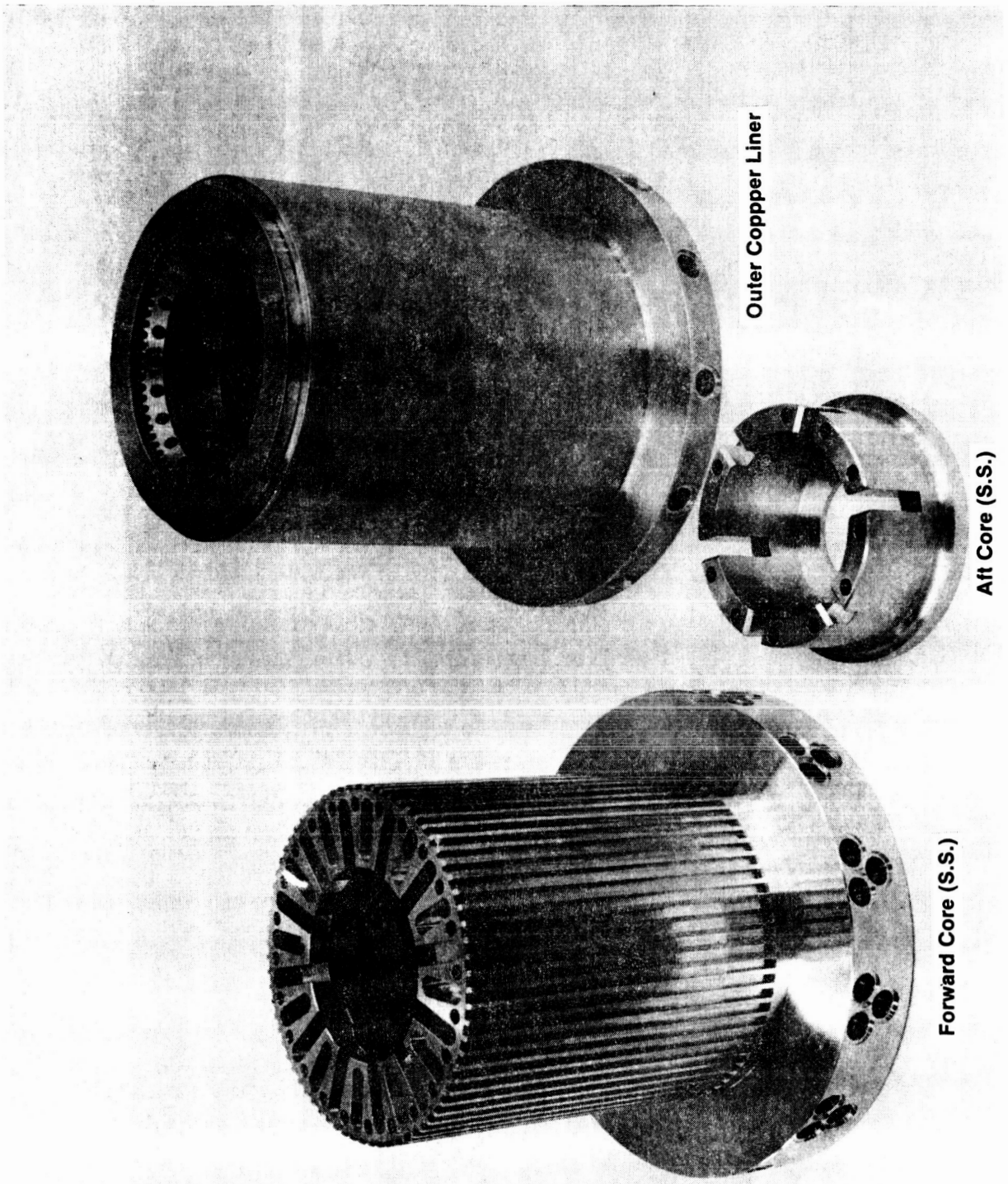

Figure 29. Primary Chamber -19 Assembly Components

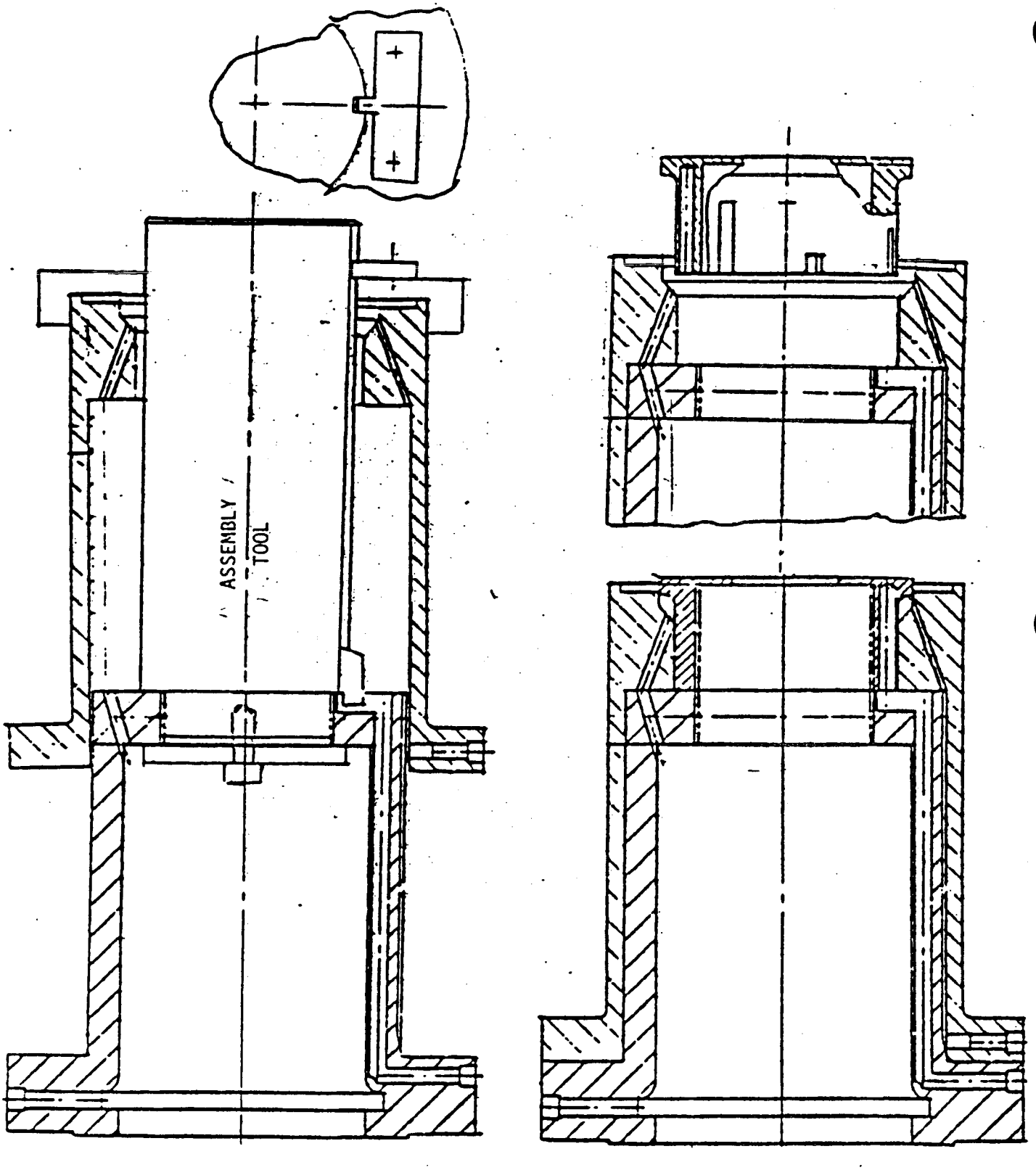

Figure 30. Primary Chamber -19 Assembly Sequence

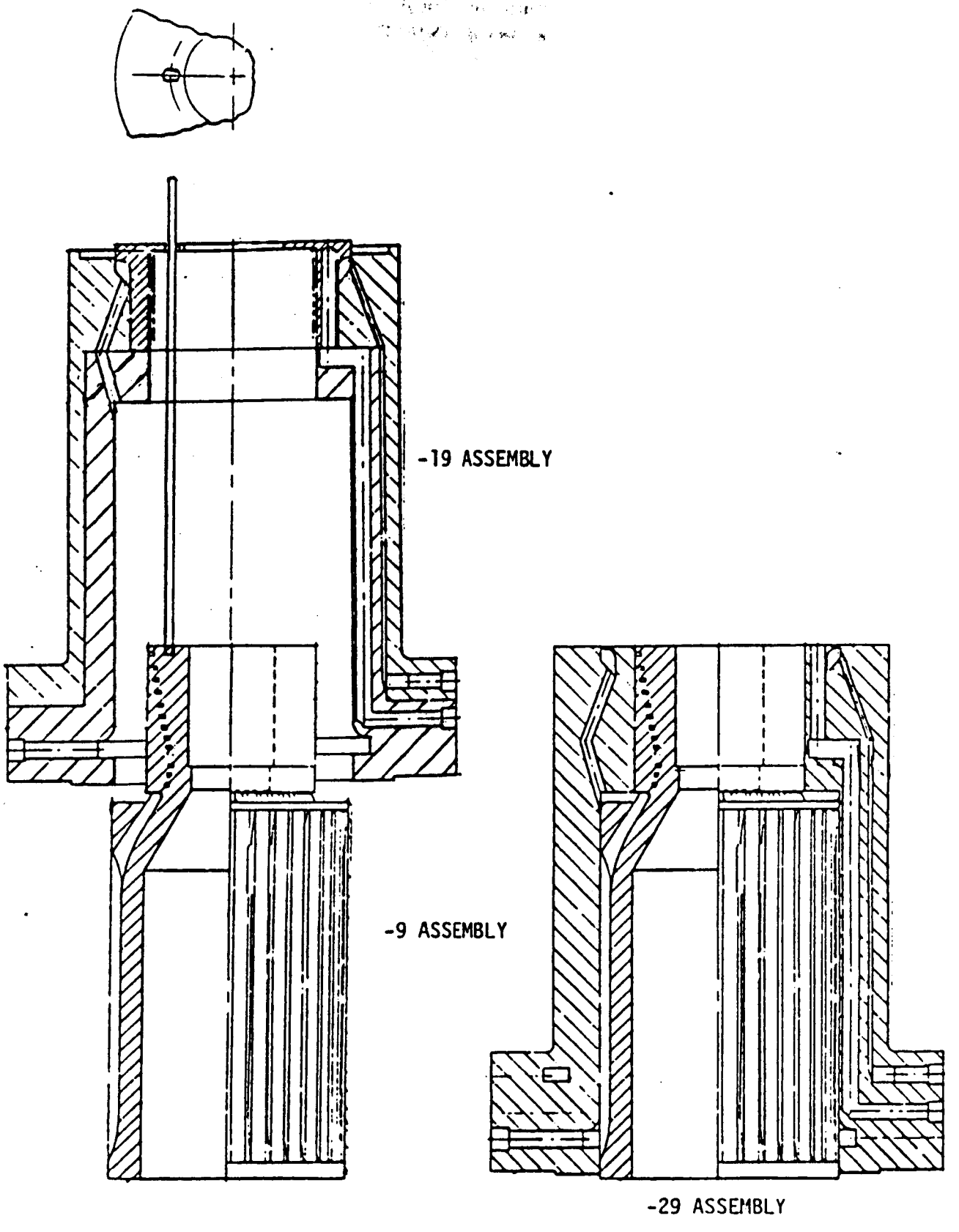

Figure 31. Primary Chamber -29 Assembly Sequence

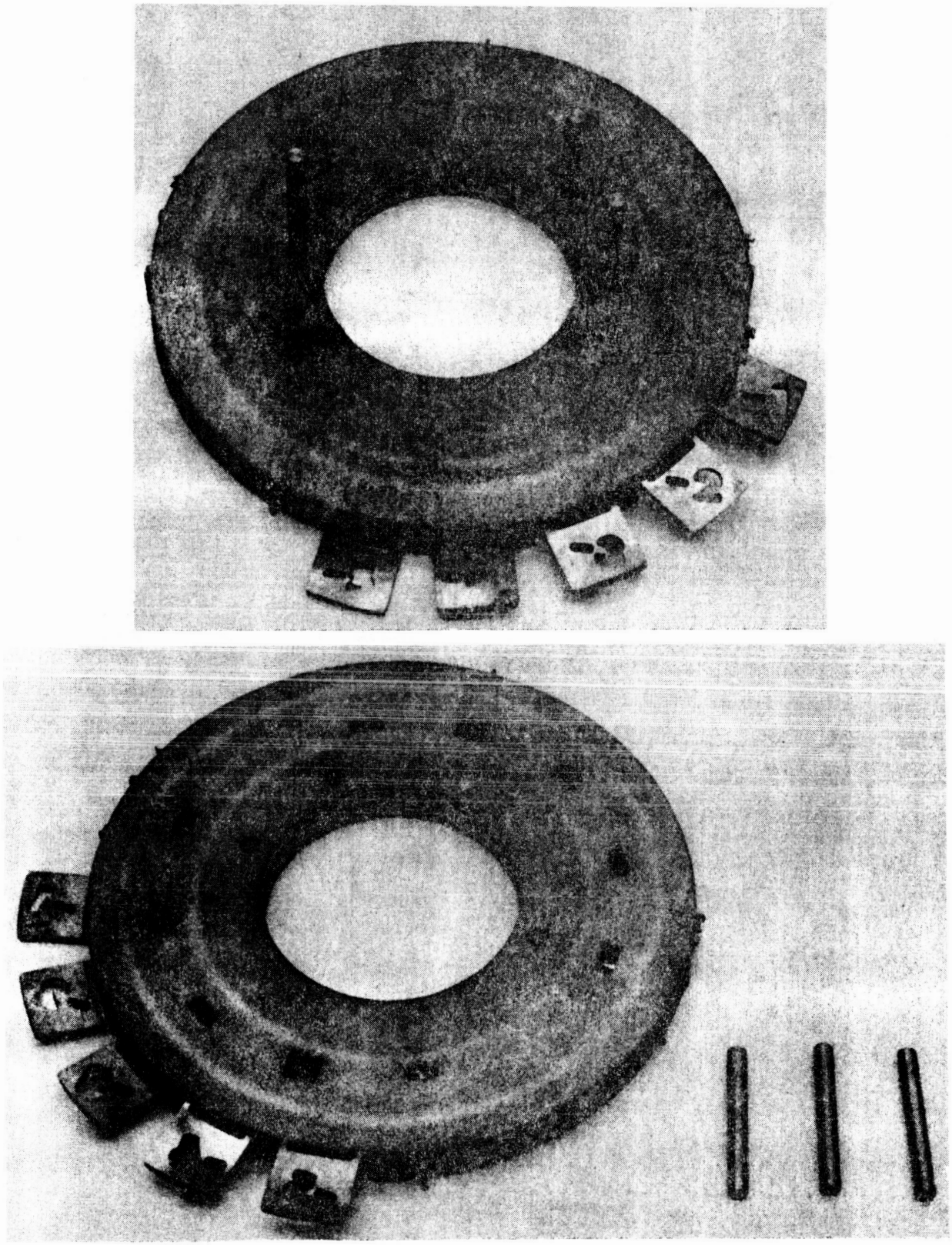

Figure 32. Primary Chamber Copper Platelet Stack

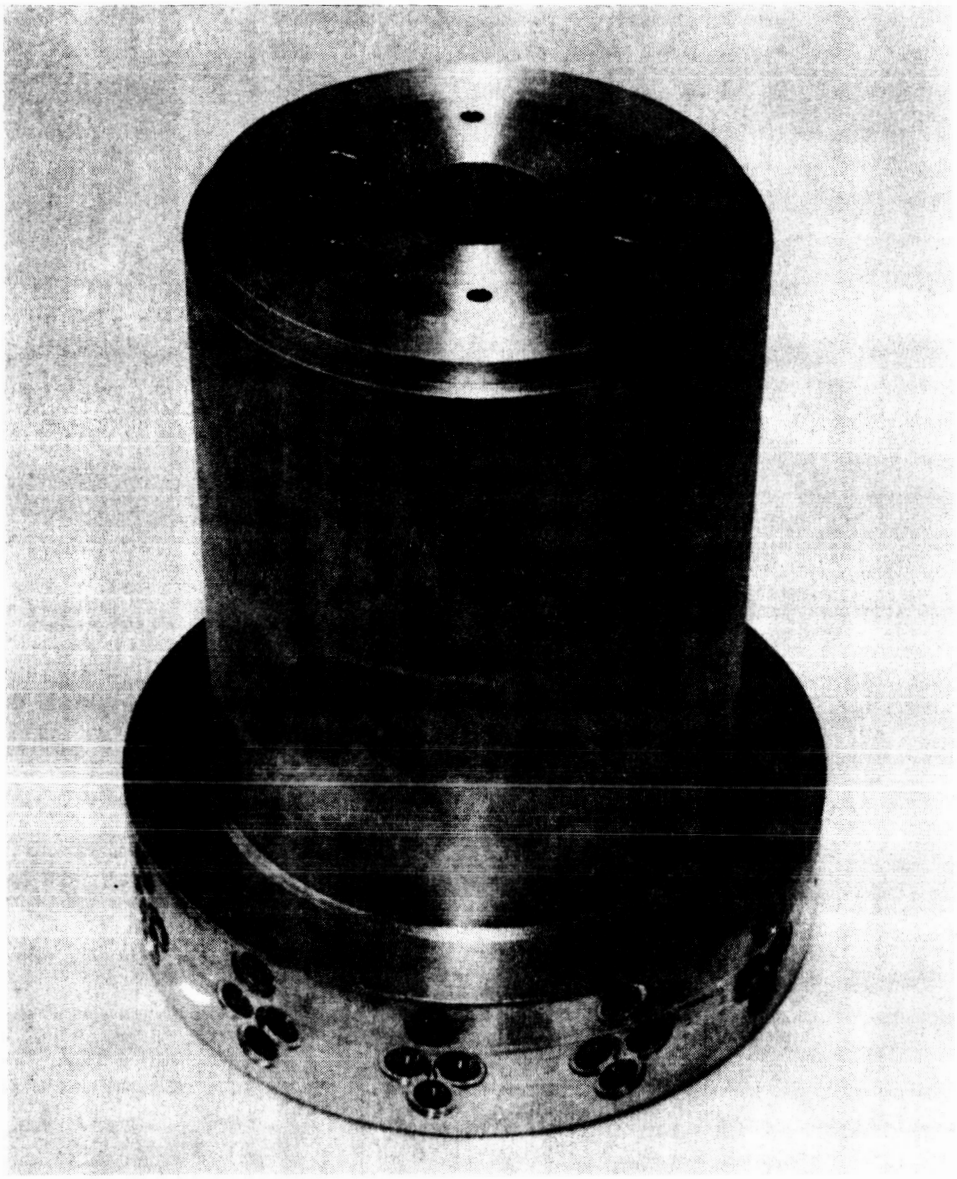

Prepared For Brazing
Copper Platelet Stack

Figure 33. Primary Chamber -39 Assembly

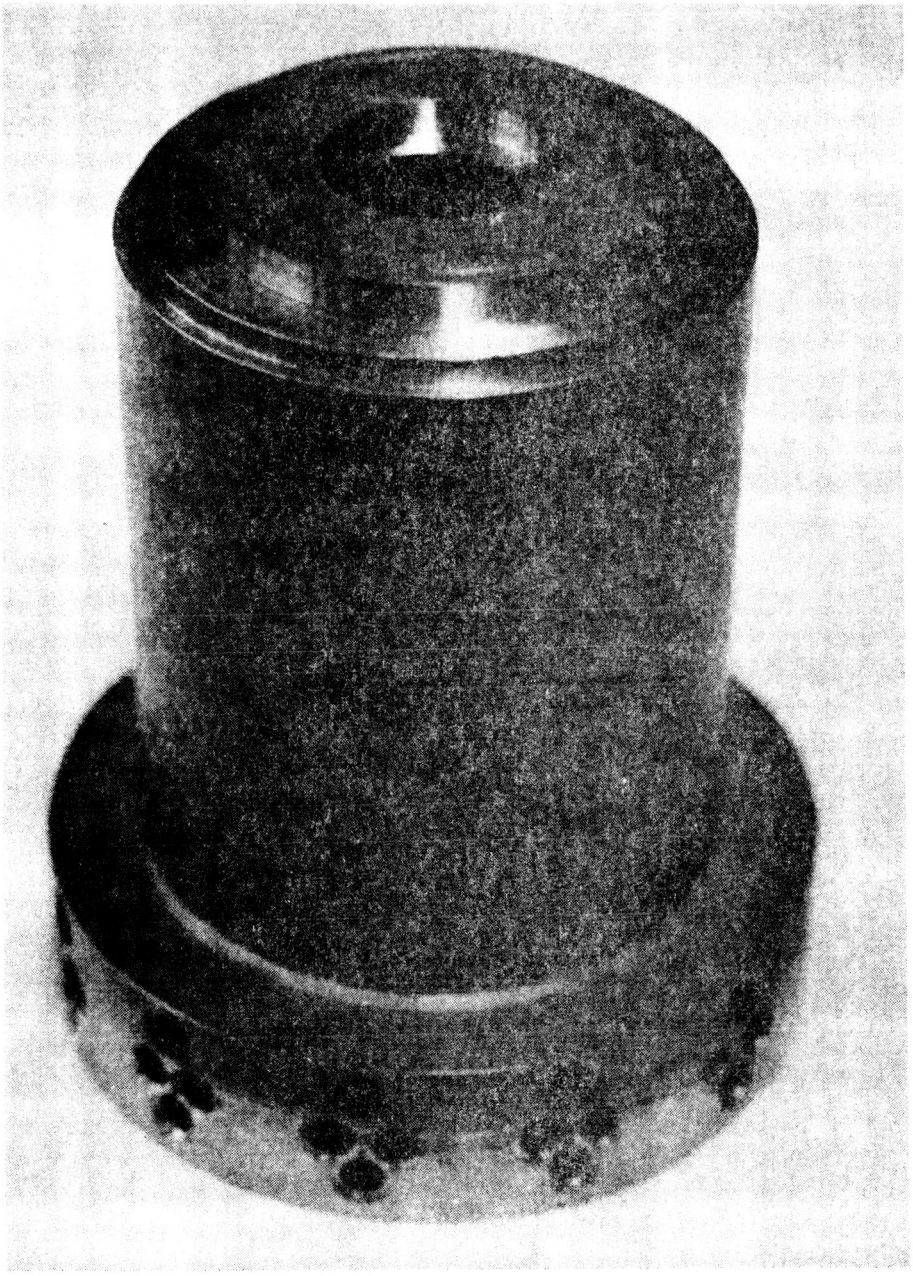

Figure 34. After Brazing Copper Platelet Stack

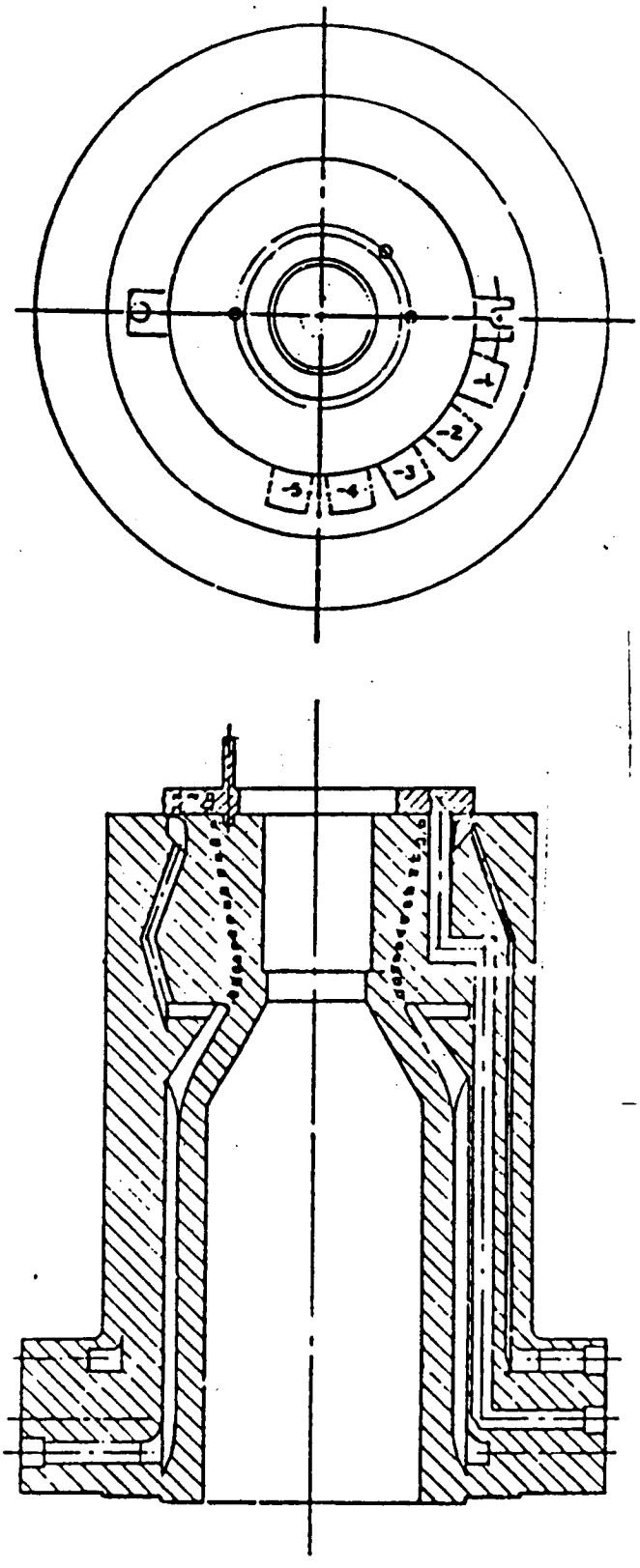

Figure 35. Schematic Sketch of -39 Assembly

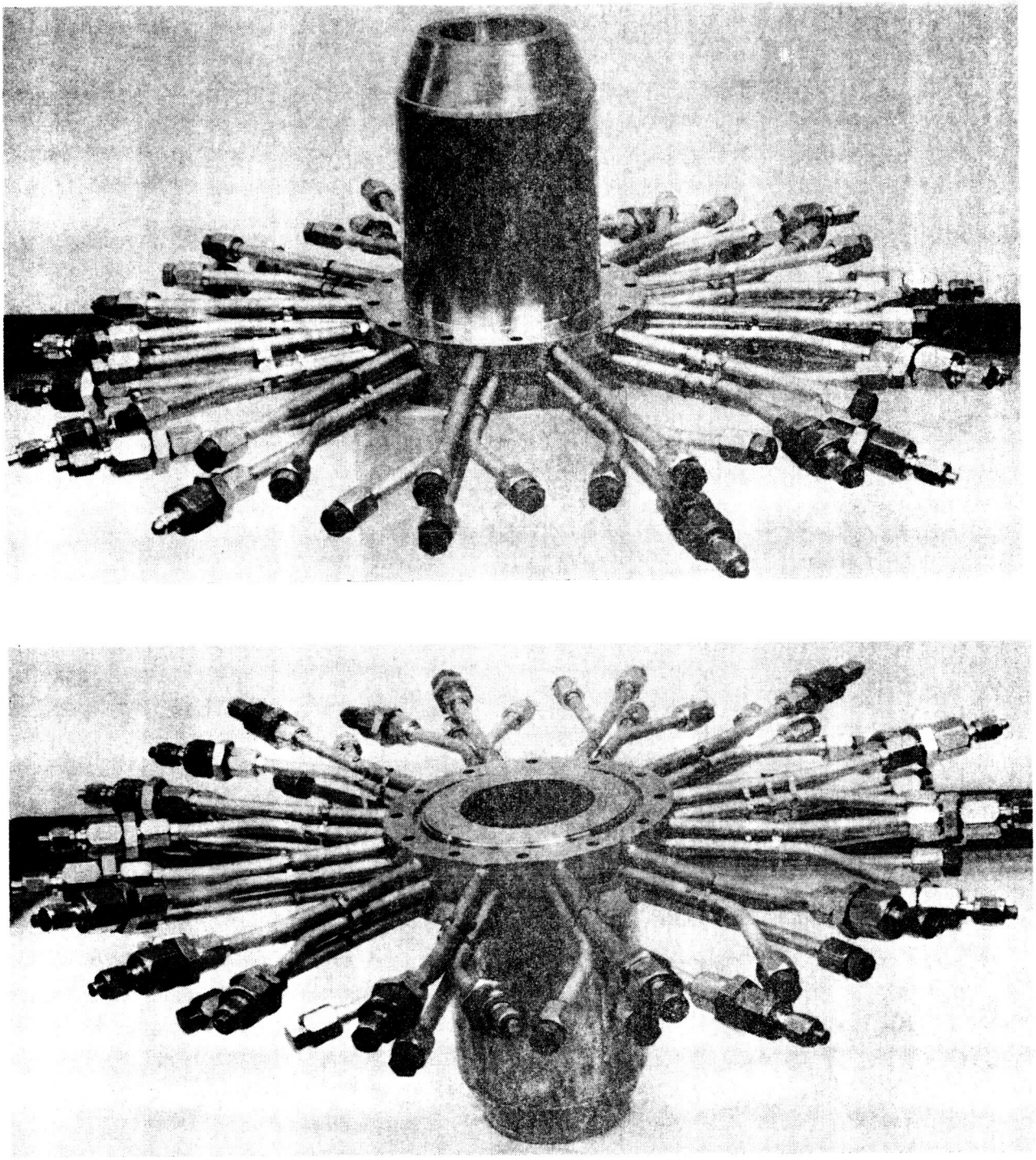

Figure 36. Primary Chamber -49 Assembly, Complete

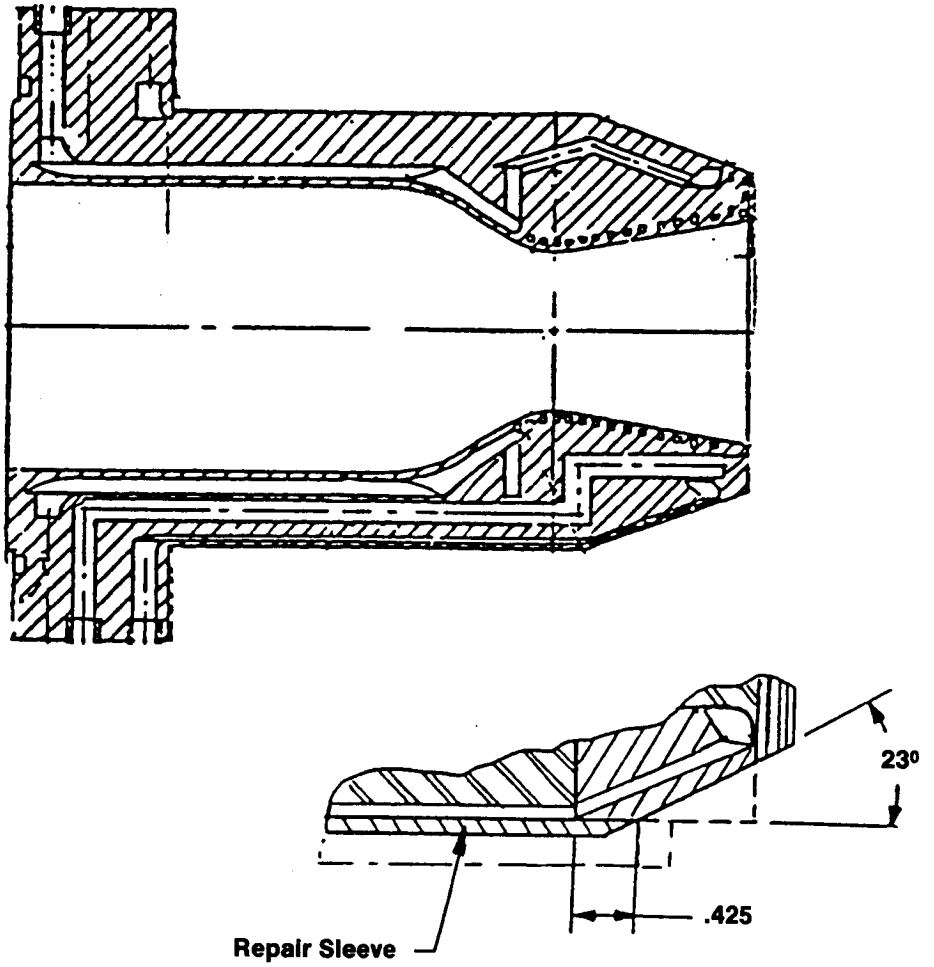

Figure 37. Primary Chamber -49 Assembly, Final Machine with Deviation

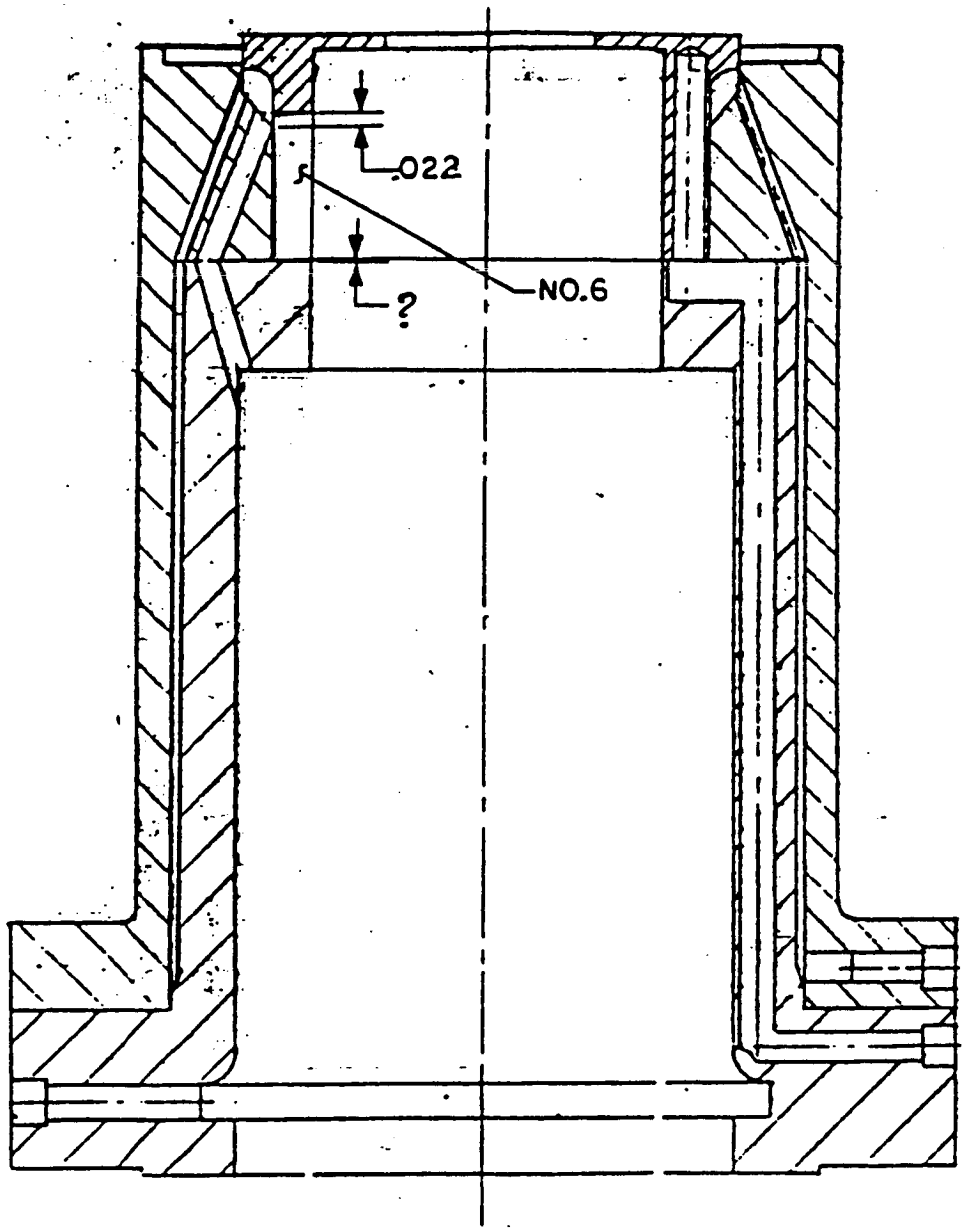

Figure 38. Primary Chamber Built-In Leak, Circuit 6 (Design Error)

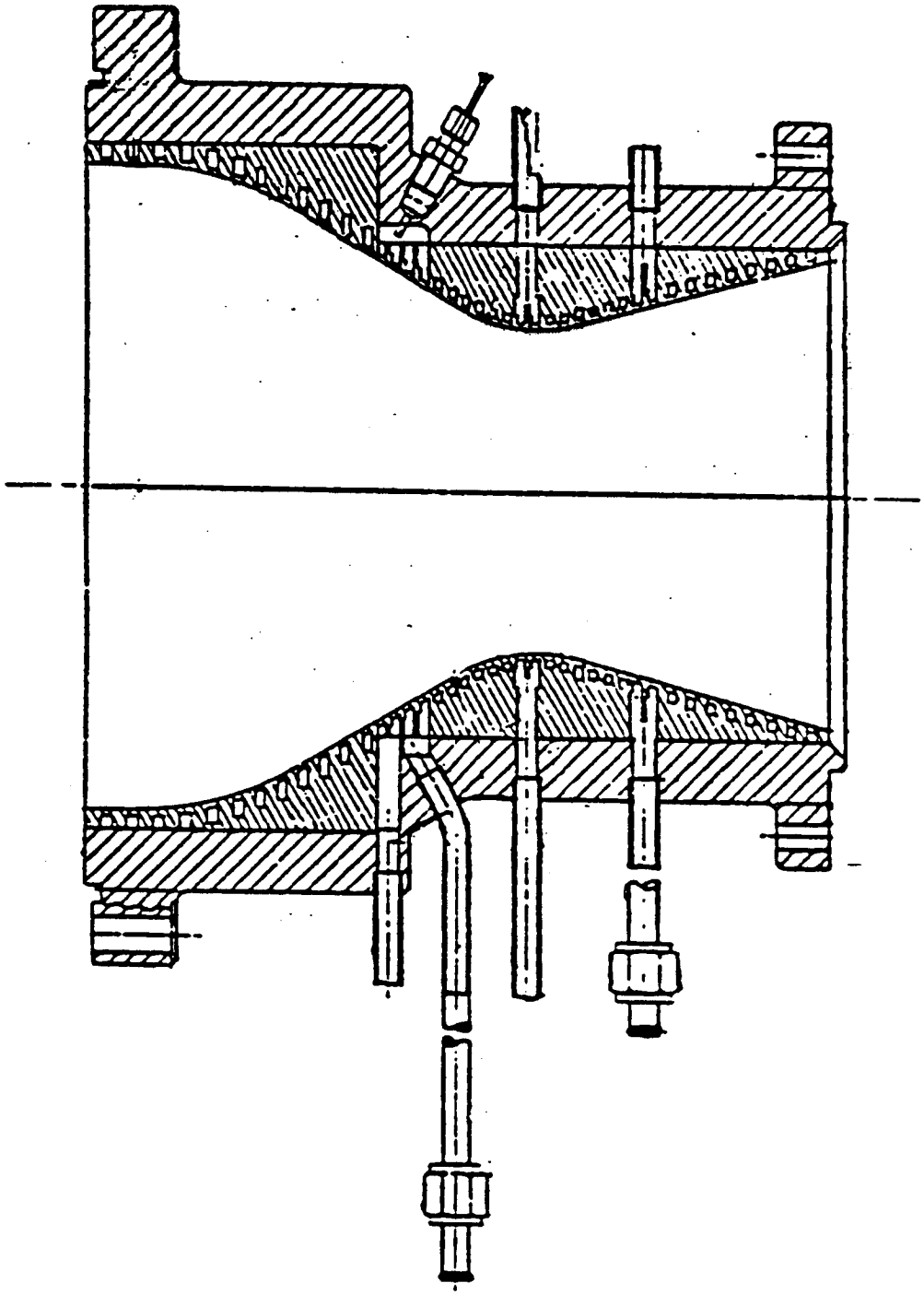

Figure 39. Secondary Chamber

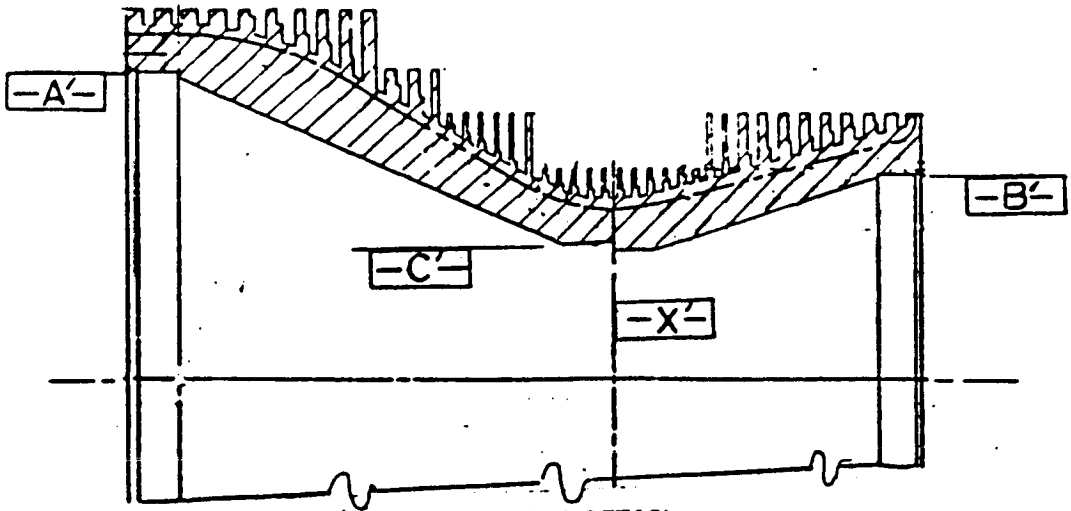

-1 CORE DETAIL
(WITH DATUMS)

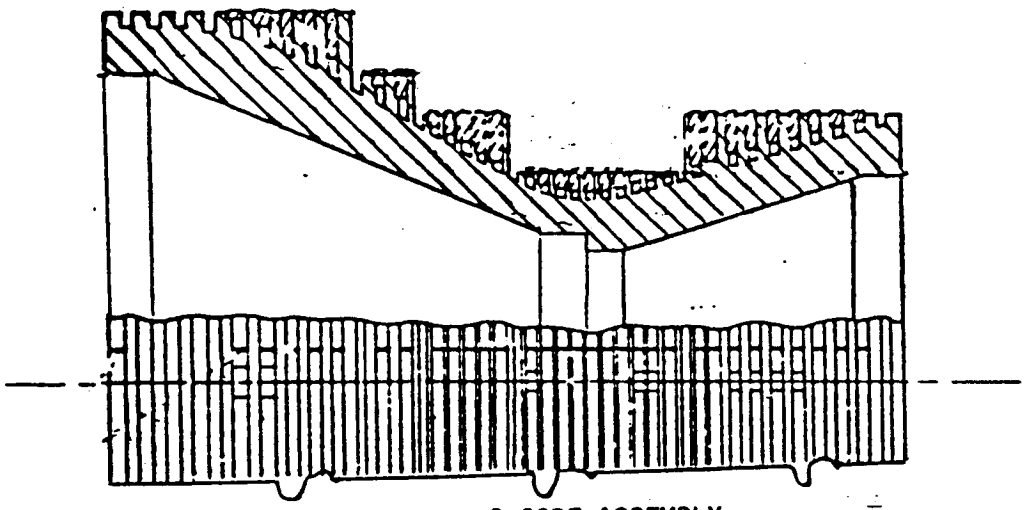

-9 CORE ASSEMBLY

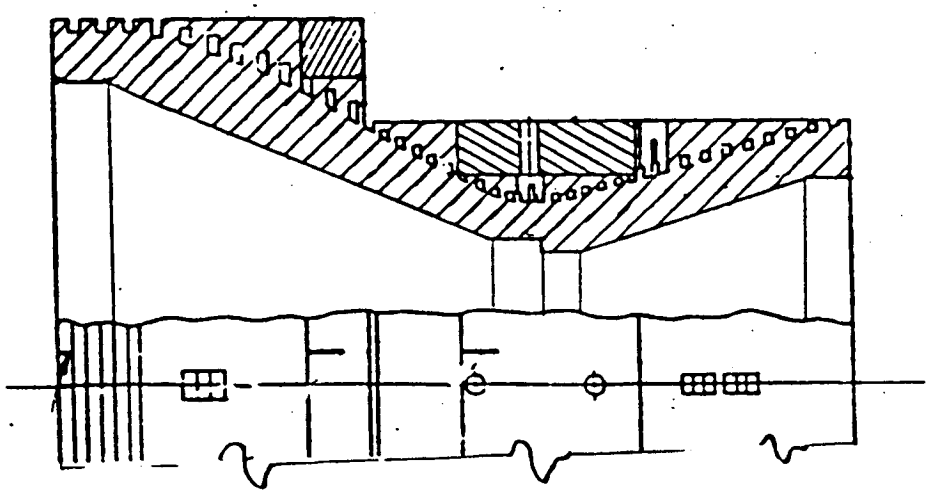

-19 CORE ASSEMBLY

Figure 40. Secondary Chamber Assembly Levels

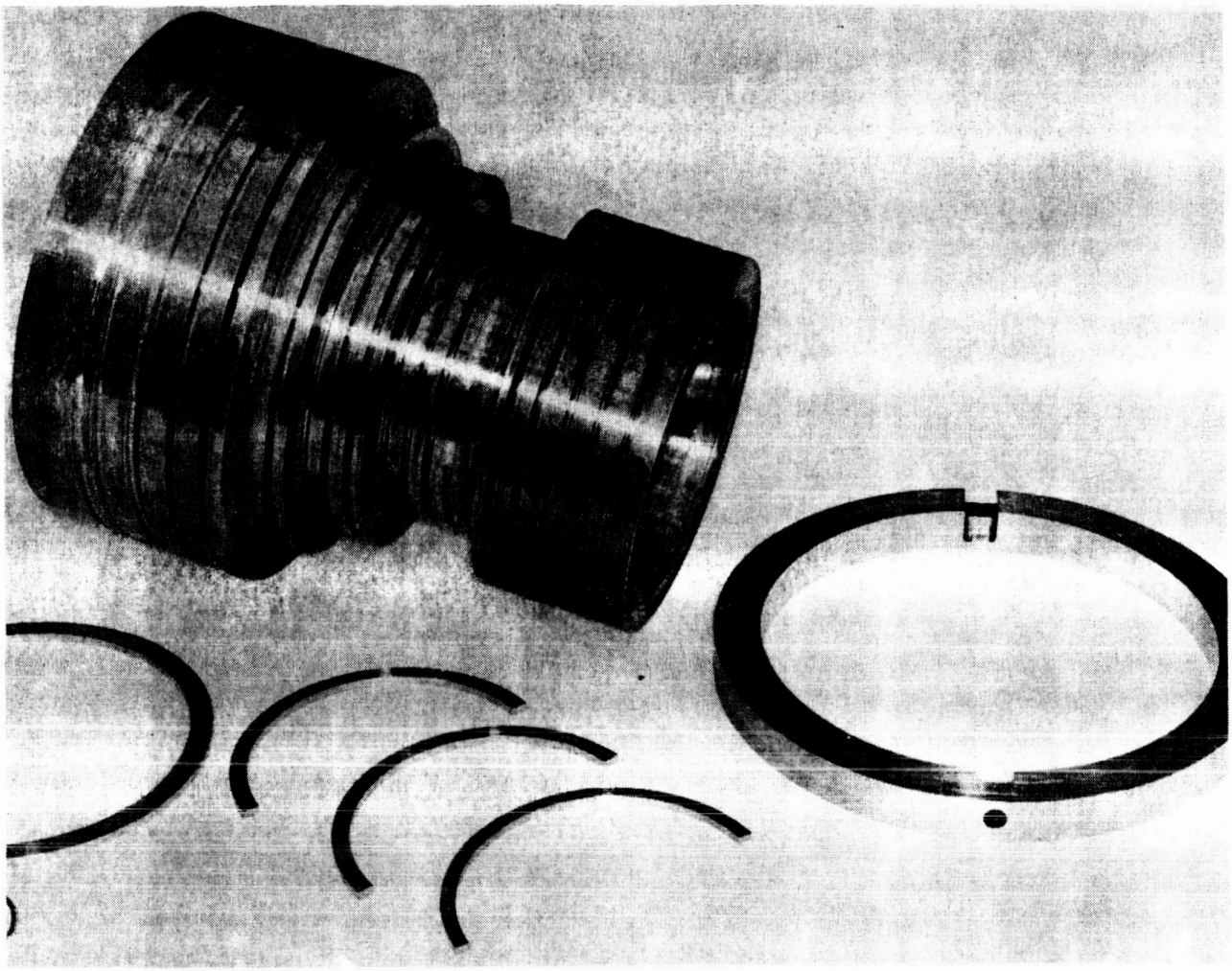

Figure 41. Secondary Chamber - Core with the First Set of Grooves, Some of the Split Rings, and -37 Insert

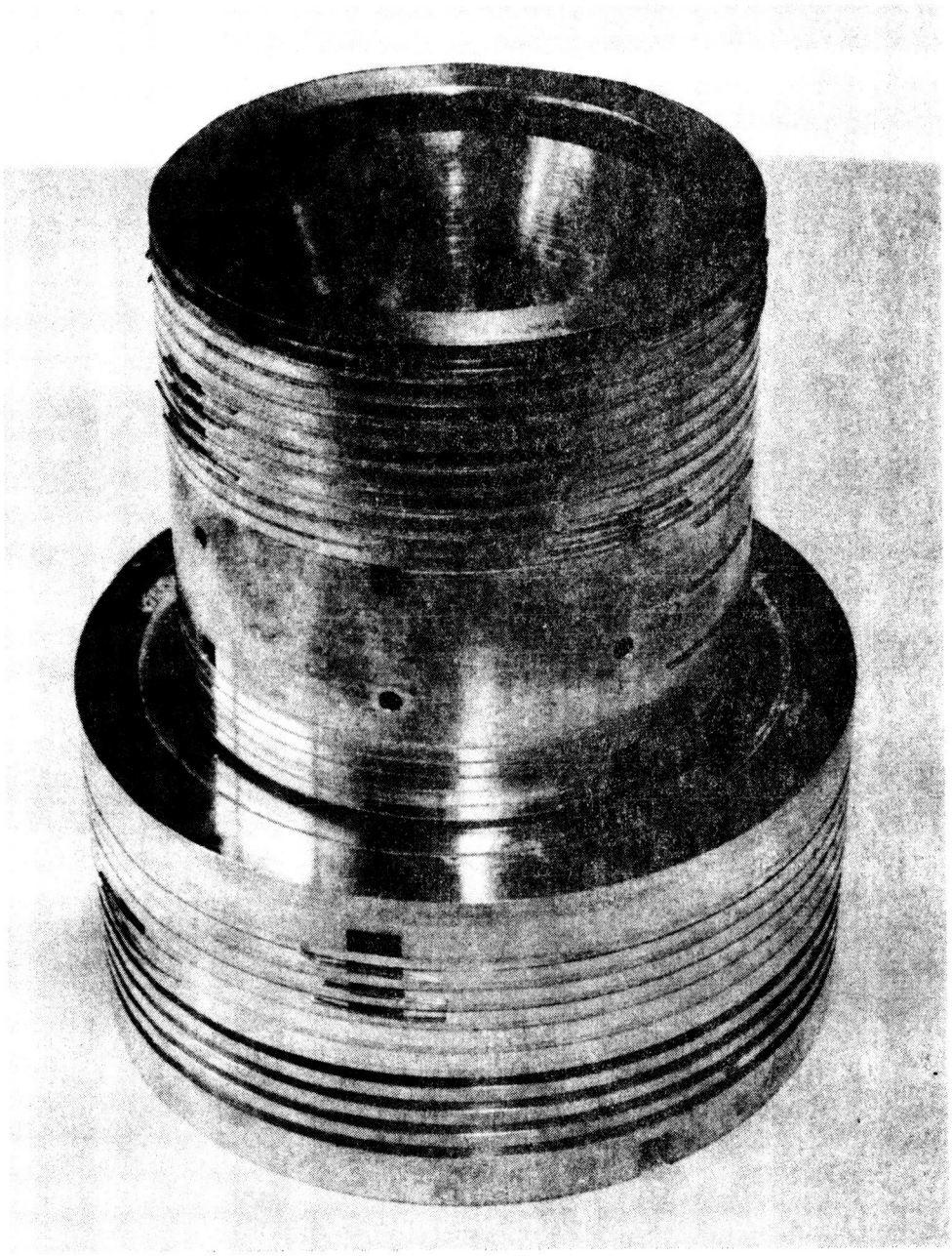

Figure 42. Secondary Chamber -19 Assembly - After Braze

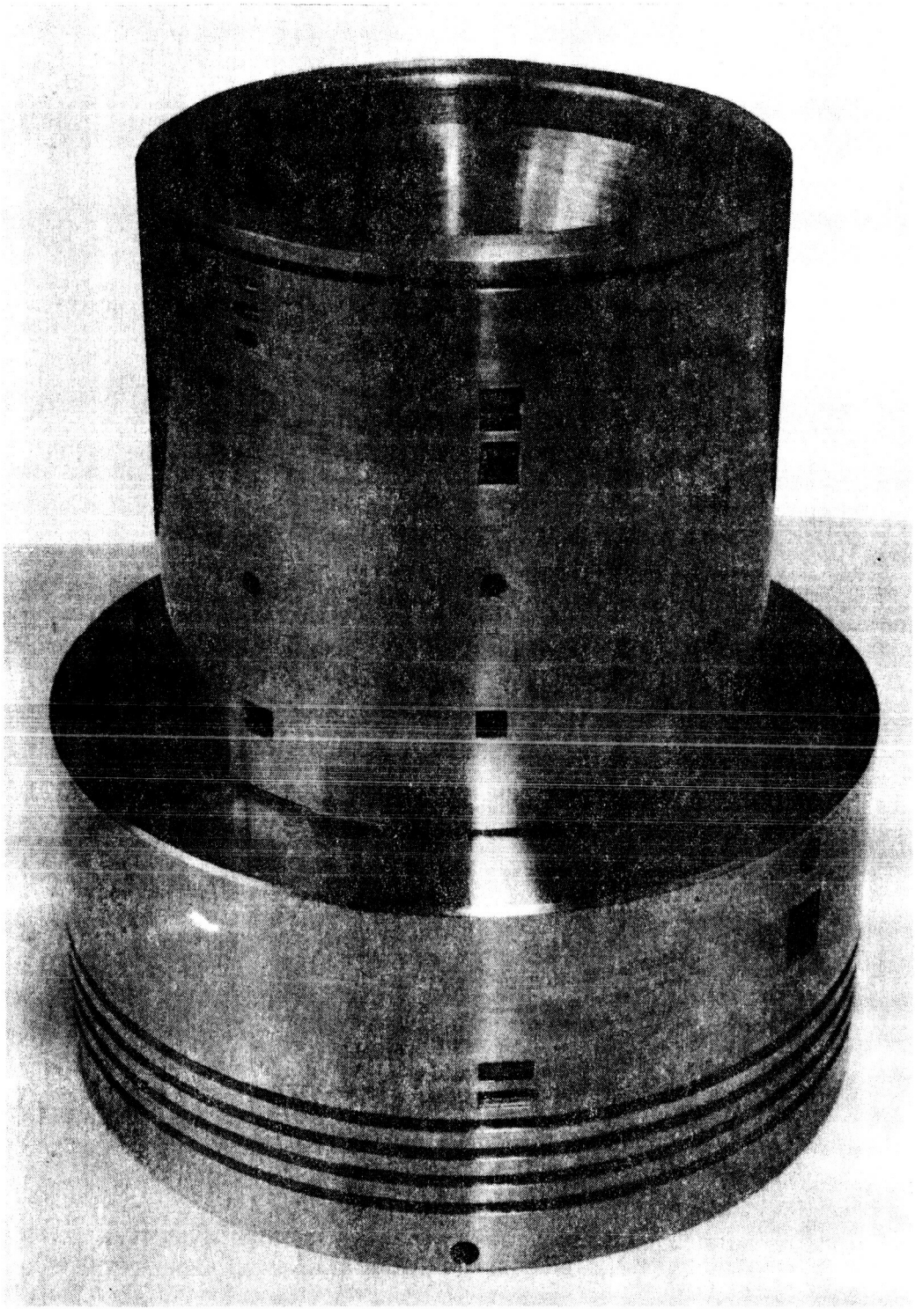

Figure 43. Secondary Chamber Machined for Inserting Into -38 Liner

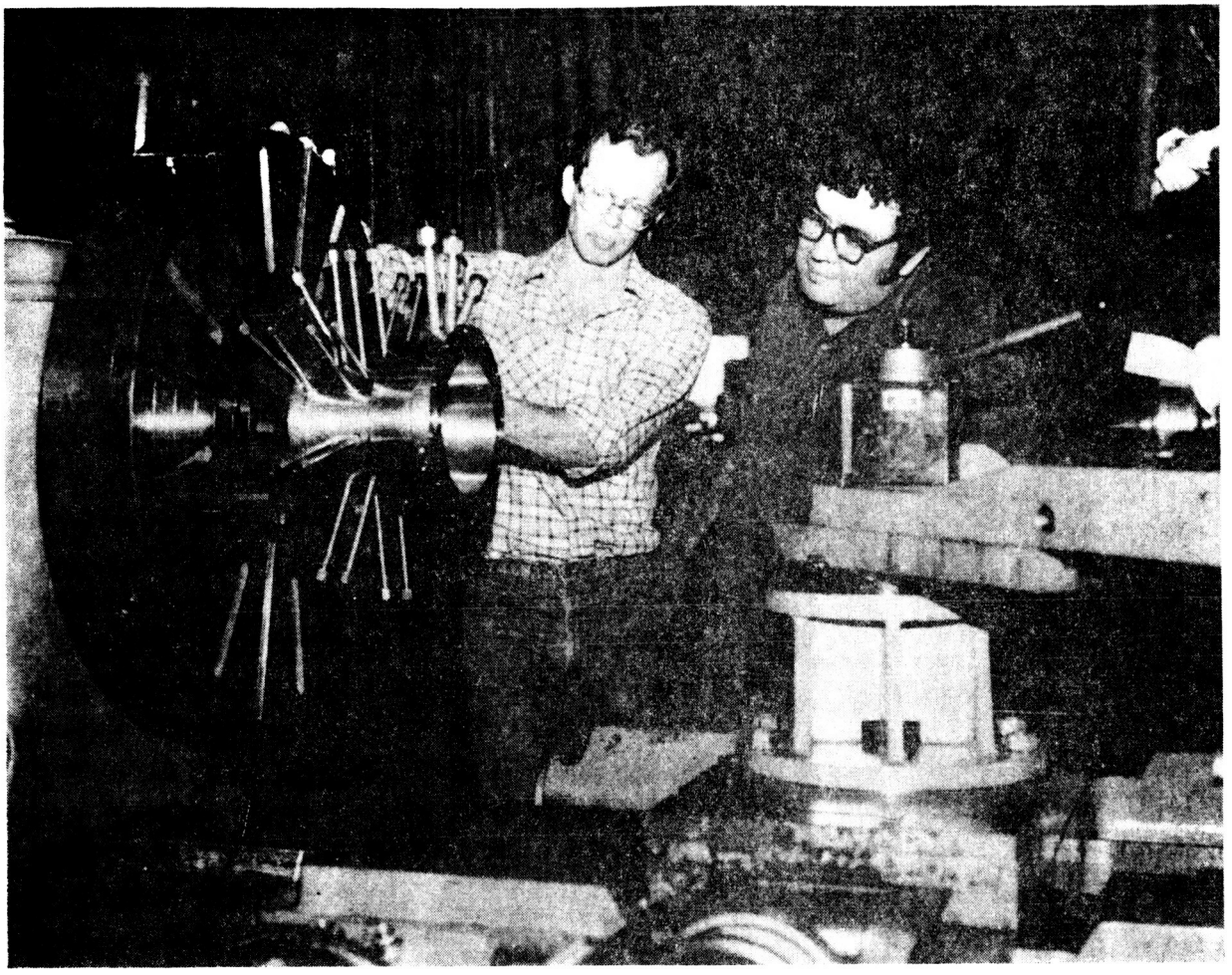

Figure 44. Photograph of Final Contouring

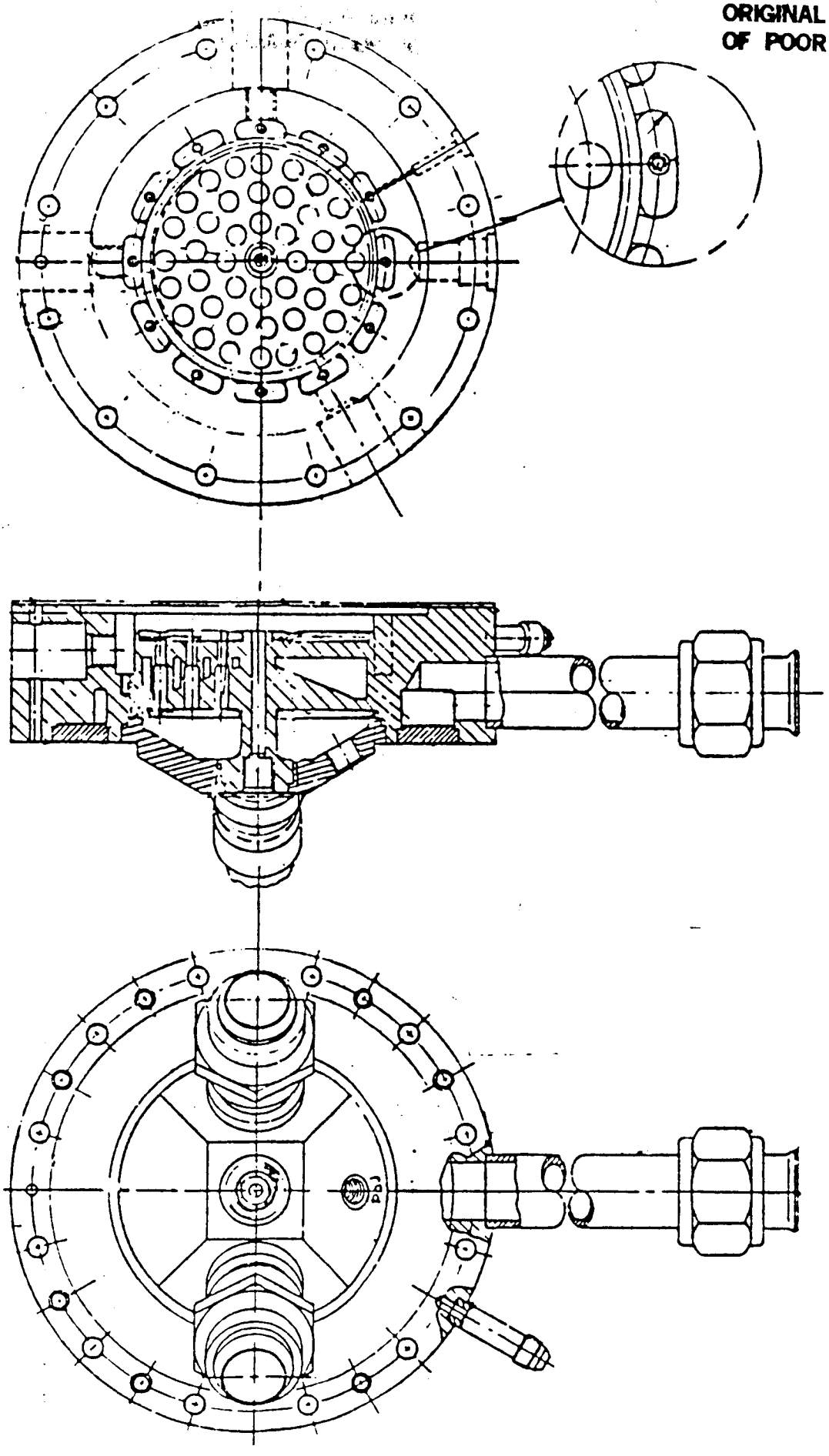

Figure 45. Primary Injector Assembly

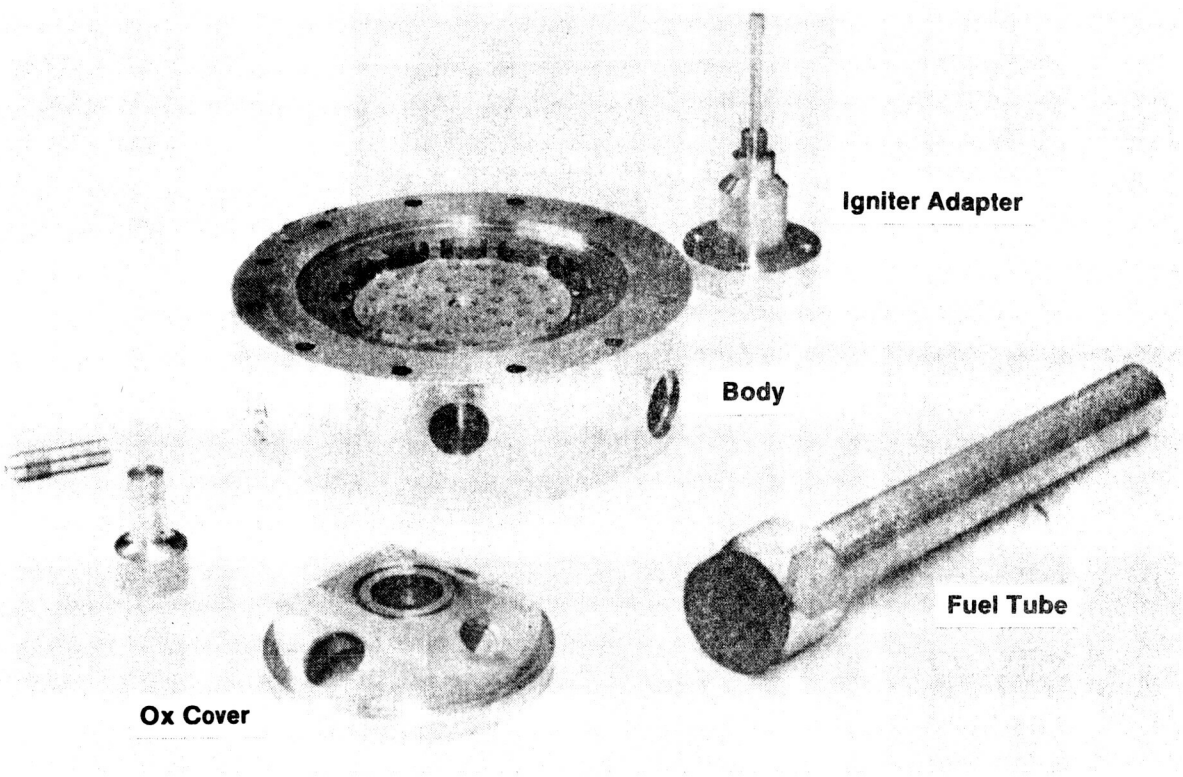

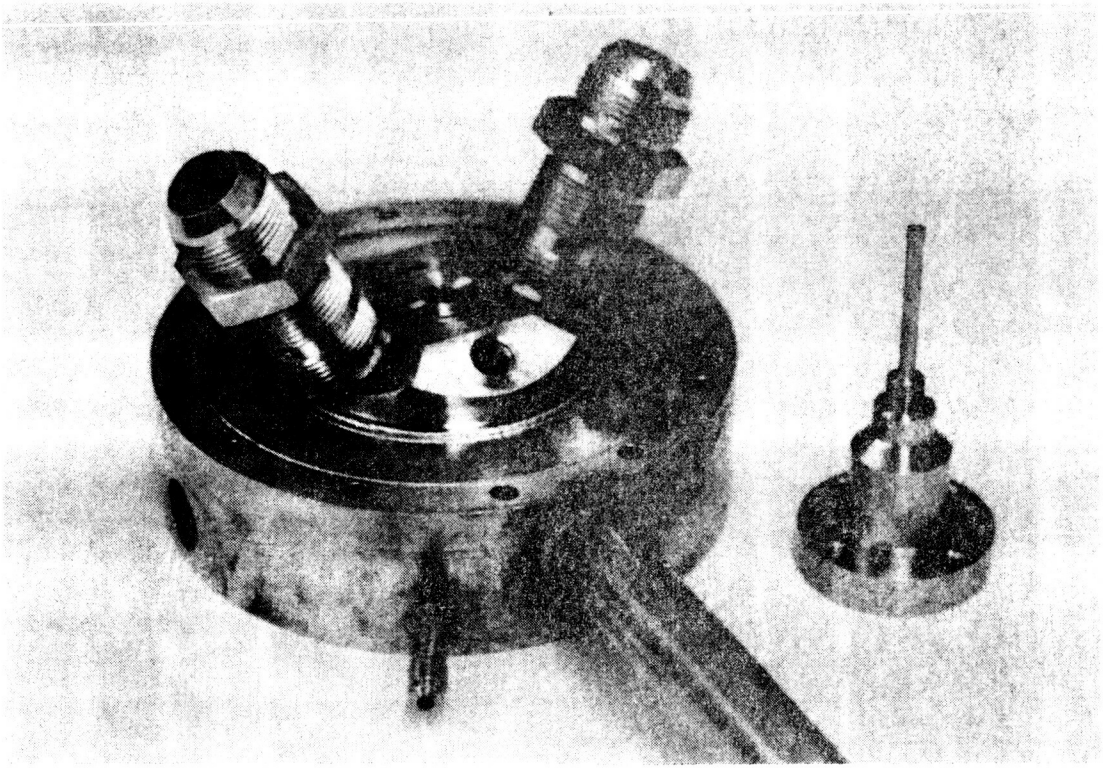

Figure 46. Assembly

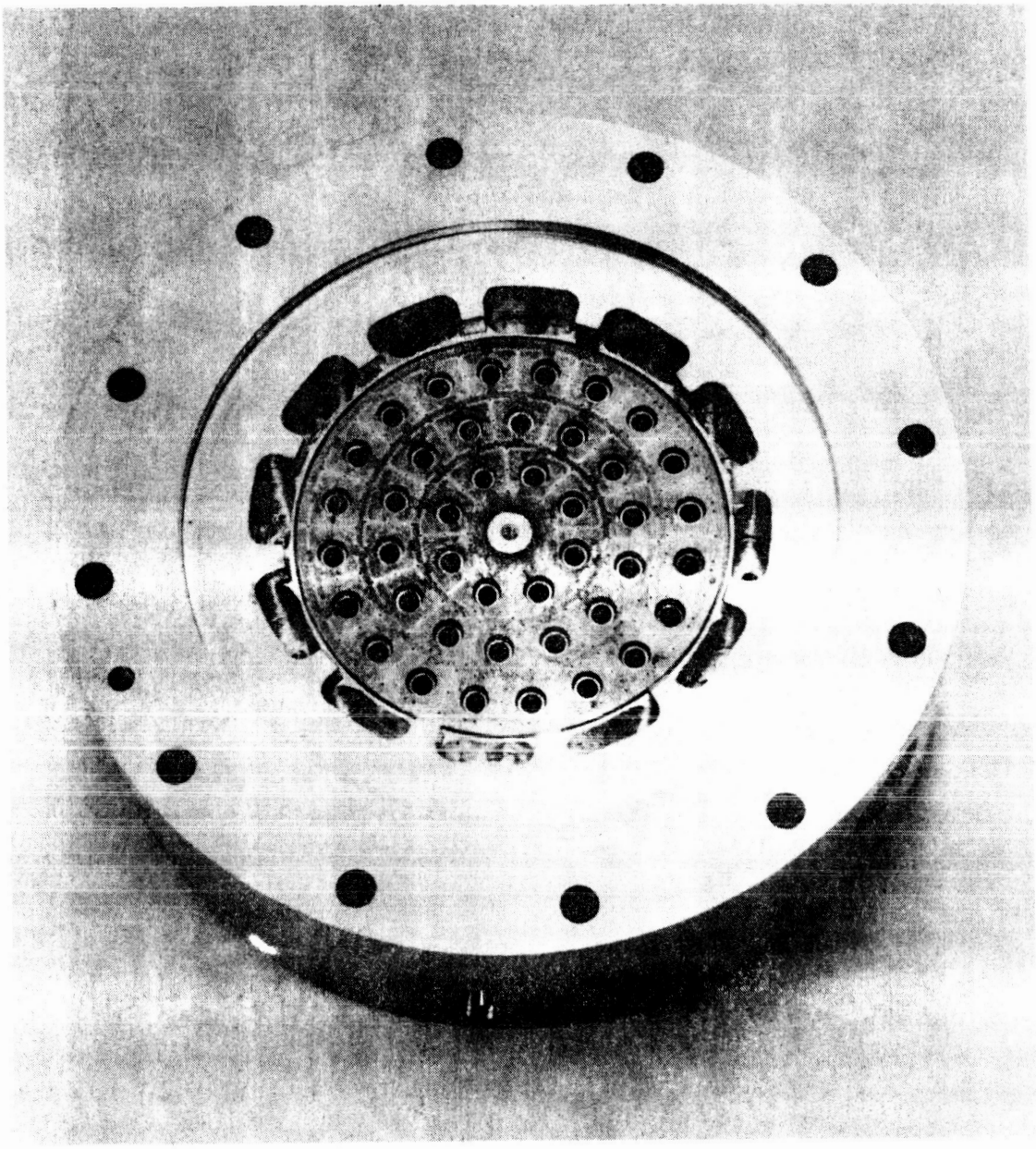

Figure 47. Primary Injector After First Braze - Face Side

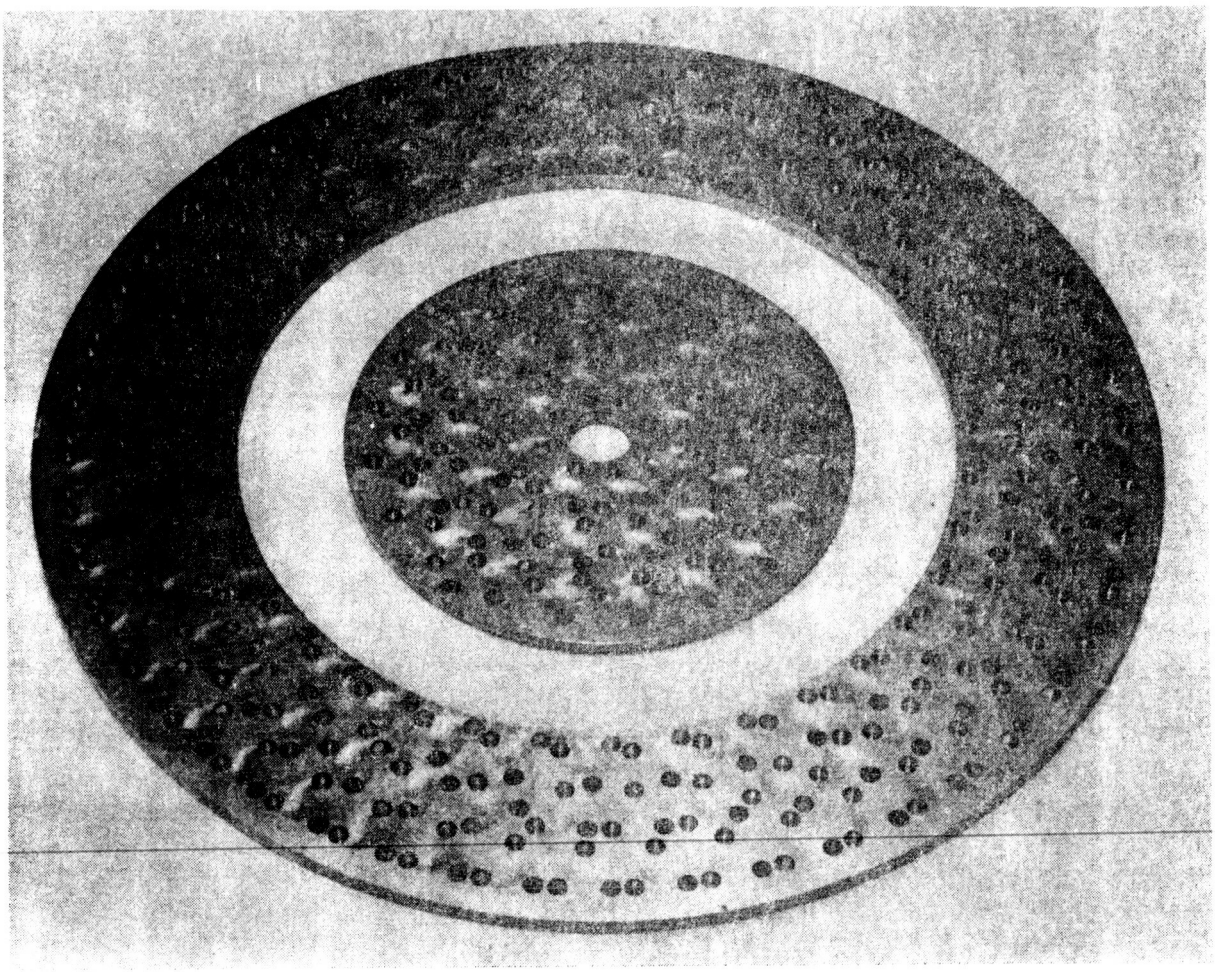

Center: Primary Injector
Outer: Secondary Injector
These Were Photoetched and Bonded as One Set

Figure 48. Machined Oxidizer Platelet Stacks

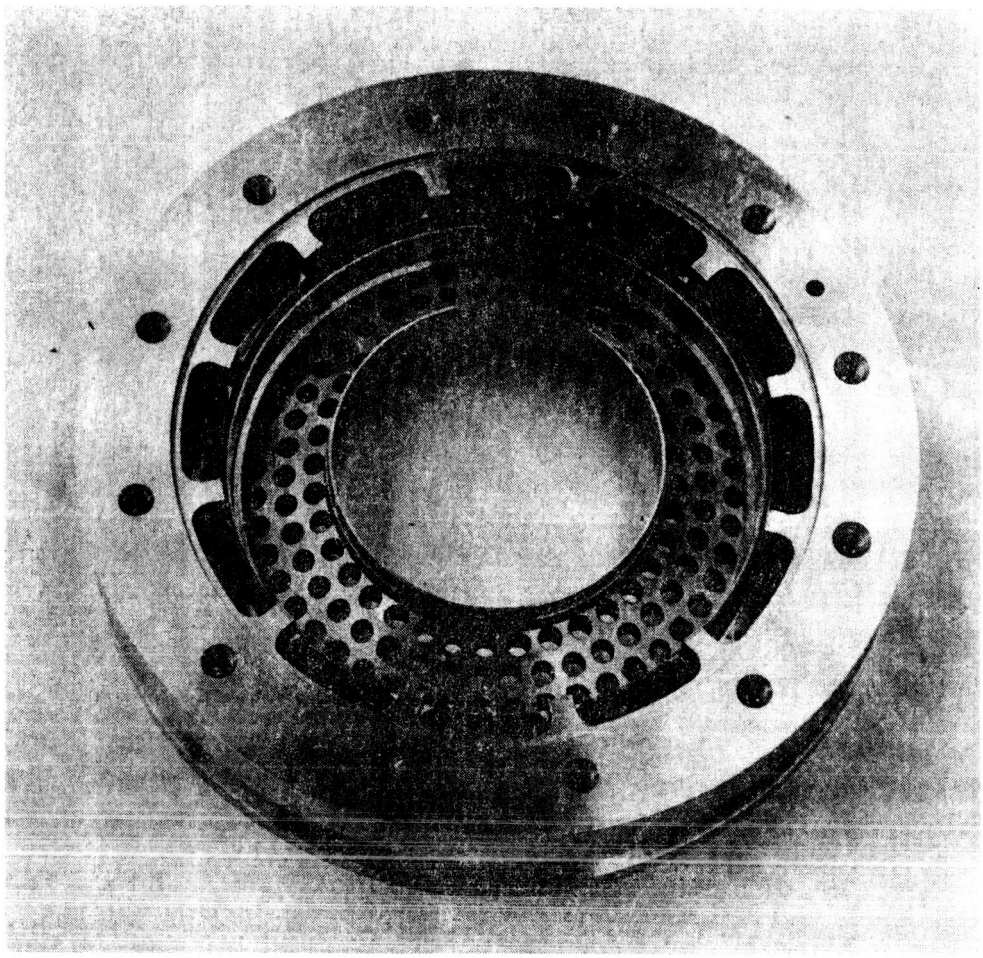

Figure 49. Secondary Injector - View of Body, Face Side Before Brazing

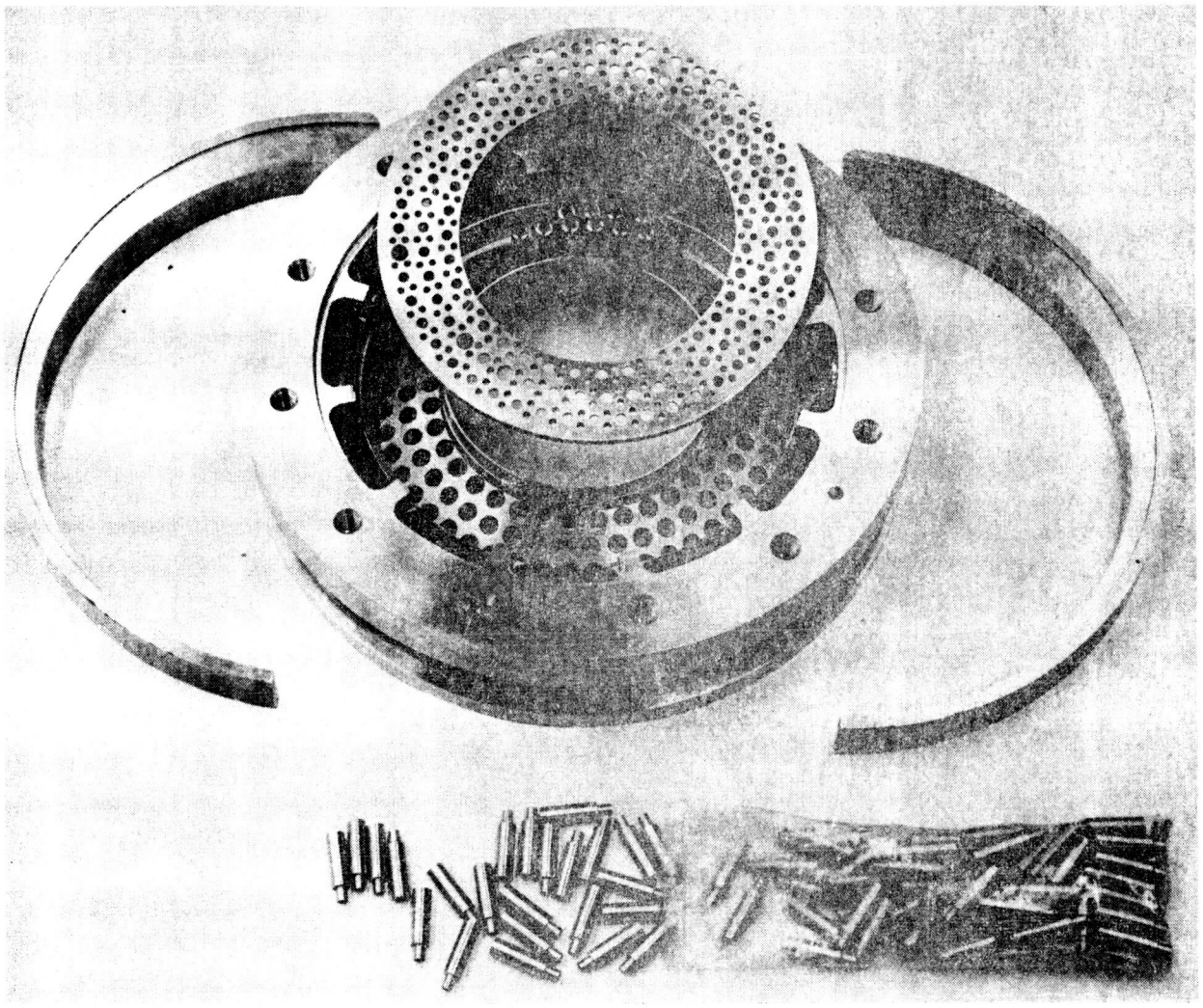

Body, Strongback, Fuel Manifold Split Rings
and Oxidizer Twirler Tubes

Figure 50. Secondary Injector - Photograph of Components

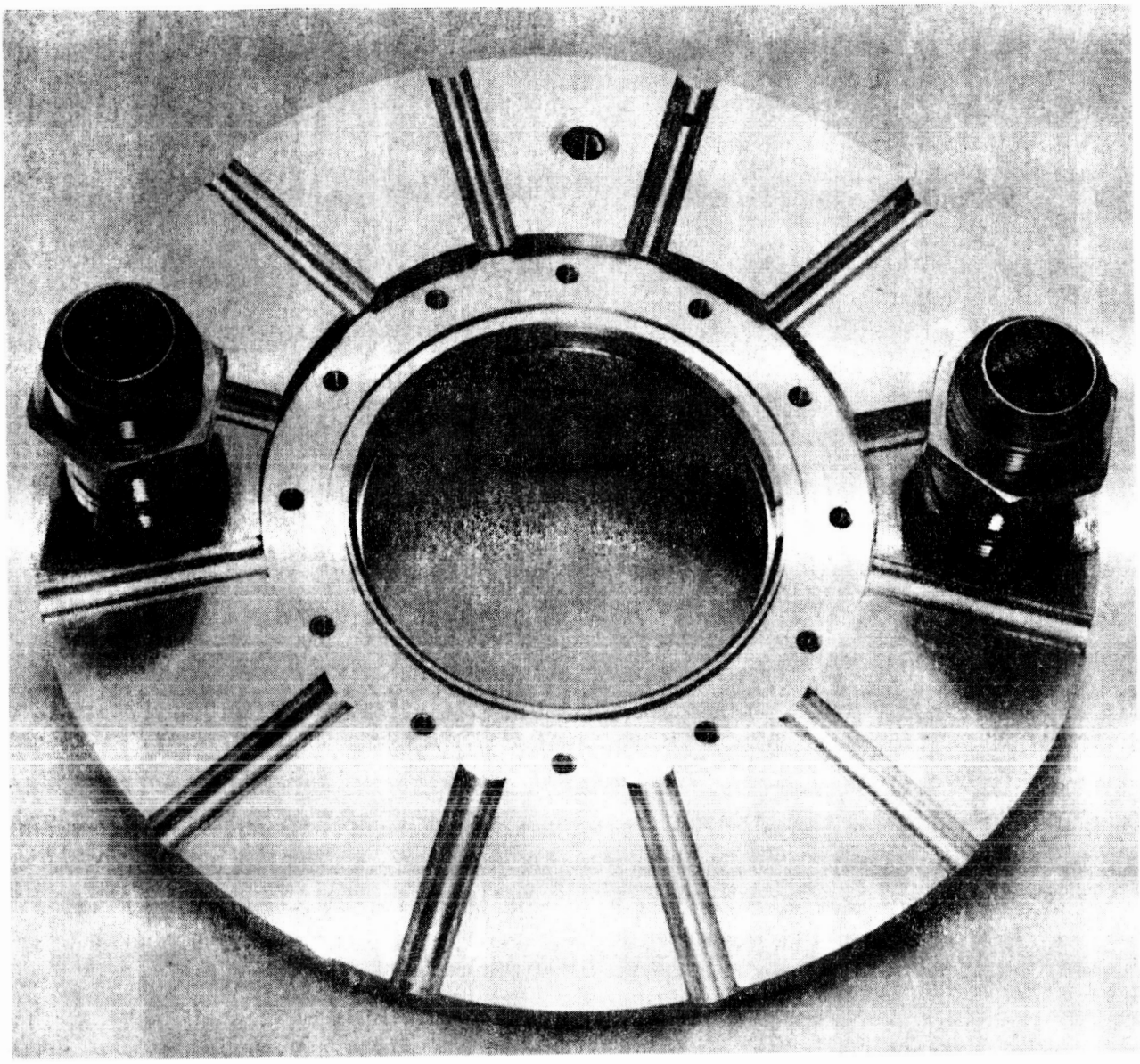

Figure 51. Secondary Injector - Oxidizer Cover External Side

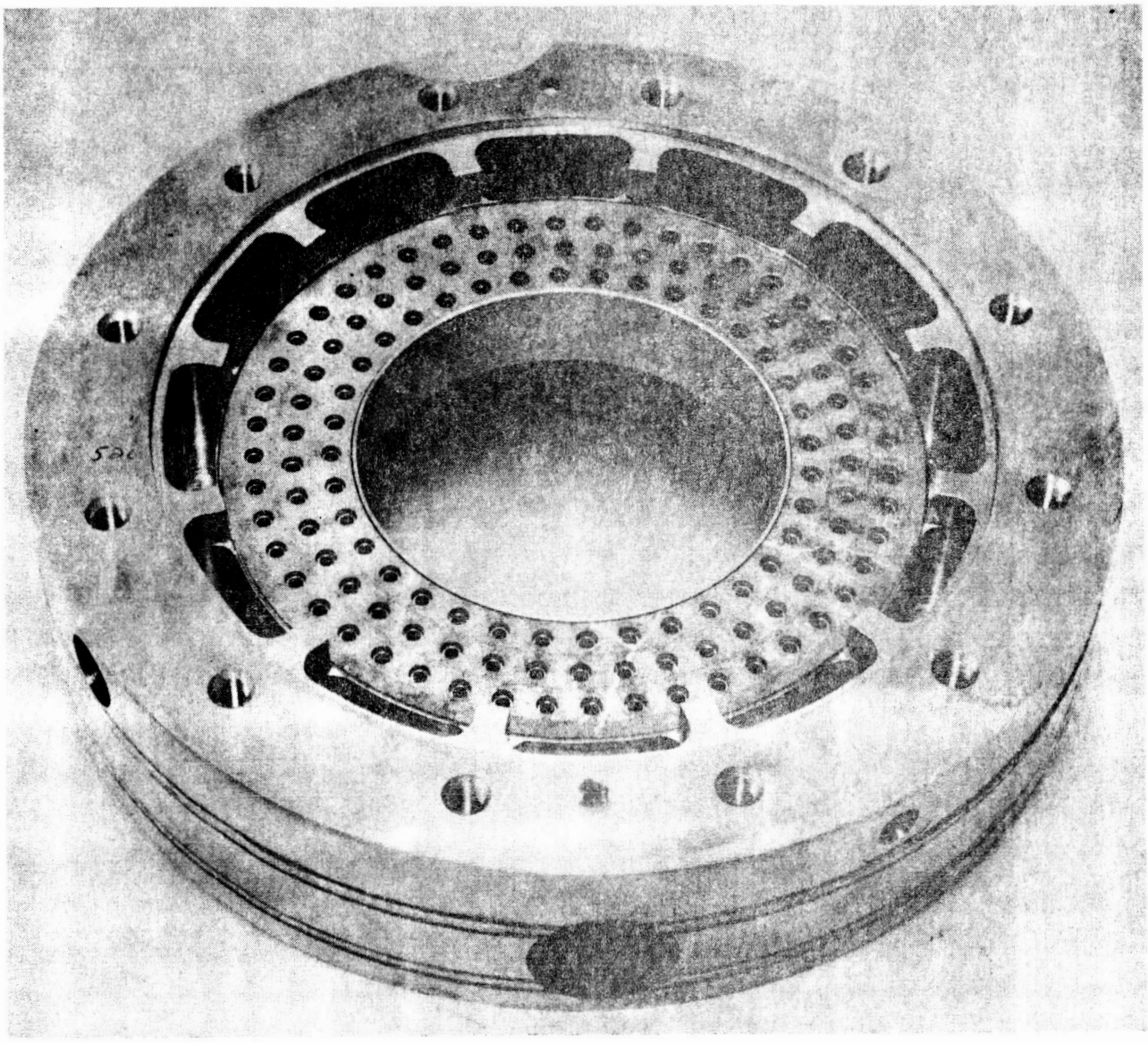

Figure 52. Secondary Injector - Face Side After First Braze

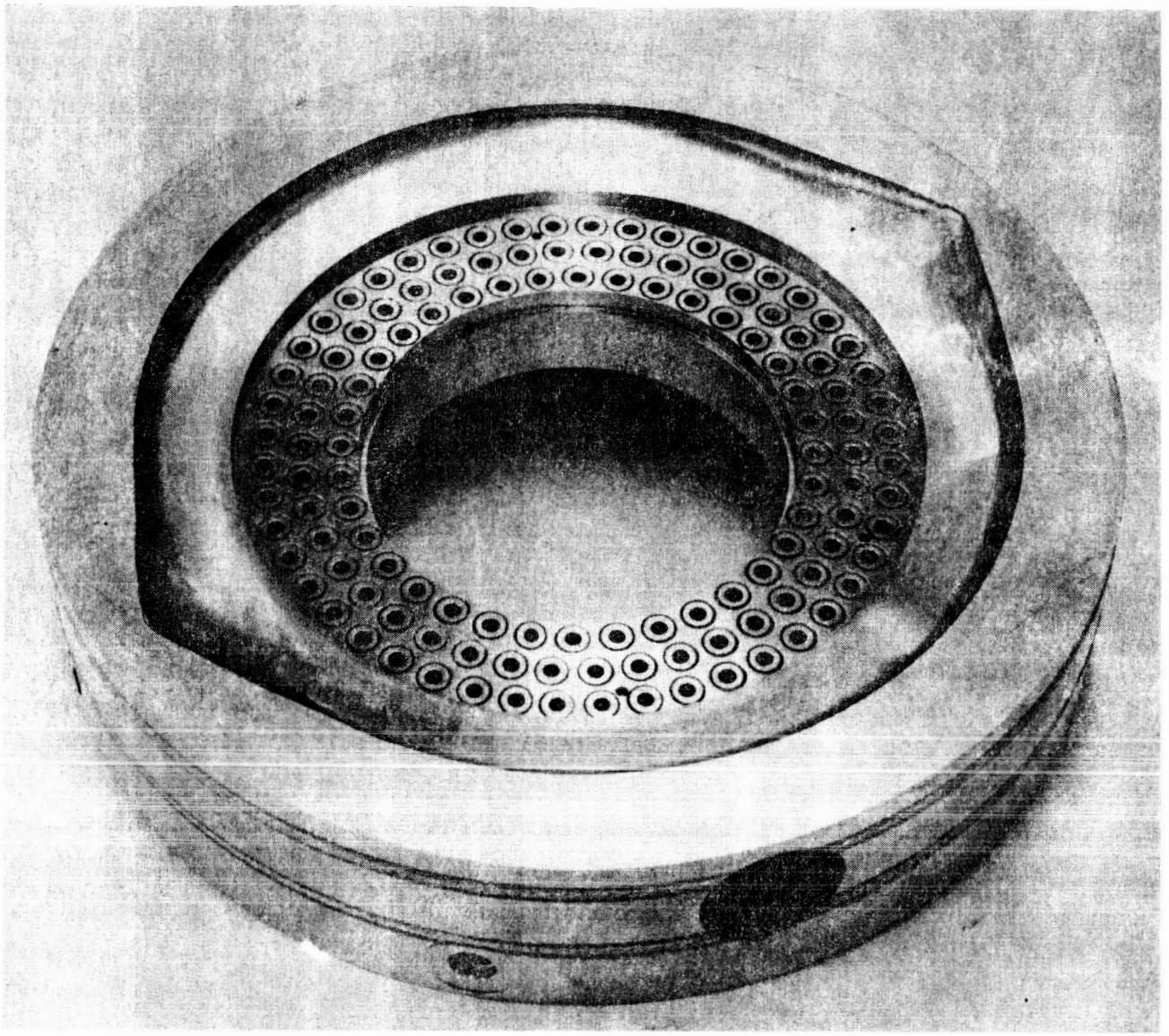

Figure 53. Secondary Injector - Oxidizer Cavity Side After First Braze

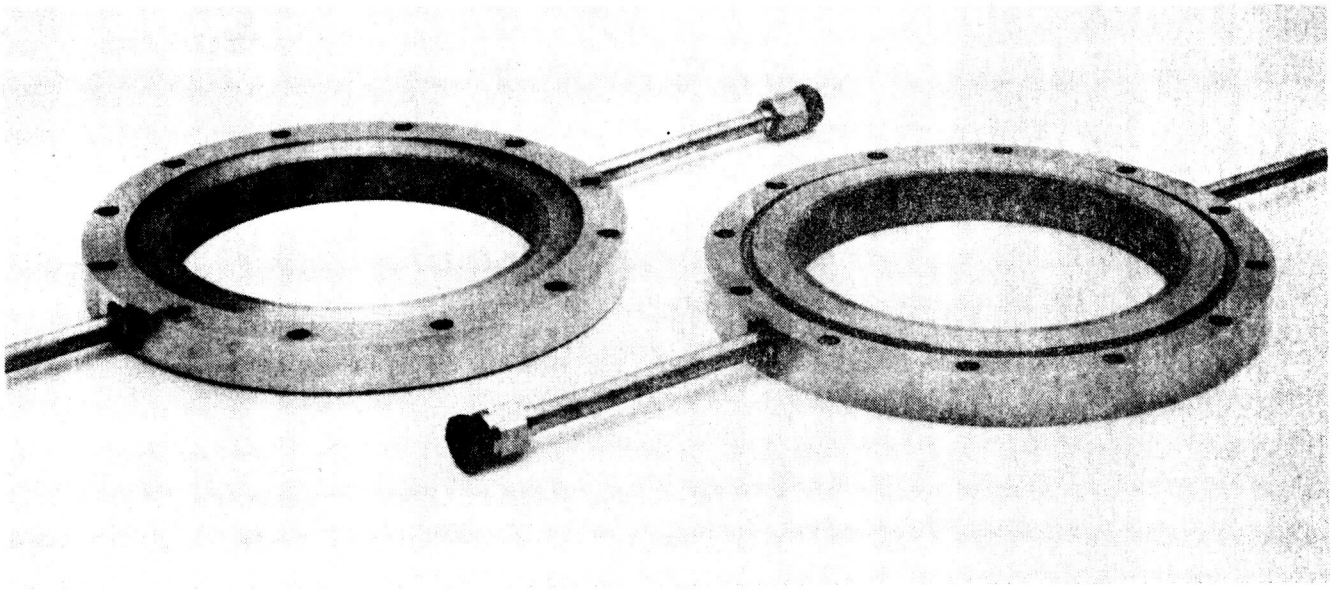

Figure 54. L' Spacer Rings Showing Both Forward and Aft Sides

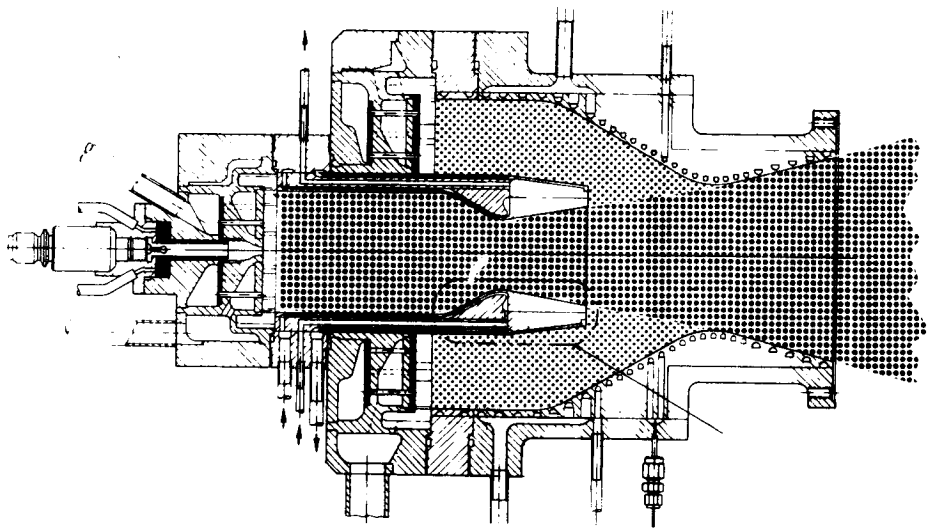

DETERMINE: C*, Φ_P & Φ_S PROFILES

CALIBRATE: COOLANT FLOWRATES

TESTS: 23

DURATION: 1 - 6 SECONDS

HOT-FIRE TEST PRIMARY CHAMBER WITH BLEED FLOW

- INSTRUMENTATION, TRANSIENTS, STABILITY
- BLEED FLOW SURVEY (PcP = 500 PSIA, MRP = 5, Le = NOMINAL)
- BLEED FLOW SURVEY (PcP = 500, MRP = 5, Le = SHORT)
- BLEED FLOW SURVEY (PcP = 500, MRP = 5, Le = LONG)
- PcP, MRP, BLEED FLOW SURVEY (PcP = 750 - 1000, MRP = 2 - 7, Le = NOMINAL)
- HOT GAS BLEED FLOW SURVEY (PcP = 500, MRP = 5, Le = NOMINAL, T_{BLEED} = 1000°F)

Figure 55. Dual Throat Thruster Thermal Model (Test Plan - Mode II Operation)

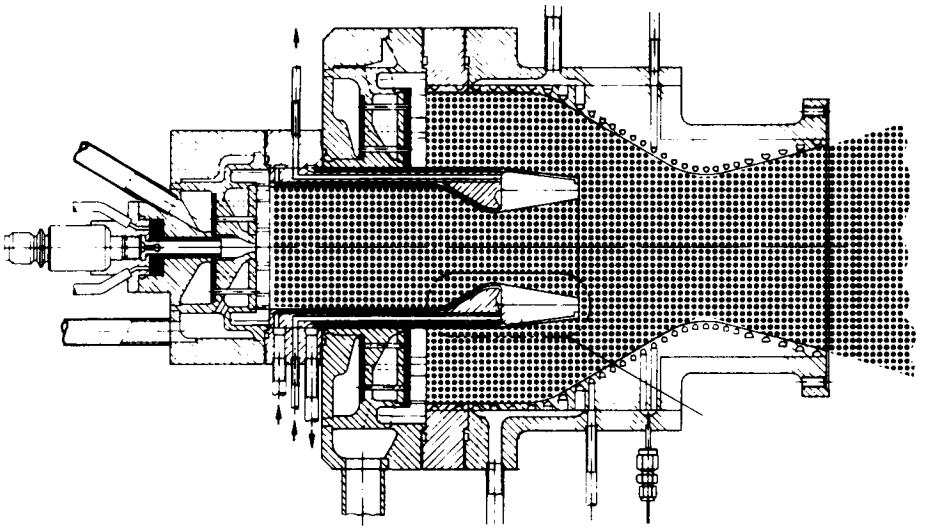

DETERMINE: C*, ϕ_P & ϕ_S PROFILES

CALIBRATE: COOLANT FLOWRATES

TESTS: 13

DURATION: 1 - 6 SECONDS

HOT-FIRE TEST BOTH CHAMBERS (PARALLEL BURN)

- INSTRUMENTATION, TRANSIENTS, STABILITY
- PC, MR SURVEY (PcP = 500-1000, MR = 2-7, PCR = 0.7)
- PCR SURVEY (PCR = 0.5 - 0.85, PcP = 500, MRP = 5)
- MR SURVEY (MRP/MRS = 7/2 - 2/7, PcP = 500, MRP = 5, PCR = 0.7)
- Le SURVEY (Le = SHORT - LONG, PcP = 500, MRP = 5, PCR - 0.7)

Figure 56. Dual Throat Thruster Thermal Model (Test Plan - Mode I Operation)

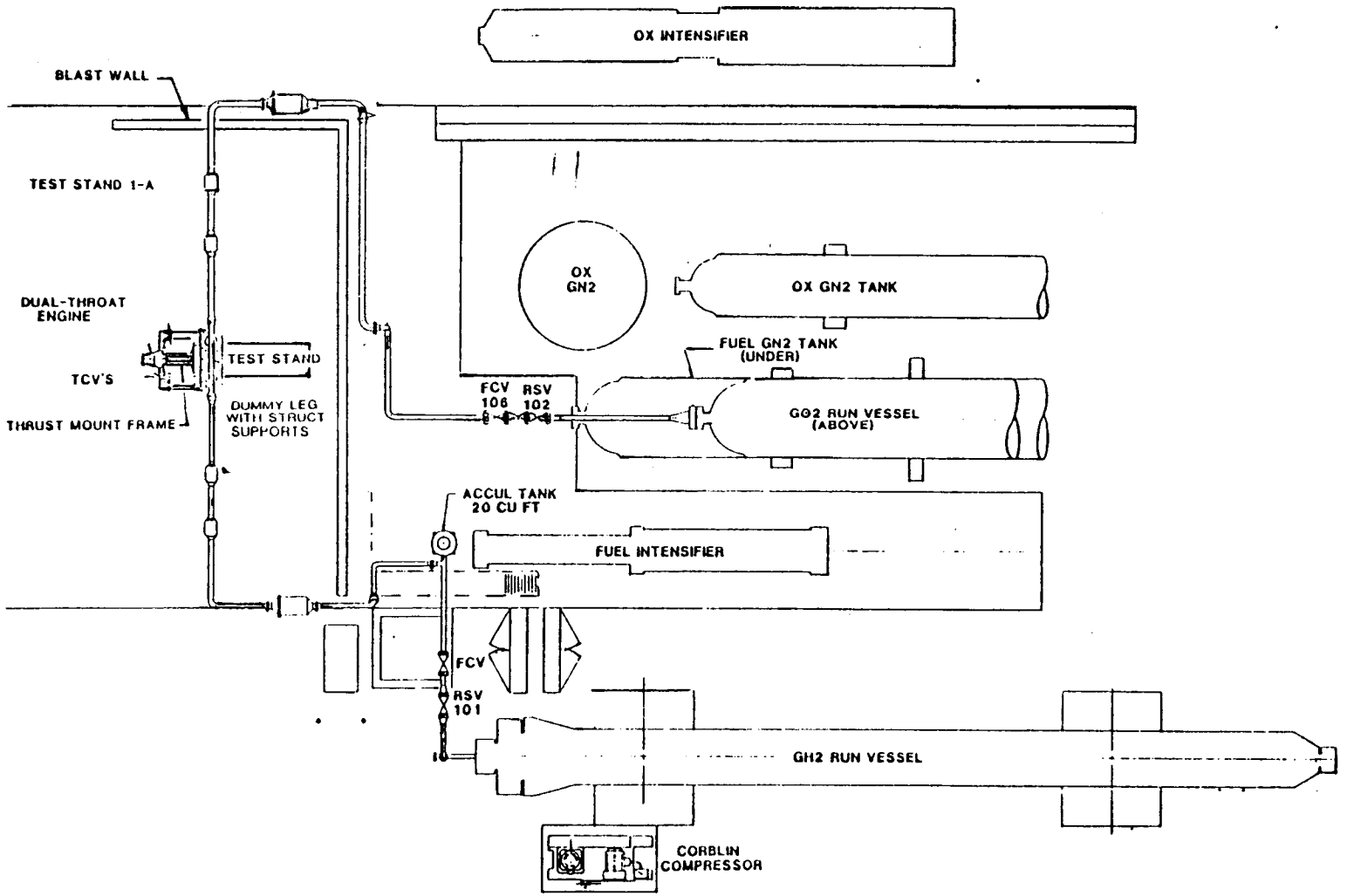

Figure 57. J-1A. Dual Throat Thruster Test Facility GO_2 and Fuel Piping Layout

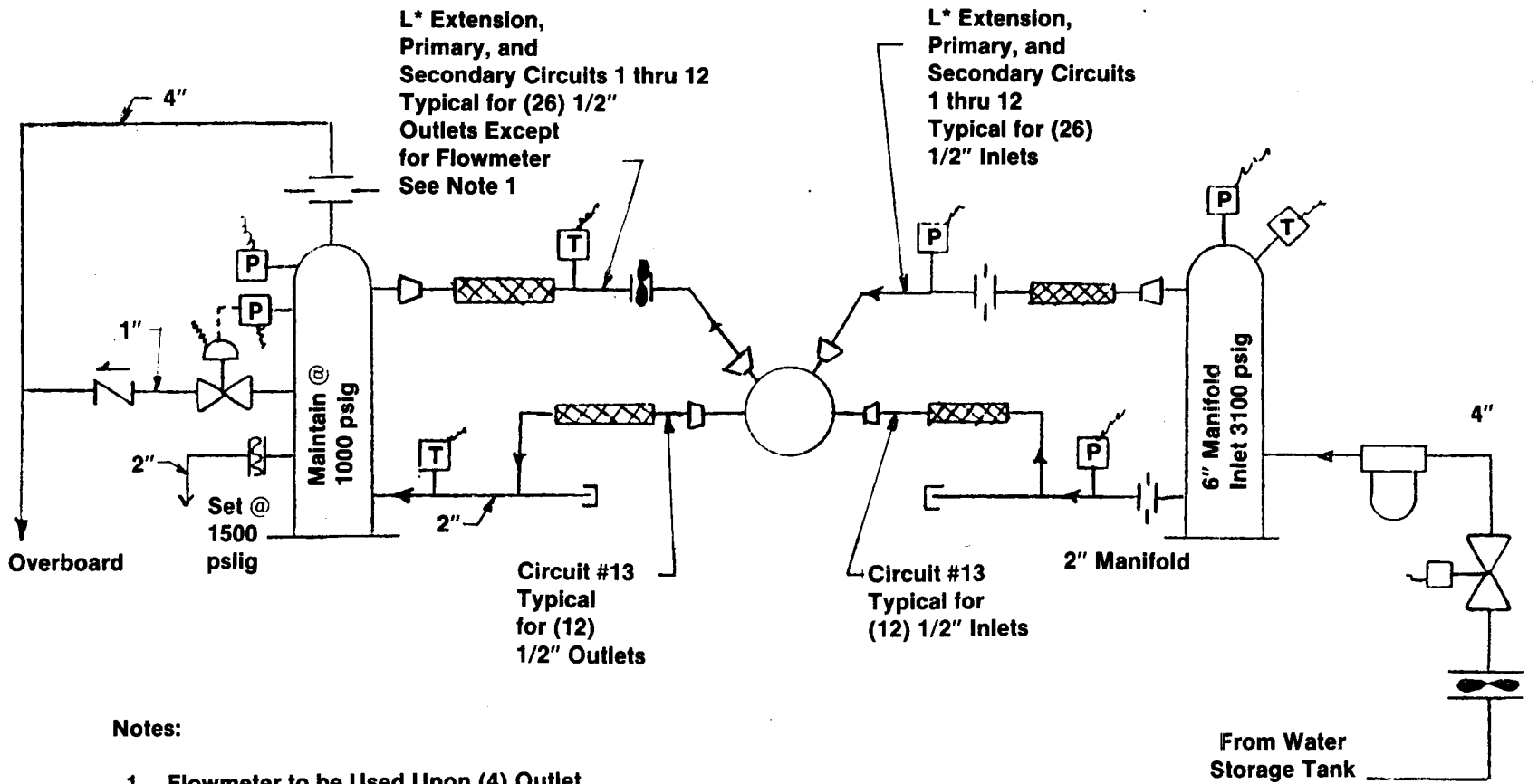

Notes:

1. Flowmeter to be Used Upon (4) Outlet Circuits Per Test. Engineering to Provide Required Circuit Numbers
2. (10) I.D. Diameters to be Provided Upstream and Downstream of Flowmeters and Orifices
3. Individual Circuits to be Flowed and KW's Established Prior to Testing

AEROJET LIQUID ROCKET COMPANY TEST DIVISION	
TEST SKETCH	
TITLE: J1A DUAL THROAT CALORIMETER TEST SET UP	
NO.:	DATE: 11-5-02
DRAWN BY: DRUTT	APPROVED:

Figure 58. J-1A Dual Throat Calorimeter Water Flow Circuits

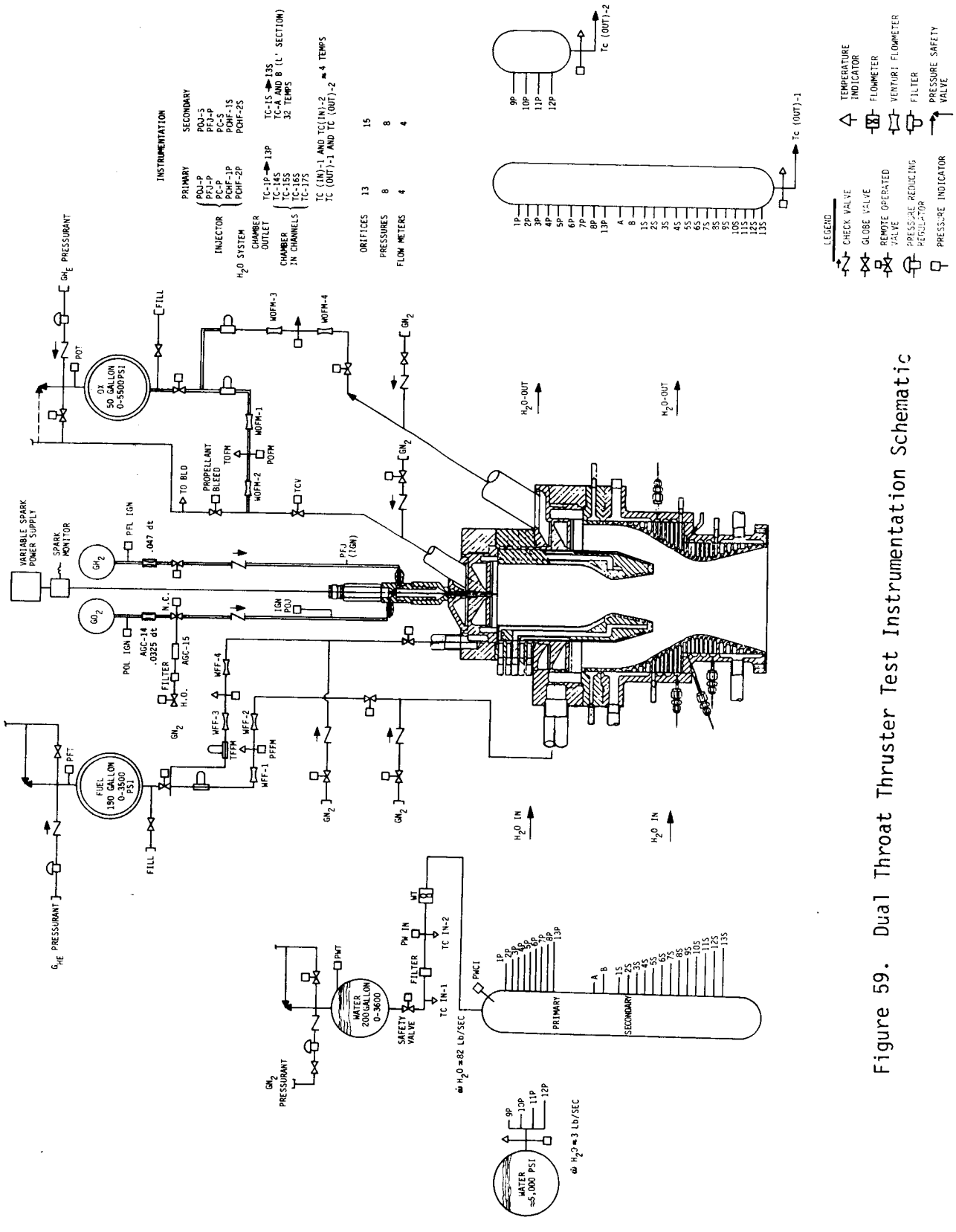

Figure 59. Dual Throat Thruster Test Instrumentation Schematic

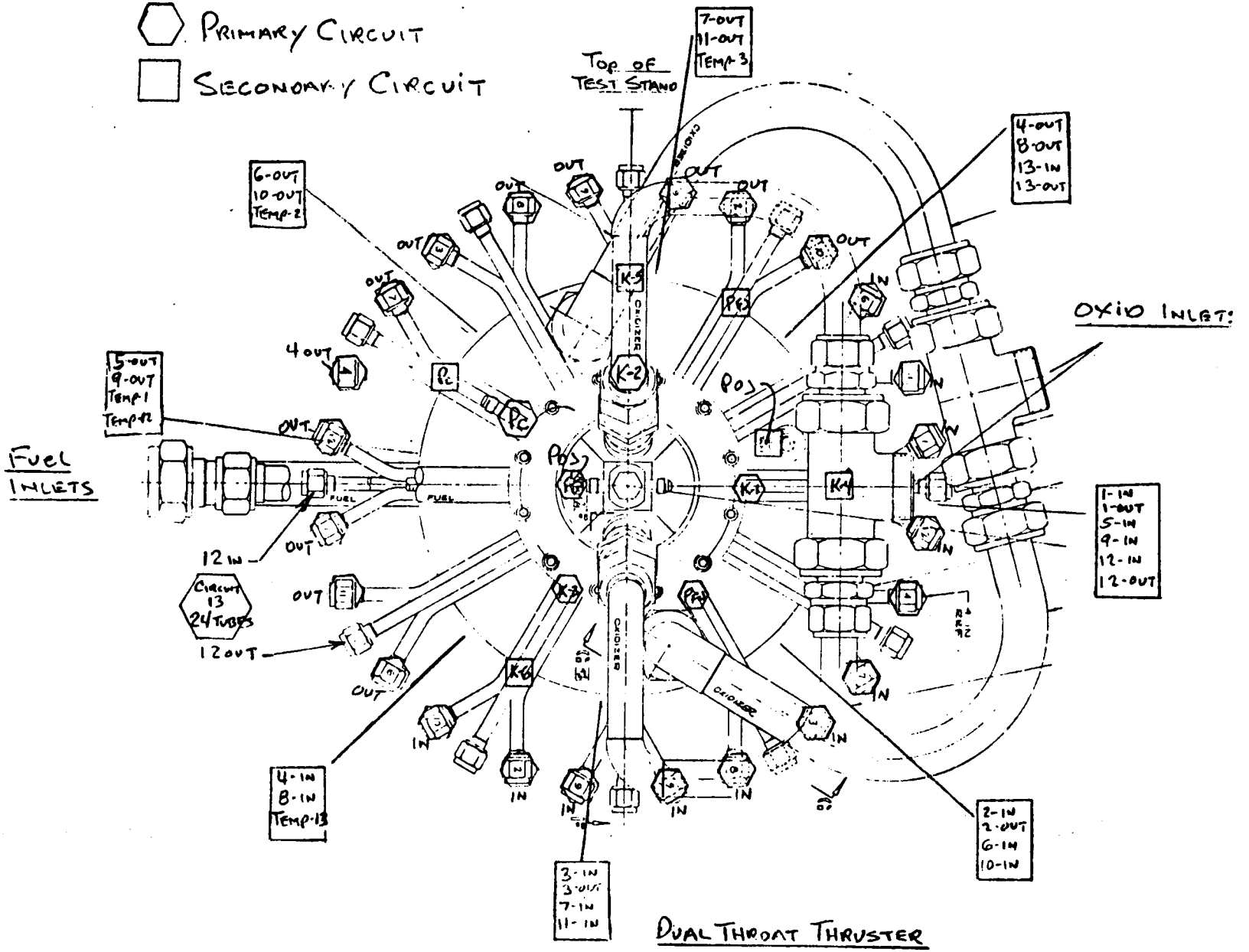
PRIMARY CIRCUIT
SECONDARY CIRCUIT
TOP OF TEST STAND
7-OUT
11-OUT
TEMP-3
4-OUT
8-OUT
13-IN
13-OUT
6-OUT
10-OUT
TEMP-2
OXIDIZER
OXIDIZER
OXIDIZER

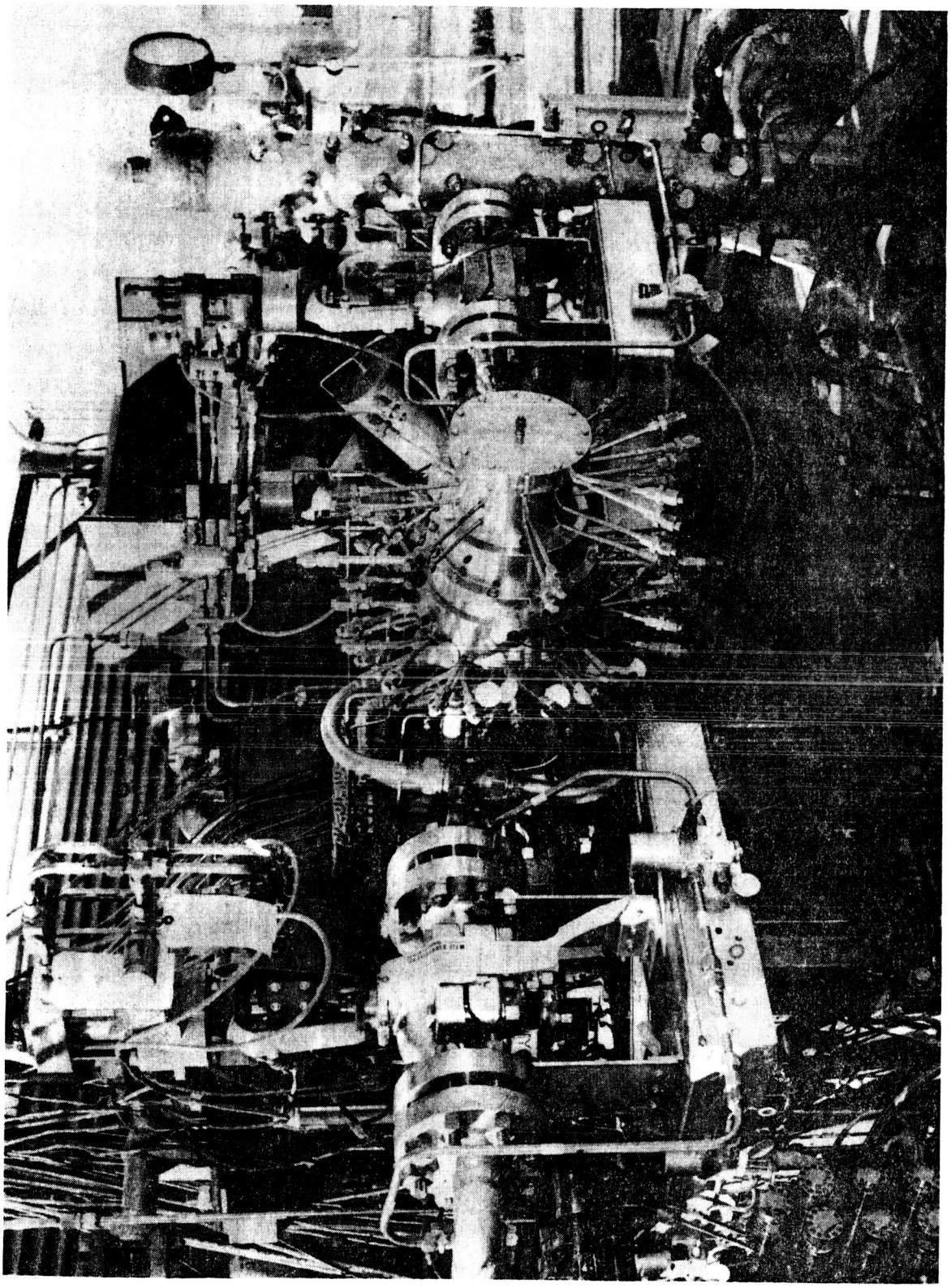

Figure 61. Dual Throat Test Setup on J-1A Test Stand (C1183 033)

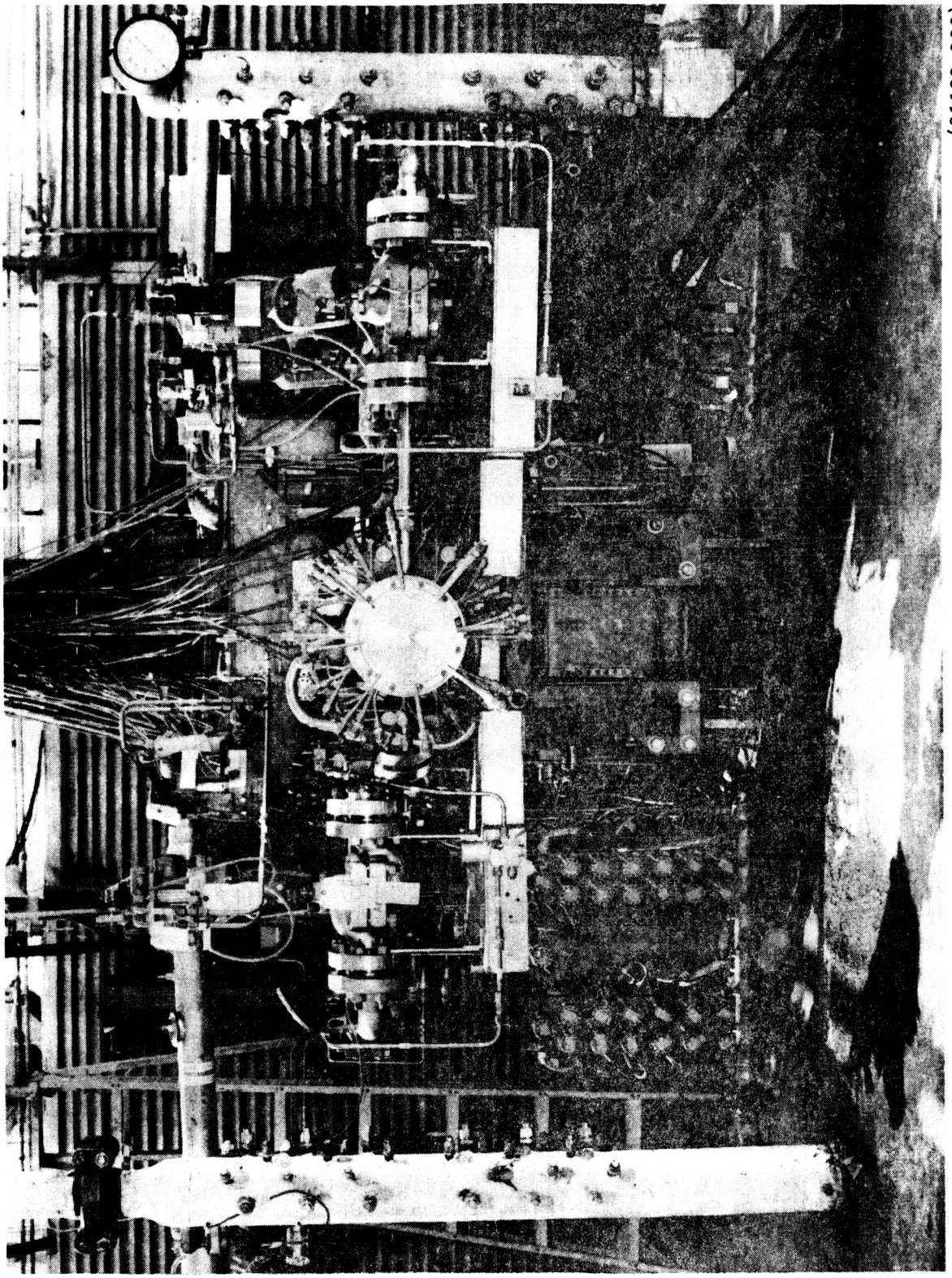

(C1183-032)

Figure 62. Dual Throat Test Setup on J-1A Test Stand

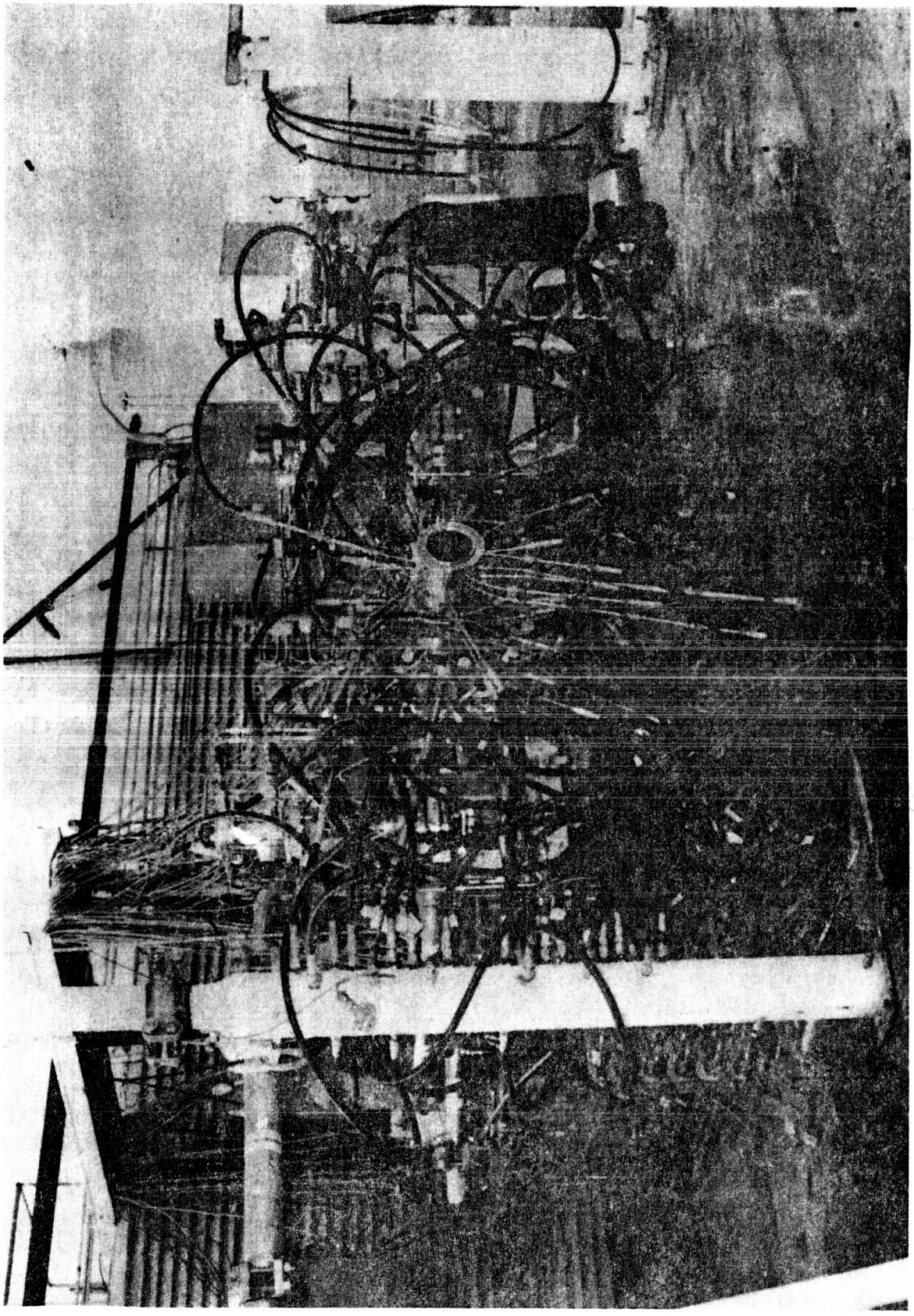

Figure 63. Dual Throat Test Setup on J-1A Test Stand (C1283 047)

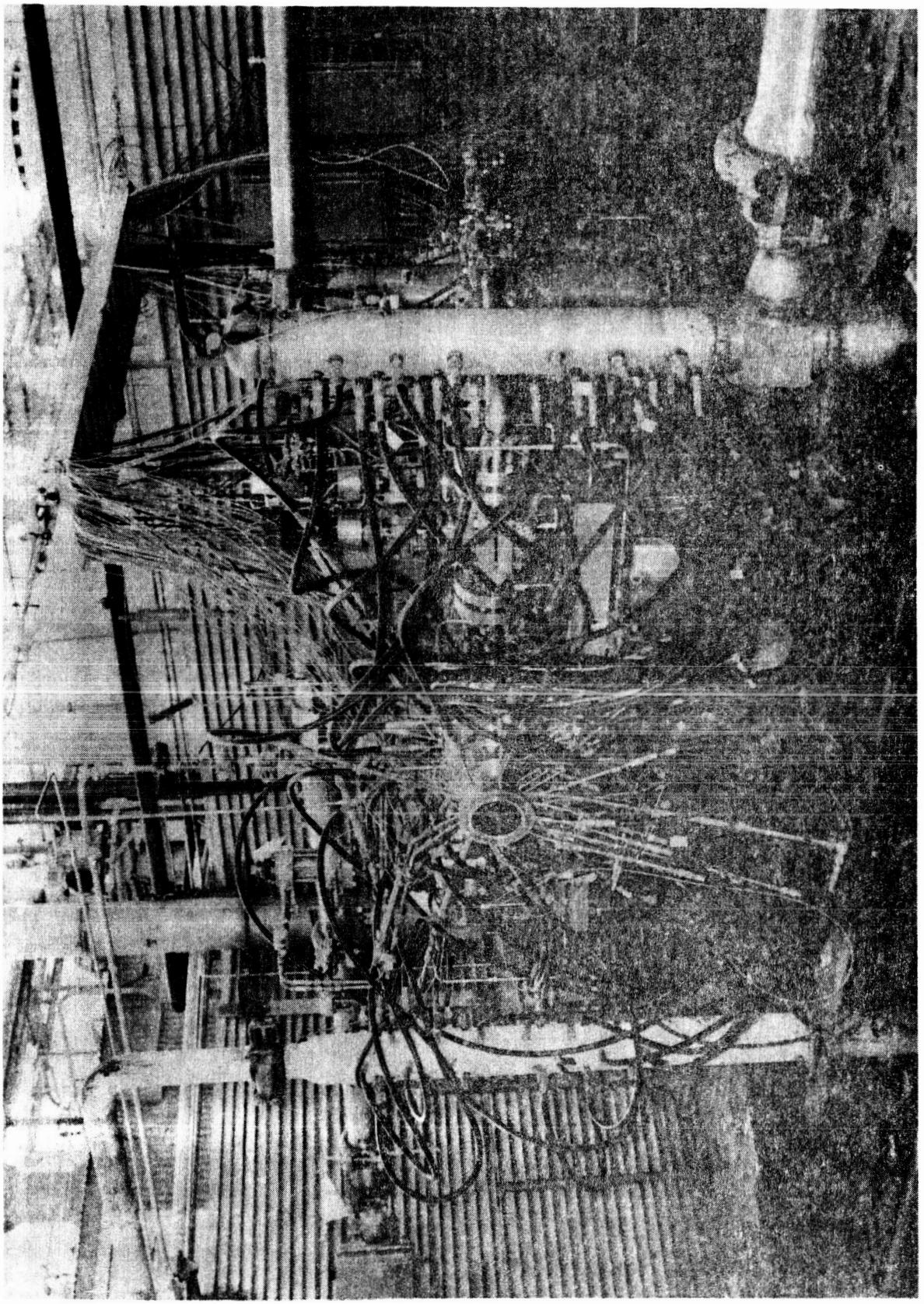

Figure 64. Dual Throat Test Setup on J-1A Test Stand (C1283 045)

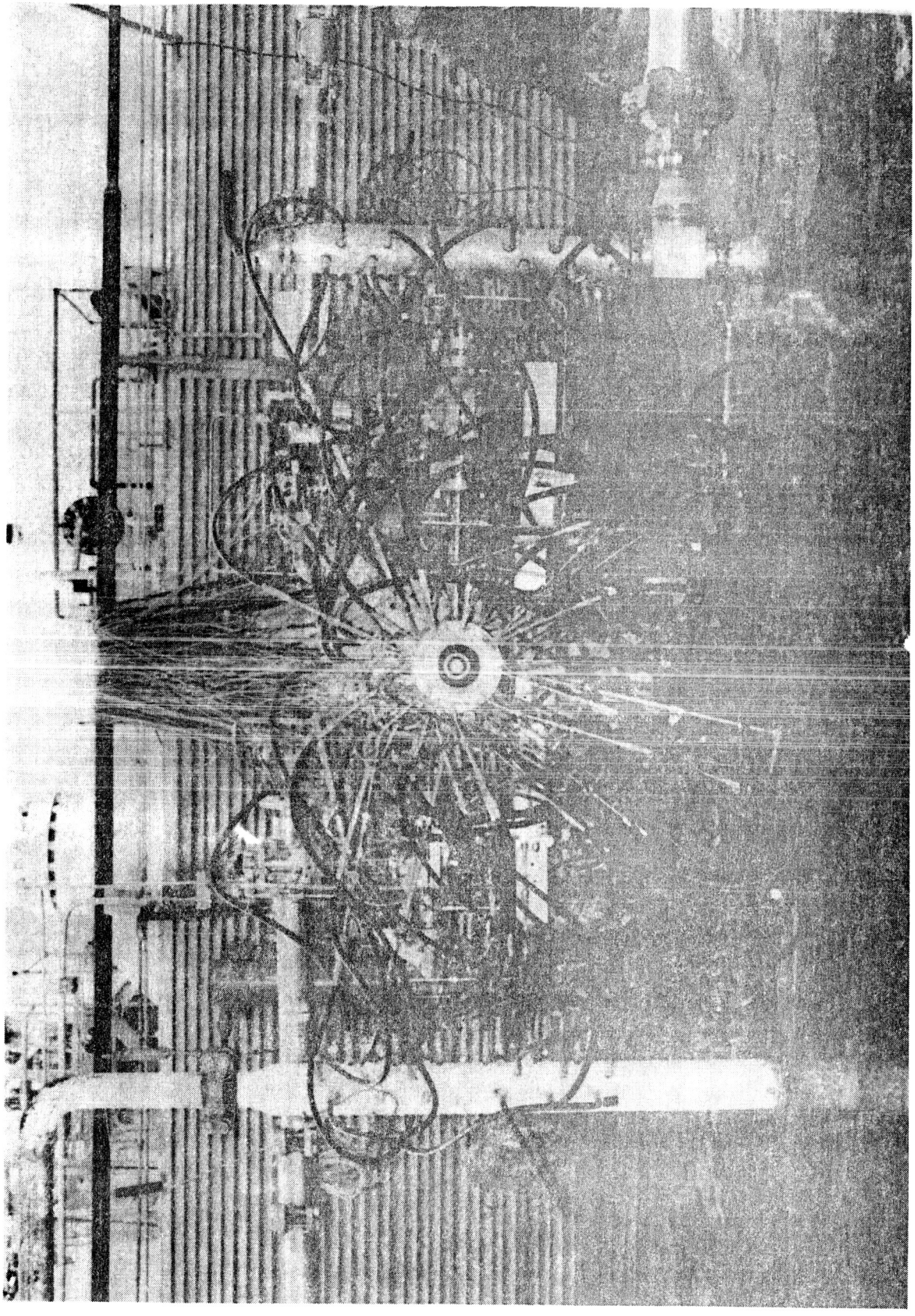

Figure 65. Dual Throat Test Setup on J-1A Test Stand (C1283 044)

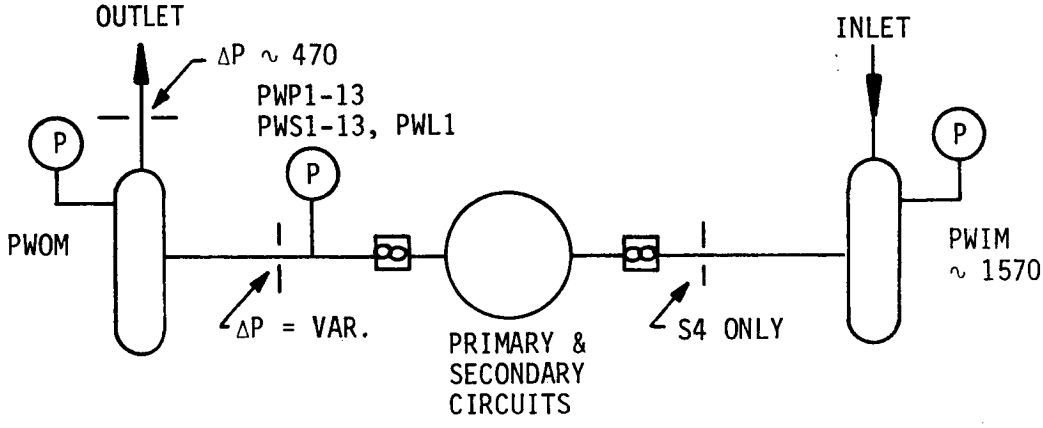

Inlet Flow Rate FWIM
Outlet Flow Rate FWOM
Inlet Water Pressure PWIM
Outlet Water Pressure PWOM

(See Table XVII for additional definitions)

Figure 66. Calibration Flow Circuit Schematic

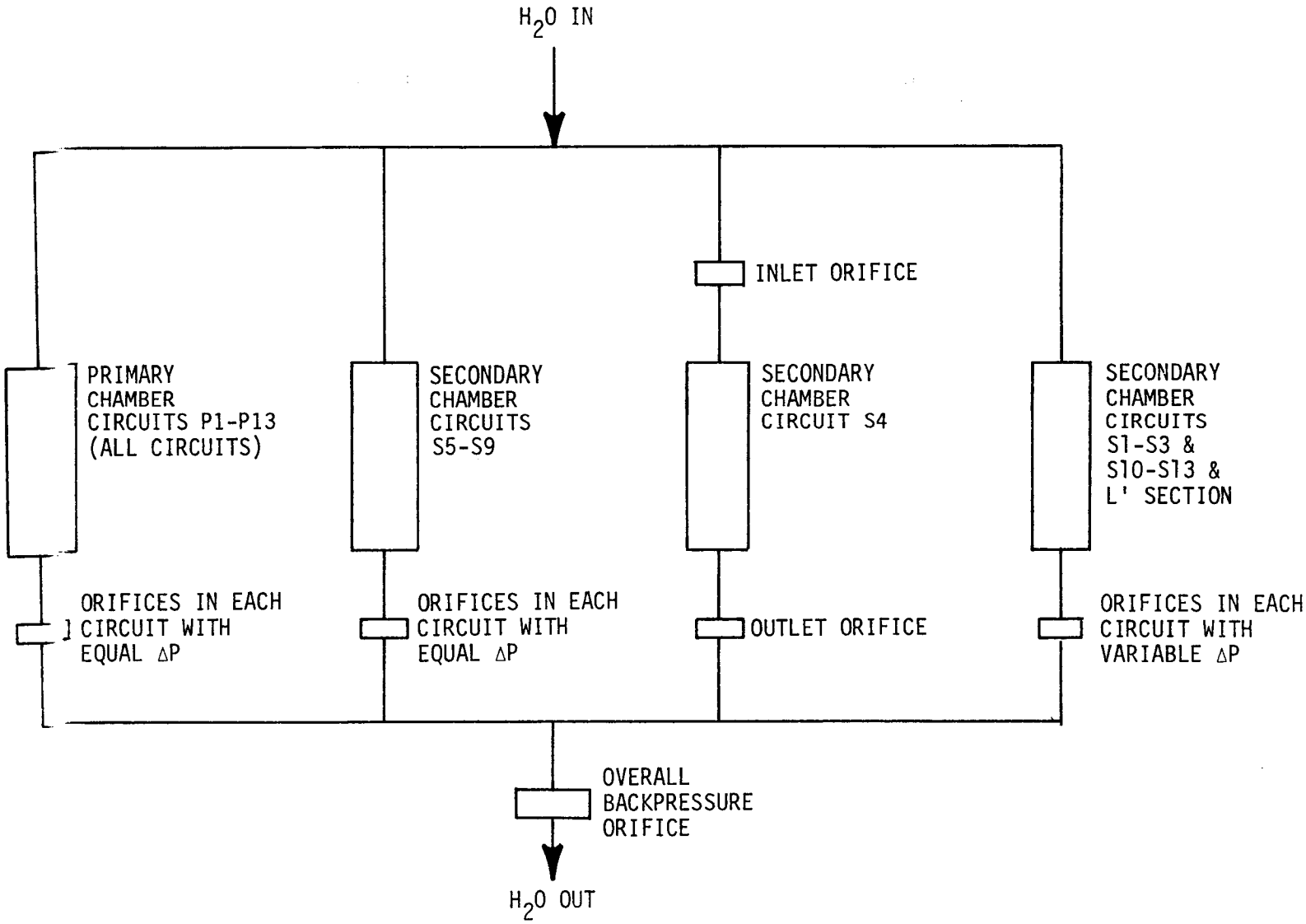

Figure 67, Dual Throat Coolant Orificing Scheme

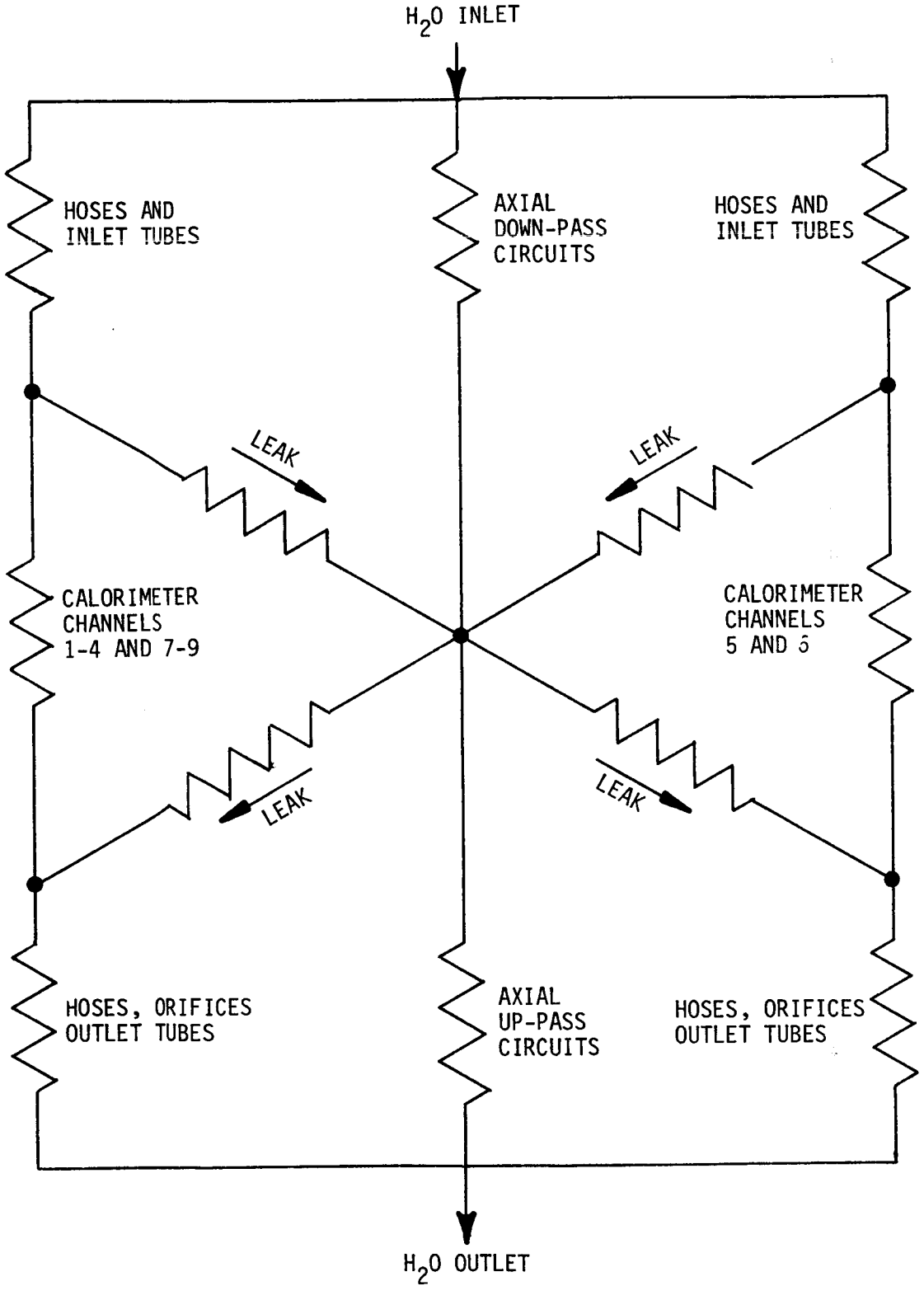

Figure 68. Hydraulic Model for the Primary Chamber Coolant System

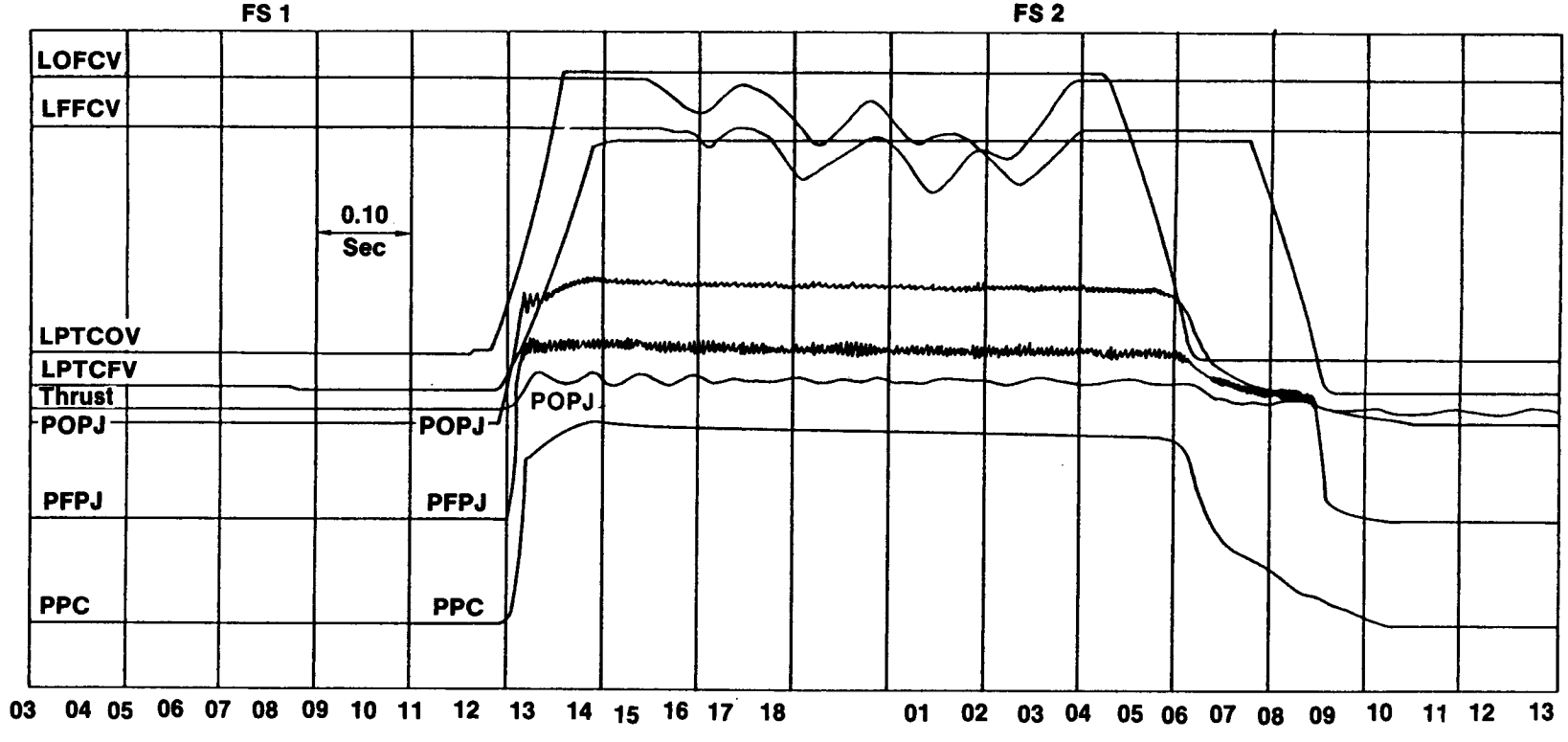

Figure 69a. Test 105 Start/Shutdown Sequence (1 of 2)

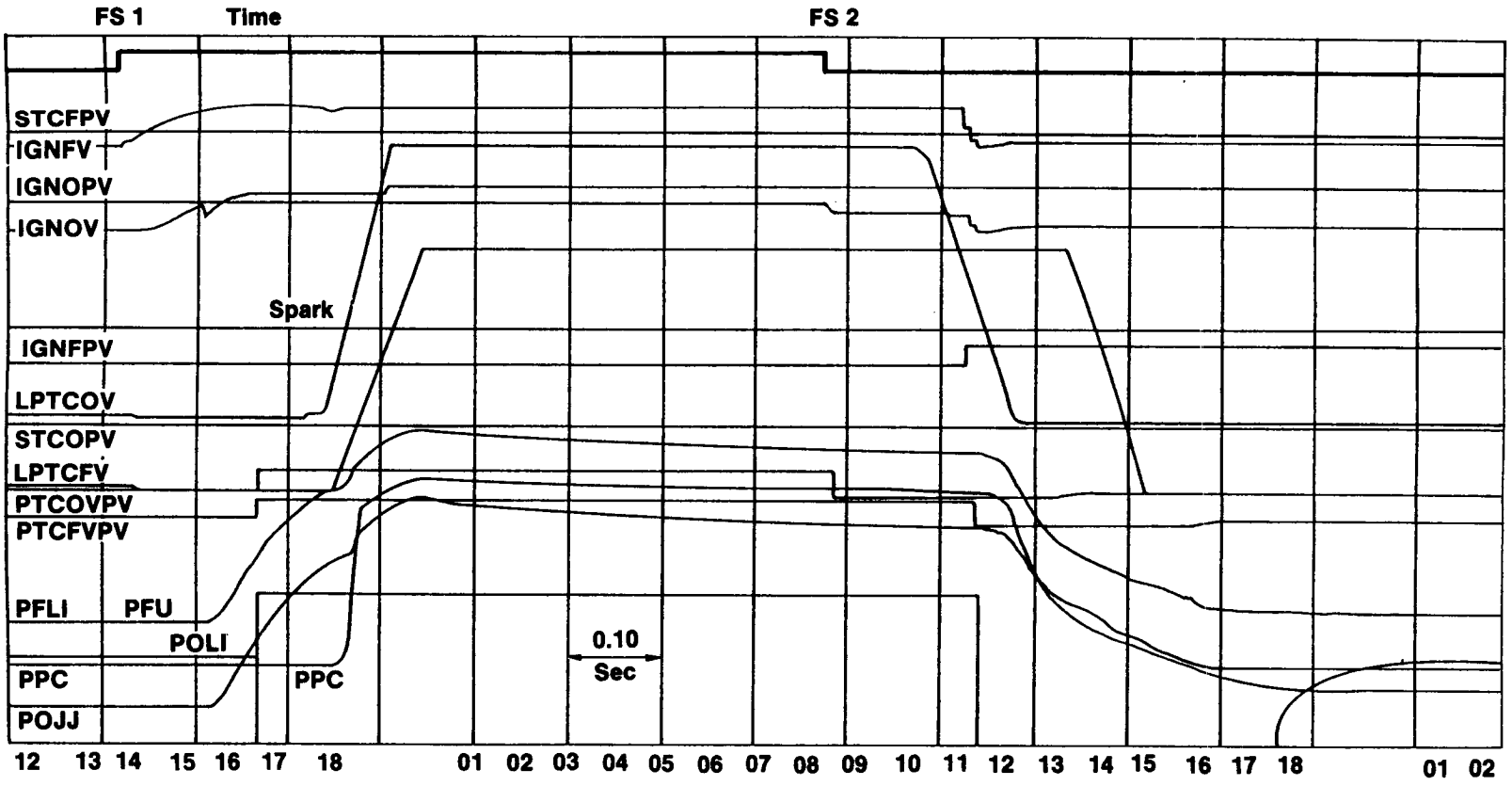

Figure 69a. Test 105 Start/Shutdown Sequence (2 of 2)

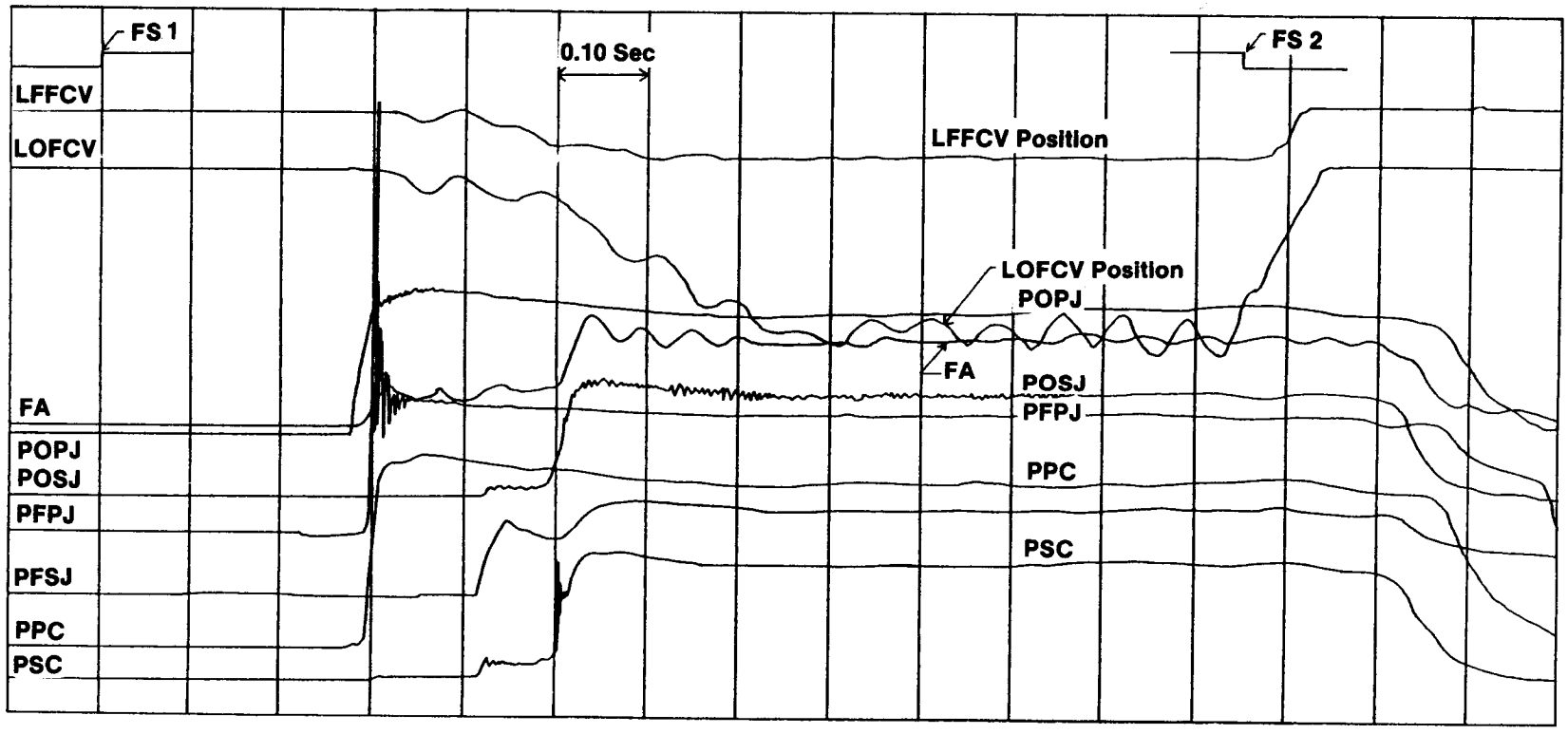

Figure 69b. Test 115/Start/Shutdown Sequence

V. DATA ANALYSIS

A. OBJECTIVES

The objectives were as follows: (1) reduce and display the test data in the form of heat flux profiles for individual tests and heat flux variations with test parameters, (2) compare model predictions with the test data to identify inconsistencies, and (3) upgrade the model so that final predictions agree with the data variations.

B. APPROACH

1. Primary Mode II and Secondary Mode I

Heat flux data from these operating regimes were interpreted in terms of turbulent pipe flow correlation coefficients. Development of a stream tube moded for the secondary flow was necessary to define freestream mass velocities and other combustion product expansion characteristics. The purpose of this approach was to show that conventional correlation coefficients could be applied to the dual throat concept for the primary chamber in Mode II and the secondary in Mode I.

2. Primary Mode I

Changes in heat flux relative to Mode II as a result of the back pressure imposed by the secondary chamber were evaluated as a function of chamber pressure ratio and nozzle spacing. Therefore, these data are presented as Φ_I/Φ_{II} . Correlation coefficient ratios are actually used to account for differences in primary chamber operating conditions between modes.

3. Primary Chamber Tip

Tip heat fuxes were correlated with the primary nozzle and secondary annulus heat fluxes just upstream of the tip.

V, B, Approach (cont.)

4. Secondary Mode II

The purpose of the data analysis task in this operating regime was to define empirical parameters or correlations in the aerodynamic and thermal models of Task I. These parameters had been tentatively defined based on cold flow tests and simulation of two-dimensional finite difference boundary layer analyses.

C. RESULTS

1. Primary Mode II

In Mode II testing the primary nozzle operates in a conventional manner, i.e., with very low ambient pressure relative to the chamber pressure. These results are considered first in order to provide a reference for evalution of the effects of the high back pressure imposed by Mode I operation. Since the main purpose of the Mode II testing was to evaluate the effect of bleed flow variations on the secondary throat region, a limited number of primary chamber operating conditions were obtained. These conditions are summarized in Table XXVI, and the measured heat flux profiles are included in Appendix B. In general, the heat flux data are consistent with the design predictions as illustrated in Figure 70 for Test 111.

All measured heat fluxes, including circuit P9 assuming no base heating, have been used to define normalized correlation coefficients from the following pipe flow model:

$$q_w = 0.026\, C_g \rho_f U_e C_p Re_{D_f}^{-0.2} Pr_f^{-0.6} (T_{aw} - T_w)$$

TABLE XXVI

MODE II TEST SUMMARY

Test Number	Primary Pc psia	Primary O/F	Bleed Flow %	Comments
111-114	530	7.1	1.4 - 3.9	Before Primary Chamber Repair
137-139	680	6.8	0 - 2.5	Repaired Primary Chamber, Leakage at Primary Tip
140-142	670	3.0	0 - 2.6	Same as 137 - 139

V, C, Results (cont.)

in which subscript f refers to property evaluation at a film temperature defined as 0.5 ($T_{aw} + T_w$). Wall temperatures were determined by two-dimensional conduction network analyses of the coolant channels for each circuit using the measured heat flux as a boundary condition. Two models were considered for the specific heat: (1) the conventional frozen specific heat from TRAN72 evaluated at the film temperature and (2) the reactive specific heat defined by

$$Cp_R = \frac{H_{aw} - H_w}{T_{aw} - T_w}$$

It was found that the frozen specific heat failed to predict the mixture ratio trends of the Primary Mode II data, i.e., a Cg dependence on mixture ratio was obtained. Use of the reactive specific heat eliminated this problem, as shown in Figure 71 by the excellent Cg agreement between Tests 137-139 at a mixture ratio of 6.8 and Tests 140-142 at a mixture ratio of 3.0. Cg variation from test to test within a series was very small except for circuit P9. Data from the latter indicate a probable base heating effect since the highest Cg is always associated with the lowest bleed flow rate; Figure 71 includes the average Cg for the higher bleed flow rates. Computer printouts from the reactive model Cg analysis are presented in Table XXVII.

The Cg data of Figure 71 indicate a number of anomalies in the spatial distributions and in the comparison between the test series before (111-114) and after (137-142) the repair of the primary chamber. The spatial distribution anomalies, such as the high values for circuit P7 on Tests 111-114 and for circuit P1 on Tests 137-139, are probably related to inadequacies in the internal leakage model. Some reduction in Cg between circuits P1 and P2 is to be expected due to flow acceleration. It is apparent from the two different Cg profiles that the hardware repair changed the internal leakage pattern. Comparison of the data of Figure 71 with heat sink chamber data

TABLE XXVII

PRIMARY SURFACE ANALYSIS MODE II TEST 111

	PC PSIA	MR	WT LB/S
PRIMARY	528.0	7.110	5.25
SECONDARY	37.0	0.000	0.21

PRESSURE RATIO = .070

CKT	Z	R	EPS	TR R	TWG R	HG THEOR	FLUX MEAS	CG	S	DEQG	AFLOWG
1	-0.201	0.884	1.06	6507.	1050.	0.744E-02	27.16	0.669	6.004	1.767	2.454
2	0.000	0.960	1.00	6494.	1010.	0.772E-02	26.52	0.626	6.206	1.720	2.324
3	0.211	0.884	1.06	6469.	970.	0.719E-02	21.73	0.549	6.419	1.768	2.455
4	0.512	0.937	1.19	6411.	915.	0.614E-02	19.10	0.566	6.725	1.874	2.758
5	0.853	0.997	1.34	6385.	910.	0.535E-02	19.06	0.651	7.071	1.994	3.123
6	1.214	1.061	1.52	6361.	820.	0.467E-02	14.80	0.572	7.437	2.121	3.534
7	1.580	1.125	1.71	6334.	940.	0.408E-02	16.49	0.749	7.810	2.251	3.978
8	1.879	1.178	1.88	6311.	830.	0.367E-02	13.13	0.654	8.113	2.356	4.359
9	2.017	1.202	1.95	6300.	750.	0.349E-02	11.31	0.584	8.253	2.404	4.541

PRIMARY SURFACE ANALYSIS MODE II TEST 112

	PC PSIA	MR	WT LB/S
PRIMARY	524.0	7.110	5.21
SECONDARY	35.0	0.000	0.19

PRESSURE RATIO = .067

CKT	Z	R	EPS	TR R	TWG R	HG THEOR	FLUX MEAS	CG	S	DEQG	AFLOWG
1	-0.201	0.884	1.06	6507.	1045.	0.739E-02	27.29	0.676	6.004	1.767	2.454
2	0.000	0.960	1.00	6494.	1000.	0.768E-02	26.22	0.622	6.206	1.720	2.324
3	0.211	0.884	1.06	6469.	960.	0.715E-02	21.43	0.544	6.419	1.768	2.455
4	0.512	0.937	1.19	6411.	920.	0.610E-02	18.73	0.559	6.725	1.874	2.758
5	0.853	0.997	1.34	6386.	895.	0.532E-02	18.75	0.642	7.071	1.994	3.123
6	1.214	1.061	1.52	6361.	820.	0.464E-02	14.63	0.569	7.437	2.121	3.534
7	1.580	1.125	1.71	6334.	925.	0.405E-02	16.23	0.740	7.810	2.251	3.978
8	1.879	1.178	1.88	6311.	825.	0.364E-02	12.81	0.641	8.113	2.356	4.359
9	2.017	1.202	1.95	6300.	740.	0.347E-02	10.99	0.570	8.253	2.404	4.541

PRIMARY SURFACE ANALYSIS MODE II TEST 113

TABLE XXVII (cont.)

	PC PSIA	MR	WT LB/S
PRIMARY	532.0	7.080	5.20
SECONDARY	33.0	0.100	0.11

PRESSURE RATIO = .062

CKT	Z	R	EPS	TR R	TWG R	HG THEOR	FLUX MEAS	CG	S	DEQG	AFLOWG
1	-0.201	0.884	1.06	6507.	1065.	0.738E-02	28.47	0.709	6.004	1.767	2.454
2	0.000	0.860	1.00	6494.	1020.	0.767E-02	27.12	0.646	6.206	1.720	2.324
3	0.211	0.884	1.06	6469.	970.	0.714E-02	22.09	0.563	6.419	1.768	2.455
4	0.512	0.937	1.19	6411.	925.	0.609E-02	18.83	0.563	6.725	1.874	2.758
5	0.853	0.997	1.34	6385.	905.	0.531E-02	19.15	0.658	7.071	1.994	3.123
6	1.214	1.061	1.52	6361.	825.	0.463E-02	14.94	0.582	7.437	2.121	3.534
7	1.580	1.125	1.71	6334.	935.	0.405E-02	16.56	0.758	7.810	2.251	3.978
8	1.879	1.178	1.88	6311.	835.	0.364E-02	13.10	0.659	8.113	2.356	4.359
9	2.017	1.202	1.95	6300.	750.	0.346E-02	11.32	0.589	8.253	2.404	4.541

PRIMARY SURFACE ANALYSIS MODE II TEST 114

	PC PSIA	MR	WT LB/S
PRIMARY	536.0	7.100	5.22
SECONDARY	31.0	0.000	0.07

PRESSURE RATIO = .058

CKT	Z	R	EPS	TR R	TWG R	HG THEOR	FLUX MEAS	CG	S	DEQG	AFLOWG
1	-0.201	0.884	1.06	6507.	1065.	0.740E-02	28.06	0.696	6.004	1.767	2.454
2	0.000	0.860	1.00	6494.	1020.	0.769E-02	26.98	0.641	6.206	1.720	2.324
3	0.211	0.884	1.06	6469.	985.	0.716E-02	22.51	0.573	6.419	1.768	2.455
4	0.512	0.937	1.19	6411.	875.	0.611E-02	20.98	0.620	6.725	1.874	2.758
5	0.853	0.997	1.34	6385.	920.	0.533E-02	19.55	0.672	7.071	1.994	3.123
6	1.214	1.061	1.52	6361.	835.	0.465E-02	15.15	0.591	7.437	2.121	3.534
7	1.580	1.125	1.71	6334.	940.	0.406E-02	16.64	0.760	7.810	2.251	3.978
8	1.879	1.178	1.88	6311.	740.	0.365E-02	13.29	0.654	8.113	2.356	4.359
9	2.017	1.202	1.95	6300.	755.	0.348E-02	11.52	0.598	8.253	2.404	4.541

PRIMARY SURFACE ANALYSIS MODE II TEST 137

	PC PSIA	MR	WT LB/S
PRIMARY	677.0	6.830	6.85
SECONDARY	40.9	0.000	0.11

PRESSURE RATIO = .059

CKT	Z	R	EPS	TR R	TWG R	HG THEOR	FLUX MEAS	CG	S	DEQG	AFLOWG
1	-0.201	0.884	1.06	6467.	1195.	0.919E-02	36.00	0.784	6.004	-1.767	2.454
2	0.000	0.860	1.00	6455.	1000.	0.954E-02	27.47	0.528	6.206	1.720	2.324
3	0.211	0.884	1.06	6430.	965.	0.888E-02	23.15	0.477	6.419	1.768	2.455
4	0.517	0.937	1.19	6372.	930.	0.759E-02	20.36	0.493	6.725	1.874	2.758
5	0.853	0.997	1.34	6347.	935.	0.661E-02	22.18	0.620	7.071	1.994	3.123
6	1.214	1.061	1.52	6322.	825.	0.577E-02	15.94	0.502	7.437	2.121	3.534
7	1.586	1.125	1.71	6295.	865.	0.504E-02	13.93	0.509	7.810	2.251	3.978
8	1.879	1.178	1.88	6273.	840.	0.453E-02	14.51	0.589	8.113	2.356	4.359
9	2.017	1.202	1.95	6262.	760.	0.432E-02	14.10	0.594	8.253	2.404	4.541

PRIMARY SURFACE ANALYSIS MODE II TEST 138

	PC PSIA	MR	WT LB/S
PRIMARY	676.0	6.840	6.84
SECONDARY	36.1	0.000	0.01

PRESSURE RATIO = .053

CKT	Z	R	EPS	TR R	TWG R	HG THEOR	FLUX MEAS	CG	S	DEQG	AFLOWG
1	-0.201	0.884	1.06	6467.	1185.	0.918E-02	37.38	0.771	6.004	1.767	2.454
2	0.000	0.860	1.00	6455.	1010.	0.953E-02	28.36	0.547	6.206	1.720	2.324
3	0.211	0.884	1.06	6430.	965.	0.887E-02	22.51	0.464	6.419	1.768	2.455
4	0.517	0.937	1.19	6372.	905.	0.758E-02	19.82	0.478	6.725	1.874	2.758
5	0.853	0.997	1.34	6347.	945.	0.660E-02	22.41	0.628	7.071	1.994	3.123
6	1.214	1.061	1.52	6322.	830.	0.576E-02	16.07	0.508	7.437	2.121	3.534
7	1.586	1.125	1.71	6295.	845.	0.504E-02	13.44	0.489	7.810	2.251	3.978
8	1.879	1.178	1.88	6273.	750.	0.453E-02	14.48	0.579	8.113	2.356	4.359
9	2.017	1.202	1.95	6262.	790.	0.431E-02	16.43	0.697	8.253	2.404	4.541

PRIMARY SURFACE ANALYSIS MODE II TEST 139

	PC PSIA	MR	WT LB/S
PRIMARY	676.0	6.805	6.84
SECONDARY	42.0	0.000	0.17

PRESSURE RATIO = .062

CKT	Z	F	EPS	TR R	TWG R	HG THEOR	FLUX MEAS	CG	S	DEQG	AFLOWG
1	-0.201	0.884	1.06	6467.	1220.	0.918E-02	38.93	0.808	6.004	1.767	2.454
2	0.009	0.869	1.00	6455.	1010.	0.953E-02	27.83	0.536	6.206	1.720	2.324
3	0.211	0.884	1.06	6430.	965.	0.987E-02	23.18	0.478	6.419	1.768	2.455
4	0.512	0.937	1.19	6372.	905.	0.758E-02	20.05	0.484	6.725	1.874	2.758
5	0.853	0.997	1.34	6347.	945.	0.660E-02	22.27	0.624	7.071	1.994	3.123
6	1.214	1.061	1.52	6322.	850.	0.576E-02	16.53	0.524	7.437	2.121	3.534
7	1.580	1.125	1.71	6295.	870.	0.504E-02	13.92	0.509	7.810	2.251	3.978
8	1.879	1.178	1.88	6273.	825.	0.453E-02	14.28	0.579	8.113	2.356	4.359
9	2.017	1.202	1.95	6262.	770.	0.431E-02	15.12	0.638	8.253	2.404	4.541

PRIMARY SURFACE ANALYSIS MODE II TEST 140

	PC PSIA	MR	WT LB/S
PRIMARY	663.0	2.950	6.30
SECONDARY	32.0	0.000	0.09

PRESSURE RATIO = .048

CKT	Z	F	EPS	TR R	TWG R	HG THEOR	FLUX MEAS	CG	S	DEQG	AFLOWG
1	-0.201	0.884	1.06	4710.	1025.	0.917E-02	28.45	0.842	6.004	1.767	2.454
2	0.009	0.869	1.00	4698.	870.	0.964E-02	20.03	0.543	6.206	1.720	2.324
3	0.211	0.884	1.06	4674.	850.	0.900E-02	16.91	0.491	6.419	1.768	2.455
4	0.512	0.937	1.19	4619.	790.	0.773E-02	14.28	0.482	6.725	1.874	2.758
5	0.853	0.997	1.34	4594.	830.	0.672E-02	16.25	0.642	7.071	1.994	3.123
6	1.214	1.061	1.52	4571.	750.	0.591E-02	11.73	0.519	7.437	2.121	3.534
7	1.580	1.125	1.71	4545.	770.	0.516E-02	10.07	0.517	7.810	2.251	3.978
8	1.879	1.178	1.88	4523.	740.	0.465E-02	10.19	0.574	8.113	2.356	4.359
9	2.017	1.202	1.95	4513.	705.	0.445E-02	10.63	0.628	8.253	2.404	4.541

TABLE XXVII (cont.)

PRIMARY SURFACE ANALYSIS MODE II TEST 141

	PC PSIA	MR	WT LB/S
PRIMARY	675.0	3.000	6.42
SECONDARY	34.0	0.000	0.16

PRESSURE RATIO = .050

CKT	Z	R	EPS	TR R	TWG R	HG THEOR	FLUX MEAS	CG	S	DEQG	AFLOWG
1	-0.201	0.884	1.06	4750.	1045.	0.926E-02	28.61	0.834	6.004	1.767	2.454
2	0.000	0.960	1.00	4737.	870.	0.974E-02	19.81	0.526	6.206	1.720	2.324
3	0.211	0.884	1.06	4713.	835.	0.911E-02	16.38	0.464	6.419	1.768	2.455
4	0.512	0.937	1.19	4658.	790.	0.782E-02	14.24	0.471	6.725	1.874	2.758
5	0.853	0.997	1.34	4633.	835.	0.680E-02	15.72	0.609	7.071	1.994	3.123
6	1.214	1.061	1.52	4609.	750.	0.597E-02	11.62	0.504	7.437	2.121	3.534
7	1.580	1.125	1.71	4583.	770.	0.522E-02	9.94	0.500	7.810	2.251	3.978
8	1.879	1.178	1.88	4561.	740.	0.470E-02	10.07	0.560	8.113	2.356	4.359
9	2.017	1.202	1.95	4551.	690.	0.450E-02	10.42	0.600	8.253	2.404	4.541

PRIMARY SURFACE ANALYSIS MODE II TEST 142

	PC PSIA	MR	WT LB/S
PRIMARY	674.0	3.050	6.41
SECONDARY	29.0	0.000	0.00

PRESSURE RATIO = .043

CKT	Z	R	EPS	TR R	TWG R	HG THEOR	FLUX MEAS	CG	S	DEQG	AFLOWG
1	-0.201	0.884	1.06	4789.	1030.	0.923E-02	28.35	0.817	6.004	1.767	2.454
2	0.000	0.960	1.00	4777.	890.	0.969E-02	20.60	0.547	6.206	1.720	2.324
3	0.211	0.884	1.06	4753.	835.	0.907E-02	16.39	0.461	6.419	1.768	2.455
4	0.512	0.937	1.19	4696.	790.	0.778E-02	14.36	0.472	6.725	1.874	2.758
5	0.853	0.997	1.34	4671.	830.	0.677E-02	16.35	0.629	7.071	1.994	3.123
6	1.214	1.061	1.52	4647.	750.	0.595E-02	11.92	0.514	7.437	2.121	3.534
7	1.580	1.125	1.71	4621.	770.	0.519E-02	9.98	0.499	7.810	2.251	3.978
8	1.879	1.178	1.88	4599.	740.	0.468E-02	10.44	0.578	8.113	2.356	4.359
9	2.017	1.202	1.95	4588.	705.	0.447E-02	11.41	0.657	8.253	2.404	4.541

from OMS and TRANSTAR I, which utilize the same reactive heat transfer model, indicate generally good agreement since the bulk of the storable propellant Cg data are in the 0.5-0.6 range.

2. Primary Mode I

In Mode I the primary nozzle operates with a very high back pressure due to its location upstream ofthe secondary throat. Therefore, it was anticipated that flow separation would occur in the primary nozzle as illustrated in Figure 72. One purpose of the test program was to vary the ratio of secondary to primary chamber pressure to determine its effect on primary nozzle heat transfer as a result of changes in the primary flow field. This was accomplished for two nozzle spacings. Table XXVIII summarizes the test conditions, grouping the tests to indicate the parametricvariations achieved. The resulting heat fluxes are included in Appendix B. Mode II Tests 111-114 were run with essentially the same primary chamber operating conditions as the first group of Mode I tests in Table XXVIII in hopes of obtaining a direct comparison of heat fluxes for the two modes of operation. However, repair of the primary chamber following Test 117 and the resultant shift in the internal leakage characteristics noted above in the discussion of Figure 131 makes such a direct comparison questionable since all but two of the Mode I tests were conducted after the repair. Therefore, heat flux comparisons are made herein using the reactive model correlation coefficients with three Mode II baselines: Tests 111-114 for the two tests prior to the repair, Tests 137-139 for the post-repair tests at a mixture ratio of 3. Table XXIX gives the primary nozzle Cg analysis output for all tests in Table XXVIII.

The Mode I testing resulted in significant heat flux increases relative to Mode II in part of the primary nozzle. Figure 73 illustrates the difference between operating modes by showing the profiles of Cg_I/Cg_{II} for chamber pressure ratios of 0.60 and 0.74 for a nozzle spacing of 2.5 in. The pressure ratio of 0.74 was the highest for which steady-state operation was achieved with the 2.5 in. spacing. Figure 73 shows that at the lower

TABLE XXVIII

MODE I TEST SUMMARY

Test Numbers	Primary Pc psia	Pressure Ratio Pc_s/Pc_p	Primary O/F	Secondary O/F	Le in.	Comments
116, 117	510 - 560	0.48	7.1 - 7.8	7.0 - 7.7	2.5	Before Primary Chamber Repair
125 - 127	490	0.65 - 0.74	6.7 - 6.9	6.8 - 7.0	2.5	Primary Chamber Repaired
130	490	0.67	3.0	6.9	2.5	Unequal Mixture Ratios
131	500	0.60	6.9	2.9	2.5	Unequal Mixture Ratios
132, 148	410, 650	0.67	3.0	3.0	2.5	Test 132 at Le = 1.5 in Operating Conditions
144 - 147	380 - 400	0.45 - 0.83	2.8 - 3.4	2.8 - 3.4	1.5	Short Nozzle Spacing

PRIMARY SURFACE ANALYSIS MODE I TEST 116

	PC PSIA	MR	WT LB/S
PRIMARY	515.0	7.910	5.27
SECONDARY	245.0	7.900	8.42

PRESSURE RATIO = .476

CKT	Z	R	EPS	TR R	TWG R	HG THEOR	FLUX MEAS	CG	S	DEQG	AFLOWG
1	-0.201	0.884	1.06	6548.	1000.	0.747E-02	25.11	0.606	6.004	1.767	2.454
2	0.000	0.860	1.00	6535.	980.	0.776E-02	25.32	0.587	6.206	1.720	2.324
3	0.211	0.884	1.06	6511.	920.	0.722E-02	19.65	0.487	6.419	1.768	2.455
4	0.512	0.937	1.19	6454.	840.	0.616E-02	15.01	0.434	6.725	1.874	2.758
5	0.853	0.997	1.34	6428.	880.	0.537E-02	17.91	0.601	7.071	1.994	3.123
6	1.214	1.061	1.52	6403.	770.	0.468E-02	12.27	0.465	7.437	2.121	3.534
7	1.580	1.125	1.71	6377.	860.	0.409E-02	13.63	0.604	7.810	2.251	3.978
8	1.879	1.178	1.88	6354.	935.	0.368E-02	17.78	0.892	8.113	2.356	4.359

PRIMARY SURFACE ANALYSIS MODE I TEST 117

	PC PSIA	MR	WT LB/S
PRIMARY	559.0	7.180	5.56
SECONDARY	267.0	7.090	8.89

PRESSURE RATIO = .478

CKT	Z	R	EPS	TR R	TWG R	HG THEOR	FLUX MEAS	CG	S	DEQG	AFLOWG
1	-0.201	0.884	1.06	6517.	1075.	0.779E-02	29.25	0.690	6.004	1.767	2.454
2	0.000	0.860	1.00	6504.	1020.	0.809E-02	28.10	0.633	6.206	1.720	2.324
3	0.211	0.884	1.06	6479.	960.	0.753E-02	21.81	0.525	6.419	1.768	2.455
4	0.512	0.937	1.19	6421.	870.	0.643E-02	16.42	0.460	6.725	1.874	2.758
5	0.853	0.997	1.34	6395.	795.	0.560E-02	20.02	0.638	7.071	1.994	3.123
6	1.214	1.061	1.52	6370.	795.	0.489E-02	13.49	0.495	7.437	2.121	3.534
7	1.580	1.125	1.71	6343.	880.	0.427E-02	14.44	0.619	7.810	2.251	3.978
8	1.879	1.178	1.88	6320.	950.	0.384E-02	18.51	0.898	8.113	2.356	4.359

PRIMARY SURFACE ANALYSIS MODE I TEST 125

	PC PSIA	MR	WT LB/S
PRIMARY	487.0	6.740	4.87
SECONDARY	316.0	6.850	11.39

PRESSURE RATIO = .649

CKT	Z	R	EPS	TR R	TWG R	HG THEOR	FLUX MEAS	CG	S	DEGG	AFLOWG
1	-0.201	0.884	1.06	6467.	1040.	0.699E-02	27.98	0.738	6.004	1.767	2.454
2	0.000	0.860	1.00	6455.	995.	0.726E-02	21.31	0.529	6.206	1.720	2.324
3	0.211	0.884	1.06	6430.	895.	0.676E-02	18.45	0.493	6.419	1.768	2.455
4	0.512	0.937	1.19	6372.	785.	0.578E-02	12.53	0.388	6.725	1.874	2.758
5	0.853	0.997	1.34	6347.	860.	0.504E-02	18.40	0.666	7.071	1.994	3.123
6	1.214	1.061	1.52	6322.	820.	0.439E-02	14.88	0.615	7.437	2.121	3.534
7	1.583	1.125	1.71	6295.	910.	0.384E-02	14.98	0.725	7.810	2.251	3.978
8	1.879	1.178	1.88	6273.	1025.	0.345E-02	21.96	1.214	8.113	2.356	4.359

PRIMARY SURFACE ANALYSIS MODE I TEST 126

	PC PSIA	MR	WT LB/S
PRIMARY	495.0	6.920	4.99
SECONDARY	321.0	7.030	11.35

PRESSURE RATIO = .648

CKT	Z	R	EPS	TR R	TWG R	HG THEOR	FLUX MEAS	CG	S	DEGG	AFLOWG
1	-0.201	0.884	1.06	6487.	1095.	0.714E-02	30.88	0.803	6.004	1.767	2.454
2	0.000	0.860	1.00	6474.	1005.	0.741E-02	26.84	0.662	6.206	1.720	2.324
3	0.211	0.884	1.06	6449.	890.	0.690E-02	18.18	0.474	6.419	1.768	2.455
4	0.512	0.937	1.19	6392.	910.	0.589E-02	12.18	0.377	6.725	1.874	2.758
5	0.853	0.997	1.34	6366.	880.	0.514E-02	18.46	0.655	7.071	1.994	3.123
6	1.214	1.061	1.52	6341.	855.	0.448E-02	16.79	0.683	7.437	2.121	3.534
7	1.583	1.125	1.71	6315.	925.	0.392E-02	15.56	0.737	7.810	2.251	3.978
8	1.879	1.178	1.88	6292.	1025.	0.352E-02	21.90	1.183	8.113	2.356	4.359

PRIMARY SURFACE ANALYSIS MODE I TEST 127

	PC PSIA	MR	WT LB/S
PRIMARY	492.0	6.920	4.96
SECONDARY	364.0	6.950	12.93

PRESSURE RATIO = .740

CKT	Z	R	EPS	TR R	TWG R	HG THEOR	FLUX MEAS	CG	S	DEGG	AFLOWG
1	-0.201	0.884	1.06	6487.	1030.	0.710E-02	27.22	0.703	6.004	1.767	2.454
2	0.000	0.860	1.00	6474.	945.	0.737E-02	23.43	0.575	6.206	1.720	2.324
3	0.211	0.884	1.06	6449.	890.	0.687E-02	17.96	0.470	6.419	1.768	2.455
4	0.512	0.937	1.19	6392.	790.	0.587E-02	12.68	0.386	6.725	1.874	2.758
5	0.853	0.997	1.34	6366.	960.	0.511E-02	22.59	0.818	7.071	1.994	3.123
6	1.214	1.061	1.52	6341.	880.	0.446E-02	17.97	0.738	7.437	2.121	3.534
7	1.580	1.125	1.71	6315.	980.	0.390E-02	17.71	0.852	7.810	2.251	3.978
8	1.879	1.178	1.88	6292.	1095.	0.350E-02	25.12	1.381	8.113	2.356	4.359

PRIMARY SURFACE ANALYSIS MODE I TEST 129

	PC PSIA	MR	WT LB/S
PRIMARY	489.0	7.100	4.94
SECONDARY	402.0	7.560	14.54

PRESSURE RATIO = .822

CKT	Z	R	EPS	TR R	TWG R	HG THEOR	FLUX MEAS	CG	S	DEGG	AFLOWG
1	-0.201	0.884	1.06	6507.	1025.	0.708E-02	27.85	0.717	6.004	1.767	2.454
2	0.000	0.860	1.00	6494.	970.	0.736E-02	25.43	0.626	6.206	1.720	2.324
3	0.211	0.884	1.06	6469.	895.	0.685E-02	19.29	0.505	6.419	1.768	2.455
4	0.512	0.937	1.19	6411.	810.	0.585E-02	14.38	0.439	6.725	1.874	2.758
5	0.853	0.997	1.34	6385.	1050.	0.510E-02	27.96	1.028	7.071	1.994	3.123
6	1.214	1.061	1.52	6361.	955.	0.445E-02	22.45	0.934	7.437	2.121	3.534
7	1.580	1.125	1.71	6334.	965.	0.389E-02	17.67	0.847	7.810	2.251	3.978
8	1.879	1.178	1.88	6311.	1060.	0.349E-02	23.96	1.307	8.113	2.356	4.359

PRIMARY SURFACE ANALYSIS MODE I TEST 130

	PC PSIA	MR	WT LB/S
PRIMARY	490.0	3.020	4.60
SECONDARY	327.0	6.960	11.37

PRESSURE RATIO = .667

CKT	Z	R	EPS	TR R	TWG R	HG THEOR	FLUX MEAS	CG	S	DEQG	AFLOWG
1	-0.201	0.884	1.06	4769.	960.	0.713E-02	23.80	0.877	6.004	1.767	2.454
2	0.000	0.860	1.00	4757.	870.	0.746E-02	18.91	0.653	6.206	1.720	2.324
3	0.211	0.884	1.06	4733.	830.	0.697E-02	15.08	0.554	6.419	1.768	2.455
4	0.512	0.937	1.19	4677.	700.	0.603E-02	8.55	0.357	6.725	1.874	2.758
5	0.853	0.997	1.34	4652.	860.	0.519E-02	17.41	0.885	7.071	1.994	3.123
6	1.214	1.061	1.52	4628.	805.	0.455E-02	14.21	0.817	7.437	2.121	3.534
7	1.580	1.125	1.71	4602.	855.	0.396E-02	12.84	0.864	7.810	2.251	3.978
8	1.879	1.178	1.88	4579.	950.	0.354E-02	18.70	1.457	8.113	2.356	4.359

PRIMARY MODE I TEST 131

	PC PSIA	MR	WT LB/S
PRIMARY	501.0	6.910	5.06
SECONDARY	298.0	2.940	9.39

PRESSURE RATIO = .595

CKT	Z	R	EPS	TR R	TWG R	HG THEOR	FLUX MEAS	CG	S	DEQG	AFLOWG
1	-0.201	0.884	1.06	6487.	1090.	0.722E-02	30.68	0.788	6.004	1.767	2.454
2	0.000	0.860	1.00	6474.	970.	0.749E-02	24.41	0.592	6.206	1.720	2.324
3	0.211	0.884	1.06	6449.	910.	0.698E-02	19.33	0.500	6.419	1.768	2.455
4	0.512	0.937	1.19	6392.	810.	0.596E-02	13.80	0.415	6.725	1.874	2.758
5	0.853	0.997	1.34	6366.	890.	0.519E-02	18.79	0.661	7.071	1.994	3.123
6	1.214	1.061	1.52	6341.	780.	0.453E-02	12.90	0.512	7.437	2.121	3.534
7	1.580	1.125	1.71	6315.	845.	0.396E-02	12.55	0.579	7.810	2.251	3.978
8	1.879	1.178	1.88	6292.	930.	0.356E-02	17.71	0.929	8.113	2.356	4.359

PRIMARY SURFACE ANALYSIS MODE I TEST 132

	PC PSIA	MR	WT LB/S
PRIMARY	414.0	2.990	3.85
SECONDARY	277.0	2.950	8.91

PRESSURE RATIO = .669

CKT	Z	R	EPS	TR R	TWG R	HG THEOR	FLUX MEAS	CG	S	DEQG	AFLOWG
1	-0.201	0.884	1.06	4750.	895.	0.622E-02	19.41	0.809	6.004	1.767	2.454
2	0.000	0.860	1.00	4737.	815.	0.651E-02	15.44	0.635	6.206	1.720	2.324
3	0.211	0.884	1.06	4713.	775.	0.609E-02	11.91	0.497	6.419	1.768	2.455
4	0.512	0.937	1.19	4657.	685.	0.525E-02	7.51	0.360	6.725	1.874	2.758
5	0.853	0.997	1.34	4632.	800.	0.453E-02	13.80	0.795	7.071	1.994	3.123
6	1.214	1.061	1.52	4608.	740.	0.398E-02	10.64	0.692	7.437	2.121	3.534
7	1.586	1.125	1.71	4583.	800.	0.346E-02	10.34	0.790	7.810	2.251	3.976
8	1.879	1.178	1.88	4561.	880.	0.309E-02	14.97	1.316	8.113	2.356	4.359

PRIMARY SURFACE ANALYSIS MODE I TEST 144

	PC PSIA	MR	WT LB/S
PRIMARY	399.0	2.600	3.87
SECONDARY	179.0	3.010	5.50

PRESSURE RATIO = .449

CKT	Z	R	EPS	TR R	TWG R	HG THEOR	FLUX MEAS	CG	S	DEQG	AFLOWG
1	-0.201	0.884	1.06	4582.	870.	0.636E-02	18.64	0.789	6.004	1.767	2.454
2	0.000	0.860	1.00	4570.	775.	0.666E-02	13.90	0.550	6.206	1.720	2.324
3	0.211	0.884	1.06	4547.	745.	0.623E-02	11.12	0.470	6.419	1.768	2.455
4	0.512	0.937	1.19	4493.	670.	0.536E-02	6.96	0.339	6.725	1.874	2.758
5	0.853	0.997	1.34	4469.	760.	0.464E-02	12.27	0.713	7.071	1.994	3.123
6	1.214	1.061	1.52	4446.	680.	0.408E-02	8.02	0.522	7.437	2.121	3.534
7	1.586	1.125	1.71	4421.	680.	0.357E-02	5.93	0.444	7.810	2.251	3.978
8	1.879	1.178	1.88	4400.	725.	0.320E-02	8.80	0.749	8.113	2.356	4.359

PRIMARY SURFACE ANALYSIS MODE I TEST 145

	PC PSIA	MR	WT LB/S
PRIMARY	397.0	2.770	3.83
SECONDARY	288.0	2.990	9.59

PRESSURE RATIO = .725

CKT	Z	R	EPS	TR R	TWG R	HG THEOR	FLUX MEAS	CG	S	DEGG	AFLOWG
1	-0.201	0.884	1.06	4552.	920.	0.630E-02	21.38	0.935	6.004	1.767	2.454
2	0.000	0.860	1.00	4541.	890.	0.656E-02	20.16	0.842	6.206	1.720	2.324
3	0.211	0.884	1.06	4518.	775.	0.618E-02	12.52	0.542	6.419	1.768	2.455
4	0.512	0.937	1.19	4464.	670.	0.533E-02	7.10	0.351	6.725	1.874	2.758
5	0.853	0.997	1.34	4440.	790.	0.460E-02	13.89	0.821	7.071	1.994	3.123
6	1.214	1.061	1.52	4417.	735.	0.404E-02	10.63	0.715	7.437	2.121	3.534
7	1.580	1.125	1.71	4392.	715.	0.354E-02	7.29	0.560	7.810	2.251	3.978
8	1.879	1.178	1.88	4371.	790.	0.316E-02	11.54	1.019	8.113	2.356	4.359

PRIMARY SURFACE ANALYSIS MODE I TEST 146

	PC PSIA	MR	WT LB/S
PRIMARY	395.0	2.780	3.82
SECONDARY	326.0	2.830	10.04

PRESSURE RATIO = .825

CKT	Z	R	EPS	TR R	TWG R	HG THEOR	FLUX MEAS	CG	S	DEGG	AFLOWG
1	-0.201	0.884	1.06	4562.	890.	0.629E-02	20.01	0.866	6.004	1.767	2.454
2	0.000	0.860	1.00	4550.	840.	0.657E-02	17.46	0.716	6.206	1.720	2.324
3	0.211	0.884	1.06	4527.	770.	0.616E-02	12.08	0.522	6.419	1.768	2.455
4	0.512	0.937	1.19	4474.	640.	0.533E-02	5.46	0.267	6.725	1.874	2.758
5	0.853	0.997	1.34	4450.	770.	0.460E-02	12.92	0.764	7.071	1.994	3.123
6	1.214	1.061	1.52	4427.	710.	0.404E-02	9.54	0.636	7.437	2.121	3.534
7	1.580	1.125	1.71	4402.	830.	0.349E-02	7.83	0.627	7.810	2.251	3.978
8	1.879	1.178	1.88	4381.	800.	0.315E-02	12.14	1.077	8.113	2.356	4.359

PRIMARY SURFACE ANALYSIS MODE I TEST 147

	PC PSIA	MR	WT LB/S
PRIMARY	381.0	3.340	3.68
SECONDARY	315.0	3.400	9.67

PRESSURE RATIO = .827

CKT	Z	R	EPS	TR R	TWG R	HG THEOR	FLUX MEAS	CG	S	DEQG	AFLOWG
1	-0.201	0.884	1.06	5045.	870.	0.590E-02	18.74	0.761	6.004	1.767	2.454
2	0.000	0.860	1.00	5032.	850.	0.614E-02	18.21	0.710	6.206	1.720	2.324
3	0.211	0.884	1.06	5006.	750.	0.576E-02	11.18	0.456	6.419	1.768	2.455
4	0.512	0.937	1.19	4947.	670.	0.495E-02	7.05	0.333	6.725	1.874	2.758
5	0.853	0.997	1.34	4921.	785.	0.429E-02	13.46	0.759	7.071	1.994	3.123
6	1.214	1.061	1.52	4895.	720.	0.376E-02	9.90	0.631	7.437	2.121	3.534
7	1.589	1.125	1.71	4868.	720.	0.329E-02	7.71	0.565	7.810	2.251	3.978
8	1.879	1.178	1.88	4844.	830.	0.293E-02	13.28	1.128	8.113	2.356	4.359

PRIMARY SURFACE ANALYSIS MODE I TEST 148

	PC PSIA	MR	WT LB/S
PRIMARY	648.0	3.120	6.31
SECONDARY	437.0	3.200	14.70

PRESSURE RATIO = .674

CKT	Z	R	EPS	TR R	TWG R	HG THEOR	FLUX MEAS	CG	S	DEQG	AFLOWG
1	-0.201	0.884	1.06	4858.	895.	0.917E-02	26.35	0.725	6.004	1.767	2.454
2	0.000	0.860	1.00	4845.	810.	0.959E-02	16.73	0.432	6.206	1.720	2.324
3	0.211	0.884	1.06	4821.	830.	0.892E-02	16.34	0.459	6.419	1.768	2.455
4	0.512	0.937	1.19	4764.	720.	0.770E-02	10.13	0.325	6.725	1.874	2.758
5	0.853	0.997	1.34	4736.	890.	0.663E-02	19.90	0.780	7.071	1.994	3.123
6	1.214	1.061	1.52	4714.	815.	0.582E-02	15.34	0.676	7.437	2.121	3.534
7	1.589	1.125	1.71	4687.	845.	0.508E-02	13.36	0.685	7.810	2.251	3.978
8	1.879	1.178	1.88	4665.	1040.	0.450E-02	19.18	1.176	8.113	2.356	4.359

pressure ratio heat fluxes are similar for the two operating modes except near the end of the nozzle, where a 60 percent increase is observed for circuit P8 in Mode I. As the pressure ratio increases the region of increased heat flux extends farther upstream and the magnitude of the perturbation near the aft end of the nozzle increases. At a pressure ratio of 0.74, heat flux perturbations in Mode I were observed as far upstream as circuit P5, and the heat flux at P8 had increased to 2.4 times the Mode II value. The high primary nozzle heat fluxes obtained during Mode I operation are the most significant result of the present contract and have serious design implications in view of the corner cooling problems at the tip of the primary nozzle.

Details of the Mode I primary nozzle heat fluxes relative to Mode II are shown in Figures 74-77 for circuits P5-P8, respectively. Upstream circuit (P2-P4) heat fluxes were generally consistent with or lower than the corresponding Mode II values. Figures 74 and 75 include data from Test 129, the highest chamber pressure ratio attempted with the 2.5 in. nozzle spacing, even though steady state conditions were not obtained due to the outlet coolant temperature for circuit P5 reaching the kill value. These results are included to show pressure ratio trends; actual heat fluxes are slightly higher. The pressure ratio trends for the nozzle spacing of 2.5 in. are shown more clearly on Figure 78, in which the mixture ratio 7 results of Figures 74-77 have been normalized to the low pressure ratio values (the low pressure ratio value for circuit P8 was assumed to be unity). Figure 78 clearly shows how the heat flux perturbation relative to Mode II increases with pressure ratio and how the point at which a perturbation is initially observed moves upstream. Heat fluxes greater than Mode I were observed at all pressure ratios tested for circuit P8. Circuit P7 indicates a pressure ratio threshold between 0.49 and approximately 0.55. Circuits P6 and P5 were not affected until the pressure ratio exceeded 0.60 and 0.65, repectively. Figures 74-77 indicate similar or less severe heat flux increases for Mode I with the 1.5 in. nozzle spacing. All tests for this spacing reached steady state

conditions, and the data at the highest pressure ratio (0.83) show a less severe heat flux increase for Mode I than the data for a 2.5 in. spacing.

The above results appear to be consistent with the flow separation and recirculation depicted in Figure 79. The gas in the secondary nozzle separates at E because of the extreme change in wall angle. During the tests chamber pressure, flowrate and mixture ratio were measured, from which the effective throat area of the secondary flow field could be calculated. With the primary nozzle in the normal position (L_e = 2.5 inches) the effective secondary throat area was much less than the area across E-F. Therefore, the secondary flow choked at T. For typical test conditions, assuming the primary gas pressure equals the secondary gas pressure, the primary flow field is slightly supersonic and the area occupied by the primary exhaust at T is slightly greater than the throat area of the primary nozzle. For test conditions where the secondary chamber presssure was 60 to 70 percent of the primary chamber pressure, the pressure of the secondary flow at E was much greater than the pressure that the primary nozzle would produce for isentropic flow to its exit at G. Therefore, the primary nozzle, being unable to flow full against the high back pressure created by the secondary nozzle, separated at some point S.

The high speed streams from both nozzles along jet boundaries EW and SW shear against the gas in the separated region. The shearing action transfers momentum from the high speed jet to the essentially stagnant gas in the separated region, entraining some of the separated gas in the shear layer. Part of the gas in the shear layer turns back at W, recirculating into the separated region, creating a circulation pattern similar to the twin vortex patern shown in Figure 79 or a more complex vortex pattern. This recirculation model agrees with the observed heat fluxes on the primary nozzle wall, which increase approaching the tip as shown in Appendix B (Figure B-11). In Figure 79, point G at the tip of the primary chamber is a stagnation point. It has a much higher heat flux than would occur for Mode II operation with attached flow to the end of the nozzle. Moving into the primary nozzle

from point G results in decreasing heat flux consistent with the establishment and growth of a reverse flow boundary layer in the separated region. Upstream of point S the heat flux is the same in both modes because the expanding gas is attached in both cases.

3. Primary Chamber Tip (Mode I)

Wake region heat fluxes were obtained directly for circuit P10 and were inferred for circuits P9 and P11 at the corners by correcting upstream heat fluxes at P8 and P12, respectively, for $(\rho_f U_e)^{0.8}$ to obtain sidewall heat fluxes in order to split the measured heat load between the sidewall and wake region. Results are presented herein relative to the primary nozzle circuit P8, the center of which is 0.23 in. from the end of the nozzle. Figure 80 shows the relative heat fluxes from circuits P10 and P11 for a nozzle spacing of 2.5 in. These heat flux ratios are seen to be independent of pressure ratio, with values of 0.80 at the center of the tip and 0.32 near the secondary corner. Figure 81 indicates essentially no change in the latter for the reduced nozzle spacing of 1.5 in., whereas the heat flux at the center increases to 92 percent of that at P8. Figure 82 for circuit P9 near the primary corner with the 2.5 in. nozzle spacing shows more data scatter but no apparent effect of pressure ratio. The data scatter for P9 no doubt reflects errors in the sidewall heat flux estimate based on P8, which is not surprising in view of the separated flow region in the primary nozzle. In all cases but one, the heat flux from P9 is lower than that at the center of the tip (P10). Figure 81 shows an increase in the relative heat flux at P9 for the 1.5 in. nozzle spacing. This increase is greater than that noted above for P10 so that at the smaller spacing the heat flux at P9 generally exceeds that at P10.

The spatial distributions for the wake region heat fluxes are highlighted in Figure 83 for both nozzle spacings using the results for Tests 132 and 146, which are typical of the data of Figures 80-82. Note that these distributions are consistent with the recirculation pattern of Figure 79, which would predict low heat fluxes near the secondary corner relative to the

primary corner. Figure 83 includes the relative fluxes for the secondary side of the primary chamber from circuit P12; all such data are included in Figure 84. Both figures clearly show the significant increase in heat flux at P12 for the shorter nozzle spacing due to higher secondary mass velocities. The corresponding increases in wake heat flux at P9 and P10 are to be expected; the surprising result is that the wake heat flux at P11 near the secondary corner is unaffected. Correlations of the relative wake heat fluxes with the secondary heat flux near the corner (P12) are shown in Figures 85-87. These figures allow prediction of the wake region heat fluxes in design applications if the sidewall heat fluxes are known.

4. Secondary Mode I

Heat flux data from the secondary chamber during Mode I operation, which are included in Appendix B, have been evaluated using the reactive pipe flow correlation used above for the primary nozzle in both modes. Data from circuit P12 on the outer surface of the primary chamber are included with the secondary chamber results at the axial distance on the secondary contour which provides the same flow area as at P12. All correlation coefficient analysis output is presented in Table XXX. An annular stream tube containing the secondary flow was used to define mass velocities and other combustion product expansion characteristics at the secondary chamber wall downstream of the physical annulus created by the primary chamber. The throat for this stream tube is assumed to occur at the physical throat of the secondary chamber, with the throat area based on one-dimensional expansion of the measured flow from the known chamber pressure. Stream tube area ratios downstream of the throat are assumed to equal the local physical area ratio of the secondary nozzle. A dividing streamline is created between the end of the primary chamber and the secondary throat; this streamline normally consists of a straight line and a circular arc through the dividing radius at the throat. The radius of curvature for the arc is defined such that its center coincides with that of the wall contour radius of curvature upstream of the throat. This dividing streamline applied to all tests with a nozzle spacing of 2.5 in. In this region and in the physical annulus between chambers, flow

TABLE XXX

SECONDARY MODE I TEST 116

	PC PSIA	MR	WT LB/S
PRIMARY	515.0	7.910	5.27
SECONDARY	245.0	7.800	8.42

PRESSURE RATIO = .476

CKT	Z	R	EPS	TR R	TWO R	HG THEOR	FLUX MEAS	CG	S	DEGG	AFLOWG
14	-5.700	3.670	3.22	6617.	900.	0.165E-02	11.32	1.200	0.000	2.655	25.078
1A	-4.653	3.670	3.22	6617.	900.	0.165E-02	7.44	0.789	1.047	2.655	25.078
1B	-3.738	3.561	3.11	6616.	840.	0.170E-02	5.51	0.562	1.971	2.628	24.210
2B	-2.939	3.263	2.81	6615.	830.	0.184E-02	6.80	0.639	2.825	2.615	21.884
12P	-2.216	2.852	2.19	6612.	760.	0.229E-02	8.26	0.616	3.658	2.339	17.063
2A	-2.208	2.847	2.18	6612.	830.	0.230E-02	7.08	0.533	3.667	2.336	17.011
3	-1.555	2.470	1.67	6602.	800.	0.290E-02	8.21	0.488	4.420	2.067	12.995
4	-1.064	2.187	1.33	6593.	793.	0.353E-02	9.02	0.440	4.988	1.863	10.324
5	-0.737	2.012	1.13	6565.	775.	0.396E-02	8.96	0.391	5.359	1.748	8.819
6	-0.409	1.906	1.01	6538.	760.	0.426E-02	8.44	0.343	5.704	1.697	7.898
7	0.000	1.860	1.00	6535.	770.	0.427E-02	8.73	0.355	6.116	1.740	7.789
8	0.246	1.876	1.02	6528.	760.	0.418E-02	7.77	0.323	6.363	1.755	7.927
9	0.573	1.948	1.10	6493.	765.	0.378E-02	8.22	0.379	6.698	1.822	8.543
10	0.901	2.036	1.20	6449.	790.	0.335E-02	8.96	0.472	7.038	1.904	9.331
11	1.228	2.124	1.30	6433.	790.	0.306E-02	7.75	0.449	7.377	1.986	10.153
12A	1.651	2.237	1.45	6414.	800.	0.273E-02	8.04	0.524	7.814	2.092	11.263
12B	2.104	2.358	1.61	6392.	775.	0.243E-02	7.57	0.556	8.283	2.206	12.520
13B	2.557	2.480	1.78	6368.	700.	0.216E-02	5.22	0.426	8.753	2.320	13.845
13A	3.011	2.601	1.96	6343.	762.	0.193E-02	7.43	0.691	9.222	2.433	15.232

SECONDARY MODE I TEST 117

	PC PSIA	MR	WT LB/S
PRIMARY	559.0	7.180	5.56
SECONDARY	267.0	7.090	8.89

PRESSURE RATIO = .478

CKT	Z	R	EPS	TR R	TWQ R	HQ THEOR	FLUX MEAS	CQ	S	DEQQ	AFLOWQ
14	-5.700	3.670	3.24	6577.	930.	0.172E-02	11.96	1.231	0.000	2.655	25.078
1A	-4.653	3.670	3.24	6577.	930.	0.172E-02	8.11	0.834	1.047	2.655	25.078
1B	-3.738	3.561	3.13	6576.	875.	0.177E-02	6.16	0.609	1.971	2.628	24.210
2B	-2.939	3.263	2.83	6575.	880.	0.192E-02	7.59	0.693	2.825	2.615	21.884
12P	-2.216	2.852	2.21	6572.	770.	0.239E-02	8.79	0.633	3.658	2.339	17.063
2A	-2.208	2.847	2.20	6572.	895.	0.240E-02	7.91	0.581	3.667	2.336	17.011
3	-1.555	2.470	1.68	6562.	730.	0.304E-02	9.10	0.514	4.420	2.060	12.959
4	-1.064	2.187	1.33	6553.	725.	0.371E-02	10.11	0.467	4.988	1.850	10.265
5	-0.737	2.012	1.13	6524.	800.	0.417E-02	10.07	0.422	5.359	1.731	8.751
6	-0.409	1.906	1.01	6497.	810.	0.448E-02	10.25	0.402	5.704	1.679	7.836
7	0.000	1.860	1.00	6494.	840.	0.450E-02	11.17	0.439	6.116	1.721	7.730
8	0.246	1.876	1.02	6486.	830.	0.440E-02	10.30	0.414	6.363	1.736	7.867
9	0.573	1.948	1.10	6451.	810.	0.399E-02	9.94	0.442	6.698	1.802	8.478
10	0.901	2.036	1.20	6406.	825.	0.353E-02	10.39	0.527	7.038	1.884	9.260
11	1.228	2.124	1.30	6391.	825.	0.322E-02	8.87	0.494	7.377	1.965	10.076
12A	1.651	2.237	1.45	6371.	850.	0.288E-02	9.00	0.567	7.814	2.069	11.177
12B	2.104	2.358	1.61	6348.	830.	0.256E-02	8.47	0.601	8.283	2.182	12.424
13B	2.557	2.480	1.78	6325.	750.	0.228E-02	5.74	0.452	8.753	2.294	13.739
13A	3.011	2.601	1.96	6300.	800.	0.203E-02	8.32	0.745	9.222	2.406	15.116

SECONDARY MODE I TEST 125

	PC PSIA	MR	WT LB/S
PRIMARY	487.0	6.740	4.87
SECONDARY	316.0	6.850	11.09

PRESSURE RATIO = .649

CKT	Z	R	EPS	TR R	TWG R	HG THEOR	FLUX MEAS	CG	S	DEGG	AFLOWG
14	-5.700	3.670	3.05	6546.	990.	0.205E-02	14.52	1.274	0.000	2.655	25.078
1A	-4.653	3.670	3.05	6546.	990.	0.205E-02	9.63	0.845	1.047	2.655	25.078
1B	-3.738	3.561	2.95	6545.	910.	0.211E-02	6.63	0.557	1.971	2.628	24.210
2B	-2.939	3.263	2.66	6544.	860.	0.229E-02	7.31	0.561	2.825	2.615	21.884
12P	-2.216	2.852	2.08	6541.	805.	0.285E-02	10.02	0.612	3.658	2.339	17.063
2A	-2.208	2.847	2.07	6541.	860.	0.286E-02	8.22	0.506	3.667	2.336	17.011
3	-1.555	2.470	1.62	6531.	880.	0.353E-02	10.94	0.549	4.420	2.117	13.268
4	-1.064	2.187	1.31	6523.	870.	0.421E-02	12.46	0.524	4.988	1.962	10.764
5	-0.737	2.012	1.14	6495.	880.	0.465E-02	13.96	0.534	5.359	1.882	9.333
6	-0.409	1.906	1.02	6468.	825.	0.500E-02	15.39	0.546	5.704	1.835	8.341
7	0.000	1.860	1.00	6465.	1000.	0.502E-02	19.28	0.703	6.116	1.881	8.213
8	0.246	1.876	1.02	6457.	855.	0.491E-02	11.96	0.435	6.363	1.898	8.359
9	0.573	1.948	1.10	6422.	835.	0.445E-02	11.46	0.461	6.698	1.970	9.009
10	0.901	2.036	1.20	6377.	840.	0.394E-02	11.68	0.535	7.038	2.059	9.839
11	1.228	2.124	1.30	6362.	830.	0.360E-02	9.45	0.475	7.377	2.148	10.706
12A	1.651	2.237	1.45	6342.	860.	0.321E-02	10.53	0.598	7.814	2.262	11.877
12B	2.104	2.358	1.61	6320.	755.	0.286E-02	7.12	0.448	8.283	2.385	13.202
13B	2.557	2.480	1.78	6296.	740.	0.254E-02	5.82	0.412	8.753	2.508	14.599
13A	3.011	2.601	1.96	6271.	790.	0.227E-02	8.48	0.682	9.222	2.631	16.062

SECONDARY MODE I TEST 126

	PC PSIA	MR	WT LB/S
PRIMARY	495.0	6.920	4.99
SECONDARY	321.0	7.030	11.35

PRESSURE RATIO = .648

CKT	Z	R	EPS	TR R	TWG R	HG THEOR	FLUX MEAS	CG	S	DEGG	AFLOWG
14	-5.700	3.670	3.05	6566.	1000.	0.209E-02	15.15	1.302	0.000	2.655	25.078
1A	-4.653	3.670	3.05	6566.	1000.	0.209E-02	9.91	0.852	1.047	2.655	25.078
1B	-3.738	3.561	2.94	6565.	920.	0.215E-02	6.80	0.559	1.971	2.628	24.210
2B	-2.939	3.263	2.66	6564.	875.	0.233E-02	7.65	0.576	2.825	2.615	21.884
12P	-2.216	2.852	2.08	6561.	830.	0.291E-02	10.98	0.659	3.658	2.339	17.063
2A	-2.208	2.847	2.07	6561.	895.	0.291E-02	9.07	0.549	3.667	2.336	17.011
3	-1.555	2.470	1.61	6551.	865.	0.359E-02	11.49	0.562	4.420	2.118	13.273
4	-1.064	2.187	1.31	6543.	850.	0.429E-02	11.75	0.482	4.988	1.965	10.773
5	-0.737	2.012	1.14	6515.	940.	0.474E-02	16.25	0.615	5.359	1.885	9.343
6	-0.409	1.906	1.02	6488.	970.	0.509E-02	17.21	0.613	5.704	1.838	8.350
7	0.000	1.860	1.00	6484.	955.	0.511E-02	17.32	0.613	6.116	1.884	8.222
8	0.246	1.876	1.02	6476.	795.	0.500E-02	9.84	0.347	6.363	1.901	8.367
9	0.573	1.948	1.10	6441.	880.	0.453E-02	13.14	0.522	6.698	1.973	9.018
10	0.901	2.036	1.20	6397.	890.	0.401E-02	13.52	0.612	7.038	2.062	9.849
11	1.228	2.124	1.30	6381.	830.	0.366E-02	9.59	0.472	7.377	2.151	10.717
12A	1.651	2.237	1.45	6361.	895.	0.327E-02	11.65	0.652	7.814	2.266	11.889
12B	2.104	2.358	1.61	6339.	745.	0.291E-02	6.66	0.410	8.283	2.389	13.215
13B	2.557	2.480	1.78	6315.	740.	0.259E-02	5.85	0.406	8.753	2.512	14.614
13A	3.011	2.601	1.96	6290.	805.	0.231E-02	8.96	0.708	9.222	2.635	16.078

SECONDARY MODE I TEST 127

	PC PSIA	MR	WT LB/S
PRIMARY	492.0	6.920	4.96
SECONDARY	364.0	6.950	12.93

PRESSURE RATIO = .740

CKT	Z	R	EPS	TR R	TWO R	HO THEOR	FLUX MEAS	CO	S	DEGO	AFLOWO
14	-5.700	3.670	3.03	6556.	1030.	0.232E-02	15.50	1.209	0.000	2.655	25.078
1A	-4.653	3.670	3.03	6556.	1030.	0.232E-02	10.41	0.812	1.047	2.655	25.078
1B	-3.738	3.561	2.92	6555.	975.	0.239E-02	7.68	0.576	1.971	2.628	24.210
2B	-2.939	3.263	2.64	6554.	930.	0.259E-02	8.83	0.606	2.825	2.615	21.884
12P	-2.216	2.852	2.06	6551.	830.	0.322E-02	10.98	0.595	3.658	2.339	17.063
2A	-2.208	2.847	2.05	6551.	935.	0.323E-02	9.98	0.550	3.667	2.336	17.011
3	-1.555	2.470	1.61	6540.	950.	0.398E-02	12.87	0.579	4.420	2.126	13.314
4	-1.064	2.187	1.31	6533.	930.	0.472E-02	14.56	0.550	4.988	1.980	10.840
5	-0.737	2.012	1.14	6506.	955.	0.521E-02	16.90	0.584	5.359	1.906	9.421
6	-0.409	1.906	1.02	6478.	990.	0.560E-02	17.86	0.581	5.704	1.859	8.413
7	0.000	1.860	1.00	6474.	1040.	0.563E-02	20.53	0.671	6.116	1.905	8.282
8	0.246	1.876	1.02	6467.	850.	0.550E-02	11.86	0.384	6.363	1.922	8.428
9	0.573	1.948	1.10	6432.	855.	0.498E-02	12.22	0.440	6.698	1.995	9.084
10	0.901	2.036	1.20	6387.	865.	0.441E-02	12.58	0.516	7.038	2.085	9.921
11	1.228	2.124	1.30	6372.	840.	0.403E-02	9.83	0.441	7.377	2.175	10.795
12A	1.651	2.237	1.45	6352.	880.	0.360E-02	11.30	0.574	7.814	2.291	11.976
12B	2.104	2.358	1.61	6329.	770.	0.320E-02	7.53	0.424	8.283	2.415	13.312
13B	2.557	2.480	1.78	6305.	750.	0.285E-02	5.95	0.376	8.753	2.540	14.721
13A	3.011	2.601	1.96	6281.	830.	0.254E-02	9.72	0.702	9.222	2.664	16.196

SECONDARY MODE I TEST 130

	PC PSIA	MR	WT LB/S
PRIMARY	490.0	3.020	4.60
SECONDARY	327.0	6.960	11.37

PRESSURE RATIO = .667

CKT	Z	R	EPS	TR R	TWG R	HG THEOR	FLUX MEAS	CG	S	DEGG	AFLOWG
14	-5.700	3.670	3.09	6556.	995.	0.209E-02	14.89	1.279	0.000	2.655	25.078
1A	-4.653	3.670	3.09	6556.	995.	0.209E-02	9.76	0.838	1.047	2.655	25.078
1B	-3.738	3.561	2.99	6556.	920.	0.216E-02	6.79	0.559	1.971	2.628	24.210
2B	-2.939	3.263	2.70	6554.	880.	0.234E-02	7.67	0.578	2.825	2.615	21.884
12P	-2.216	2.852	2.11	6551.	820.	0.291E-02	10.45	0.627	3.658	2.339	17.063
2A	-2.208	2.847	2.10	6551.	900.	0.292E-02	9.38	0.569	3.667	2.336	17.011
3	-1.555	2.470	1.63	6541.	920.	0.362E-02	12.13	0.596	4.420	2.104	13.194
4	-1.064	2.187	1.31	6533.	915.	0.434E-02	14.15	0.580	4.988	1.935	10.645
5	-0.737	2.012	1.13	6505.	950.	0.482E-02	16.68	0.623	5.359	1.846	9.195
6	-0.409	1.906	1.02	6478.	975.	0.518E-02	17.21	0.604	5.704	1.798	8.226
7	0.000	1.860	1.00	6474.	1015.	0.520E-02	19.68	0.693	6.116	1.844	8.103
8	0.246	1.876	1.02	6467.	940.	0.508E-02	11.47	0.408	6.363	1.860	8.246
9	0.573	1.948	1.10	6432.	960.	0.461E-02	12.32	0.489	6.698	1.931	8.888
10	0.901	2.036	1.20	6387.	970.	0.408E-02	12.77	0.578	7.038	2.018	9.707
11	1.228	2.124	1.30	6372.	830.	0.373E-02	9.55	0.463	7.377	2.105	10.562
12A	1.651	2.237	1.45	6352.	875.	0.333E-02	10.98	0.603	7.814	2.217	11.717
12B	2.104	2.358	1.61	6329.	745.	0.296E-02	6.70	0.406	8.283	2.337	13.024
13B	2.557	2.480	1.78	6305.	730.	0.263E-02	5.62	0.383	8.753	2.458	14.403
13A	3.011	2.601	1.96	6281.	790.	0.235E-02	8.40	0.651	9.222	2.578	15.846

SECONDARY MODE I TEST 131

	PC PSIA	MR	WT LB/S
PRIMARY	501.0	6.910	5.06
SECONDARY	298.0	2.940	9.39

PRESSURE RATIO = .595

CKT	Z	R	EPS	TR R	TWQ R	HQ THEOR	FLUX MEAS	CQ	S	DEQQ	AFLOWQ
14	-5.700	3.670	3.04	4766.	880.	0.193E-02	11.78	1.568	0.000	2.655	25.078
1A	-4.653	3.670	3.04	4766.	880.	0.193E-02	7.38	0.982	1.047	2.655	25.078
1B	-3.738	3.561	2.93	4766.	830.	0.200E-02	5.20	0.661	1.971	2.628	24.210
2B	-2.939	3.263	2.65	4764.	805.	0.217E-02	6.05	0.704	2.825	2.615	21.884
12P	-2.216	2.852	2.07	4761.	755.	0.271E-02	8.19	0.753	3.658	2.339	17.063
2A	-2.208	2.847	2.06	4761.	830.	0.271E-02	7.52	0.707	3.667	2.336	17.011
3	-1.555	2.470	1.61	4751.	845.	0.333E-02	9.76	0.750	4.420	2.122	13.296
4	-1.064	2.187	1.31	4744.	830.	0.397E-02	11.11	0.715	4.988	1.973	10.810
5	-0.737	2.012	1.14	4718.	880.	0.437E-02	14.02	0.837	5.359	1.896	9.386
6	-0.409	1.906	1.02	4692.	894.	0.469E-02	14.21	0.798	5.704	1.849	8.384
7	0.000	1.860	1.00	4688.	905.	0.471E-02	15.28	0.858	6.116	1.896	8.255
8	0.246	1.876	1.02	4681.	760.	0.466E-02	8.68	0.475	6.363	1.912	8.401
9	0.573	1.948	1.10	4647.	780.	0.422E-02	9.43	0.578	6.698	1.985	9.054
10	0.901	2.036	1.20	4604.	780.	0.374E-02	9.56	0.668	7.038	2.075	9.889
11	1.228	2.124	1.30	4590.	750.	0.343E-02	7.03	0.534	7.377	2.164	10.760
12A	1.651	2.237	1.45	4571.	790.	0.305E-02	8.35	0.724	7.814	2.280	11.936
12B	2.104	2.358	1.61	4549.	690.	0.274E-02	4.88	0.462	8.283	2.403	13.268
13B	2.557	2.480	1.78	4526.	680.	0.244E-02	4.19	0.446	8.753	2.527	14.672
13A	3.011	2.601	1.96	4503.	725.	0.217E-02	6.37	0.776	9.222	2.651	16.142

SECONDARY MODE I TEST 132

	PC PSIA	MR	WT LB/S
PRIMARY	414.0	3.000	3.85
SECONDARY	277.0	2.950	8.91

PRESSURE RATIO = .669

CKT	Z	R	EPS	TR R	TWG R	HG THEOR	FLUX MEAS	CG	S	DEGG	AFLOWG
14	-5.700	3.670	2.98	4776.	880.	0.185E-02	11.35	1.573	0.000	2.655	25.078
1A	-4.653	3.670	2.98	4776.	880.	0.185E-02	6.97	0.966	1.047	2.655	25.078
1B	-3.738	3.561	2.87	4775.	830.	0.192E-02	4.93	0.652	1.971	2.628	24.210
2B	-2.939	3.263	2.60	4774.	760.	0.209E-02	5.70	0.680	2.825	2.615	21.884
12P	-2.216	2.852	2.02	4771.	740.	0.260E-02	7.20	0.686	3.658	2.339	17.063
2A	-2.208	2.847	2.02	4771.	775.	0.260E-02	7.06	0.679	3.667	2.336	17.011
3	-1.555	2.470	1.59	4761.	835.	0.316E-02	9.10	0.733	4.420	2.144	13.415
4	-1.064	2.187	1.31	4754.	825.	0.373E-02	10.44	0.712	4.988	2.017	11.005
5	-0.737	2.012	1.05	4708.	885.	0.437E-02	13.66	0.818	5.359	1.796	8.822
6	-0.409	1.906	1.02	4701.	875.	0.440E-02	12.97	0.771	5.704	1.909	8.565
7	0.000	1.860	1.00	4698.	885.	0.442E-02	14.13	0.839	6.116	1.957	8.426
8	0.246	1.876	1.02	4690.	755.	0.436E-02	8.16	0.475	6.363	1.974	8.575
9	0.573	1.948	1.10	4657.	760.	0.396E-02	8.38	0.543	6.698	2.049	9.242
10	0.901	2.036	1.20	4614.	770.	0.351E-02	8.80	0.652	7.038	2.141	10.094
11	1.228	2.124	1.30	4599.	720.	0.322E-02	5.95	0.476	7.377	2.234	10.983
12A	1.651	2.237	1.45	4580.	770.	0.286E-02	7.48	0.686	7.814	2.353	12.184
12B	2.104	2.358	1.61	4559.	665.	0.257E-02	4.14	0.414	8.283	2.480	13.544
13B	2.557	2.480	1.78	4536.	670.	0.229E-02	3.82	0.432	8.753	2.608	14.977
13A	3.011	2.601	1.96	4512.	700.	0.204E-02	5.36	0.690	9.222	2.736	16.478

SECONDARY MODE I TEST 148

	PC PSIA	MR	WT LB/S
PRIMARY	648.0	3.120	6.31
SECONDARY	437.0	3.200	14.70

PRESSURE RATIO = .674

CKT	Z	R	EPS	TR R	TWQ R	HQ THEOR	FLUX MEAS	CQ	S	DEQQ	AFLOWQ
14	-5.700	3.670	2.86	4995.	825.	0.273E-02	14.82	1.301	0.000	2.655	25.078
1A	-4.653	3.670	2.86	4995.	825.	0.273E-02	6.90	0.606	1.047	2.655	25.078
1B	-3.738	3.561	2.76	4994.	1060.	0.277E-02	10.93	1.002	1.971	2.628	24.210
2B	-2.939	3.263	2.49	4993.	870.	0.304E-02	8.37	0.667	2.825	2.615	21.884
12P	-2.216	2.852	1.94	4989.	780.	0.381E-02	9.94	0.620	3.658	2.339	17.063
2A	-2.208	2.847	1.94	4989.	890.	0.379E-02	9.90	0.637	3.667	2.336	17.011
3	-1.555	2.470	1.56	4979.	910.	0.453E-02	12.94	0.702	4.420	2.192	13.682
4	-1.064	2.187	1.30	4972.	910.	0.523E-02	14.82	0.697	4.988	2.118	11.442
5	-0.737	2.012	1.05	4926.	940.	0.610E-02	17.28	0.711	5.359	1.918	9.235
6	-0.409	1.906	1.02	4918.	950.	0.614E-02	17.32	0.711	5.704	2.038	8.937
7	0.000	1.860	1.00	4914.	1005.	0.615E-02	20.35	0.846	6.116	2.089	8.779
8	0.246	1.876	1.02	4906.	940.	0.604E-02	12.29	0.513	6.363	2.107	8.934
9	0.573	1.948	1.10	4871.	805.	0.553E-02	11.23	0.499	6.698	2.188	9.629
10	0.901	2.036	1.20	4826.	795.	0.491E-02	10.72	0.541	7.038	2.286	10.516
11	1.228	2.124	1.30	4811.	790.	0.449E-02	9.03	0.500	7.377	2.385	11.443
12A	1.651	2.237	1.45	4791.	800.	0.401E-02	9.55	0.597	7.814	2.512	12.694
12B	2.104	2.358	1.61	4768.	750.	0.358E-02	7.57	0.527	8.283	2.648	14.110
13B	2.557	2.480	1.78	4745.	705.	0.320E-02	5.45	0.422	8.753	2.785	15.604
13A	3.011	2.601	1.96	4720.	750.	0.285E-02	7.79	0.689	9.222	2.921	17.167

SECONDARY MODE I TEST 146 LE=1.5

	PC PSIA	MR	WT LB/S
PRIMARY	395.0	2.780	3.82
SECONDARY	326.0	2.930	10.04

PRESSURE RATIO = .825

CKT	Z	R	EPS	TR R	TWG R	HG THEOR	FLUX MEAS	EC	S	WEGG	AFLOWG
1A	-4.653	3.670	3.17	4676.	900.	0.206E-02	8.29	1.068	1.047	2.655	25.078
1B	-3.738	3.561	2.88	4675.	900.	0.225E-02	8.29	0.974	1.971	2.456	22.776
2B	-2.939	3.263	2.15	4672.	905.	0.301E-02	7.06	0.807	2.825	1.928	16.98[illegible]
2A	-2.298	2.847	1.62	4662.	865.	0.383E-02	10.00	0.687	3.667	1.659	12.819
3	-1.555	2.470	1.19	4640.	950.	0.501E-02	11.94	0.629	4.420	1.387	9.393
12P	-1.428	2.396	1.11	4623.	955.	0.520E-02	13.19	0.691	4.568	1.335	8.784
4	-1.064	2.187	1.00	4600.	930.	0.557E-02	14.59	0.710	4.988	1.329	7.901
5	-0.737	2.012	1.00	4600.	935.	0.545E-02	16.18	0.805	5.359	1.467	7.931
6	-0.409	1.906	1.00	4600.	695.	0.537E-02	14.31	0.719	5.754	1.604	7.911
7	0.000	1.860	1.00	4600.	880.	0.527E-02	14.32	0.730	5.116	1.776	7.901
8	0.246	1.876	1.02	4592.	710.	0.523E-02	6.85	0.337	6.363	1.792	8.041
9	0.573	1.948	1.13	4559.	775.	0.472E-02	9.41	0.527	6.698	1.869	8.666
10	0.901	2.036	1.21	4517.	770.	0.419E-02	9.09	0.579	7.038	1.944	9.465
11	1.228	2.124	1.30	4503.	725.	0.384E-02	6.40	0.441	7.377	2.028	10.299
12A	1.651	2.237	1.45	4484.	770.	0.342E-02	7.87	0.625	7.814	2.136	11.425
12B	2.164	2.358	1.61	4463.	680.	0.306E-02	4.86	0.414	8.283	2.252	12.7[illegible]
13B	2.557	2.480	1.78	4441.	665.	0.273E-02	3.78	0.366	8.753	2.368	14.044
13A	3.011	2.601	1.96	4418.	705.	0.243E-02	5.82	0.644	9.222	2.484	15.451

SECONDARY MODE I TEST 145 LE=1.5

	PC PSIA	MR	WT LB/S
PRIMARY	397.0	2.770	3.83
SECONDARY	288.0	2.990	9.50

PRESSURE RATIO = .725

CKT	Z	P	EPS	TR R	TWG R	HG THEOR	FLUX MEAS	CG	S	DEQG	AFLOWG
1A	-4.653	3.670	3.17	4805.	1315.	0.192E-02	10.13	1.389	1.047	2.655	25.078
1B	-3.738	3.561	2.88	4805.	865.	0.214E-02	4.64	0.541	1.971	2.456	22.776
2B	-2.939	3.263	2.15	4802.	815.	0.283E-02	6.21	0.558	2.825	1.928	16.981
2A	-2.208	2.847	1.62	4792.	910.	0.361E-02	9.45	0.671	3.667	1.650	12.819
3	-1.555	2.470	1.19	4769.	830.	0.473E-02	11.12	0.597	4.420	1.387	9.393
12P	-1.428	2.396	1.11	4752.	920.	0.493E-02	12.11	0.642	4.568	1.335	8.784
4	-1.064	2.187	1.00	4727.	890.	0.527E-02	13.06	0.646	4.988	1.329	7.901
5	-0.737	2.012	1.00	4727.	930.	0.515E-02	15.98	0.817	5.359	1.467	7.901
6	-0.409	1.906	1.00	4727.	900.	0.507E-02	14.47	0.746	5.714	1.604	7.901
7	0.001	1.860	1.00	4727.	845.	0.499E-02	12.87	0.664	6.116	1.776	7.901
8	0.246	1.876	1.02	4720.	705.	0.493E-02	6.72	0.339	6.363	1.792	8.041
9	0.573	1.948	1.10	4686.	790.	0.445E-02	9.83	0.568	6.698	1.860	8.666
10	0.901	2.036	1.20	4643.	790.	0.394E-02	9.68	0.637	7.038	1.944	9.465
11	1.228	2.124	1.30	4628.	720.	0.362E-02	6.07	0.429	7.377	2.028	10.299
12A	1.651	2.237	1.45	4609.	775.	0.322E-02	7.93	0.642	7.814	2.136	11.425
12B	2.104	2.358	1.61	4587.	665.	0.289E-02	4.27	0.376	8.283	2.252	12.70
13B	2.557	2.480	1.78	4564.	645.	0.258E-02	3.32	0.328	8.753	2.368	14.044
13A	3.011	2.601	1.96	4540.	700.	0.230E-02	5.66	0.642	9.222	2.484	15.451

SECONDARY MODE I TEST 144 LE=1.5

	PC PSIA	MR	WT LB/S
PRIMARY	399.0	2.800	3.87
SECONDARY	179.9	3.010	5.50

PRESSURE RATIO = .449

CKT	Z	R	EPS	TR R	TWG R	HG THEOR	FLUX MEAS	CG	S	DEQG	AFLOWG
1A	-4.653	3.670	3.17	4826.	730.	0.127E-02	7.46	1.436	1.047	2.655	25.078
1B	-3.738	3.561	2.88	4825.	720.	0.139E-02	3.16	0.553	1.971	2.456	22.776
2B	-2.939	3.263	2.15	4822.	720.	0.184E-02	4.20	0.556	2.825	1.928	16.989
2A	-2.208	2.847	1.62	4811.	770.	0.235E-02	6.03	0.631	3.667	1.650	12.819
3	-1.555	2.471	1.19	4789.	735.	0.307E-02	7.46	0.599	4.420	1.387	9.393
12P	-1.428	2.396	1.11	4772.	795.	0.321E-02	8.30	0.651	4.568	1.335	8.784
4	-1.064	2.187	1.00	4747.	775.	0.343E-02	9.01	0.662	4.988	1.329	7.991
5	-0.737	2.012	1.00	4747.	775.	0.336E-02	9.93	0.744	5.359	1.467	7.991
6	-0.439	1.906	1.00	4747.	765.	0.330E-02	9.33	0.709	5.734	1.604	7.991
7	0.000	1.860	1.00	4747.	765.	0.324E-02	9.65	0.748	6.116	1.776	7.991
8	0.246	1.876	1.02	4739.	675.	0.319E-02	5.50	0.424	6.363	1.792	8.041
9	0.573	1.948	1.10	4706.	695.	0.289E-02	6.45	0.556	6.698	1.860	8.666
10	0.901	2.036	1.20	4662.	695.	0.256E-02	6.28	0.617	7.038	1.944	9.465
11	1.228	2.124	1.30	4647.	670.	0.235E-02	4.63	0.493	7.377	2.028	10.299
12A	1.651	2.237	1.45	4626.	700.	0.209E-02	5.62	0.684	7.814	2.136	11.425
12B	2.104	2.358	1.61	4606.	635.	0.187E-02	3.52	0.474	8.283	2.252	12.701
13B	2.557	2.480	1.78	4583.	625.	0.167E-02	2.81	0.426	8.753	2.368	14.044
13A	3.011	2.601	1.96	4559.	645.	0.149E-02	4.05	0.695	9.222	2.484	15.451

SECONDARY MODE I TEST 147 LE=1.5

	PC PSIA	MR	WT LB/S
PRIMARY	381.0	3.340	3.68
SECONDARY	315.0	3.400	9.67

PRESSURE RATIO = .827

CKT	Z	R	EPS	TR R	TWG R	HG THEOR	FLUX MEAS	CG	S	DEGG	AFLOWS
1A	-4.653	3.670	3.17	5166.	900.	0.193E-02	8.47	1.031	1.047	2.655	25.078
1B	-3.738	3.561	2.88	5165.	900.	0.211E-02	8.47	0.941	1.971	2.456	22.776
2B	-2.939	3.263	2.15	5161.	865.	0.280E-02	7.31	0.607	2.825	1.928	16.988
2A	-2.208	2.847	1.62	5150.	935.	0.357E-02	10.11	0.671	3.667	1.656	12.819
3	-1.555	2.470	1.19	5126.	875.	0.468E-02	11.83	0.595	4.420	1.387	9.393
12P	-1.428	2.396	1.11	5108.	965.	0.488E-02	13.55	0.671	4.568	1.335	8.784
4	-1.064	2.187	1.00	5081.	915.	0.522E-02	14.07	0.647	4.988	1.329	7.931
5	-0.737	2.012	1.03	5081.	930.	0.511E-02	15.93	0.750	5.359	1.467	7.931
6	-0.409	1.906	1.00	5081.	890.	0.504E-02	14.16	0.671	5.734	1.604	7.931
7	0.000	1.860	1.00	5081.	875.	0.494E-02	14.06	0.677	6.116	1.776	7.931
8	0.246	1.876	1.02	5073.	745.	0.487E-02	8.09	0.384	6.363	1.792	8.041
9	0.573	1.948	1.10	5037.	765.	0.441E-02	9.00	0.482	6.698	1.869	8.666
10	0.901	2.036	1.20	4990.	760.	0.392E-02	8.84	0.534	7.038	1.944	9.465
11	1.228	2.124	1.30	4975.	720.	0.359E-02	6.07	0.398	7.377	2.028	10.299
12A	1.651	2.237	1.45	4954.	770.	0.319E-02	7.76	0.581	7.814	2.136	11.429
12B	2.104	2.358	1.61	4931.	690.	0.285E-02	5.15	0.426	8.283	2.252	12.730
13B	2.557	2.480	1.78	4906.	670.	0.255E-02	3.97	0.368	8.753	2.368	14.044
13A	3.011	2.601	1.96	4880.	705.	0.227E-02	5.79	0.611	9.222	2.484	15.451

area are calculated on a plane for which the angle between the normal to the plane and the chamber centerline is equal to the average of the wall angles where the plane intersects the walls.

For the nozzle spacing of 1.5 in., the calculated secondary flow stream tube throat areas were slightly greater than the secondary flow area at the end of the primary chamber. These tests were originally planned to have the latter area slightly larger than the stream tube throat area. In the stream tube model the throat area was set equal to the annular flow area at the end of the primary chamber, with a constant flow area assumed between these two locations. The effect of the small flow area at the end of the primary chamber is clearly seen in the high heat fluxes upstream of the physical throat in Figures 69 to 69c for Tests 144-147.

Average correlation coeffcients for the two secondary mixture ratios tested with a nozzle spacing of 2.5 in. are shown in Figure 88. A signficant injector effect is observed which decays over the first 2.4 in. of the secondary wall (the wall starts at -6.2 in. on Figure 88). This heat flux perturbation is typical of swirl co-axial injector elements. Correlation coefficients downstream of the injector-affected region are generally consistent with the range of primary Mode II values, Figure 71, and with data from other programs. However, contrary to the primary Mode II results, use of the reactive specific heat does not result in agreement between the two mixture ratios. Erratic behavior of the correlation coefficients is noted downstream of the throat, with alternating regions of low and high values. The high coefficients at the end of the nozzle may be due to heating of the end wall, but the other perturbations are presumed to be caused by the oblique shock wave emanating from the separation point in the primary nozzle. Note that the data from circuit P12 are reasonably consistent with the secondary chamber data.

Average correlation coefficients from the four tests with a nozzle spacing of 1.5 in. are shown in Figure 89. Results are similar to those of Figure 88 for the 2.5 in. spacing, except the length of the injector

perturbation is shorter. It may be that the high coefficients at -4.65 in. on Figure 88 are caused by a slight discontinuity between the one-inch L' section and the secondary chamber, with the injector effect decaying very rapidly as indicated by Figure 89. The uniform flow area assumption noted above for the secondary stream tube between the end of the primary chamber and the physical throat results in consistent correlation coefficients for three of the four data points in this region. The higher coefficient at circuit S5 appears to be qualitatively consistent with the shape of the sonic line which can be expected to start at the tip of the primary chamber.

5. Secondary Mode II

Heat flux profiles for the secondary chamber during Mode II operation are included in Appendix B (Figures B-1 to B-10). Comparison of results for the three test series summarized in Table XXVI reveal inconsistencies which are attributed to leakage from the tip of the primary chamber during the second and third series. For example, heat fluxes for Tests 137 and 139 are lower for comparable bleed flows than Tests 111-114 even though the former are at higher primary chamber pressures. Therefore, the data analysis effort has been limited to Tests 111-114. Figures 1B-1 to B-4 in Appendix B show that the maximum heat flux is always at the throat even though the variation in bleed flow is shifting the primary plume impingement point. Figure 90 shows that the peak heat flux is sensitive to the bleed flow rate; it more than doubles when the bleed flow is reduced from 3.9 percent to 1.4 percent. Even at the lowest bleed flow the maximum heat flux is only about half the Mode I flux, which exceeds 15 Btu/in^2 sec for pressure ratios of 0.60 and higher. Figure 91 reveals that the flux profile also changes shape as the bleed flow changes; the relative heat fluxes immediately upstream (S6) and downstream (S8) of the throat are shown as a function of bleed flow rate. As expected, the relative downstream heat flux increases and the upstream flux decreases as the bleed flow increases and shifts the impingement point downstream.

V, C, Results (cont.)

The purpose of the data analysis task for the secondary chamber in Mode II was to fit the aerodynamic and thermal models of Task I and the previous contract, Reference 2, to the test data, thereby confirming or redefining the empirical parameters in these models. Three empirical parameters appear in the Aerodynamic Bleed Flow Model, Reference 2, two of which have previously been based on correlation of cold flow data:

(1) The plume scaling factor is a multipler in the similarity parameter of the plume correlation, and has a value of 1.2 for the nozzle spacings tested herein based on cold flow data;

(2) The Nash factor is used in the recompression criteria relating the pressure behind the plume attachment shock to the recirculation region pressure, and it was determined to be 0.4 based on cold flow data;

(3) The jet spreading factor affects the thickness of the shear layer and is based on a correlation developed by Korst, Reference 13.

The thermal model includes two empirical parameters; the initial energy thickness of the boundary layer, and the entrainment fraction which controls the mixing rate after the shear layer becomes a wall jet downstream of the impingement point. Entrainment fraction values were expected to be similar to those for injection of a film coolant into a supersonic flow, Reference 14.

Initial comparisons of model predictions and data from Test 111 and 113 made it clear that it would be very difficult to match the data using the velocity mixing function of Figure 92. Therefore, the latter was changed to start at the relative velocity of the streamline in the shear layer and increase rapidly to unity. These early studies also revealed that the sensitivity of the recirculation region pressure to bleed flow was much greater than predicted. Furthermore, it was clear that the heat flux profiles would be much easier to predict if the impingement point location from the

aerodynamic model could be shifted upstream. Therefore, a survey of the effect of the Nash factor and the plume scaling factor was undertaken. It was determined that reducing the Nash factor to 0.2 accomplished both objectives. Figure 93 shows the predicted recirculation pressures as a function of bleed flow rate for the original cold flow Nash factor of 0.4 as well as the recommended value of 0.2. Agreement of the latter model with the measured pressures is seen to be very good.

Parametric studies with the heat transfer model indicated the heat flux predictions were relatively insensitive to the entrainment fraction except near the plume attachment point. This is caused by the offsetting effects of increased adiabatic wall temperature and reduced heat transfer coefficient as the mixture ratio at the wall is increased. As a result, subsequent predictions were based on a typical entrainment fraction of 0.03 from the data of Reference 14, and the initial boundary layer energy thickness remained as the empirical parameter with which to match measured heat fluxes. Figure 94 shows that reasonably good agreement with the entire nozzle heat flux profile is obtained for Test 113 when the initial or attachment point boundary layer energy thickness is adjusted such that the predicted throat heat flux matches the measured flux. Matching the throat heat flux was accomplished with an initial boundary energy layer thickness equal to only three percent of the shear layer energy thickness. This result is consistent with the Task I analysis presented in Figure 95, which found that matching the downstream predictions from a two-dimensional finite difference boundary layer program required a very small initial thickness in the current integral boundary layer model.

It was planned that the initial energy thickness would be specified as a fraction of the shear layer energy thickness at the attachment point. However, Figure 90 shows that such a prescription does not give the correct sensitivity of the heat flux prediction to bleed flow rate. Increasing the initial boundary layer thickness to 20 percent of the shear layer value allows the first data point downstream of the attachment point to be

V, C, Results (cont.)

During Mode I operation the primary throat is choked, but the primary nozzle is unable to flow full against the high back pressure imposed by the secondary chamber. Large increases in heat flux relative to Mode II observed near the end of the primary nozzle are consistent with the twin vortex recirculation pattern of Figure 79 in the separated region, which includes the wake region downstream of the end of the primary chamber. As the secondary chamber pressure increases, the region of increased heat flux extends farther upstream and the perturbation at the end of the nozzle increases.

Unsymmetrical heating of the tip of the primary chamber is caused by the flow separation in the primary nozzle and the resultant recirculation pattern noted above.

Secondary chamber heat fluxes during Mode I operation can be predicted with the secondary flow stream tube model used herein and correlation coefficients consistent with other applications. High heat fluxes observed near the swirl coaxial element injector are consistent with previous experience. Rapid decreases and increases with axial distance of correlation coefficients in the secondary nozzle are probably caused by oblique shock waves created by the flow separation in the primary nozzle.

Heat fluxes in the secondary throat region during Mode II operation are easily limited to values well below Mode I fluxes using small bleed flow rates, e.g., two percent of the primary flow for the geometry tested. Therefore, primary plume attachment is not a thermal design issue.

Although the analytical model of Mode II can predict secondary nozzle heat fluxes under limited test conditions, it does not exhibit the correct sensitivity to bleed flow rate. Additional model development is required to account for velocity components normal to the wall. A Nash factor of 0.2 in the aerodynamic model results in very good prediction of the recirculation region pressure and its sensitivity to bleed flow rate.

predicted for Test 111, the highest bleed flow point on Figure 151. However, as shown on Figure 96, predicted heat fluxes farther downstream are too high as would be expected from the Task I analysis noted above. For Test 111 the predicted plume attachment point is downstream of the secondary throat, so the maximum heat flux observed is in the recirculation region. The present aerodynamic model does not provide a description of the flow field in the recirculation region, so meaningful heat fluxes cannot be predicted upstream of the plume attachment point.

A model prediction is now shown for lowest bleed flow on Figure 90 (Test 114) due to a TDE convergence failure. A solution was obtained for the cold flow Nash factor of 0.4, but not for the recommended value of 0.2. The lower Nash factor moved the plume attachment point farther upstream of the secondary throat and, therefore, increased the wall angle and forced the flow to turn through a larger angle. A large reduction in flow angle results in intersections of the right characteristics in a method of characteristics solution, and TDE has a limited capability for handling such intersections.

The aerodynamic model and the use of TDE to define flow parameters at the secondary wall are intended primarily for bleed flows near the blow-off value, so that little or no turning of the flow is required at the plume attachment point and any shocks are very weak. Testing on the present program included bleed flows well below the blow-off value. It is apparent that to obtain a more general model and predict the current test data that impingement flow effects, i.e., velocity components normal to the wall, must be considered both upstream and downstream of the predicted attachment point.

D. CONCLUSIONS

Heat fluxes during conventional operation of the primary nozzle (Mode II) are consistent with data from other applications. Use of an enthalpy-based model, rather than the product of temperature difference and a frozen specific heat, is required to predict the effect of mixture ratio.

includes the wake region downstream of the end of the primary chamber. As the secondary chamber pressure increases, the region of increased heat flux extends farther upstream and the perturbation at the end of the nozzle increases.

Unsymmetrical heating of the tip of the primary chamber is caused by the flow separation in the primary nozzle and the resultant recirculation pattern noted above.

Secondary chamber heat fluxes during Mode I operation can be predicted with the secondary flow stream tube model used herein and correlation coefficients consistent with other applications. High heat fluxes observed near the swirl coaxial element injector are consistent with previous experience. Rapid decreases and increases with axial distance of correlation coefficients in the secondary nozzle are probably caused by oblique shock waves created by the flow separation in the primary nozzle.

Heat fluxes in the secondary throat region during Mode II operation are easily limited to values well below Mode I fluxes using small bleed flow rates, e.g., two percent of the primary flow for the geometry tested. Therefore, primary plume attachment is not a thermal design issue.

Although the analytical model of Mode II can predict secondary nozzle heat fluxes under limited test conditions, it does not exhibit the correct sensitivity to bleed flow rate. Additional model development is required to account for velocity components normal to the wall. A Nash factor of 0.2 in the aerodynamic model results in very good prediction of the recirculation region pressure and its sensitivity to bleed flow rate.

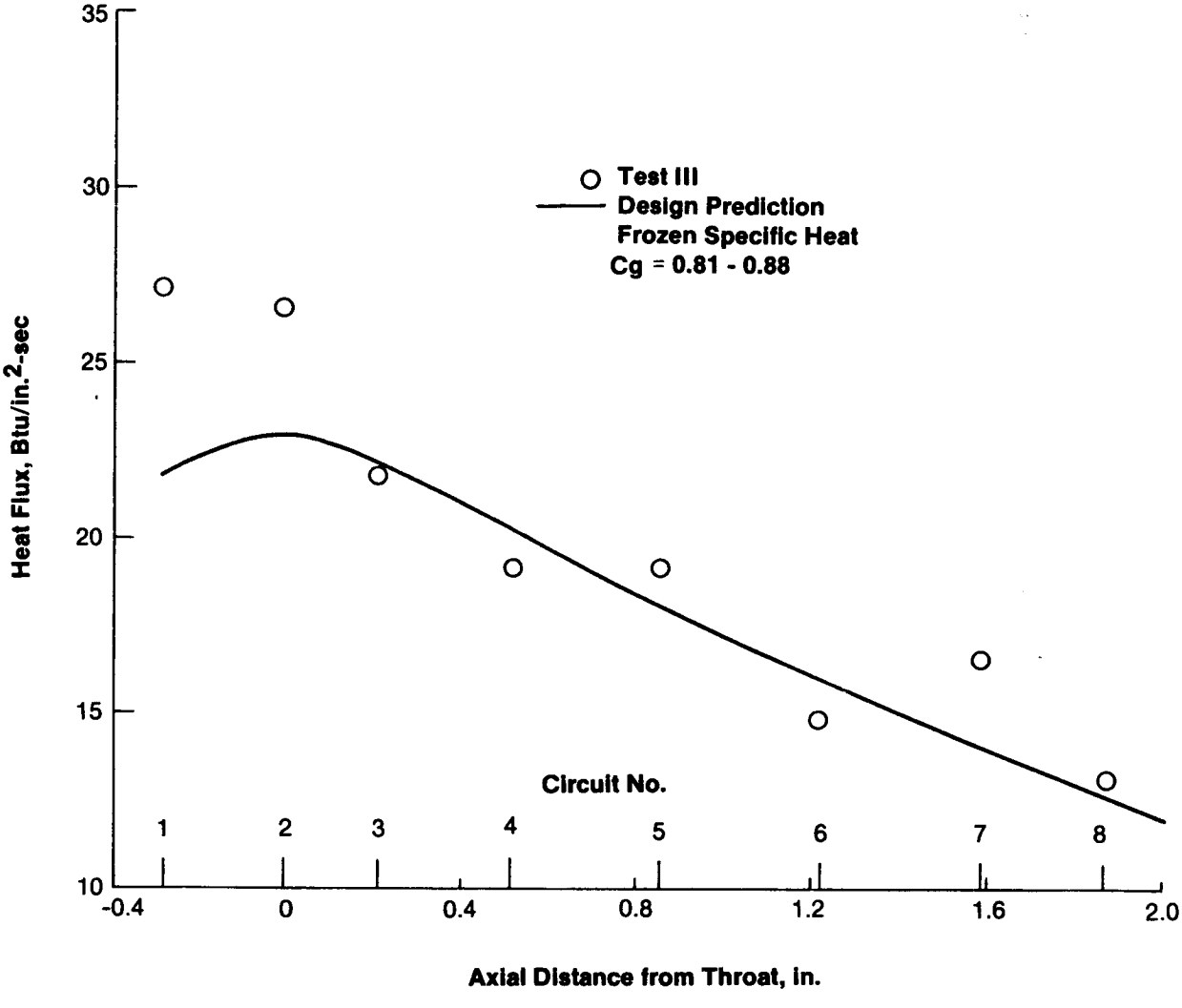

Figure 70. Mode II Primary Nozzle Heat Fluxes

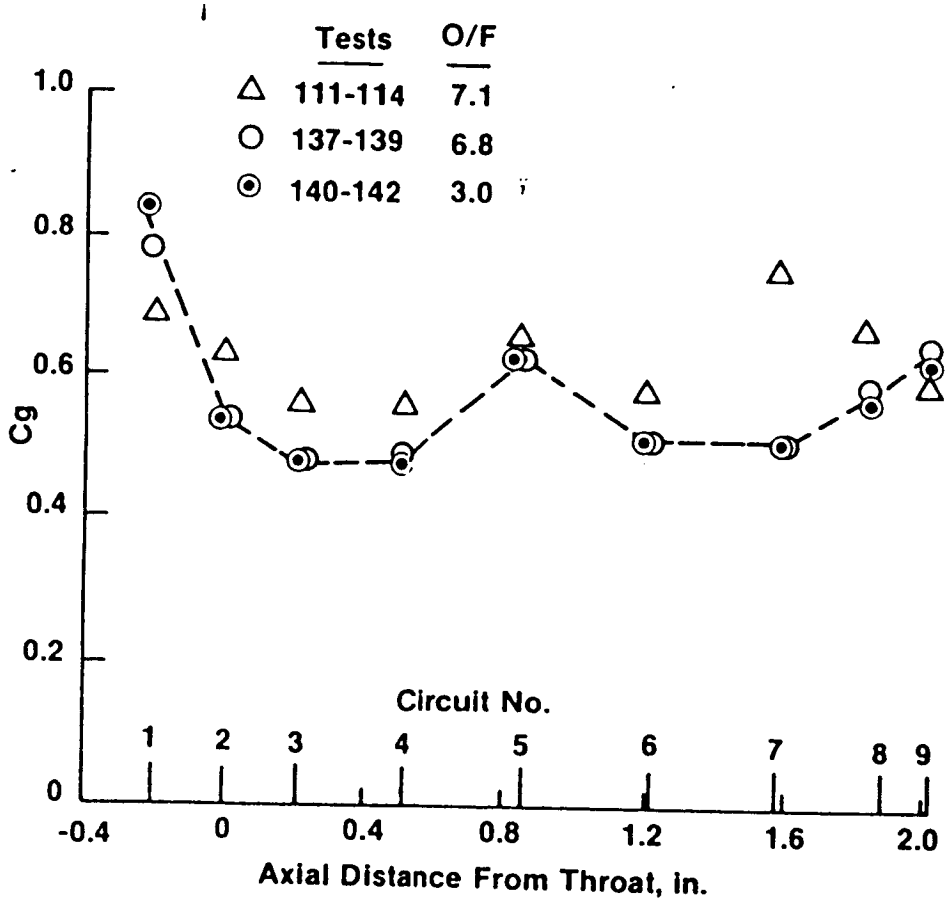

Figure 71. Mode II Primary Nozzle Correlation Coefficients

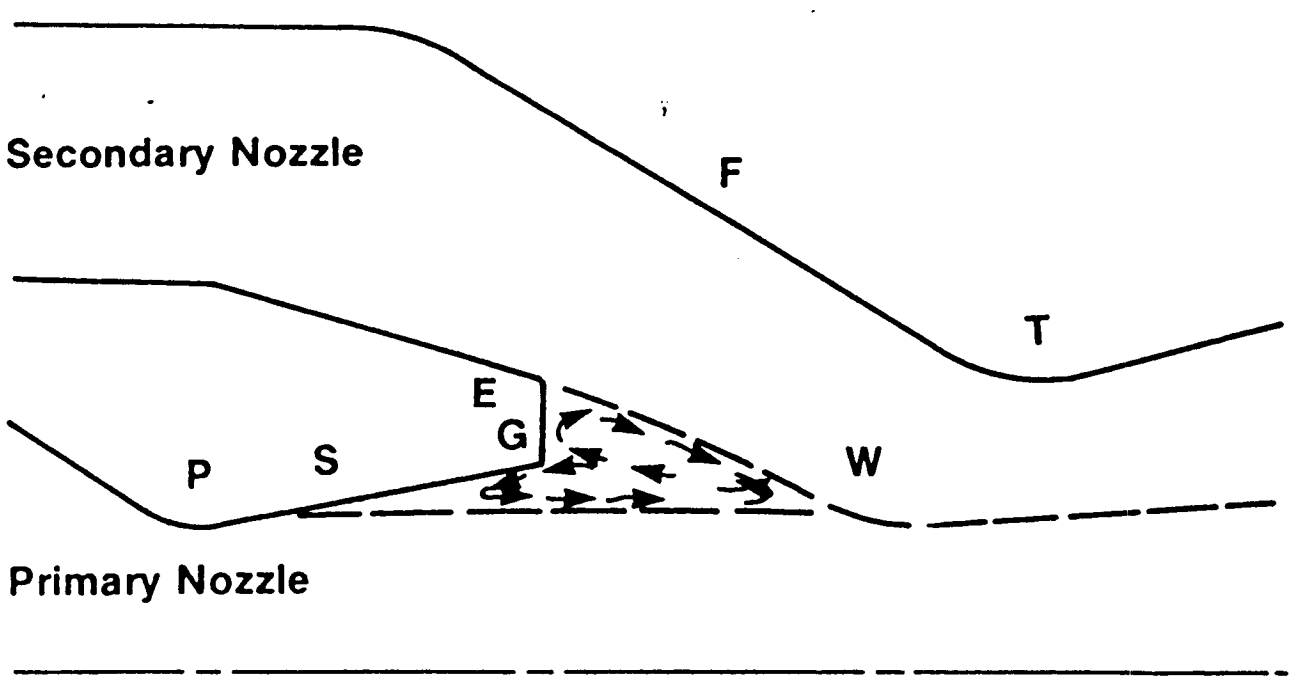

Figure 72. Mode I Flow Separation and Recirculation Pattern

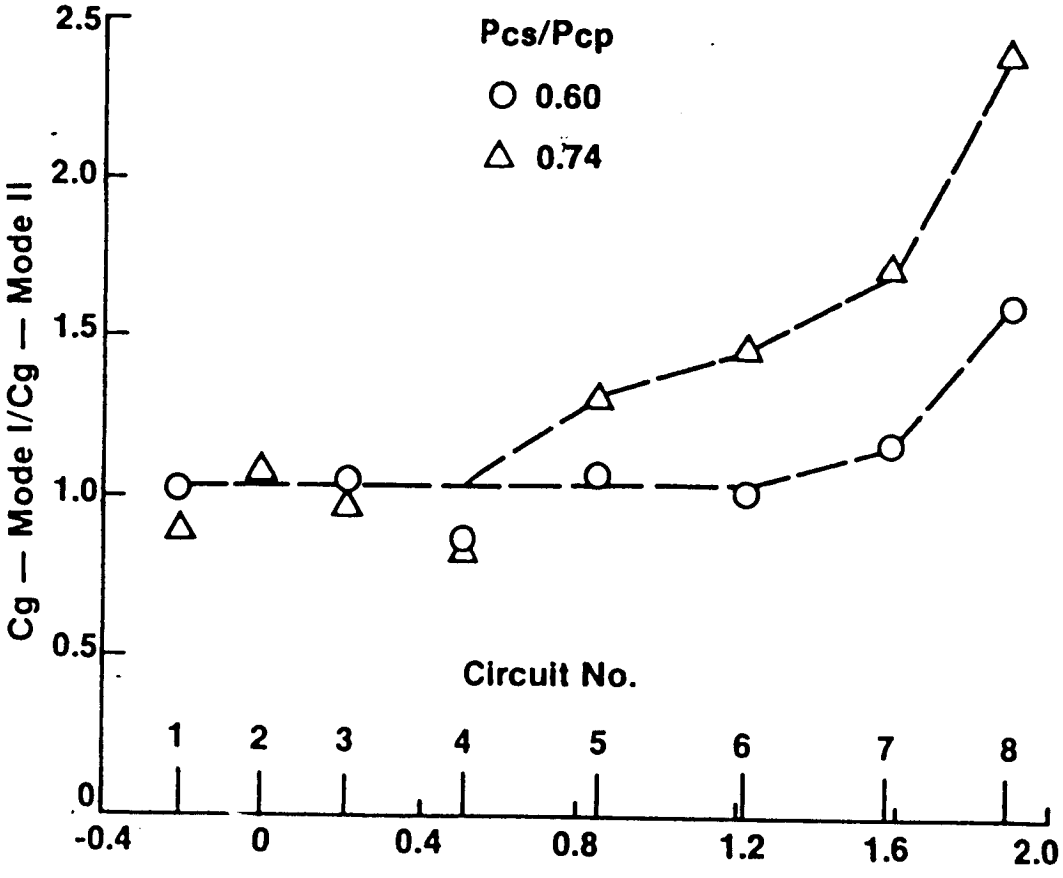

Figure 73. Primary Nozzle Mode I Heat Fluxes Relative to Mode II

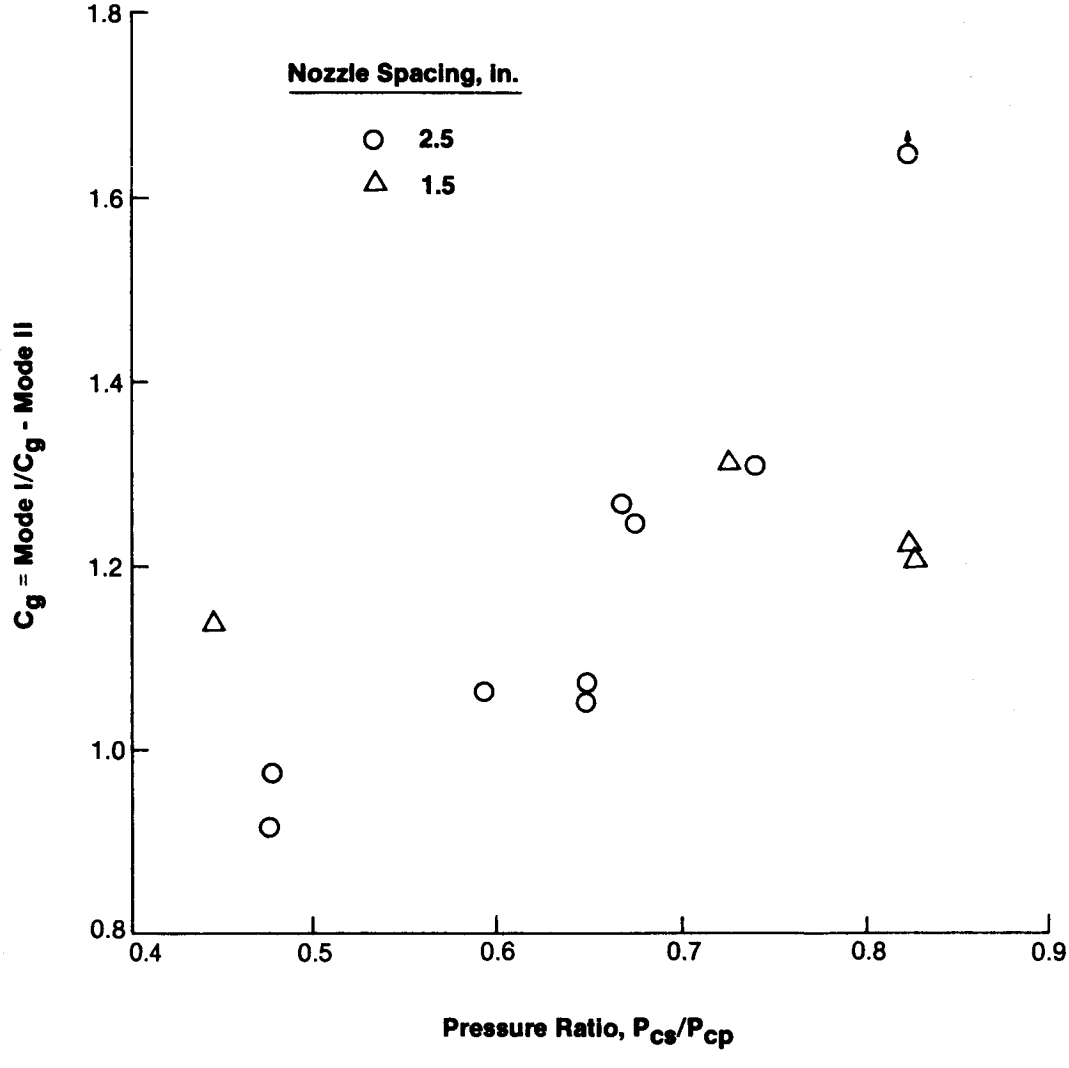

Figure 74. Effect of Pressure Ratio on Mode I Primary Nozzle Heat Fluxes, Circuit P5

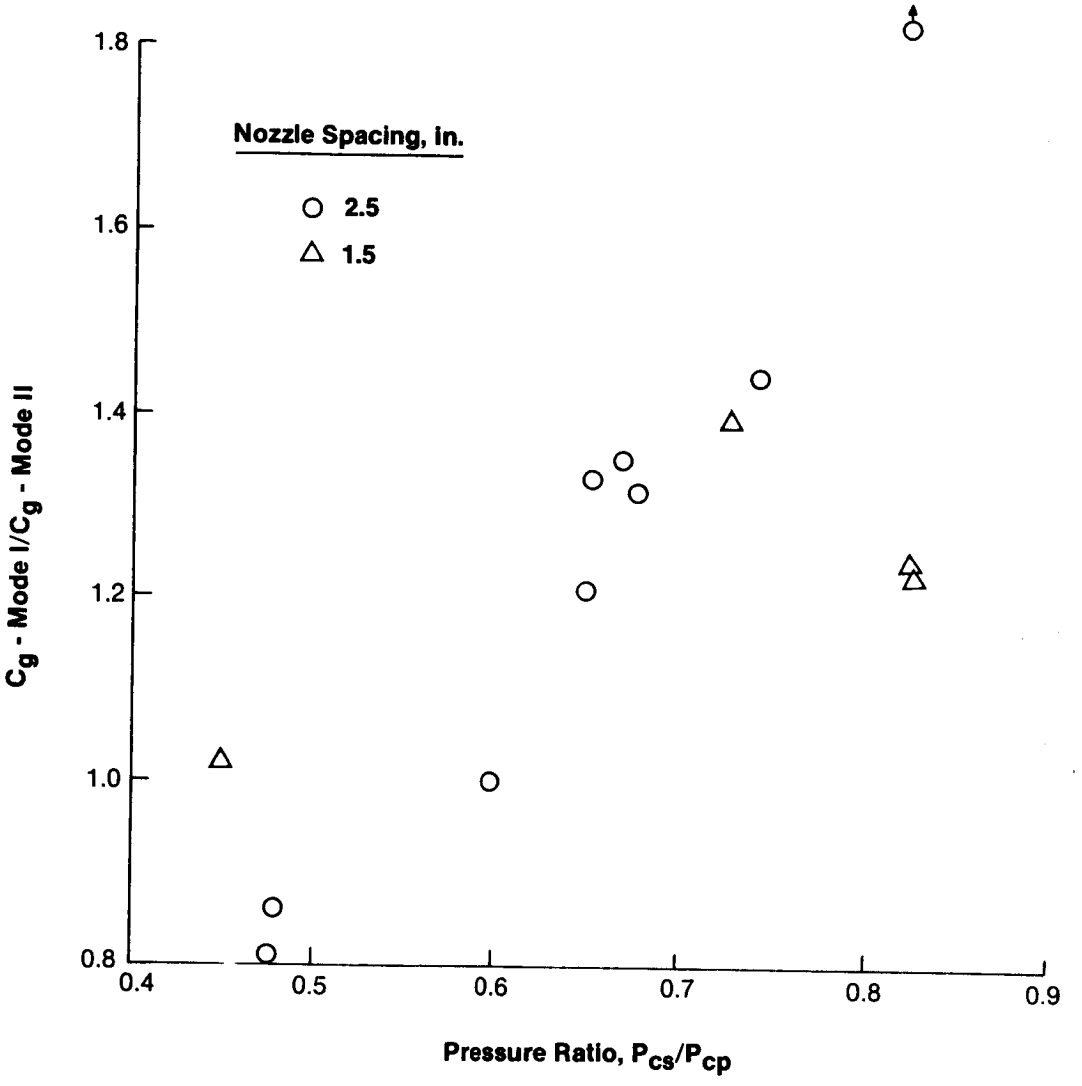

Figure 75. Effect of Pressure Ratio on Mode I Primary Nozzle Heat Fluxes, Circuit P6

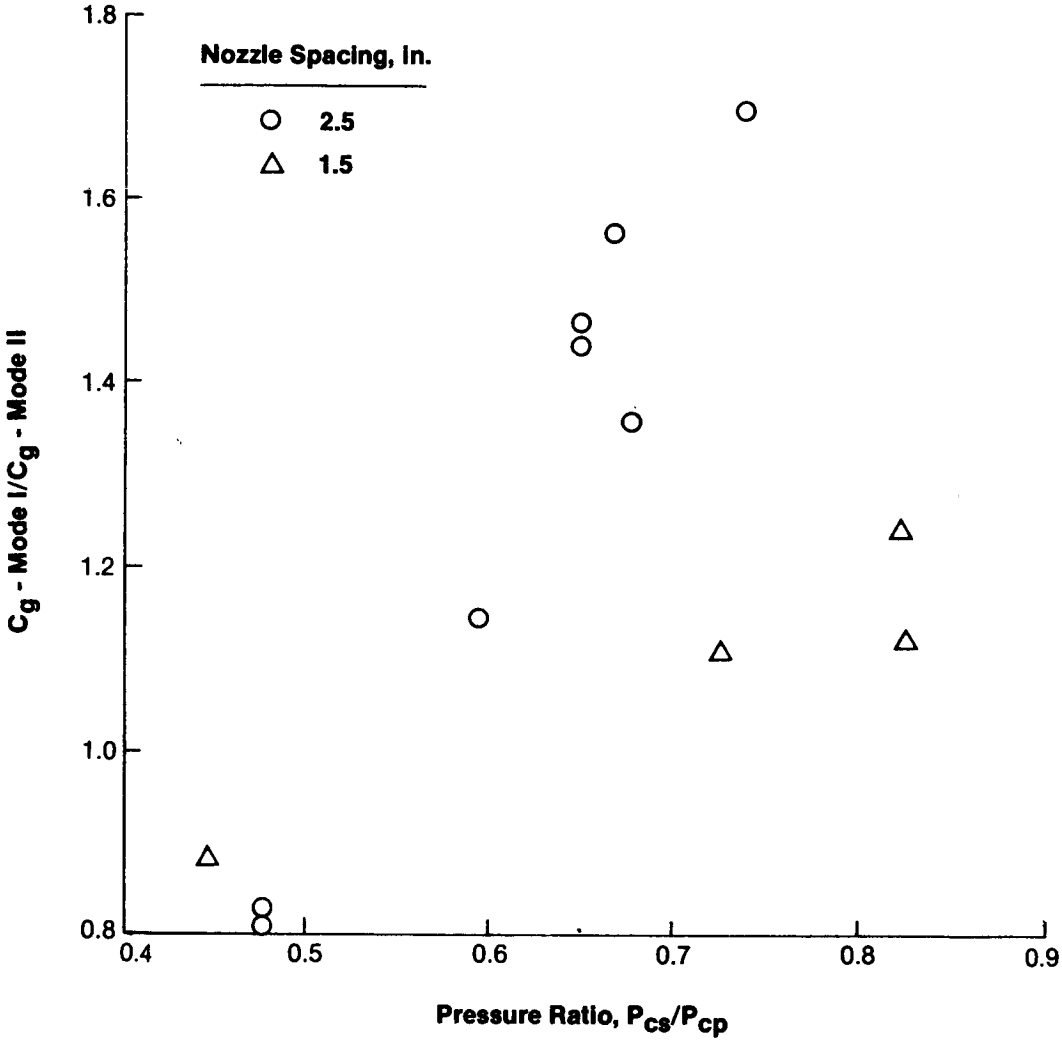

Figure 76. Effect of Pressure Ratio on Mode I Primary Nozzle Heat Fluxes, Circuit P7

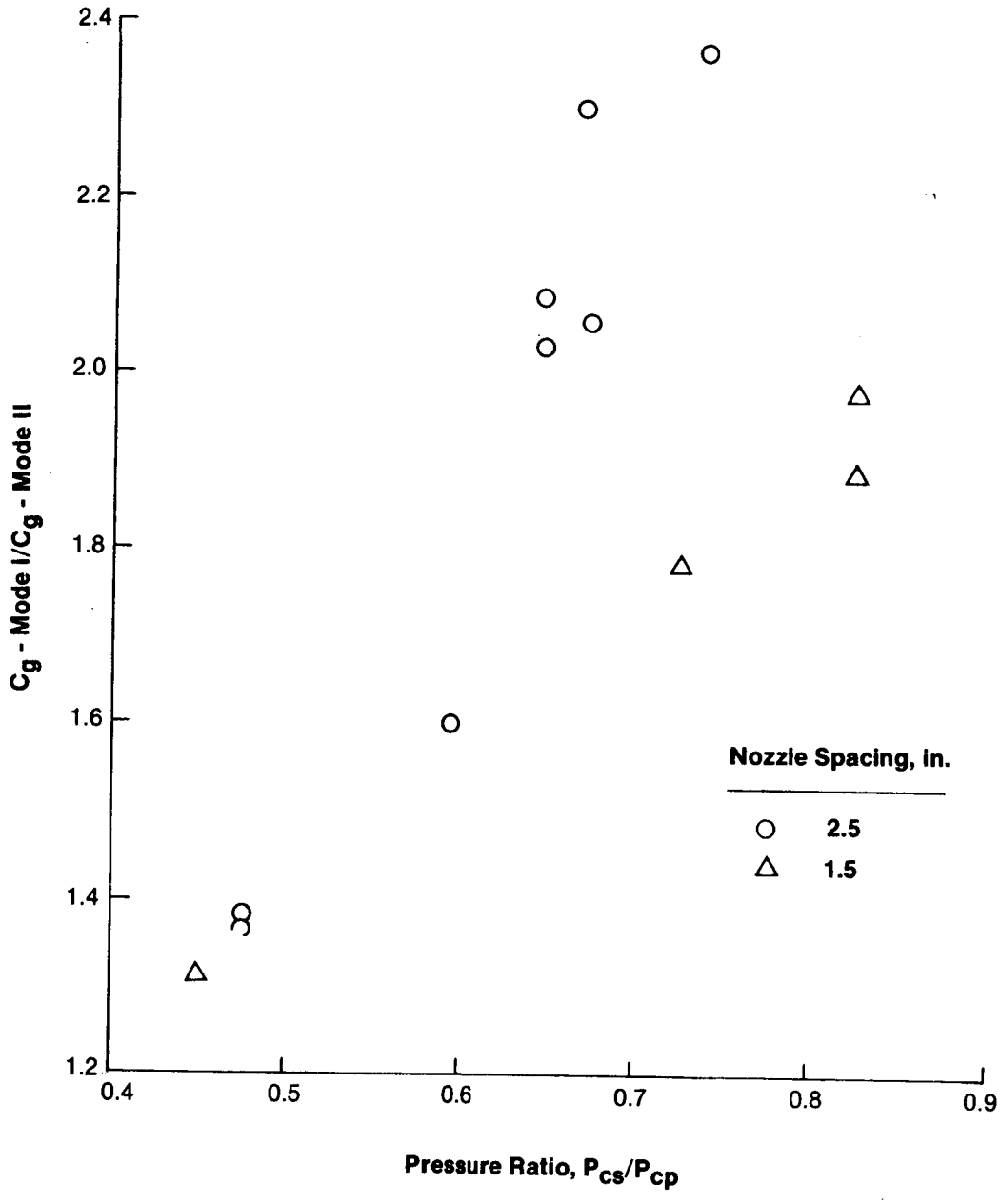

Figure 77. Effect of Pressure Ratio on Mode I Primary Nozzle Heat Fluxes, Circuit P8

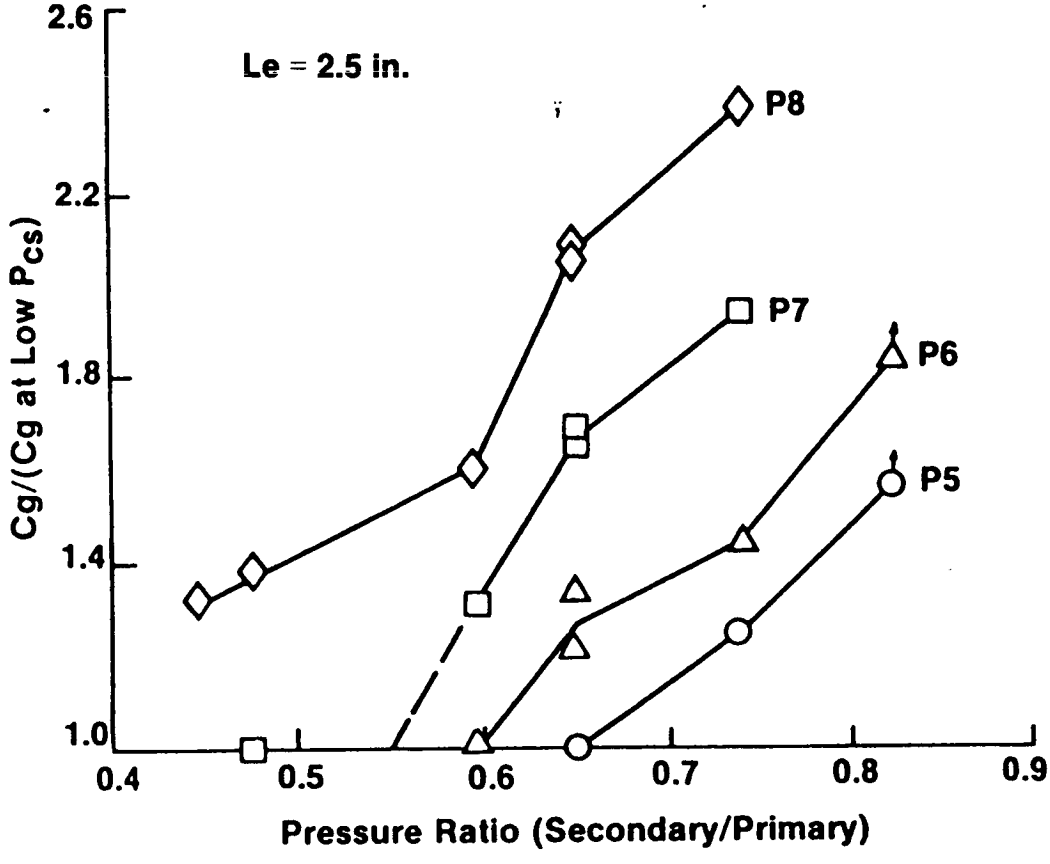

Figure 78. Effect of Pressure, Ratio On Mode I Primary Nozzle Heat Fluxes

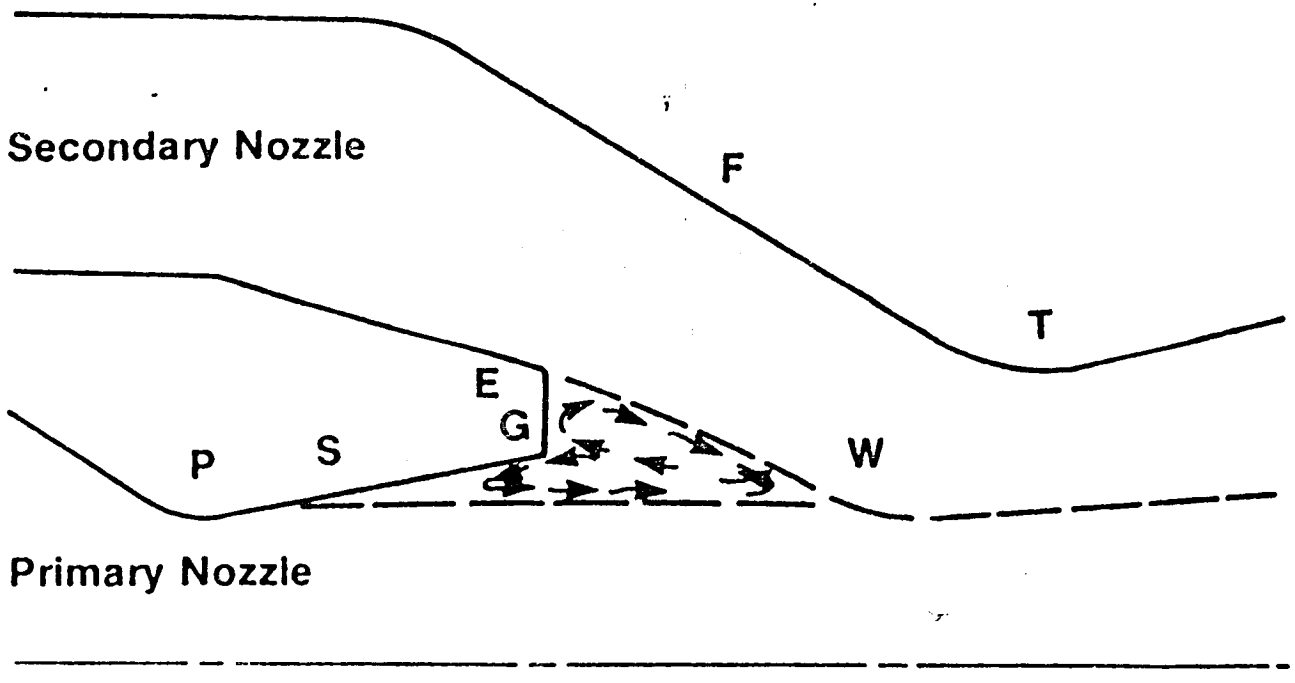

Figure 79. Mode I Flow Separation and Recirculation Pattern

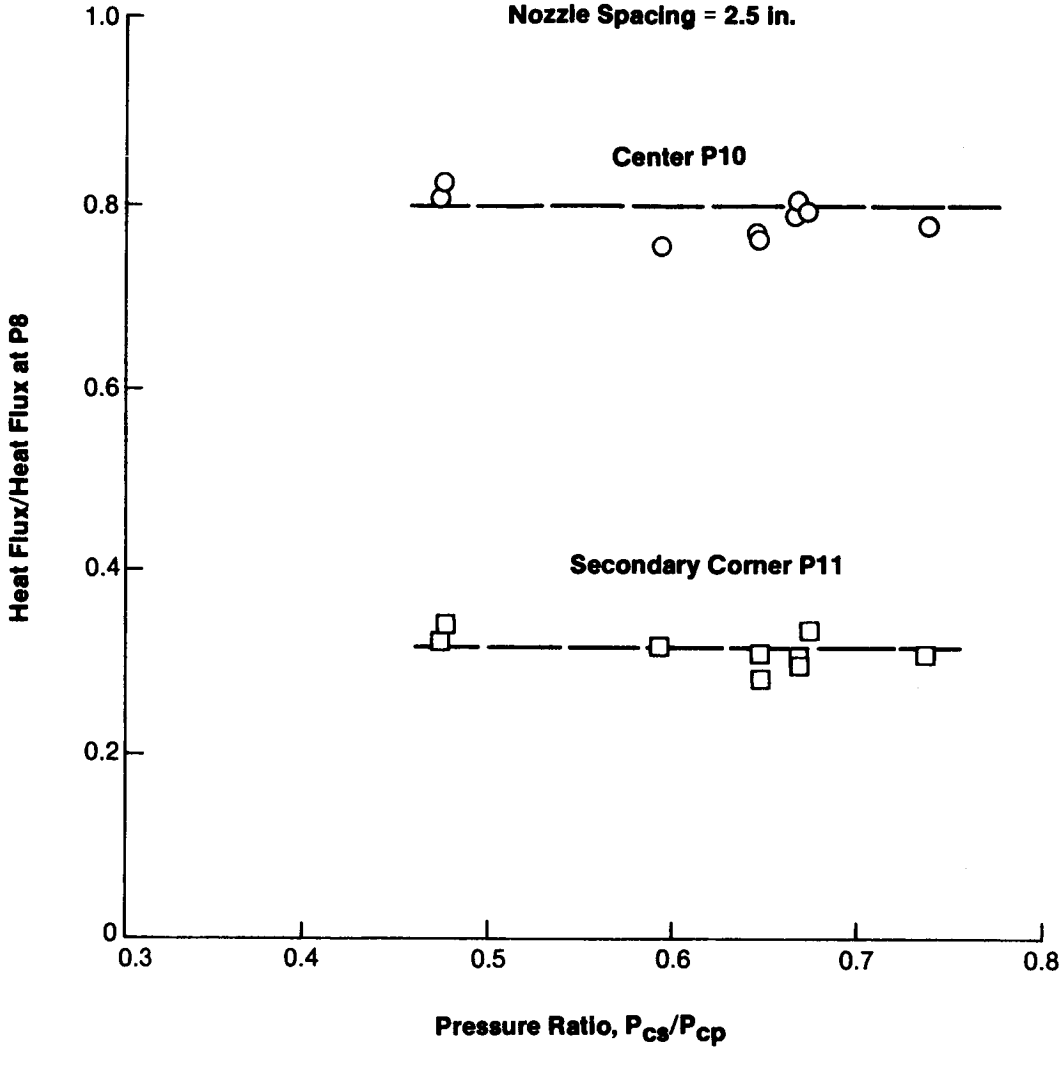

Figure 80. Mode I Primary Chamber Tip Heat Fluxes

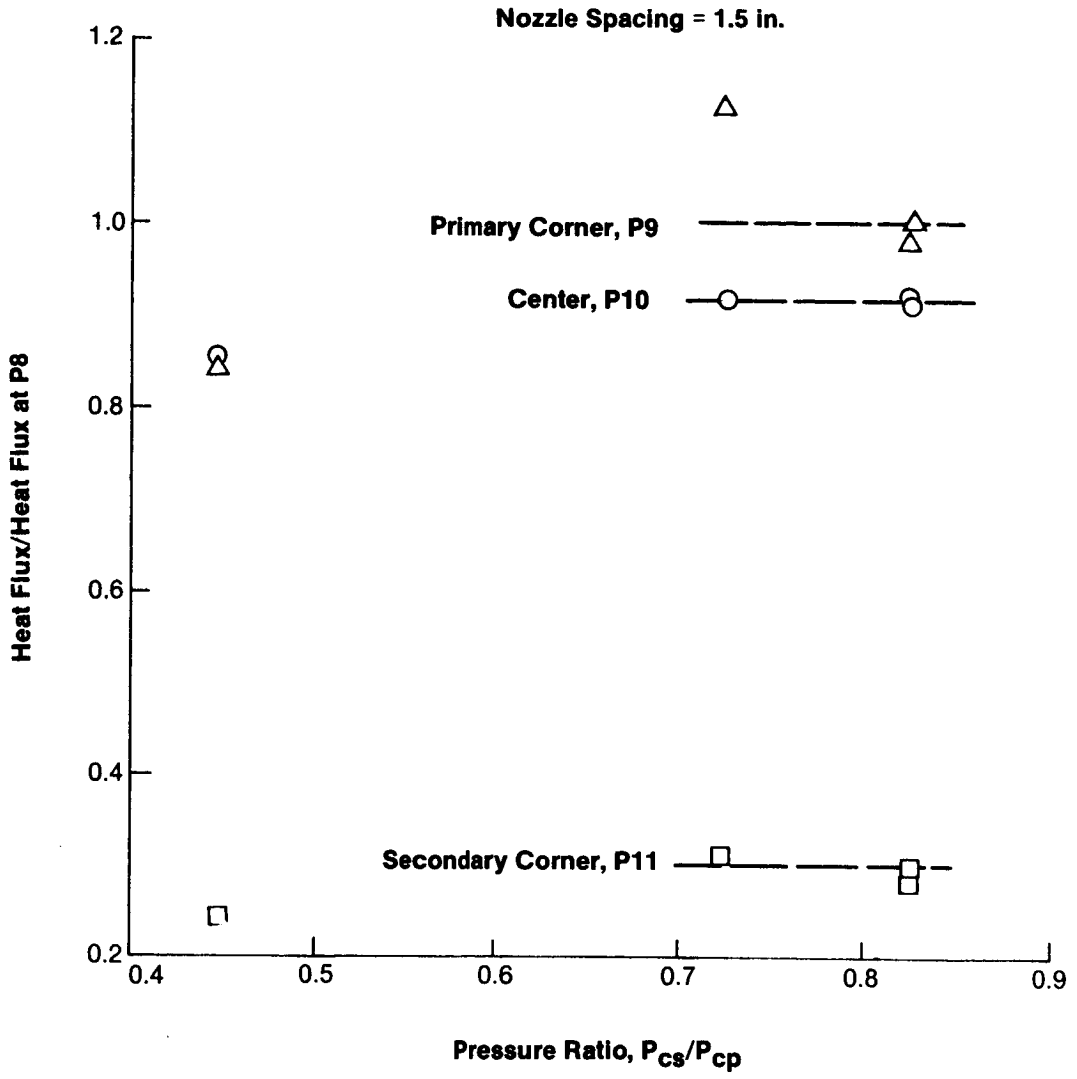

Figure 81. Mode I Primary Chamber Tip Heat Fluxes

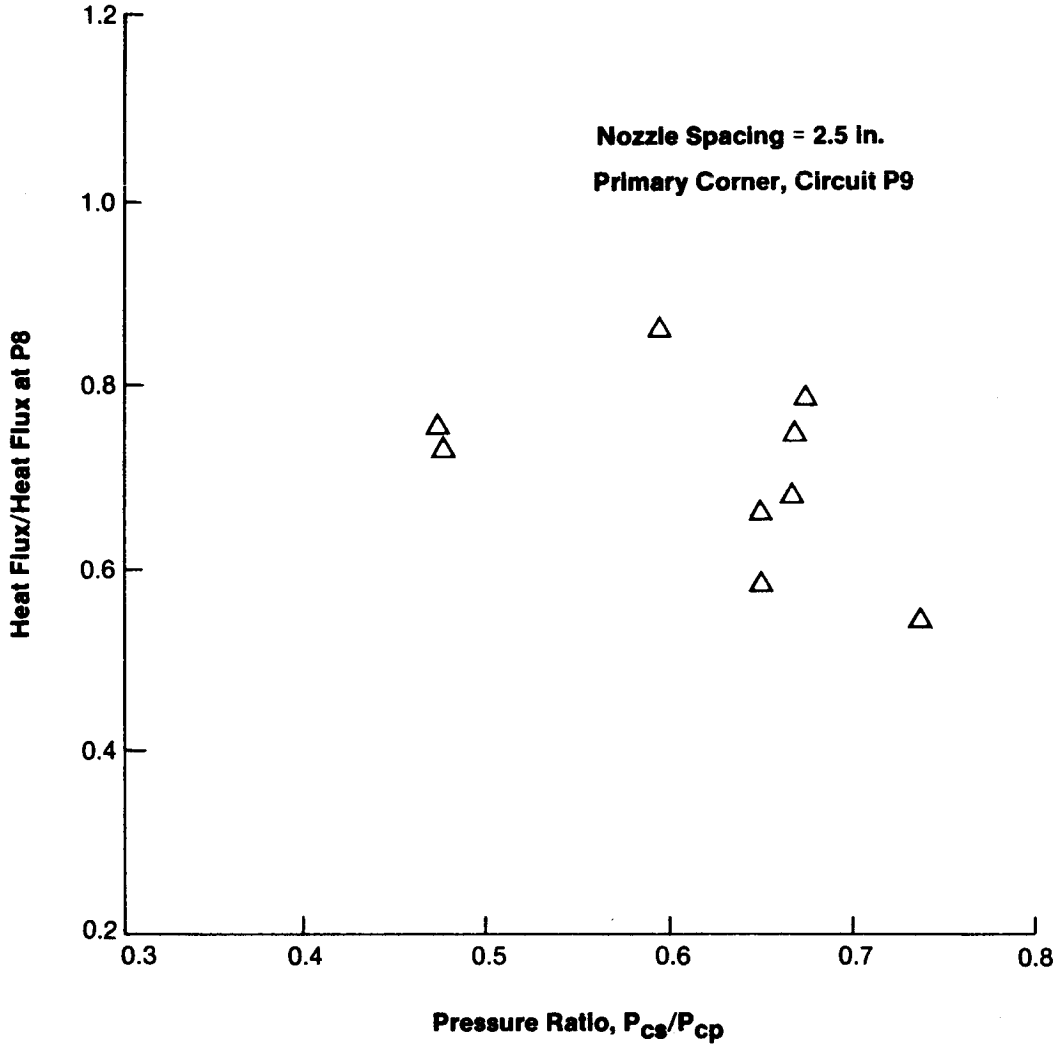

Figure 82. Mode I Primary Chamber Tip Heat Fluxes

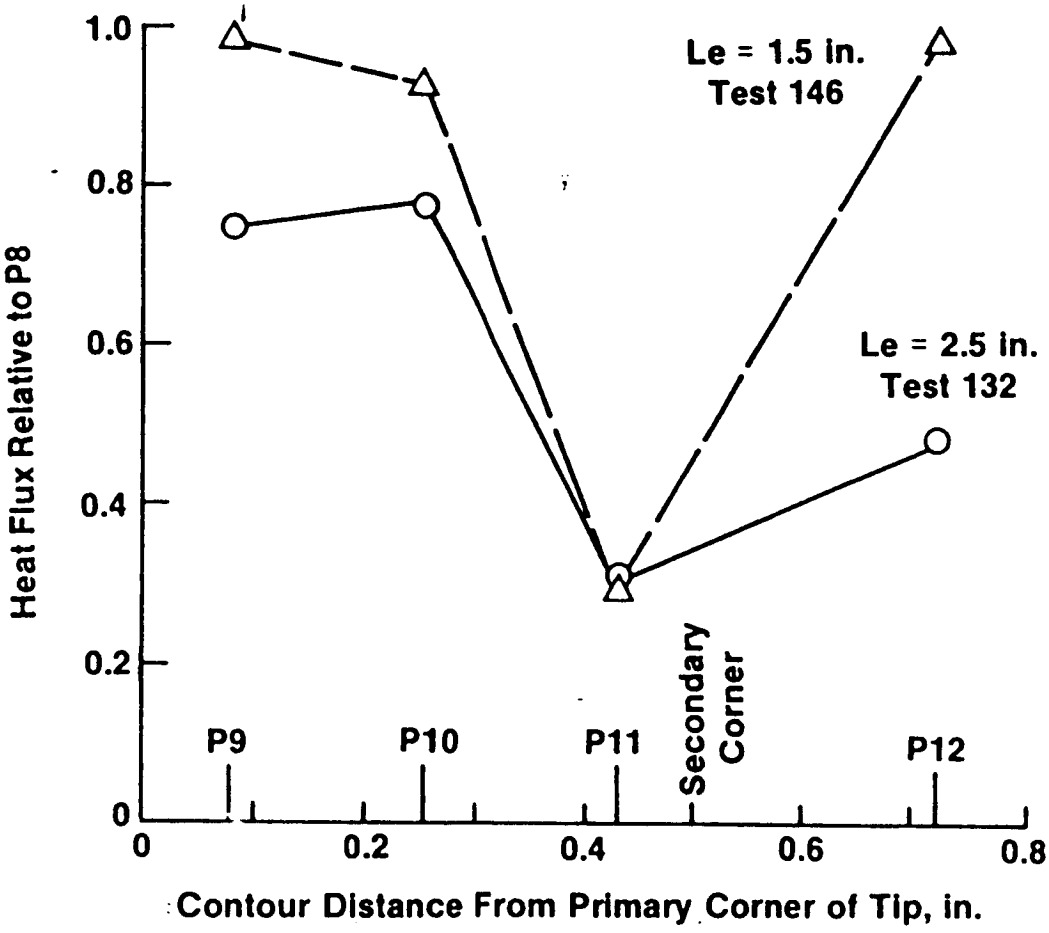

Figure 83. Mode I Primary Nozzle Tip Heat Flux Distribution

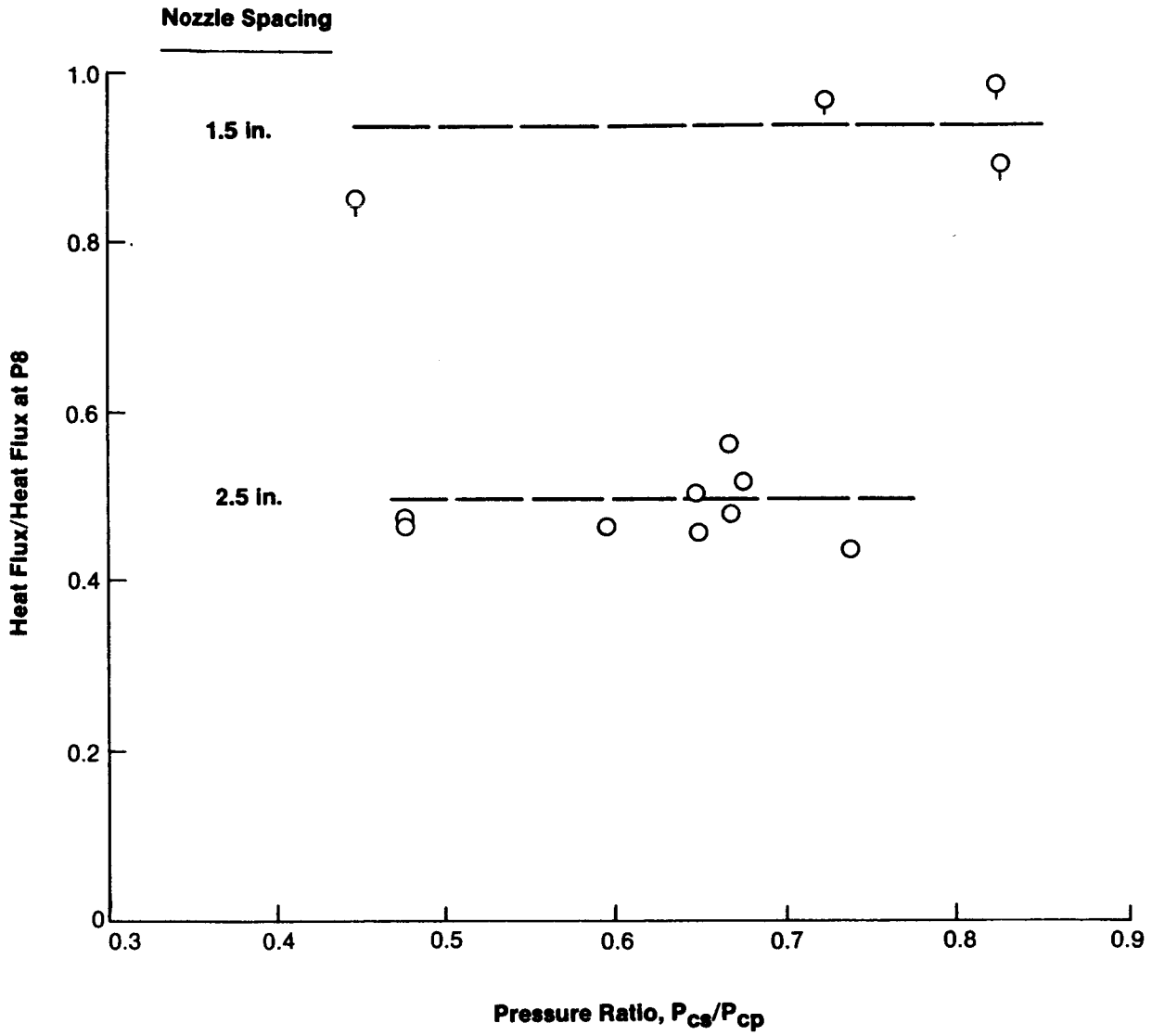

Figure 84. Mode I Primary Chamber Outer Wall Heat Fluxes (Circuit P12)

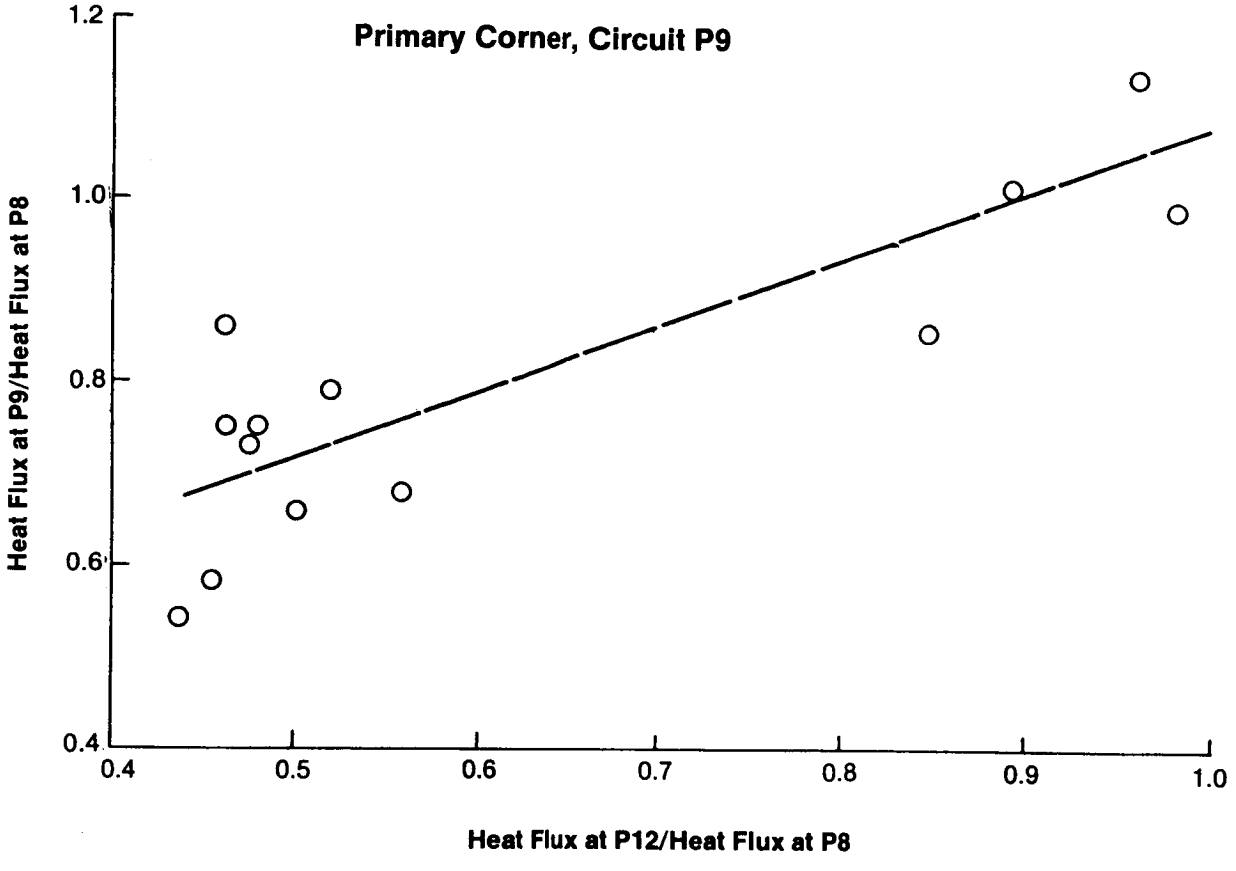

Figure 85. Mode I Primary Chamber Tip Heat Flux Correlation With Secondary Heat Flux

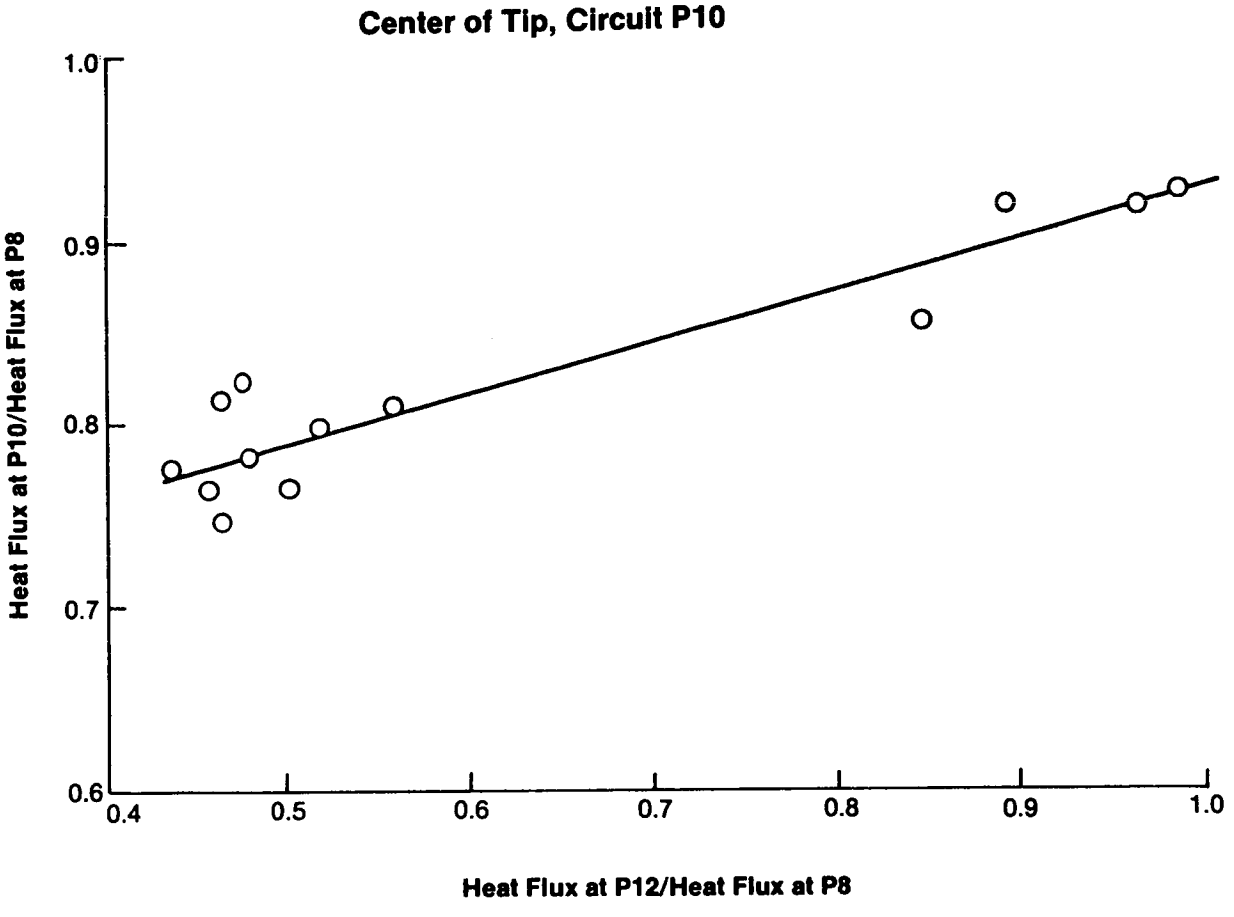

Figure 86. Mode I Primary Chamber Tip Heat Flux Correlation With Secondary Heat Flux

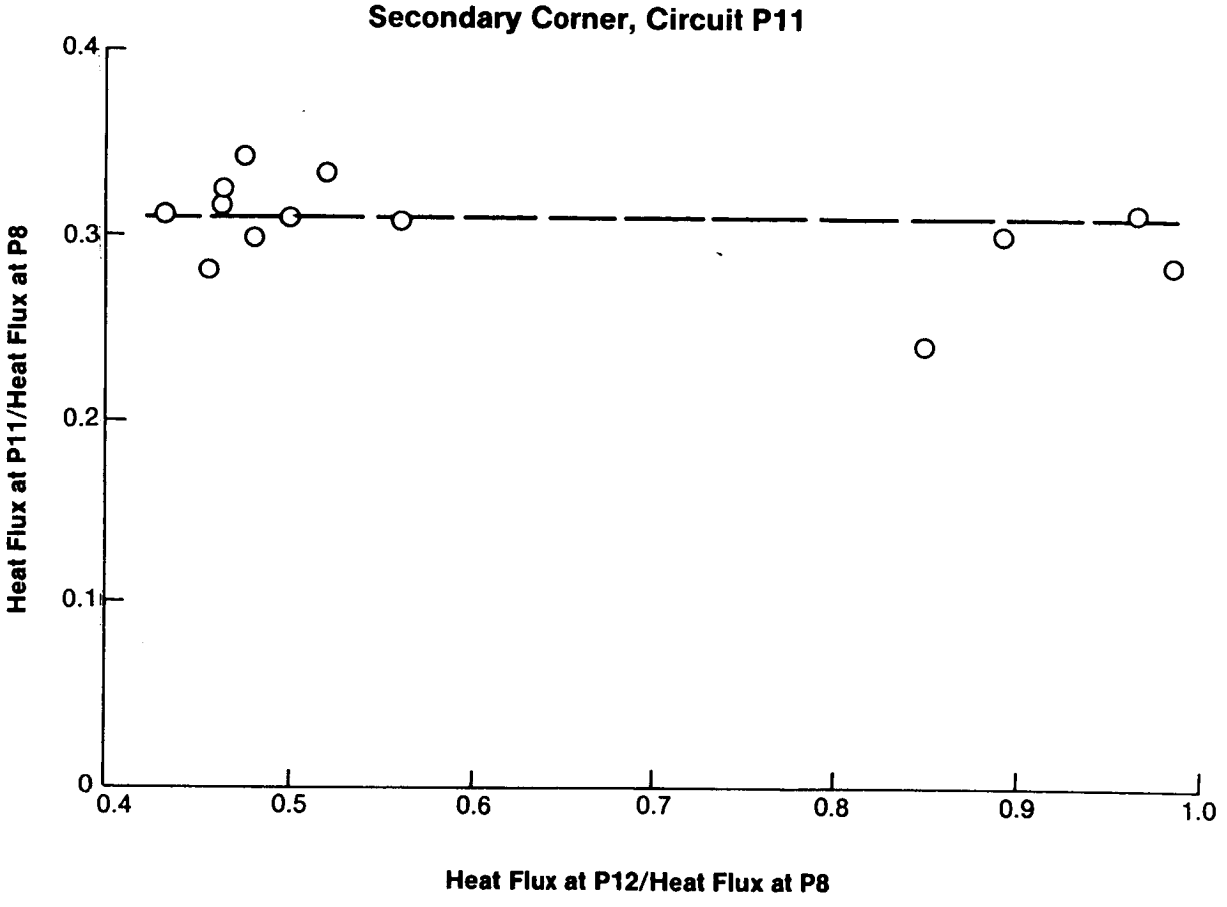

Figure 87. Mode I Primary Chamber Tip Heat Flux Correlation With Secondary Heat Flux

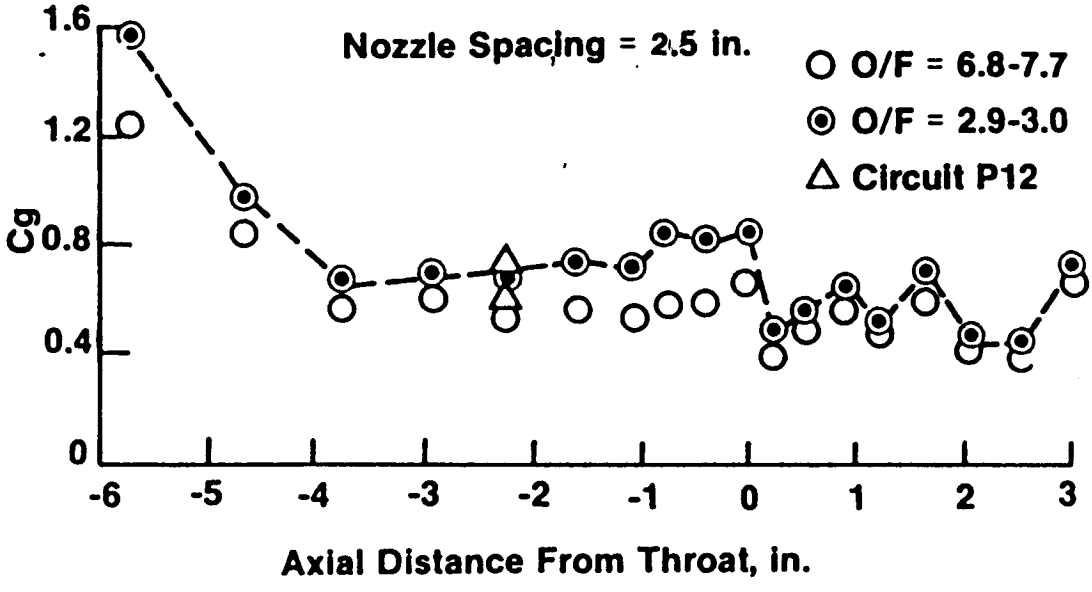

Figure 88. Mode I Secondary Chamber Correlation Coefficients

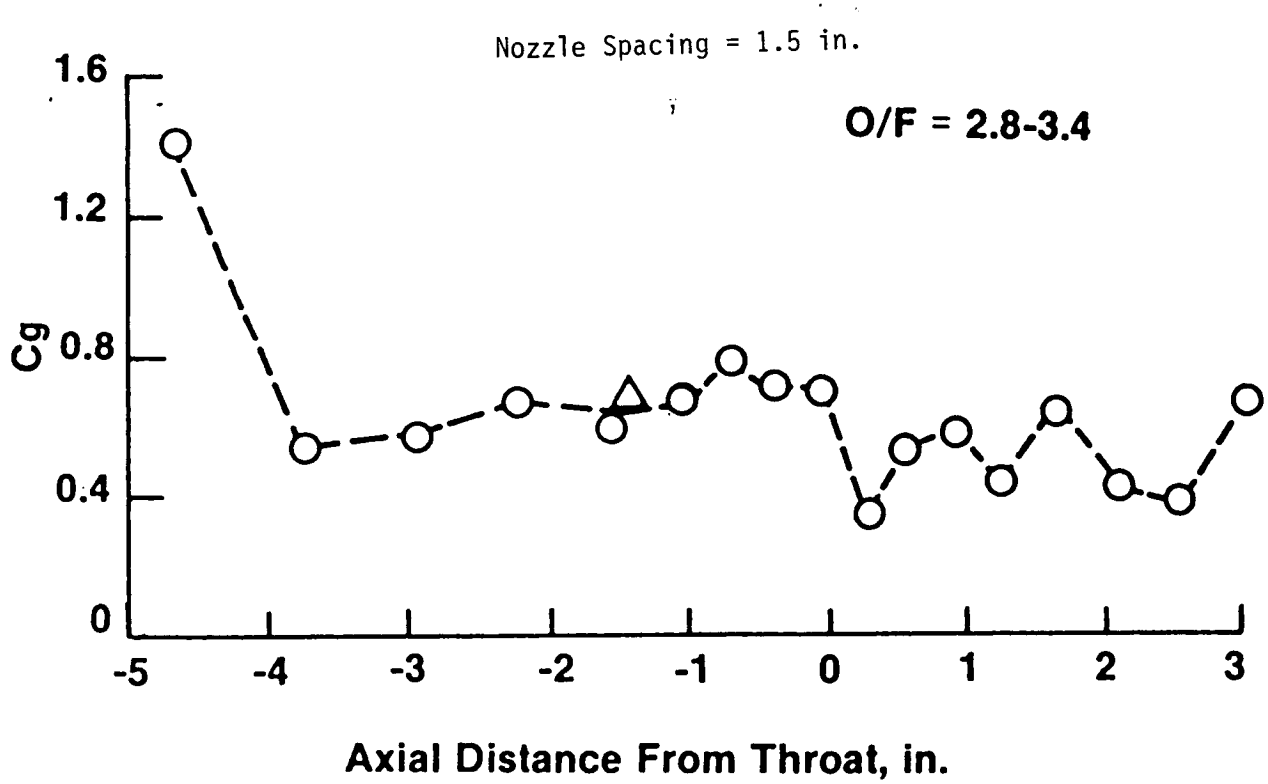

Figure 89. Mode I Secondary Chamber Correlation Coefficients

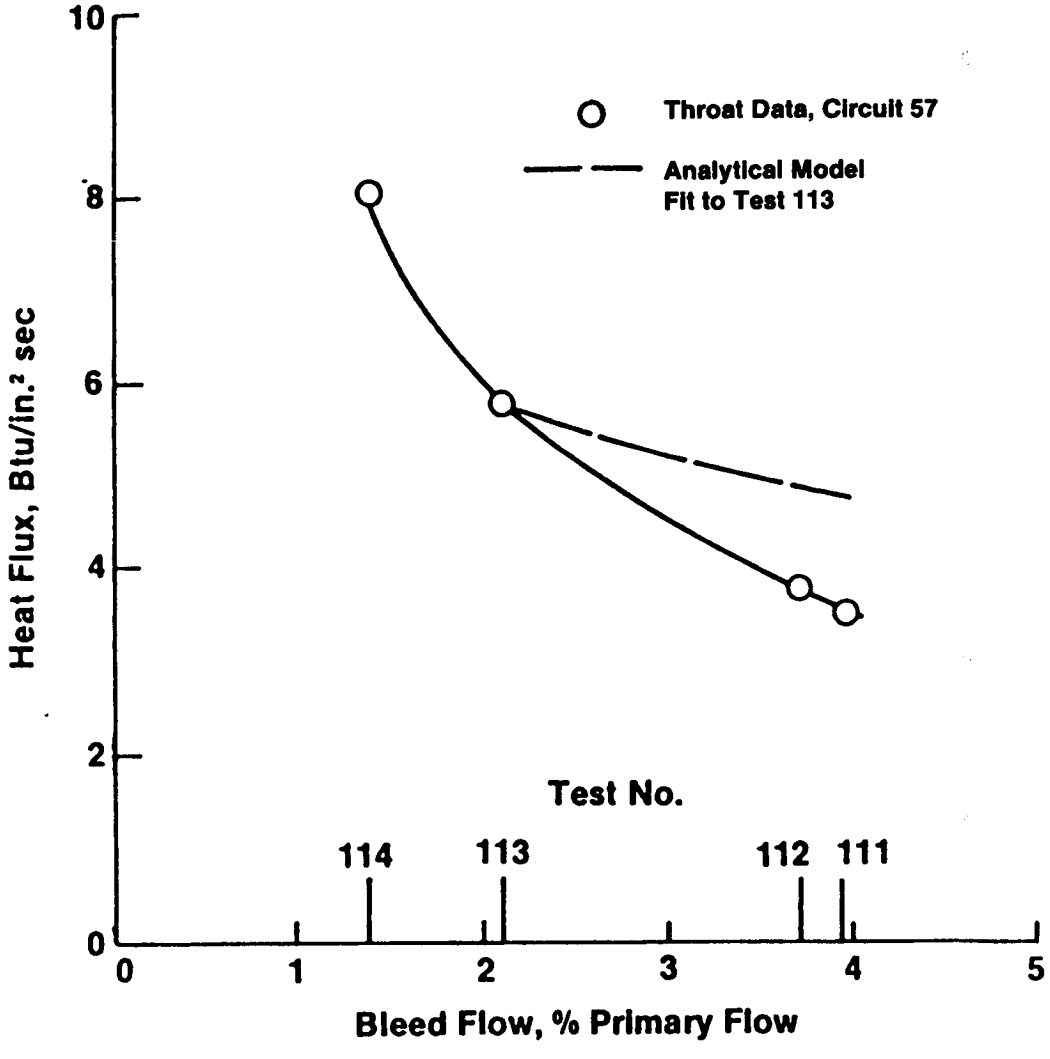

Figure 90. Effect Of Bleed Flow On Maximum Mode II Secondary Heat Flux

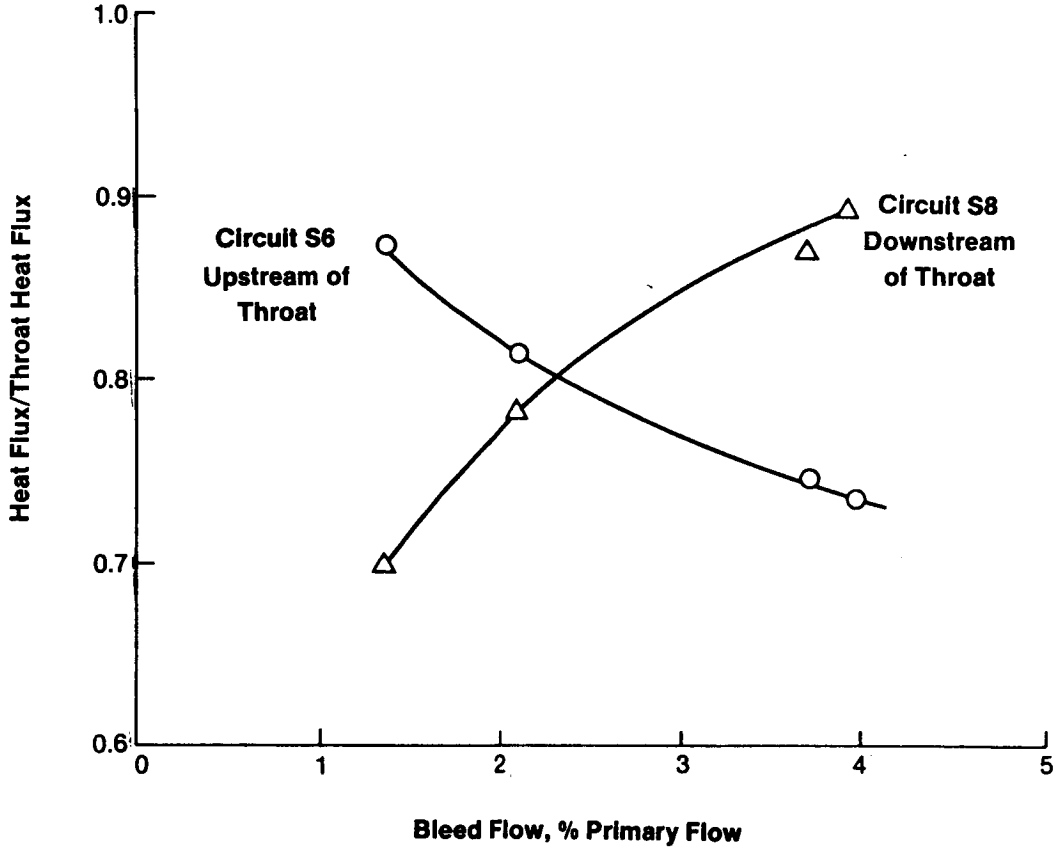

Figure 91. Effect of Bleed Flow on Secondary Nozzle Heat Flux Profile

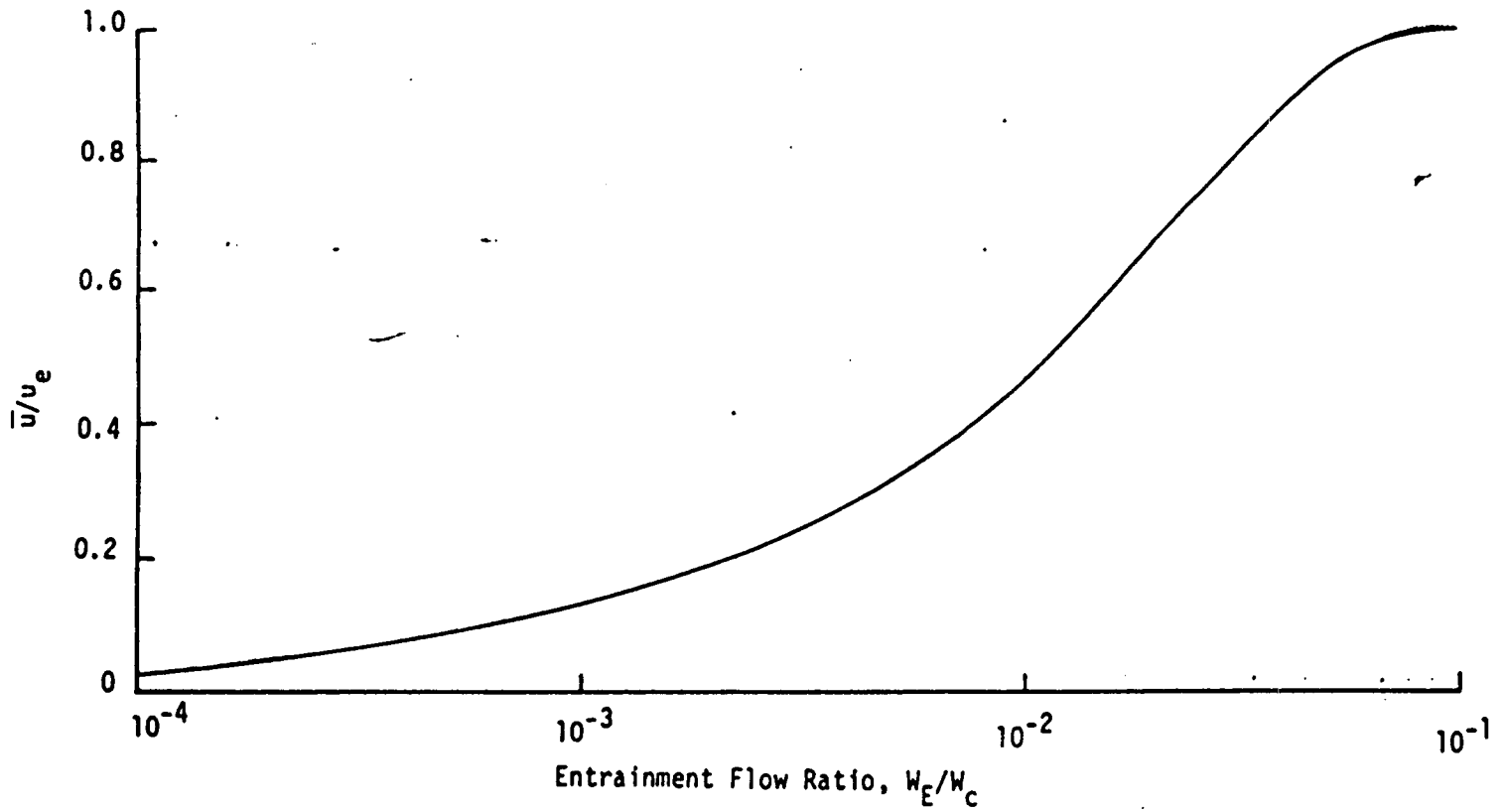

Figure 92. Effective Velocity Correlation for the Mode II Boundary Layer Heat Transfer Model

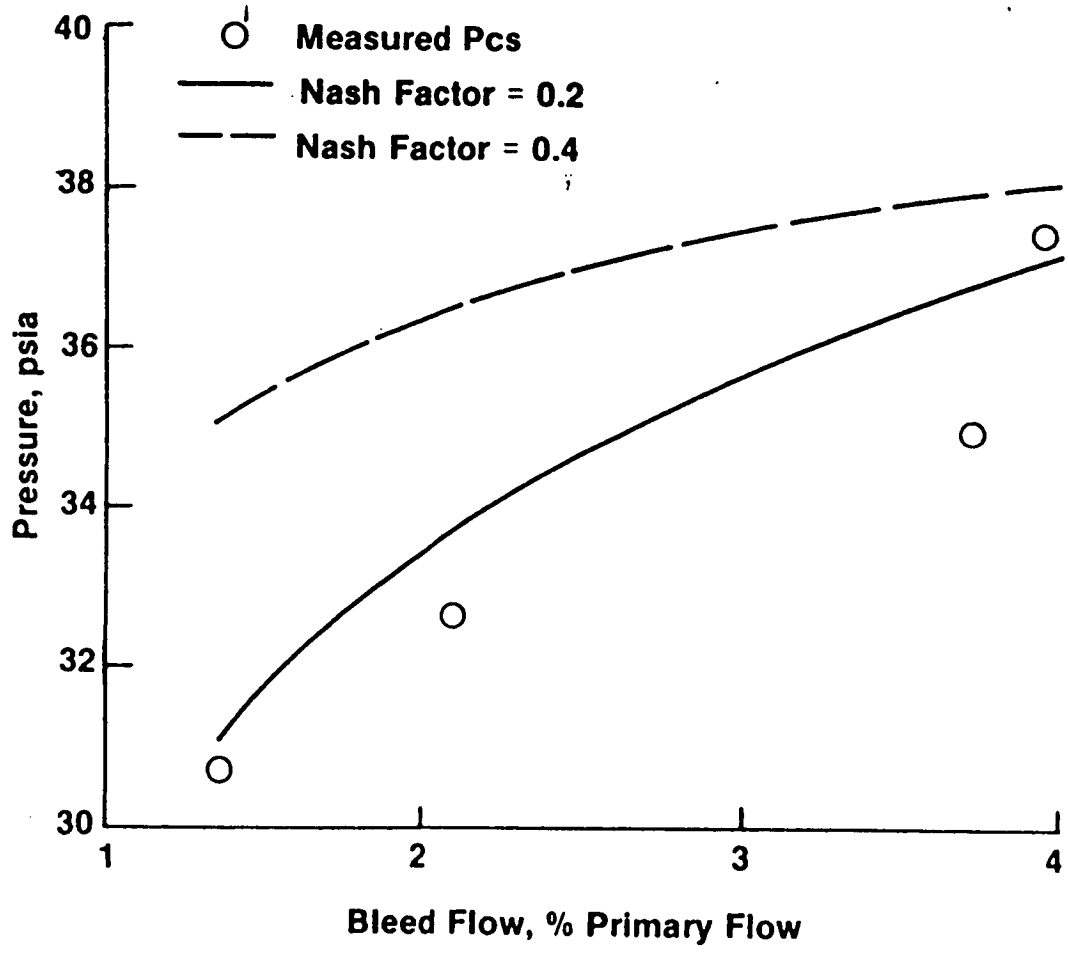

Figure 93. Effect of Bleed Flow On Recirculation Pressure

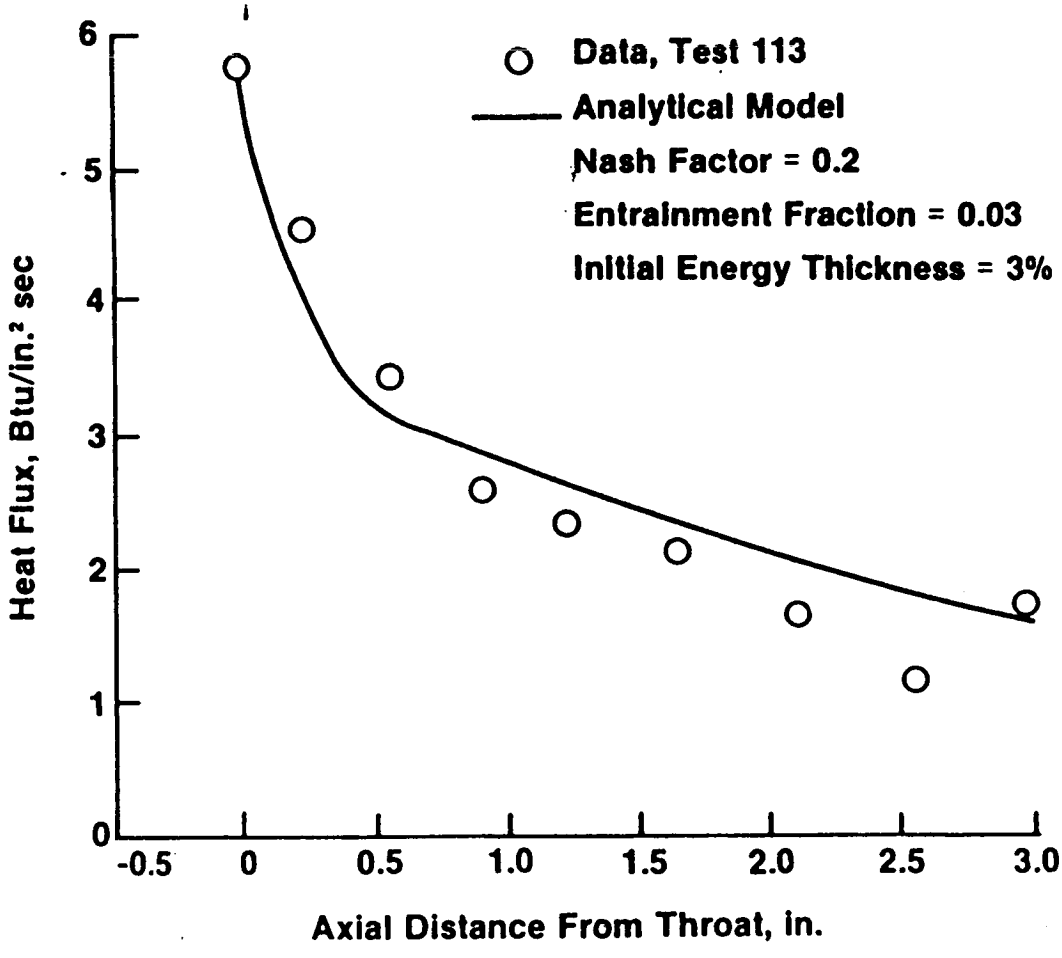

Figure 94. Comparison of Measured and Predicted Secondary Mode II Heat Flux Profiles with 2.1% Bleed Flow

$$St_1 = \frac{q_w}{\rho_{aw} u_e C_p (T_{aw} - T_w)}$$

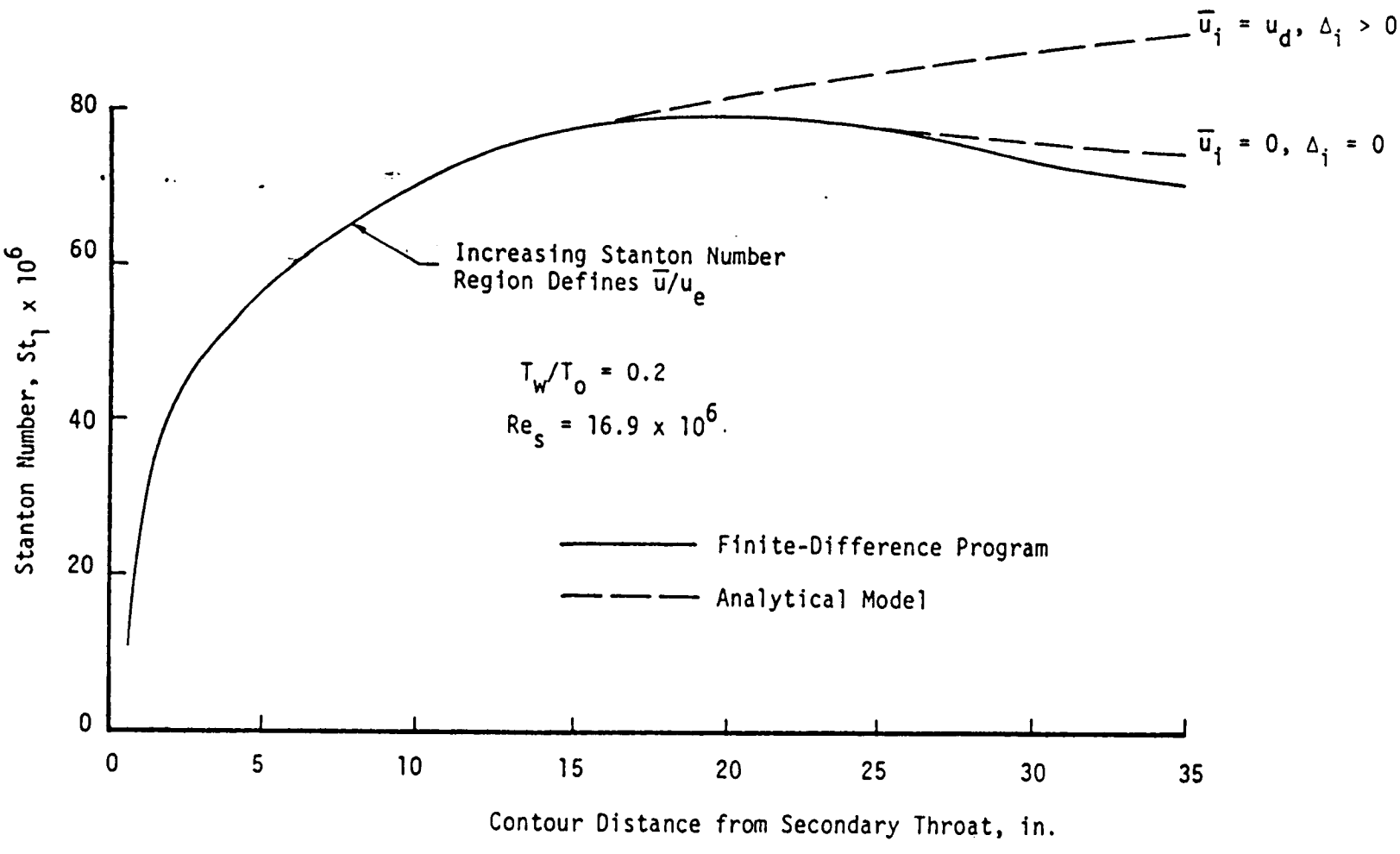

Figure 95. Stanton Numbers From Finite-Difference Boundary Layer Program Define Heat Transfer Model Parameters

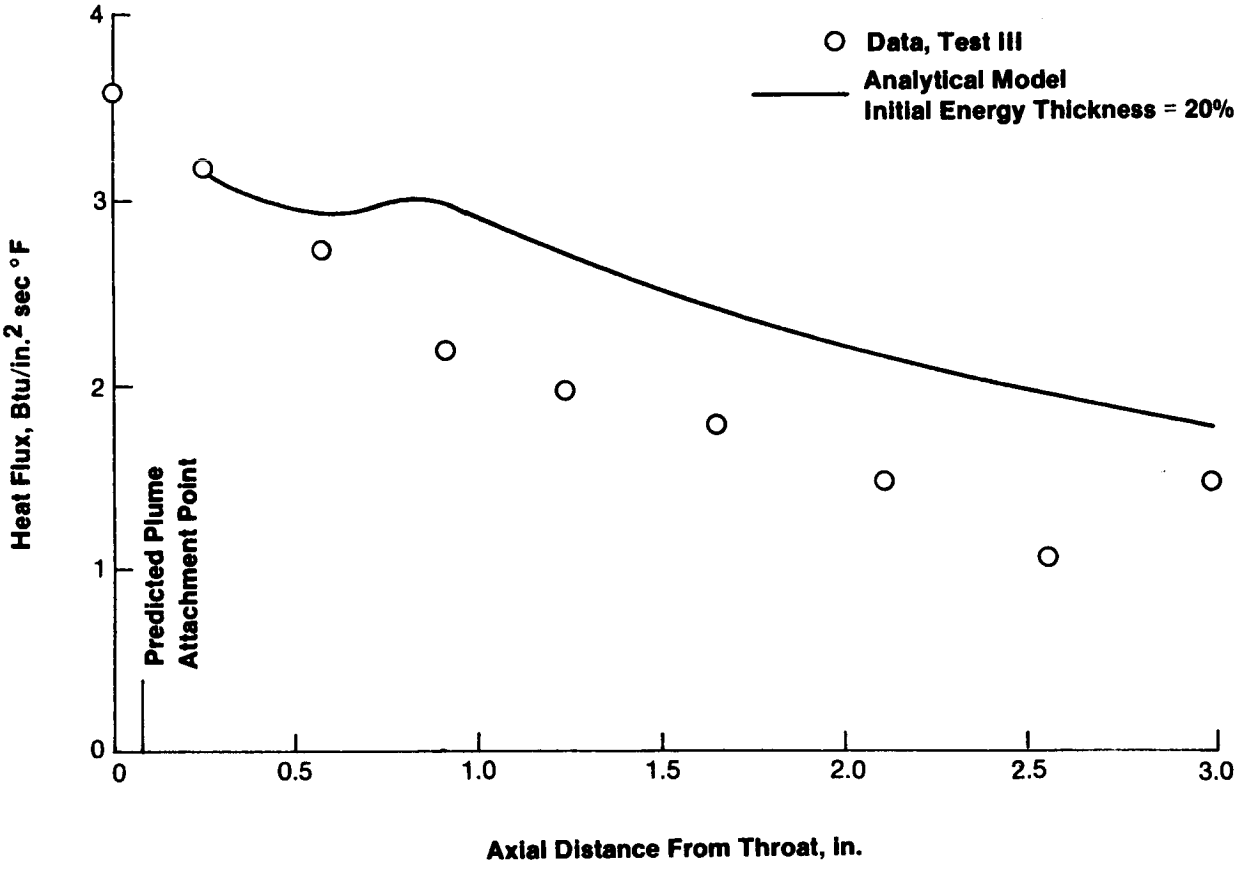

Figure 96 . Comparison of Measured and Predicted Secondary Mode II Heat Flux Profiles With 3.9% Bleed Flow

VI. THERMAL ANALYSIS

A. OBJECTIVES

The thermal model was to be assessed for its capability to analyze the dual throat thrusters described in Table XXXI. These engines operate over a broad range of thrust and chamber pressure coupled with the use of both hydrogen and methane as coolants.

B. APPROACH

Maximum gas-side wall temperatures were determined from the cycle life/creep criteria given in Figure 97. In this figure the difference between the maximum gas-side temperature and the average nickel closeout temperature is plotted as a function of closeout temperature. For closeout temperatures less than 239°K (-30°F), a cycle life of 100 cycles determines the allowable gas-side temperature. For closeout temperatures above 239K, creep limits the maximum gas-side wall temperature to 811K (1000°F). The two line segment shown in Figure 97 are input to the computer program (SCALET), and the maximum gas-side wall temperature limitation automatically determines the local channel depth provided the resultant depth/width ratio is within the 10:1 limit.

Maximum allowable channel widths were initially defined by the gas-side wall strength criteria of Figure 98; considering cold startup (i.e., cold walls, no chamber pressure and coolant inlet pressure throughout the channel) as well as steady state operation. Channel widths were generally set at the maximum allowed by this structural criteria in order to maximize the flow area obtainable within the channel aspect ratio limit of 10:1. The throat land widths were set at a minimum of .030 in. for cases 1 through 6 in order to improve cooling capability and maximize the number of coolant channels. In Cases 7 and 8, the primary chamber throat diameter necessitated using smaller throat land widths (.020 in.) in order to provide adequate cooling for these chambers. In all eight cases, the coolant flow Mach number was limited to 0.3 to minimize flow maldistribution.

TABLE XXXI

DUAL THROAT THRUSTERS

Parameter	1	2	3	4	5	6	7	8
Thrust lb	600K	600K	600K	600K	600K	600K	15K	15K
Thrust Ratio	1.5	3.0	1.5	3.0	1.5	3.0	5.0	10.0
Primary Chamber Pressure, psia	4000	4000	4000	4000	3000	3000	1500	1500
Pc Ratio	.7	.7	.7	.7	.7	.7	.7	.7
Propellants Primary:	LOX/LH_2	LOX/LH_2	LOX/LCH_4	LOX/LCH_4	LOX/LH_2	LOX/LH_2	LOX/LH_2	LOX/LH_2
Secondary:	LOX/RP-1	LOX/RP-1	LOX/LCH_4	LOX/LCH_4	LOX/LH_2	LOX/LH_2	LOX/LH_2	LOX/LH_2
Mixture Ratio Primary:	6.0	6.0	3.5	3.5	6.0	6.0	6.0	6.0
Secondary:	2.8	2.8	3.5	3.5	6.0	6.0	6.0	6.0
Coolant	LH_2	LH_2	LCH_4	LCH_4	LH_2	LH_2	LH_2	LH_2
Primary Nozzle Area Ratio	1.5	3.0	1.25	2.5	1.5	2.5	1.5	1.5
Nozzle Spacing Le/r_{tp}	1.5	1.75	1.10	1.5	2.0	2.0	3.95	3.09

VI, B, Approach (cont.)

As shown schematically in Figure 99, three cooling circuits were used with each case analyzed. Circuit #1 cooled most of the primary chamber. The coolant inlet was located at an area ratio in the primary nozzle and the outlet at the primary injector. Circuit #2 began at the termination of circuit #1 and cooled the inner annulus. Circuit #3 cooled the secondary chamber. The coolant inlet was at a nozzle area ratio 8:1 and the outlet at the secondary injector. The inability to cool the lip region to temperatures below 1000°F and within acceptable pressure drop and Mach number limits necessitated the investigation of a combination of transpiration and regenerative cooling. The lip region transpiration cooling requirements were based on ATC platelet technology using the blockage correlation of Figure 100, developed from the hydrogen and helium cooling data of Reference 16. Copper platelet and slot dimensions were assumed to be identical to those tested in Reference 16, with the coolant flow selected to provide a platelet surface temperature of 1000°F. Internal cooling effects were defined by a platelet fin model coupled through finite heat transfer coefficients to the coolant energy equation. Thus, the coolant and the wall were not in equilibrium as in many transpiration cooling analyses.

C. RESULTS

Table XXXII summarizes the individual circuit pressure drops and the tip transpiration cooling amounts required for each case. The primary nozzle Cg profile used for all eight cases was derived from the hot fire test data (see Figure 78). Table XXXIII summarizes the values used. The following sections describe each case in detail. In the successful design cases the Mach number limit, wall strength criteria, and cycle life requirements were met with minimum pressure drops and selected coolant flow fractions in each circuit.

TABLE XXXII

CIRCUIT PRESSURE AND TIP TRANSPIRATION SUMMARY

	P, psia			Tip Transpiration Cooling Flowrates lbms	
	Circuit #1	Circuit #2	Circuit #3		Results
Case 1	625	1215	200	4.19*	Successful Design
Case 2	600	325	350	0.41	Successful Design
Case 3	>2000	-	-	-	Convergenge Failure
Case 4	>2500	-	-	-	Convergenge Failure
Case 5	225	860	325	0.84	Successful Design
Case 6	310	350	350	0.32	Successful Design
Case 7	-	-	-	-	Convergenge Failure Insufficient Coolant
Case 8	-	-	-	-	Convergence Failure Insufficient Coolant

*This coolant amount is the total required to cool the tip and part of the primary nozzle to the interface area ratio 1.35.

TABLE XXXIII

PRIMARY NOZZLE Cg PROFILE

$Cg = 0.8 \times F$

Location	F
First part of nozzle	1.14
About midpoint	1.36
2/3 - 3/4	1.80
Tip	2.24

VI, C, Results (cont.)

1. Case 1

Figure 101 shows the resulting circuit pressure drop versus the percent of primary circuit hydrogen flow. The primary nozzle area ratio was 1.5. The primary circuit coolant flows from area ratio 1.25 in the primary nozzle to the primary injector. Figure 101 shows that circuit #2 is the dominant pressure drop circuit, cooling the primary nozzle high heat flux region.

The interface area ratio where circuit #2 stopped cooling the primary nozzle and where transpiration cooling took over was varied and the resulting transpiration cooling amounts noted in Table XXIV. As expected, the larger the regeneratively cooled surface area of circuit #2, the larger its pressure drop. Similarly, the larger the surface area that transpiration cooling was used, the larger the coolant amount required. As reported in Table XXXII the design point pressure drop for Circuit #1 is 625 psia, 1215 psia for Circuit #2 and 200 psia for #3. The corresponding coolant flow fractions for each circuit are 0.25, 0.25, and 0.20, respectively.

2. Case 2

This case had a less severe thermal environment compared to Case 1 since its primary nozzle area ratio (ε = 3.0) was larger than in Case 1. Figure 102 shows the resulting circuit pressure drop versus the percent of the hydrogen flow in the primary chamber. The primary circuit coolant flows from area ratio 1.60 in the primary nozzle to the primary injector. Figure 102 shows that this circuit defines the system pressure drop. The design point gives 600 psia pressure drop for Circuit #1 and a 325 psia and 350 psia for Circuits #2 and #3, respectively. Transpiration cooling the tip requires only 0.41 lbm/s of hydrogen. The coolant flow fractions are 0.30, 0.20, and 0.30 for Circuits #1, #2, and #3.

TABLE XXXIV

CASE 1. TRANSPIRATION NOZZLE COOLING

Interface Area Ratio	Nozzle Coolant Flow lb/s	Nozzle Tip Coolant Flow Required lb/s
1.25	4.85	6.30
1.35	2.74	4.19

3. Cases 3 and 4

In these two cases both the primary and secondary propellants were LOX/CH_4. In both cases, it was found that there was not enough methane to cool both the inner annulus circuit and the secondary surface circuit. The interface area ratio where the primary circuit inlet and the inner annulus circuit inlet meet was 1.10 for Case 3 and 1.30 for Case 4. As shown in Figure 103, the required primary circuit pressure drop quickly grew to >3000 psia with larger coolant flow fractions. The Case 4 results were worse since there was a reduction in primary chamber fuel flow. In both cases, the inner annulus flow required for coolant Mach number control and wall temperature below 1000°F was unobtainable. it is clear that cooling limitations in all three circuits were encountered.

4. Case 5

Figure 104 shows the resulting circuit pressure drop versus the percent of the hydrogen flow in the primary chamber. The primary circuit coolant flows from area ratio 1.25 in the primary nozzle to the primary injector. Figure 104 shows that for this Case 5 geometry the inner annulus circuit defines the system pressure drop. The minimum pressure drop design point gives a 225 psia pressure drop for Circuit #1 and 860 psia and 325 psia pressure drop for Circuits #2 and #3, respectively. The coolant flow fractions are 0.20, 0.20, ad 0.20 for Circuits #1, #2, and #3. Transpiration cooling the tip requires 0.84 lbm/s of hydrogen.

5. Case 6

Figure 105 shows the resulting pressure drop versus the fraction of the hydrogen flow in the primary chamber. The primary circuit coolant flows from area ratio 1.3 in the primary nozzle to the primary injector. Figure 105 shows that for this geometry and available propellant flow, the secondary circuit defines the system pressure drop. The design point gives a 310 psia

pressure drop for circuit #1, 310 psia and 350 psia pressure drop for circuits #2 and #3, respectively. The coolant flow fractions are 0.15, 0.20, and 0.50 for Circuits #1, #2, and #3. Transpiration cooling the tip requires only .32 lbm/s of hydrogen.

6. Cases 7 and 8

The primary and secondary propellants for these two cases were LOX/LH_2. In both cases it was found that there was not enough hydrogen to cool both the inner annulus and secondary surface. The interface area ratio was 1.25 for both cases. As shown in Figure 106, the pressure drop incurred in cooling the primary circuits for both cases was relatively small. Unfortunately, the inner annulus and secondary circuit flow required for coolant Mach number control and wall temperatures below 1000°F was unavailable.

D. CONCLUSIONS

It is possible to cool all 600 Klbf thrust designs for which hydrogen was available as the coolant, although transpiration cooling of the tip of the primary nozzle is required due to the high Mode I heat fluxes observed in the test program. With a low thrust split (1.5) and high primary chamber pressure (4000 psia), it is necessary to transpiration cool part of the primary nozzle as well (Case 1). Even in this case the transpiration cooled flow represents only 2.8 percent of the Mode II hydrogen flow, so performance degradation should be very small; in all other cases the transpiration coolant flow is well below one percent.

It is not possible to cool the methane design or the 15 Klbf thrust designs at the specified chamber pressures. The poor cooling characteristics of methane made it impossible to control coolant Mach number and pressure drop. At the low thrust level there is insufficient coolant relative to the heat load to limit coolant bulk temperatures.

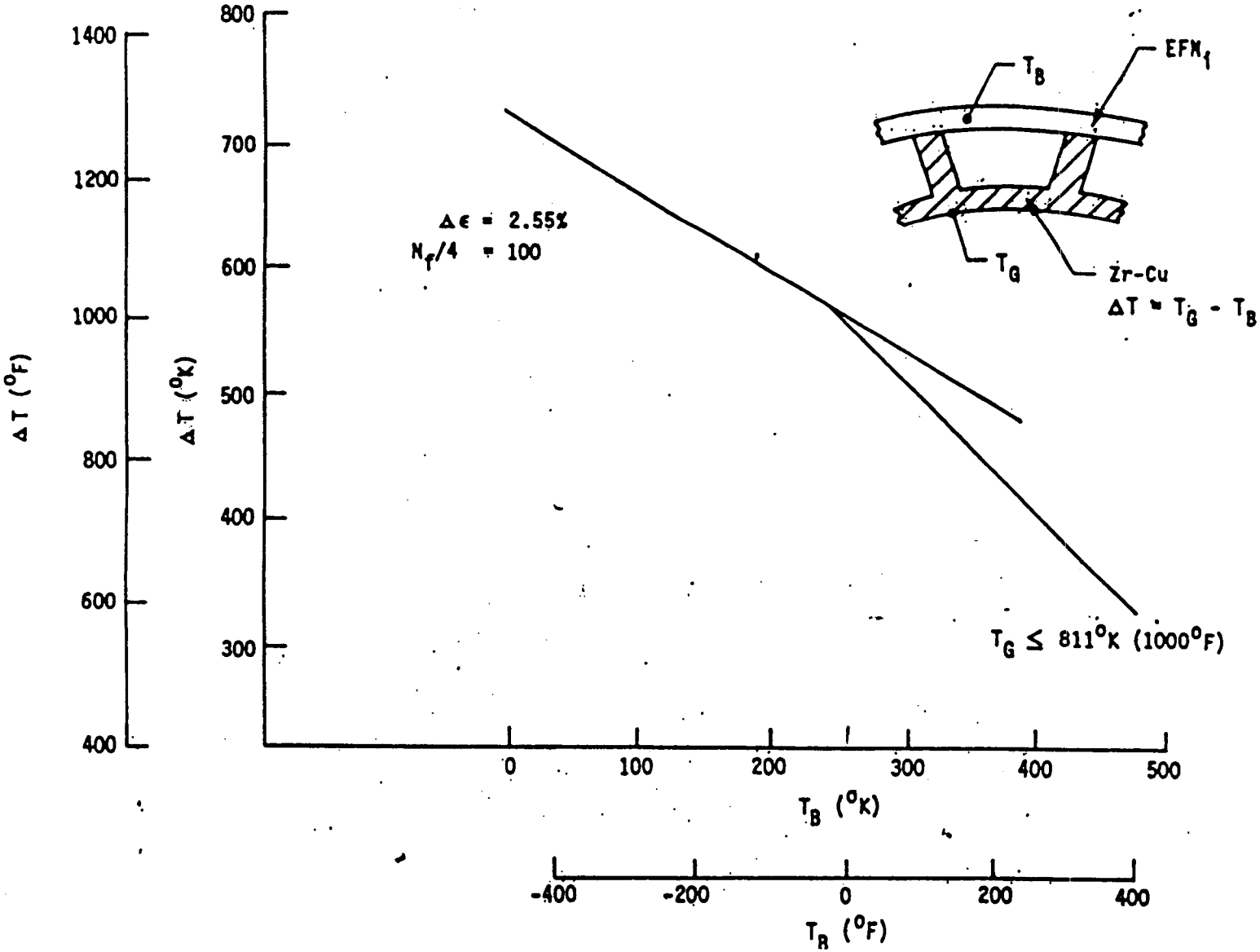

Figure 97. Cycle Life/Creep Wall Termperature Criteria

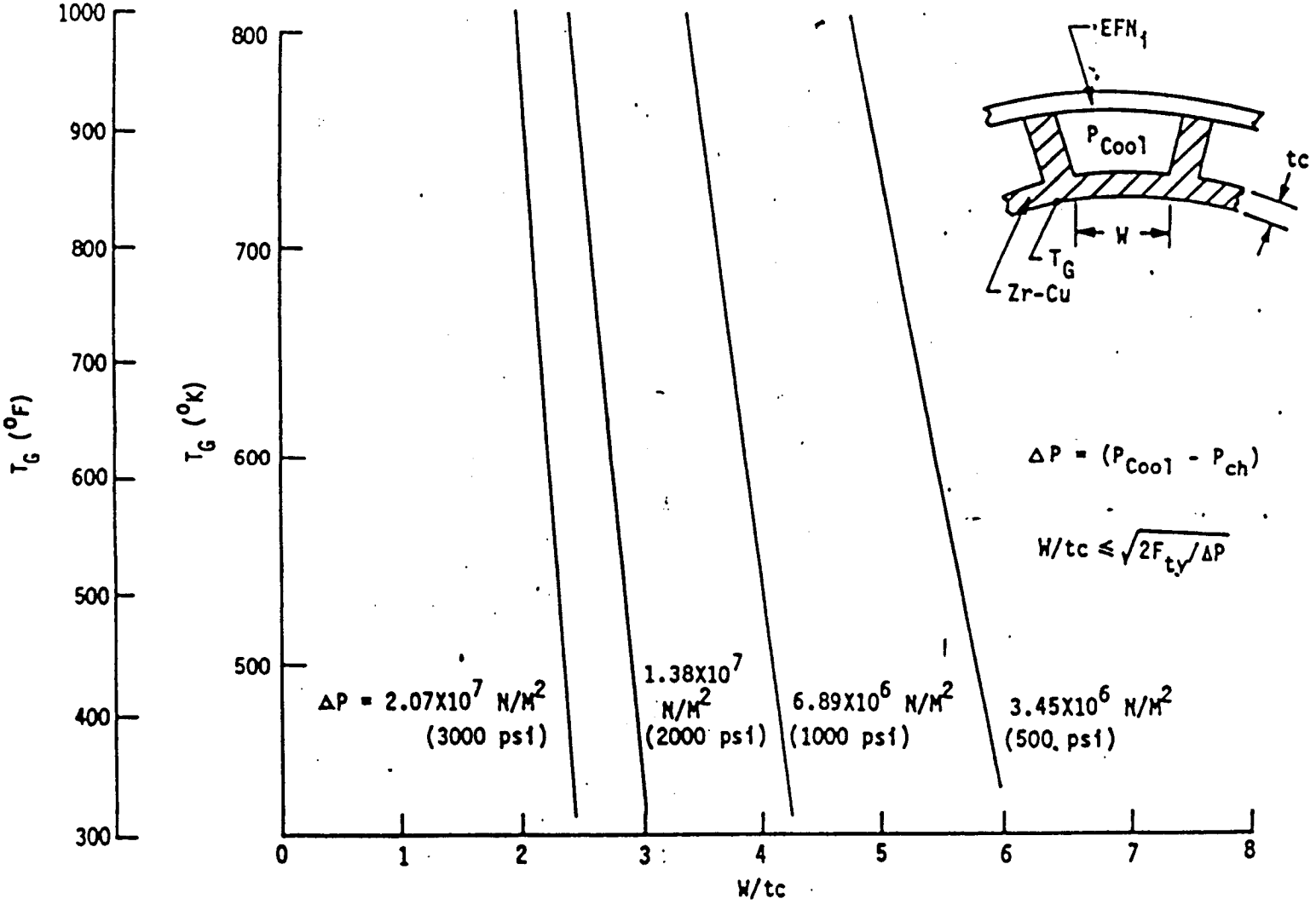

Figure 98. Zr-Cu Chamber Wall Strength Criteria

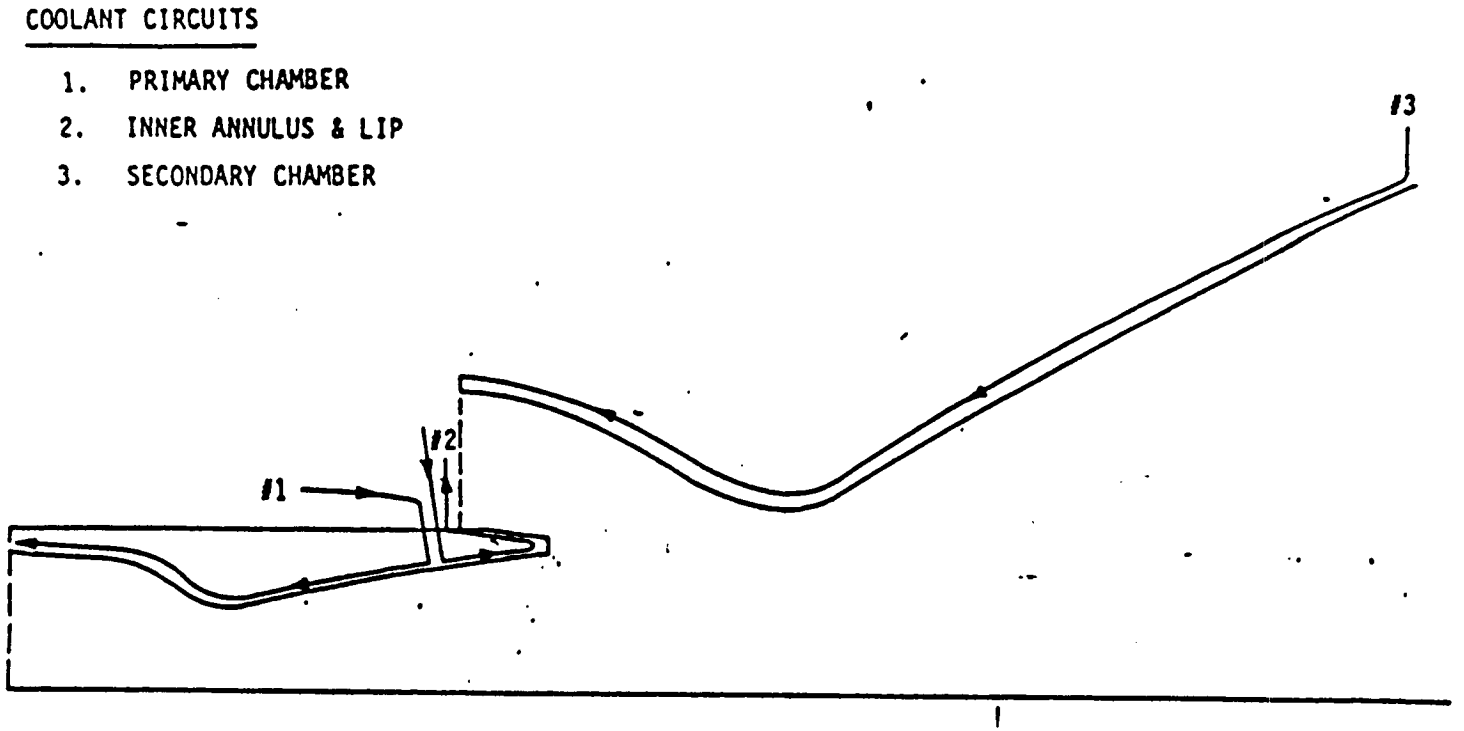

Figure 99. Dual Throat Coolant Flow Schematic

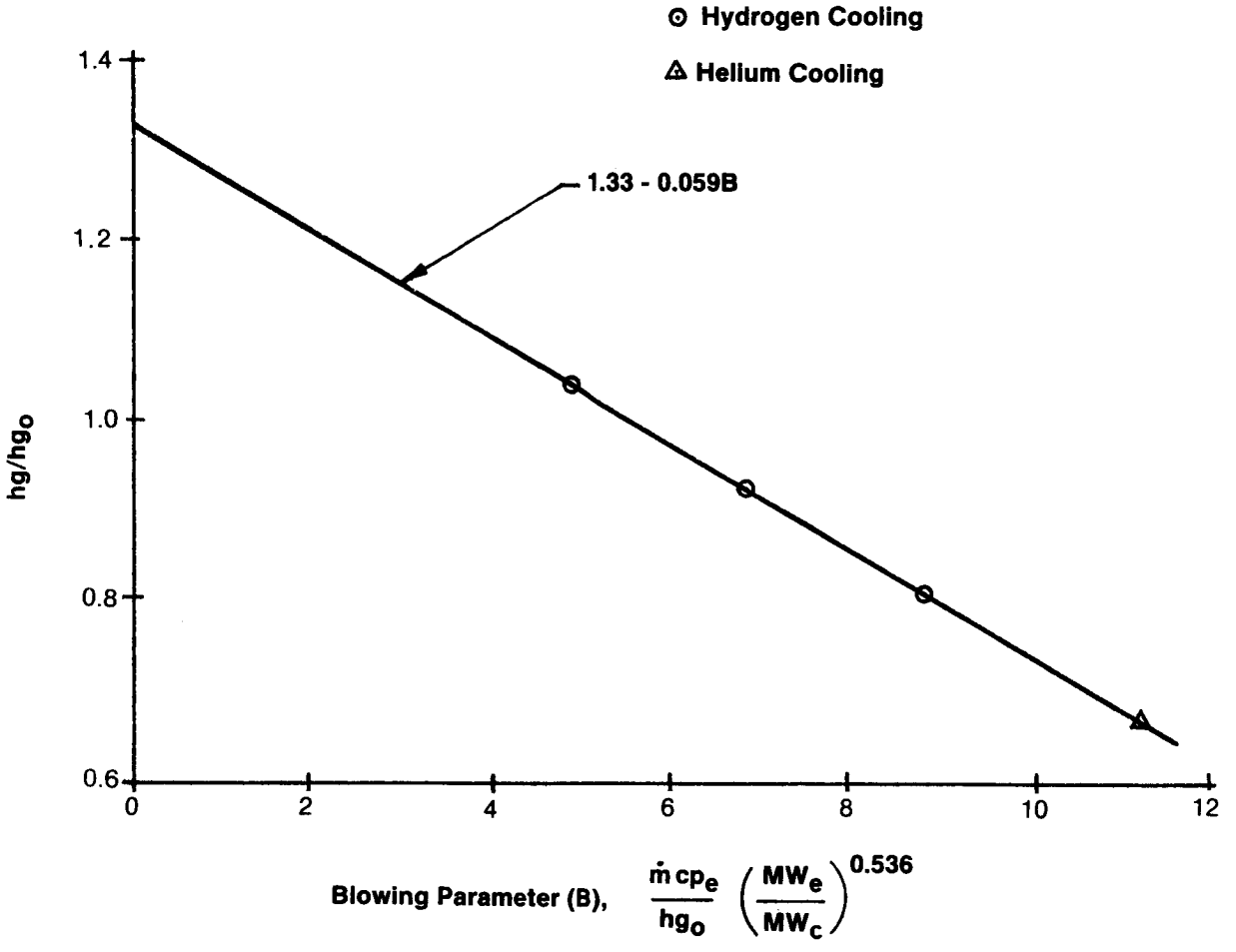

Figure 100. Correlation of Transpiration Cooling Data Contract NAS3-21029

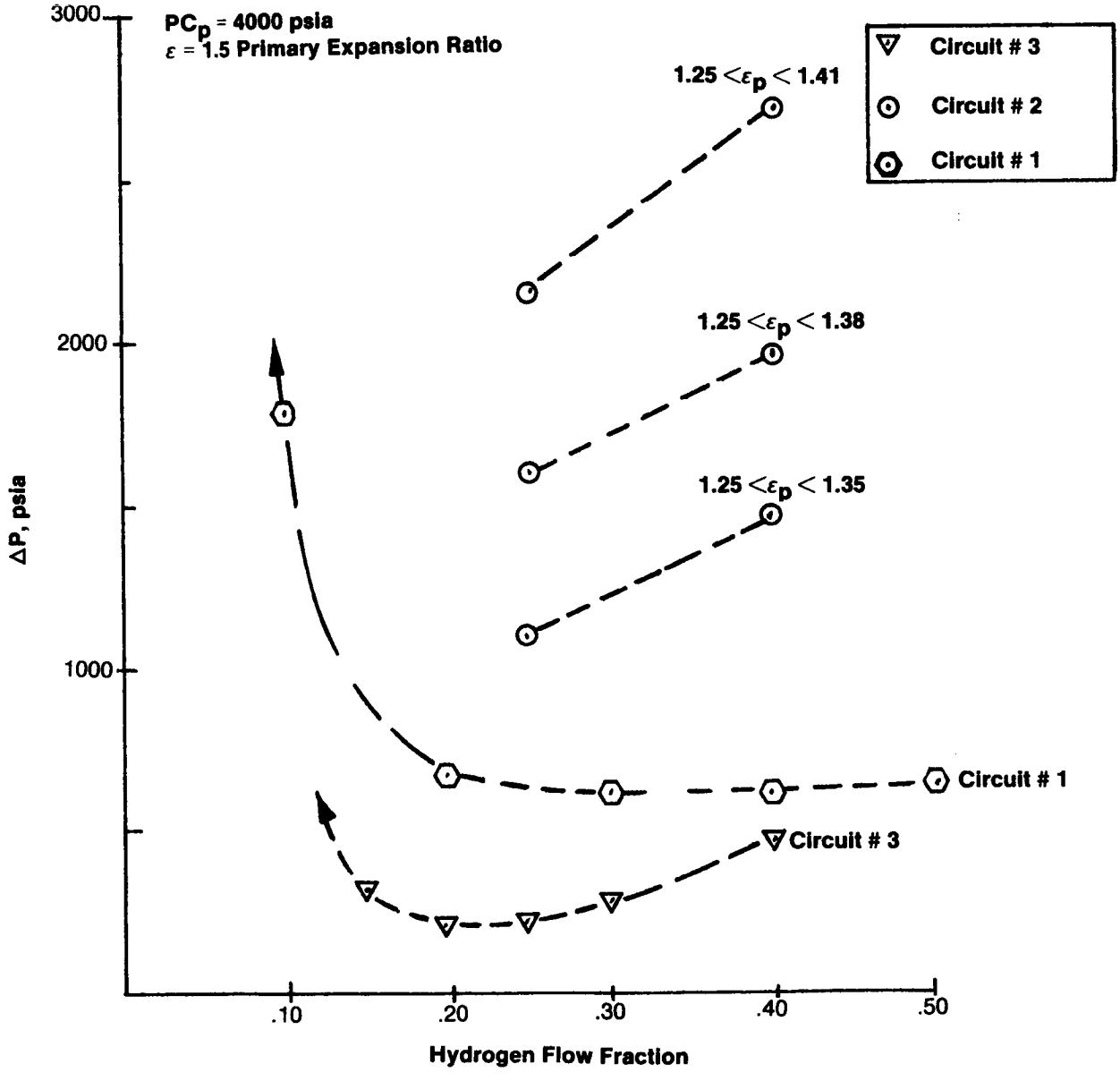

Figure 101. Case One LOX/LH_2 Primary, LOX/RP-1 Secondary

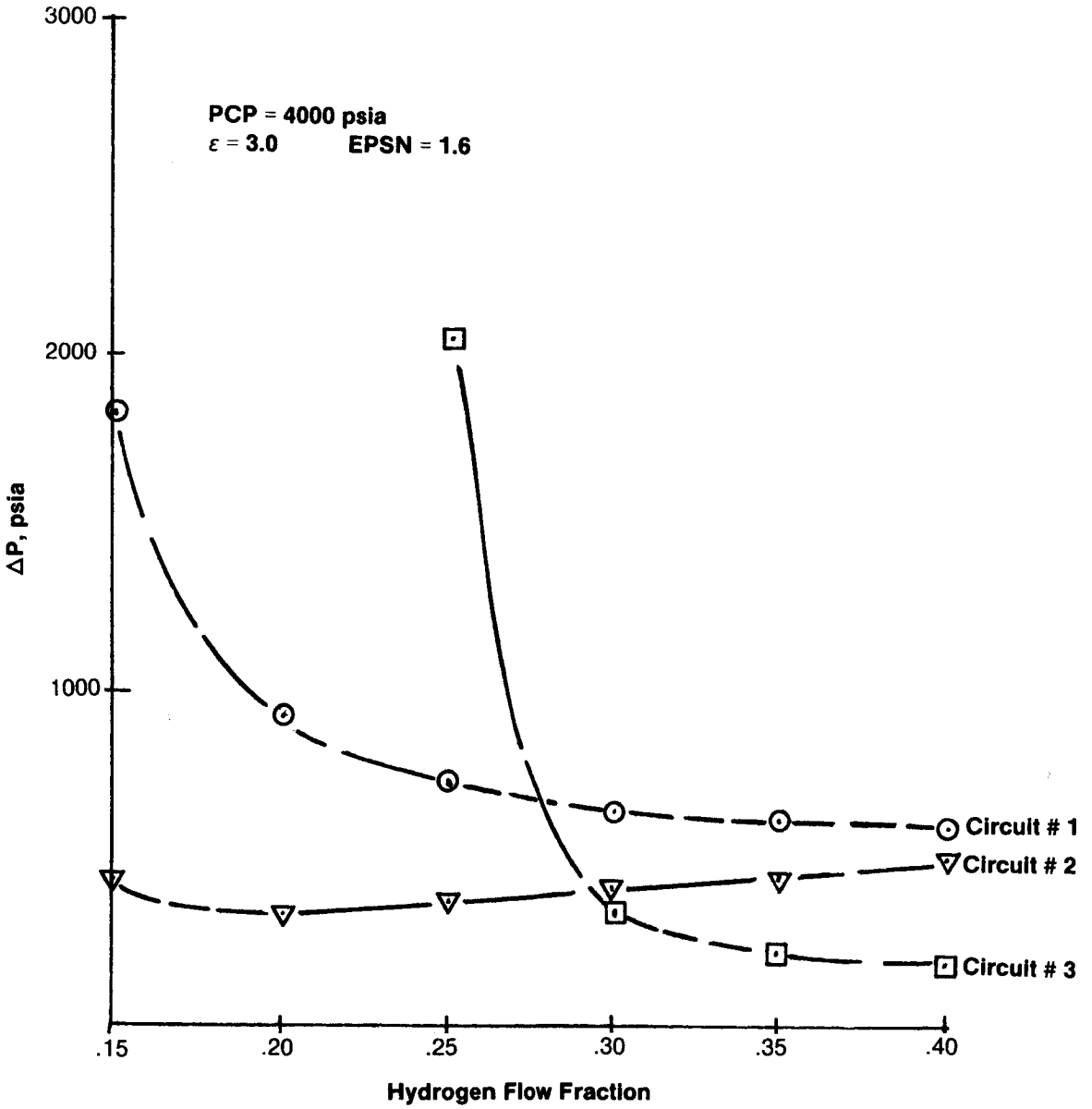

Figure 102. Case 2 LOX/LH_2 (P), LOX/RP-1 (S)

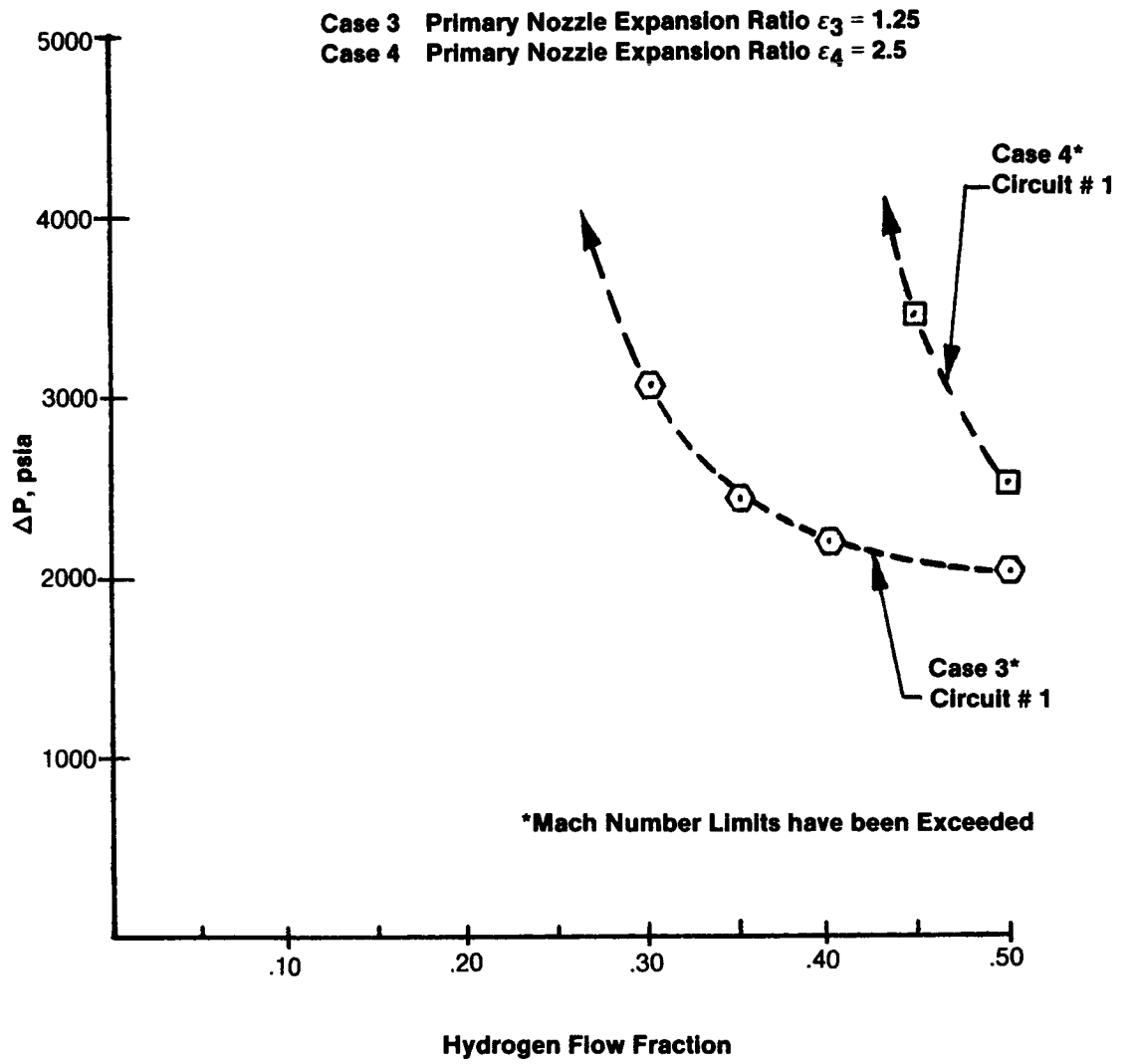

Figure 103. Case 3 and Case 4 LOX/CH_4 Propellants

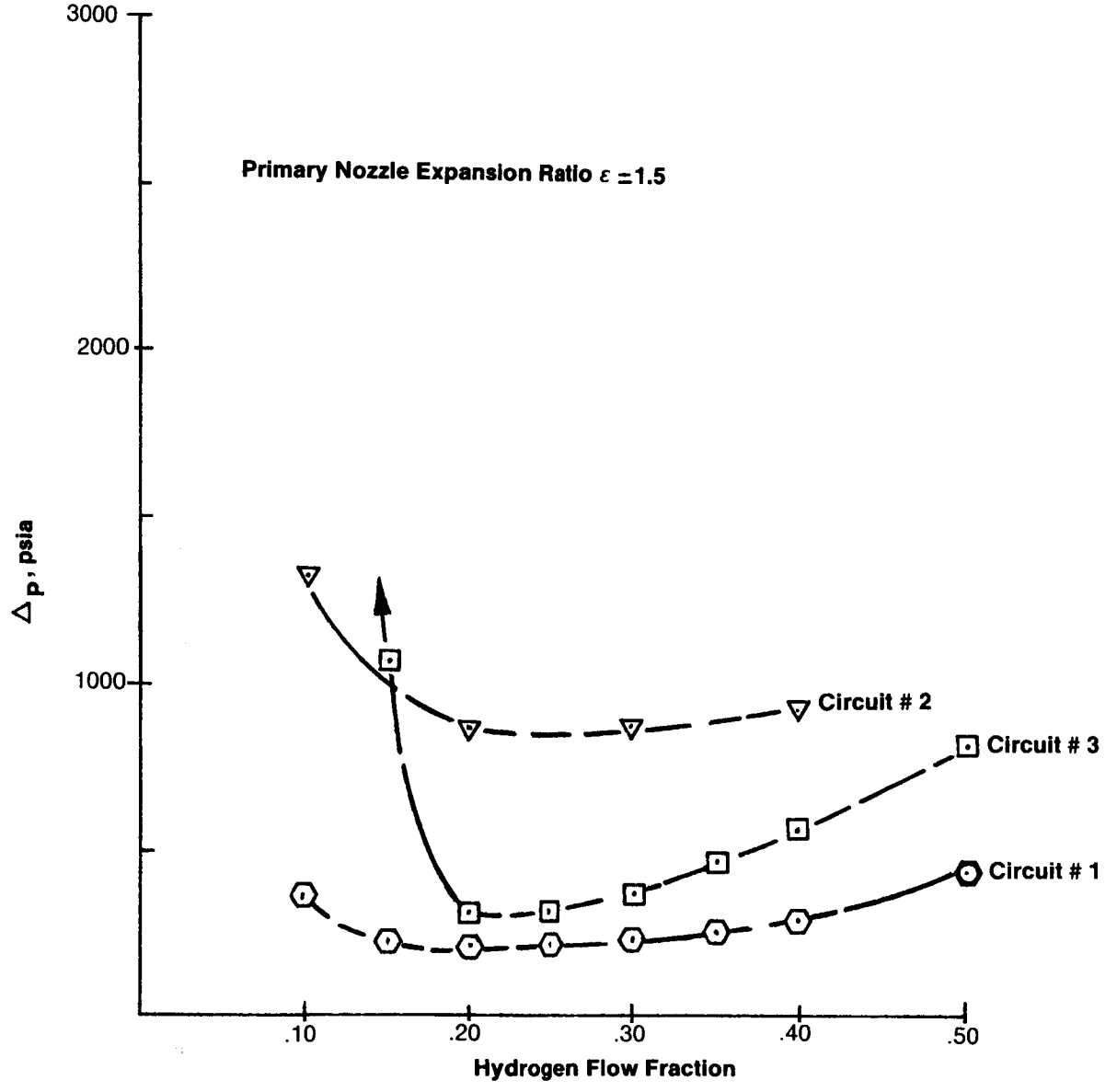

Figure 104. Case 5 LOX/LH_2

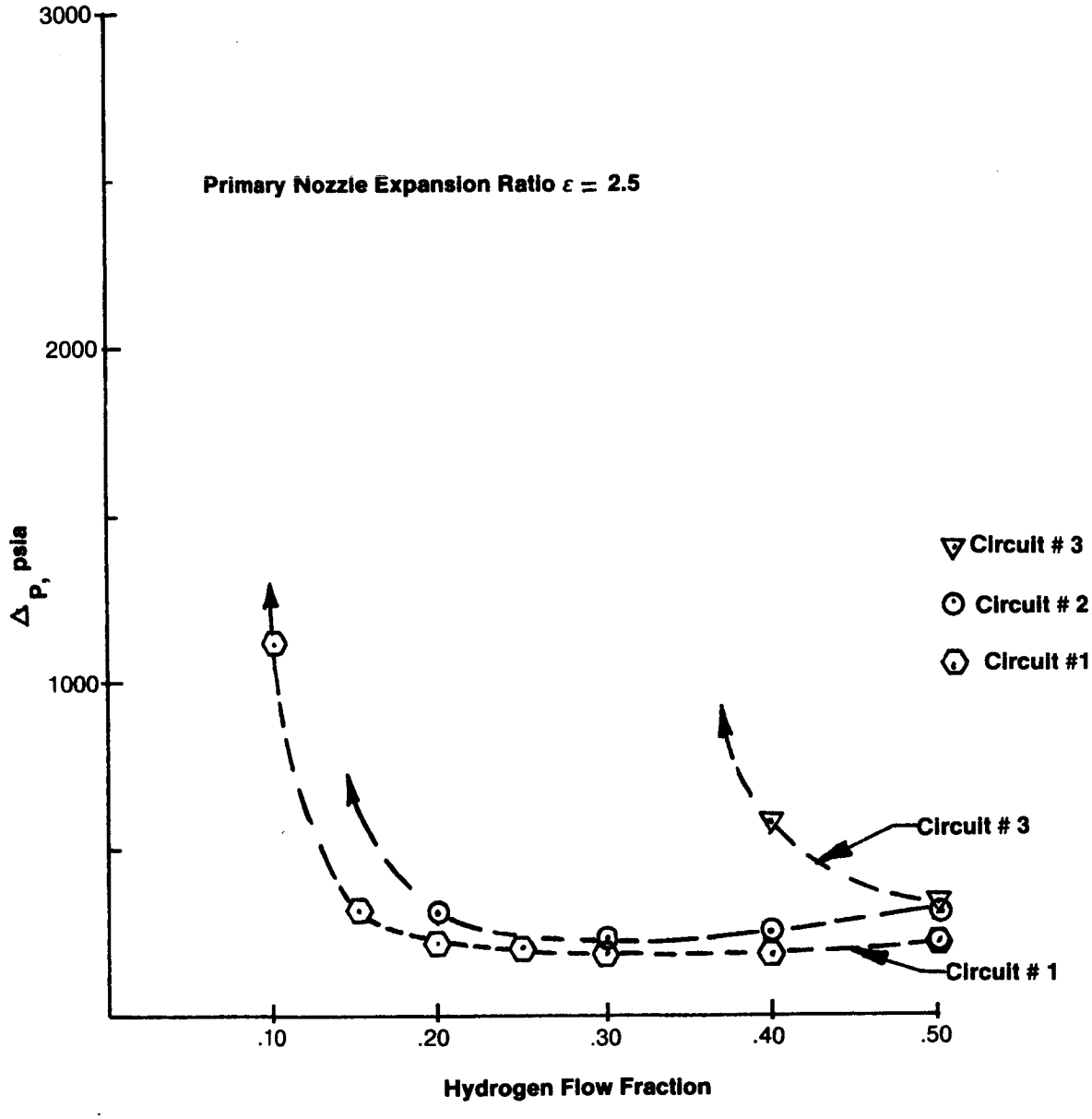

Figure 105. Case 6 LOX/LH_2

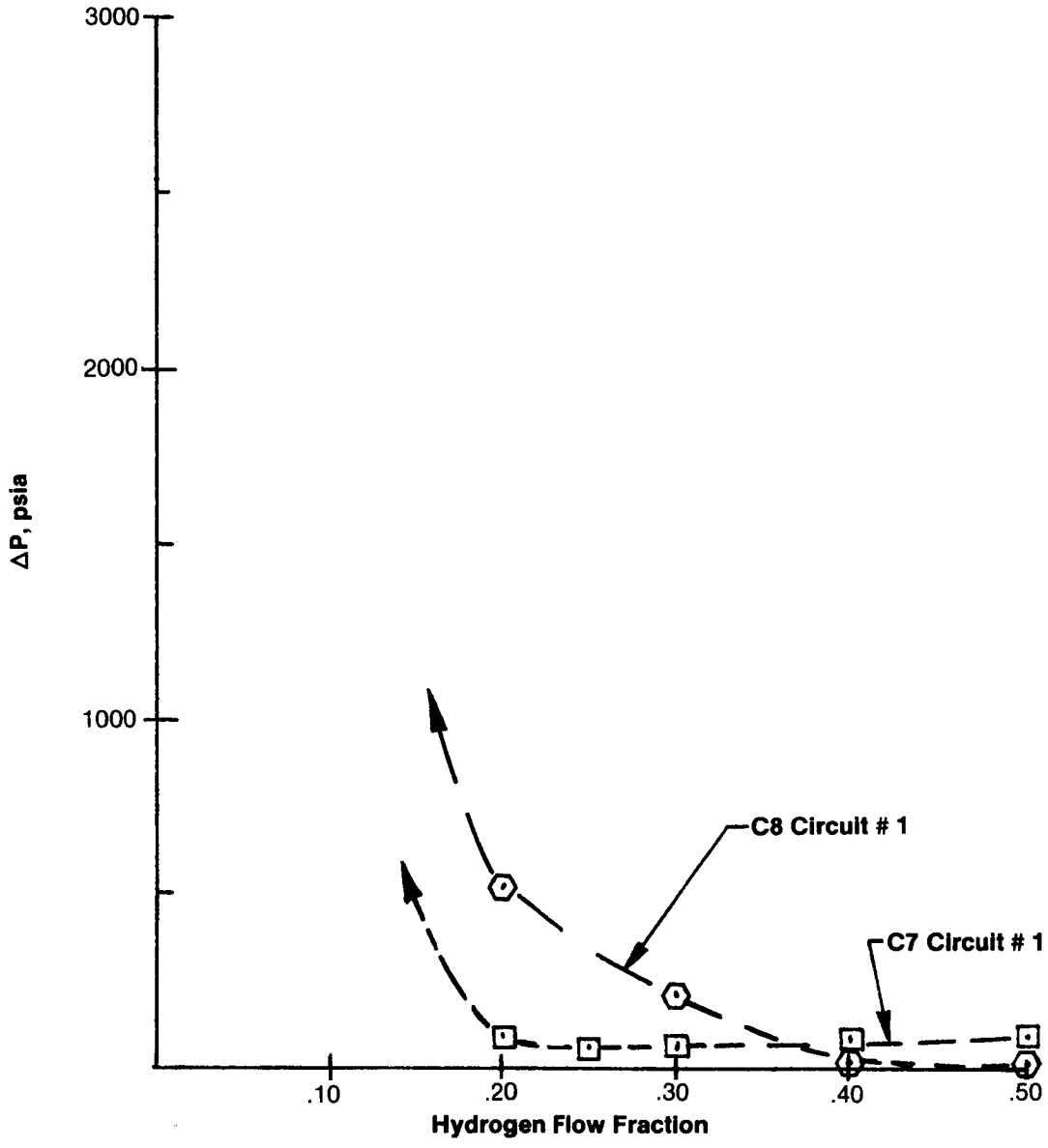

Case 7 Primary Nozzle Expansion Ratio ε_7 =
Case 8 Primary Nozzle Expansion Ratio ε_8 =

Figure 106. Case 7 and Case 8 LOX/LH_2 Propellants

VII. DISCUSSION OF RESULTS

A. RESULTS SUMMARY

A thermal model of the dual throat thruster was developed as an aid in the design analysis of future dual throat engines. The initial model was based on established methods for conventional chambers and on the aerodynamic data from cold flow dual throat tests. The model needed verification under hot fire conditions.

Dual throat hardware was designed and fabricated to gather heat transfer (calorimetric) data. Because of the unique dual throat configuration and the need for calorimetric data collection, the thruster design was very complex. Fabrication and assembly required exact interface matching and a total of ten braze cycles.

Testing of the dual throat hardware included a considerable amount of water flow calibration because of the interchannel leakage in the primary chamber. An external leakage problem that occurred on the thirteenth hot fire test required repairs to the hardware before testing could be resumed. Despite the problems, a very successful test program was accomplished, marking the first time a cooled dual throat thruster was hot fired.

The dual throat hardware was tested burning gaseous oxygen and hydrogen at primary (inner) chamber pressures from 380 to 680 psia. Heat flux profiles were obtained from the calorimetric cooling channels in the inner nozzle, outer or secondary chamber, and the tip of the inner nozzle. Secondary chamber hydrogen bleed flow rates were varied during Mode II operation to study the efect on primary plume impingement. Heat fluxes in the plume impingement region near the secondary throat were of well below Mode I values with a bleed flow as low as 1.4 percent of the primary flow. Since the primary nozzle operates in a conventional manner during Mode II, heat fluxes were consistent with other nozzle data.

The ratio of secondary/primary chamber pressures was varied from less than 0.5 to over 0.8 for each of two nozzle spacings during Mode I operation to define the effects of various back pressures on the primary nozzle flow and the wake region at its tip. The primary throat operated with choked flow in all cases. Heat fluxes near the end of the primary nozzle were significantly higher than for conventional nozzle operation and increased with pressure ratio such that a flux approximately equal to the throat heat flux was measured at a pressure ratio of 0.74 for the larger nozzle spacing. Unsymmetrical heating of the primary nozzle tip was observed, with the maximum heat flux for the smaller nozzle spacing approximately equal to that in the primary nozzle just upstream of the tip. Secondary chamber heat fluxes in Mode I were consistent with predictions based on a simple secondary flow stream tube model.

B. CONCLUSIONS

The fabrication of the dual throat calorimetric hardware established the feasibility of the assembly of dual throat chambers by conventional means. The problems associated with the calorimetric hardware were unique. The basic steps in assembly, however, would be similar for a regeneratively cooled dual throat chamber. The problems encountered during assembly indicated alternate procedures that will be beneficial for future builds of dual throat chambers.

Conclusions from the heat transfer analysis are as follows:

1. Heat fluxes during conventional operation of the primary nozzle (Mode II) are consistent with data from other applications. Use of an enthalpy-based model, rather than the product of temperature difference and a frozen specific heat, is required to predict the effect of mixture ratio.

2. During Mode I operation the primary throat is choked, but the primary nozzle is unable to flow full against the high back pressure imposed by the secondary chamber. Large increases in heat flux relative to Mode II observed near the end of the primary nozzle are consistent with the twinvortex recirculation pattern in the separated region, which includes the wake region downstream of the end of the primary chamber. As the secondary chamber pressure increases, the region of increased heat flux extends farther upstream and the perturbation at the end of the nozzle increases.

3. Unsymmetrical heating of the tip of the primary chamber is caused by the flow separation in the primary nozzle and the resultant recirculation pattern noted above.

4. Secondary chamber heat fluxes during Mode I operation can be predicted with the secondary flow stream tube model used herein and correlation coefficients consistent with other applications. High heat fluxes observed near the swirl coaxial element injector are consistent with previous experience. Rapid decreases and increases with axial distance of correlation coefficients in the secondary nozzle are probably caused by oblique shock waves created by the flow separation in the primary nozzle.

5. Heat fluxes in the secondary throat region during Mode II operation are easily limited to values well below Mode I fluxes using small bleed flow rates, e.g., less than two percent of the primary flow for the geometry tested. Therefore, primary plume attachment is not a thermal design issue.

6. The aerodynamic model of Mode II provides good prediction of the recirculation region pressure and its sensitivity to bleed flow.

7. Although the analytical thermal model of Mode II can predict secondary nozzle heat fluxes under limited test conditions, it does not exhibit the correct sensitivity to bleed flow rate.

Conclusions from the design studies of Task 2 are as follows:

1. It is possible to cool the 600klbf thrust designs specified which have hydrogen available as the coolant, although transpiration cooling of at least the tip of the primary nozzle is required in all cases. Transpiration coolant flows are less than 2.8 percent of the primary hydrogen flow, resulting in a performance loss of less than 0.8 sec.

2. It was not possible to cool the 600klbf thrust methane cases or the 15klbf thrust hydrogen cases for the chamber pressures specified with the nozzle spacings and primary area ratios selected. However, these geometric parameters were optimized to minimize Mode II bleed flow requirements rather than chamber cooling.

C. RECOMMENDATIONS

Recommendations for further effort with dual throat engines are as follows:

1. Additional testing is required to define the Mode I primary nozzle environment for prototype design:

- Added area ratios and nozzle spacings
- Engine effects
- Rounded tips, streamlined tips and transpiration-cooled tips

2. Develop an aerodynamic model of Mode I for correlatio of primary nozzle heat transfer data

3. Refine the Mode II secondary analytical model

- Account for velocity components normal to the wall
- Develop a flow field model of the recirculation region

VII, B, Conclusions (cont.)

4. Investigate low-cost methods of heat flux measurement

5. Alternate fabrication methods (including the utilization of platelets) should be demonstrated.

6. Transpiration-regenerative cooling of the critical areas of the dual throat chamber should be demonstrated.

7. A system study should be conducted to optimize the engine cycle and determine Pc, thrust, and thrust ratio capability in the light of the heat transfer results and bleed flow requirements.

REFERENCES

1. O'Brien, C. J., "Dual-Fuel, Dual-Throat Engine Preliminary Analysis", Aerojet Liquid Rocket Company, Report 32967F, Contract NAS 8-32967, August 1979

2. G. M. Meagher, Dual Nozzle Aerodynamic and Cooling Analysis Study, Final Report, Contract NAS 8-33553, ALRC Report 33553-F, 27 Feb. 1981

3. Rousar, D. C. and Ewen, R. L., "Comubstion Effects on Film Cooling," NASA CR-135052, 24 February 1977

4. R. L. Ewen and G. M. Meagher, Dual Throat Thruster Thermal Model, User's Manual (First Draft), Contract NAS8-34136, 8 Dec. 1981

5. Hixon, B. A., Beckwith, J. E. and Bushnell, D. M., "Computer Program for Compressible Laminar or Turbulent Nonsimilar Boundary Layers," NASA TM X-2140, April 1971

6. I. E. Beckwith and D. M. Bushnell, Calculation by a Finite Difference Method of Supersonic Turbulent Boundary Layers with Tangential Slot Injection, NASA TN D-6221, April 1971

7. "Hydrogen-Oxygen Auxiliary Propulsion for the Space Shuttle, Volume I: High Pressure Thrusters," NASA CR-120895, Contract NAS 3-14354, 30 January 1973.

8. "Investigation of Gaseous Propellant Combustion and Associated Injector/Chamber Design Guidelines (Part I) and Handbook for Design of Gaseous Propellant Injectors and Combustion Chambers (Part II)," NASA CR-121234, Contract NAS 3-14379, 31 July 1973.

9. LaBotz, R. J., and Blubaugh, A. L., "Integrated Thruster Assembly Program," Aerojet Liquid Rocket Company, NASA Report CR-134509, Contract NAS 3-15850, November 1973.

10. Matthews, L. W., "Dual Throat Thruster Engine Manufacturing Report," Contract NAS 8-34136, Aerojet TechSystems Manufacturing Technology Report ME83:004, 20 December 1983.

11. Lundgren, R. B, Nickerson, G. R., and O'Brien, C. J., "Dual Throat Thruster Cold Flow Analysis," Aerojet Liquid Rocket Company Report 32666F, Contract NAS 8-32666, August 1978.

12. Valler, H. W., "High Density Fuel Combustion and Cooling Investigation," Contract NAS 3-21020, Final Report, September 1980.

13. Korst, H. H., et al, "Research on Transonic and Supersonic Flow of a Real Fluid at Abrupt Increases in Cross Sectin," ME Technical Report 392-5, University of Illinois.

14.

15. Ambrok, G. S., "Approximate Solution of Equations for the Thermal Boundary Layer with Variations in Boundary Layer Structure," Soviet Physics (Technical Physics) Volume 2, 1957, pp. 1979, 1986.

16. Valler, H. W., "Performance of a Transpiration-Regenerative Cooled Rocket Thrust Chamber," NASA CR-159742, September 1979.

17. Rousar, D. C., and Ewen, R. L., "Hydrogen Film-Cooling Investigation," NASA CR-121235, August 1973.

18. Mayer, E., "Analysis of Convective Heat Transfer in Rocket Nozzles," ARS Journal, Volume 31, 1961, pp. 911-917.

APPENDIX A

SECONDARY MODE II THERMAL MODEL

Nomenclature

1. English Letters

Cp	Specific heat
hg	Combustion product heat transfer coefficient
he	Effective fin heat transfer coefficient in lip model
H	Total enthalpy
I	Shear layer integrals in aerodynamic bleed flur model, Ref. 2
k	Thermal conductivity in the lip model; entrainment fraction in the secondary Mode II thermal model
l	Length of the shear layer
MR	Mixture ratio
qw	Heat flux to the wall
Pr	Prandtl number
r	radius; r_m is the radius of the mixing layer interface
R_C	Radius of curvature
Re	Reynolds number
St	Stanton number
t_w	Wall thickness
t_{lip}	Thickness of tip of primary nozzle
T	Static temperature
T_o	Total temperture
u	Velocity; $\bar{u}$ is an effective velocity in the secondary Mode II thermal model
w	Flow rate; w_c is the initial mixing layer flow rate and W_E is the primary flow intrained in the mixing layer
x	Distance along the wall in the secondary Mode II thermal model
y	Coordinate normal to the shear layer
Y	Primary gas concentration in the shear layer

2. Greek Letters

Δ	Boundary Layer Energy Thickness
η	Dimensionless coordinate y/e in the shear layer, film coolant effectiveness in the mixing layer downstream of the shear layer downstream of the shear layer

θ	Mixing layer profile shape factor
μ	Viscosity
ρ	Density
σ	Shear layer spreading rate parameter
ϕ	Dimensionless velocity u/ue in the shear layer

3. Subscripts

aw	Adiabatic walldd streamline in the shear layer, the streamline which divides the recirculating flow from that which exists the nozzle
e	Freestream or primary edge of the shear layer or mixing layer
f	Evaluated at the film temperature, 0.5 (T_{aw} + T_w)
i	Initial condition for the mixing layer
j	j streamline in the shear layer; the composition on the primary side of this streamline is primary gas only
p	Primary
r	Recirculation region
s	Secondary
w	At the wall

A thermal model of the region downstream of the primary plume attachment point has been developed by extending the shear layer of the aerodynamic bleed flow model in the form of a mixing layer similar to that used in the ATC film cooling model of Reference 3. Heat transfer to the wall is based on an integral model of the thermal boundary layer. Details of these models shown schematically in Figure A-1, are presented below.

A. MIXING LAYER INITIAL CONDITIONS

Initial conditions for the mixing layer and wall boundary layer analyses downstream of the primary plume impingement point are defined by the shear layer of the aerodynamic bleed flow model, Reference 2. The initial mixing layer extends from the "d" streamline, which is the boundary of the recirculation flow, to the shear layer edge coordinate η_e defined such that the concentration of primary gas Y_e is 0.99. From the definition of Y_e,

$$Y_r (1 - \Phi_e) + \Phi_e = 0.99$$

or

$$\Phi_e = 0.5 [1 + \text{erf} (\eta_e)] = \frac{0.99 - Y_r}{1 - Y_r}$$

in which subscript r refers to the recirculation zone. For the small values of Y_r normally obtained η_e is approximately 1.65, compared with the value of 3.0 used in the bleed flow model.

1. "d" Streamline Conditions

The bleed flow model calculates the "d" streamline coordinate η_d and the corresponding velocity ratio Φ_d. All other parameters of interest at this location, which become the initial wall conditions for the mixing layer, follow from Φ_d and the recirculation region parameters. Thus, the primary gas concentration is

$$Y_d = Y_r (1 - \Phi_d) + \Phi_d$$

A, Mixing Layer Initial Conditions (cont.)

and the total enthalpy is

$$H_d = Y_d\, H_p + (1 - Y_d)\, H_{bleed}$$

Assuming the bleed flow is a mixture of the primary propellants, the mixture ratios MR_r and MR_d can be calculated from the primary gas concentrations using the defining relation

$$\frac{1}{1 + MR} = \frac{Y}{1 + MR_p} + \frac{1-Y}{1 + MR_s}$$

which yields

$$MR = \frac{1 + MR_p}{1 + (1-Y)\,\dfrac{MR_p - MR_s}{1 + MR_s}} - 1$$

Three options are included for the calculation of total temperatures. In the reactive option, a built-in table derived from ODE for O_2/H_2 systems, defines temperature as a function of mixture ratio, enthalpy and pressure. This table is used to obtain both To_d and the recirculation region temperature; the latter requires H_r, which is calculated like H_d above with Y_r replacing Y_d. A non-reactive, constant specific heat option utilizes the recirculation region temperature T_r from the bleed flow model. In this case

$$To_d = \frac{H_r(1-\Phi_d) + \Phi_d\, C_{pp}\, To_p}{c_{ps}\,(1-Y_d) + c_{pp}\, Y_d}$$

in which the recirculation enthalpy is

$$H_r = [C_{ps}\,(1-Yr) + C_{pp}\, Yr]\, T_r$$

A, Mixing Layer Initial Conditions (cont.)

The third option merely uses an input table of temperature vs mixture ratio.

2. Mixing Layer Parameters

A number of initial mixing layer parameters must be defined from the bleed flow model. The thickness of the mixing layer at the plume impingement point is

$$y_e = \frac{\ell}{\sigma} (\eta_e - \eta_d)$$

in which ℓ is the length of the shear layer and σ is the spreading rate parameter. The initial flow in the mixing layer is defined as

$$W_c = 2\pi r_w \int_0^{y_e} \rho u \, dy$$

$$2\pi r_w \frac{\rho_e u_e \ell}{\sigma} \int_{y_d}^{\eta_e} \frac{\rho}{\rho_e} \Phi \, d\eta$$

Since the bleed flow W_s can be expressed in the same way with the upper limit of integration being the "j" streamline,

$$\frac{W_c}{W_s} = \frac{I_1 (\eta_e) - I_1(\eta_d)}{I_1 (\eta_j) - I_1(\eta_d)}$$

Although not used at present, the recirculation flow can be caluclated as

$$\frac{W_r}{W_s} = \frac{I_1 (\eta_d)}{I_1 (\eta_j) - I_1 (\eta_d)}$$

A, Mixing Layer Initial Conditions (cont.)

The mixing layer model requires a concentration profile shape factor Θ relating the bulk and wall concentrations. Therefore, an initial valve Θ_i must be obtained from the shear layer results. From its definition

$$\Theta_i = \frac{1 - \overline{Y}}{1 - Y_d}$$

in which

$$\overline{Y} = \frac{\int_0^{y_e} \rho u \, Y \, dy}{\int_0^{y_e} \rho u \, dy}$$

However, a shear layer mass balance requires that

$$W_s = 2\pi \, r_w \int_0^{y_e} \rho u \, (1-Y) \, dy$$

Therefore

$$\Theta_i = \frac{1}{1 - Y_d} \cdot \frac{W_s}{W_c}$$

In order to provide a reference for the initial energy thickness of the wall boundary layer, the energy thickness Δ_s of the shear layer is of interest. By definition,

$$\Delta_s = \int_0^{y_e} \frac{\rho}{\rho_e} \Phi \frac{H_p - H}{H_p - H_d} \, dy$$

$$= \int_0^{y_e} \frac{\rho}{\rho_e} \Phi \frac{1 - \Phi}{1 - \Phi_d} \, dy$$

$$= \frac{\ell}{(1-\Phi_d) \, \sigma} \int_{\eta_d}^{\eta_e} \frac{\rho}{\rho_e} \Phi \, (1 - \Phi) \, d\eta$$

A, Mixing Layer Initial Conditions (cont.)

In terms of the bleed flow model integrals and the plume boundary temperature ratio,

$$\Delta_s = \frac{(T/T_o)_p \ell}{(1 - \Phi_d)\sigma} [I_1(\eta_e) - I_1(\eta_d) - I_3(\eta_e) + I_e(\eta_d)]$$

From the definition of the "j" streamline

$$I_1(\eta_j) = I_1(\eta_e) - I_3(\eta_e)$$

so

$$\Delta_s = \frac{(T/T_o)_p \ell}{(1 - \Phi_d)\sigma} [I_1(\eta_j) - I_1(\eta_d) + I_3(\eta_d)]$$

The revised aerodynamic bleed flow model computer program provides the following output parameters:

Y_r, T_r/T_{o_p}, W_r/W_s, η_d, Φd, η_e, Φ_e, y_e, W_c/W_s, and Δ_s. Initial condition parameters calculated within the thermal model include H_r, MR_r, Y_d, H_d, MR_d, T_{o_d} and Θ_i.

B. MIXING LAYER MODEL

A modification of the ATC gas film cooling model, Reference 3, is used to represent the mixing layer and predict wall mixture ratios and adiabatic wall temperatures. Yhe modification was necessary to account for the different initial conditions provided by the free shear layer upstream compared to the injection of pure film coolant. In this model, the film coolant effectiveness is defined in terms of the concentration Y of primary gas,

B, Mixing Layer Model (cont.)

$$\eta = \frac{1 - Y_w}{1 - Y_d}$$

as a result of which the wall mixture ratio is

$$MR_w = \frac{1 + MR_p}{1 + \eta\,(1 - Y_d)\,\dfrac{MR_p - MR_s}{1 + MR_s}} - 1$$

The effectiveness is calculated from the entrainment flow W_E into the mixing layer as

$$\eta = \frac{\Theta_i}{\Theta\,(1 + \dfrac{W_E}{W_C})}$$

in which Θ is a mixing layer profile shape factor, Θ_i is its initial value and W_C is the initial flow in the mixing layer.

Following the film cooling model approach, the shape factor Θ is determined from

$$\frac{\Theta - \Theta_i}{\Theta_\infty - \Theta_i} = f_1(W_E/W_C)$$

This function and the asymptotic shape factor Θ_∞ have been determined from adiabatic 2-D boundary layer analyses. Figure A-1a shows the shape factor W_E/W_C from these results. The effect of Reynolds number is seen to be relatively small and has been neglected. An asymptotic shape factor of 0.545 is indicated, compared with a value of 0.485 for the standard supersonic film cooling model (Reference 17). If the edge of the mixing layer were defined as Y = 0.999 instead of 0.99, the asymptotic Θ would be about 0.51. Thus, the present results are considered to be consistent with the standard film cooling model.

B, Mixing Layer Model (cont.)

The adiabatic wall boundary layer analyses indicate the imperfect recovery of kinetic energy has a negligible effect on the adiabatic wall enthalpy. Thus the latter may be calculated directly from the primary and "d" streamline total enthalpies and the film coolant effectiveness, i.e.,

$$\frac{H_p - H_{aw}}{H_p - H_d} = \eta$$

The entrainment mass flux into the mixing layer is defined as a fraction of the freestream mass velocity; therefore,

$$W_E = \int_0^x 2\pi\, r_m\, k\, \rho_e u_e\, dx$$

in which k is the entrainment fraction and r_m the radius of the mixing layer-freestream interface. Entrainment fractions inferred from one of the adiabatic 2-D boundary layer analyses are shown in Figure A-2; they increase with axial distance and appear to reach an asymptotic value of about 0.022.This asymptotic value is in excellent agrement with the supersonic film cooling data of Reference 17. However, film cooling data generally show somewhat higher entrainment fractions near the injection point, followed by a decay to the asymptotic value. It is expected that the actual interaction of the bleed flow shear layer with the secondary wall will not yield the low initial entrainment fractions of Figure A-2.

Three options are available for obtaining adiabatic wall temperatures: a reactive model limited to O_2/H_2 systems, which uses a built-in table of temperature vs MR_w, H_{aw} and pressure; a non-reactive, constant specific heat model; and an input table of adiabatic wall temperature vs wall mixture ratio. For the non-reactive option

$$T_{aw} = T_{o_p} - \eta \frac{C_{p_d}}{C_{p_w}} (T_{o_p} - T_{o_d})$$

B, Mixing Layer Model (cont.)

in which

$$C_{p_w} = \eta\, C_{p_d} + (1 - \eta)\, C_{pp}$$

$$C_{p_d} = C_{p_s}\ (1 - Y_d) + C_{pp}\, Y_d$$

C. HEAT TRANSFER MODELS

1. Primary Plume Impingement Region

An analytical Stanton number model similar to those of Ambrok, Reference 15, and Mayer, Reference 18, is used to predict the wall heat flux downstream of the primary plume impingement point,

$$q_w = \rho_f\, u\, C_{p_f}\, St\, (T_{aw} - T_w)$$

in which $\bar{u}$ is an effective velocity at the edge of the wall boundary layer. In this model

$$St = C\, Pr^{-0.6} \left[\overline{Re} + \left(\frac{A_i\, Pr^{0.6}}{1.25\, CA}\, Re_{\Delta_i}\right)^{1.25}\right]^{-0.2}$$

in which

$$\overline{Re} = \frac{1}{A^{1.25}} \int_0^x A^{1.25}\, \frac{\rho_f\, \bar{u}}{\mu_f}\, dx$$

$$A = r_w \mu_f\, C_{p_f}\, (T_{aw} - T_w)$$

C, Heat Transfer Models (cont.)

and Δ_i is the initial energy thickness of the thermal boundary layer. The correlation coefficient C is usually taken as the flat plate value of 0.0296. This Stanton number model is like TBL with an interaction exponent of zero; however, the Blasius skin friction law and a modified Reynolds analogy replace the Coles skin friction law and Von Karman analogy of TBL.

It was proposed that the effective velocity u is related to the mixing layer entrainment flow as follows:

$$\frac{\frac{\bar{u}}{u_e} - \Phi_d}{1 - \Phi_d} = f_2 (W_E/W_C)$$

in which Φ_d is the "d" steamline velocity ratio from the bleed flow model. The function of entrainment flow ratio was to be developed such that the 2-D cold wall boundary layer analysis results are predicted. These results are shown in Figure 95 in the form of a Stanton number based on u_e and the adiabatic wall density, i.e.,

$$St_1 = St \quad \frac{\bar{u}}{u_e} \cdot \frac{\delta_f}{\rho_{aw}}$$

St_1 increases significantly due to the increase in velocity near the wall resulting from the shear layer to wall boundary layer transition, then decreases as in a normal boundary layer. The selection of the function f_2 (W_E/W_C), a reference film temperature for property evaluation and a prescription for the initial energy thickness in terms of shear layer characteristics such that the results of Figure 95 are predicted, was required to complete the model.

The best fit of the two-dimensional heat transfer results was obtained with an initial energy thickness of zero and an initial effective velocity of zero and is shown in Figure 95. A model with the initial velocity

equal to the "d" streamline value from the aerodynamic bleed flow model, as proposed above, along with a positive initial energy thickness did not yield an asymptotic region of decreasing Stanton number (See Figure 95). The proposed correlation for the effective velocity in terms of the entrainment flow ratio from the mixing layer model is shown in Figure 92.

Two-dimensional boundary layer analyses were conducted for two initial boundary layer thicknesses. The correlation coefficient C in the Stanton number model was found to be strongly dependent on this thickness, which is equal to y_e from the shear layer model. Since the spreading rate parameter in the shear layer model has not been empirically verified, the test data of Task III are required to finalize the correlation coefficient in the boundary layer model.

2. Recirculation Region

Development of a good heat transfer model for the recirculation region is beyond the scope of this contract, since the aerodynamic model does not provide a description of the flow field. Therefore, a very simple turbulent pipe flow model has been included in the computer program:

$$q_w = \rho_e u_e C_p C_g Re D_e^{-0.2} Pr^{-0.6} (T_r - T_w)$$

in which the mass velocity $\rho_e u_e$ is based on the bleed flow W_s and all properties are evaluated at MR_r and the recirculation gas temperature T_r.

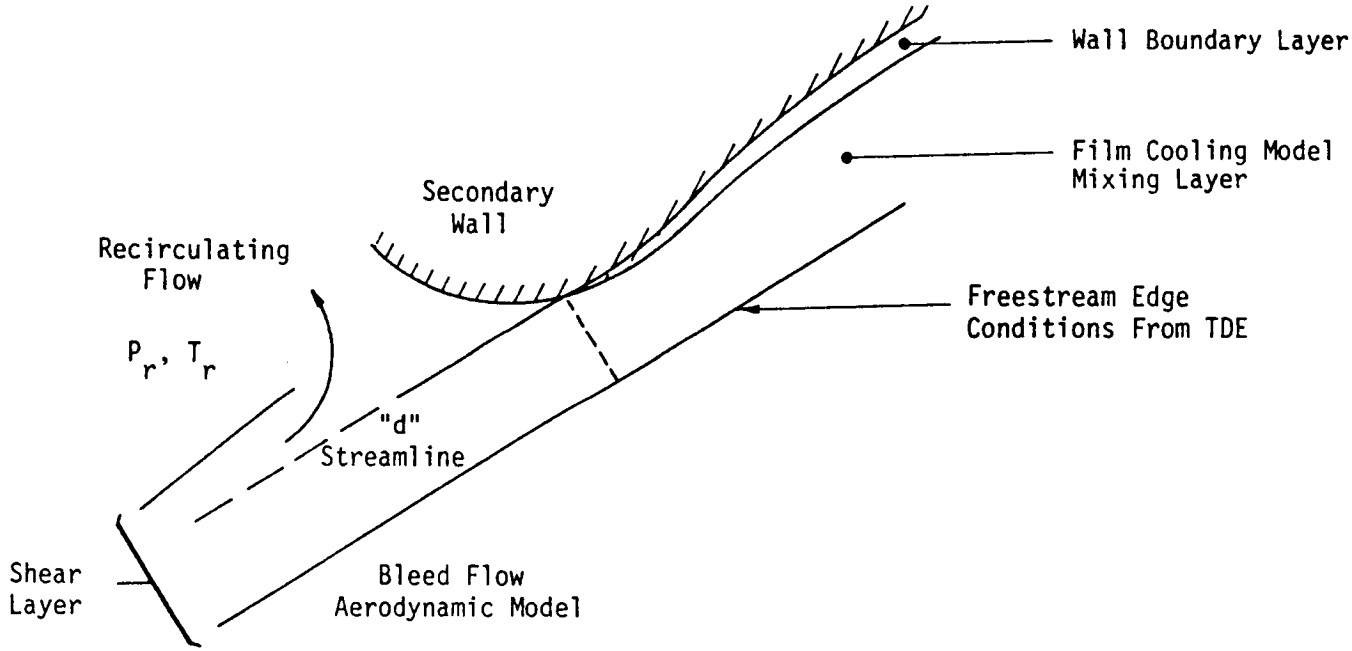

Figure A-1 Mode II Thermal Model is a Continuation of the Aerodynamic Bleed Flow Model Shear Layer

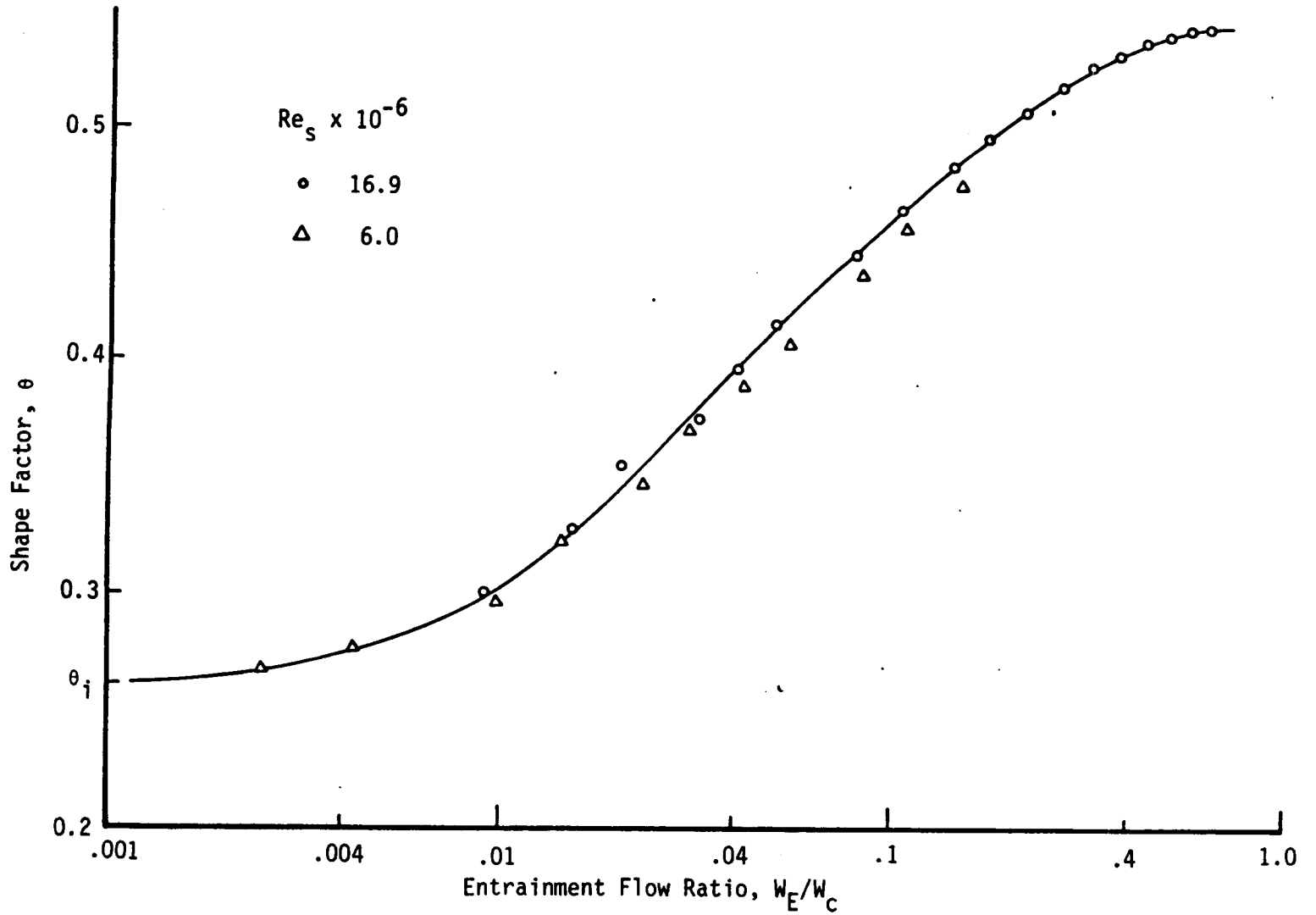

Figure A-1a Mixing Layer Shape Factors from Finite-Difference Boundary Layer Analysis

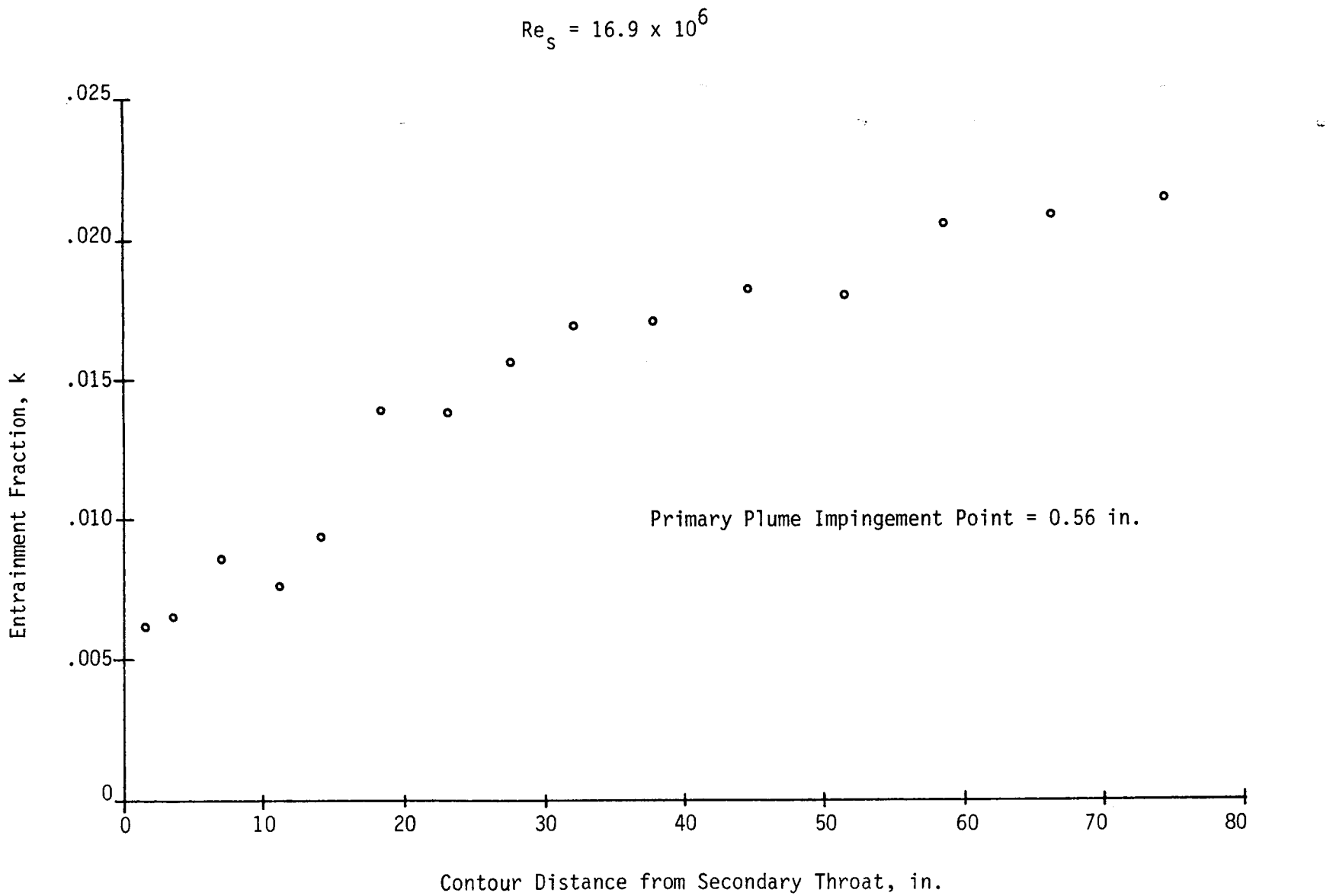

Figure A-2. Entrainment Fractions from Finite-Difference Mixing Layer Analysis

APPENDIX B

TEST SUMMARY DATA

TABLE B-1

DUAL THROAT THRUSTER DATA NOMENCLATURE

Symbol	Paramater
PPC	Primary Chamber Pressure
PSC	Secondary Chamber Pressure
PWIM	Water Inlet Manifold Pressure
PWOM	Water Outlet Manifold Pressure
POIJ	Igniter Oxygen Manifold Pressure
PFIJ	Igniter Hydrogen Manifold Pressure
POPJ	Primary Injector Oxygen Manifold Pressure
PFPJ	Primary Injector Hydrogen Manifold Pressure
POSJ	Secondary Injector Oxygen Manifold Pressure
PFSJ	Secondary Injector Hydrogen Manifold Pressure
TWP-10-12	Primary Chamber Calorimeter Circuit Temperature
TWP-13	Primary Chamber Axial Circuit Temperature
TWS-1 to 13	Secondary Chamber Calorimeter Circuit Temperature

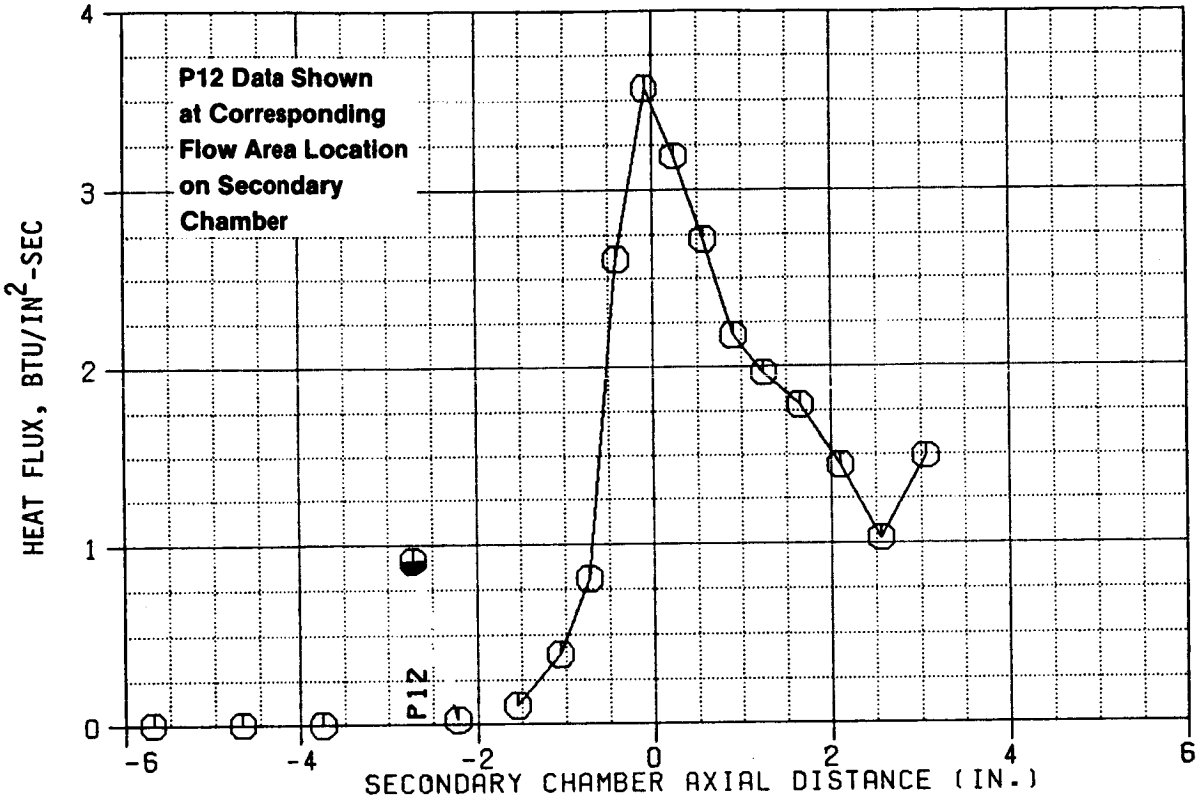

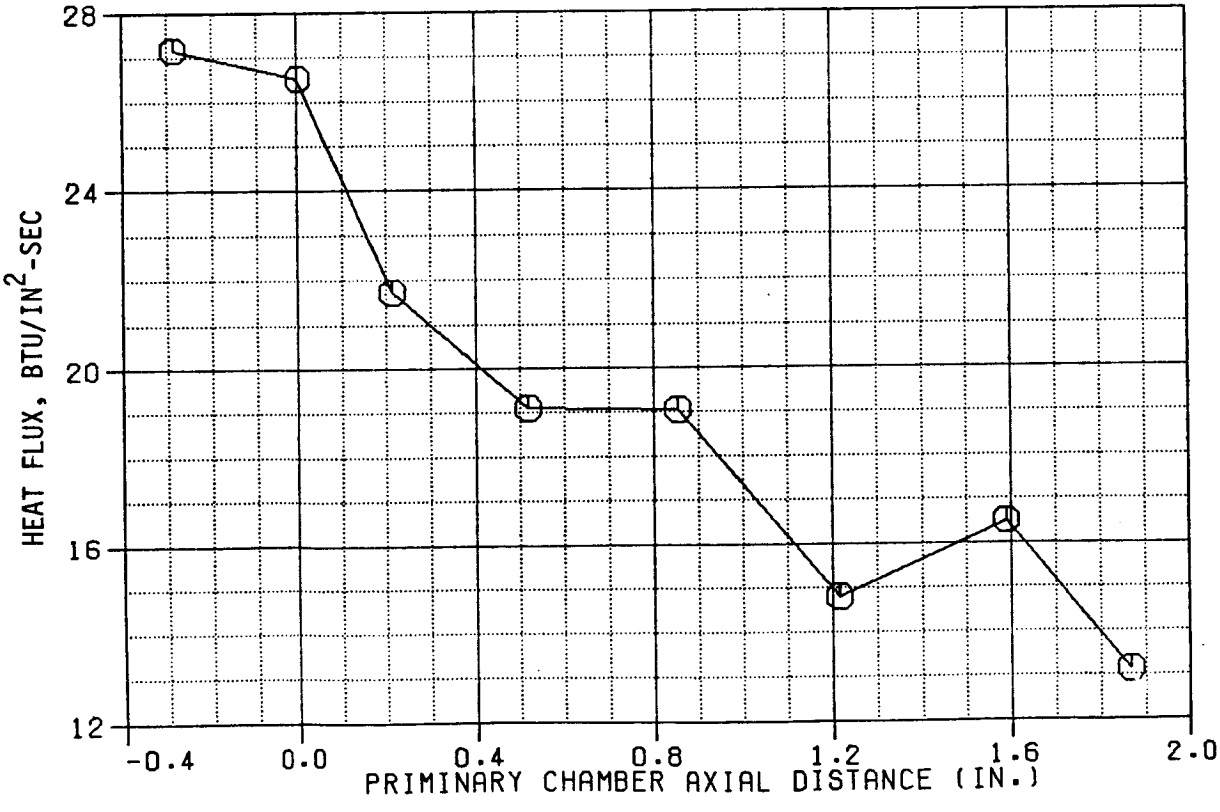

Figure B-1. Test 111 Heat Flux Profiles

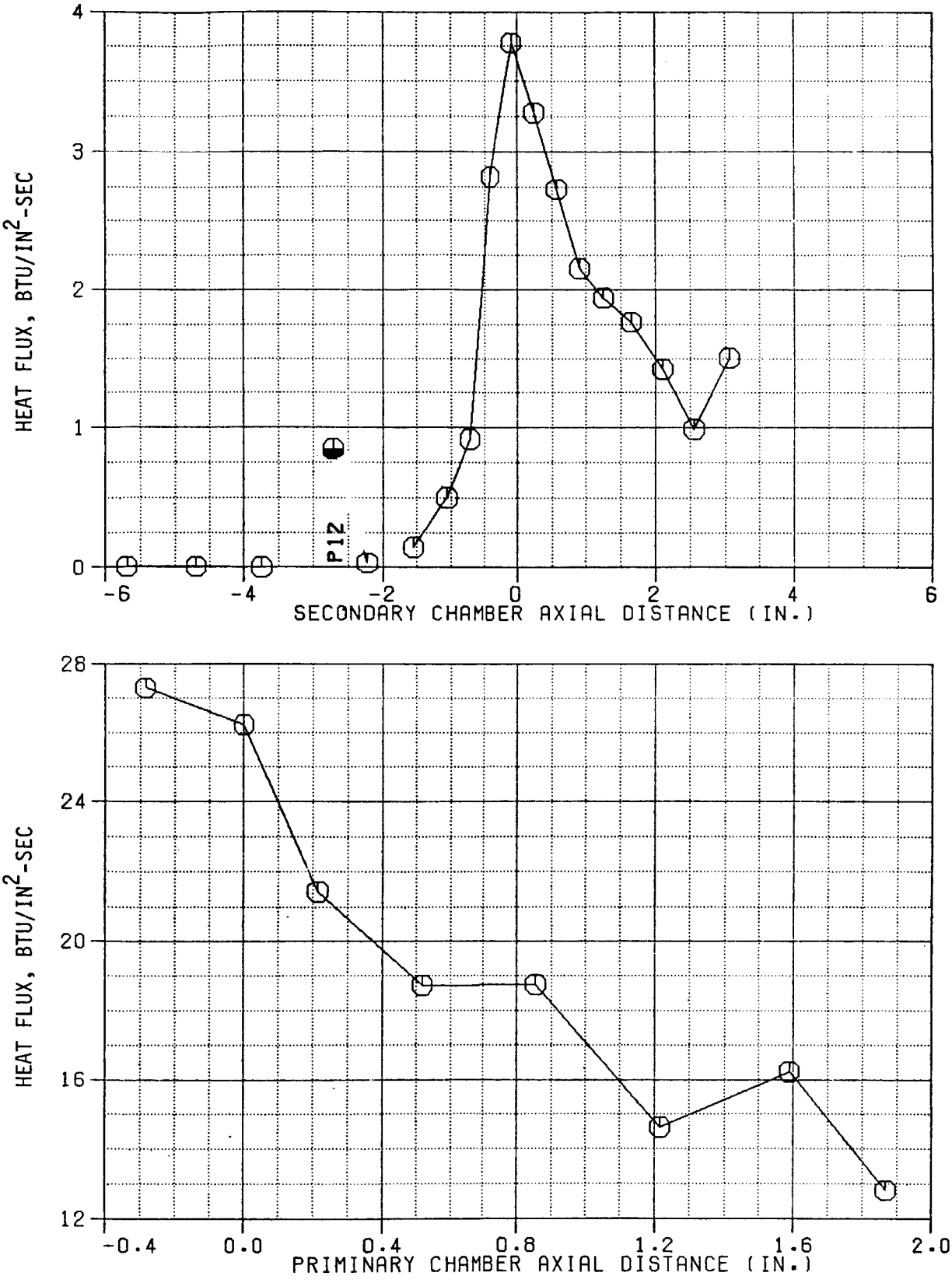

Figure B-2. Test 112 Heat Flux Profiles

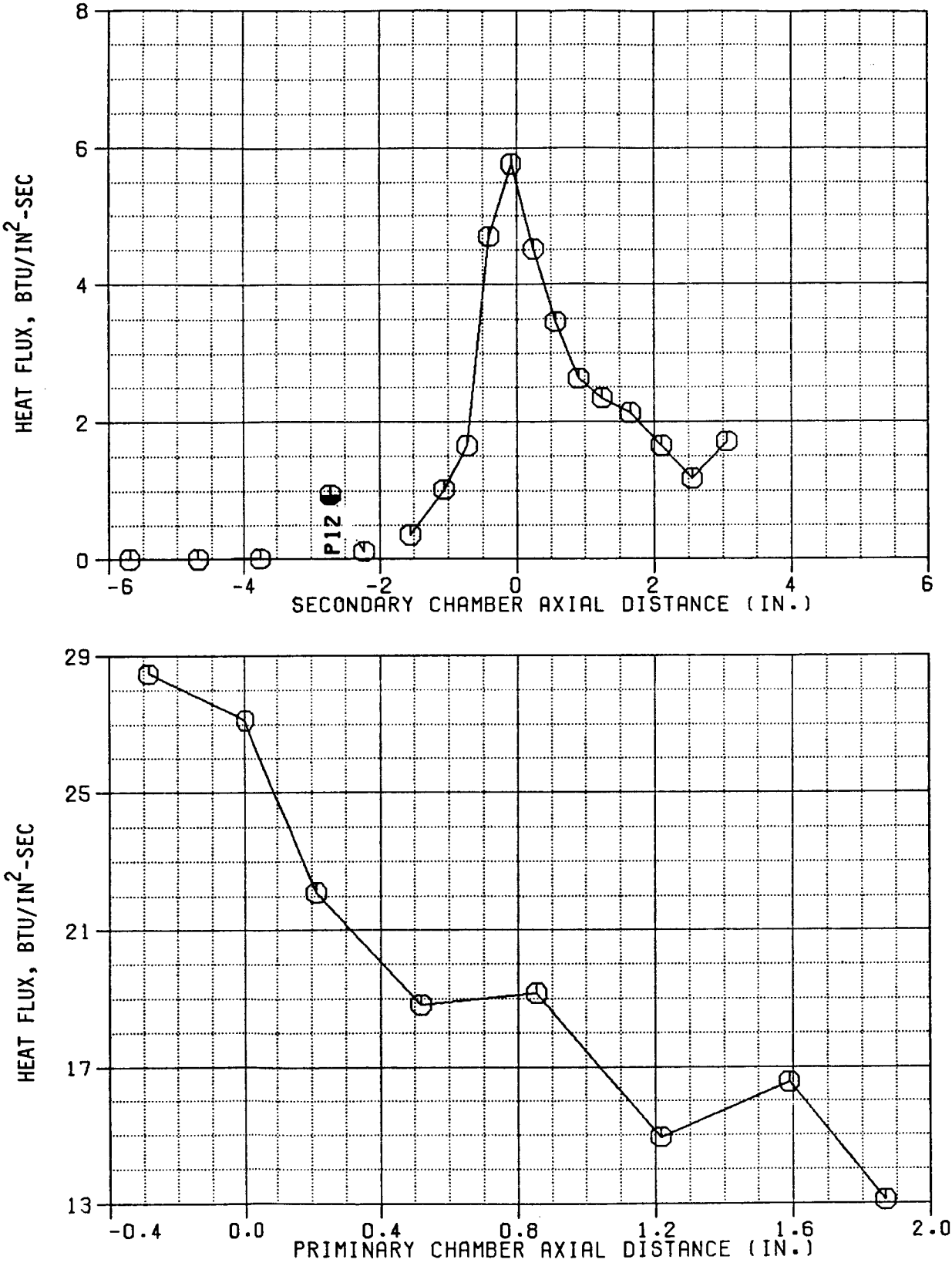

Figure B-3. Test 113 Heat Flux Profiles

C-4

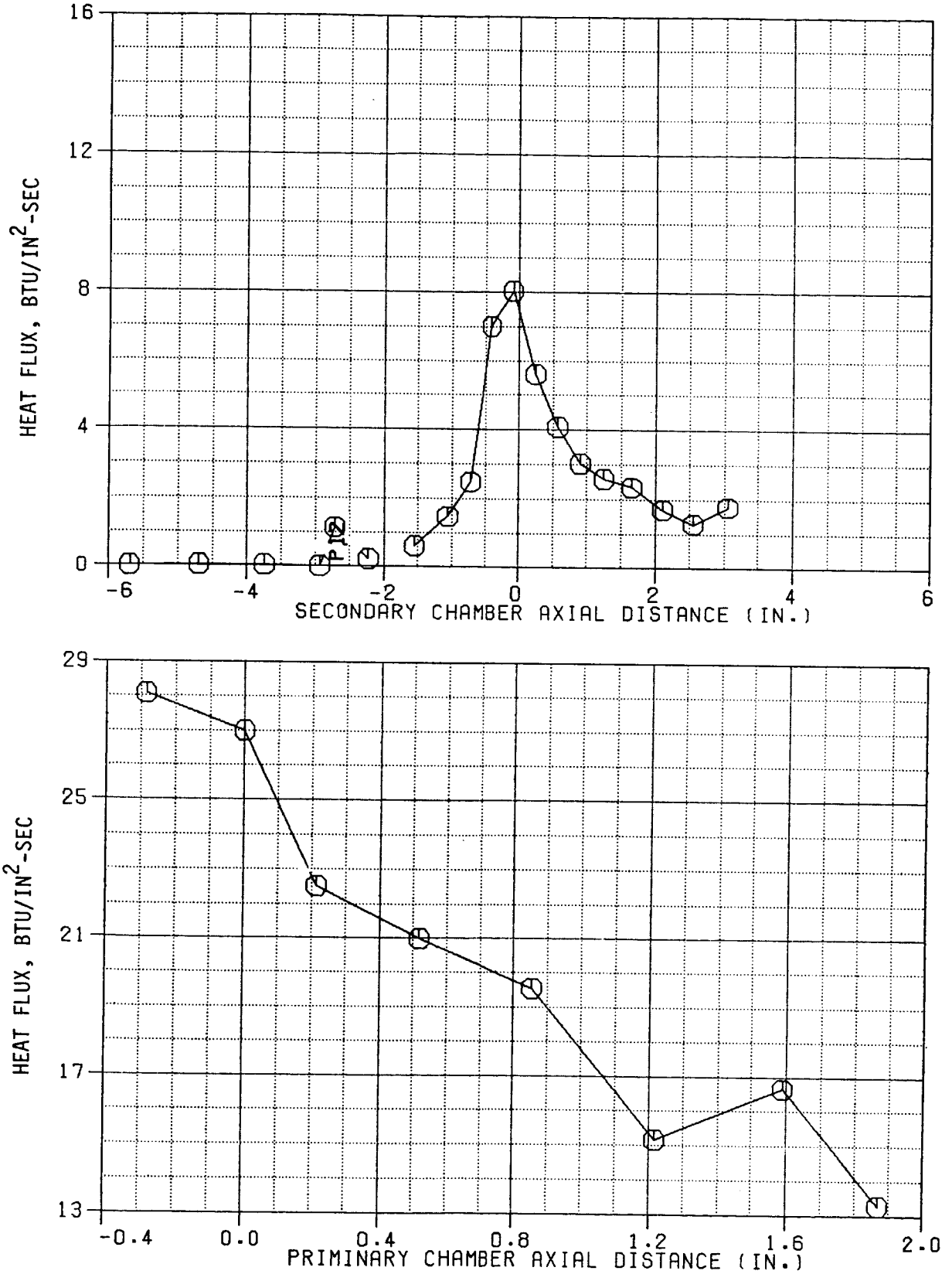

Figure B-4. Test 114 Heat Flux Profiles

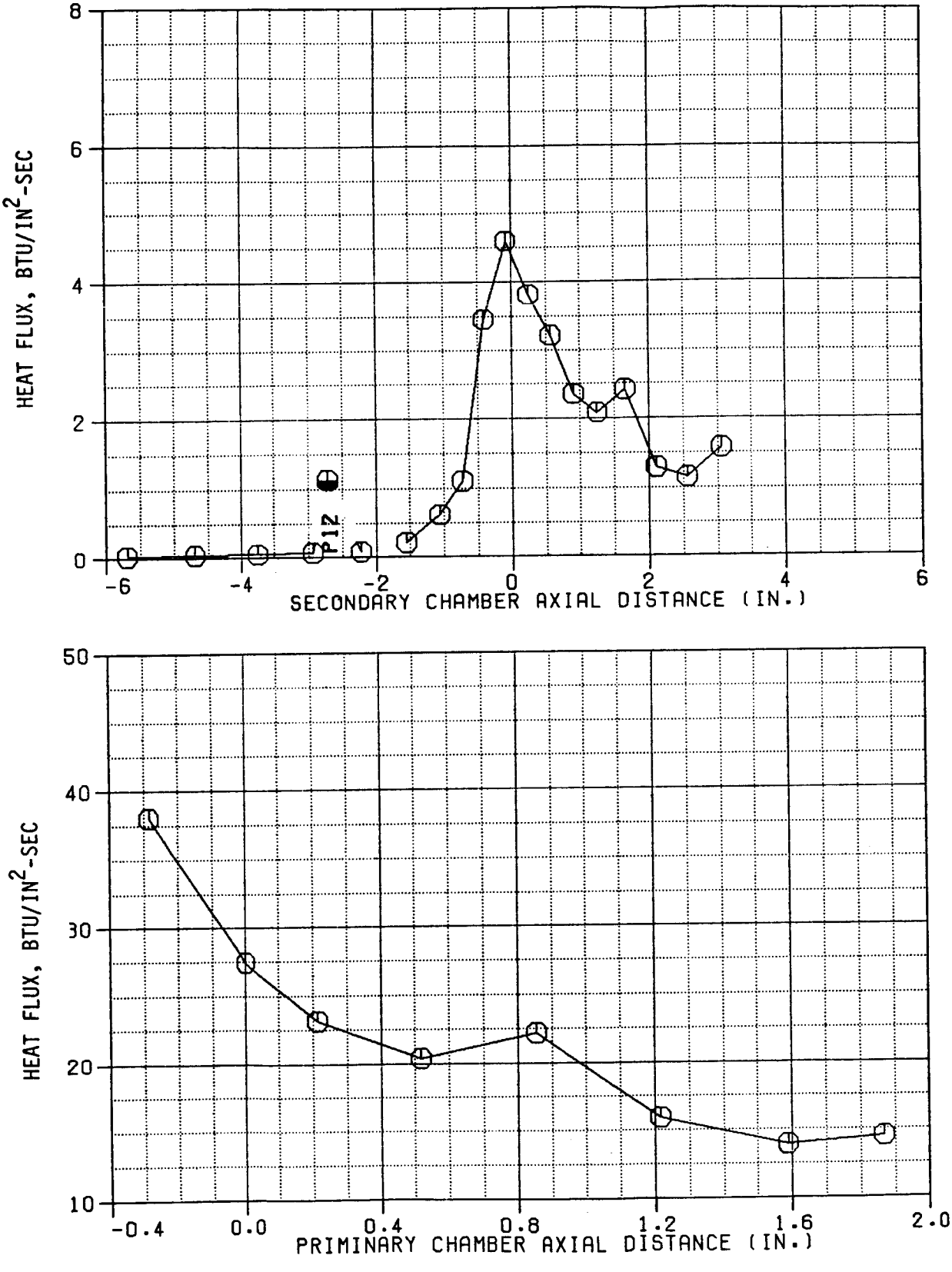

Figure B-5. Test 137 Heat Flux Profiles

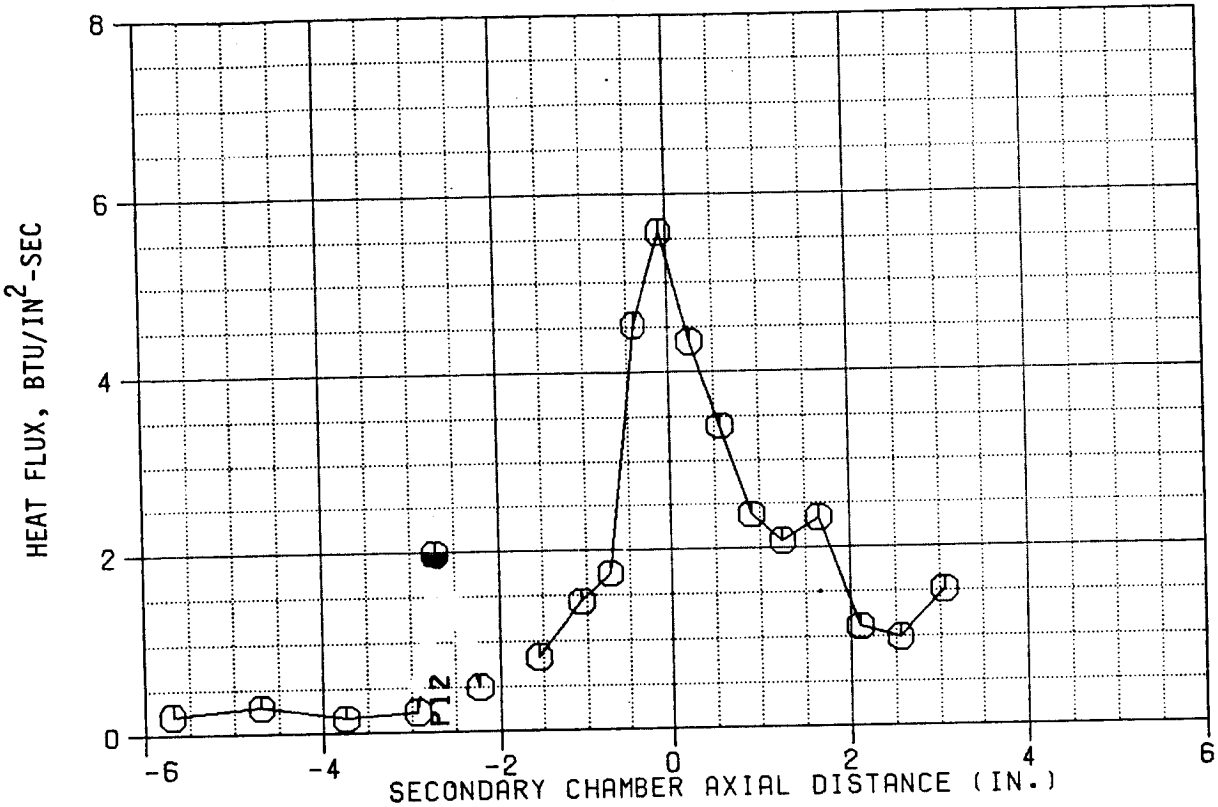

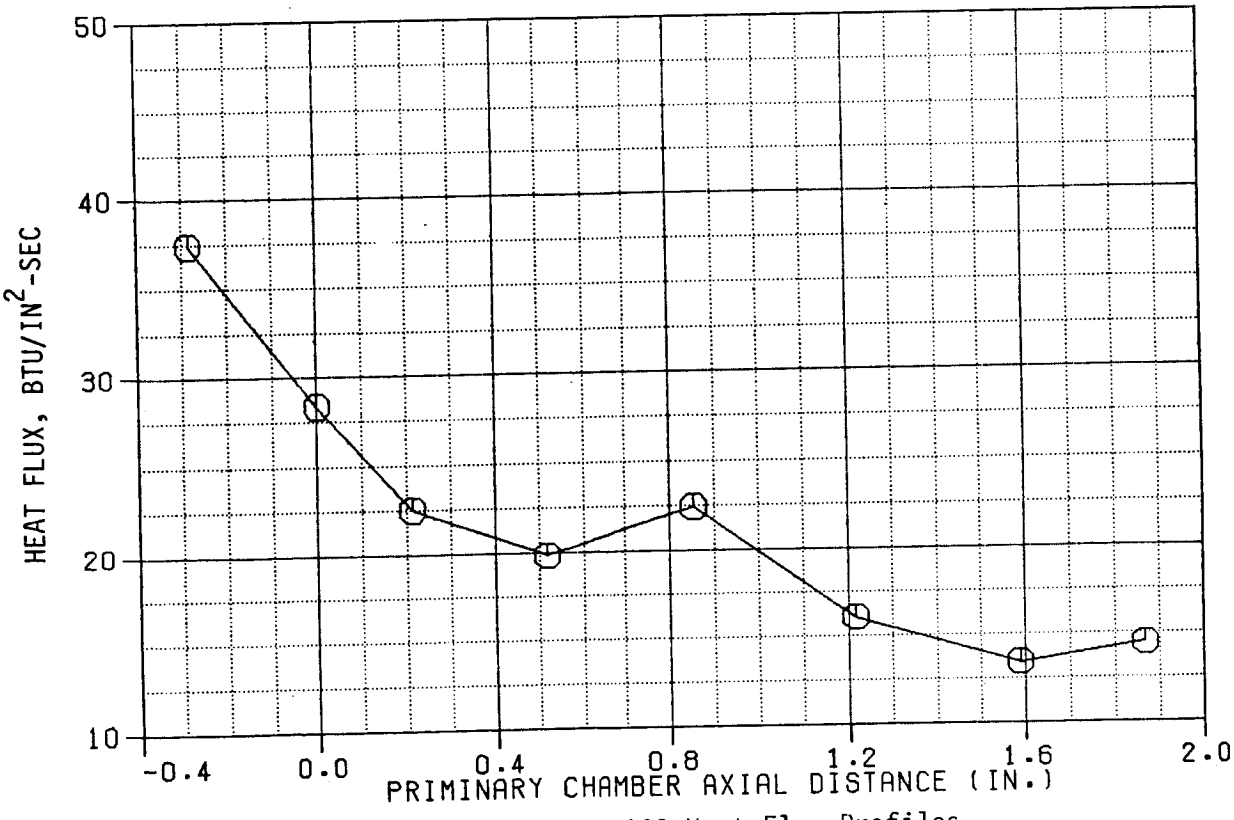

Figure B-6. Test 138 Heat Flux Profiles

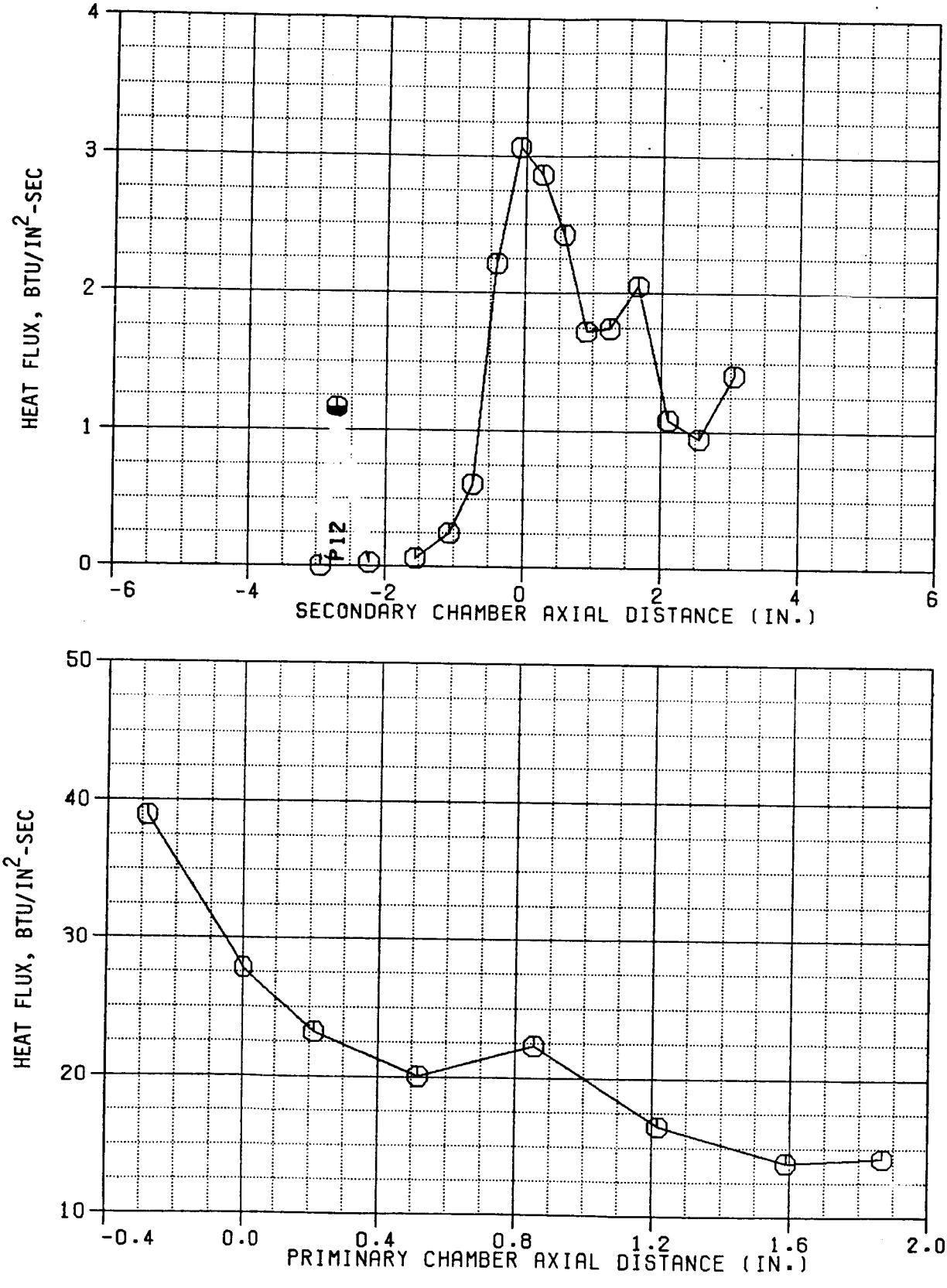

Figure B-7. Test 139 Heat Flux Profiles

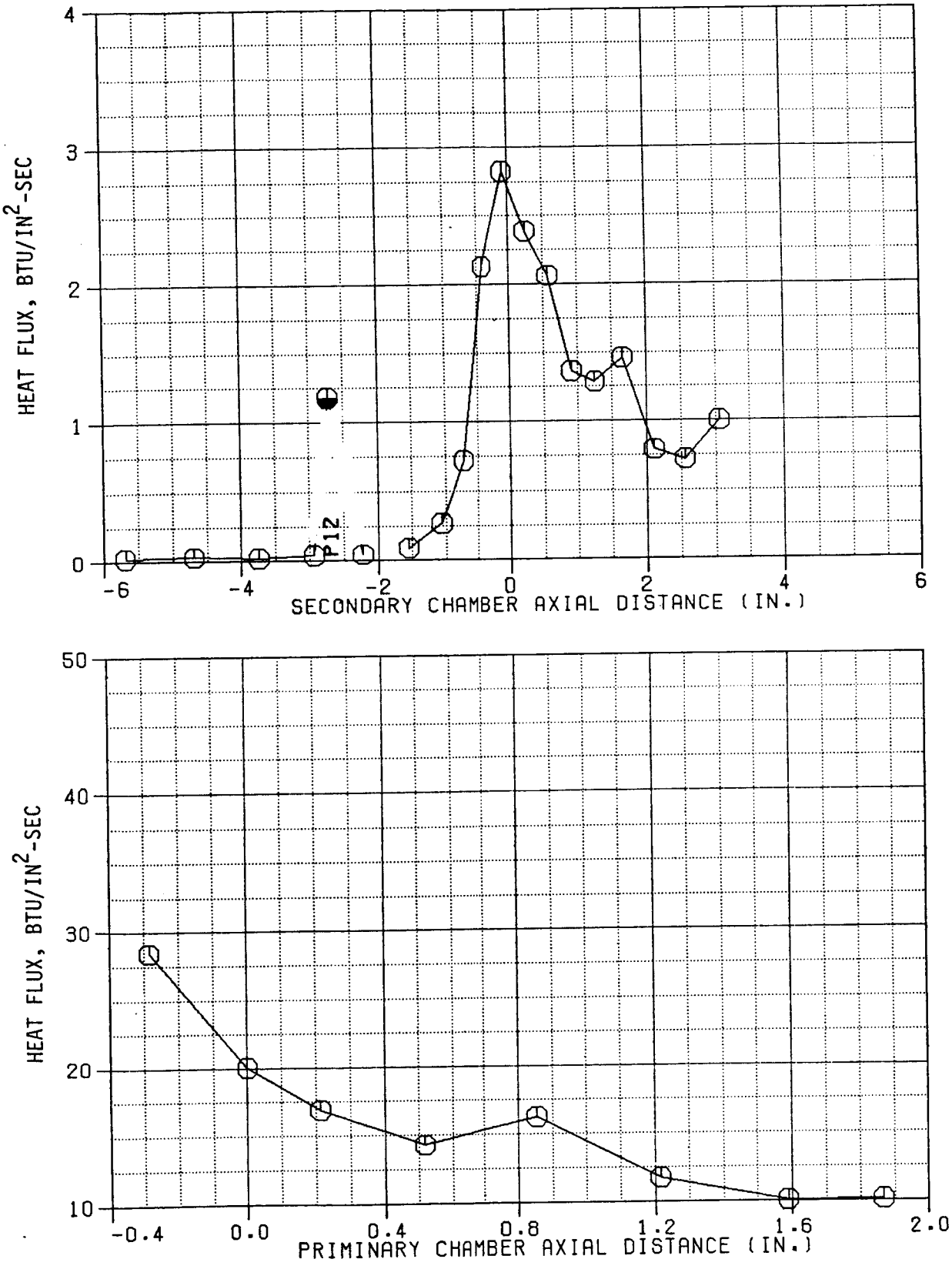

Figure B-8. Test 140 Heat Flux Profiles

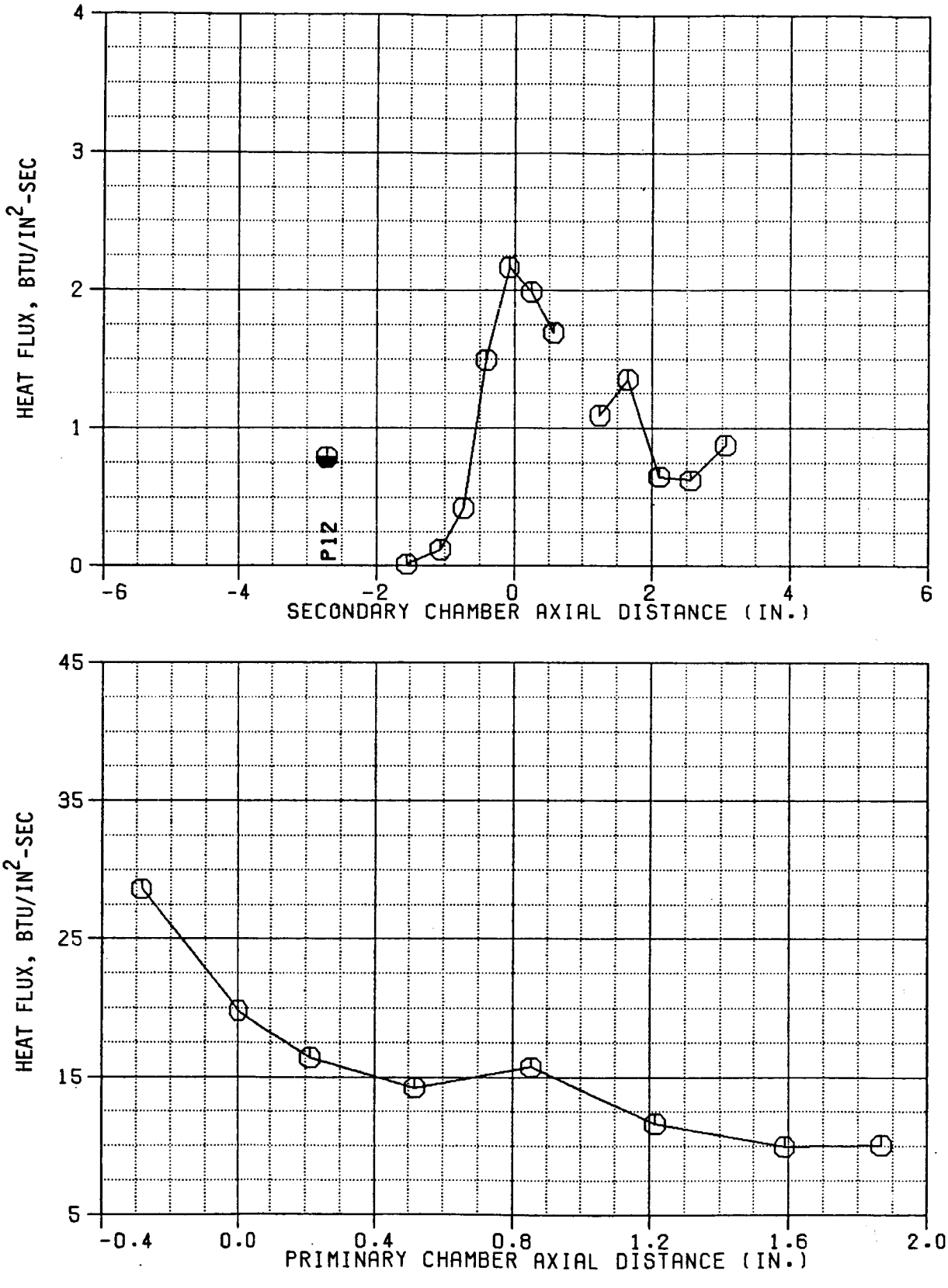

Figure B-9. Test 141 Heat Flux Profiles

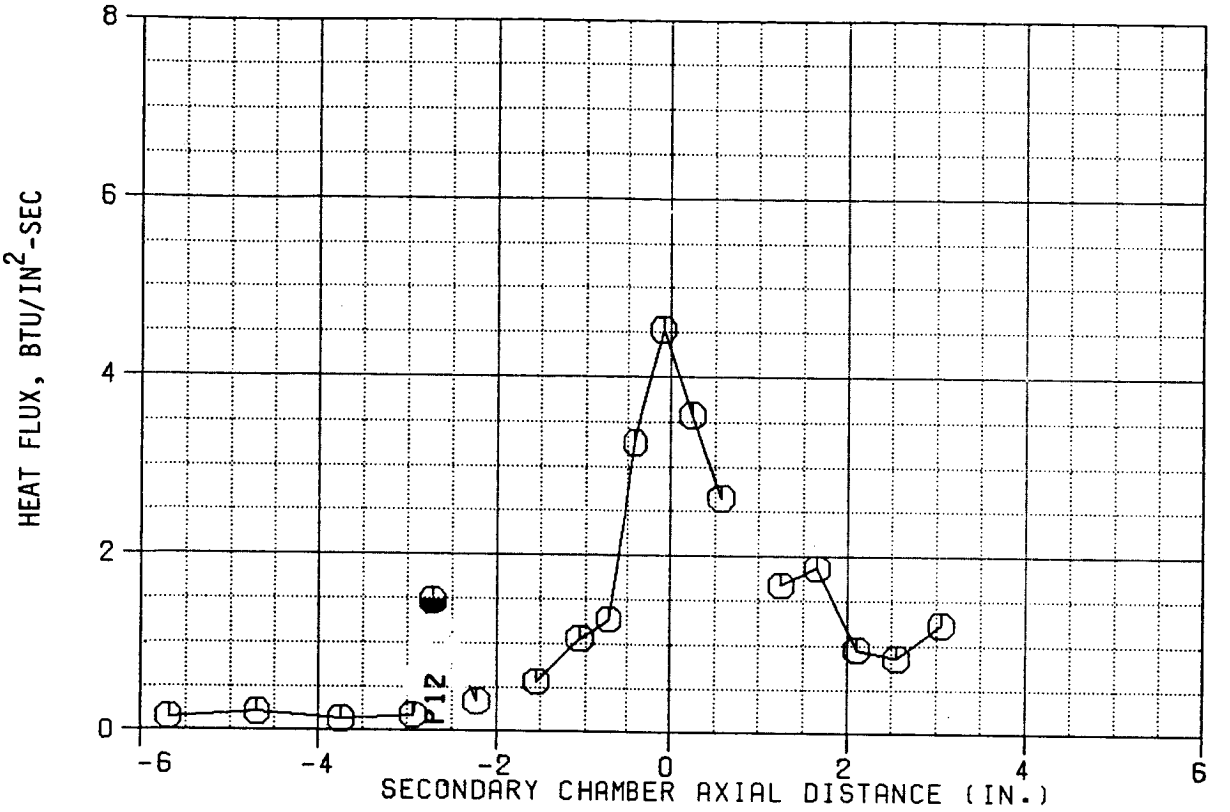

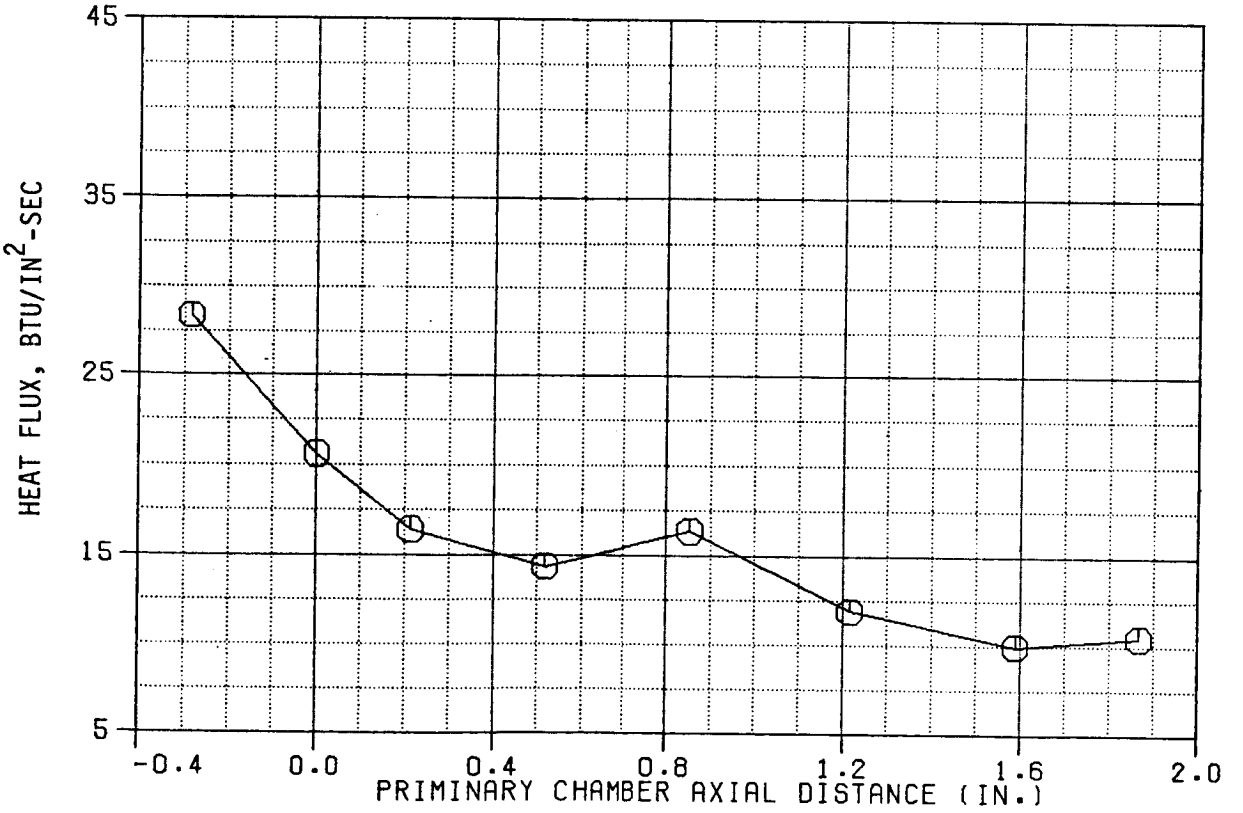

Figure B-10. Test 142 Heat Flux Profiles

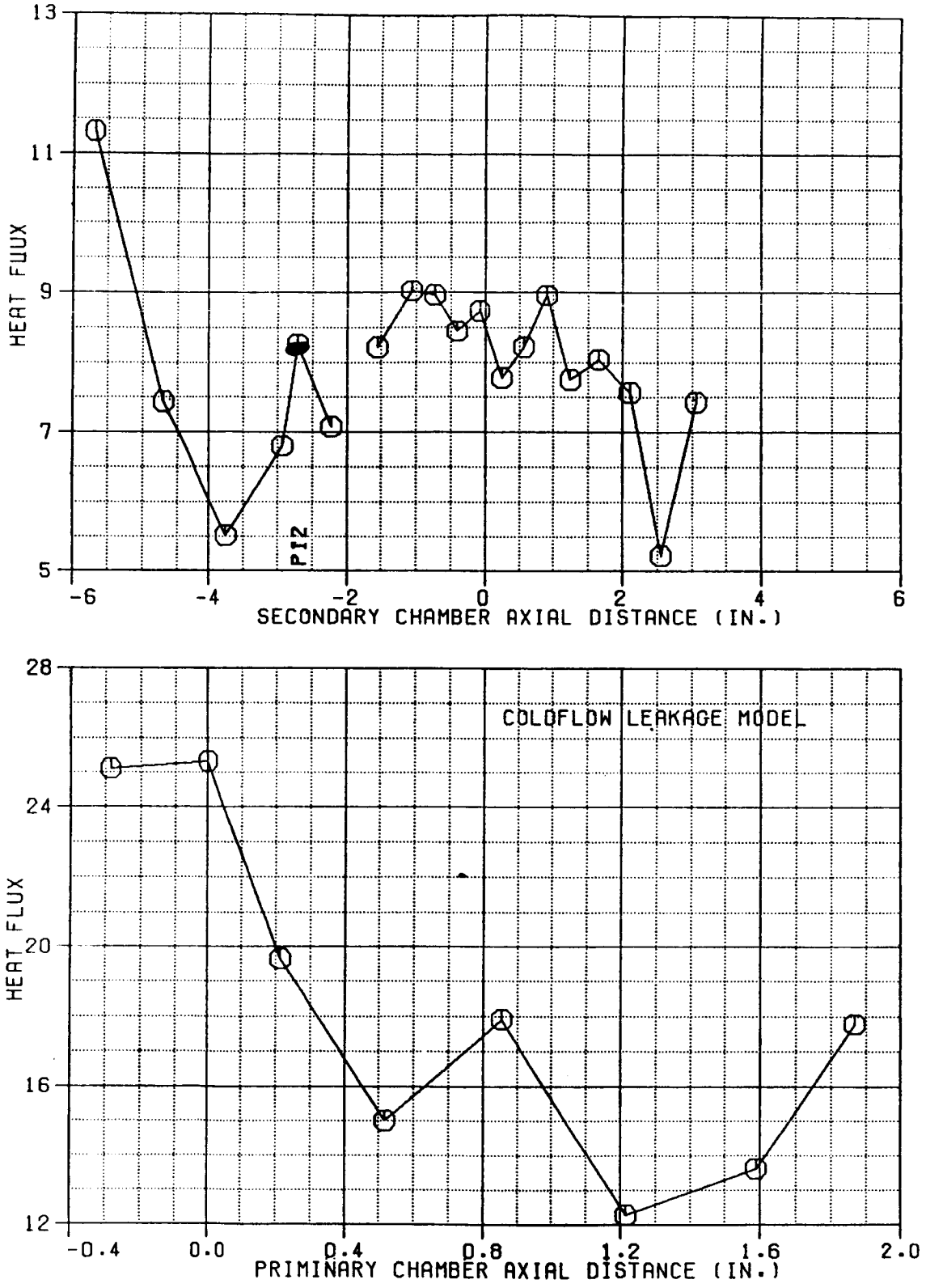

Figure B-11. Test 116 Heat Flux Profiles

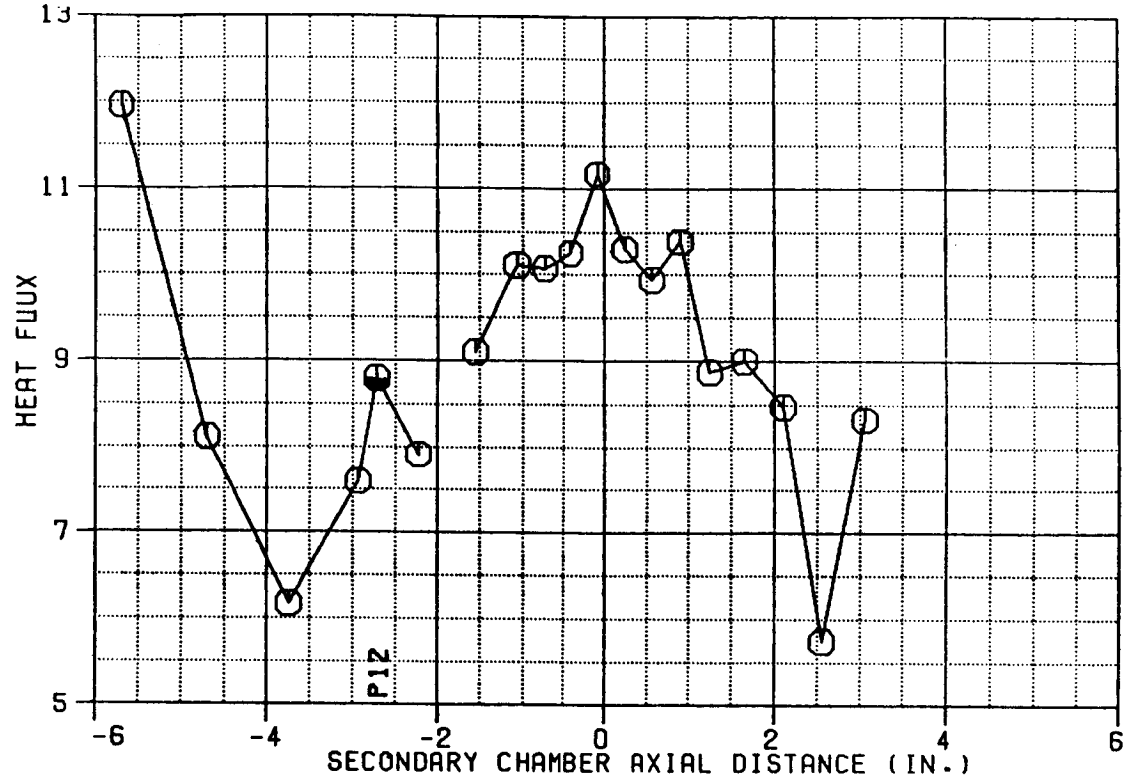

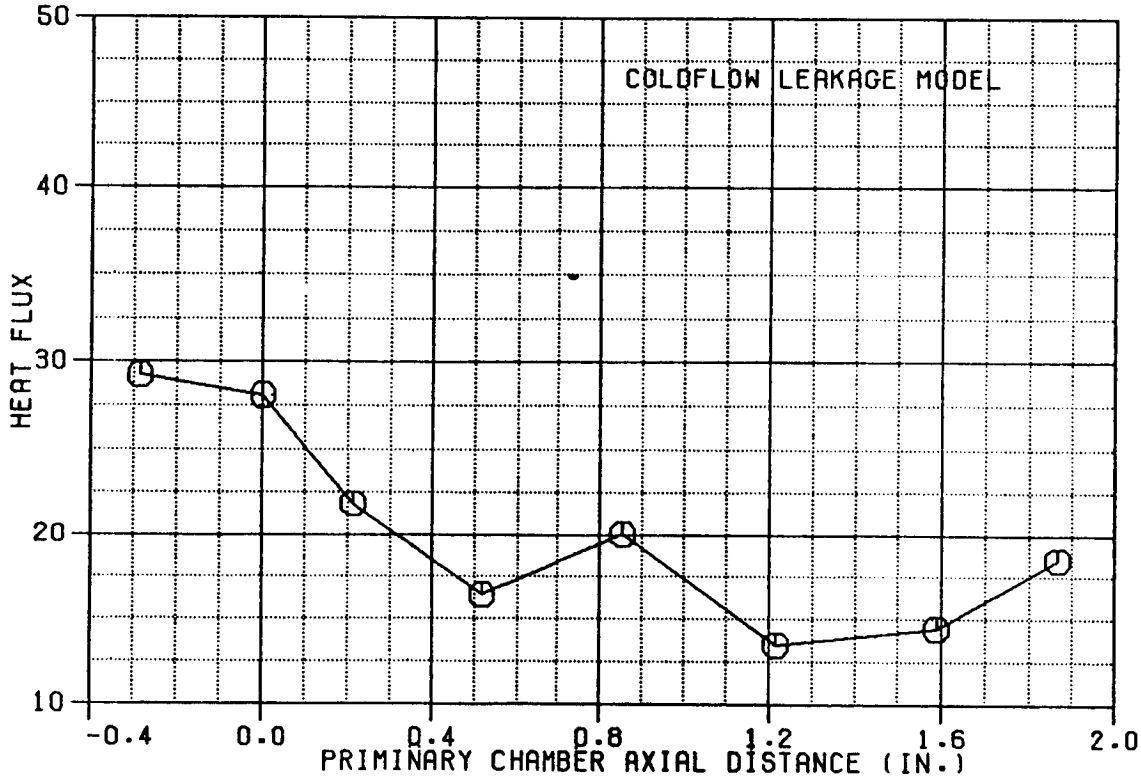

Figure B-12. Test 117 Heat Flux Profiles

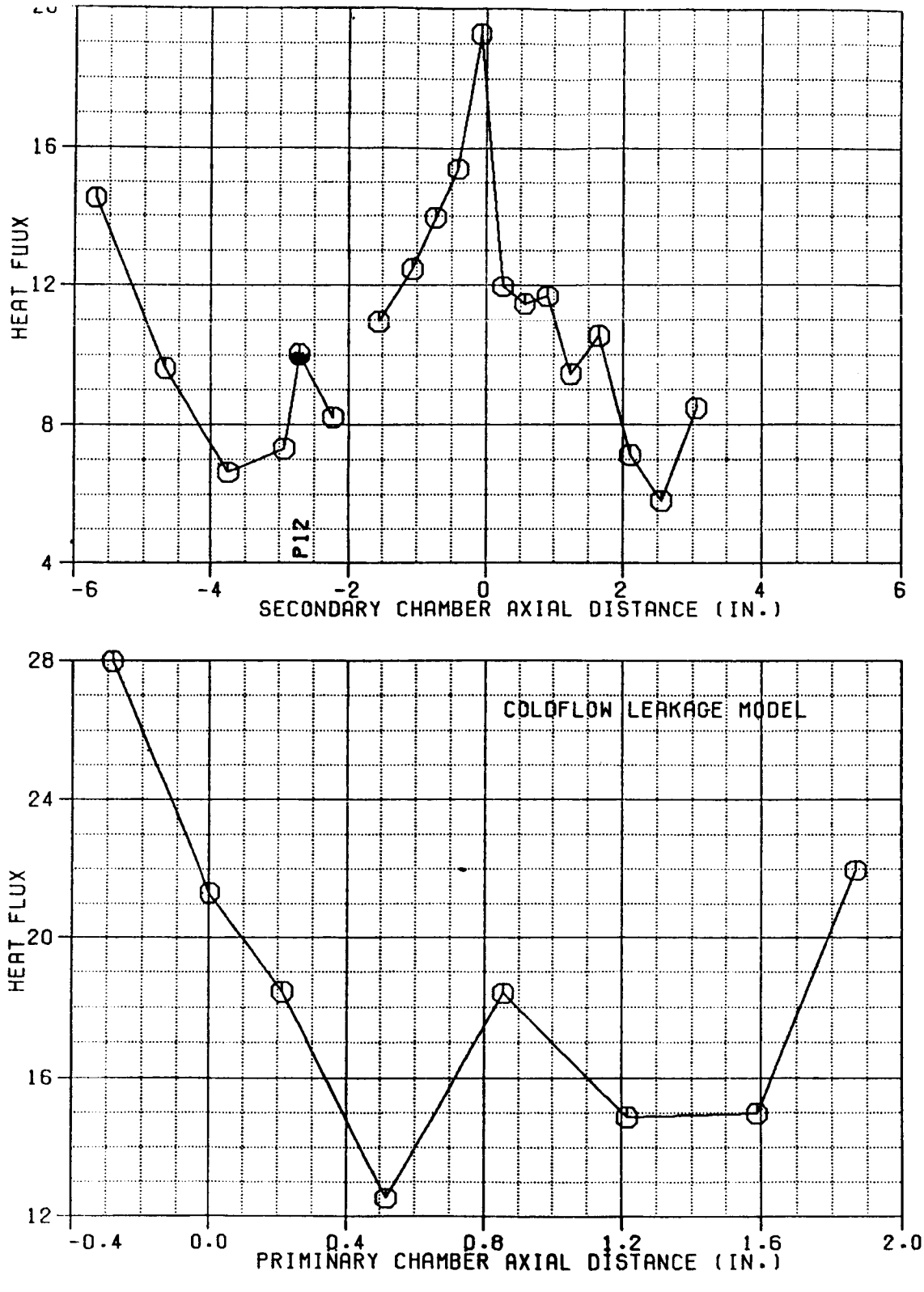

Figure B-13. Test 125 Heat Flux Profiles

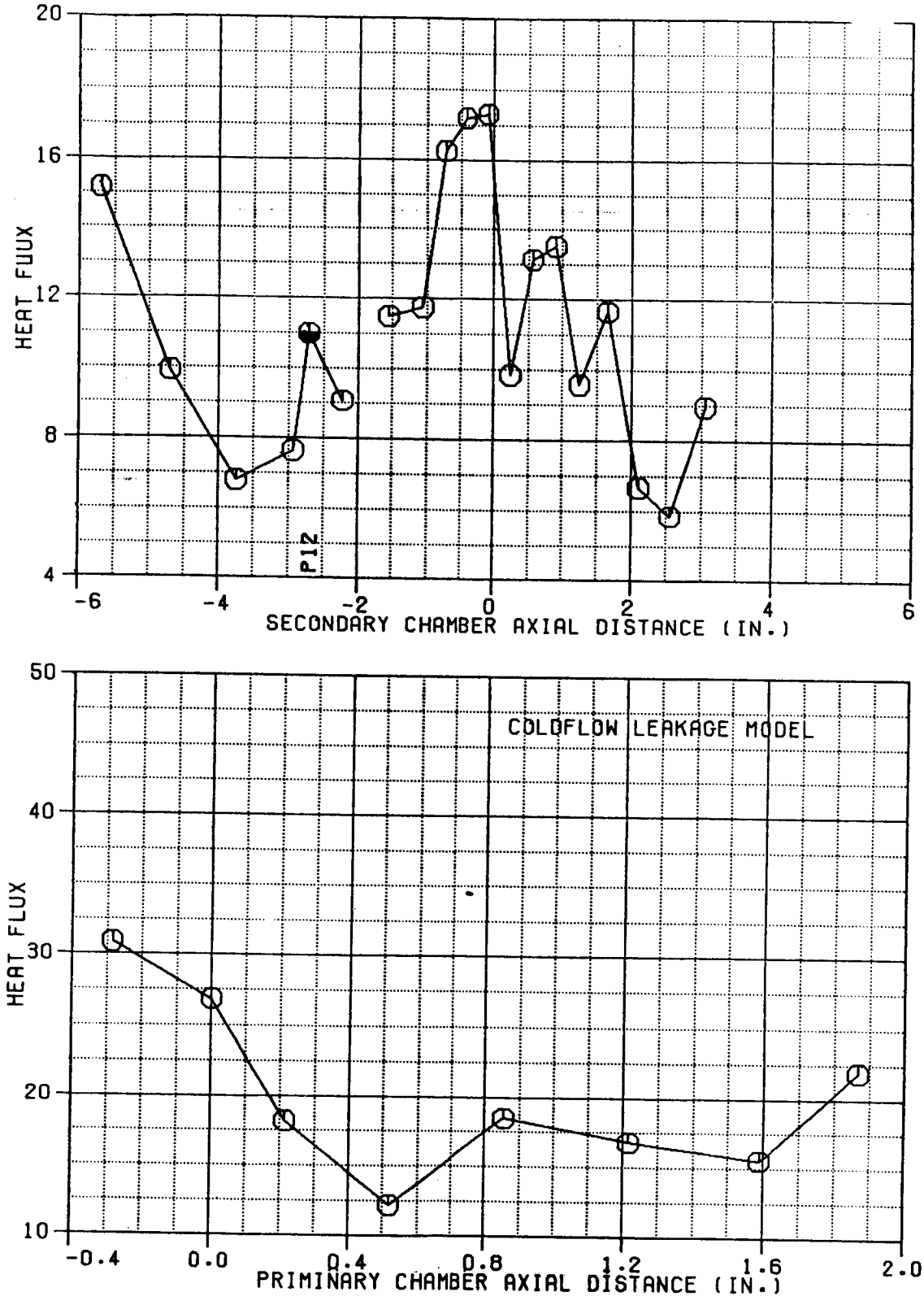

Figure B-14. Test 126 Heat Flux Profiles

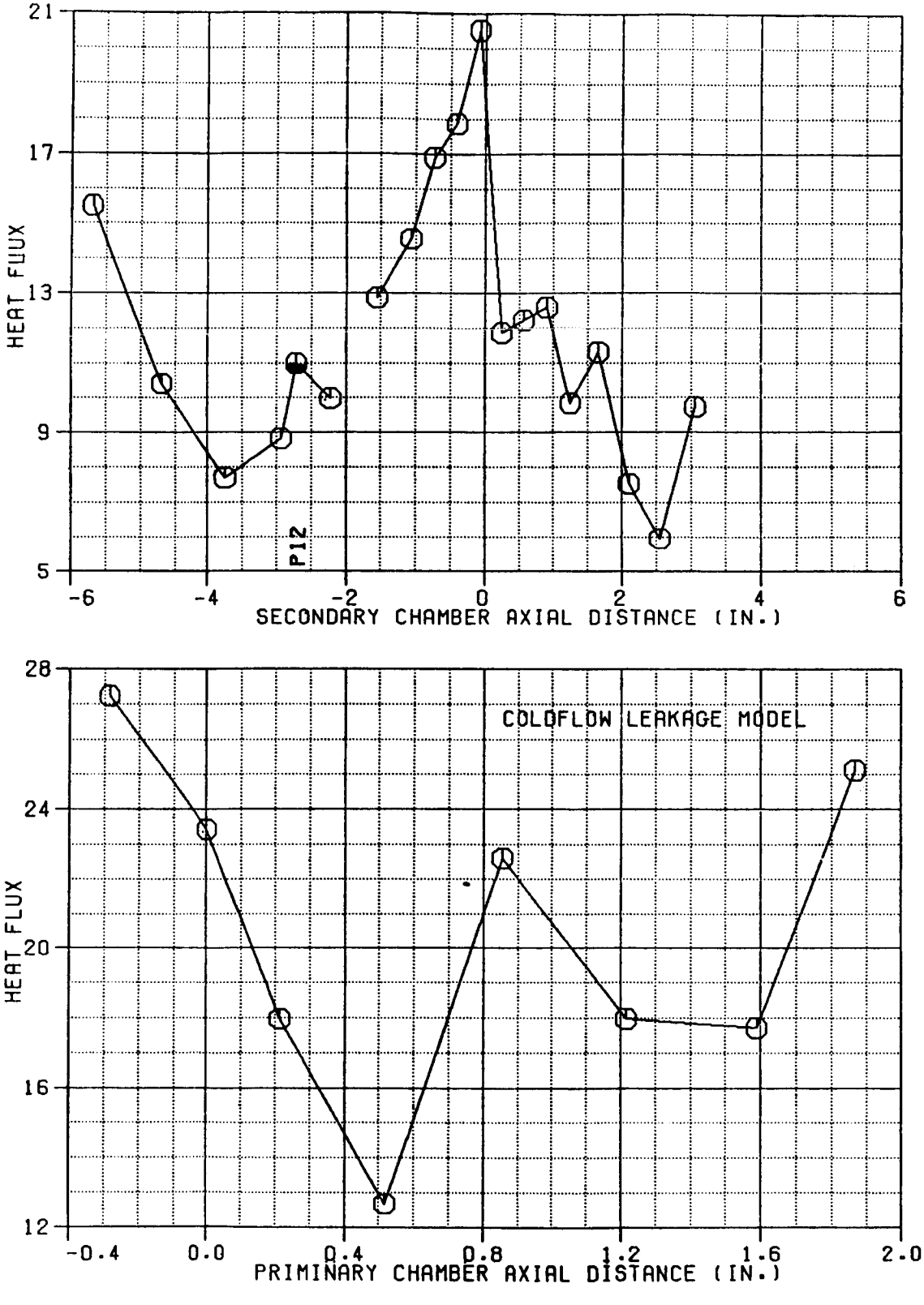

Figure B-15. Test 127 Heat Flux Profiles

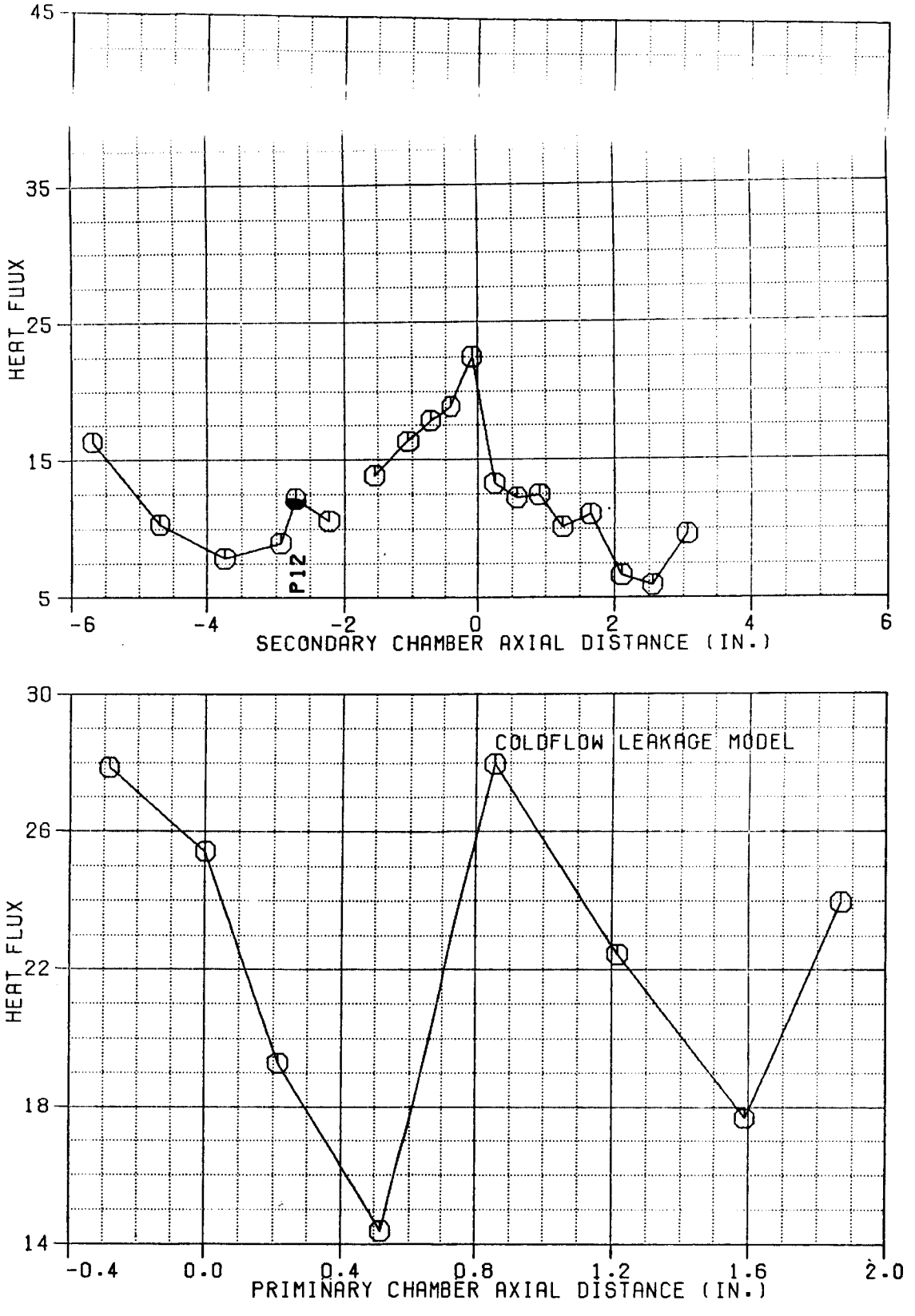

Figure B-16. Test 129 Heat Flux Profiles

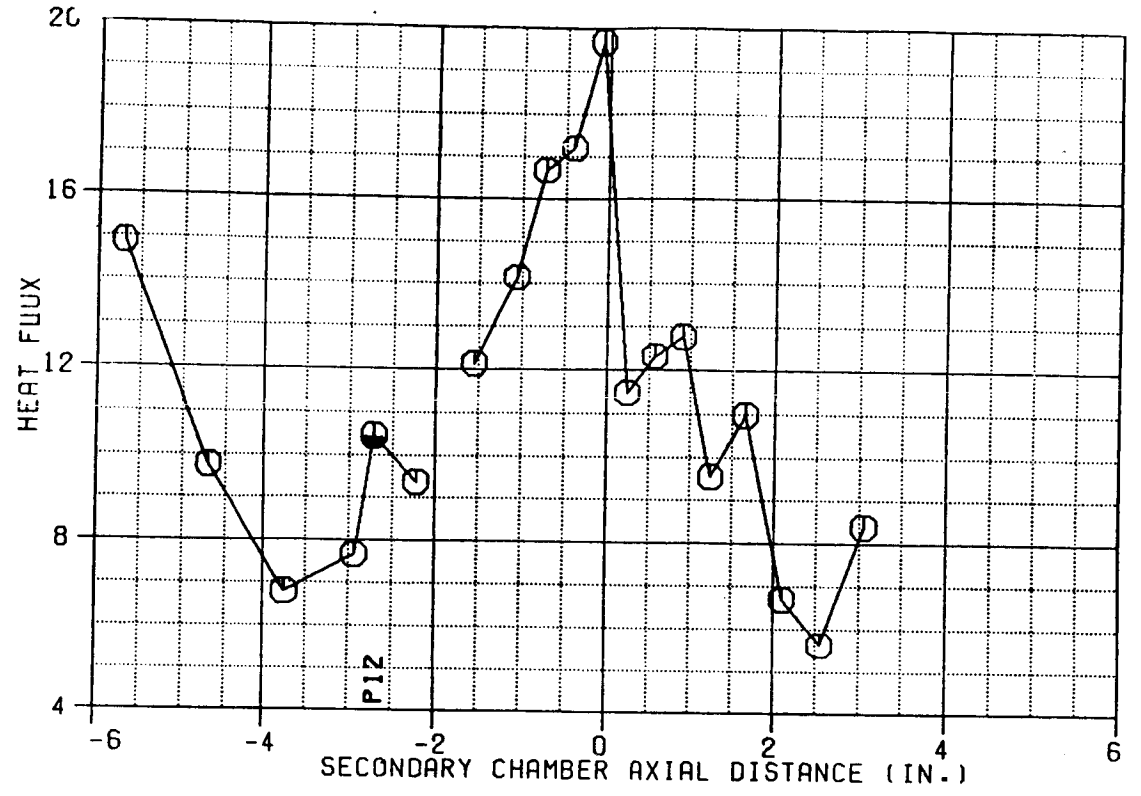

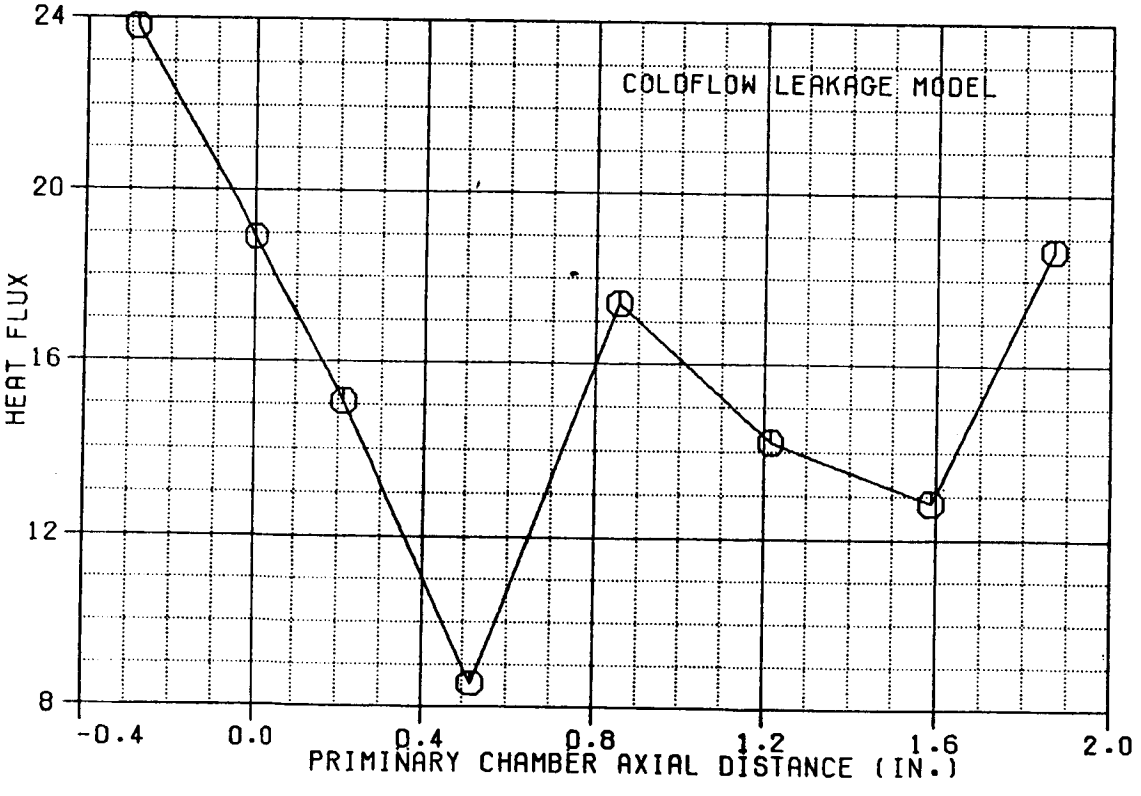

Figure B-17. Test 130 Heat Flux Profiles

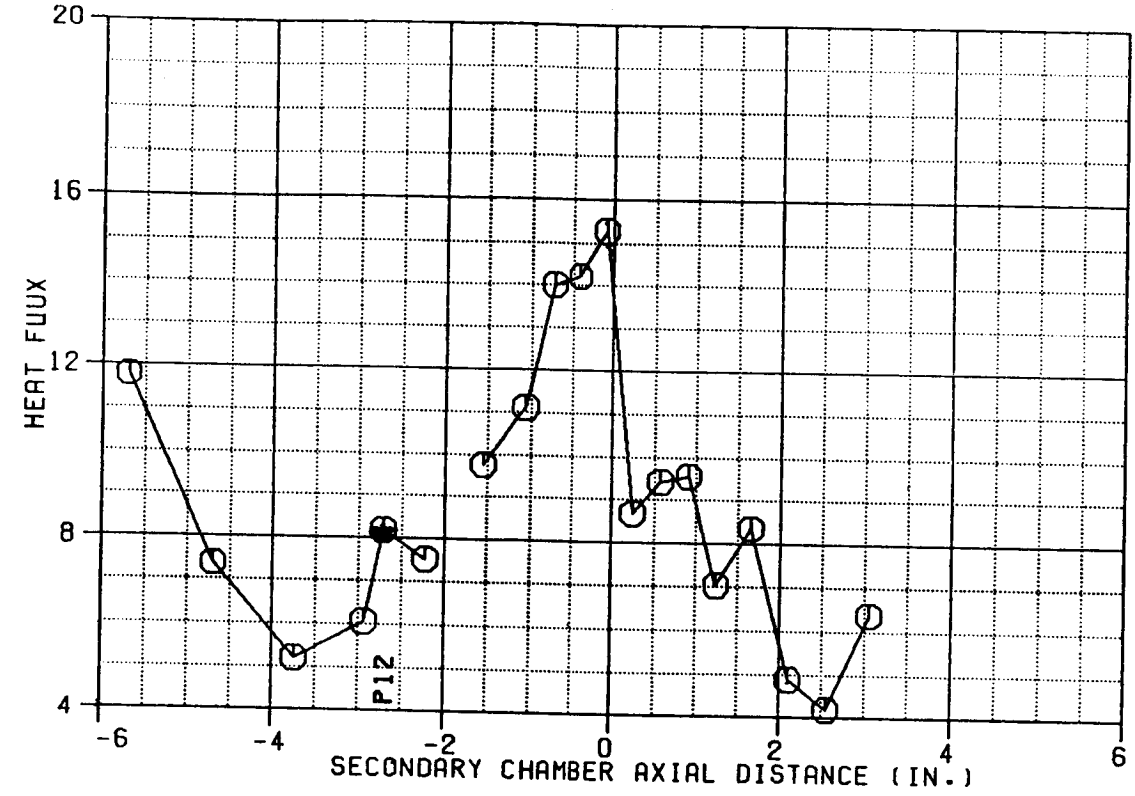

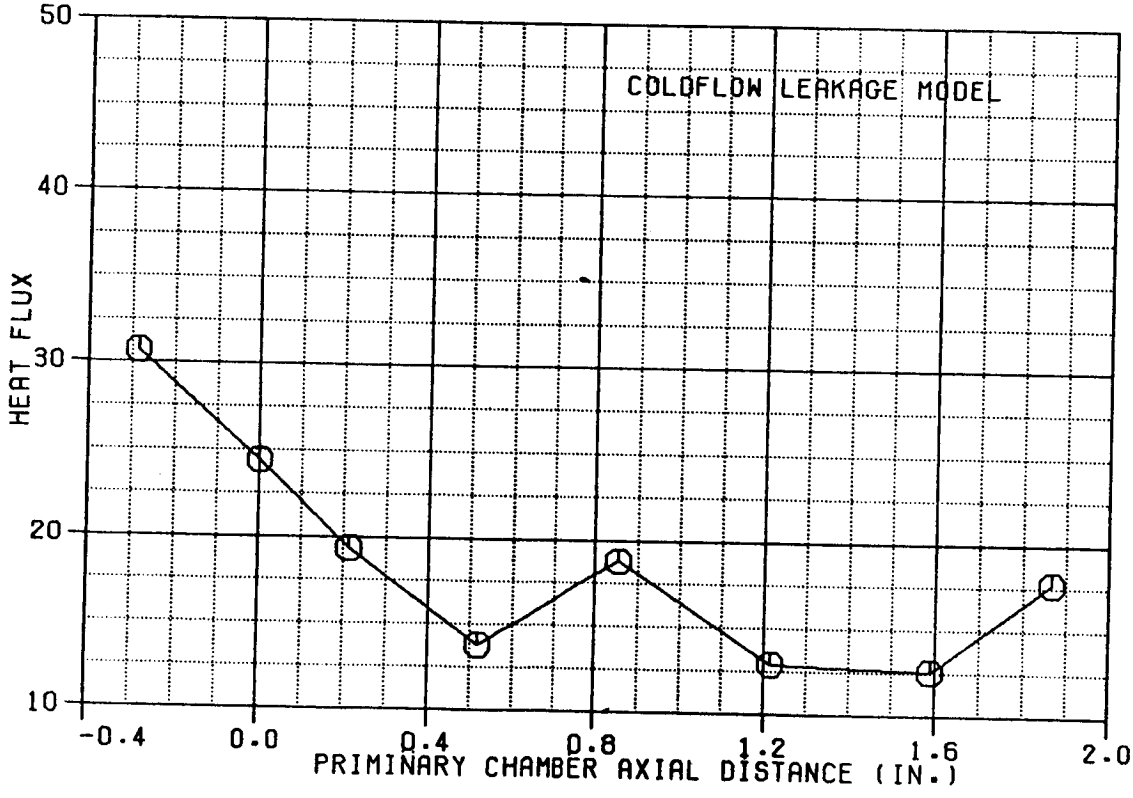

Figure B-18. Test 131 Heat Flux Profiles

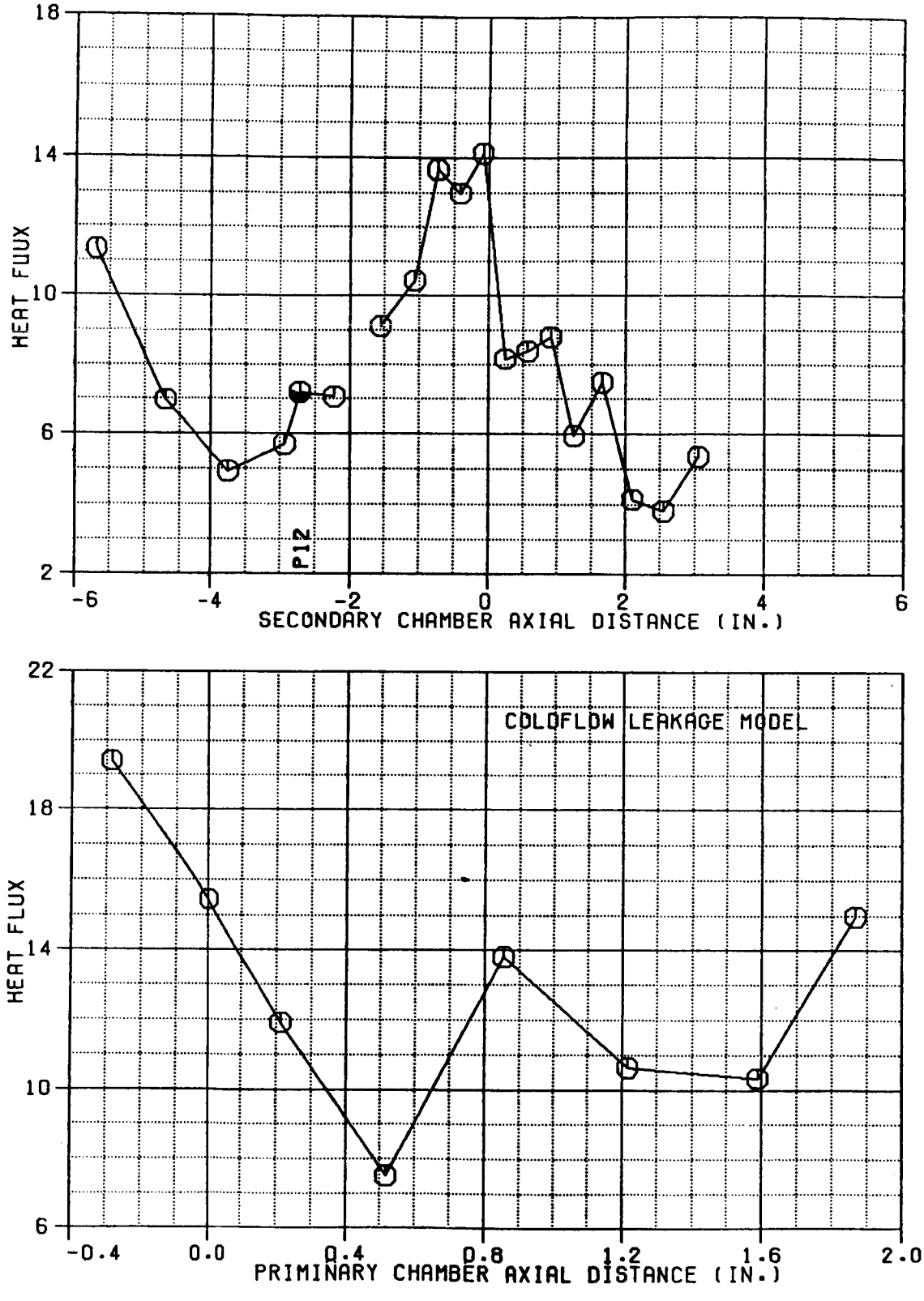

Figure B-19. Test 132 Heat Flux Profiles

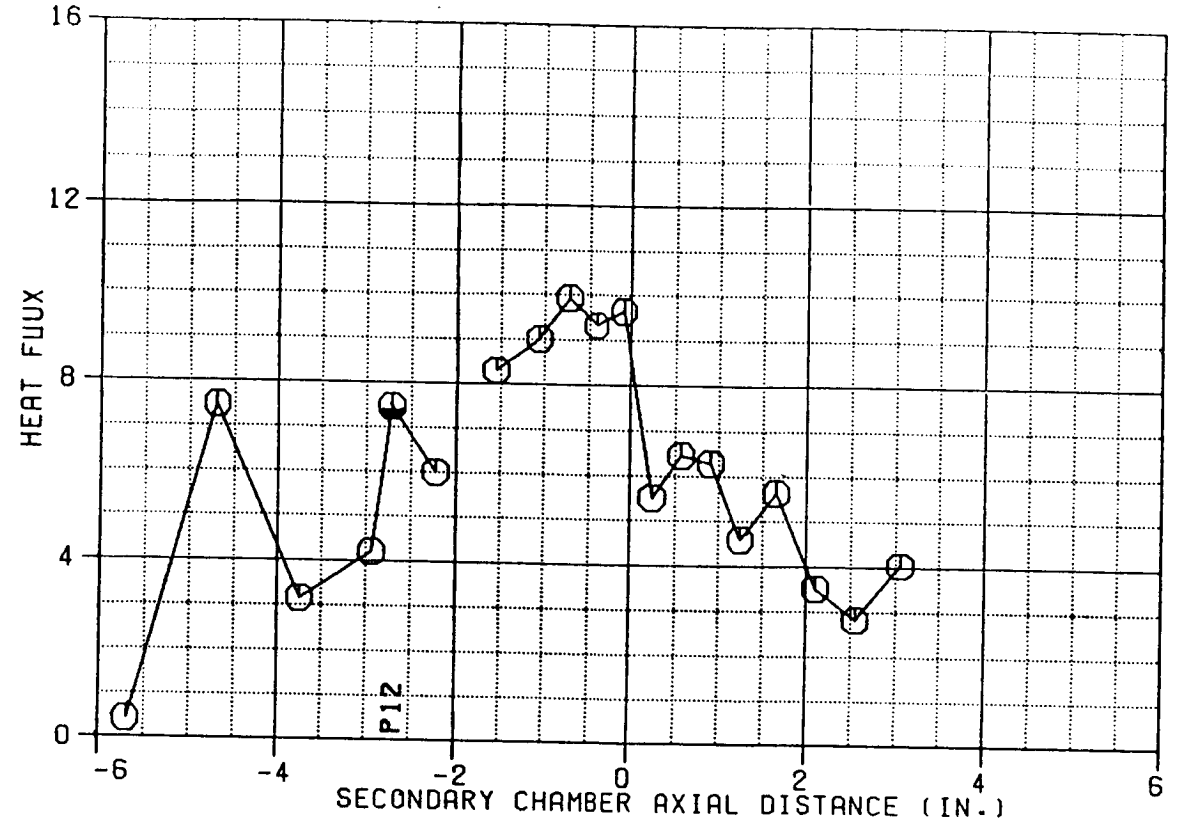

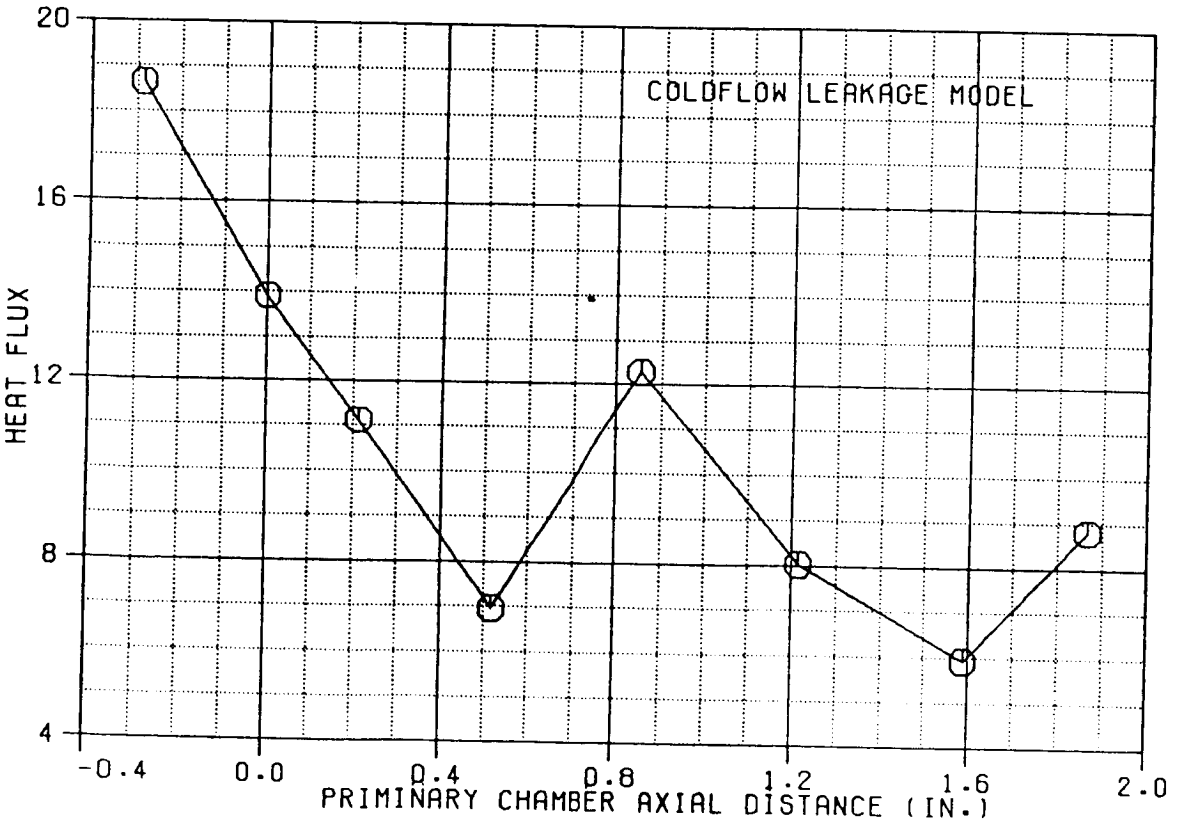

Figure B-20. Test 144 Heat Flux Profiles

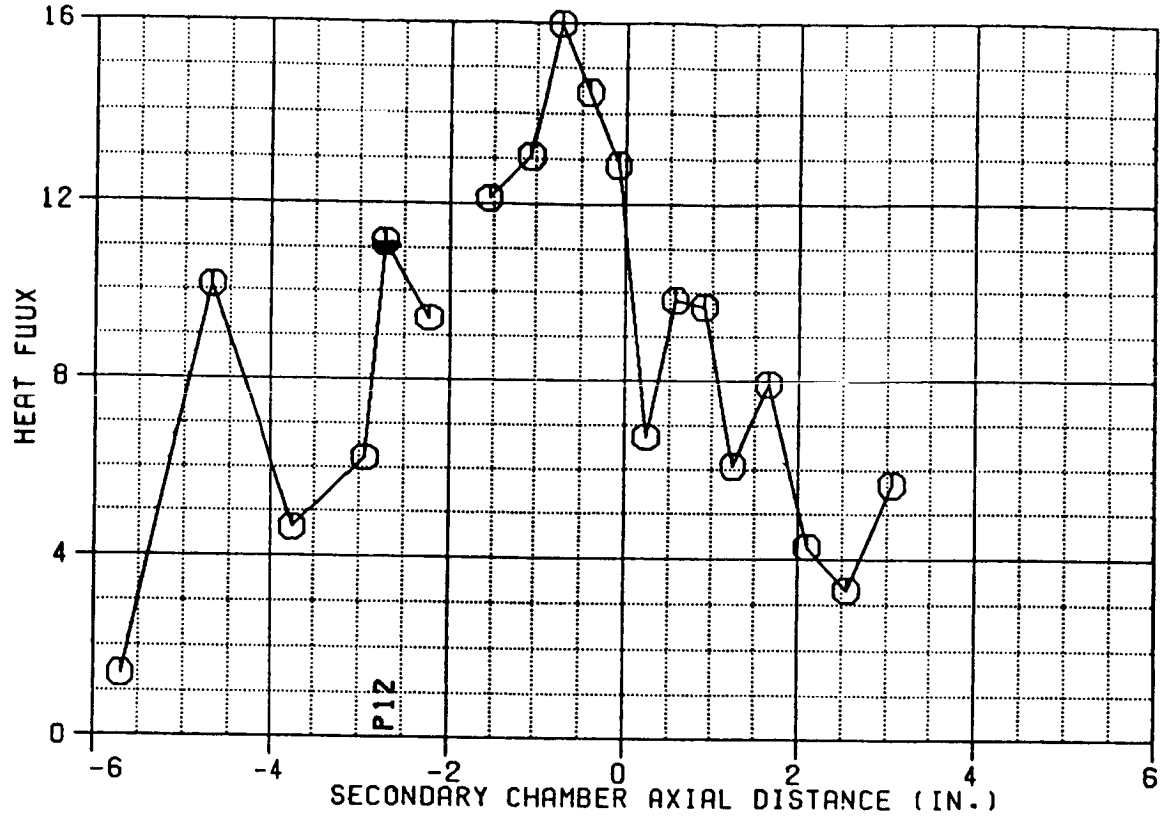

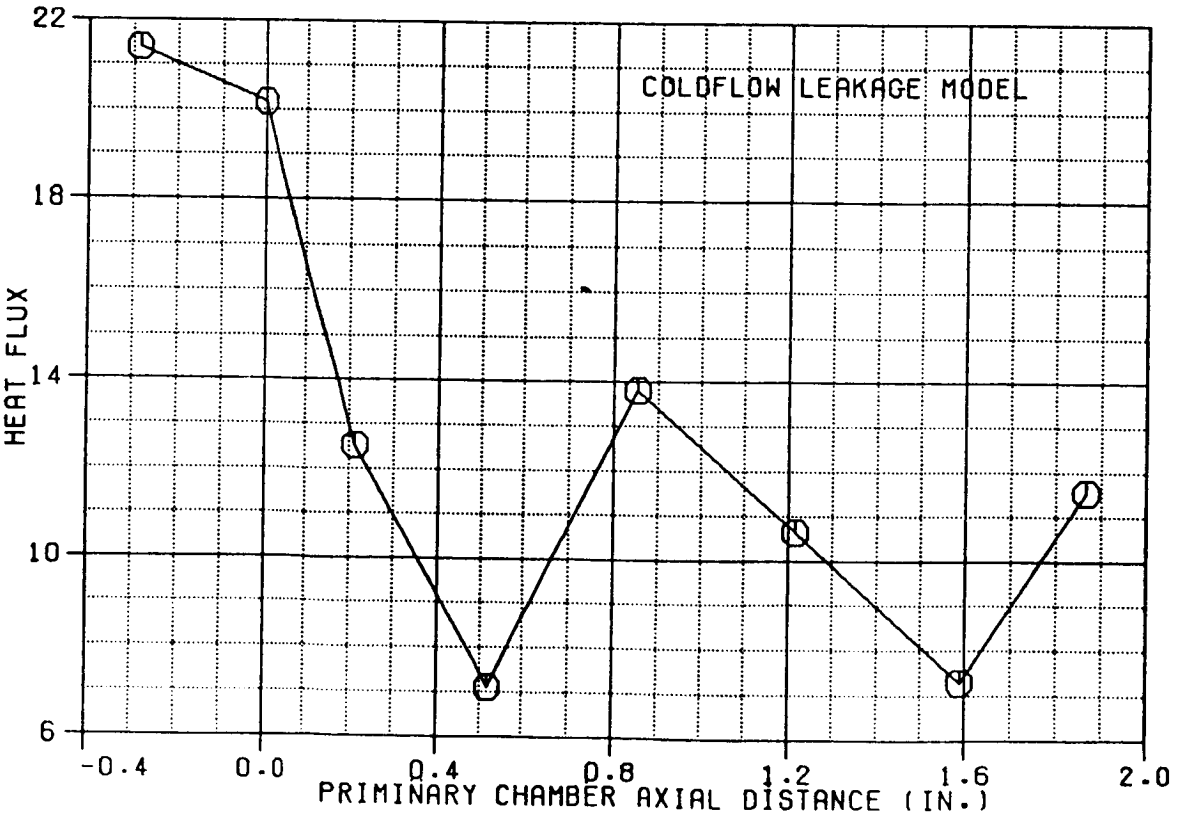

Figure B-21. Test 145 Heat Flux Profiles

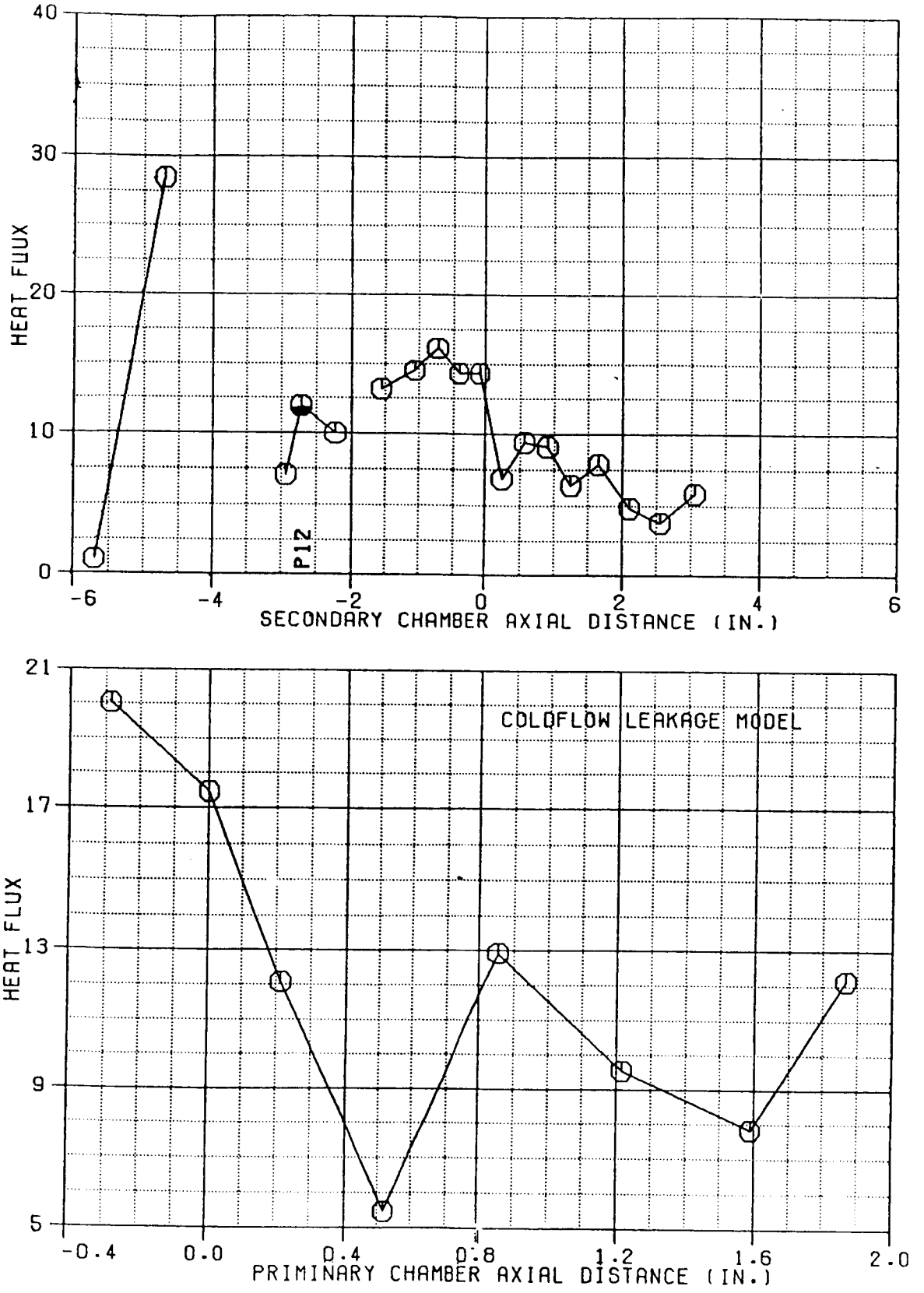

Figure B-22. Test 146 Heat Flux Profiles

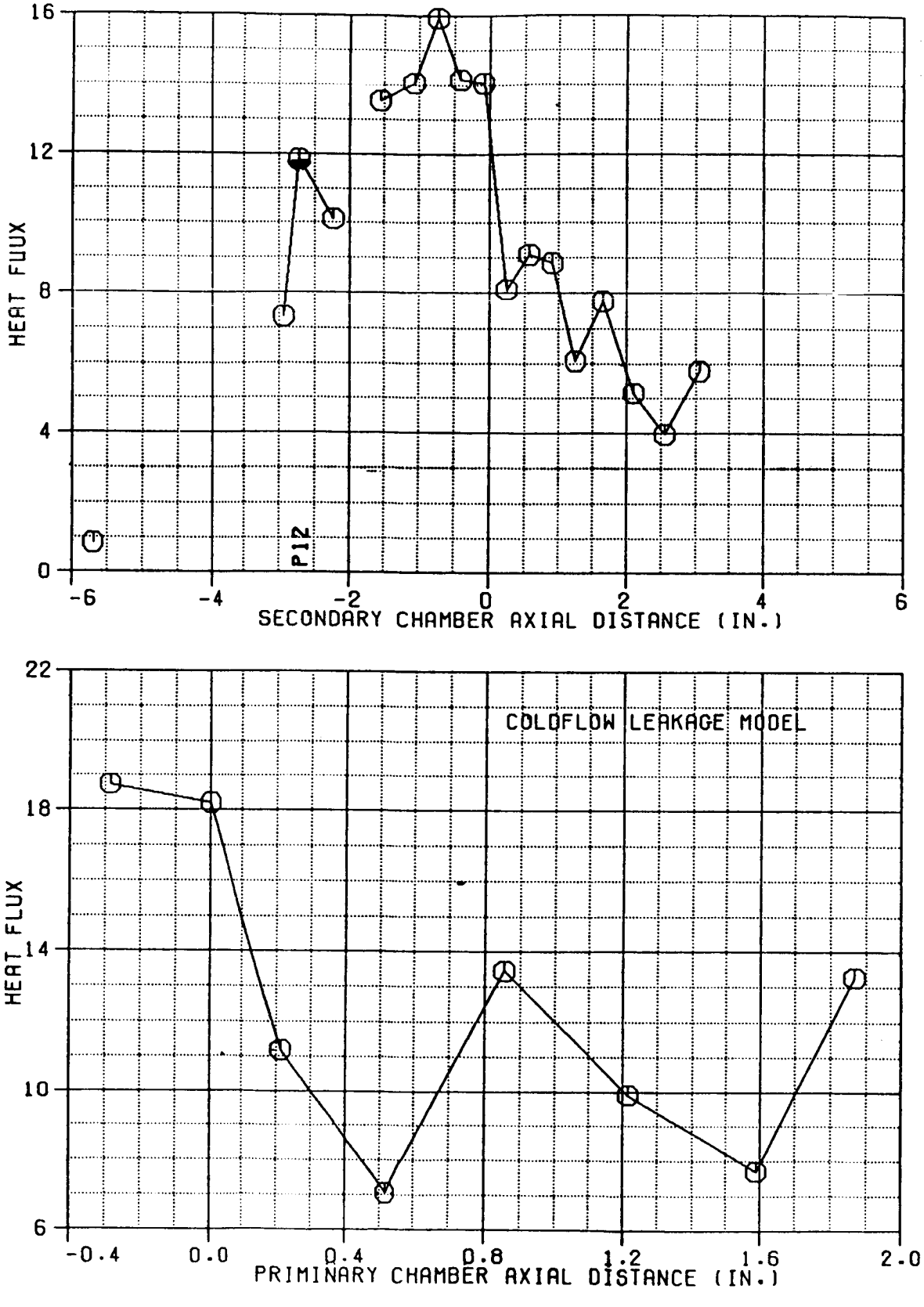

Figure B-23. Test 147 Heat Flux Profiles

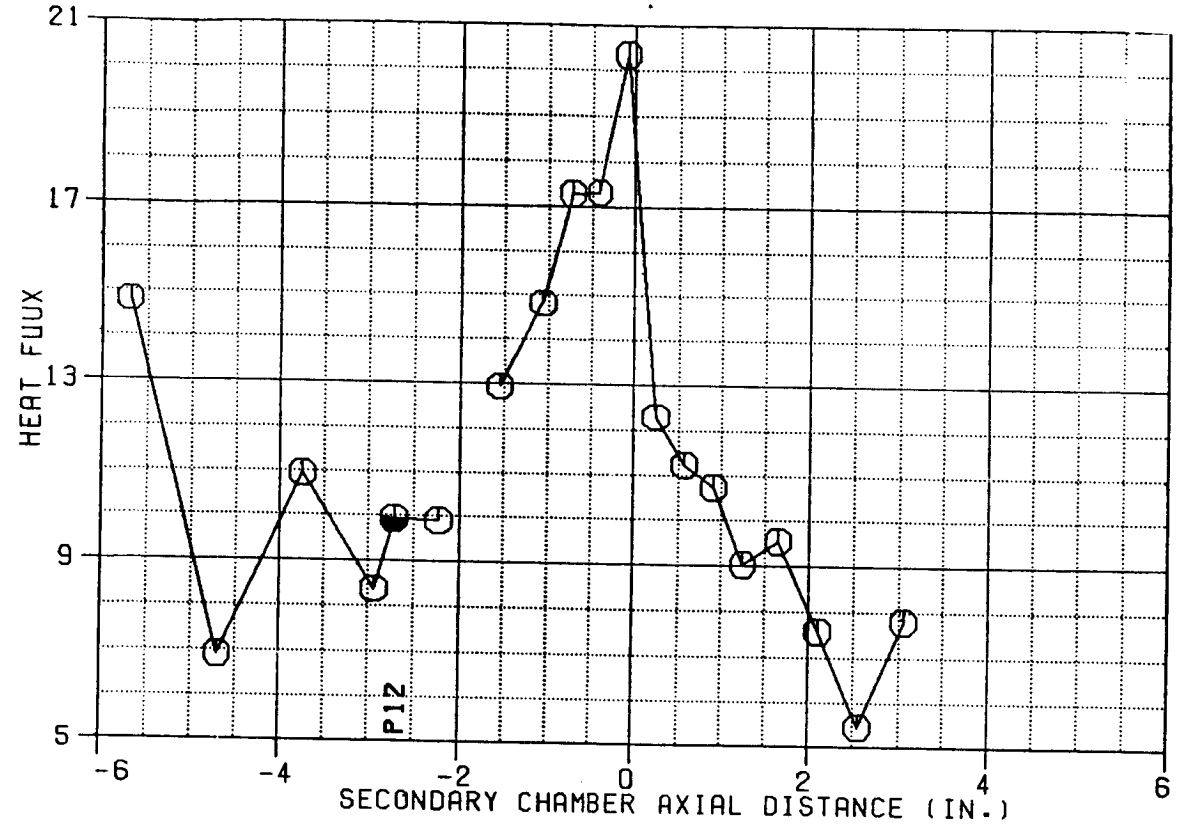

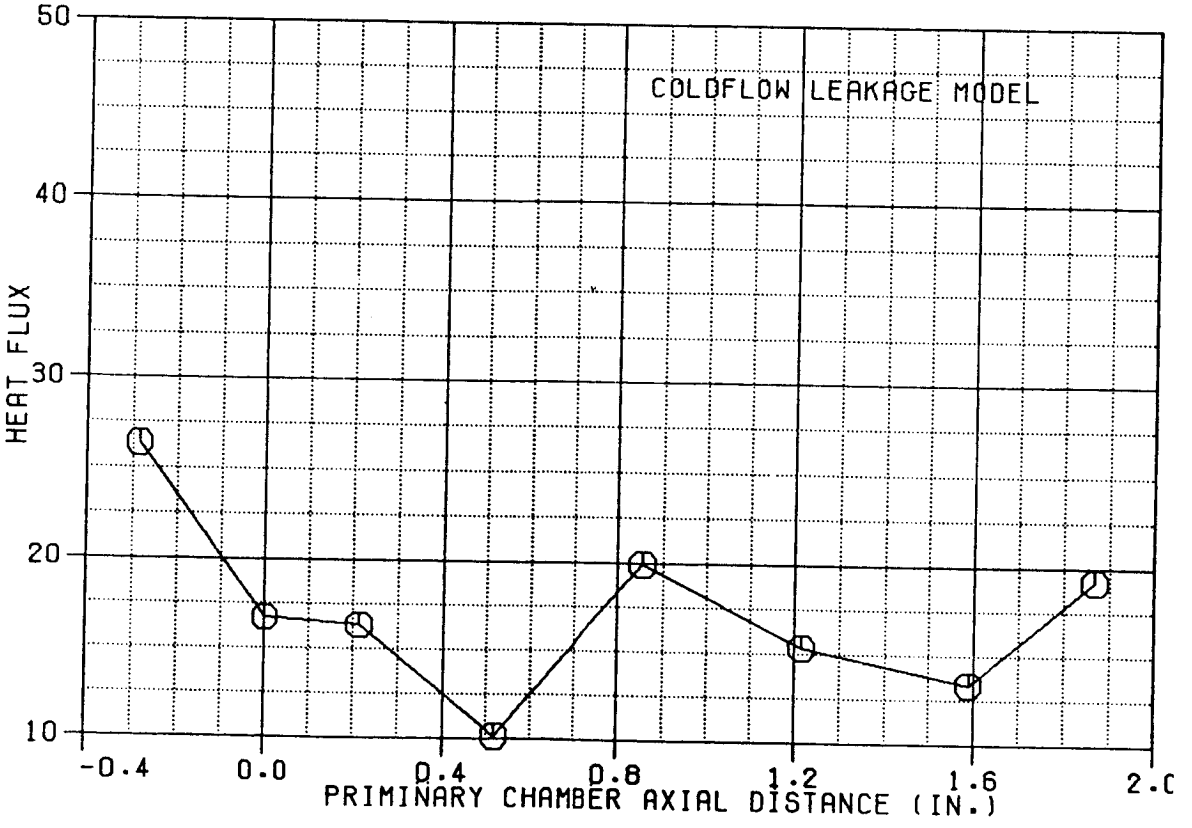

Figure B-24. Test 148 Heat Flux Profiles

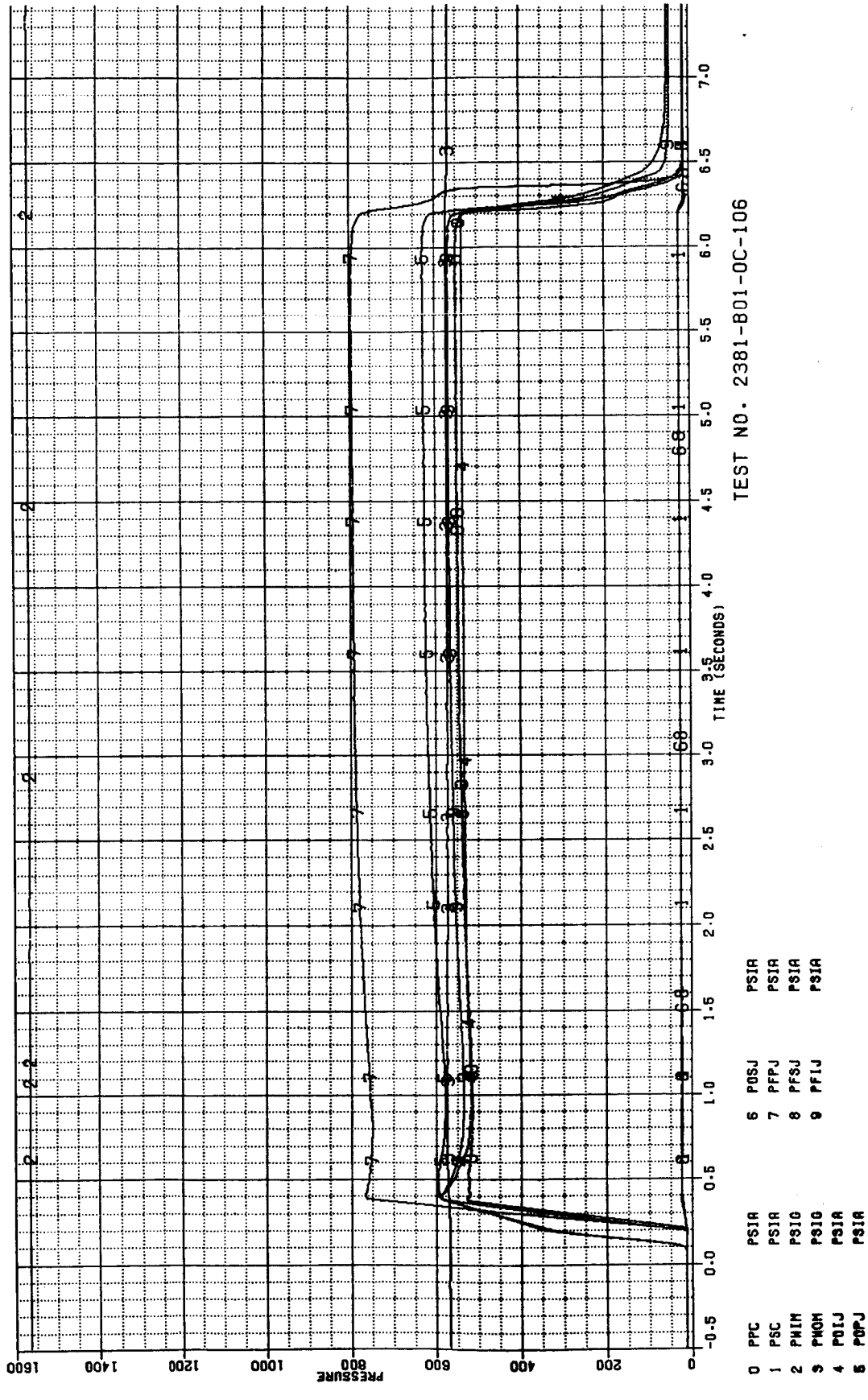

Figure B-25. Test 106 Pressure Data Summary

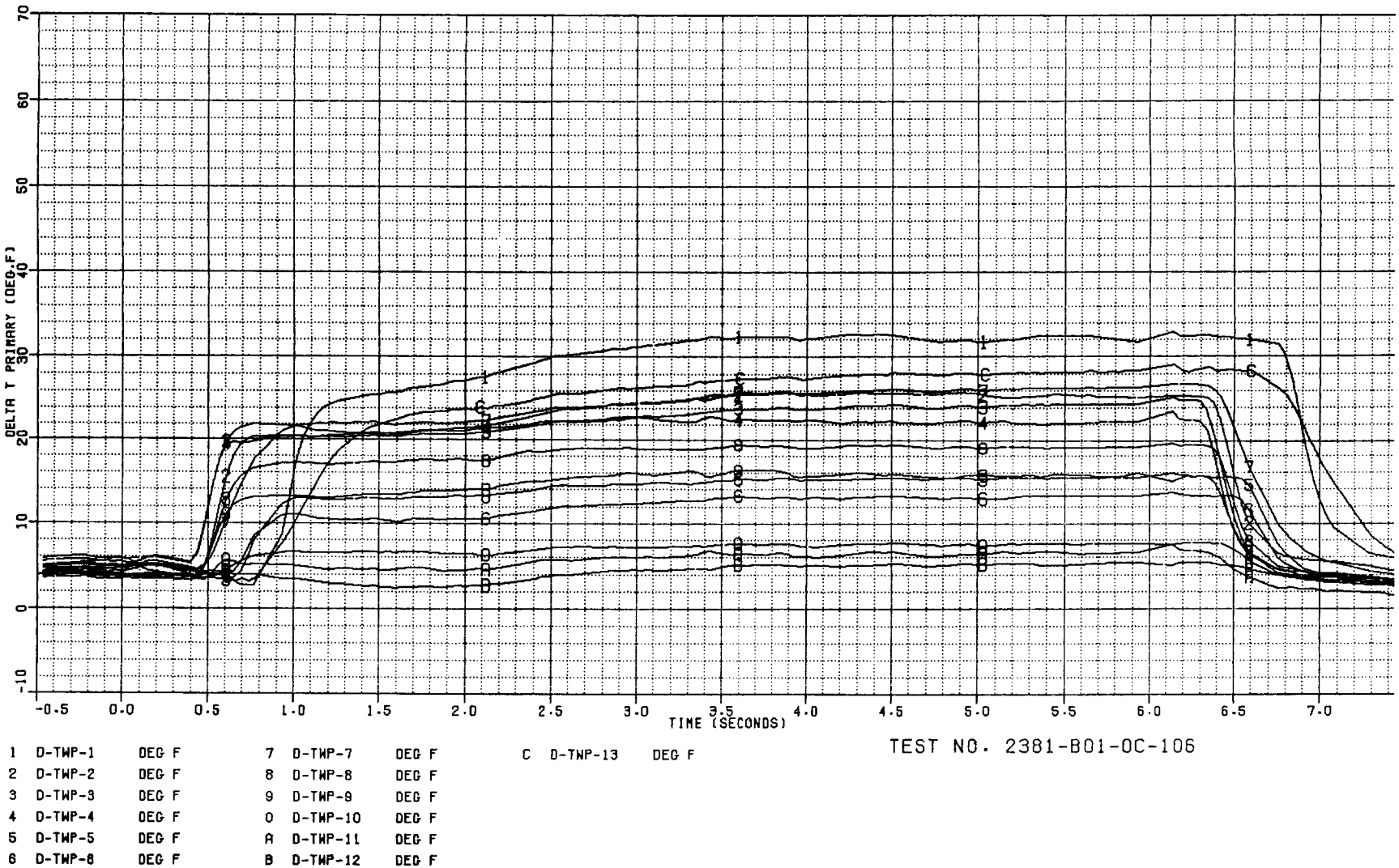

Figure B-26. Test 106 Primary Chamber Temperature Data Summary

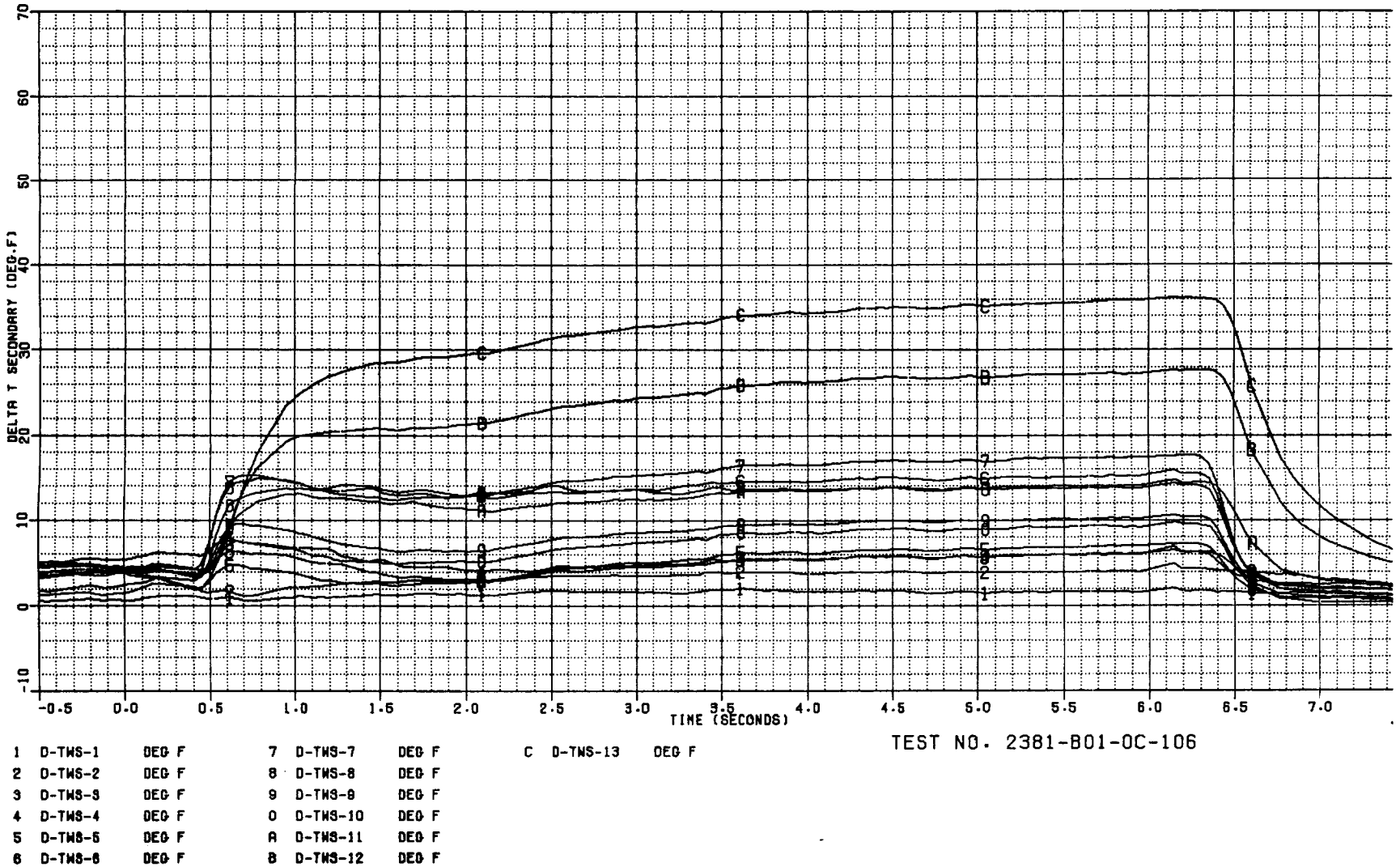

Figure B-27. Test 106 Secondary Chamber Temperature Data Summary

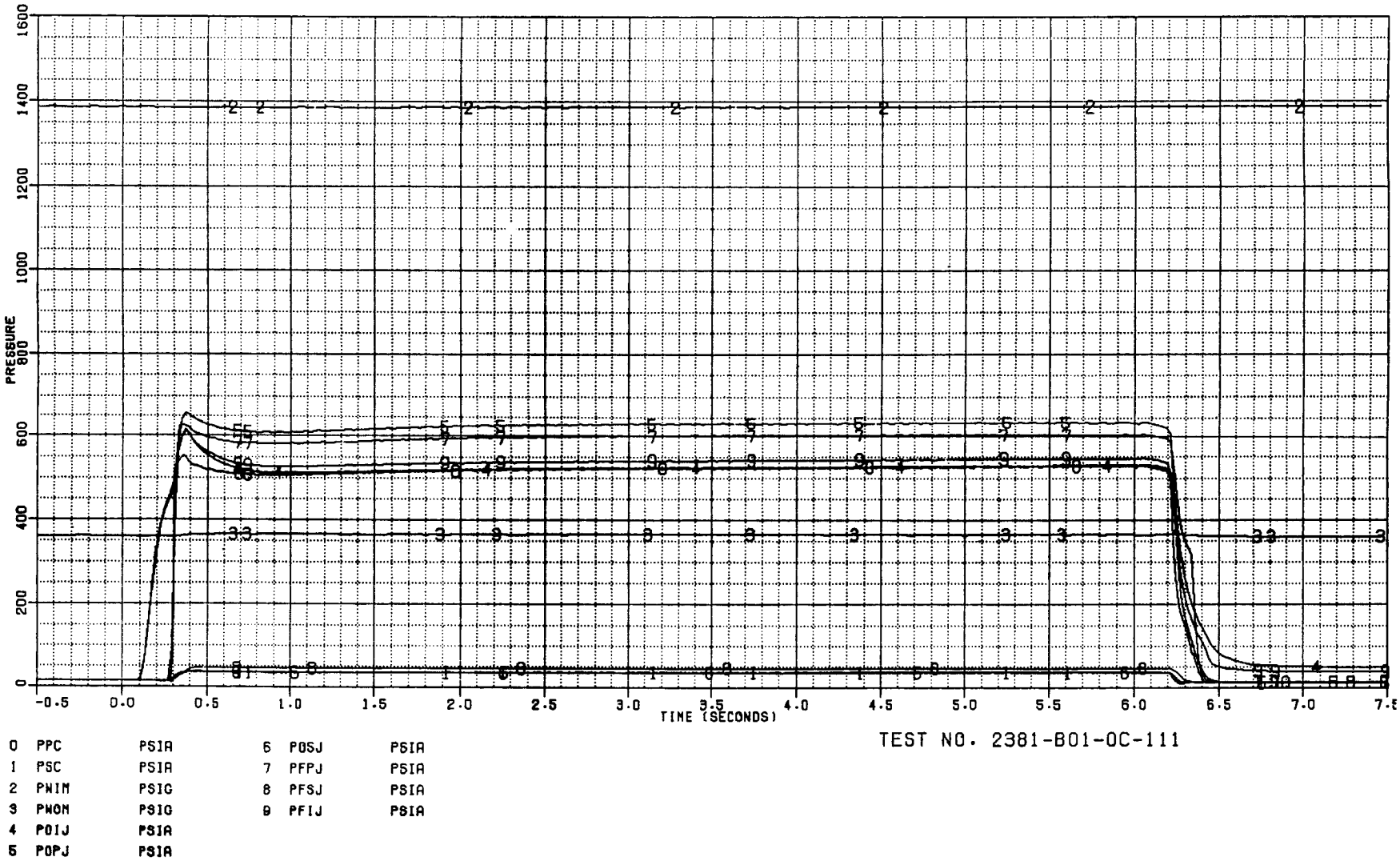

Figure B-28. Test 111 Pressure Data Summary

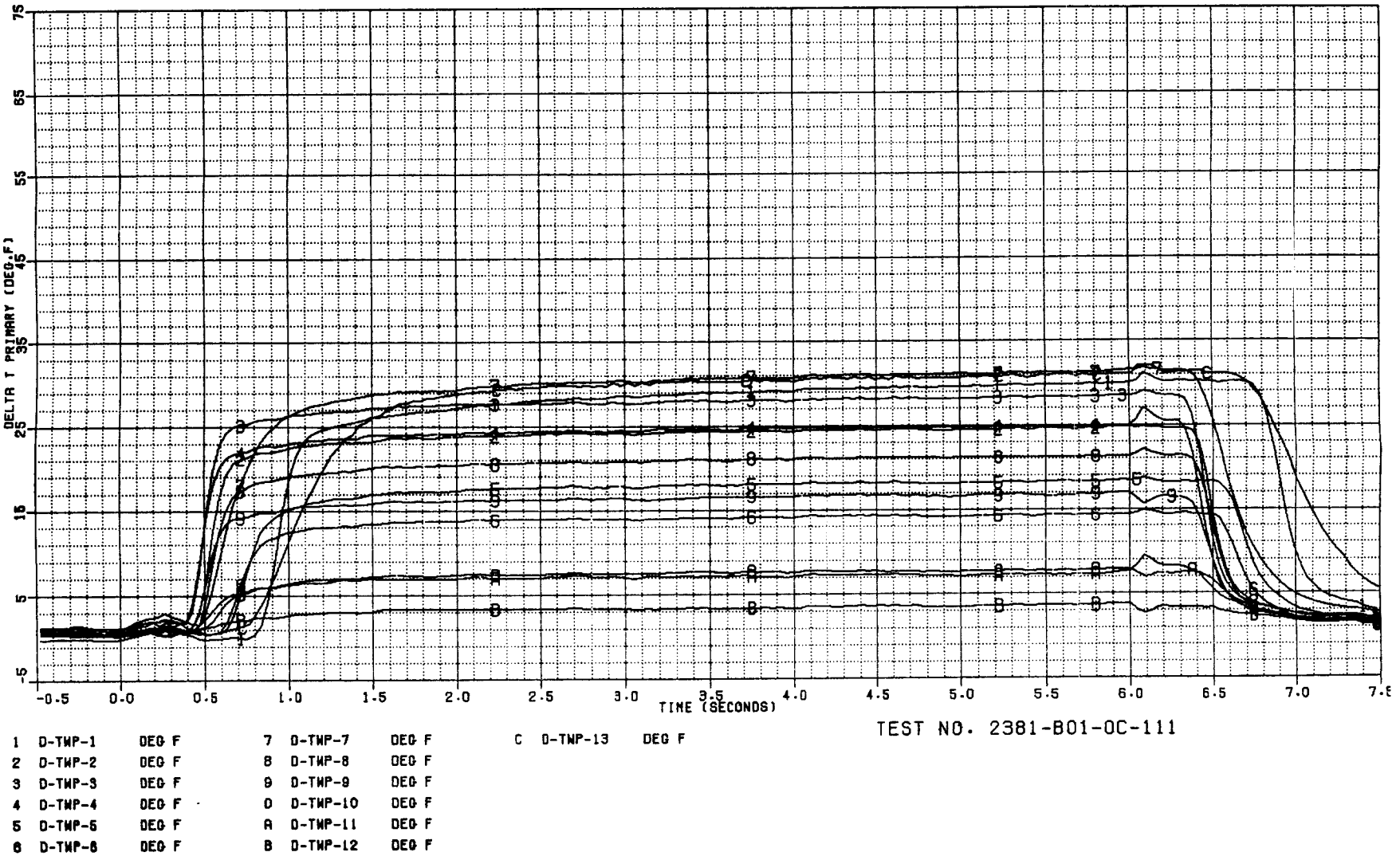

Figure B-29. Test 111 Primary Chamber Temperature Data Summary

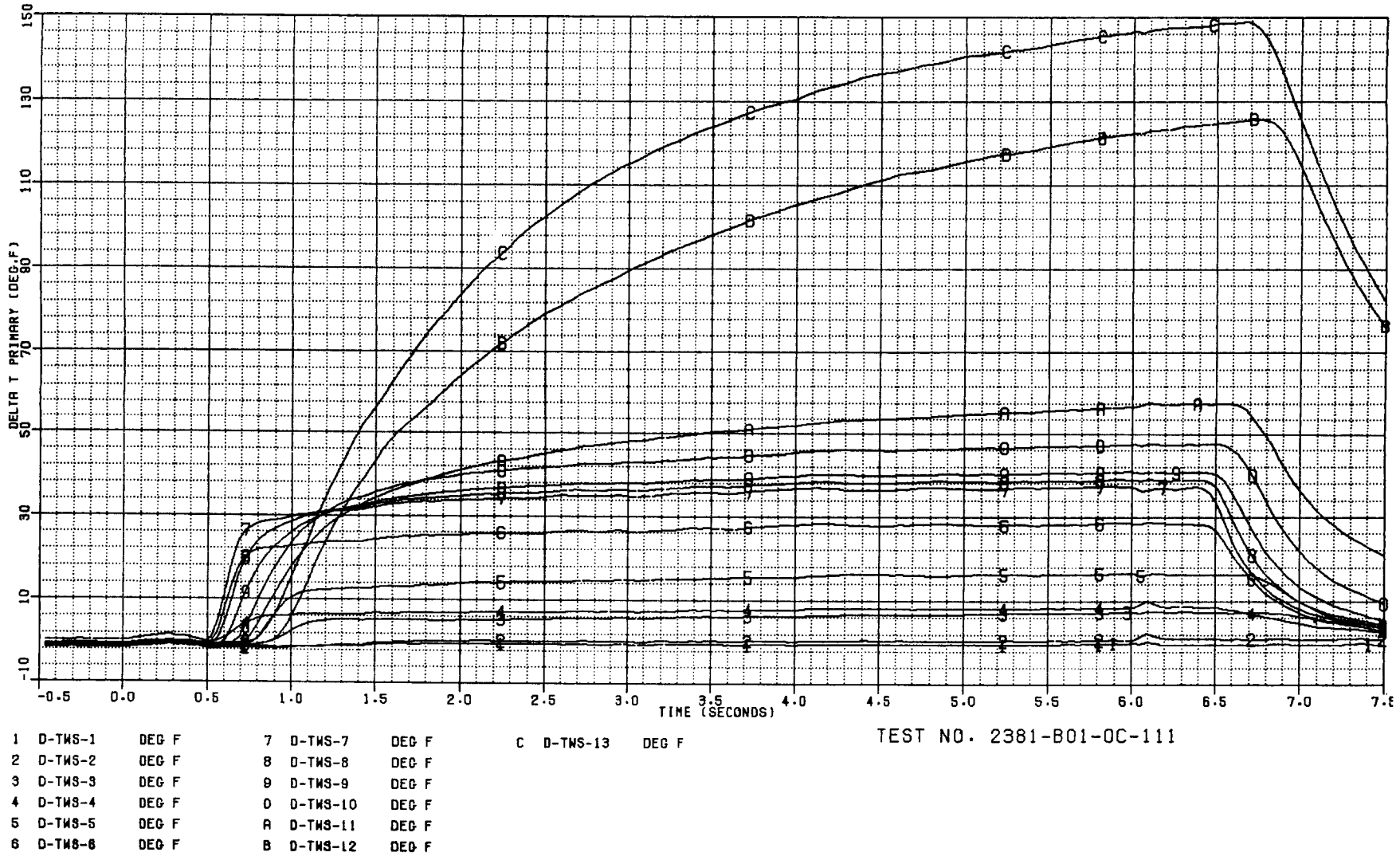

Figure B-30. Test 111 Secondary Chamber Temperature Data Summary

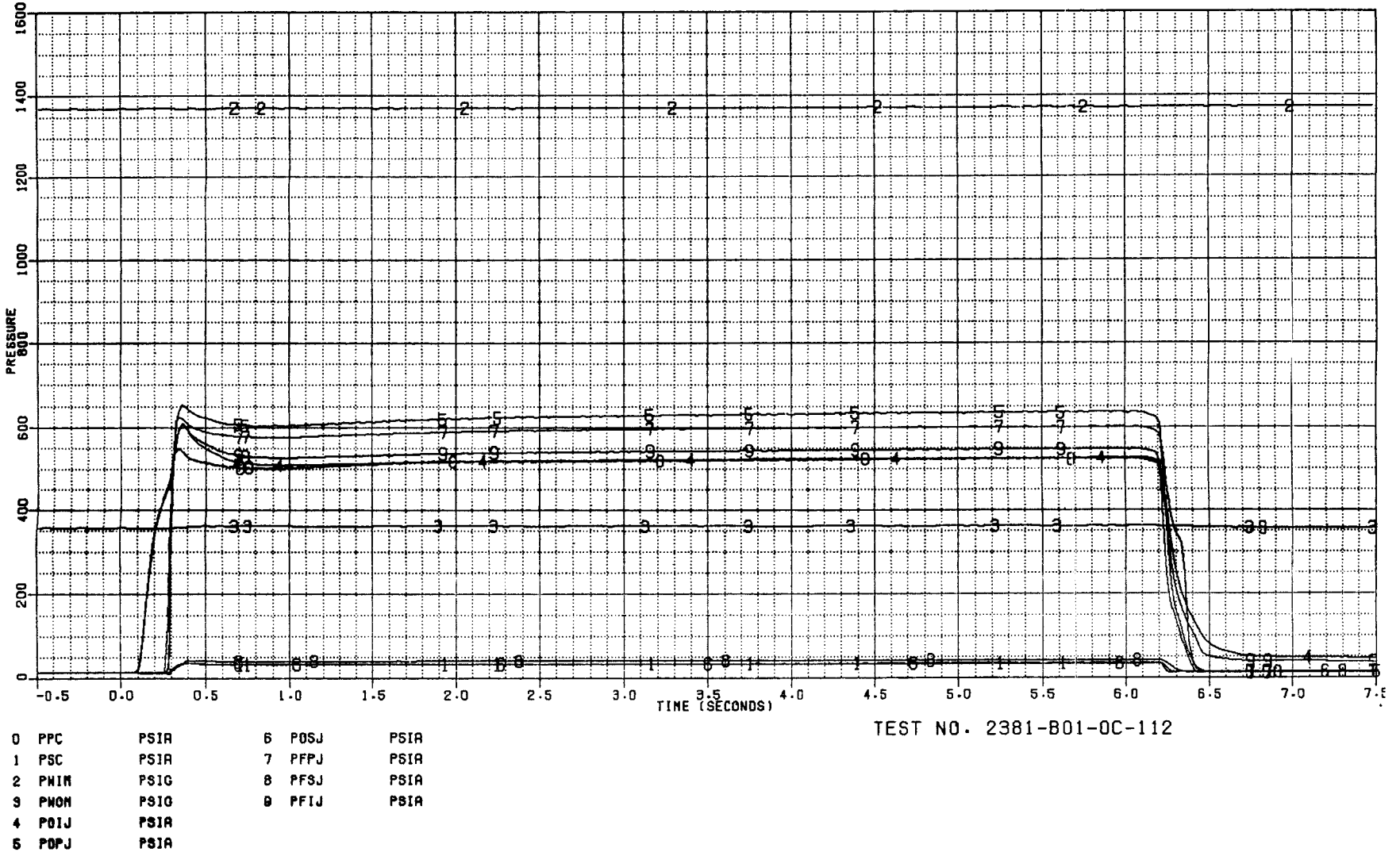

Figure B-31. Test 112 Primary Pressure Data Summary

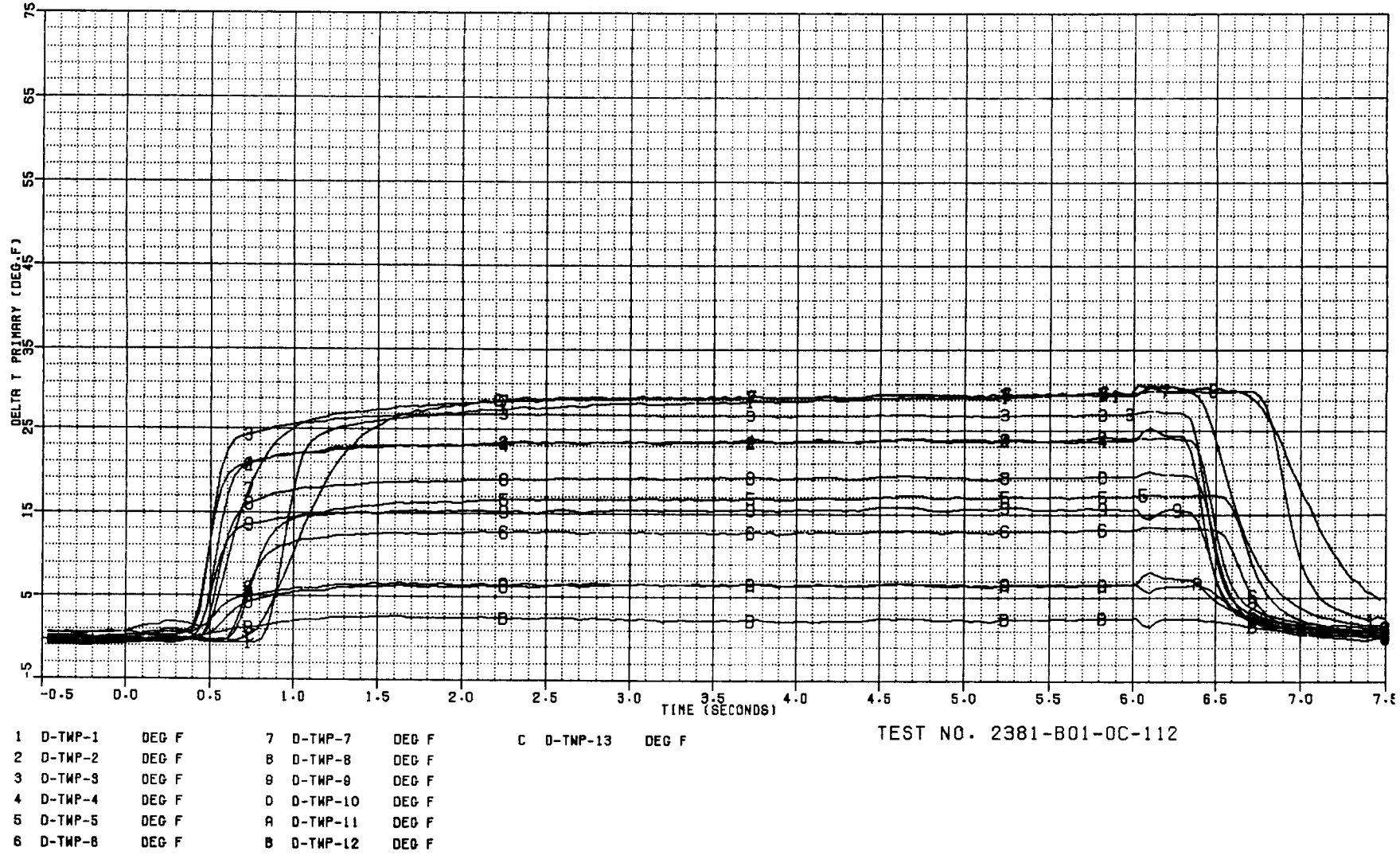

Figure B-32. Test 112 Primary Chamber Temperature Data Summary

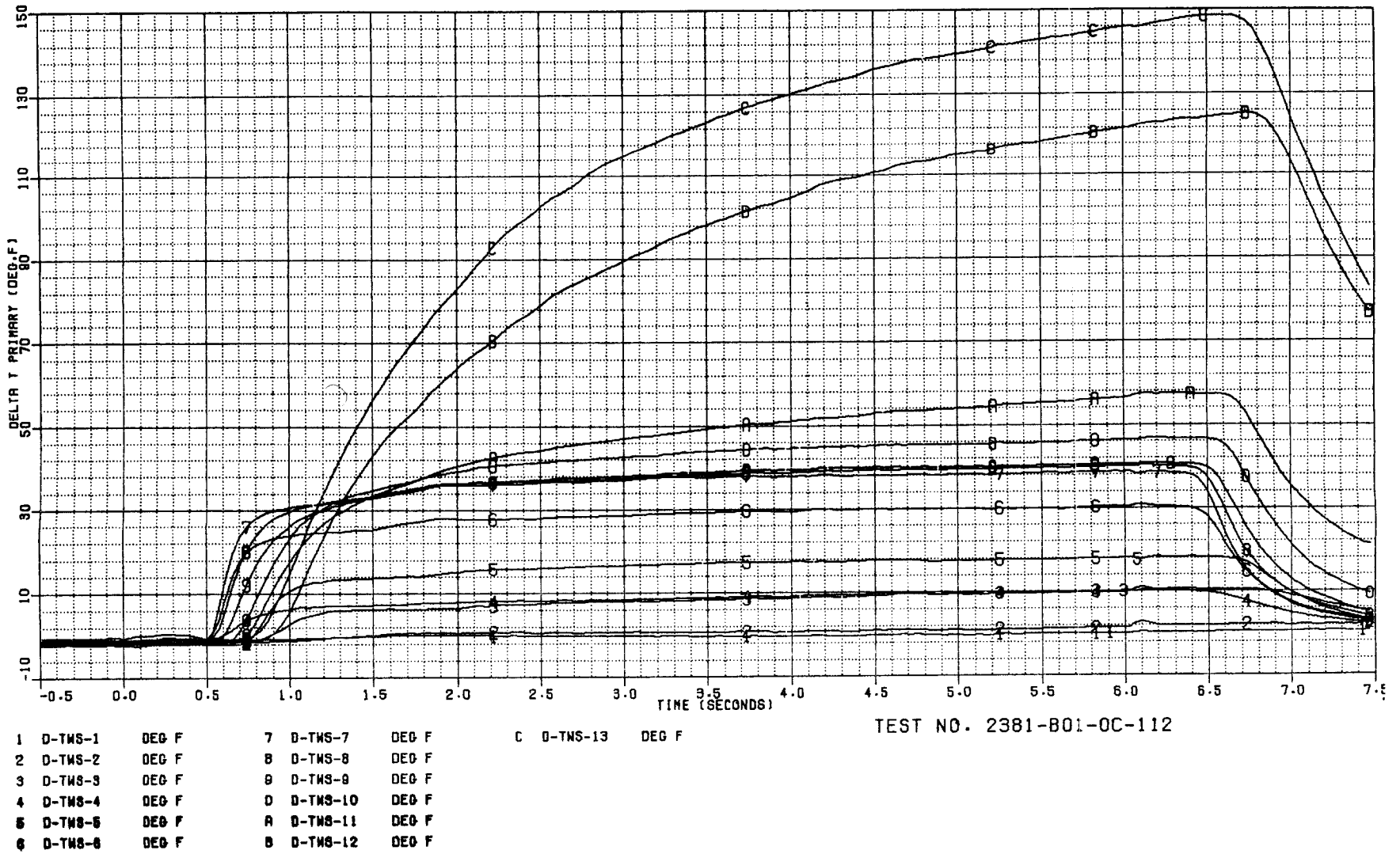

Figure B-33. Test 112 Secondary Chamber Temperature Data Summary

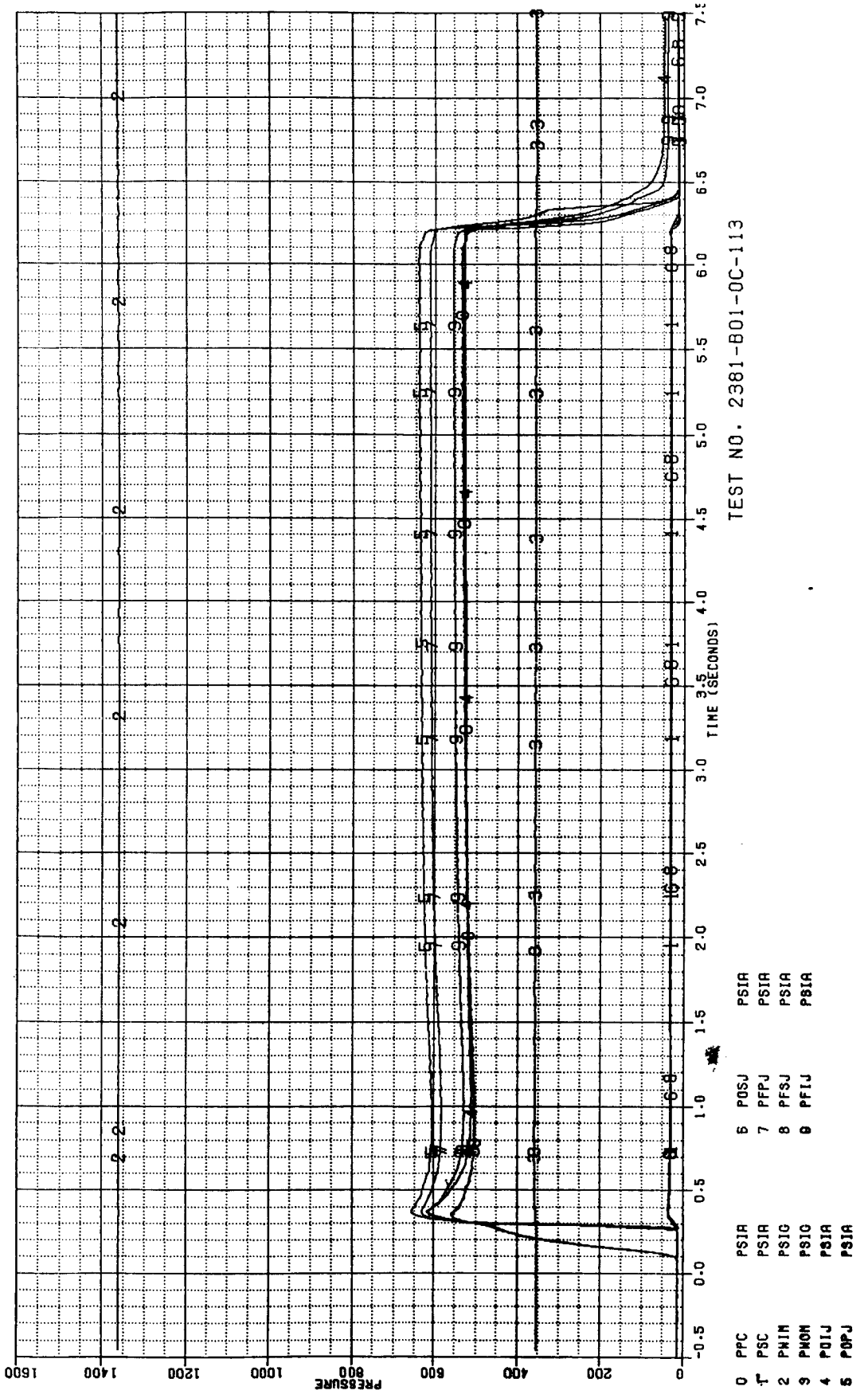

Figure B-34. Test 113 Pressure Data Summary

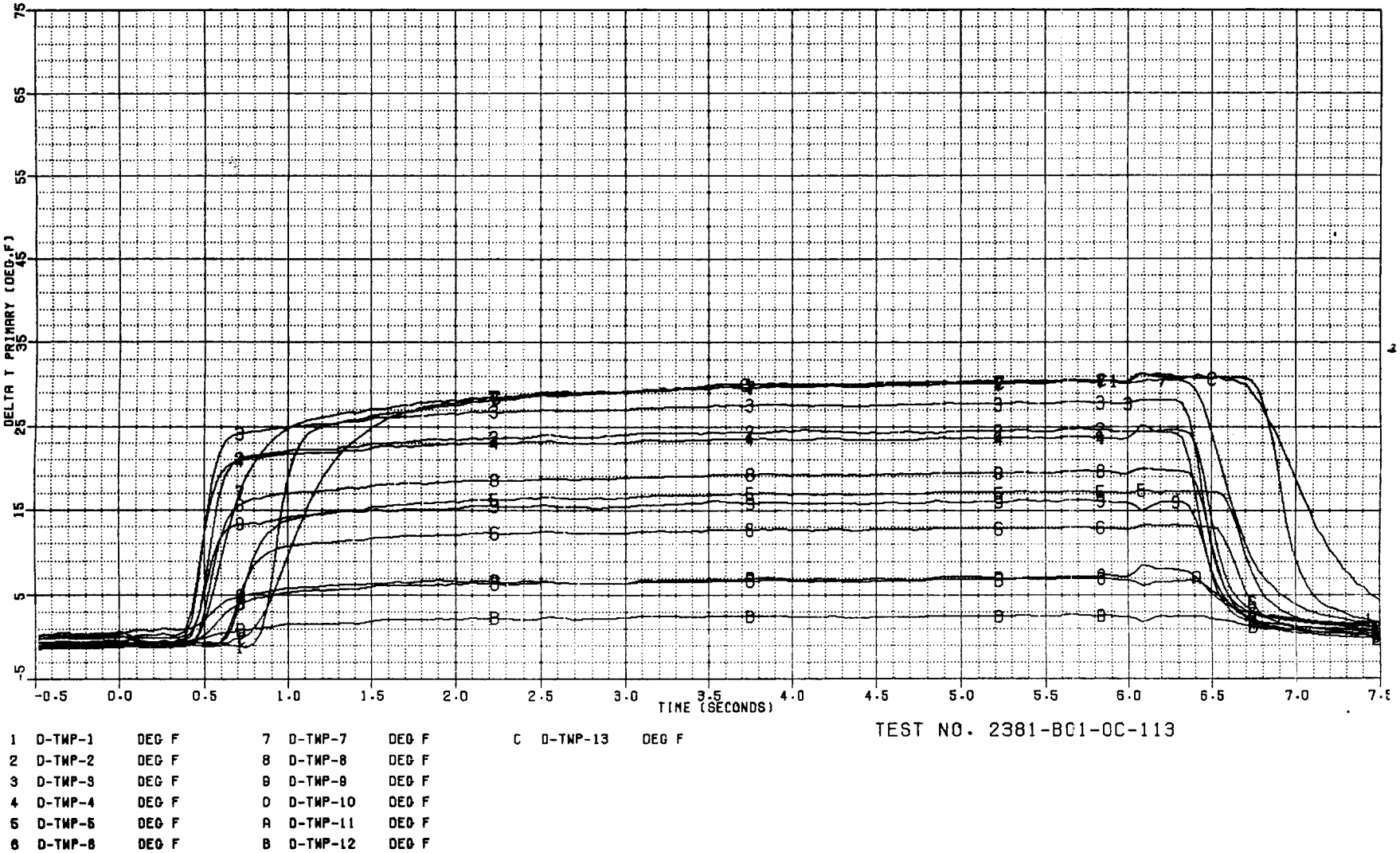

Figure B-35. Test 113 Primary Chamber Temperature Data Summary

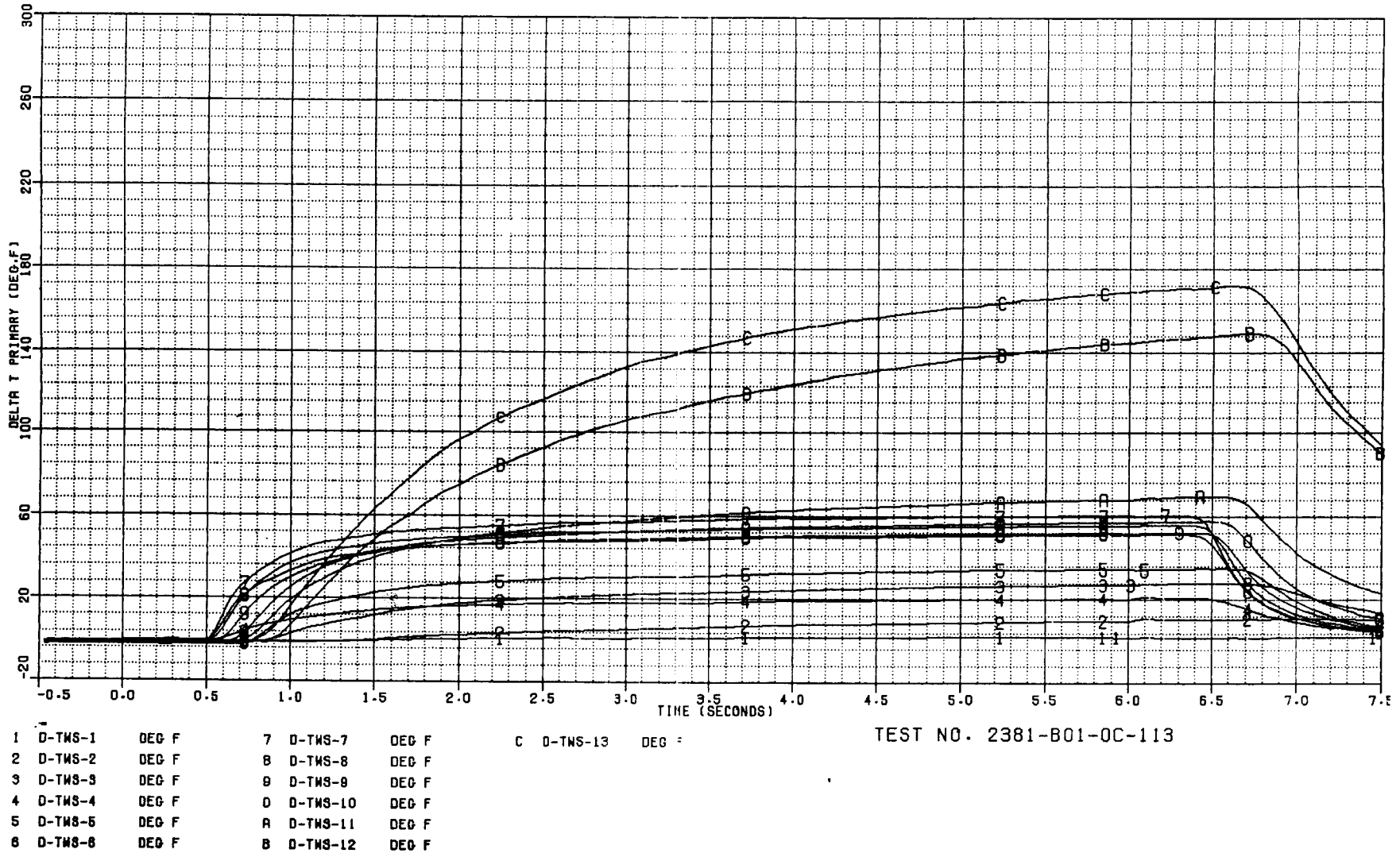

Figure B-36. Test 113 Secondary Chamber Temperature Data Summary

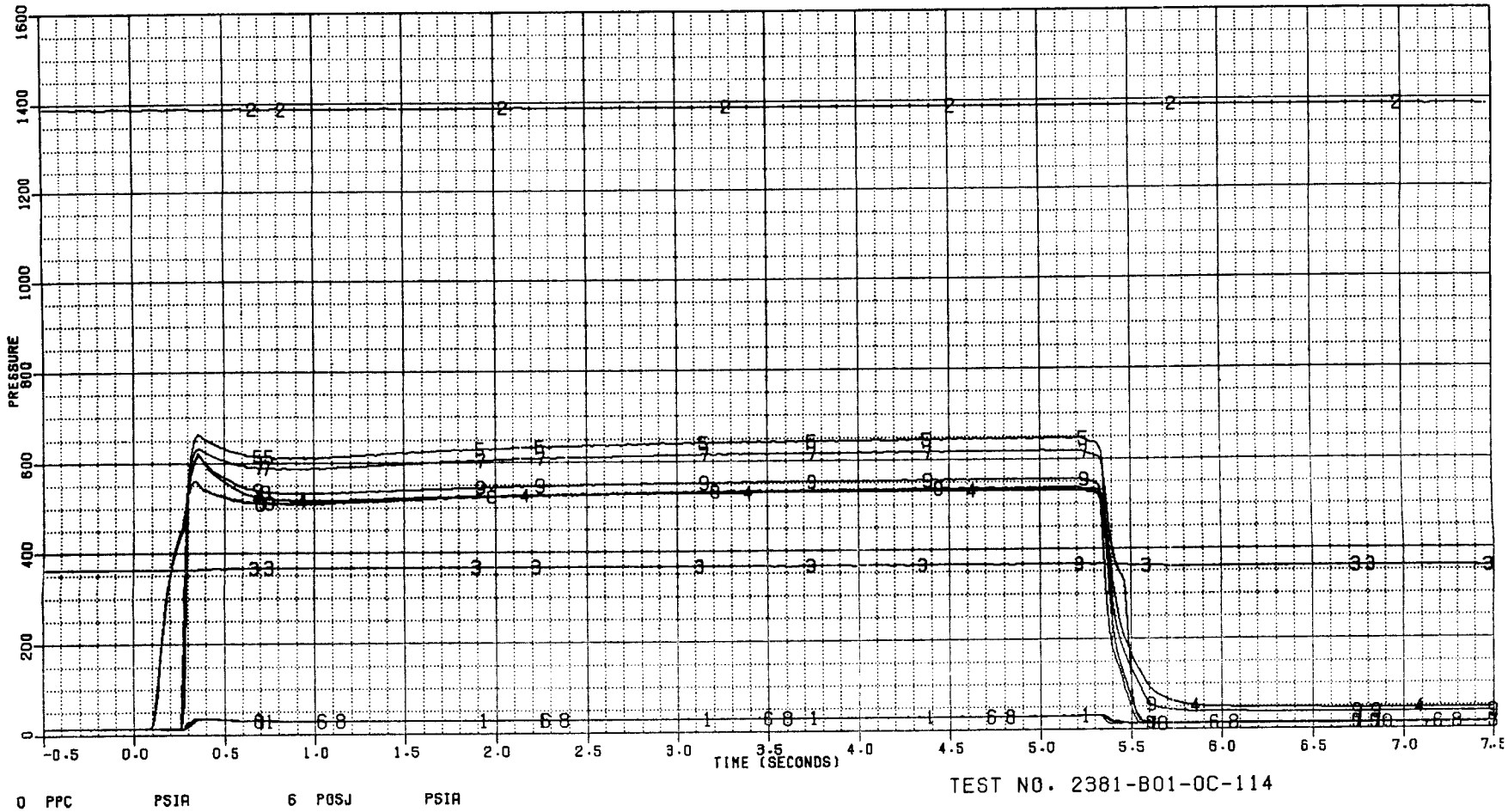

Figure B-37. Test 114 Pressure Data Summary

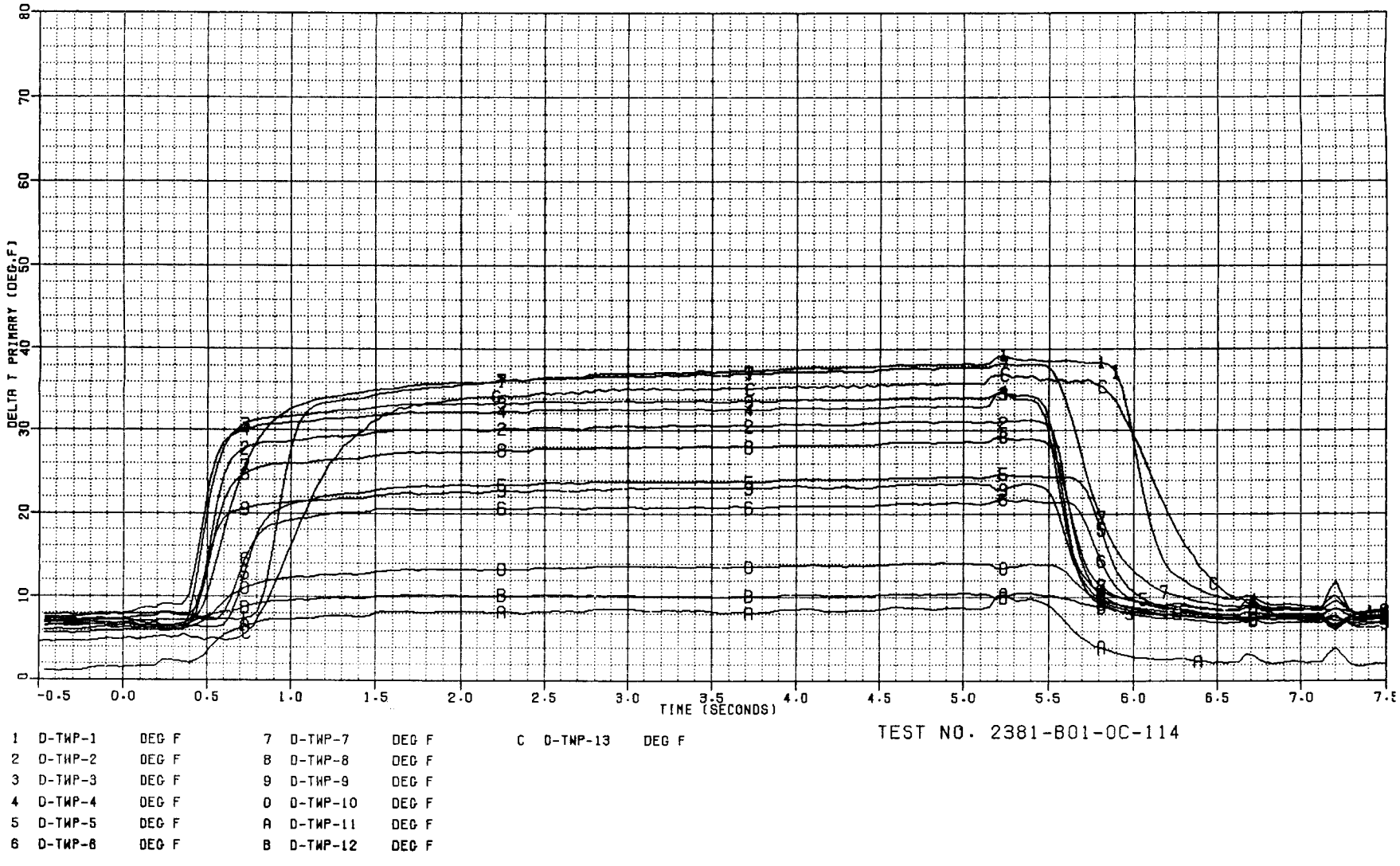

Figure B-38. Test 114 Primary Chamber Temperature Data Summary

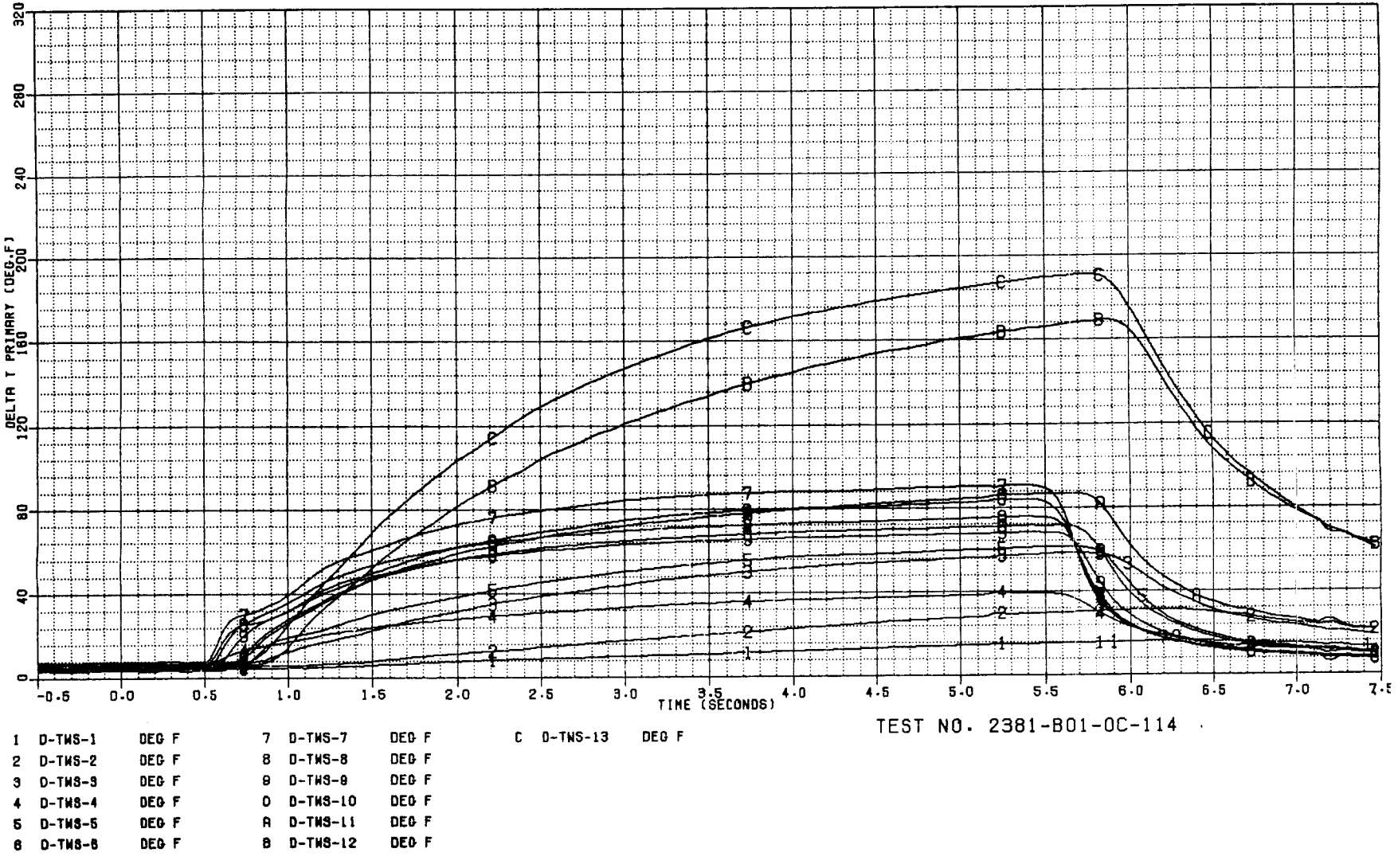

Figure B-39. Test 114 Secondary Chamber Temperature Data Summary

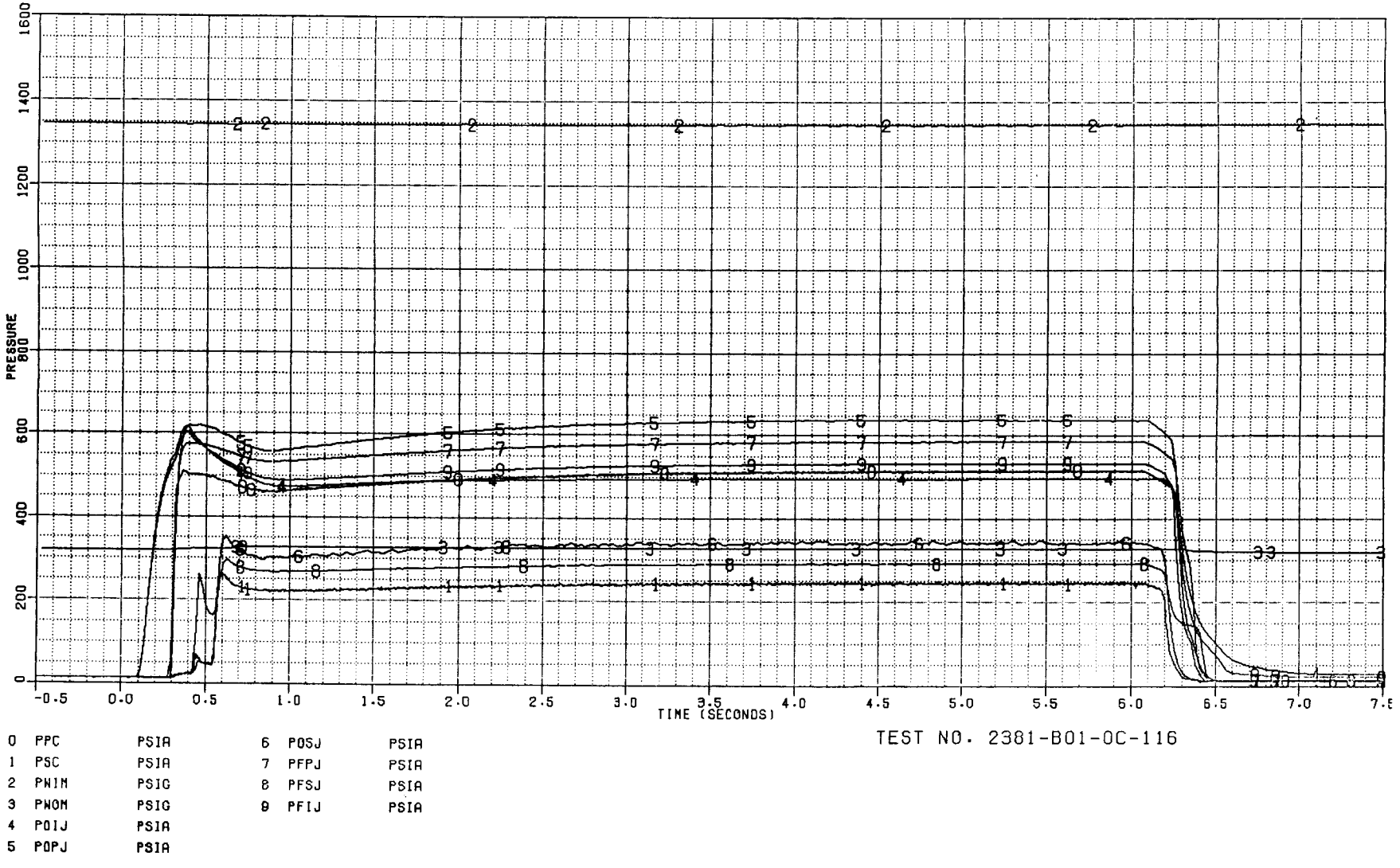

Figure B-40. Test 116 Pressure Data Summary

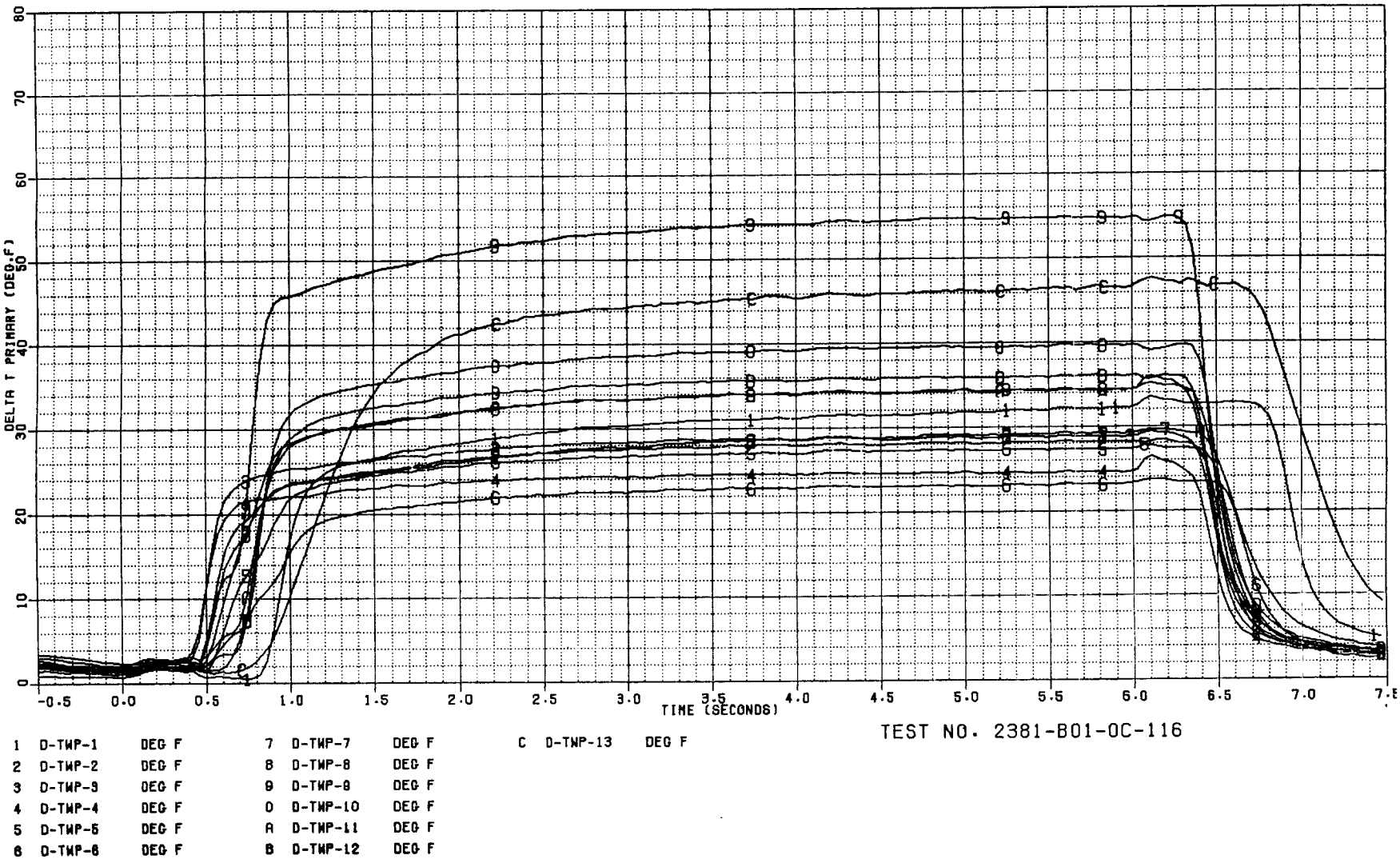

Figure B-41. Test 116 Primary Chamber Temperature Data Summary

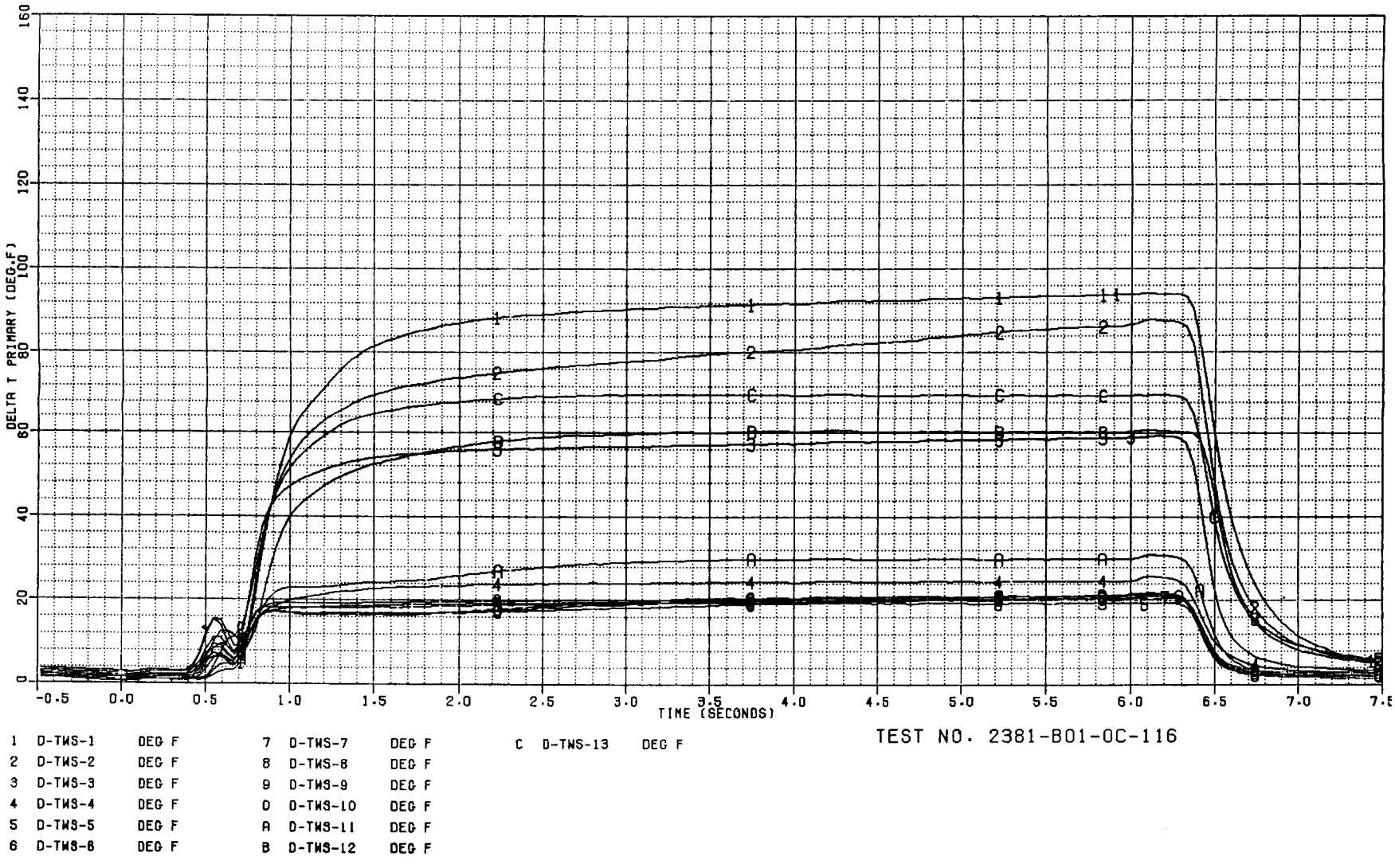

Figure B-42. Test 116 Secondary Chamber Temperature Data Summary

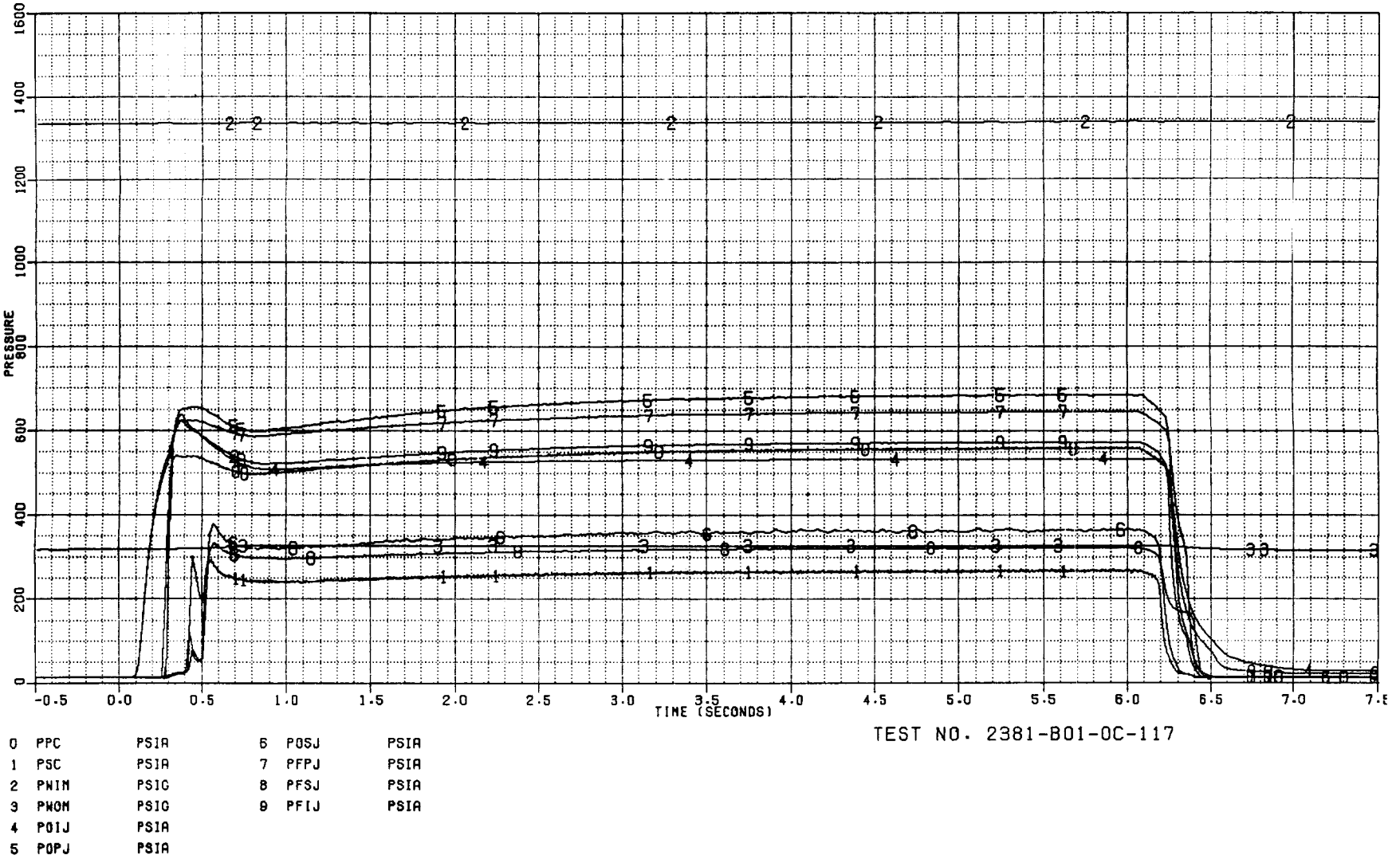

Figure B-43. Test 117 Pressure Data Summary

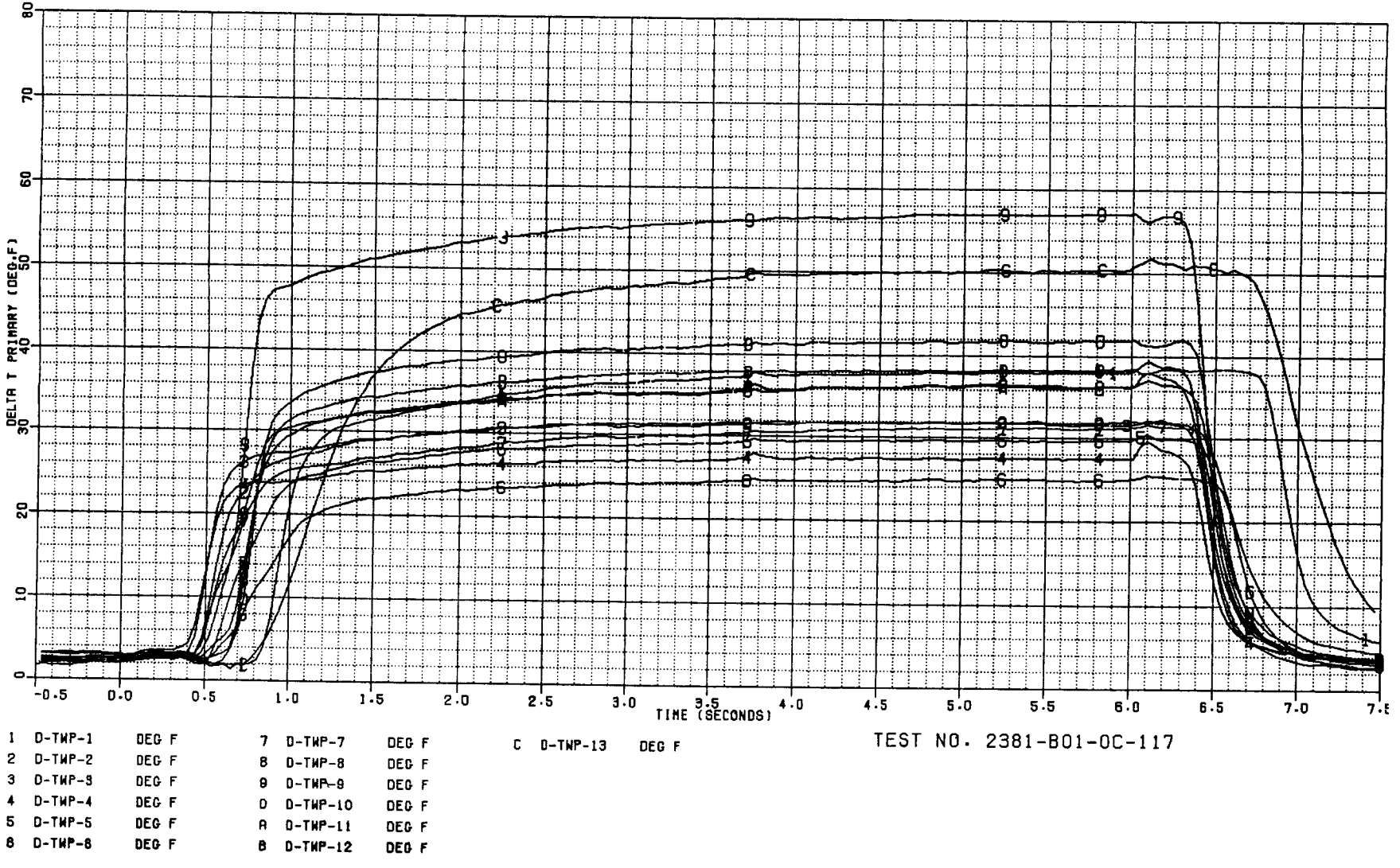

Figure B-44. Test 117 Primary Chamber Temperature Data Summary

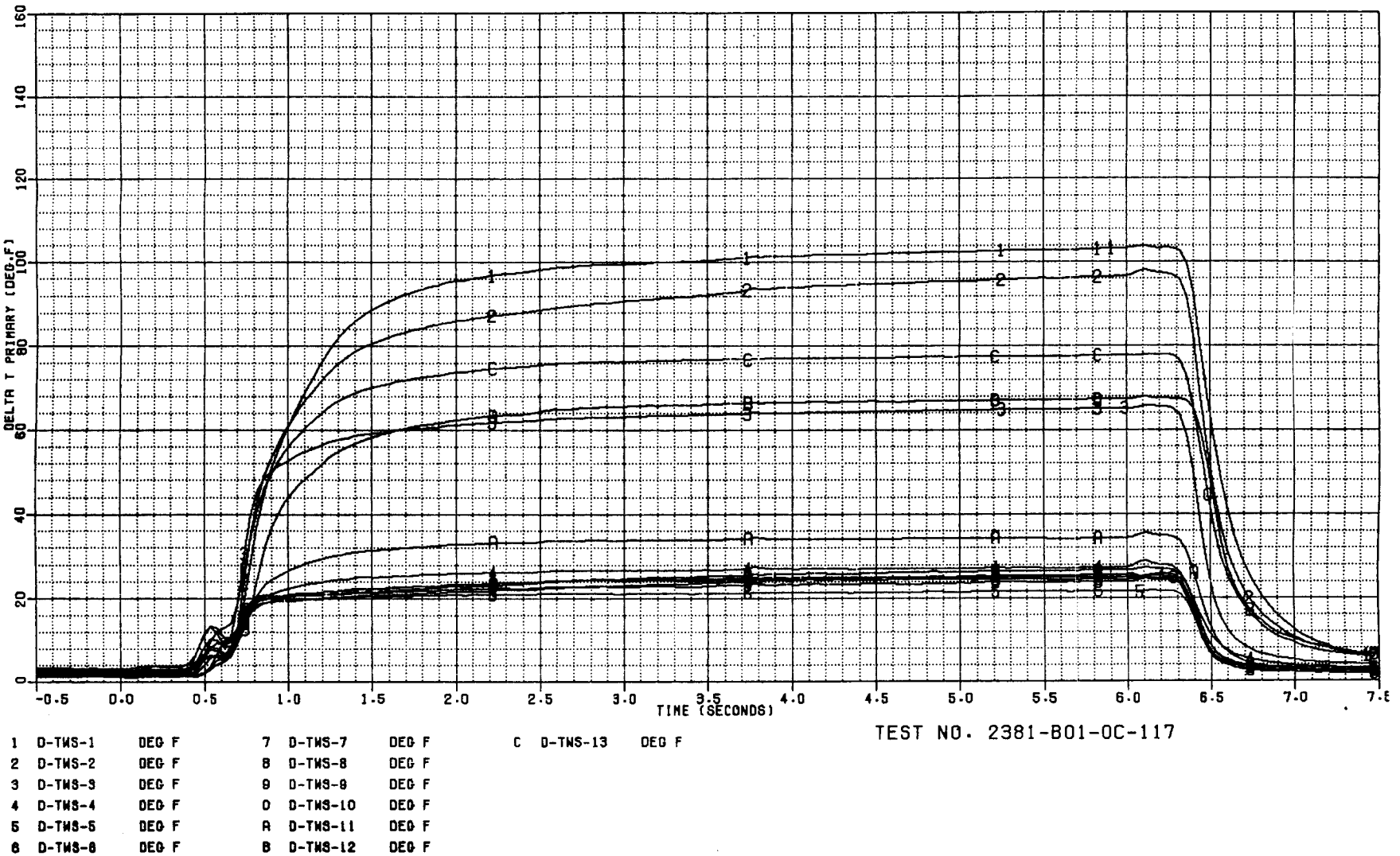

Figure B-45. Test 117 Secondary Chamber Temperature Data Summary

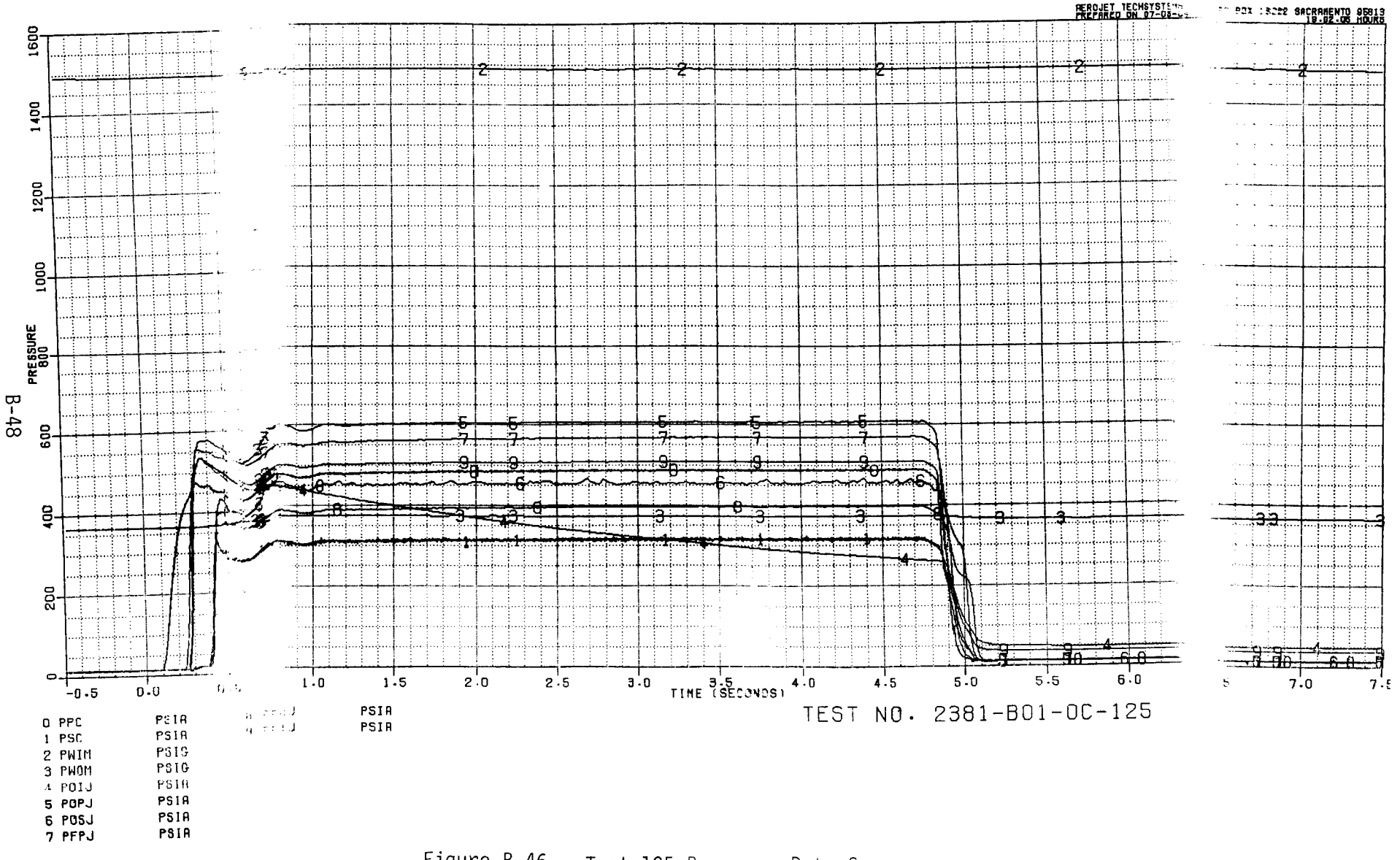

Figure B-46. Test 125 Pressure Data Summary

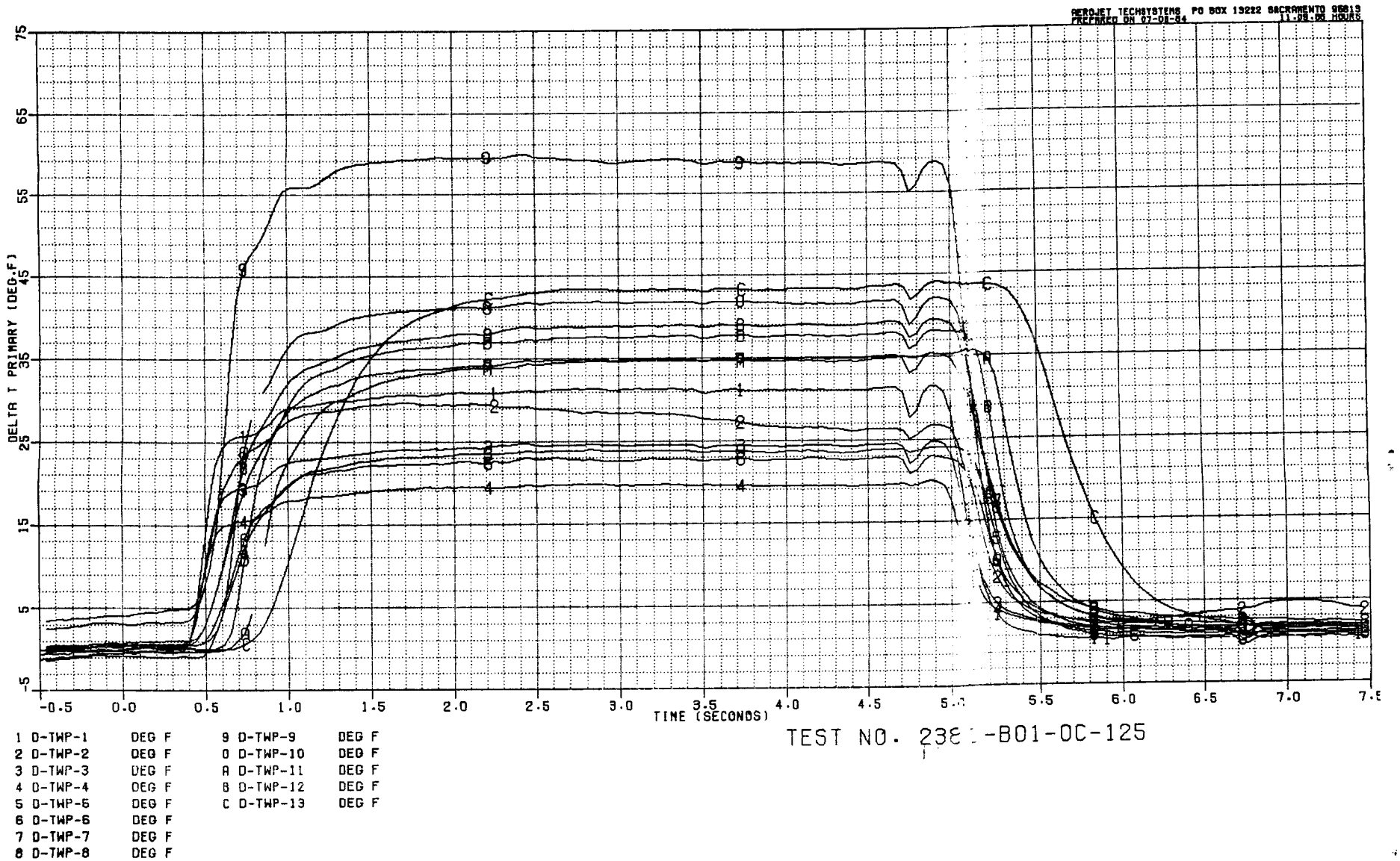

Figure B-47. Test 125 Primary Chamber Temperature Data Summary

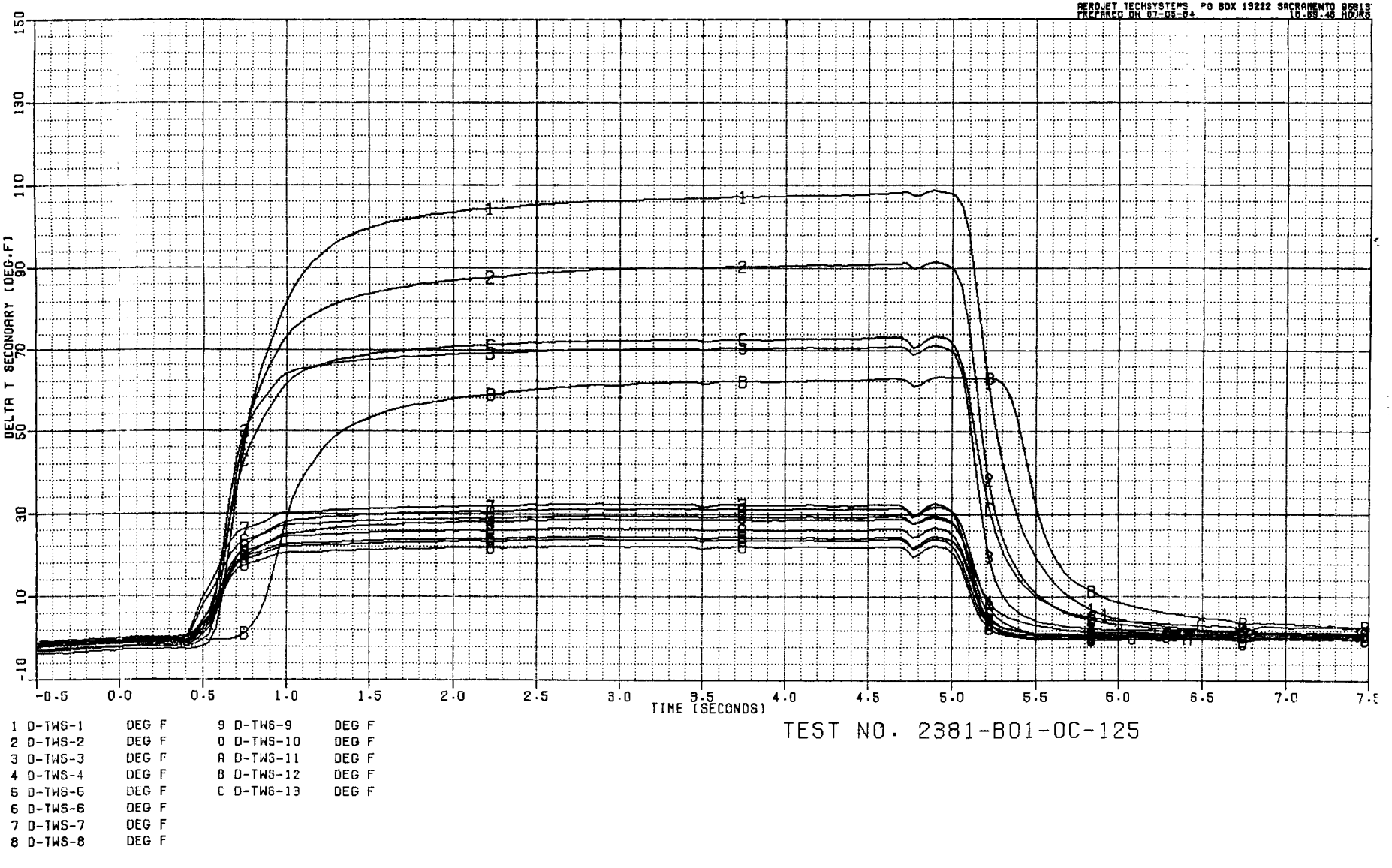

Figure B-43. Test 125 Secondary Chamber Temperature Data Summary

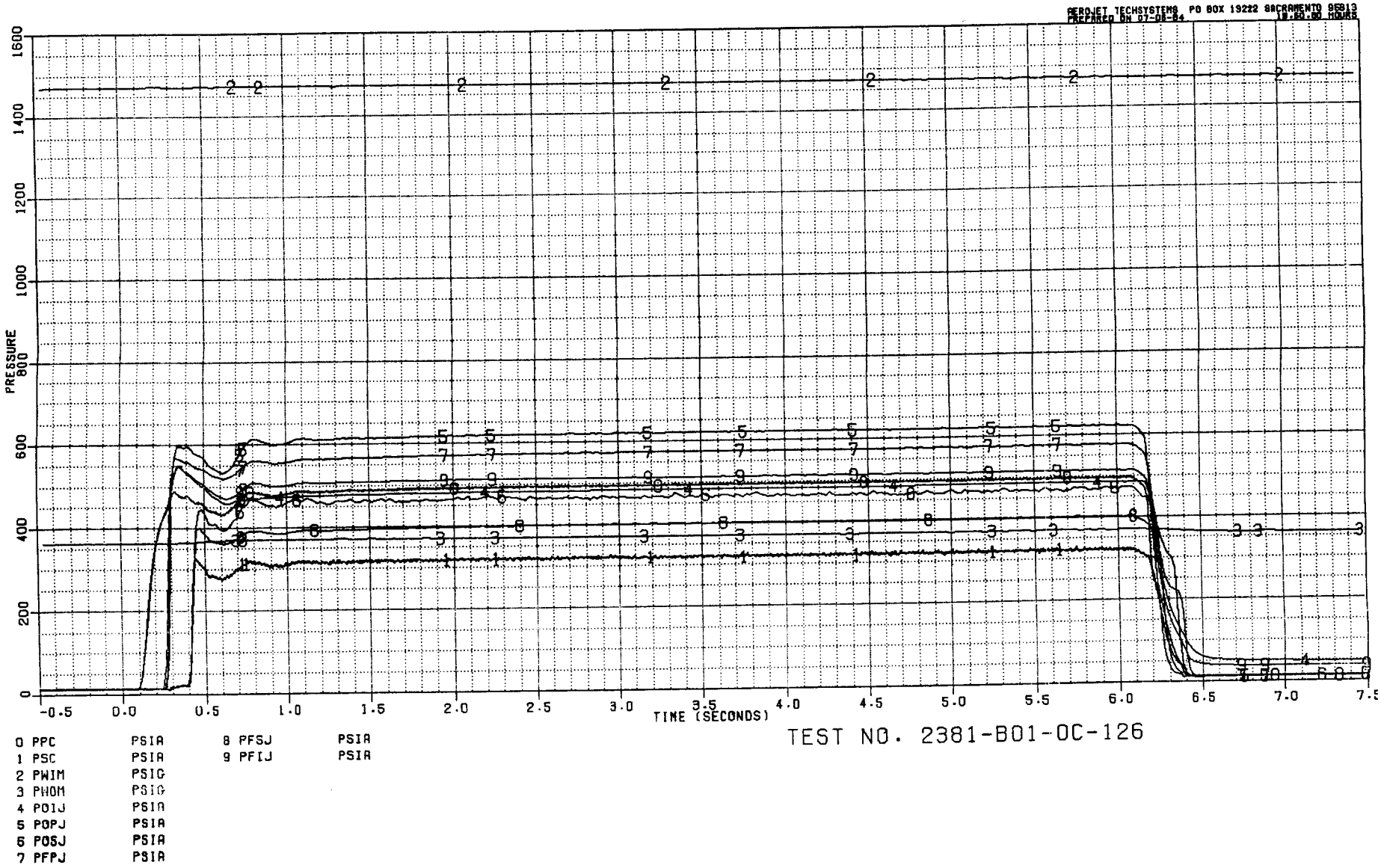

Figure B-49. Test 126 Pressure Data Summary

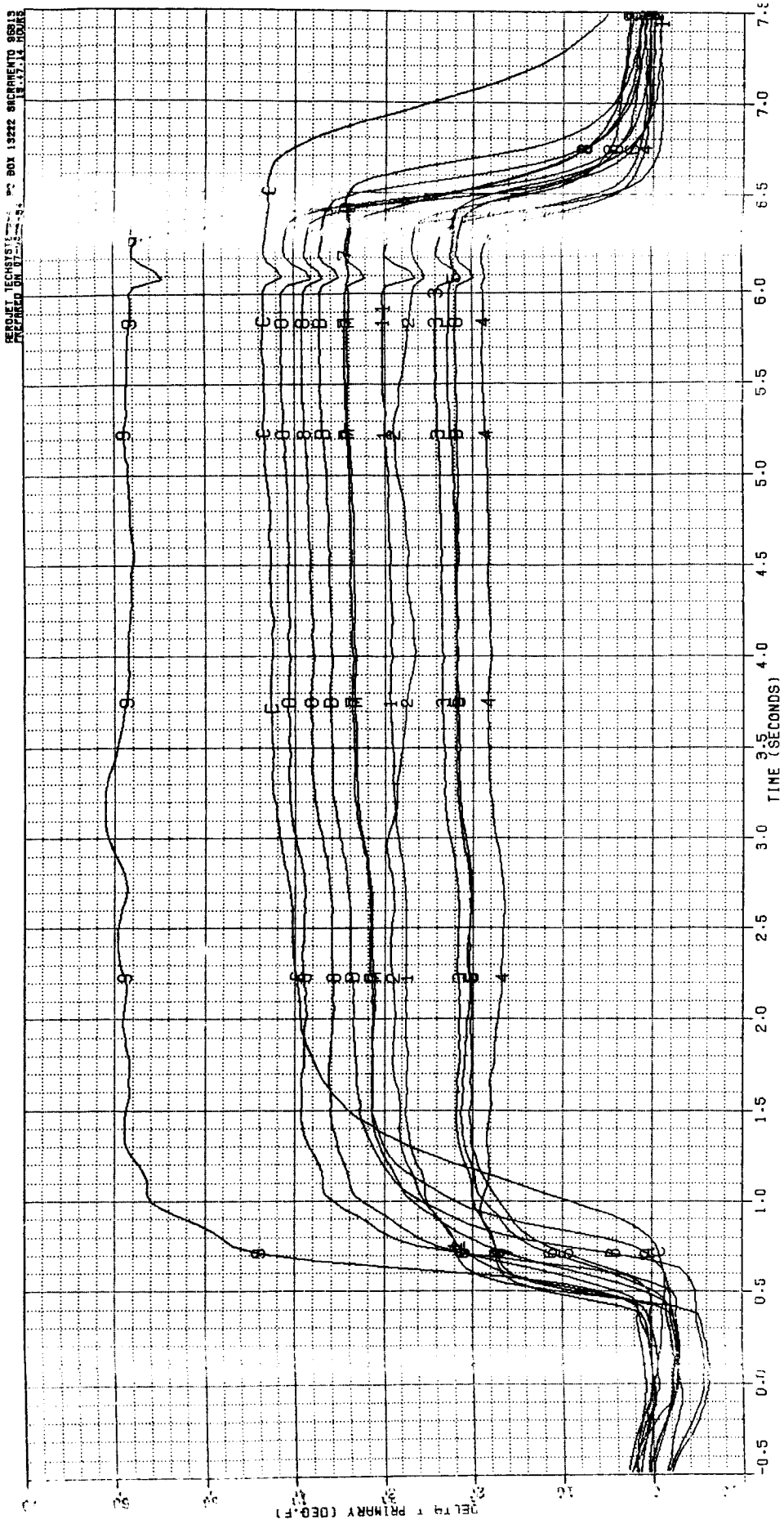

Figure B-50. Test 126 Primary Chamber Temperature Data Summary

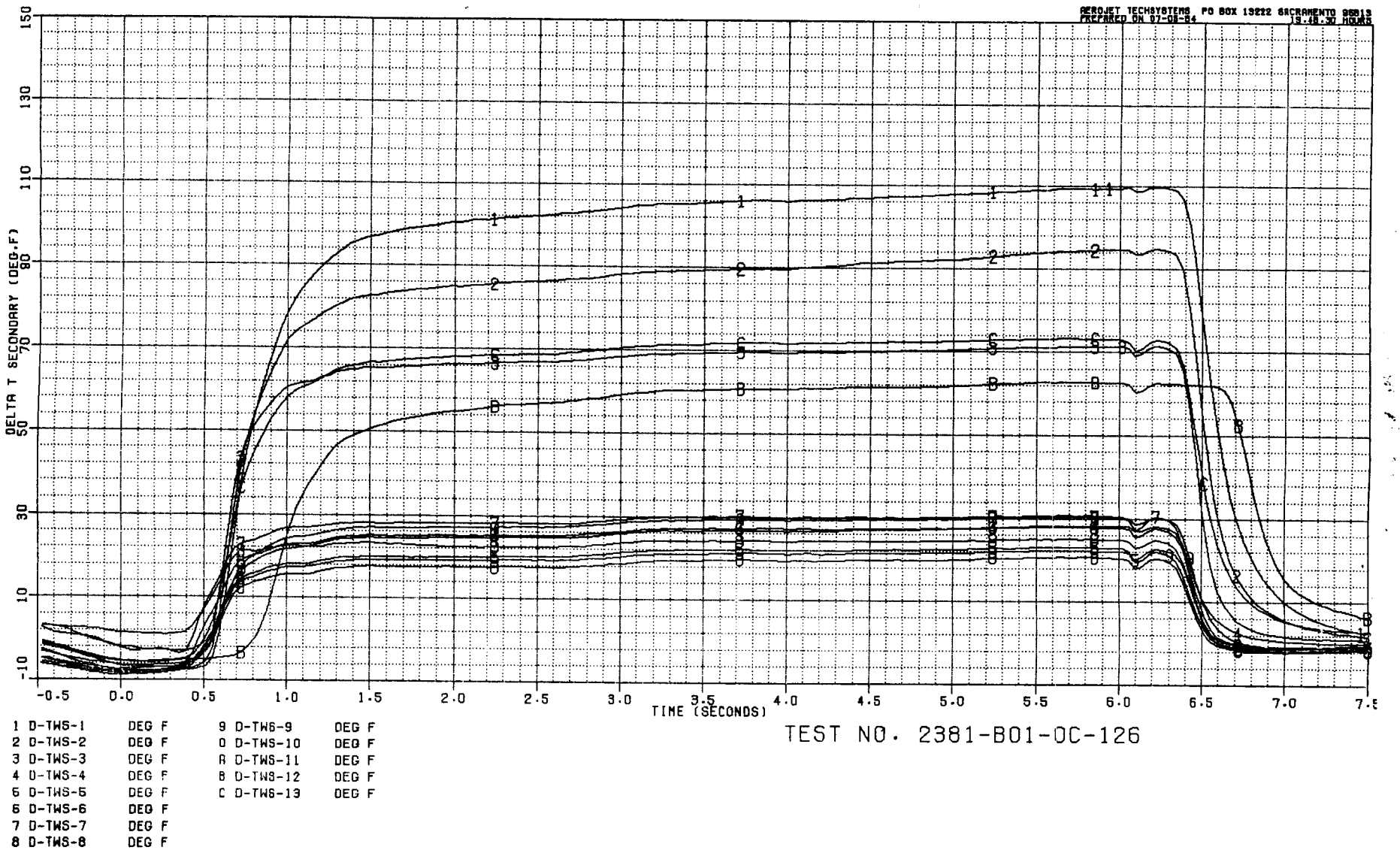

Figure B-51. Test 126 Secondary Chamber Temperature Data Summary

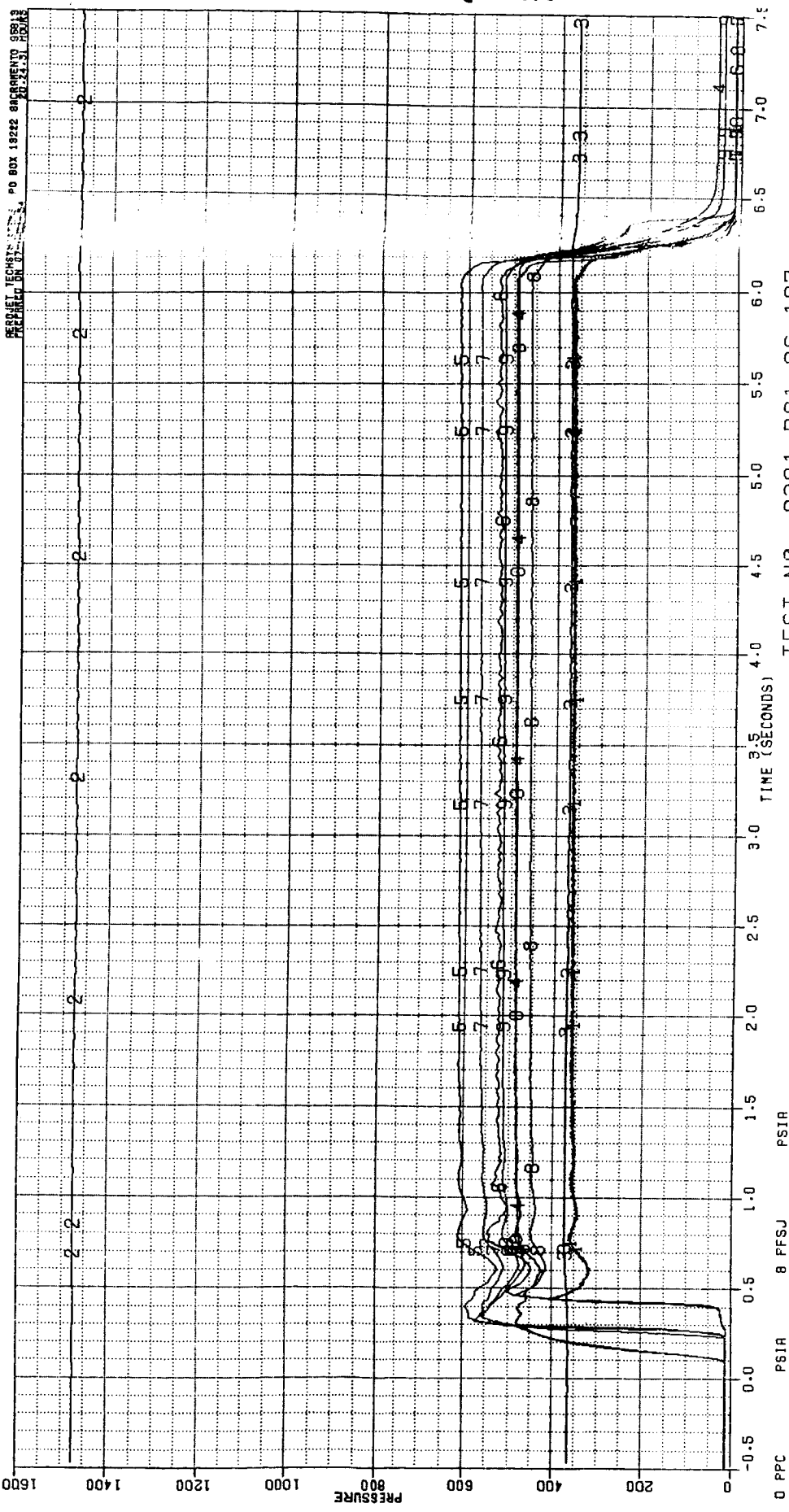

Figure B-52. Test 127 Pressure Data Summary

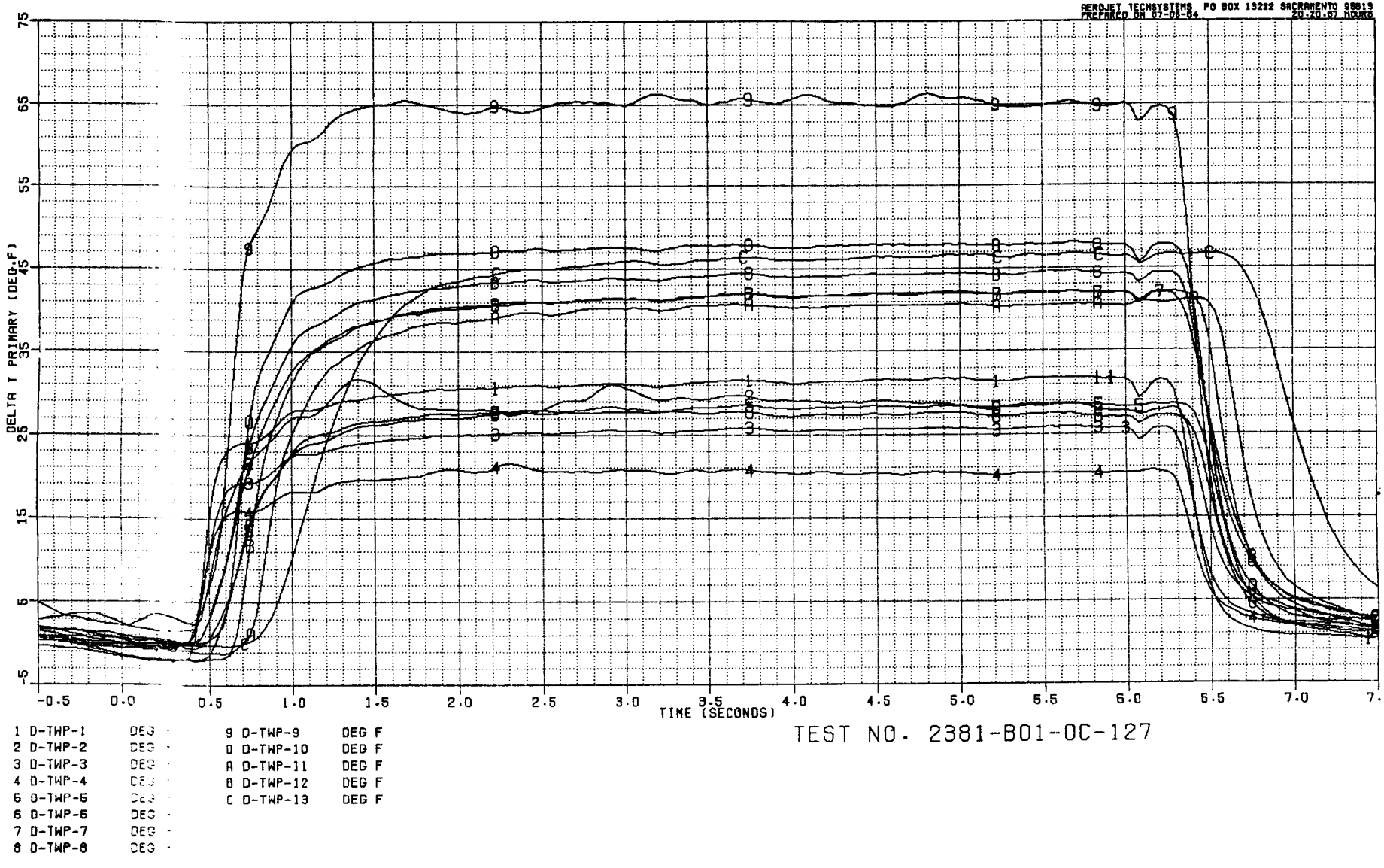

Figure B-53. Test 127 Primary Chamber Temperature Data Summary

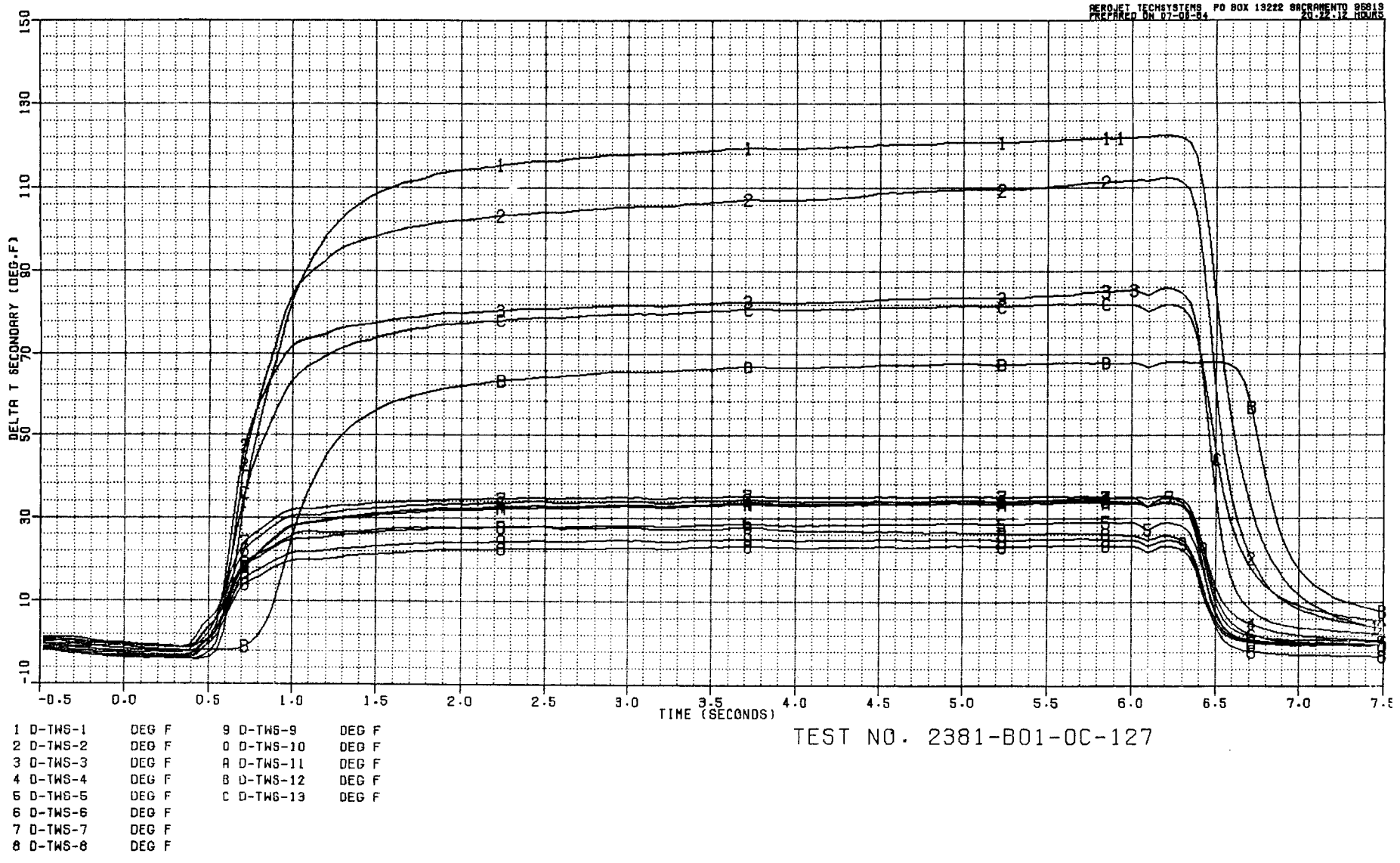

Figure B-54. Test 127 Secondary Chamber Temperature Data Summary

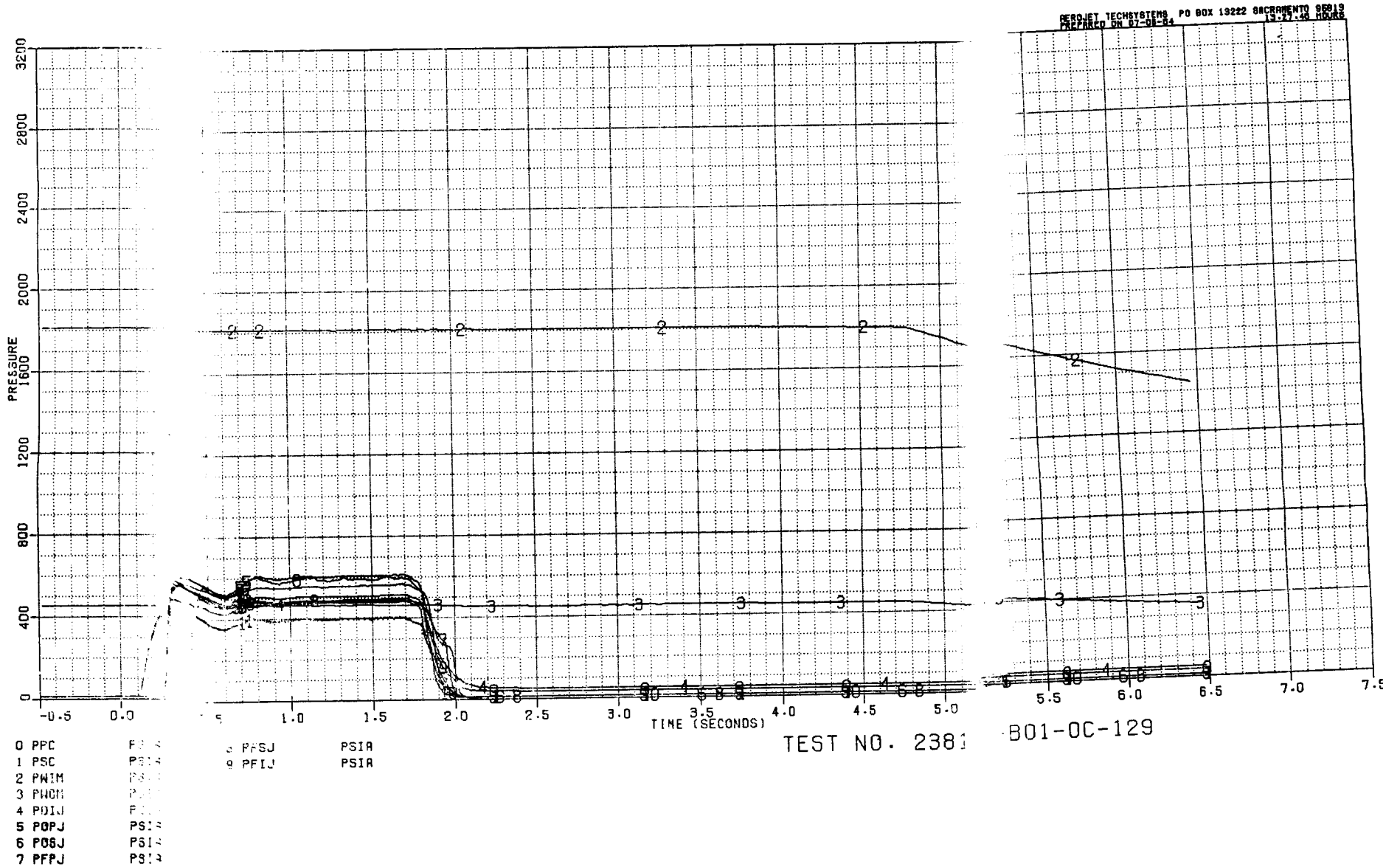

Figure B-55 Test 129 Pressure Data Summary

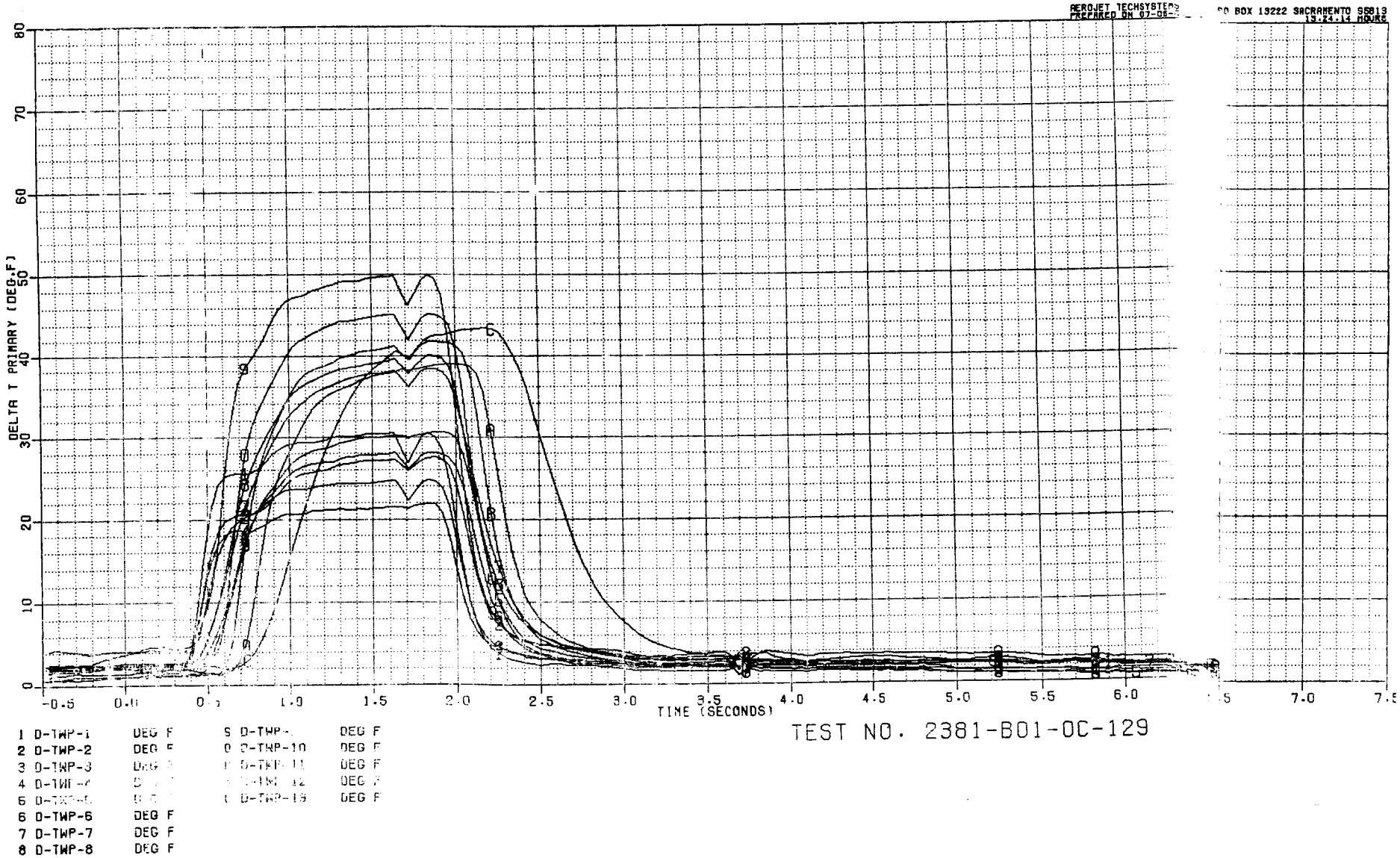

Figure B-56. Test 129 Primary Chamber Temperature Data Summary

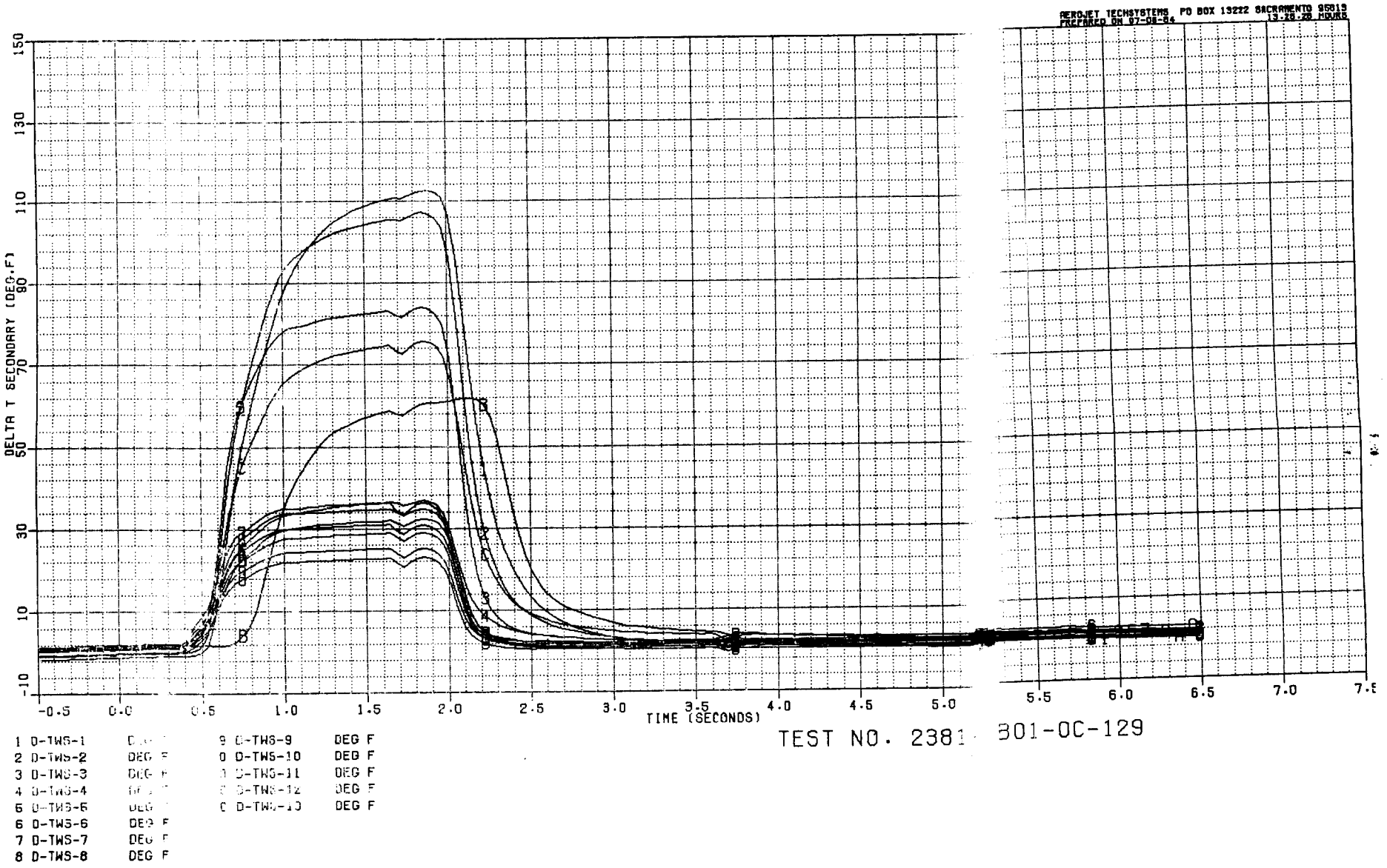

Figure B-57. Test 129 Secondary Chamber Temperature Data Summary

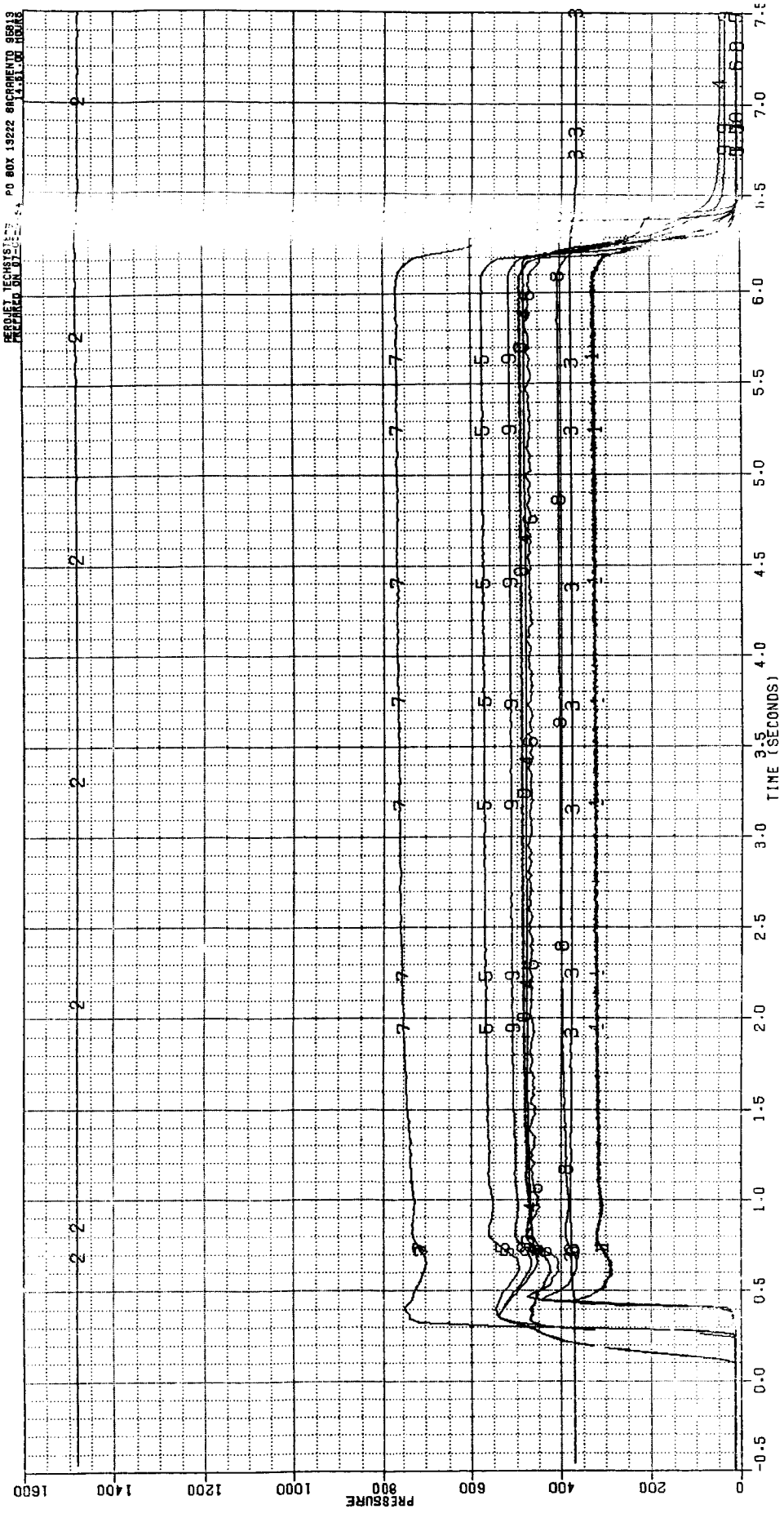

Figure B-58. Test 130 Pressure Data Summary

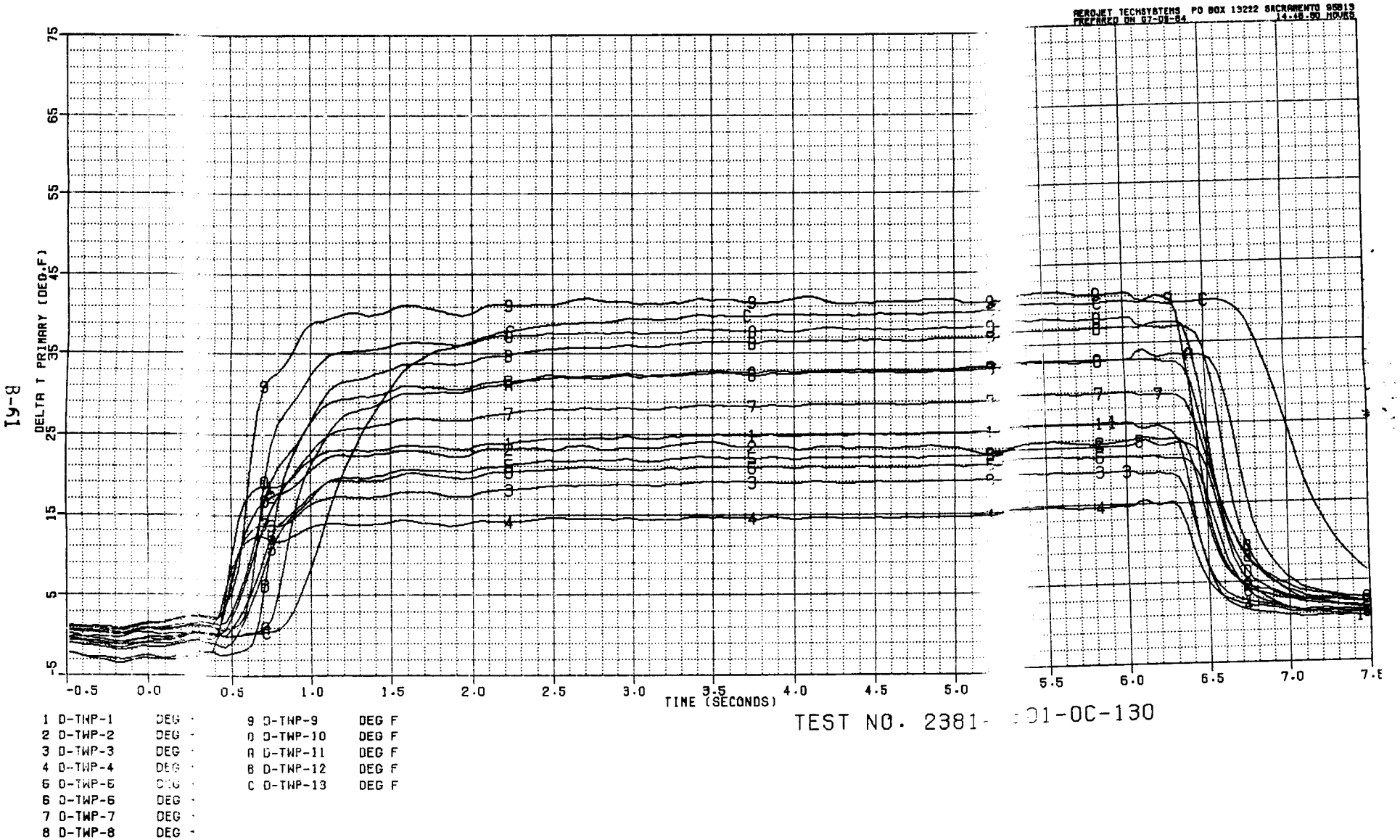

Figure B-59. Test 130 Primary Chamber Temperature Data Summary

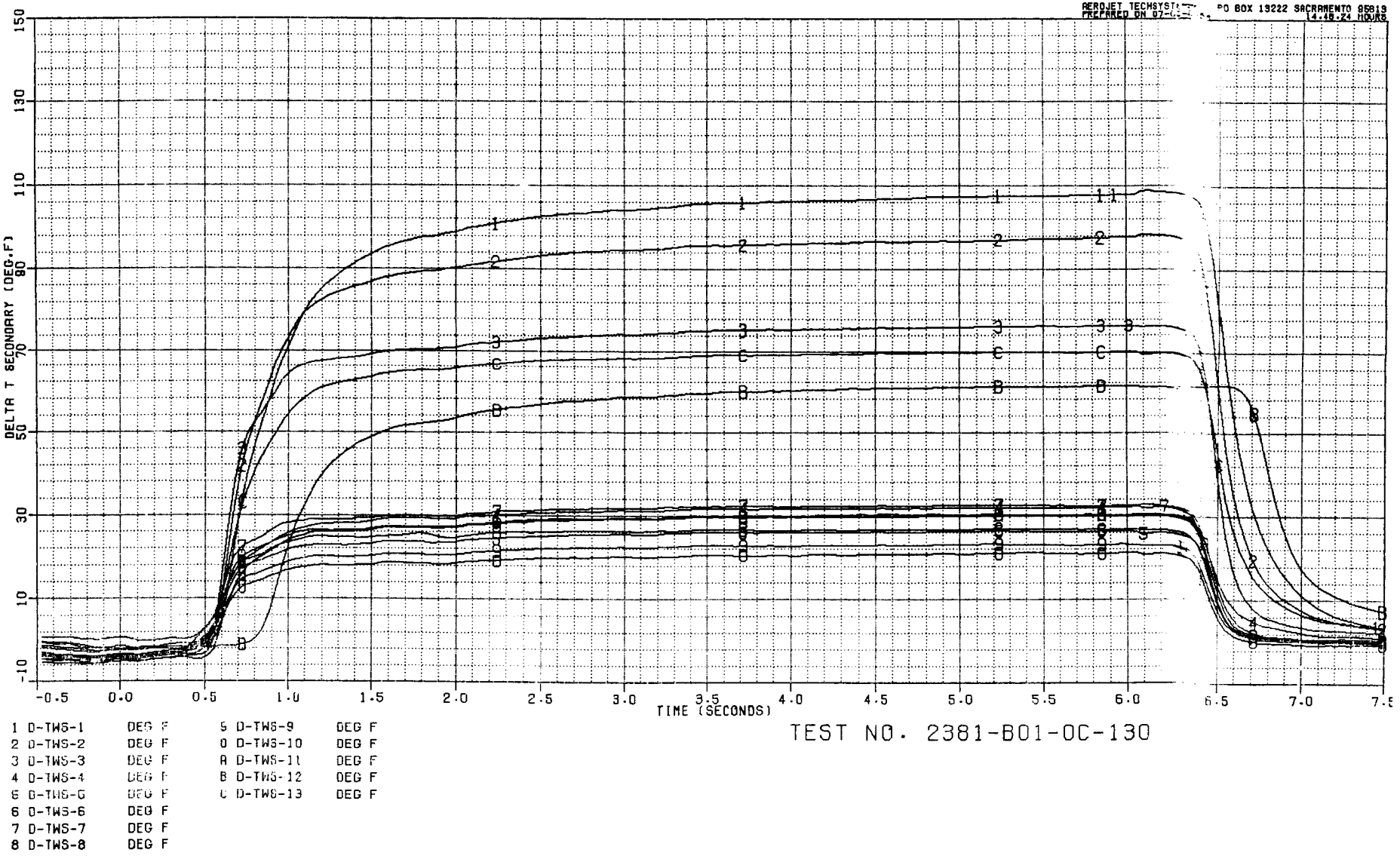

Figure B-60. Test 130 Secondary Chamber Temperature Data Summary

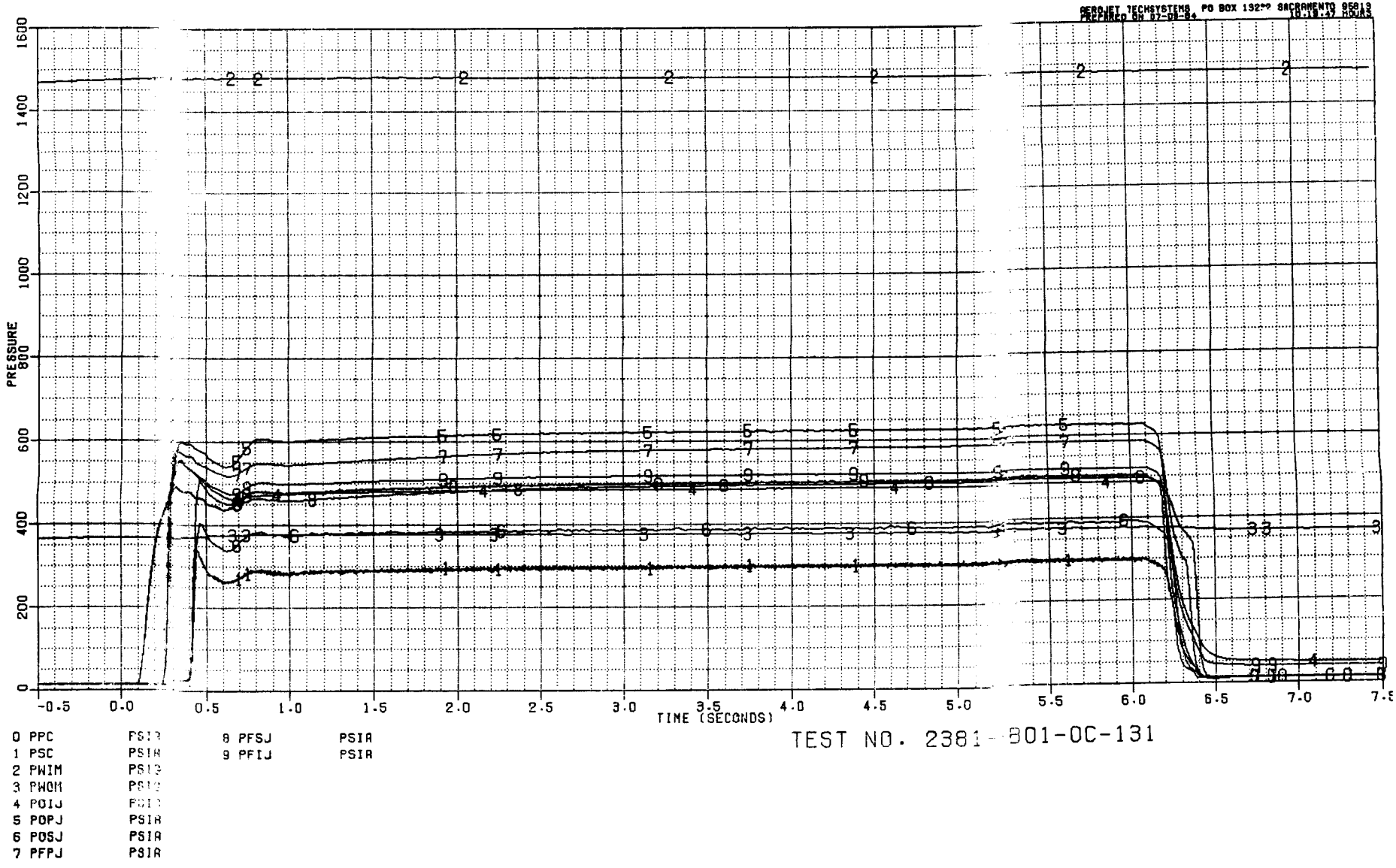

Figure B-61. Test 131 Pressure Data Summary

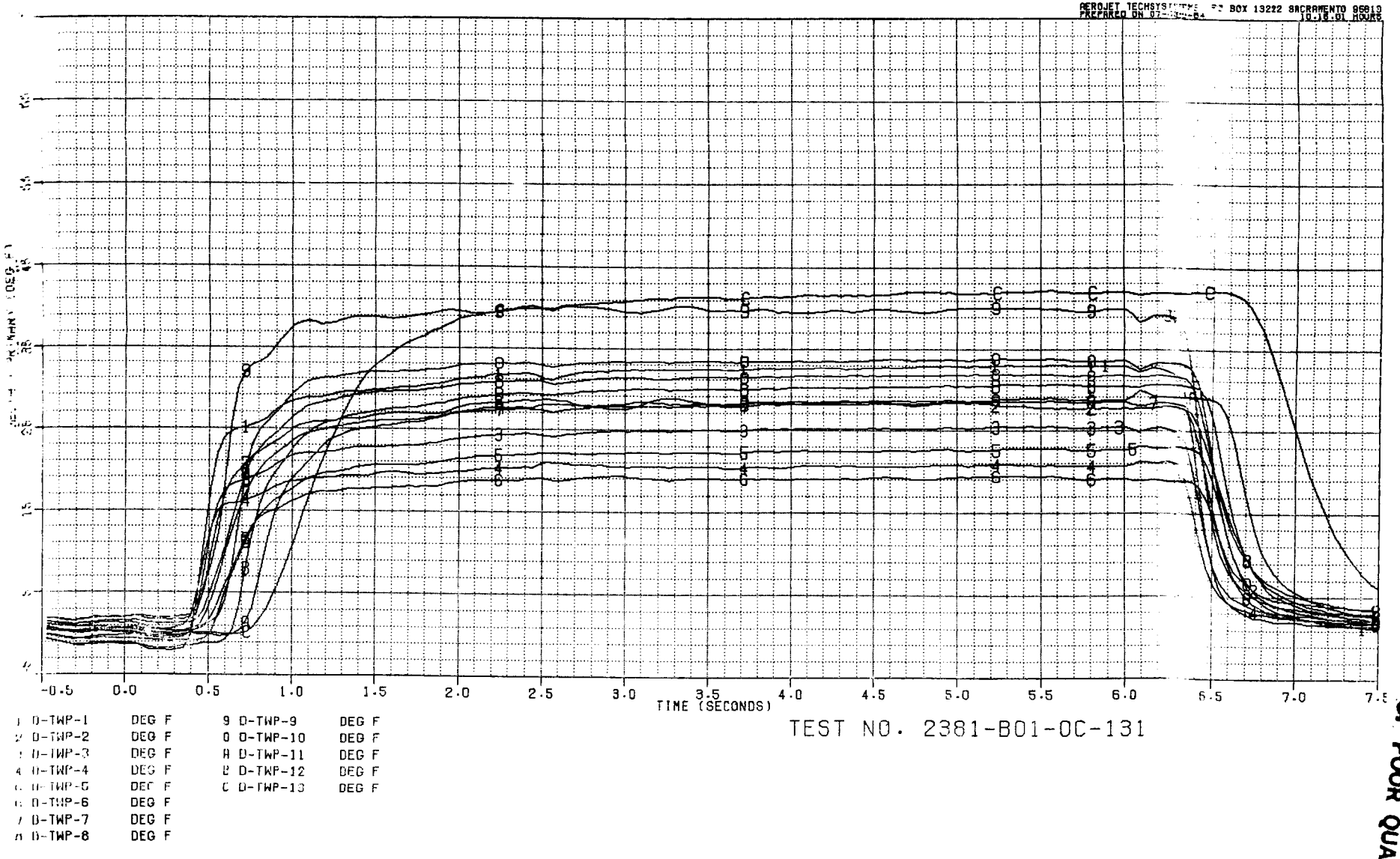

Figure B-62. Test 131 Primary Chamber Temperature Data Summary

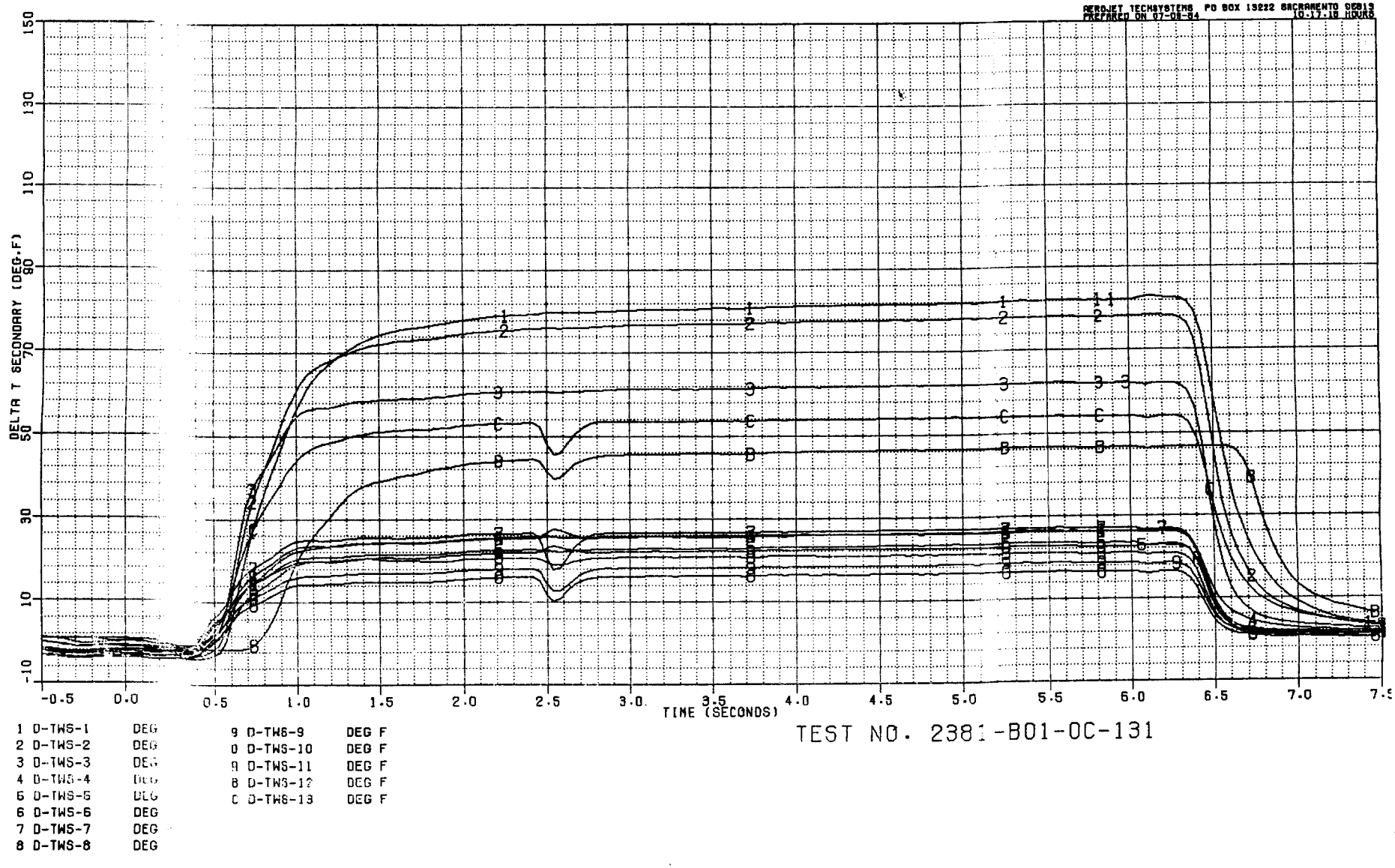

Figure B-63. Test 131 Secondary Chamber Temperature Data Summary

ORIGINAL PAGE IS
OF POOR QUALITY

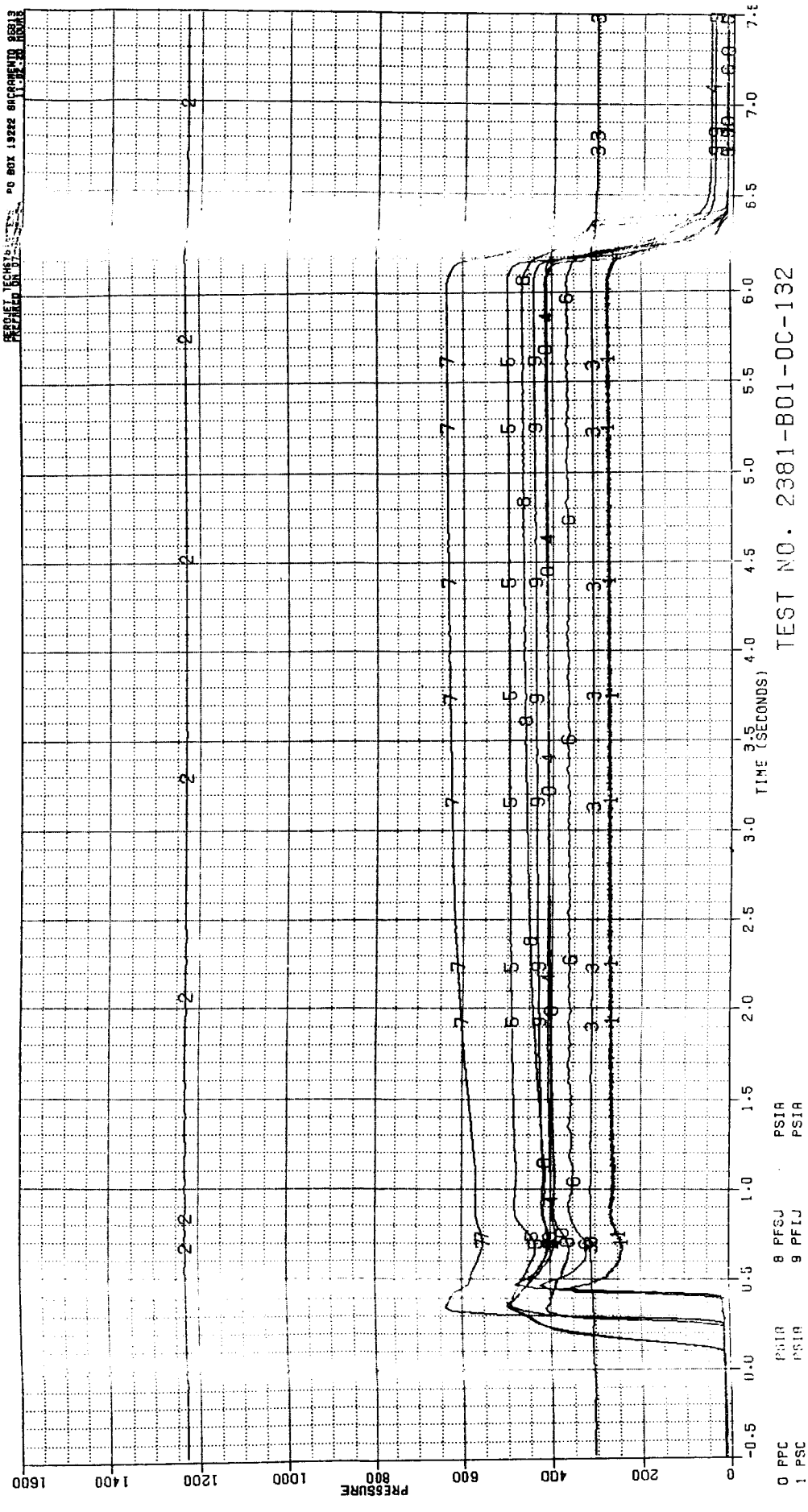

Figure B-64. Test 132 Pressure Data Summary

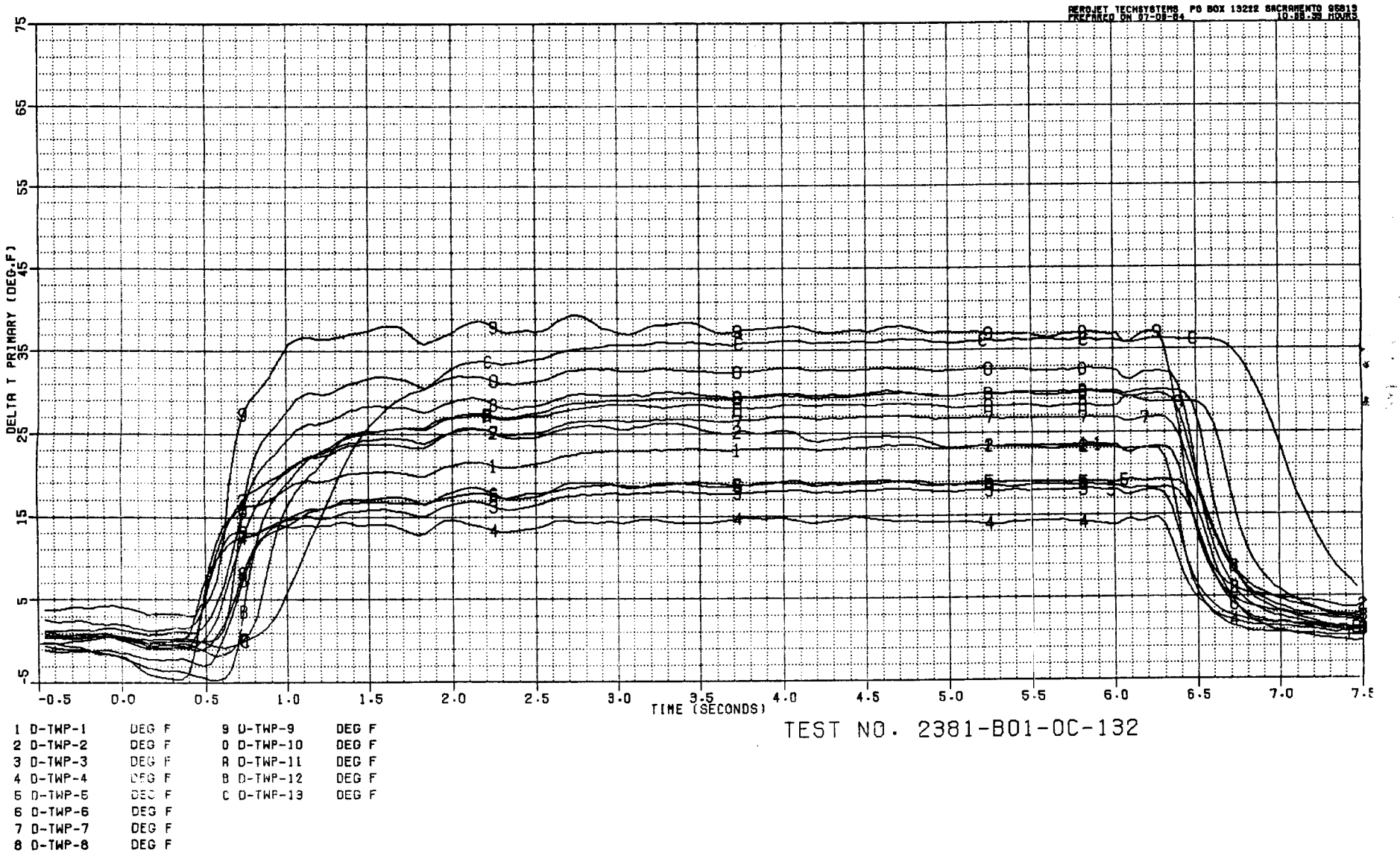

Figure B-65. Test 132 Primary Chamber Temperature Data Summary

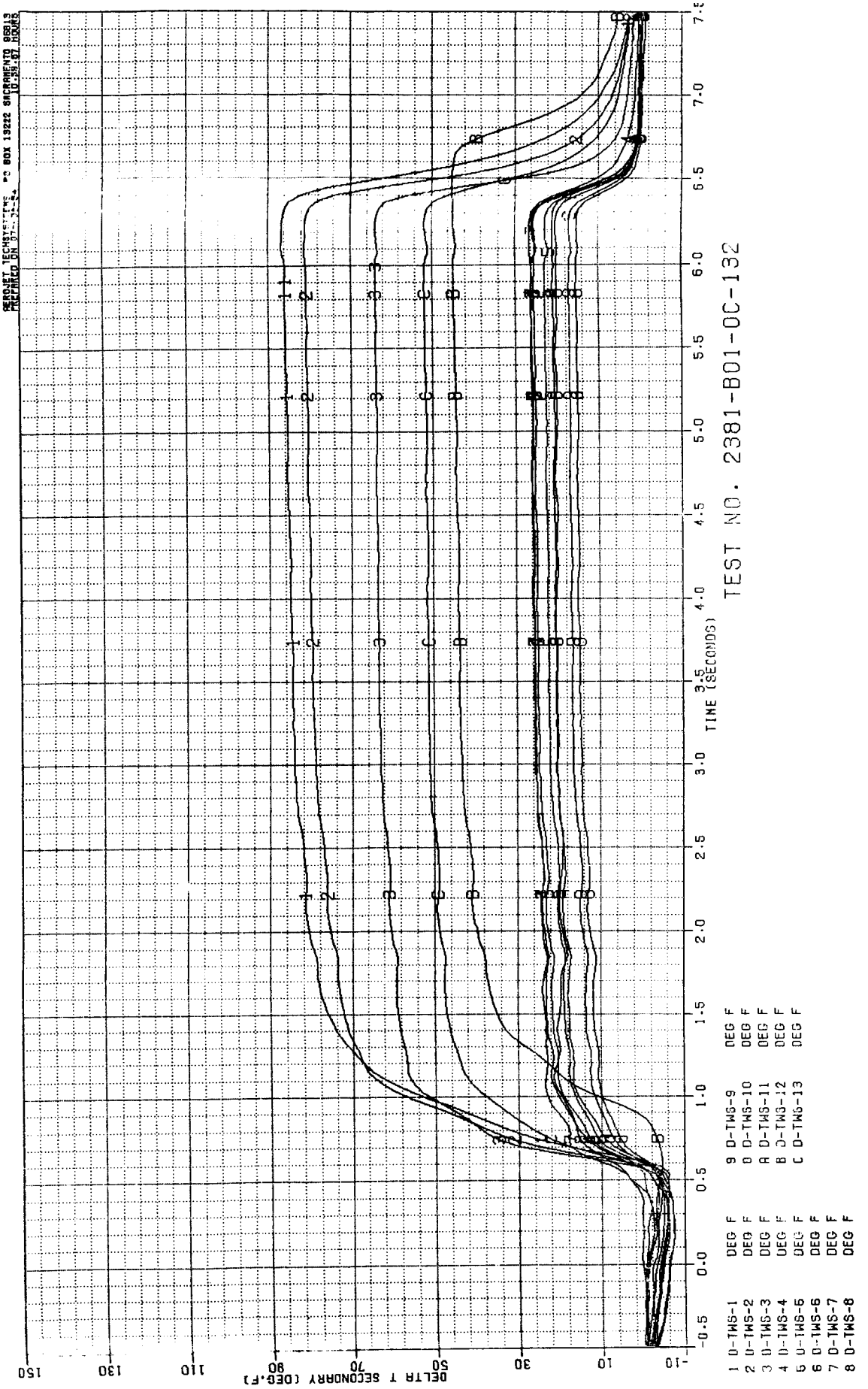

Figure B-66. Test 132 Secondary Chamber Temperature Data Summary

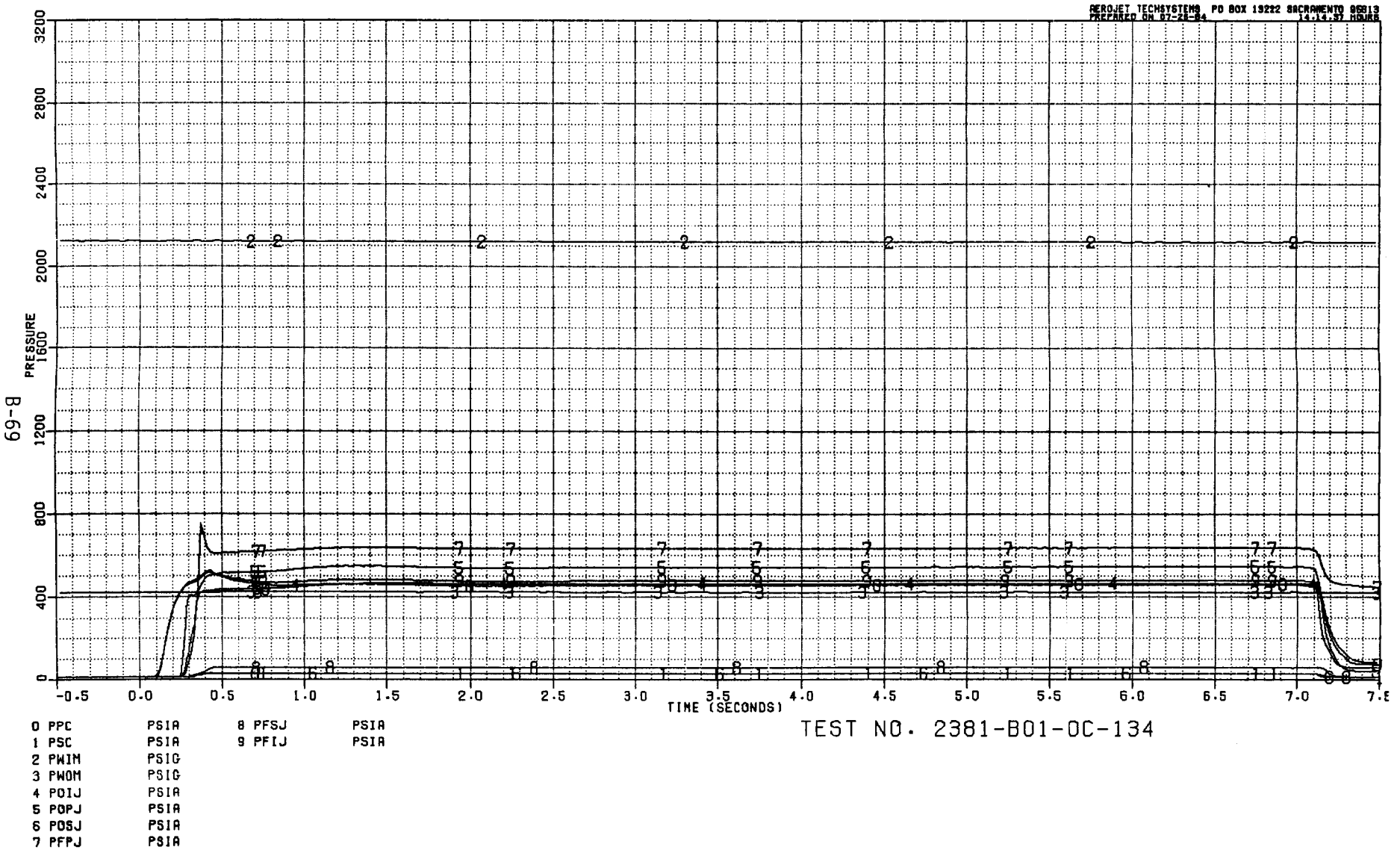

Figure B-67. Test 134 Pressure Data Summary

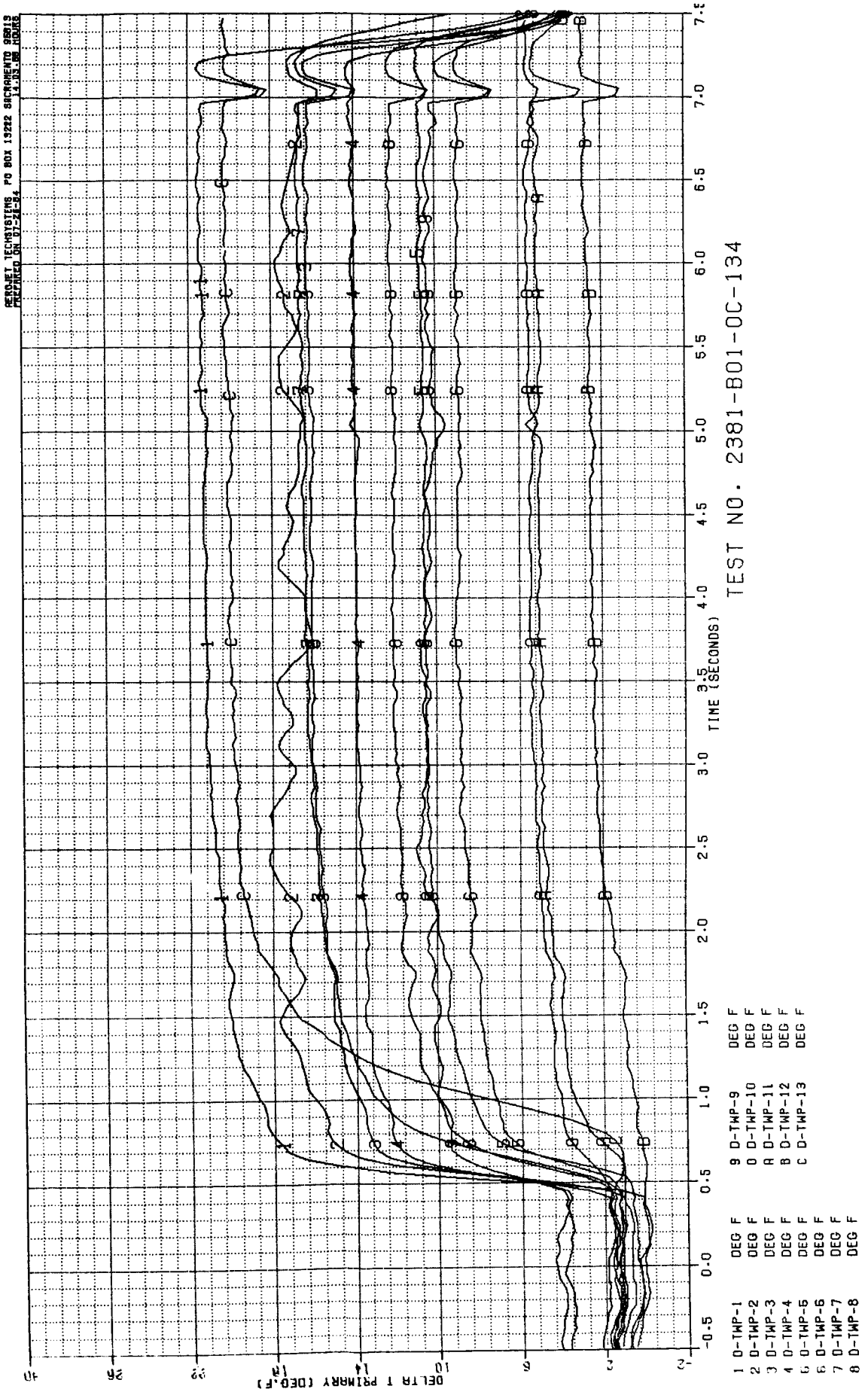

Figure B-68. Test 134 Primary Chamber Temperature Data Summary

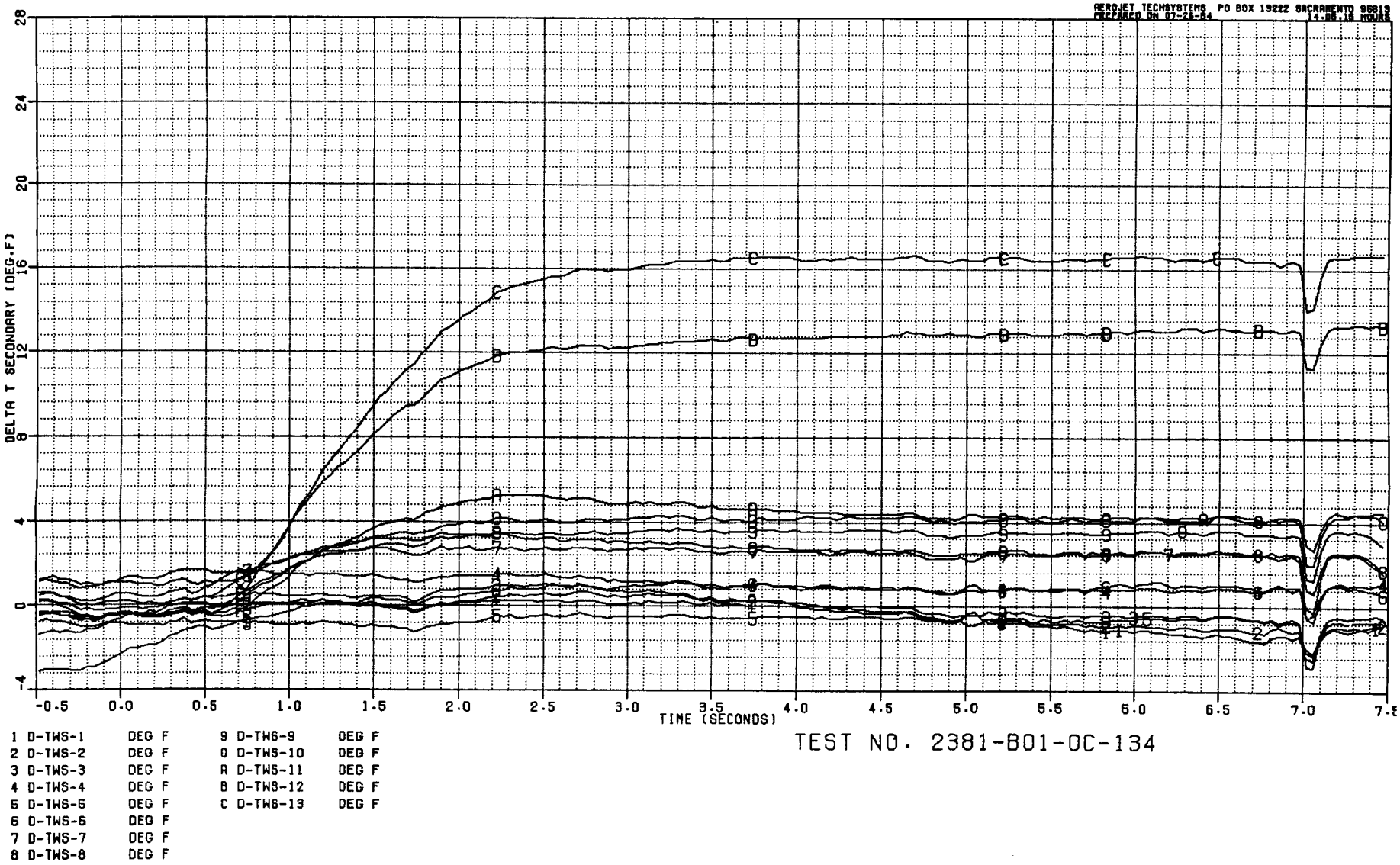

Figure B-69. Test 134 Secondary Chamber Temperature Data Summary

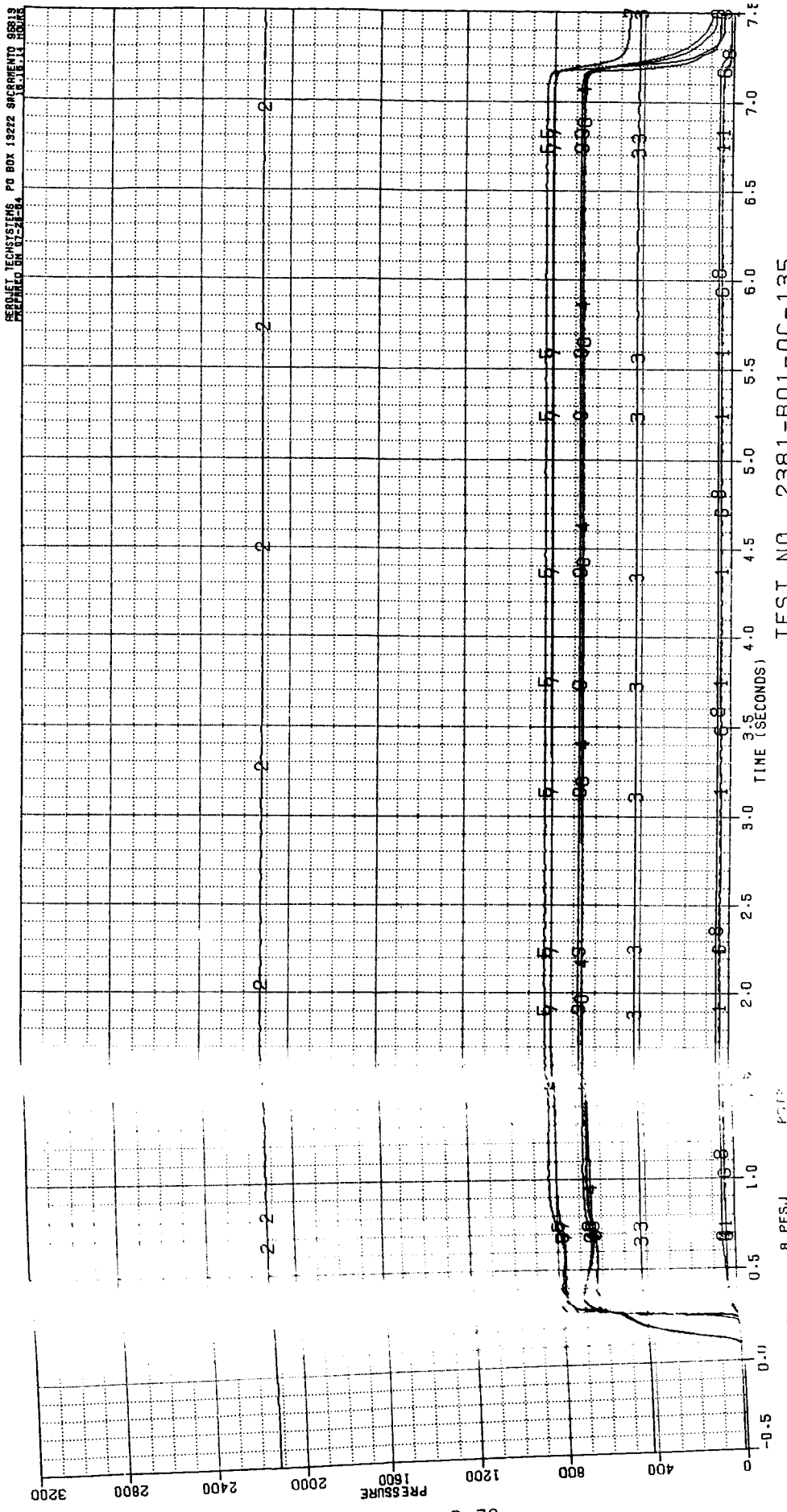

Figure B-70. Test 135 Pressure Data Summary

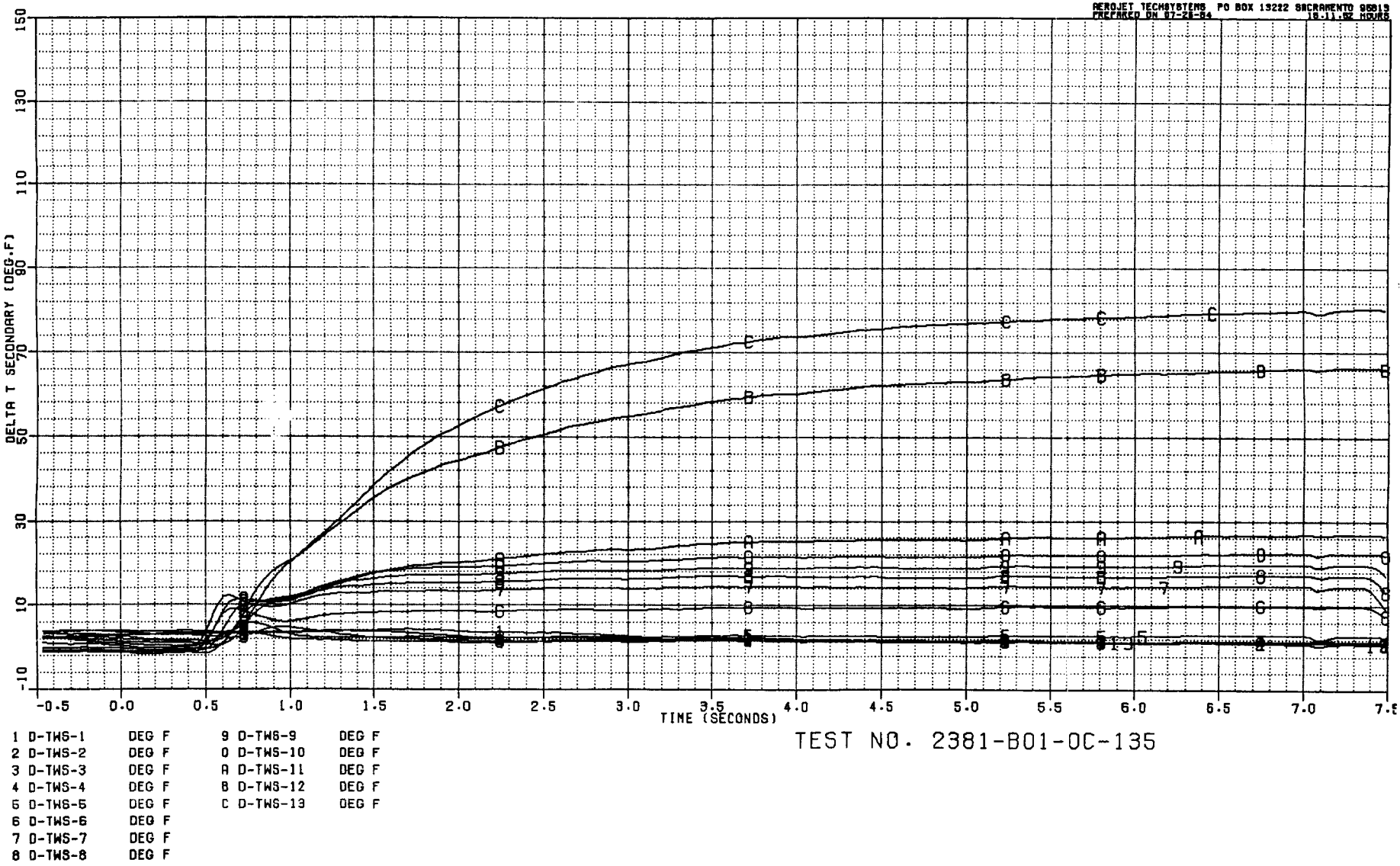

Figure B-71. Test 135 Primary Chamber Temperature Data Summary

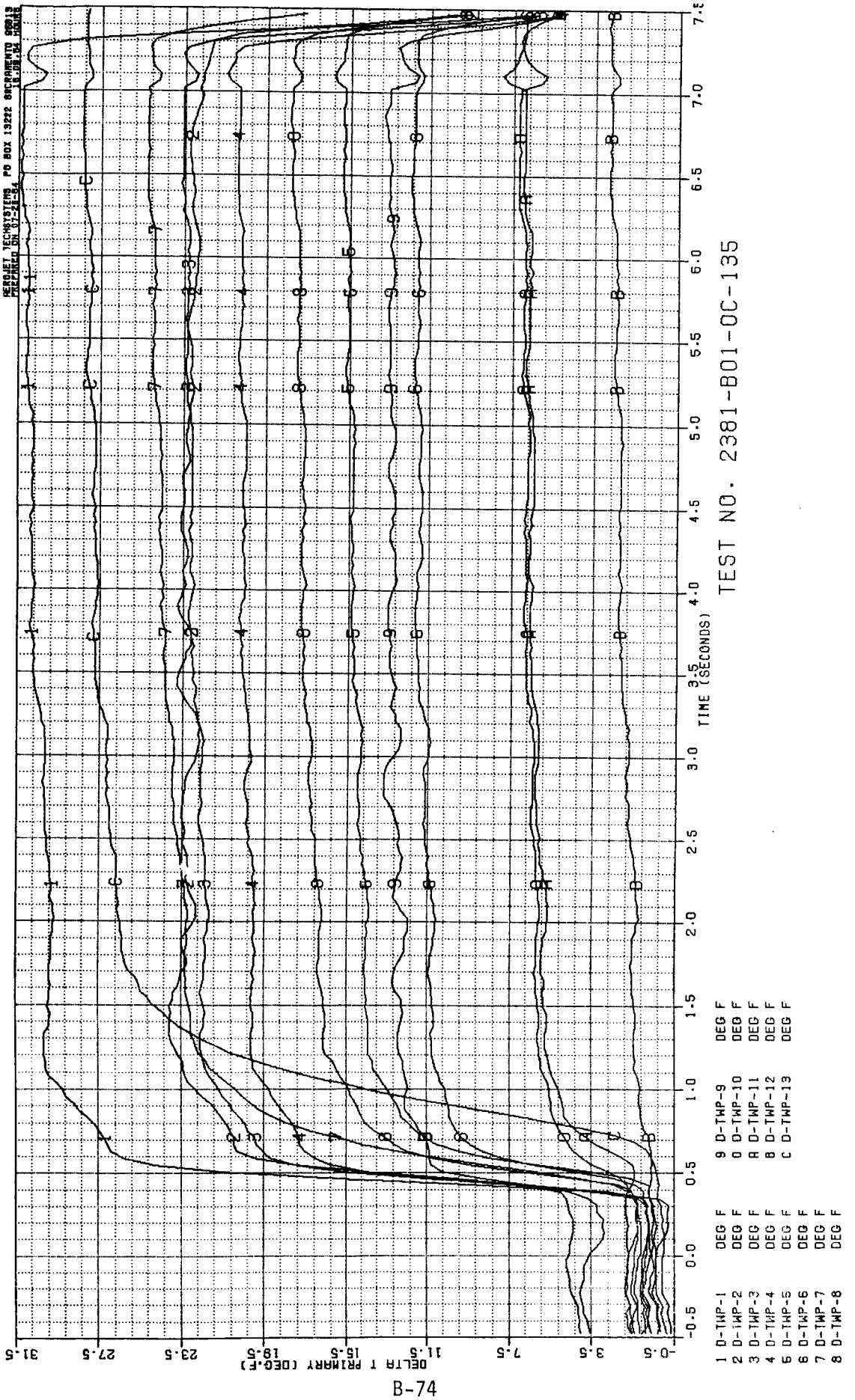

Figure B-72. Test 135 Secondary Chamber Temperature Data Summary

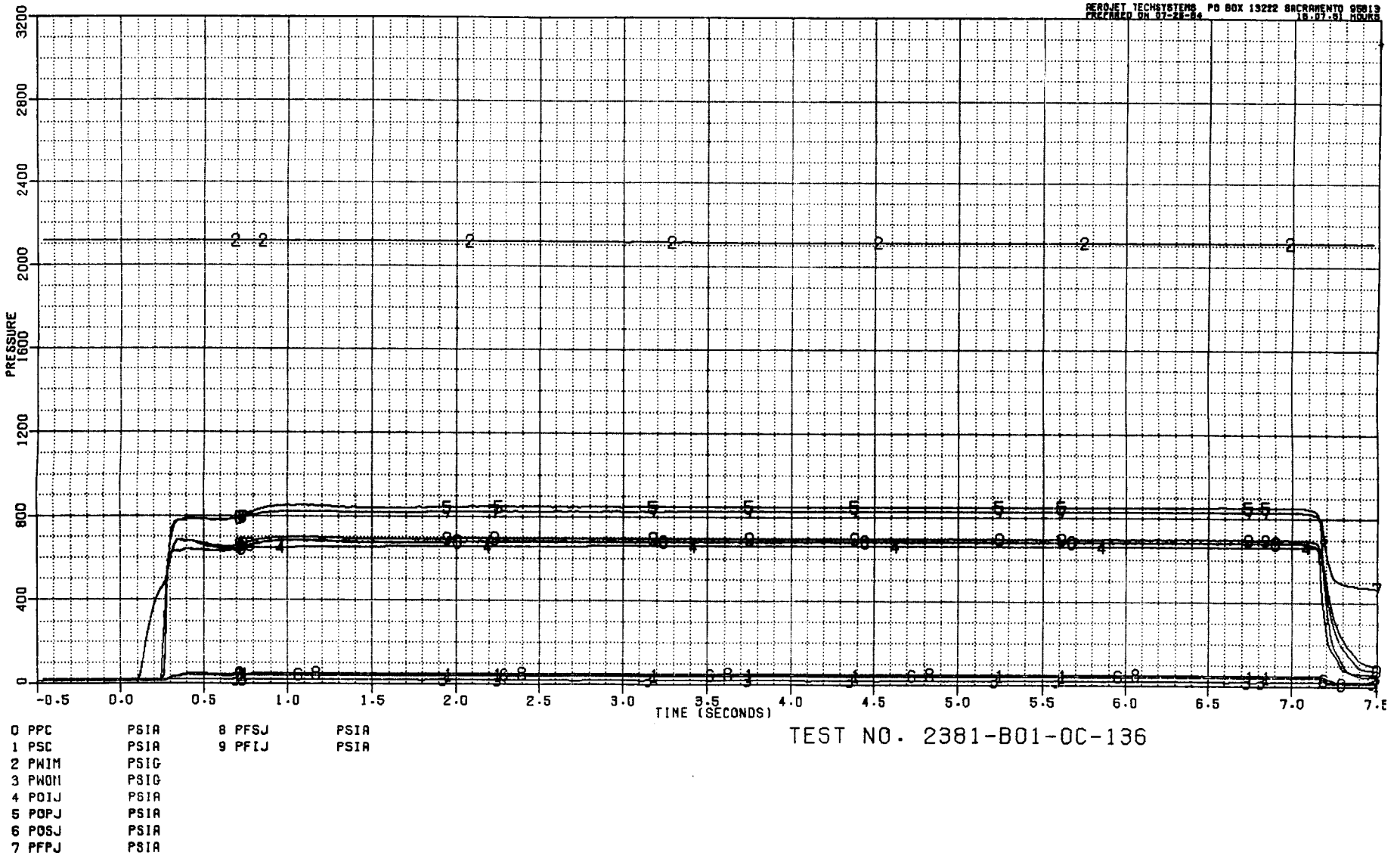

Figure B-73. Test 136 Pressure Data Summary

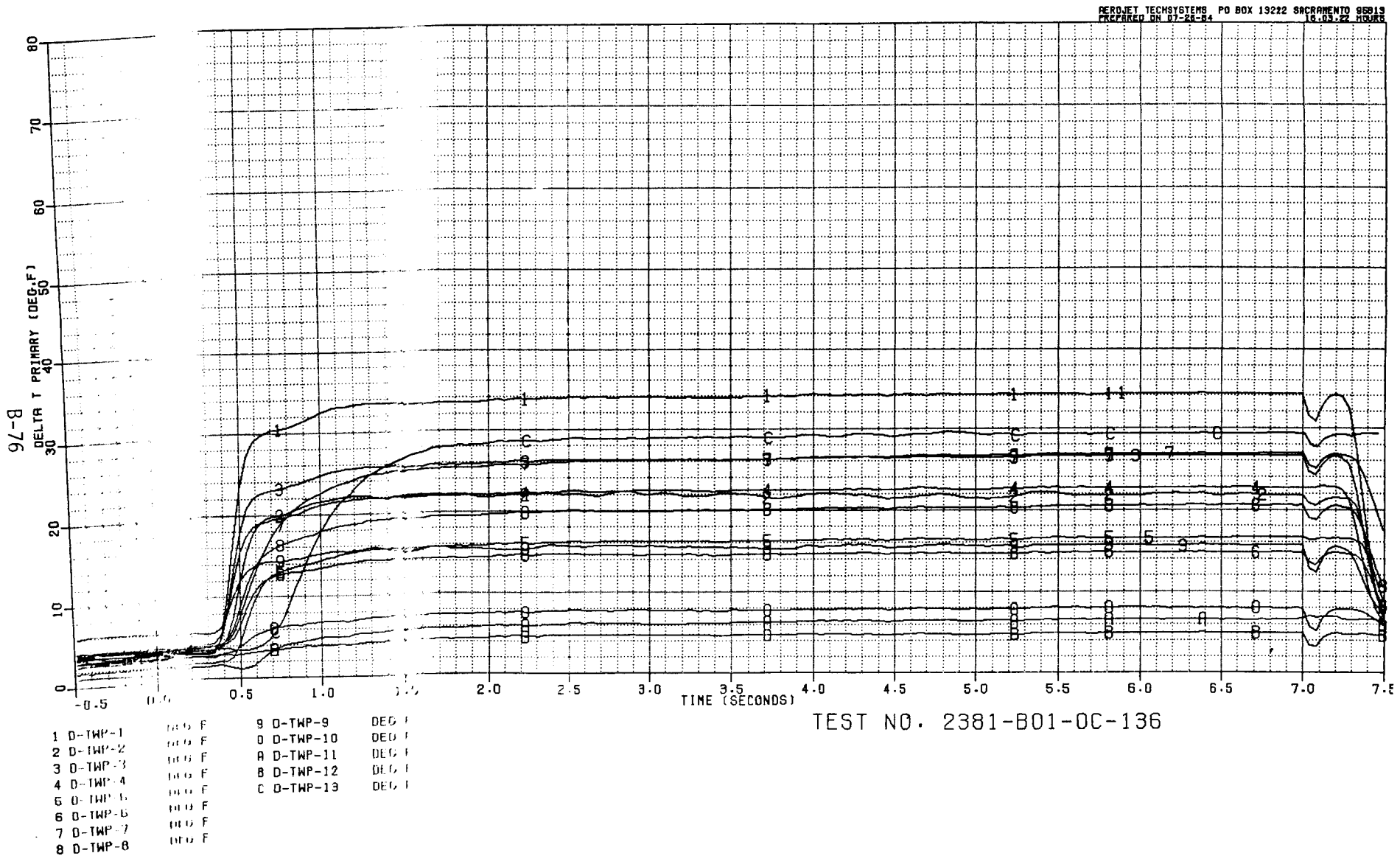

Figure B-74. Test 136 Primary Chamber Temperature Data Summary

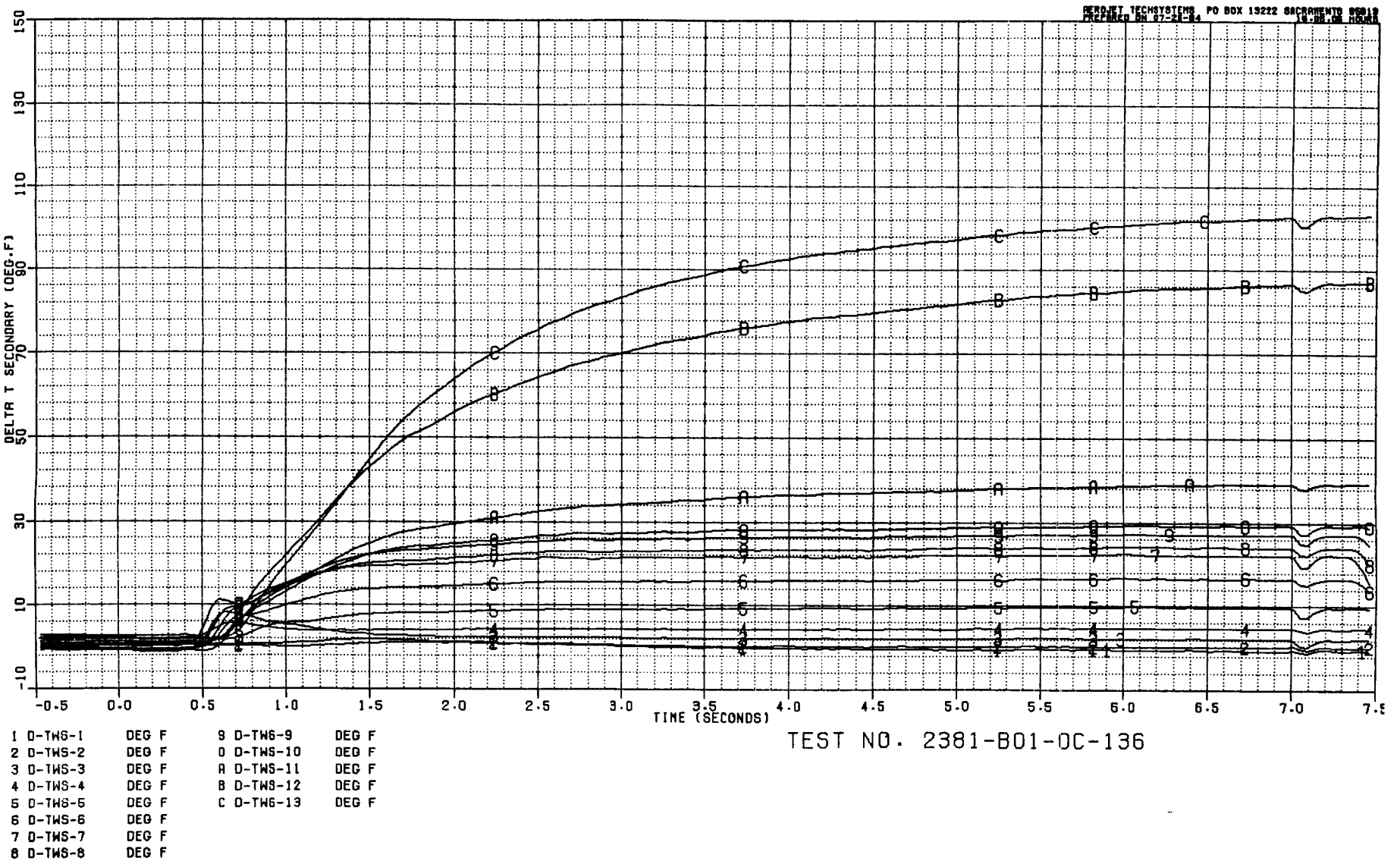

Figure B-75. Test 136 Secondary Chamber Temperature Data Summary

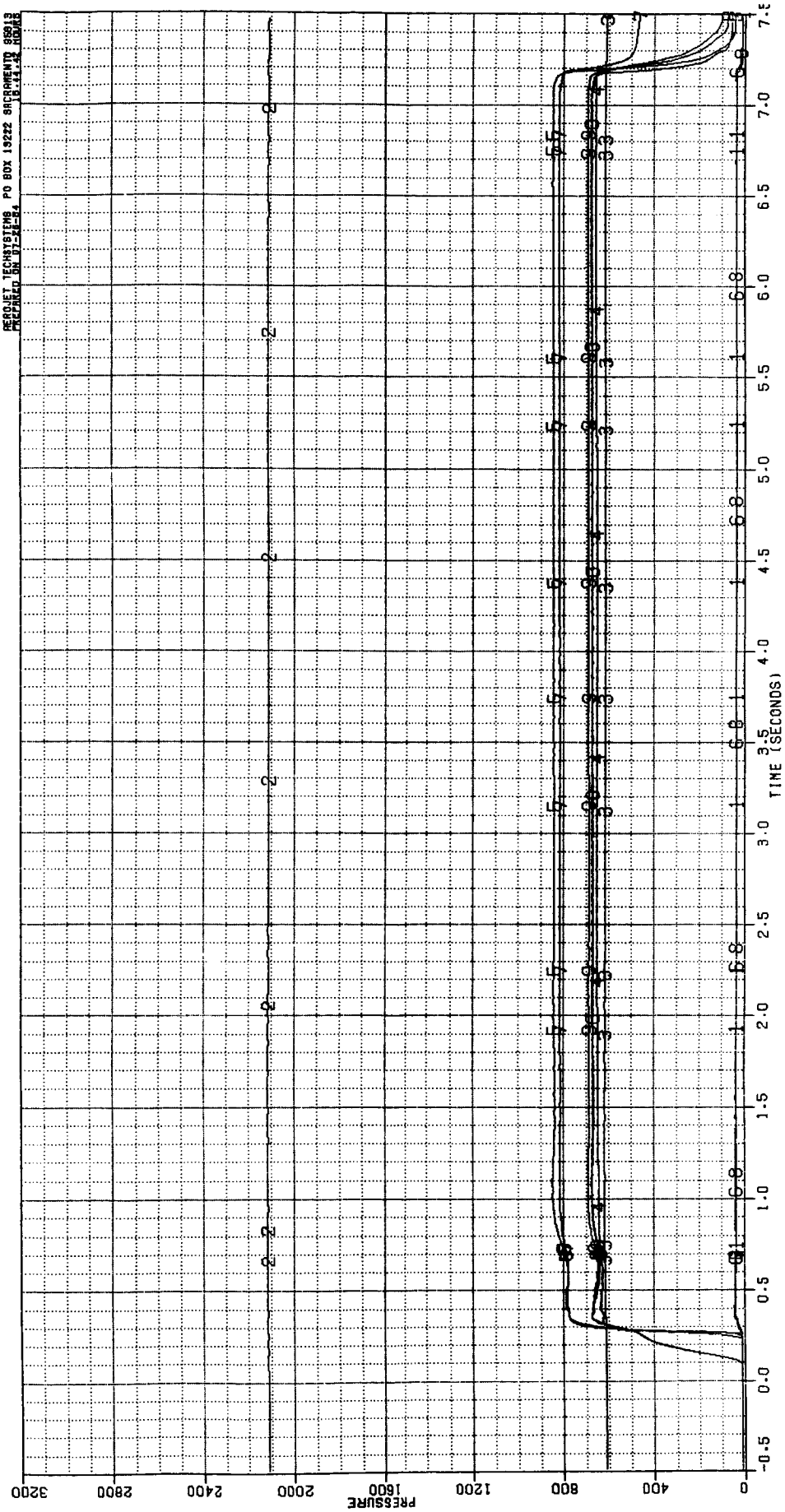

Figure B-76. Test 137 Pressure Data Summary

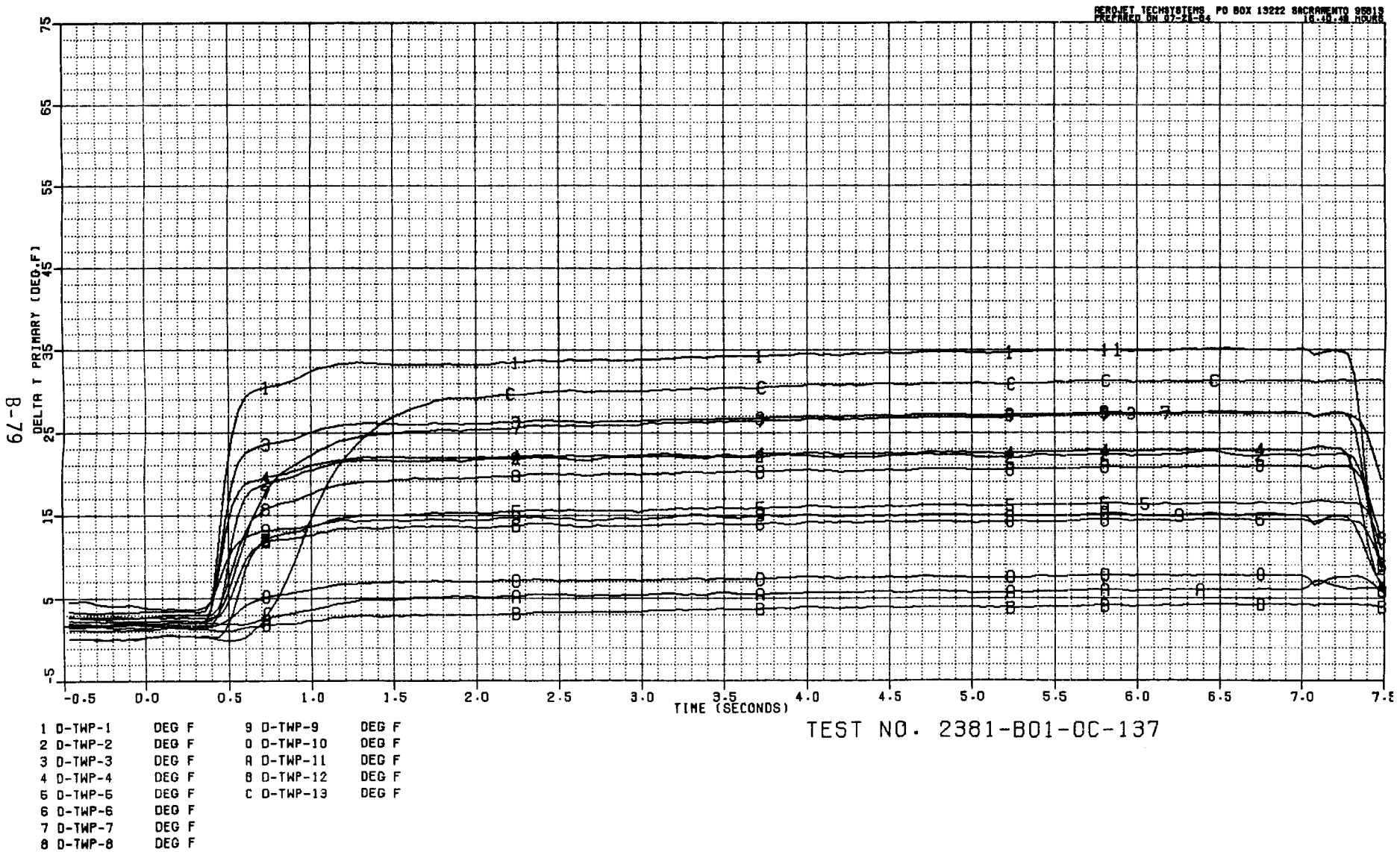

Figure B-77. Test 137 Primary Chamber Temperature Data Summary

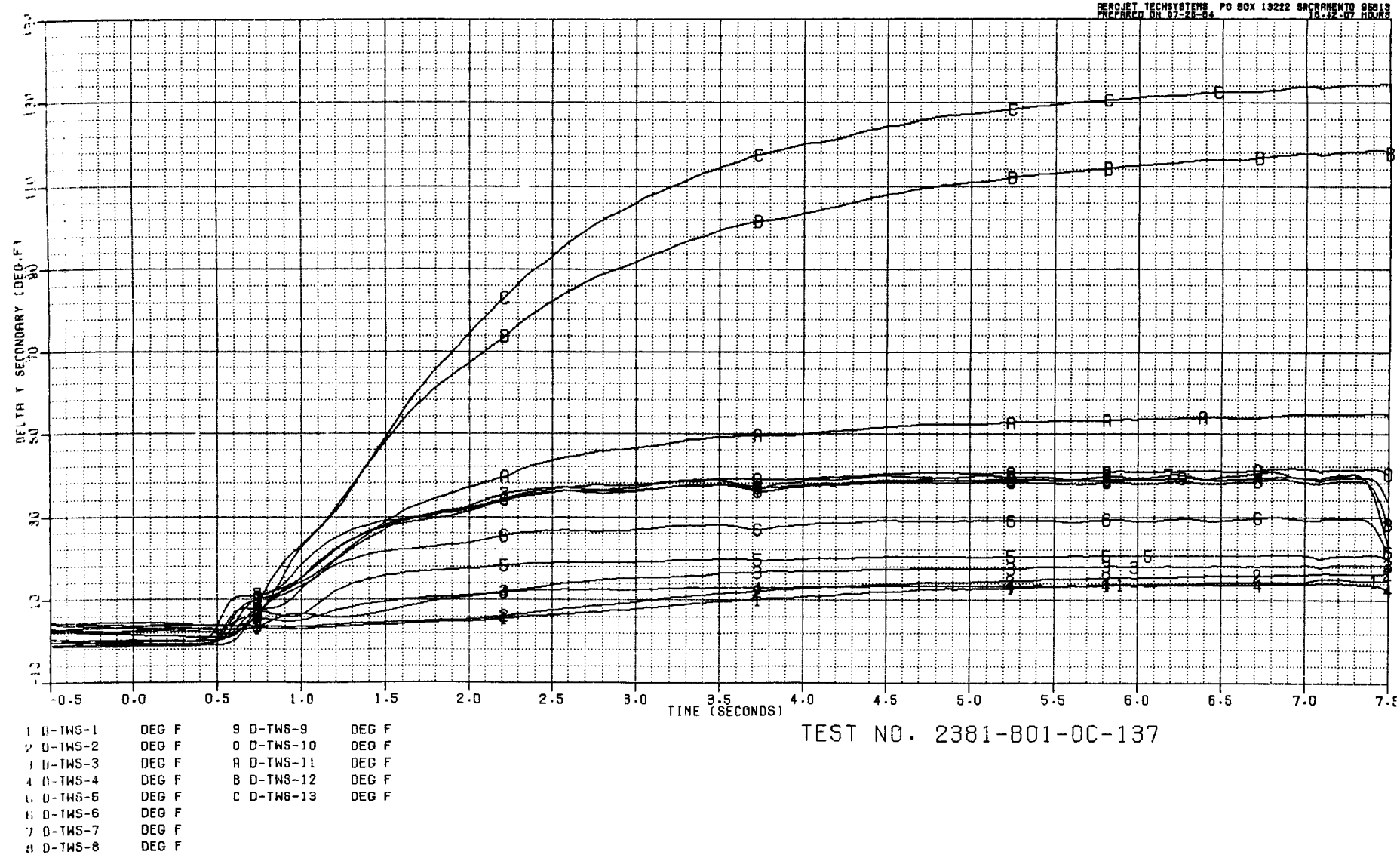

Figure B-78. Test 137 Secondary Chamber Temperature Data Summary

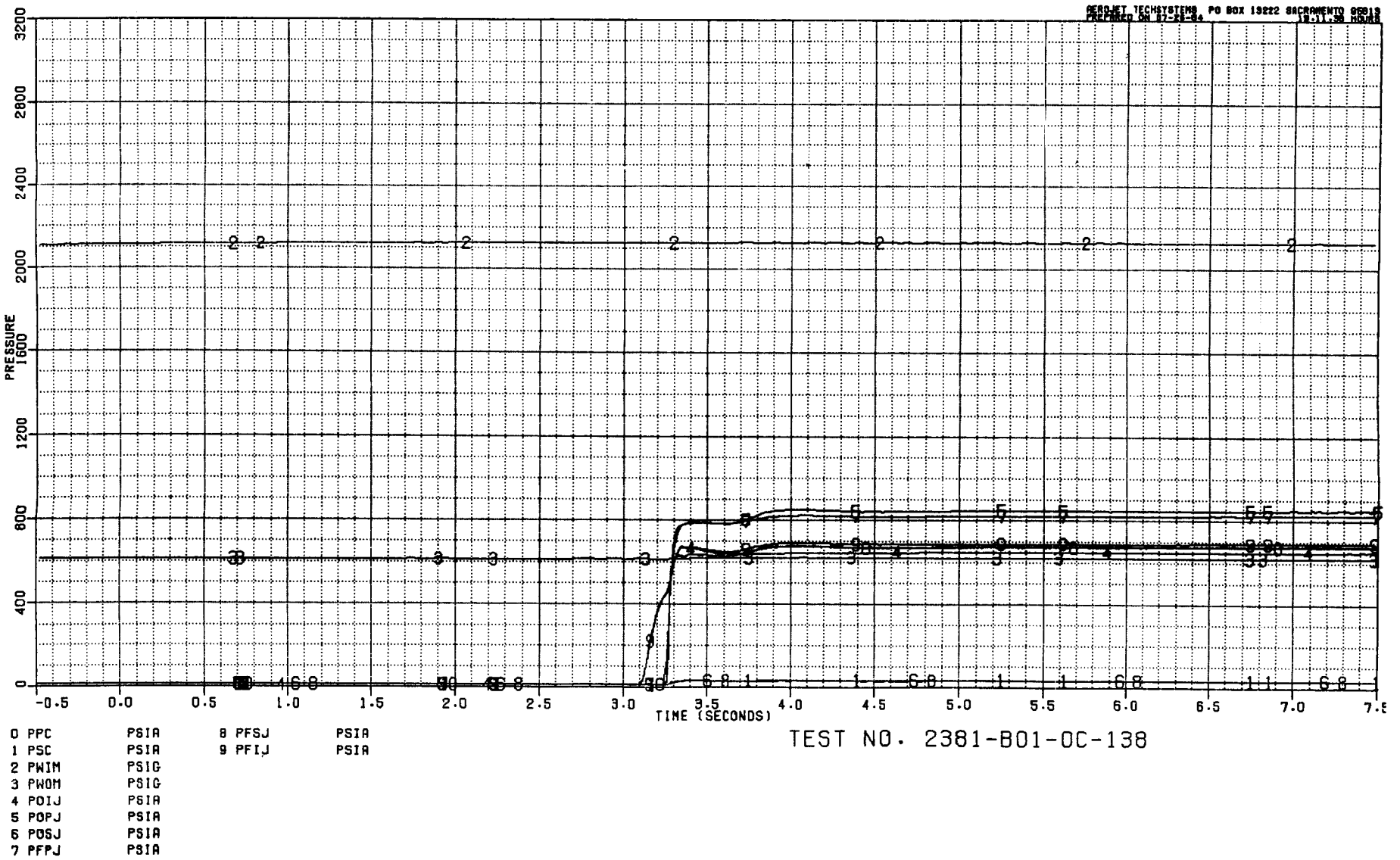

Figure B-79. Test 138 Pressure Data Summary

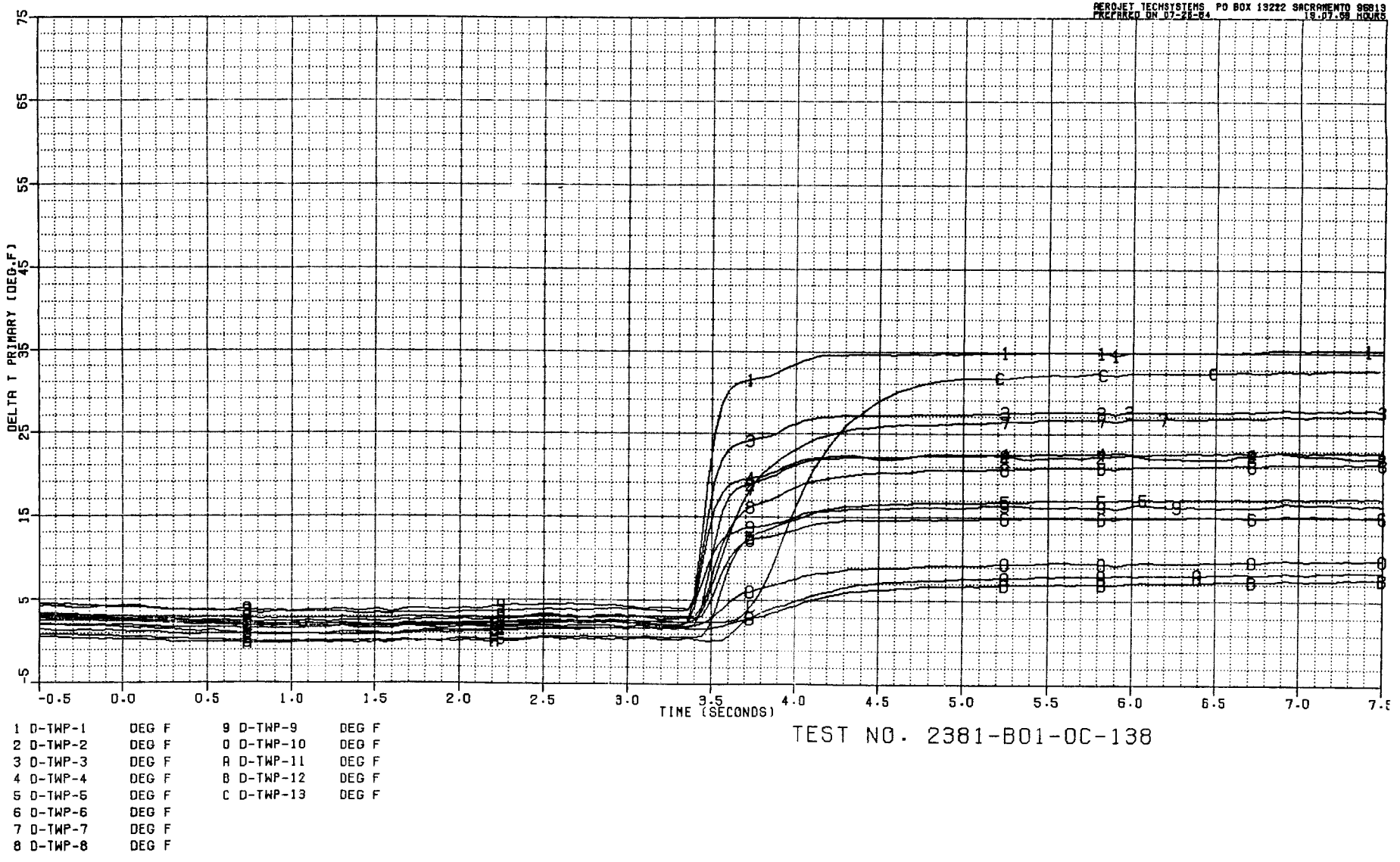

Figure B-80. Test 138 Primary Chamber Temperature Data Summary

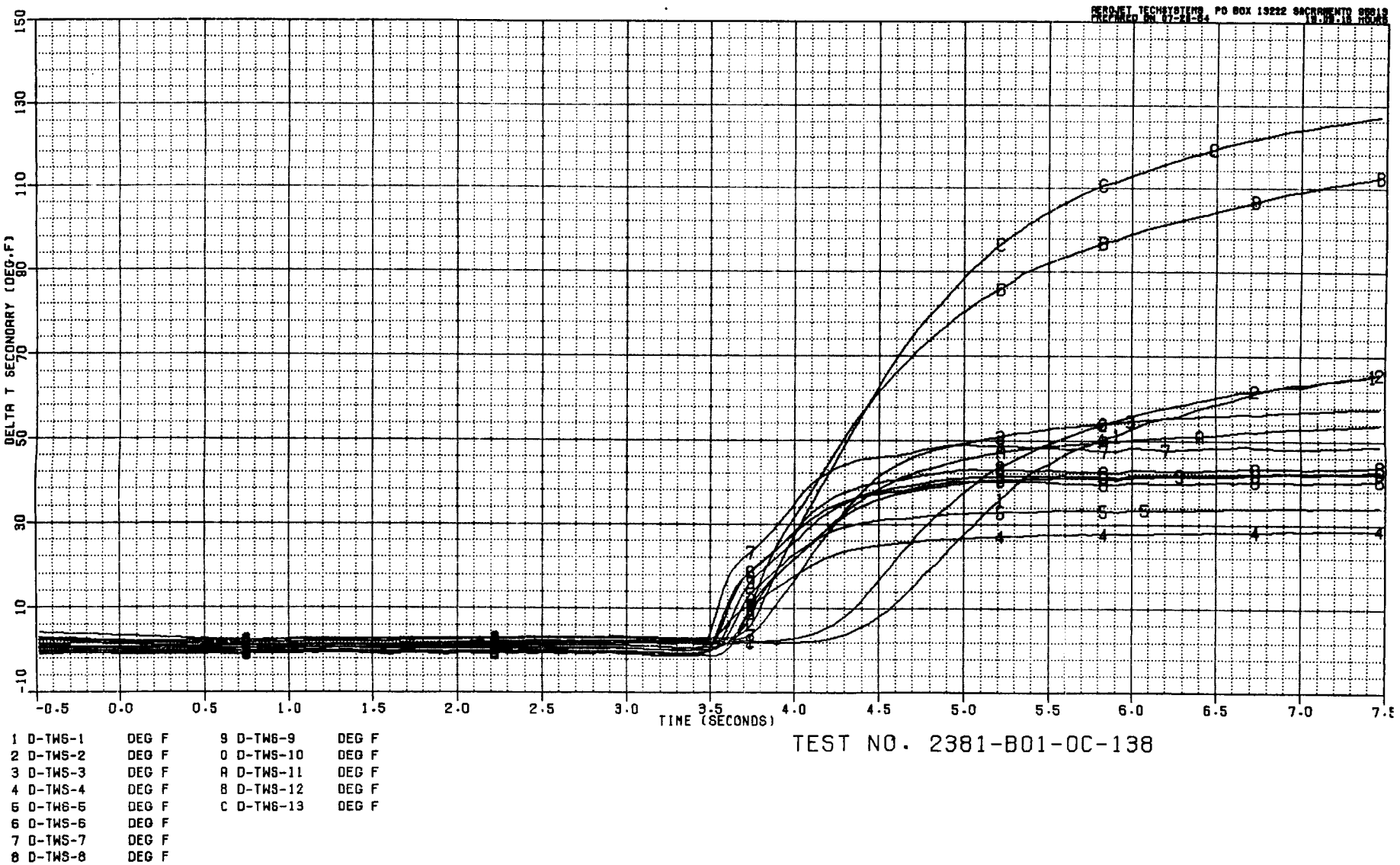

Figure B-81. Test 138 Secondary Chamber Temperature Data Summary

ORIGINAL PAGE IS
OF POOR QUALITY

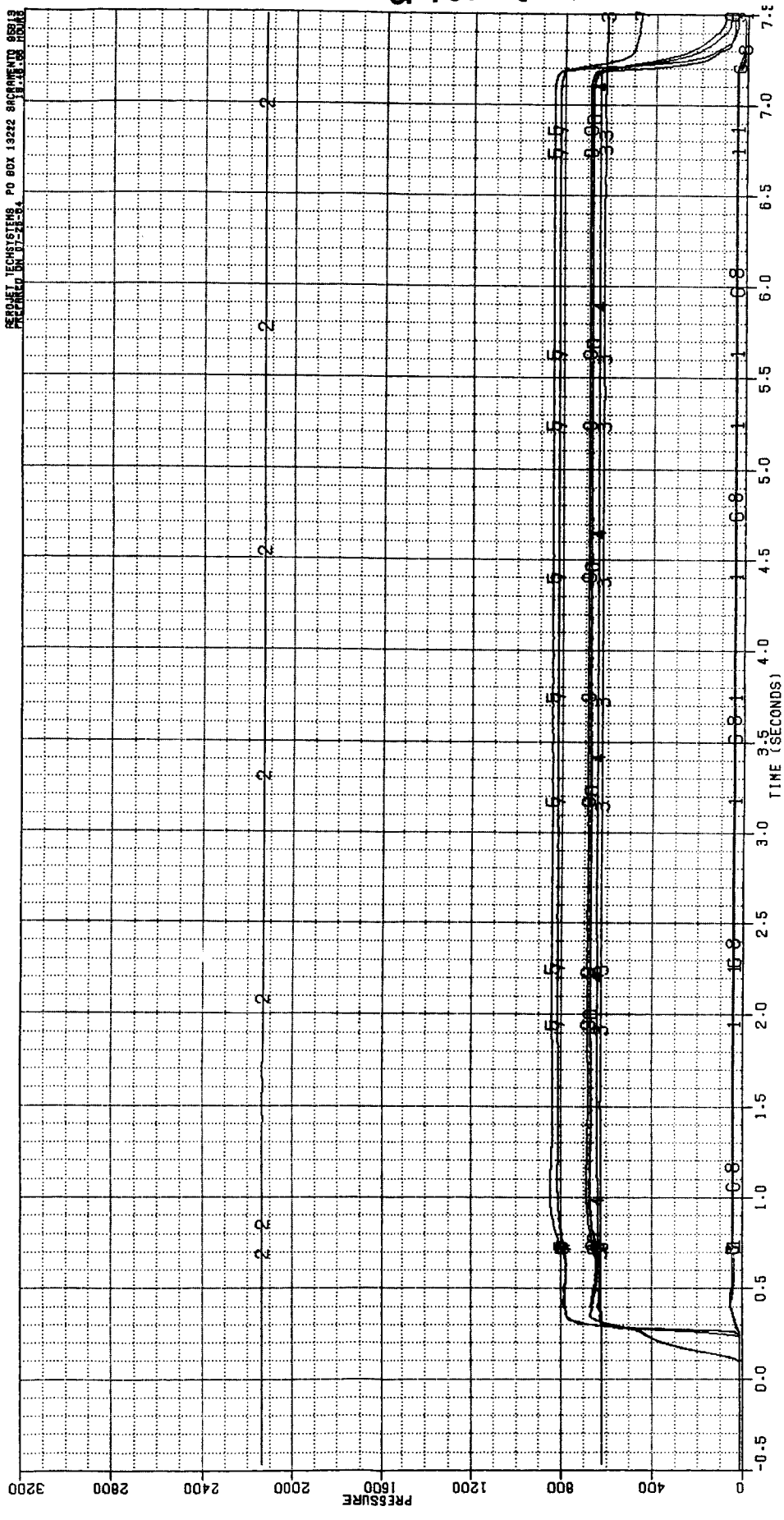

Figure B-82. Test 139 Pressure Data Summary

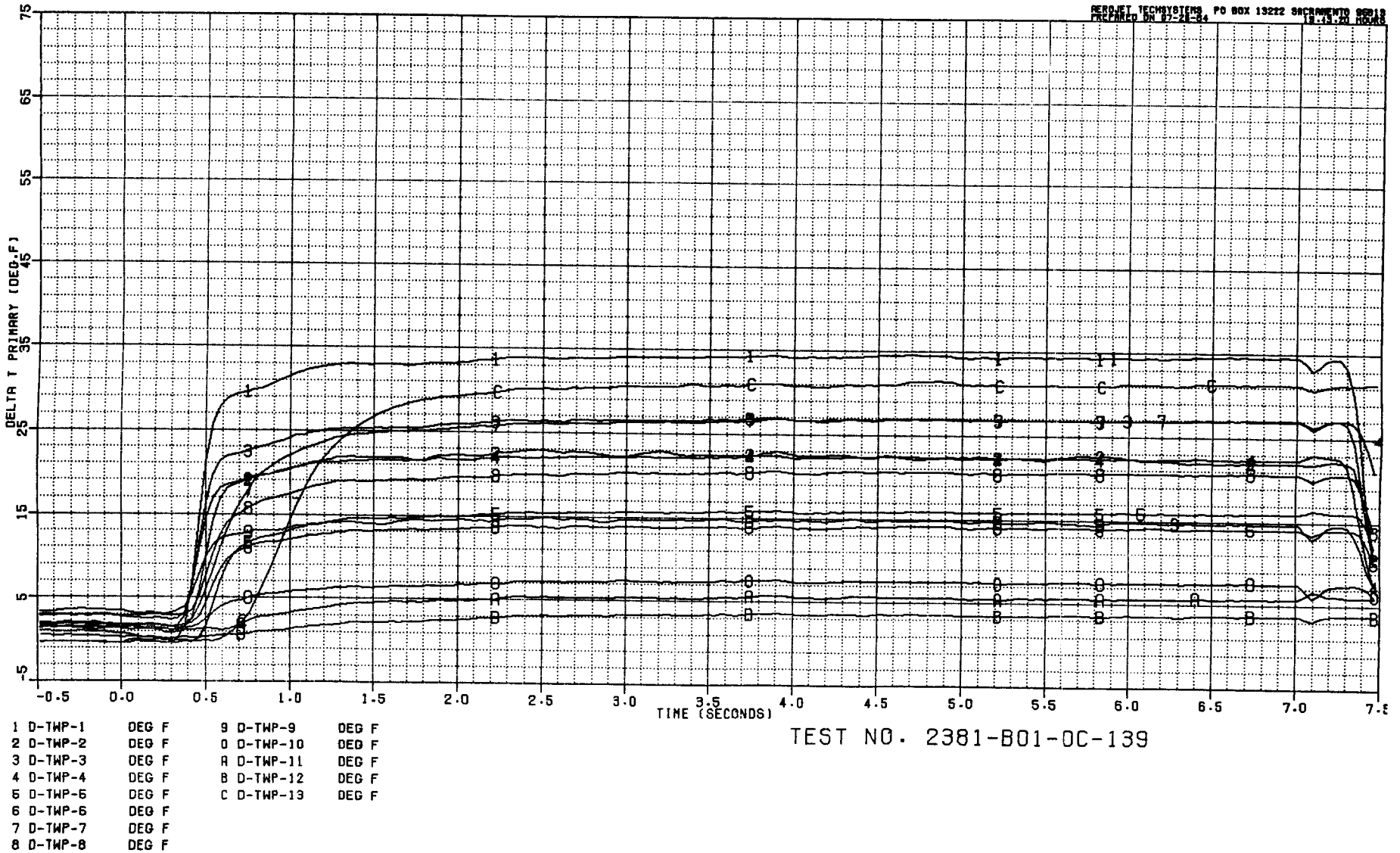

Figure B-83. Test 139 Primary Chamber Temperature Data Summary

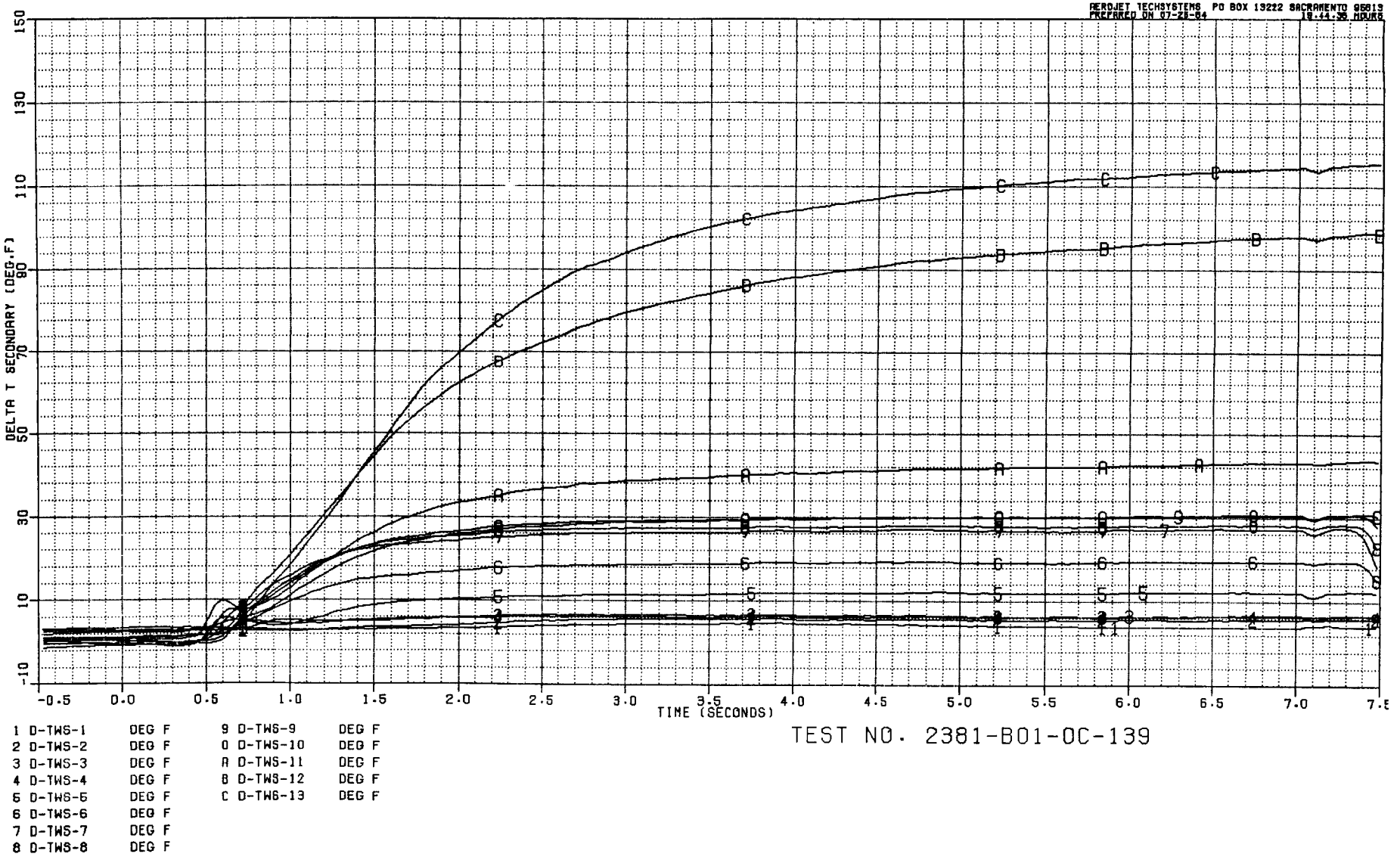

Figure B-84. Test 139 Secondary Chamber Temperature Data Summary

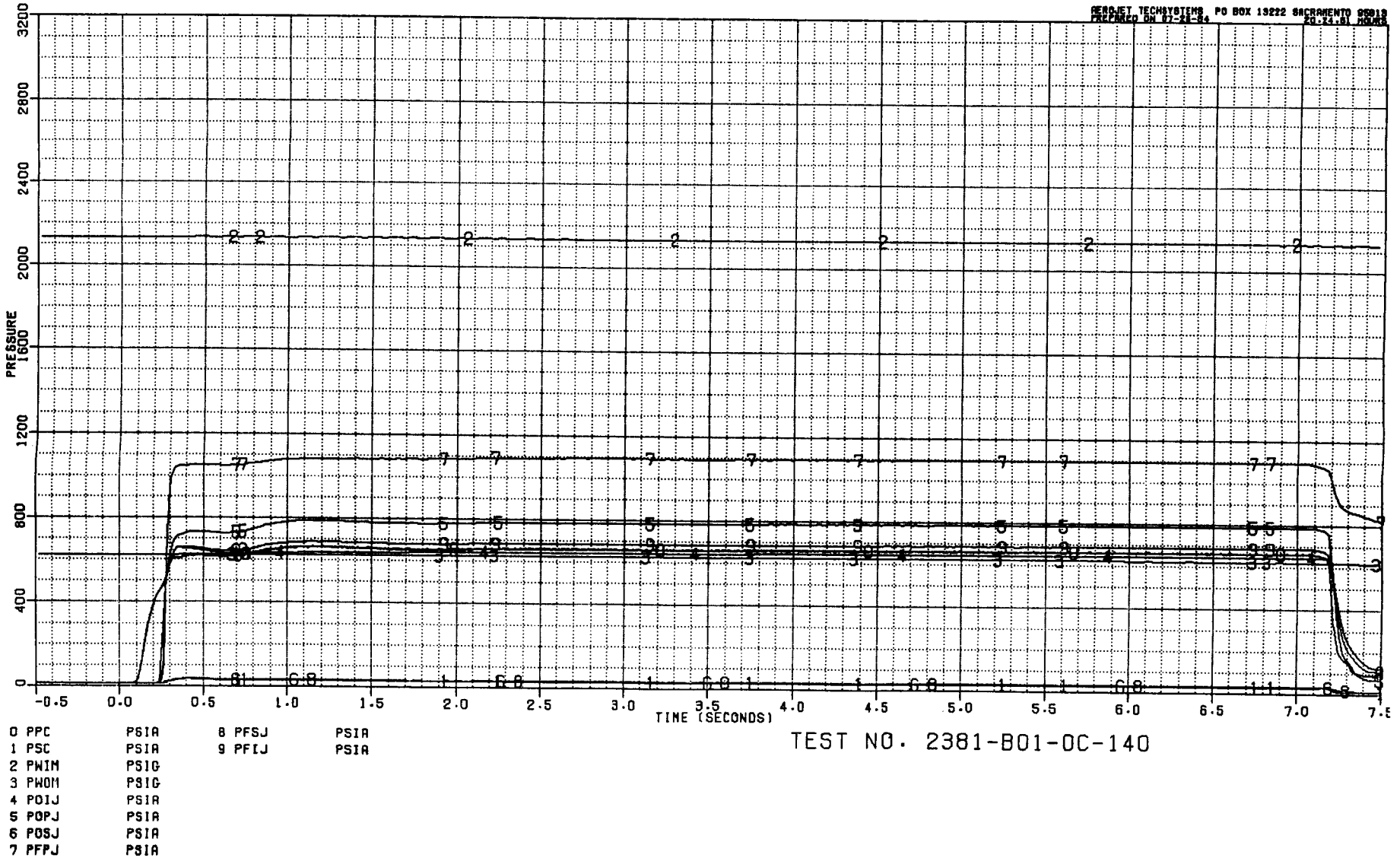

Figure B-85. Test 140 Pressure Data Summary

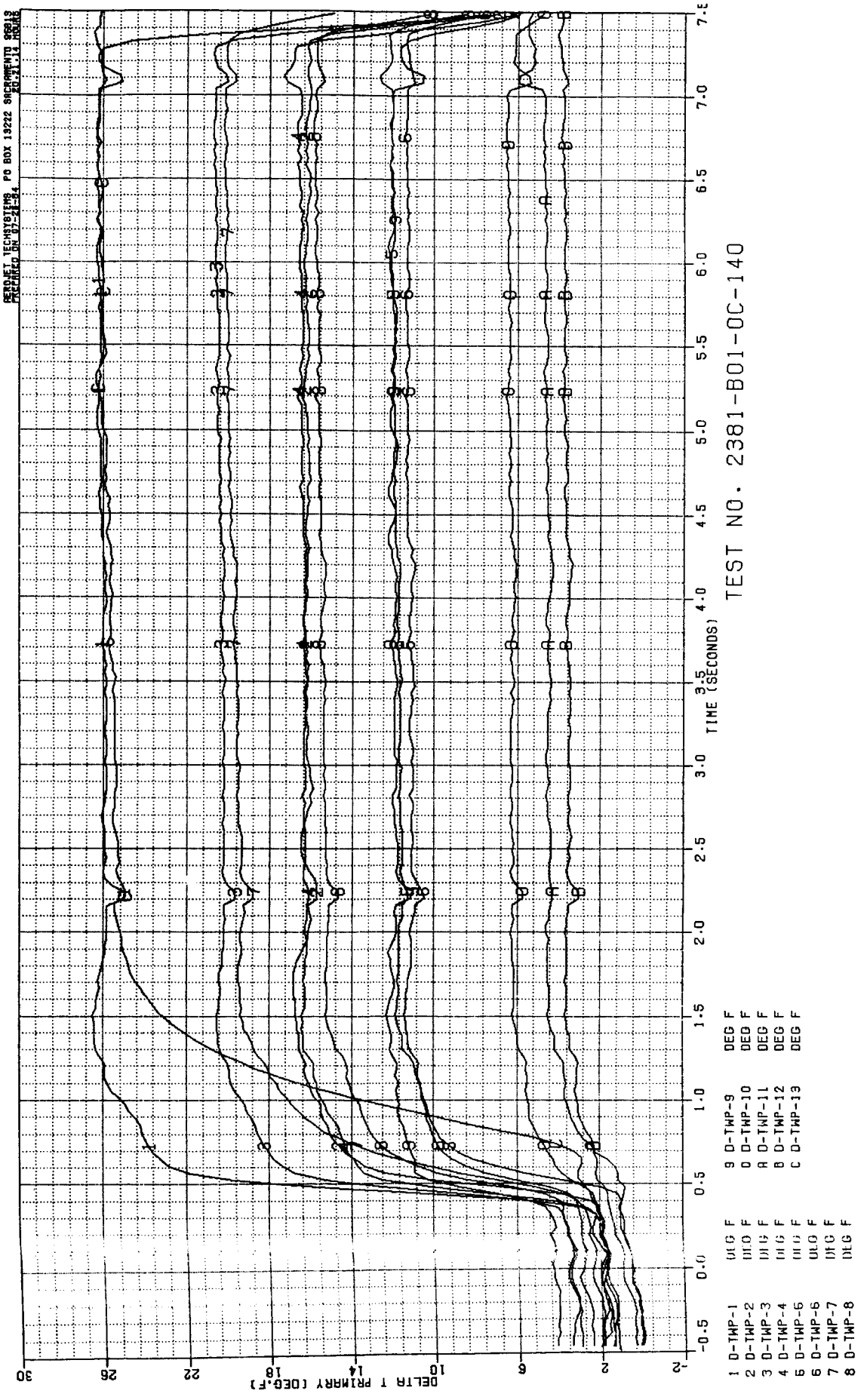

Figure B-86. Test 140 Primary Chamber Temperature Data Summary

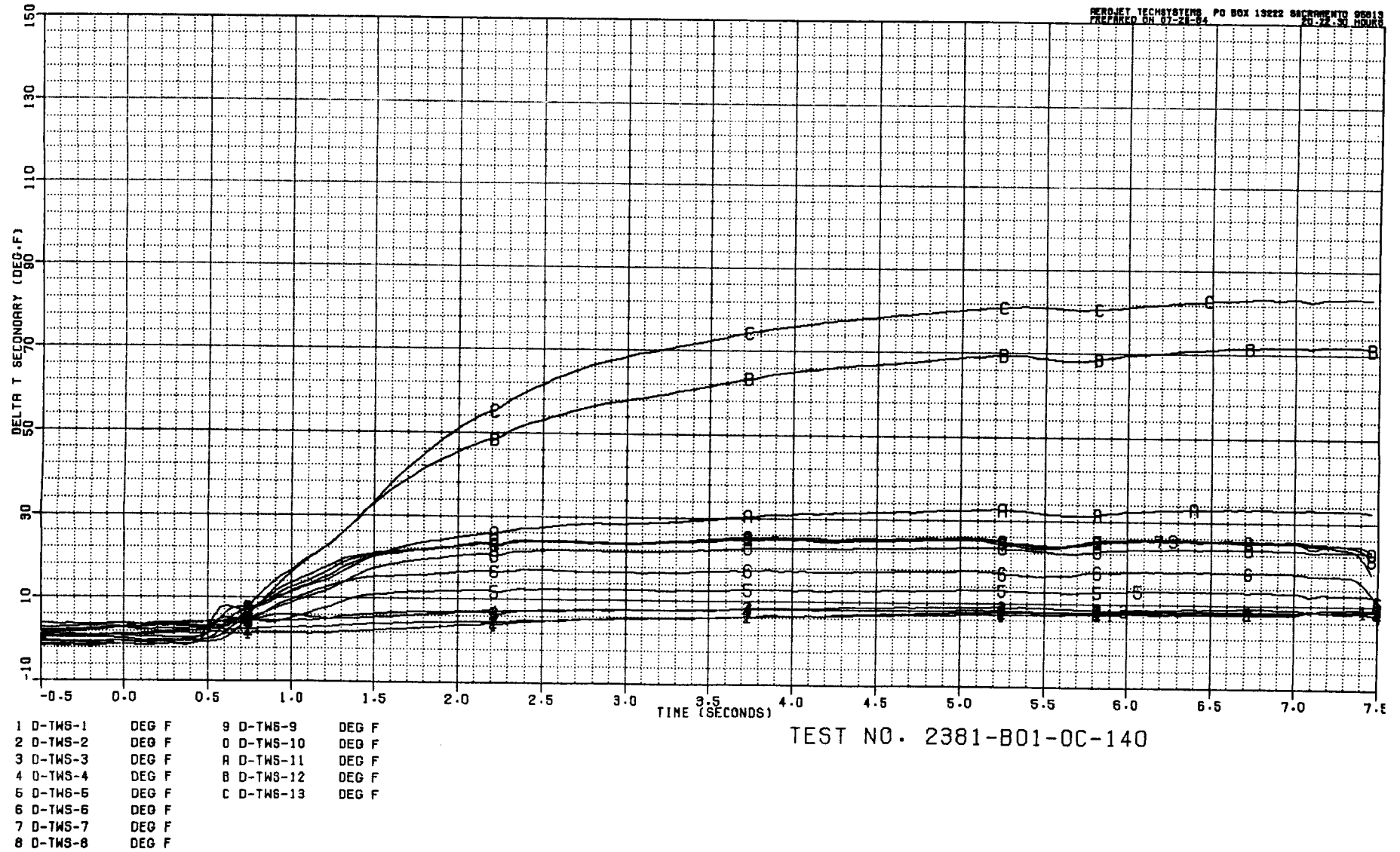

Figure B-87. Test 140 Secondary Chamber Temperature Data Summary

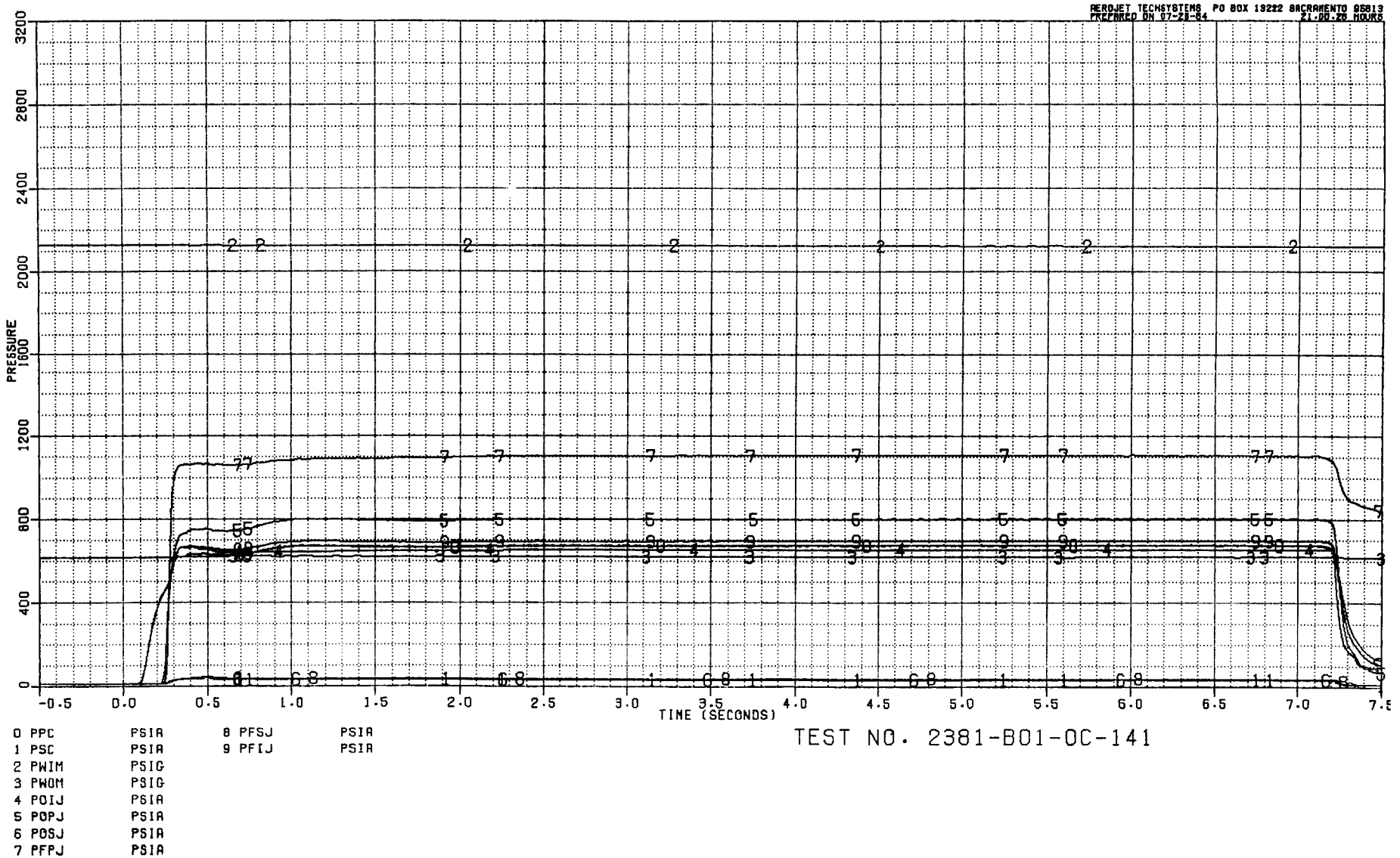

Figure B-88. Test 141 Pressure Data Summary

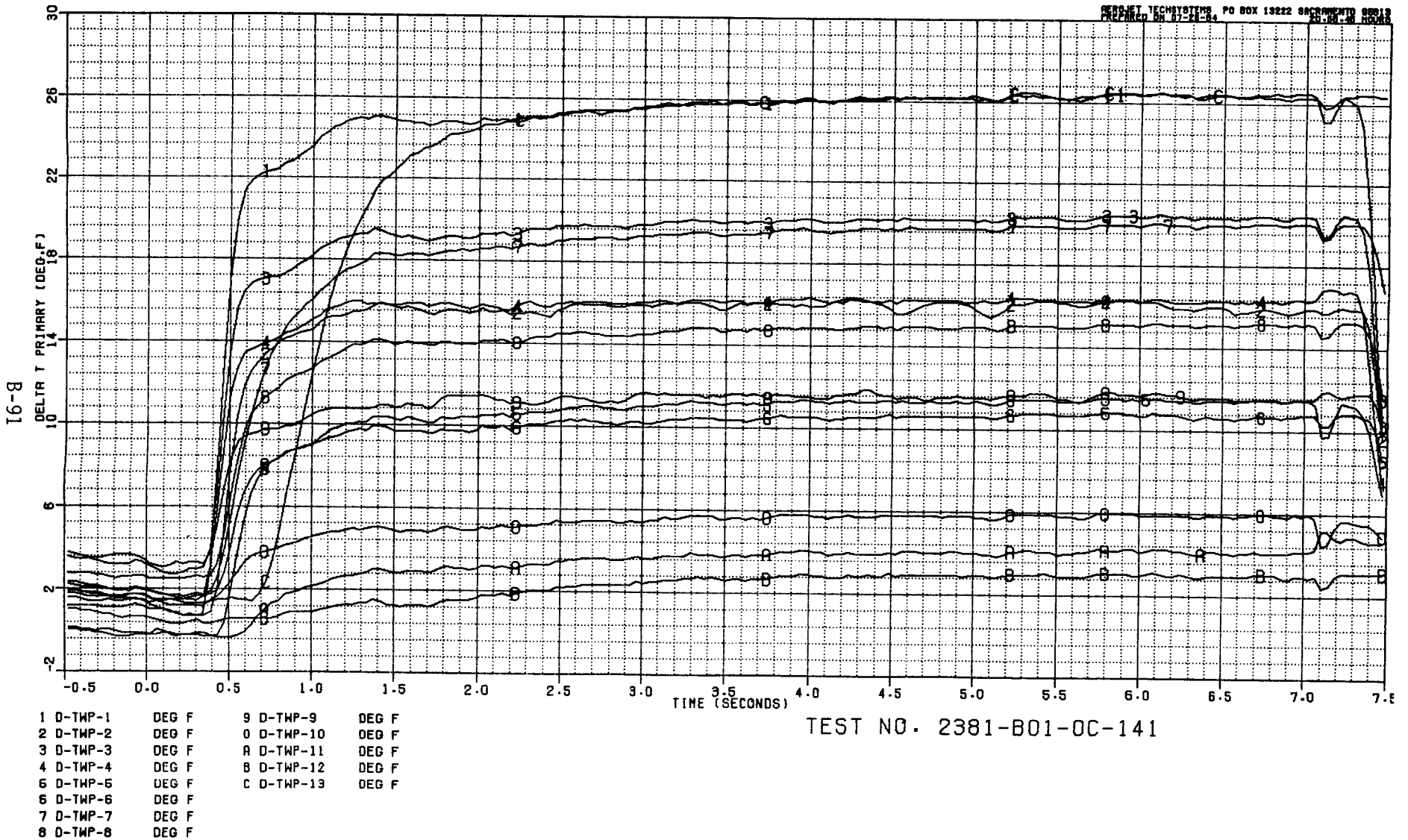

Figure B-89. Test 141 Primary Chamber Temperature Data Summary

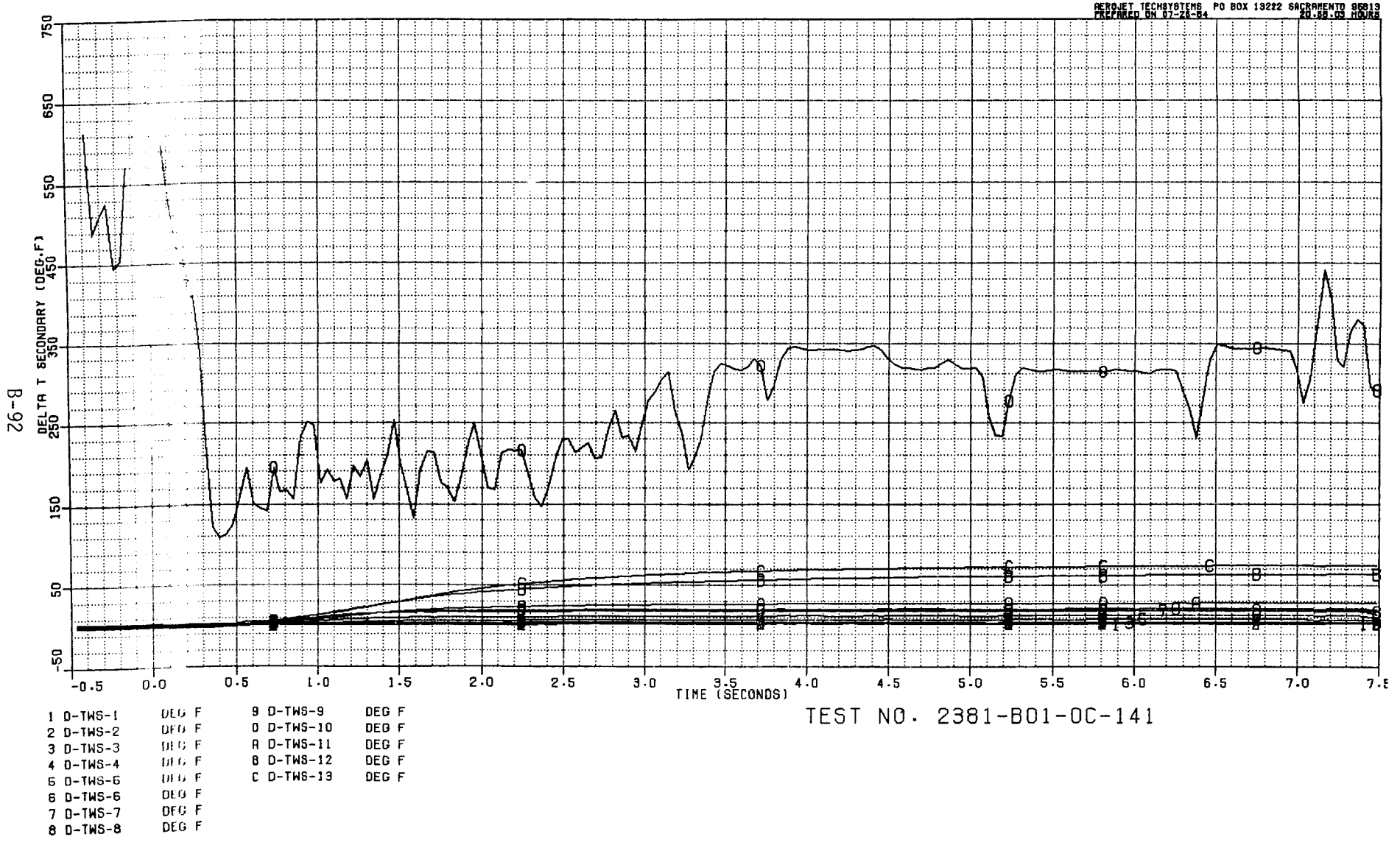

Figure B-90. Test 141 Secondary Chamber Temperature Data Summary

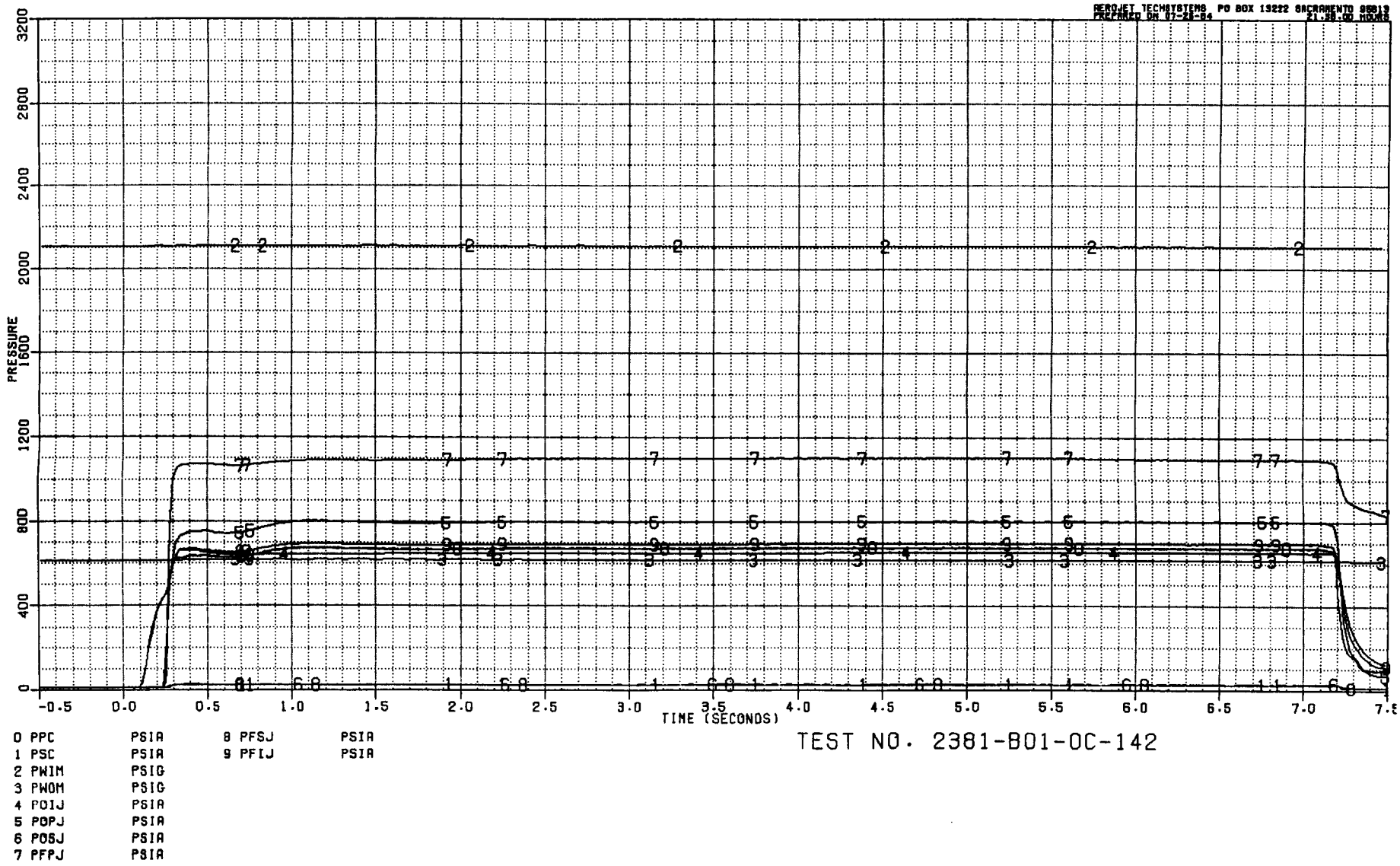

Figure B-91. Test 142 Pressure Data Summary

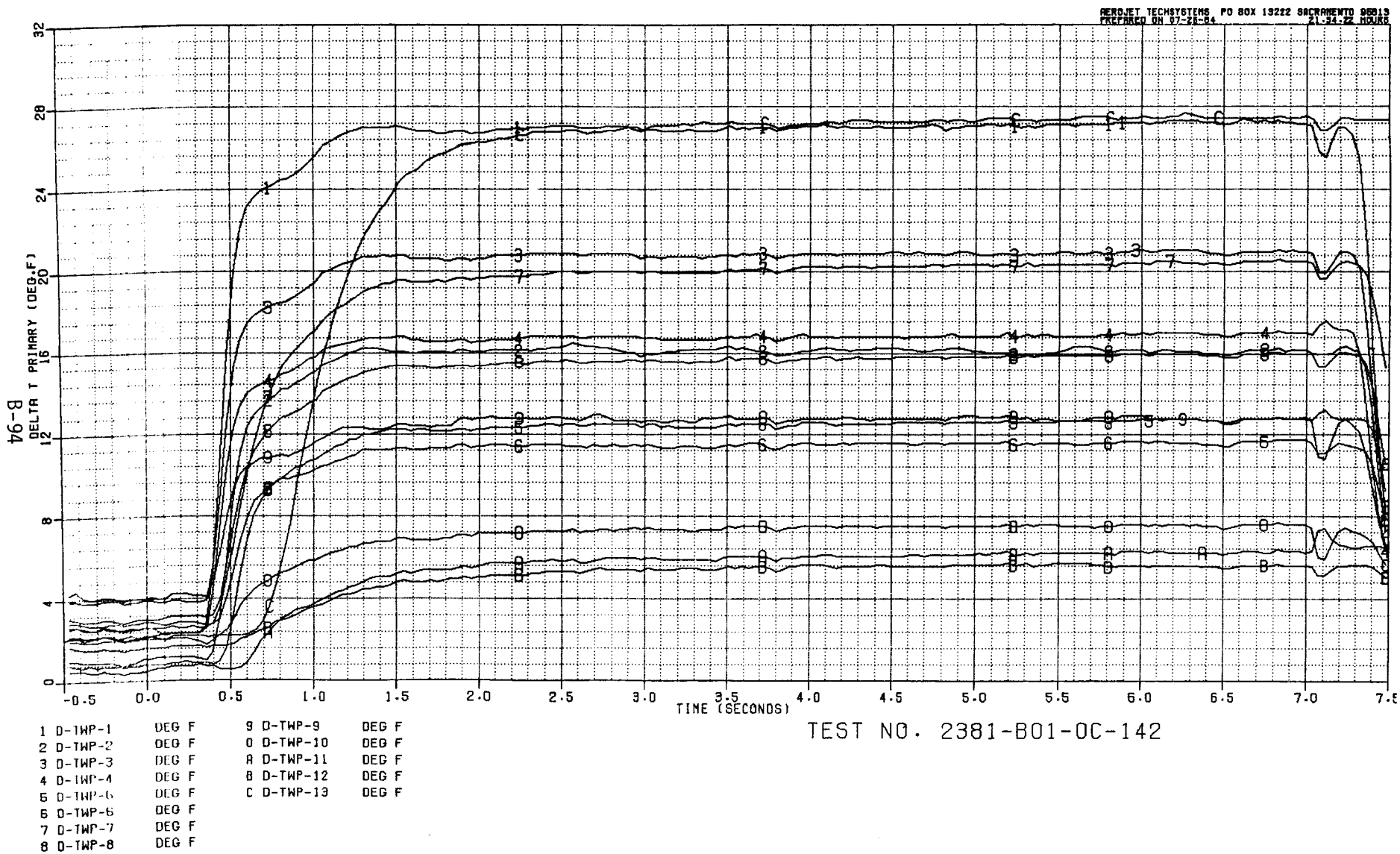

Figure B-92. Test 142 Primary Chamber Temperature Data Summary

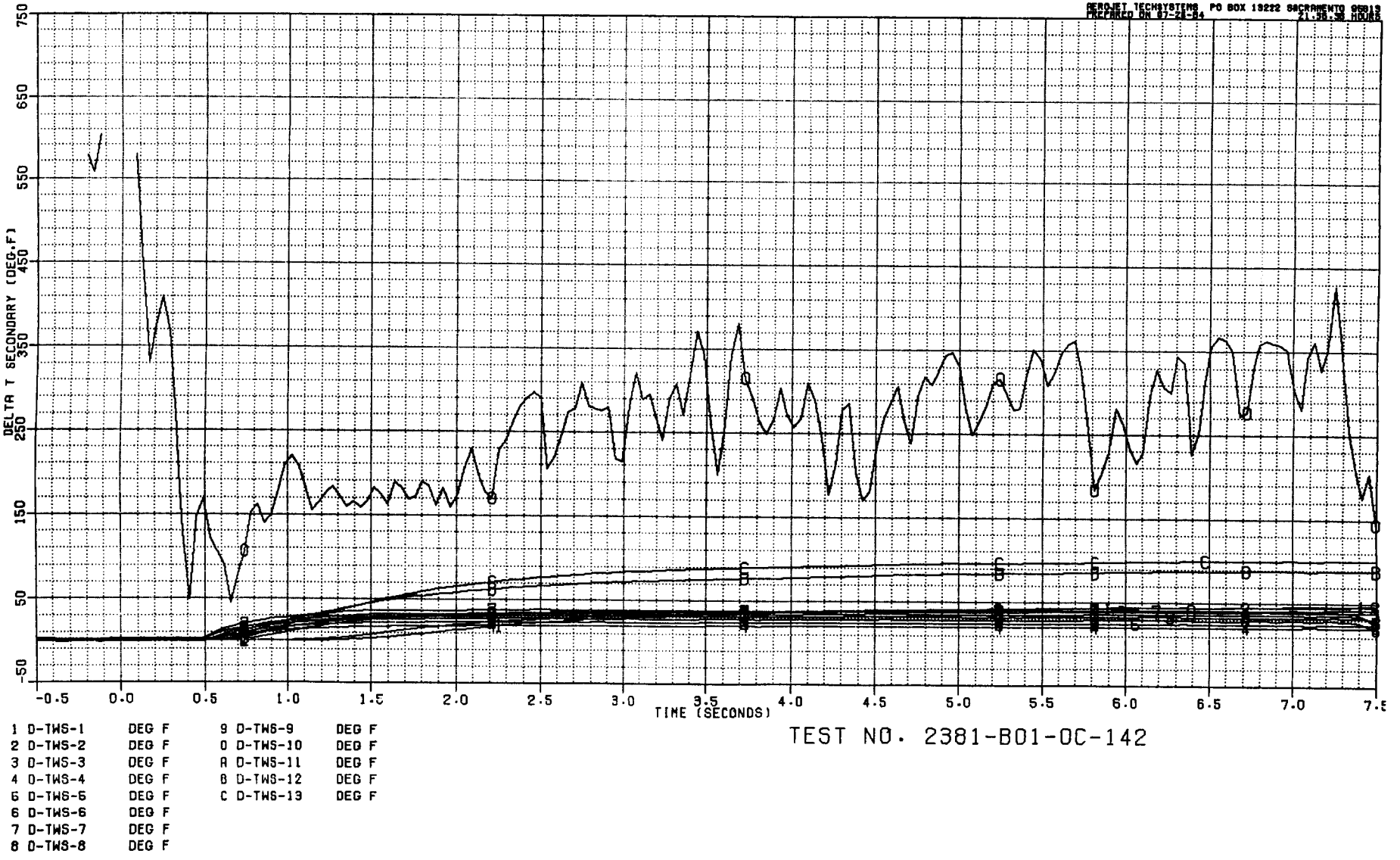

Figure B-93. Test 142 Secondary Chamber Temperature Data Summary

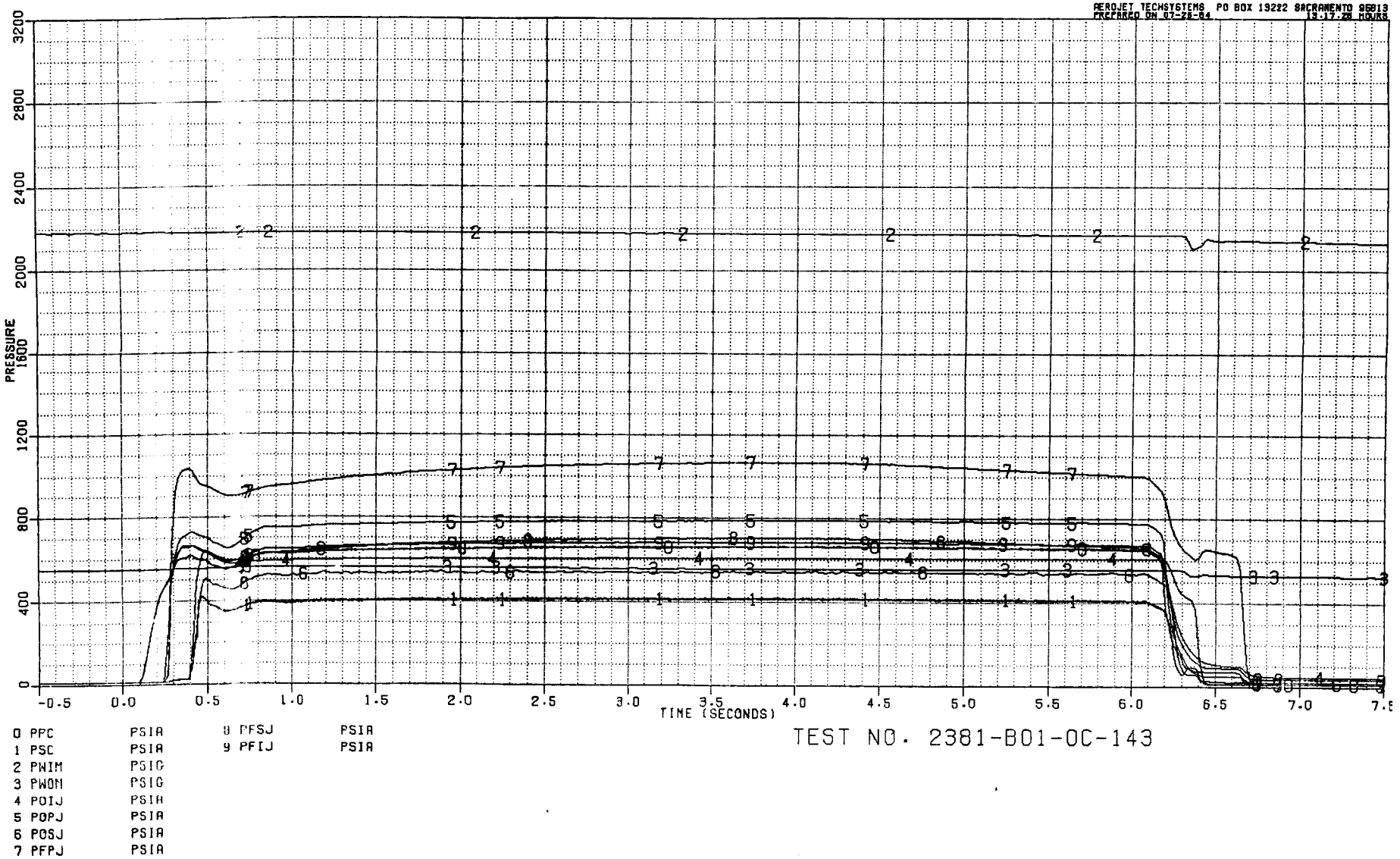

Figure B-94. Test 143 Pressure Data Summary

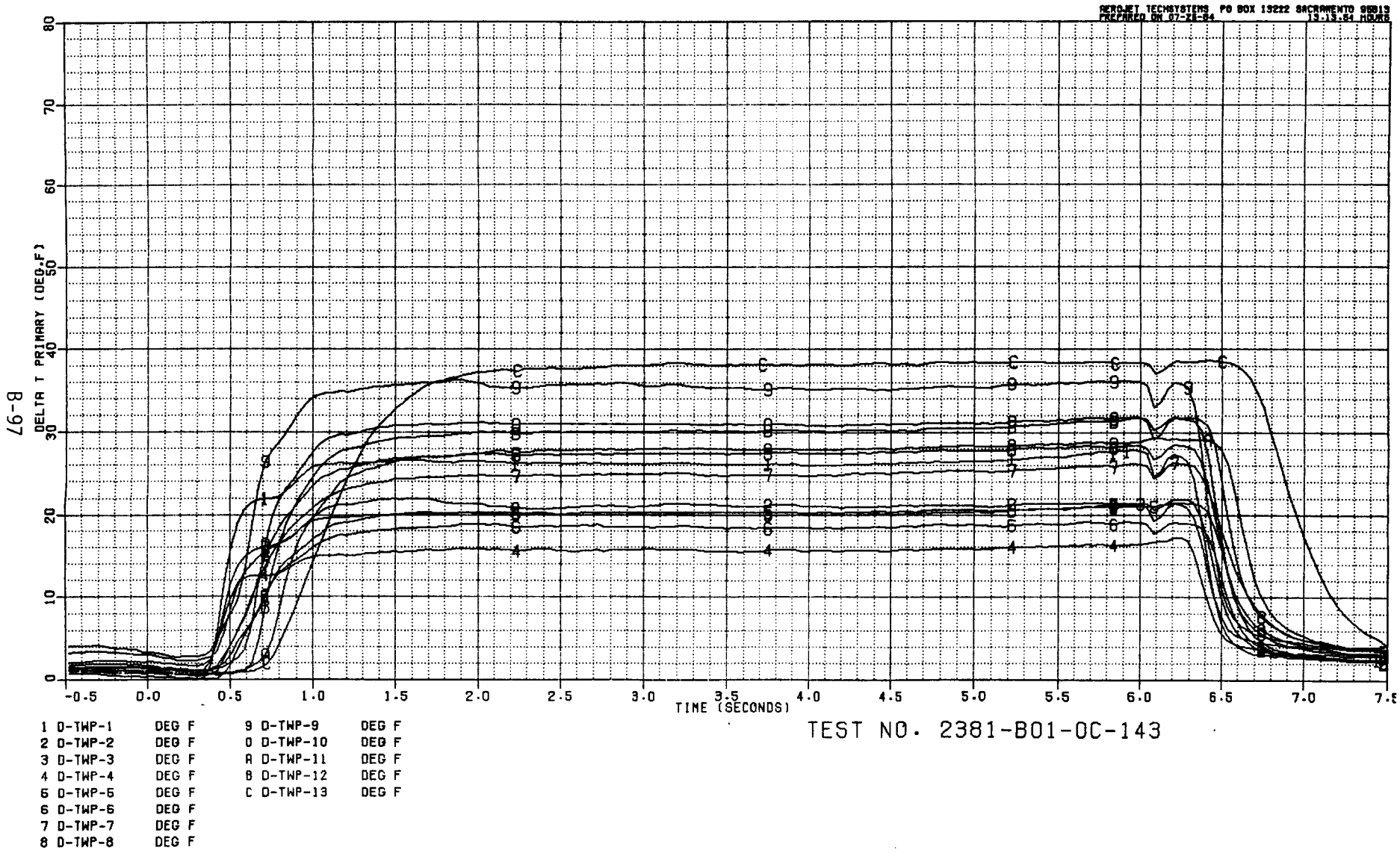

Figure B-95. Test Primary Chamber Temperature Data Summary

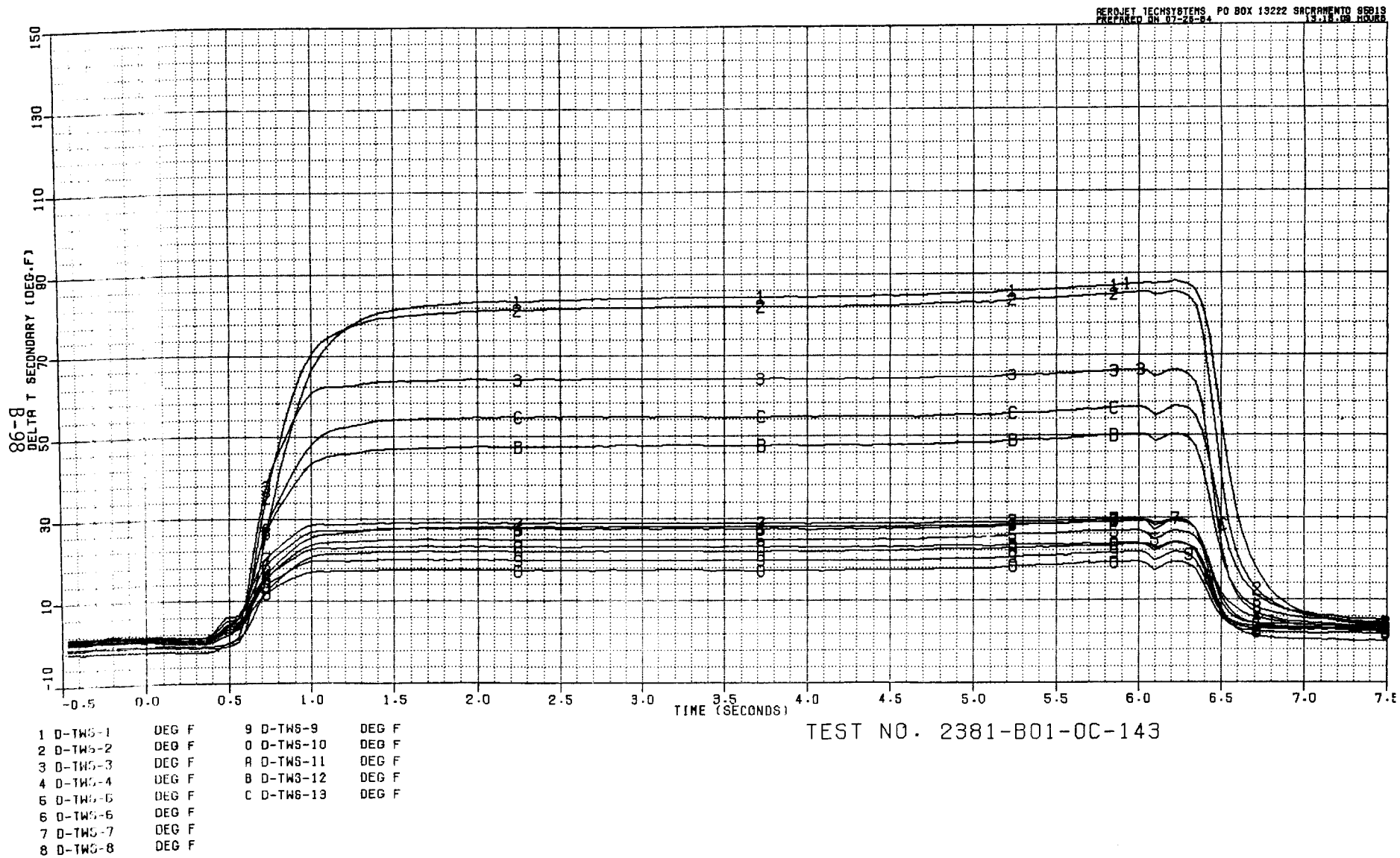

Figure B-96. Test 143 Secondary Chamber Temperature Data Summary

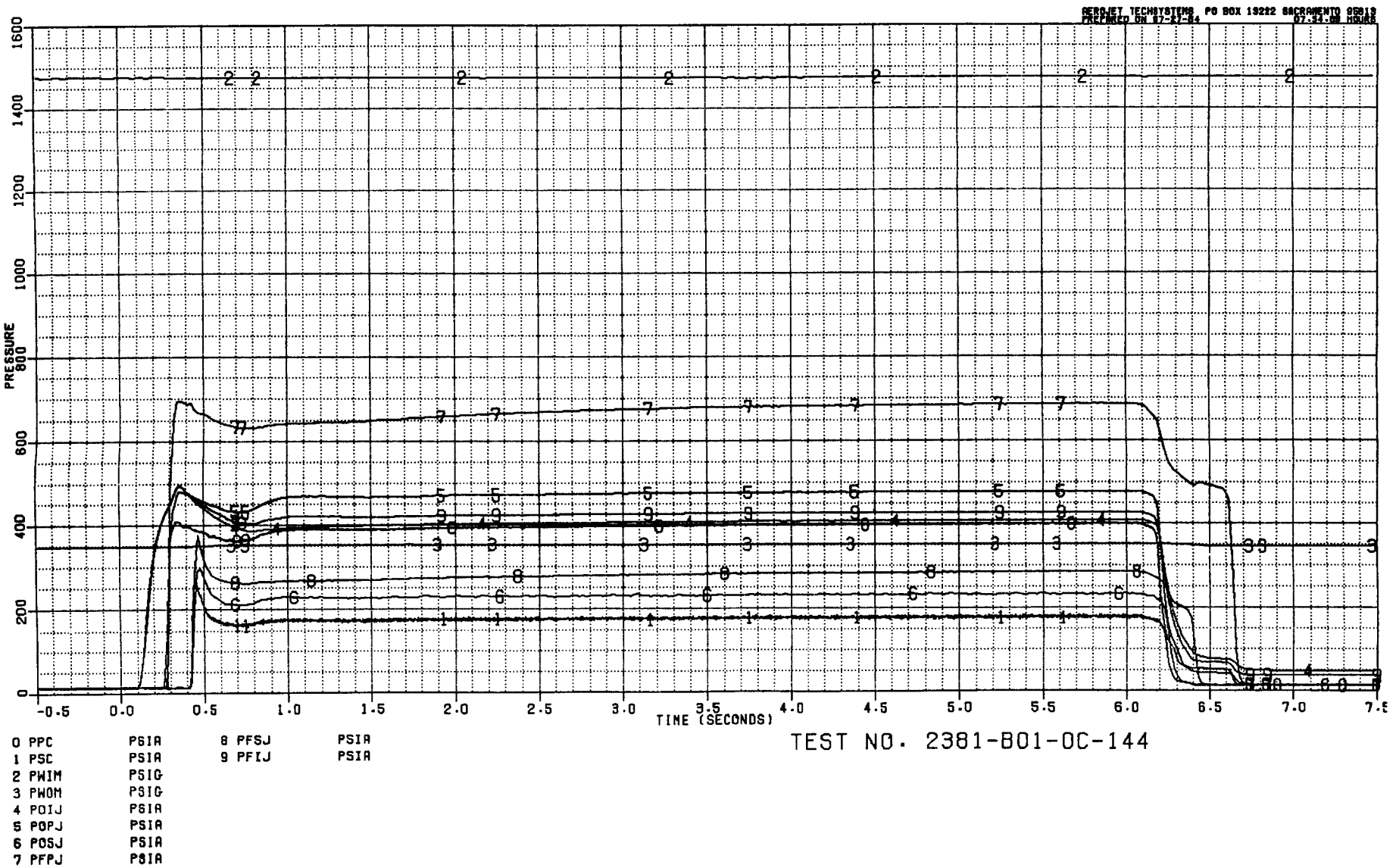

Figure B-97. Test 144 Pressure Data Summary

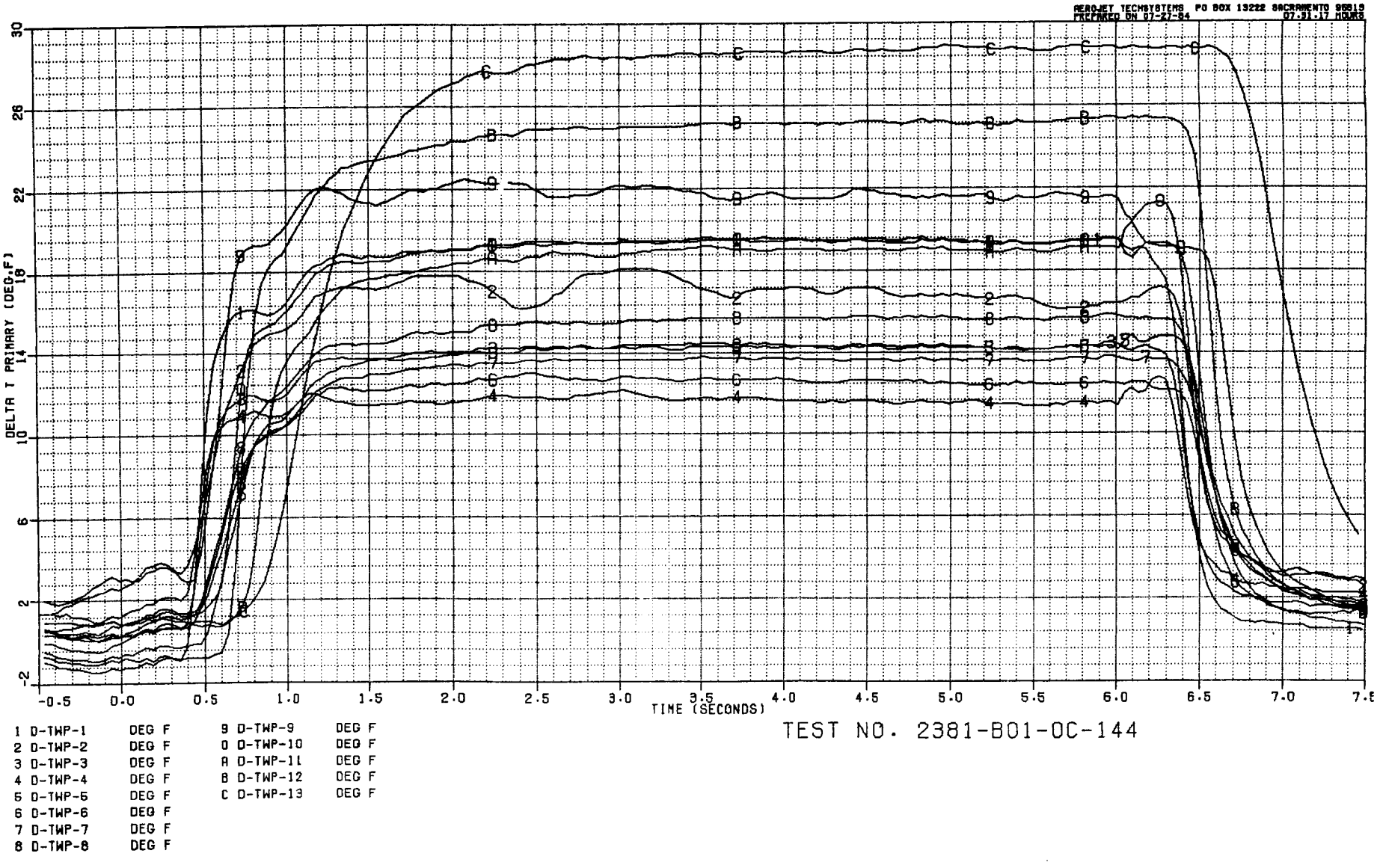

Figure B-98. Test 144 Primary Chamber Temperature Data Summary

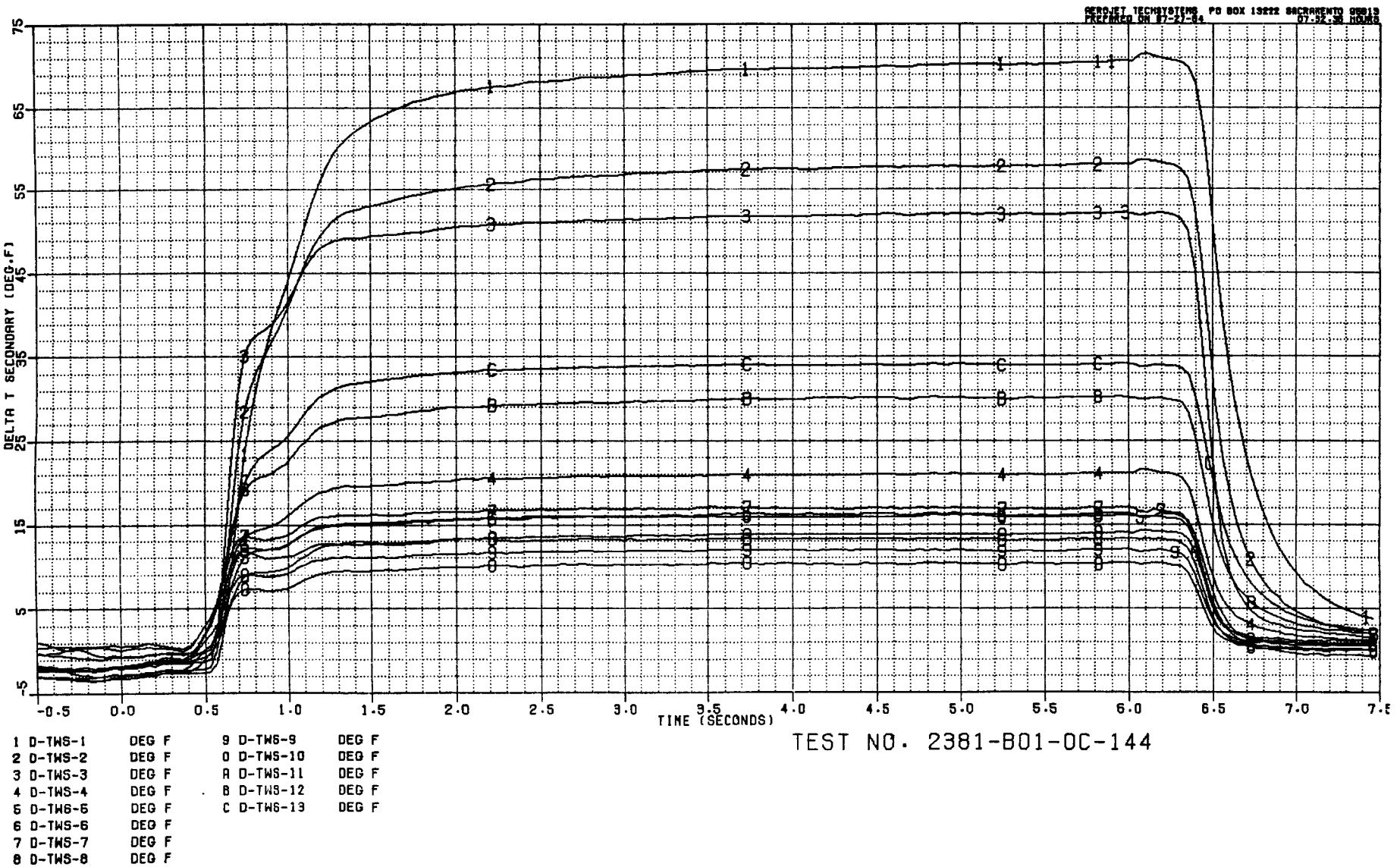

Figure B-99. Test 144 Secondary Chamber Temperature Data Summary

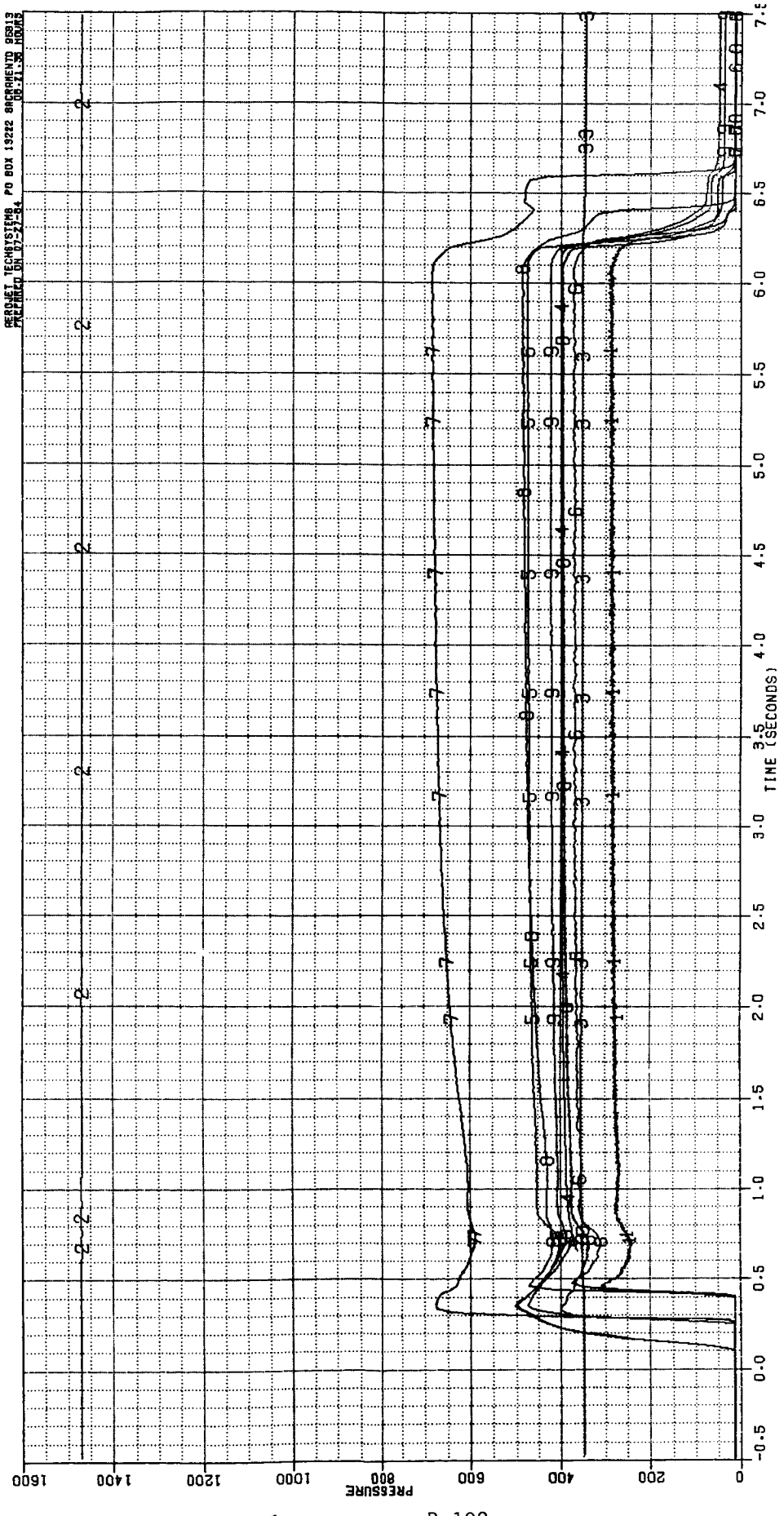

Figure 100. Test 145 Pressure Data Summary

C-5

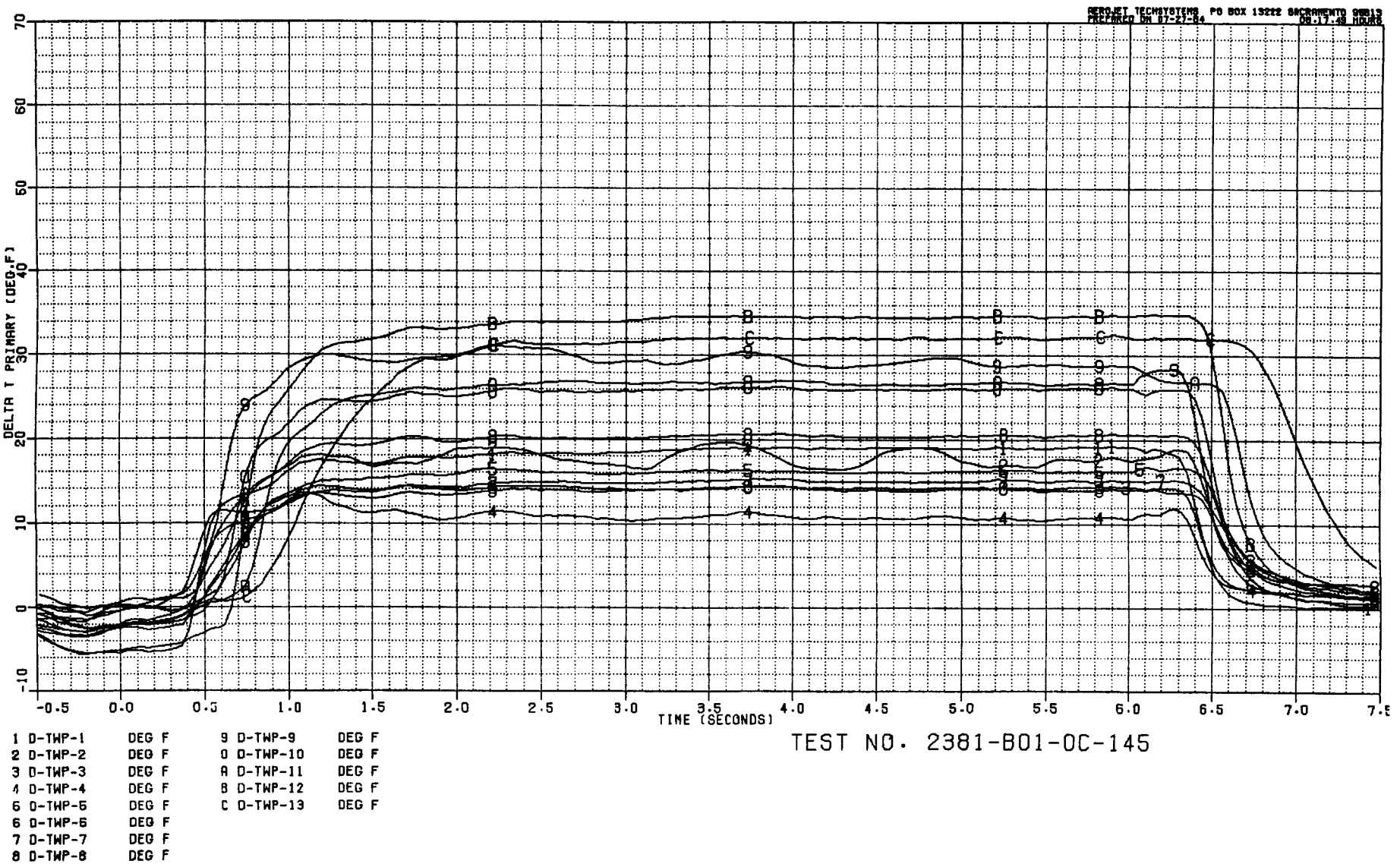

Figure B-101. Test 145 Primary Chamber Temperature Data Summary

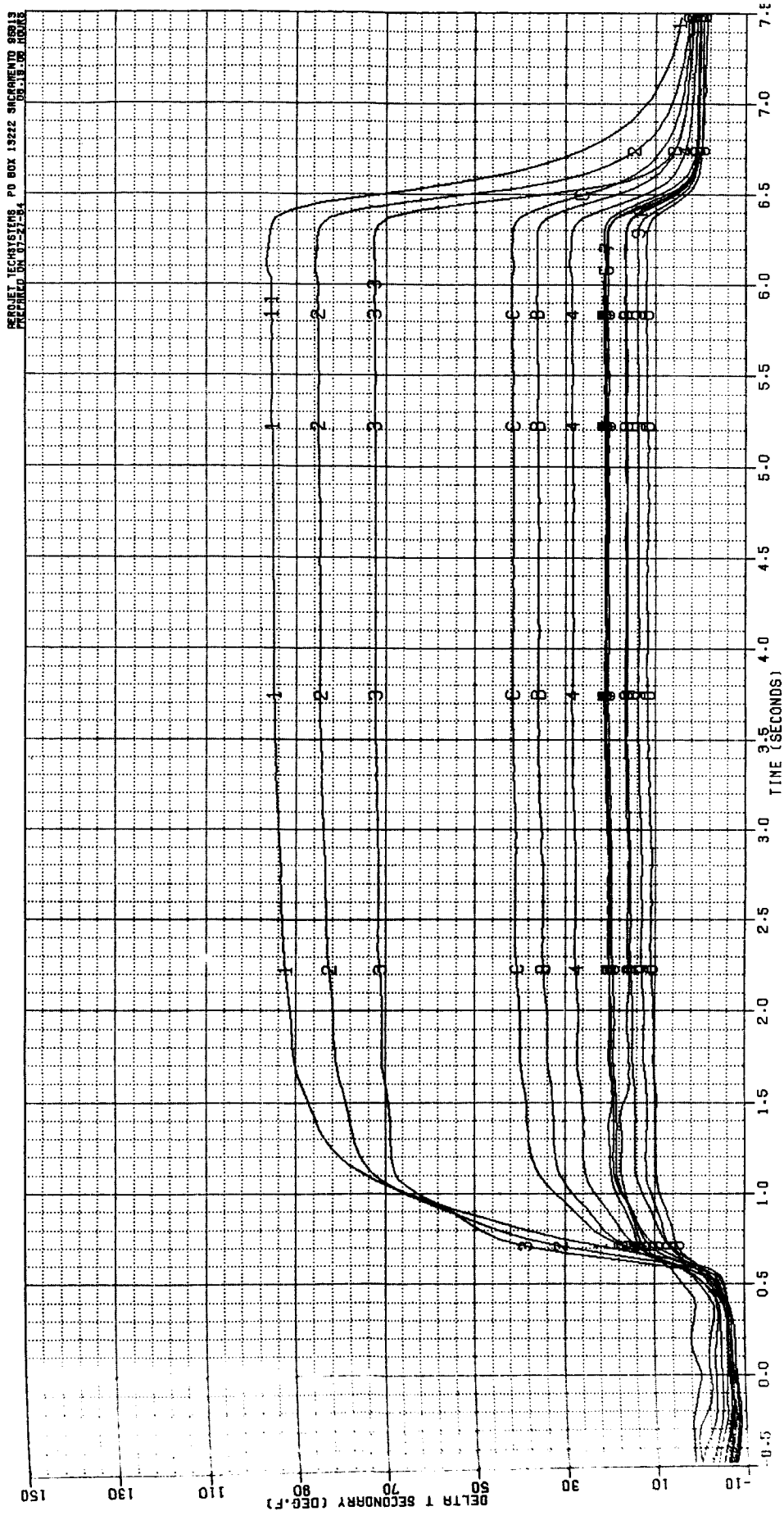

Figure B-102. Test 145 Secondary Chamber Temperature Data Summary

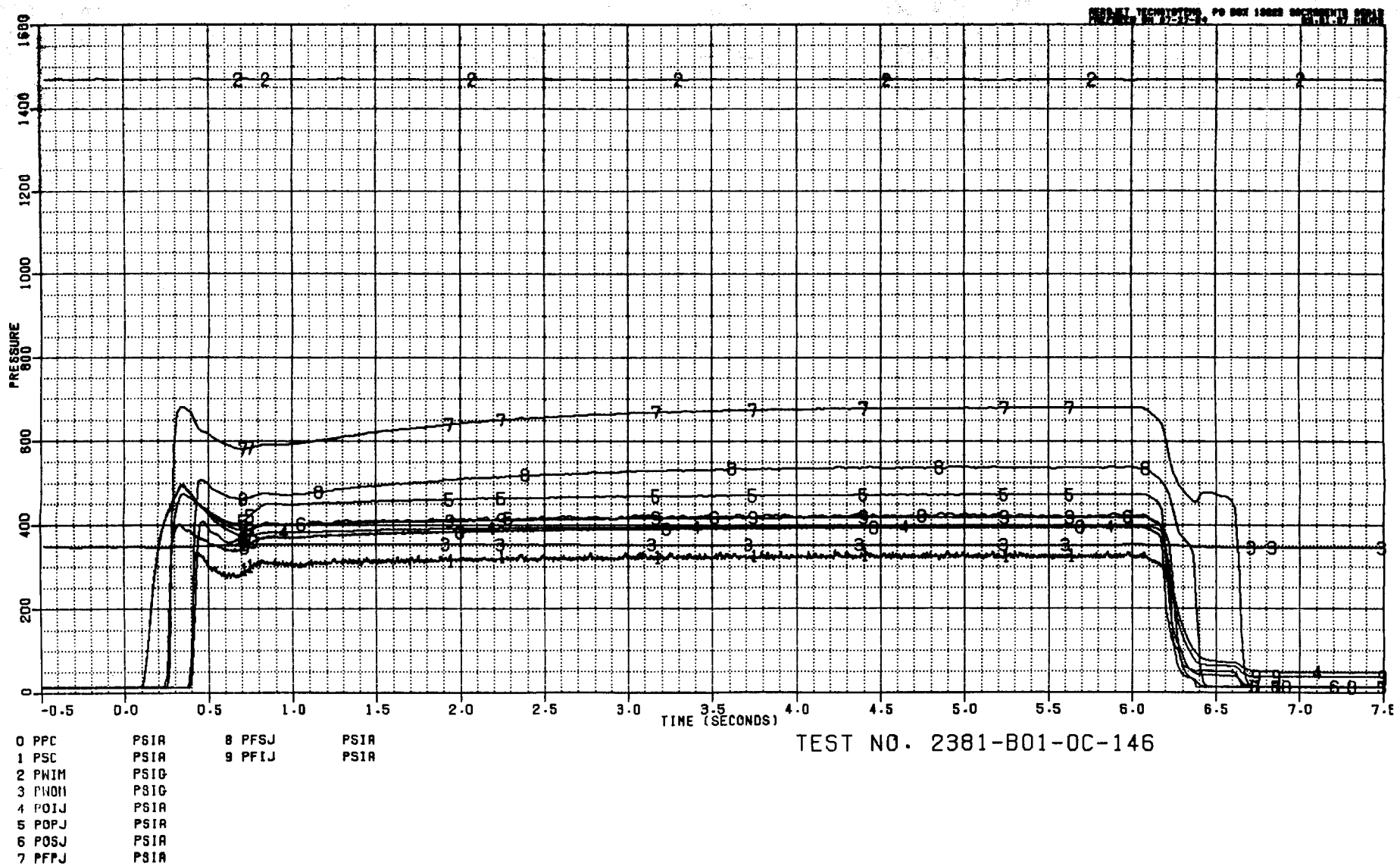

Figure B-103. Test 146 Pressure Data Summary

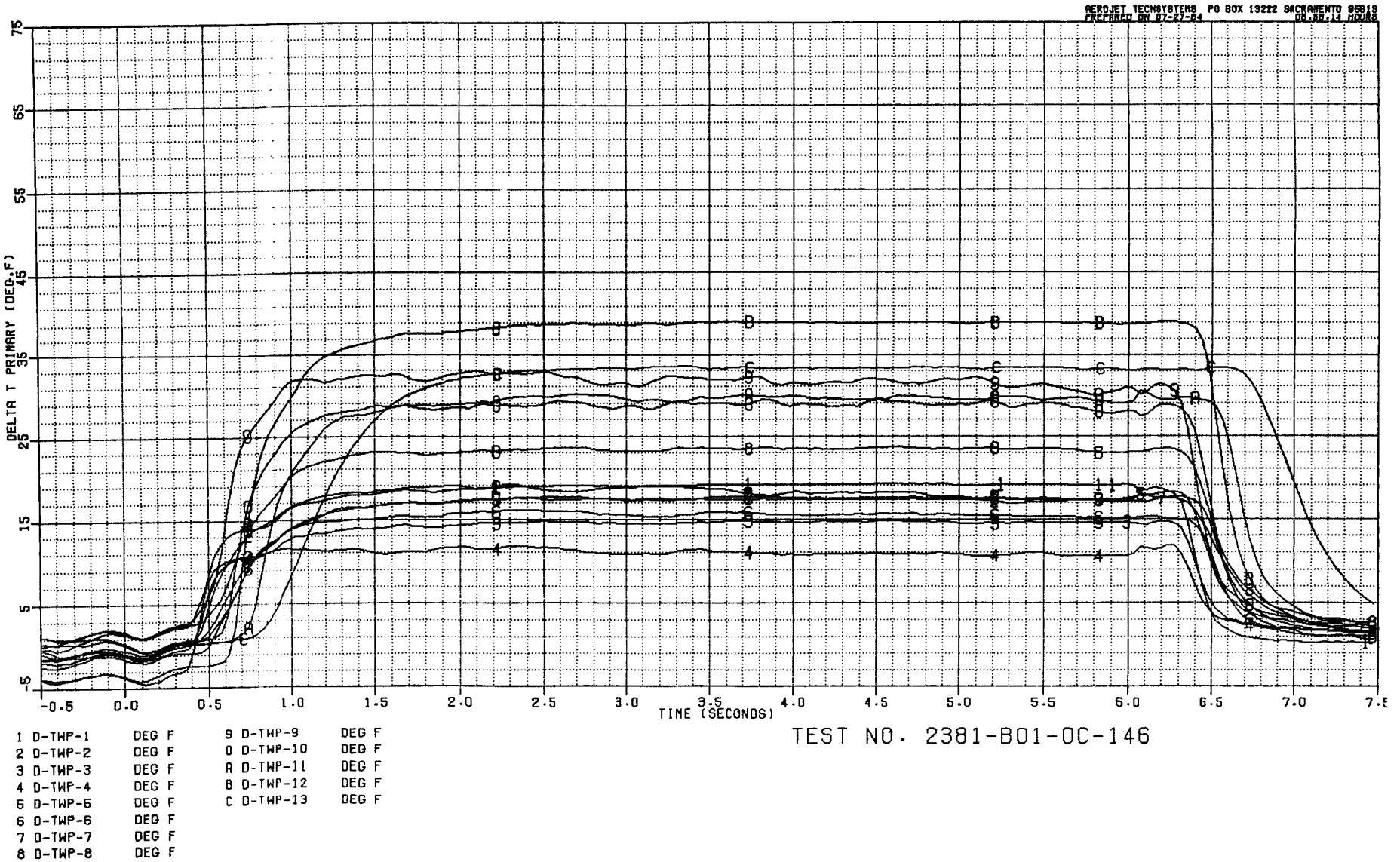

Figure B-104. Test 146 Primary Chamber Temperature Data Summary

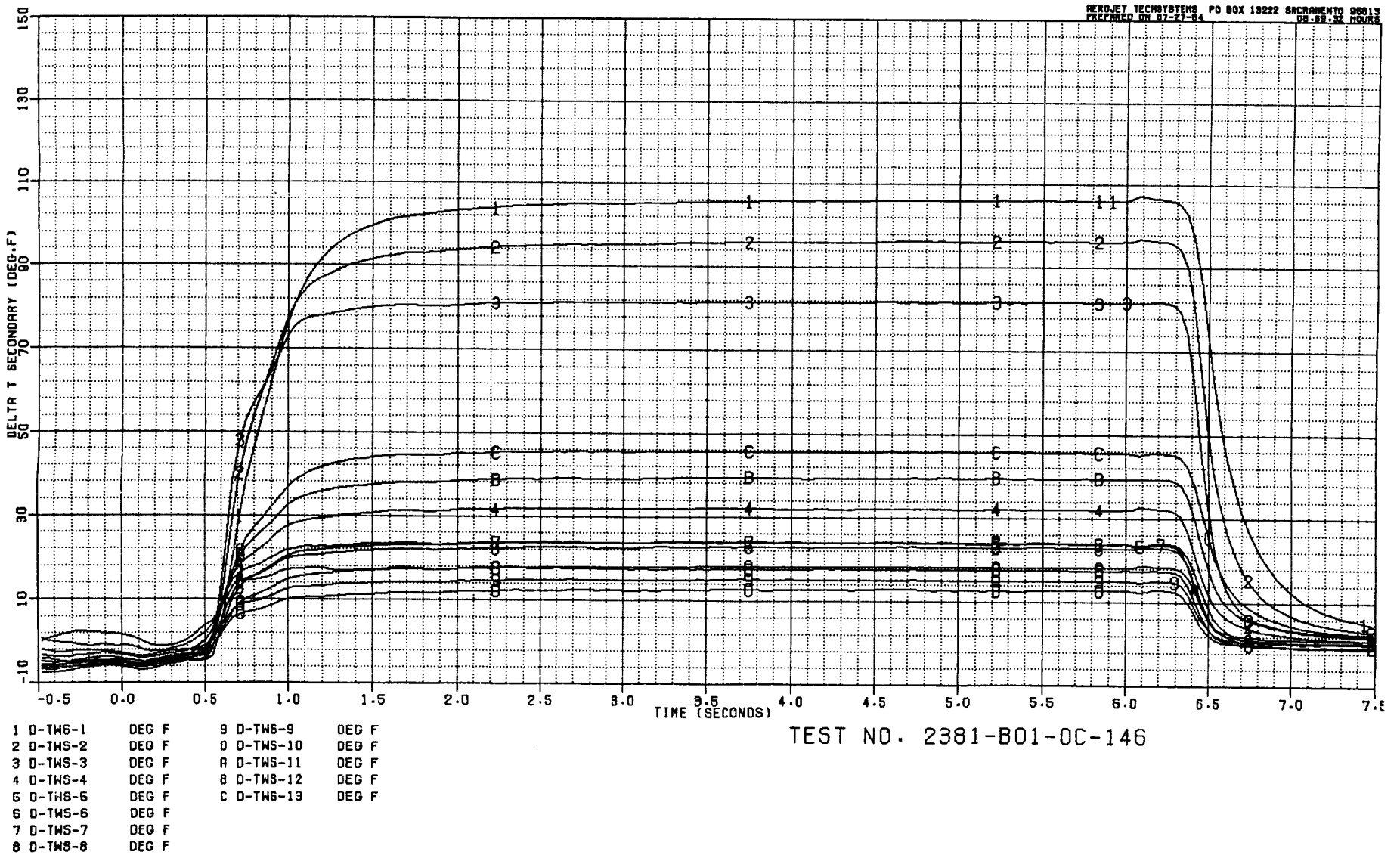

Figure B-105. Test 146 Secondary Chamber Temperature Data Summary

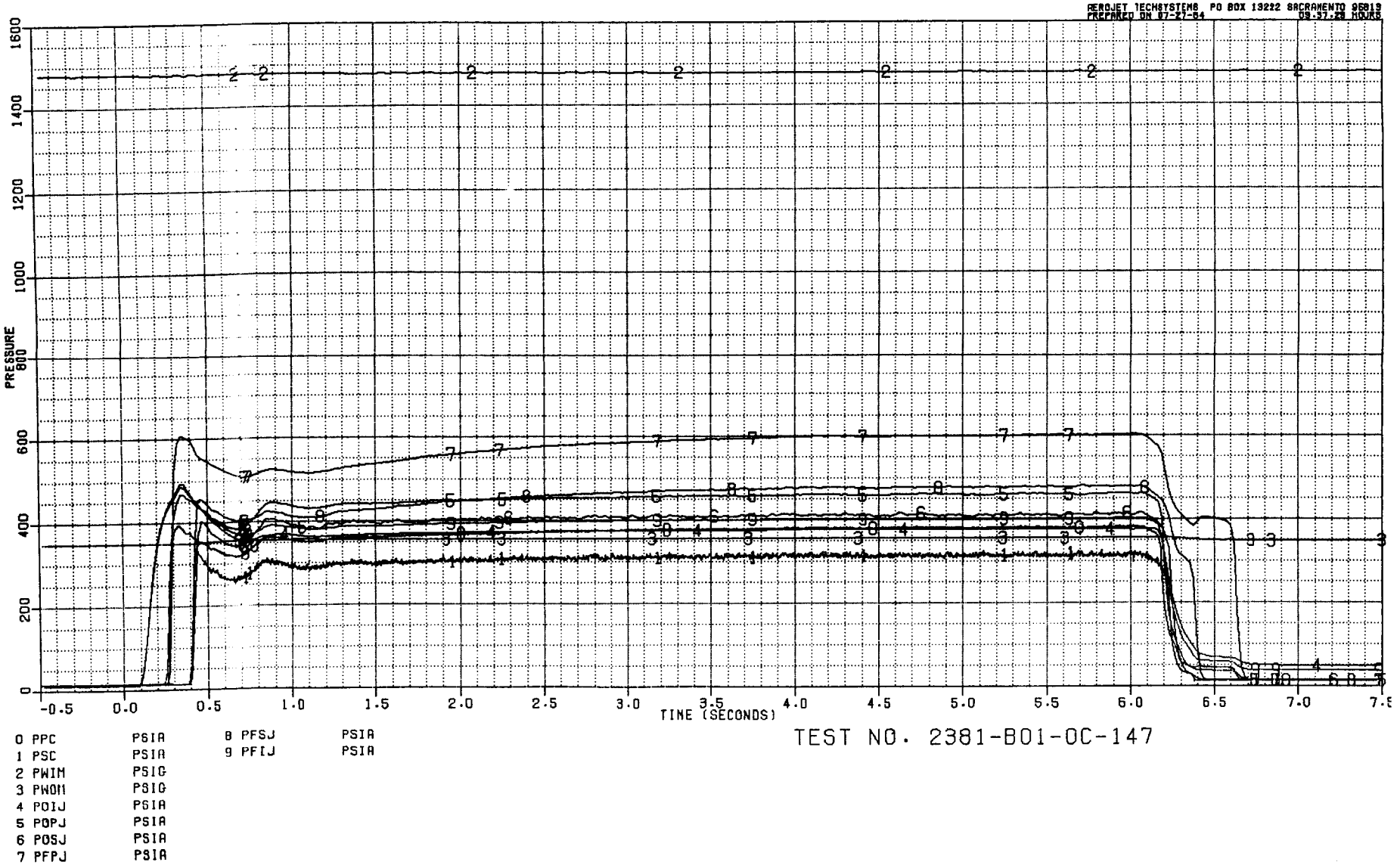

Figure B-106. Test 147 Pressure Data Summary

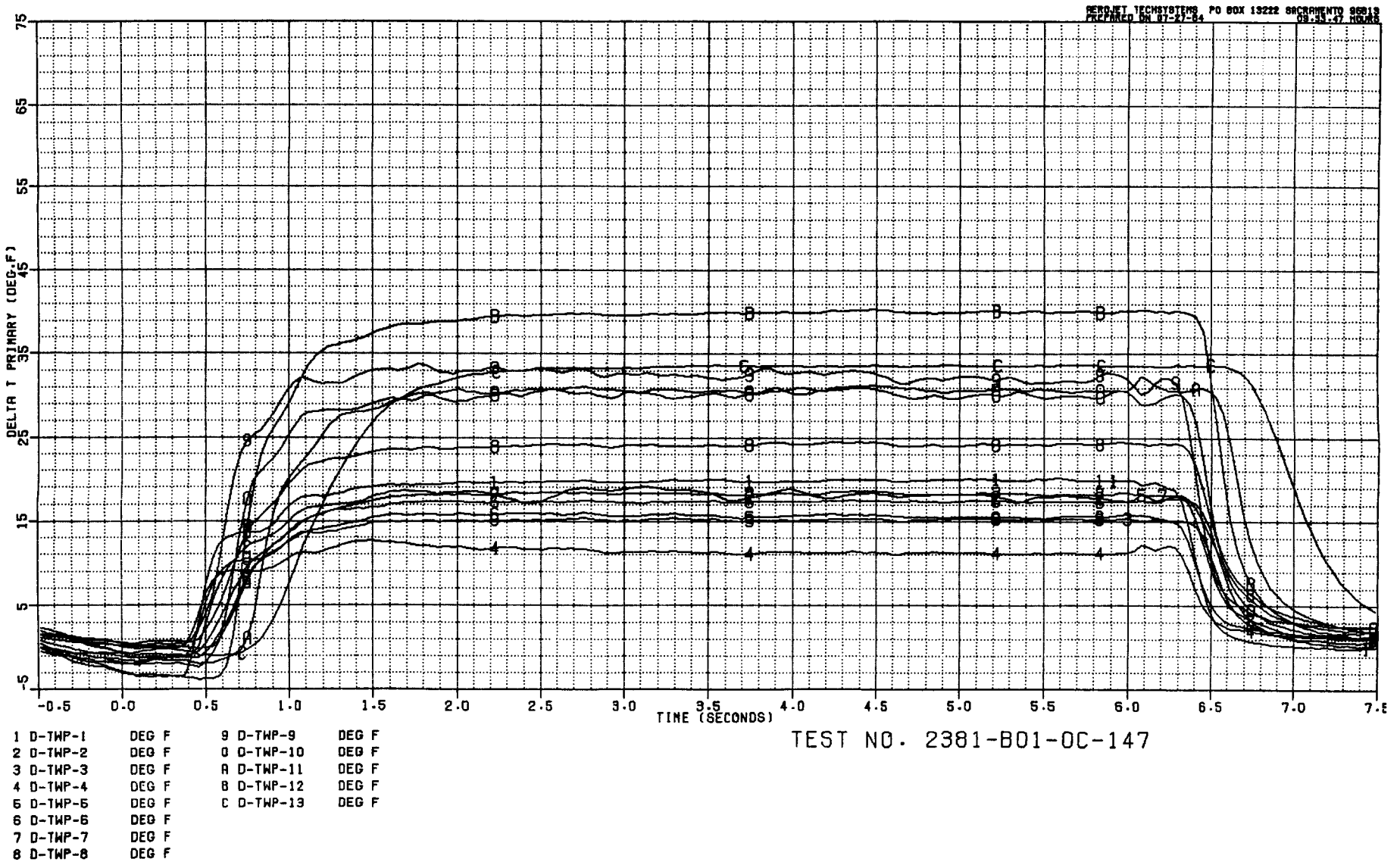

Figure B-107. Test 147 Primary Chamber Temperature Data Summary

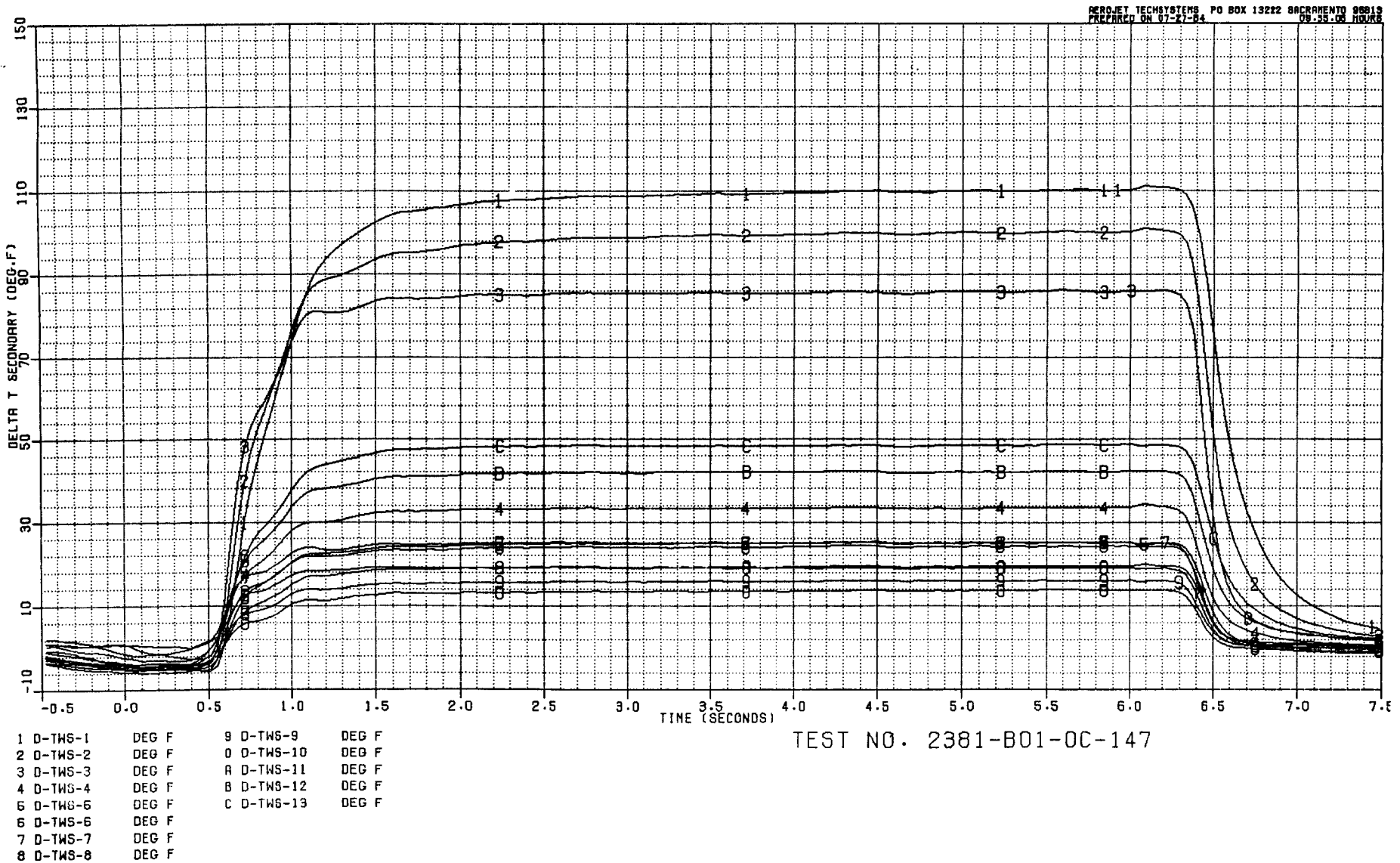

Figure B-108. Test 147 Secondary Chamber Temperature Data Summary

APPENDIX C

COLD FLOW DATA

COLD FLOW DATA

- Objective: Define Leaks Between Axial and Calorimeter Circuits

- Primary Circuit

  12 Calorimeter Channels
  Axial Circuit

- Low Pressure Runs

  ΔP = ~ 20 to ~ 60 psid

- 9 Configurations Flowed

  9 Combinations f

  - Axial and Calorimeter Inlets and Outlets Blocked
  - Axial Flowed in Reverse
  - Axial Inlet Orificed

TABLE C-1

MODELED 4 COLD FLOW CASES:

- All Circuits Flowing 1
- Cal. Outlets Capped (Inlets Pressurized) 3
- Cal. Inlets Capped 6
- All Following, Orifice on Axial Inlet 8

With Current Model Unable to Model Capping of Either the Inlet or Outlet of Axial Circuit

TABLE C-2

COMPARISON OF MODEL RESULTS WITH COLD FLOW DATA

Cold Flow Test	Maximum % Δ $\left(\frac{Kw_{meas} - Kw_{model}}{Kw_{meas}}\right)$
1	10%
3	2.8%
6	10.3%
8	19%

TABLE C-3

	1			6			
CAL	Kw_{meas}	Kw_{model}	% Δ	Cal	Kw_{meas}	Kw_{model}	% Δ
1	.0474	.0488	+3.0	1	.0208	.0198	-4.8
2	.0238	.0257	+8.0	2	.0146	.0135	-7.5
3	.0368	.0377	+2.4	3	.0067	.0061	-9.0
4	.0487	.0490	+0.6	4	.0255	.0244	-4.3
5	.0714	.0756	+5.9	5	.0632	.0613	-3.0
6	.0789	.0796	+0.9	6	.0704	.0664	-5.7
7	.038	.0414	+8.9	7	.0107	.0115	+7.5
8	.028	.0266	-5.0	8	.0160	.0149	-6.9
9	.0208	.0213	+2.4	9	.0113	.0113	0
10	.0219	.0202	-7.8	10	.0132	.0133	+0.8
11	.0278	.0252	-9.4	11	.0153	.0156	+2.0
12	.0261	.0235	-10.0	12	.0146	.0161	+10.3
εKw_{cal}	.470	.475	+1.1	εKw_{cal}	.269	.274	+ 1.9
Axial	.785	.779	-0.8	Axial	.66	.707	+7.1
Total	1.255	1.253	-0.2	Total	.929	.981	+5.6

TABLE C-4

8

CAL	Kw_{meas}	Kw_{model}	% Δ
1	.0431	.0459	+6.5
2	.0215	.0234	+8.8
3	.0349	.0374	+7.2
4	.0397	.0446	+12.3
5	.0515	.0613	+19.0
6	.0538	.0633	+17.7
7	.0359	.0397	+10.6
8	.0243	.0241	-0.8
9	.0189	.0194	+2.6
10	.0177	.0177	0
11	.0216	.0225	-4.2
12	.0185	.0205	+10.8
Kw_{cal}	.381	.4196	+10.1
Axial	.895	.823	-8.0
Total	1.276	1.243	-2.6

3

Axial Only - Cal Outlets CAPP

$Kw_{x_{meas}}$ = .822

Δ = +2.8%

$Kw_{x_{model}}$ = .845

TABLE C-5

MODEL RESULTS

Cal Channel #	$\frac{\dot{\omega}_{Cal.\ Ch.}}{\dot{\omega}\ Outlet}$
1	.7898
2	.7164
3	.9180
4	.7427
5	.4708
6	.4370
7	.8666
8	.6859
9	.7038
10	.5995
11	.6396
12	.5781

TABLE C-6

DUAL THROAT PRIMARY CHAMBER COLD FLOW

HYDRAULIC ADMITTANCES $K_W = \dot{W} / \Delta P_Y$

Calor No.	Test No.	All Flow Forward	Axial Flow Forward	Axial Outlets Capped	Axial Only Cal Out Capped	Reverse Axial All Flow	Reverse Axial Flow Capped Cal. In.	Forward Axial Flow Capped Cal. In.	Capped Axial Inlets Open Outlets	Orif .4" on Axial Inlets	Orif .4 on Axial Inlets & Capped Outlets	Full Inst. Flow Meters TC
		1	1 Rep.	2	3	4	5	6	7	8	9	
1		.0497	.0474	.0502	-	.0436	.0143	.0208	.0443	.0431	.0556	.0522
2		.0258	.0238	.0262	-	.0218	.00705	.0146	.0217	.0215	.0292	.0369
3		.0374	.0368	.0394	-	.0339	.0039	.0067	.0378	.0349	.0397	.0465
4			.0487	.0576	-	.0400	.0195	.0255	.0341	.0397	.0569	.0600
5			.0714	.0841	-	.0507	.0376	.0632	.0276	.0515	.0886	.0750
6		.0791	.0789	.0954	-	.0494	.0391	.0704	.0313	.0538	.0906	.0791
7		.038	-	.0388	-	.0344	.0063	.0107	.0343	.0359	.0396	.0487
8		.028	-	.0288	-	.0242	.0084	.0160	.0205	.0243	.0808	.0864
9		.0208	-	.0204	-	.0186	.0065	.0113	.0165	.0189	.0223	.0330
10		.0219	-	.0212	-	.0180	.0067	.0132	.0151	.0177	.0229	.0291
11		.0278	-	.0258	-	.0227	.0076	.0153	.0151	.0216	.0287	.0305
12		.0261	-	.0281	-	.0195	.0072	.0146	.0177	.0185	.0291	.0380
ΣK_W Cal			.470	.52	-	.38	.1655 Leak 61.5%	.269 Leak 100%	.316	.381	To High	.5654
$K_{W_{Axial}}$ =		.785	785	-	.822	.91	.683	.66	.252 Leak	.895 .517 w/o orif ΔP	- .95 = .51 Better	.83 w/cal out copped
$K_{W_{TOT}}$ =			1.255	.52	-	1.29	.849	.929	.568	1.276	-	1.395

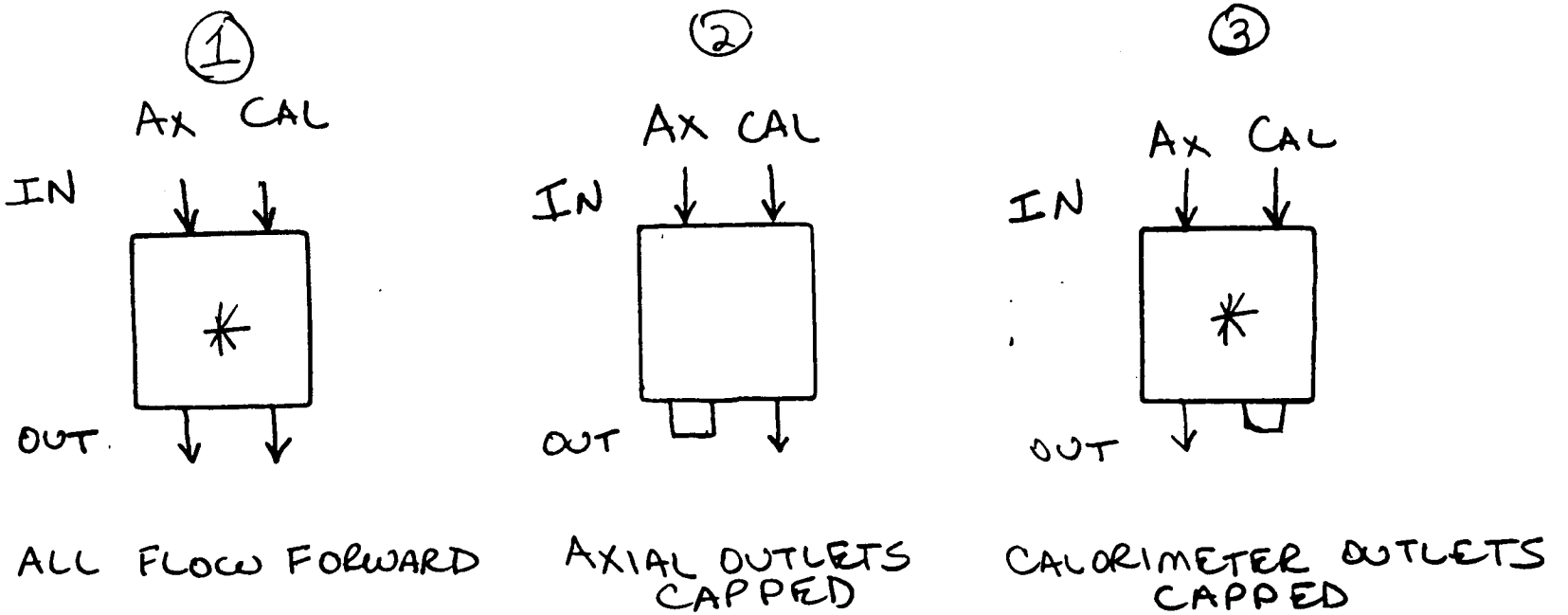
1
AX CAL
IN
OUT
ALL FLOW FORWARD
2
AX CAL
IN
OUT
AXIAL OUTLETS CAPPED
3
AX CAL
IN
OUT
CALORIMETER OUTLETS CAPPED
4
AX CAL
IN
OUT
REVERSE AXIAL FLOW
5
AX CAL
IN
OUT
REVERSE AXIAL, CALOR. INLETS CAPPED
6
AX CAL
IN
OUT
FORWARD AXIAL CALOR. INLETS CAPPED

Figure C-1

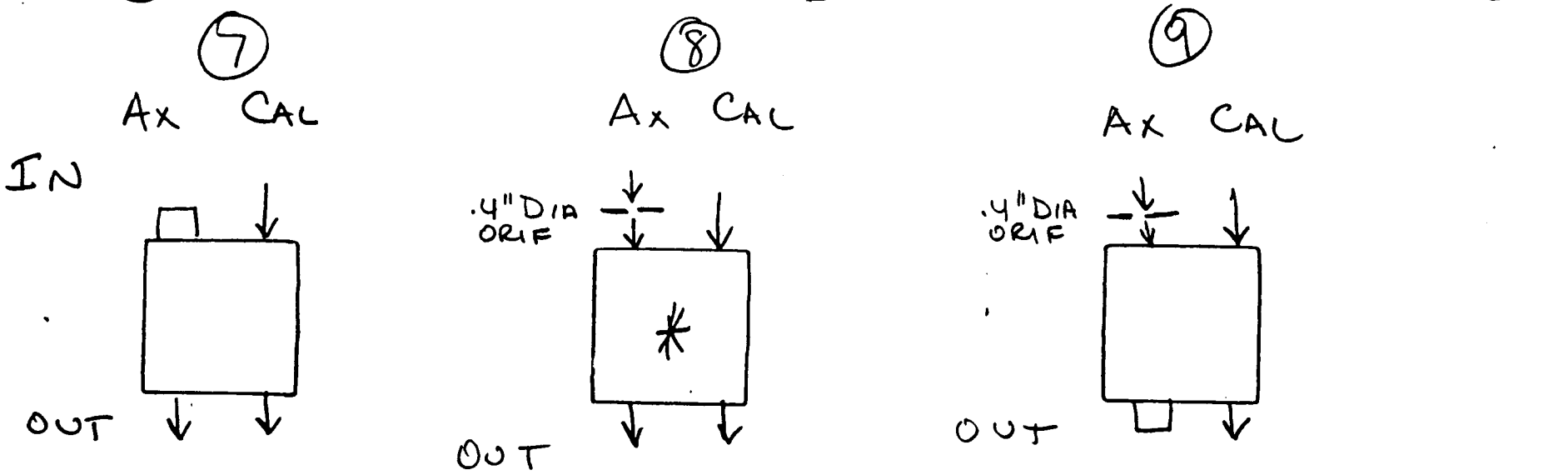

* INDICATES THE DATA USED TO CALIBRATE THE MODEL

Figure C-1 (cont.)

ORIGINAL PAGE IS
OF POOR QUALITY

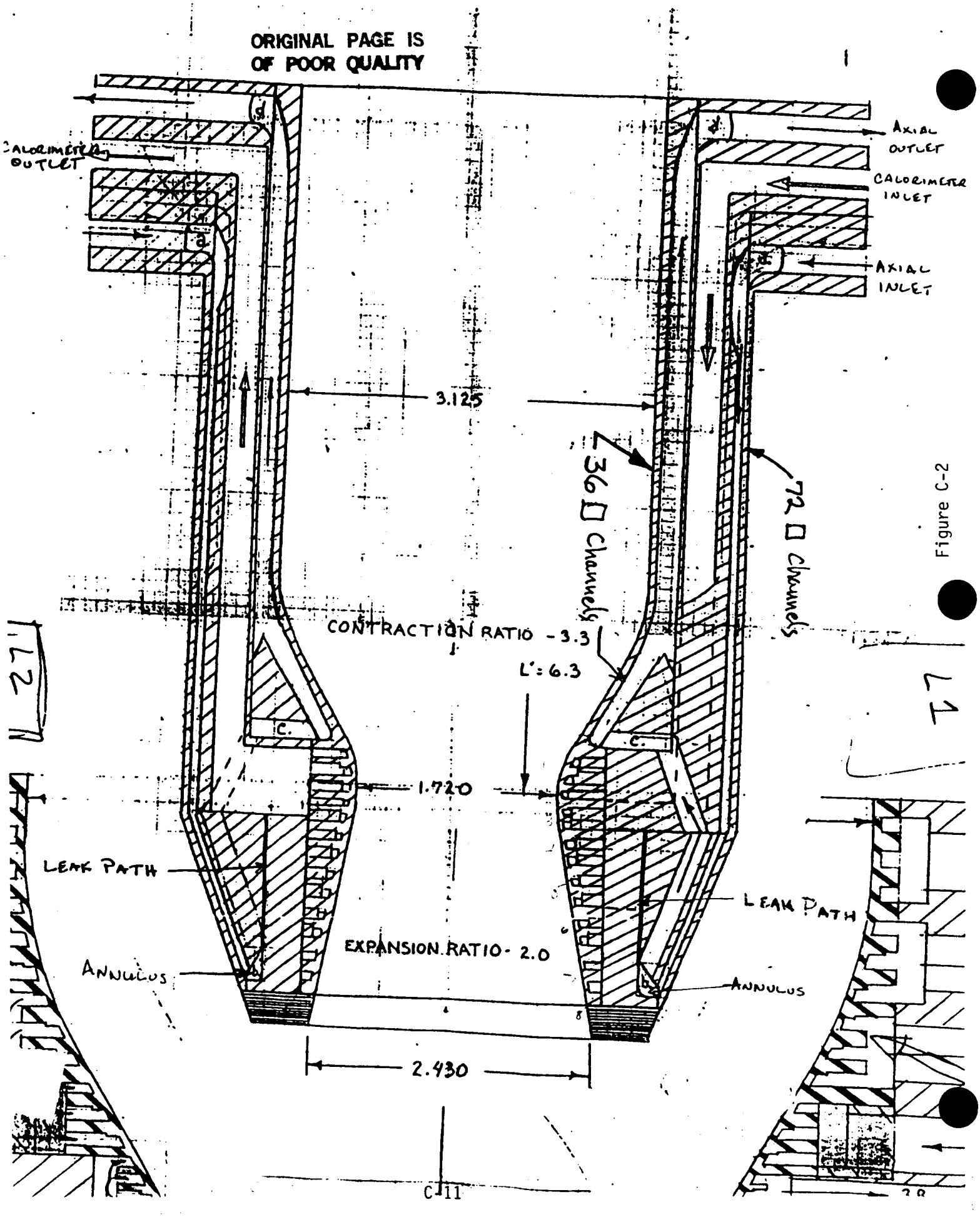

Figure C-2

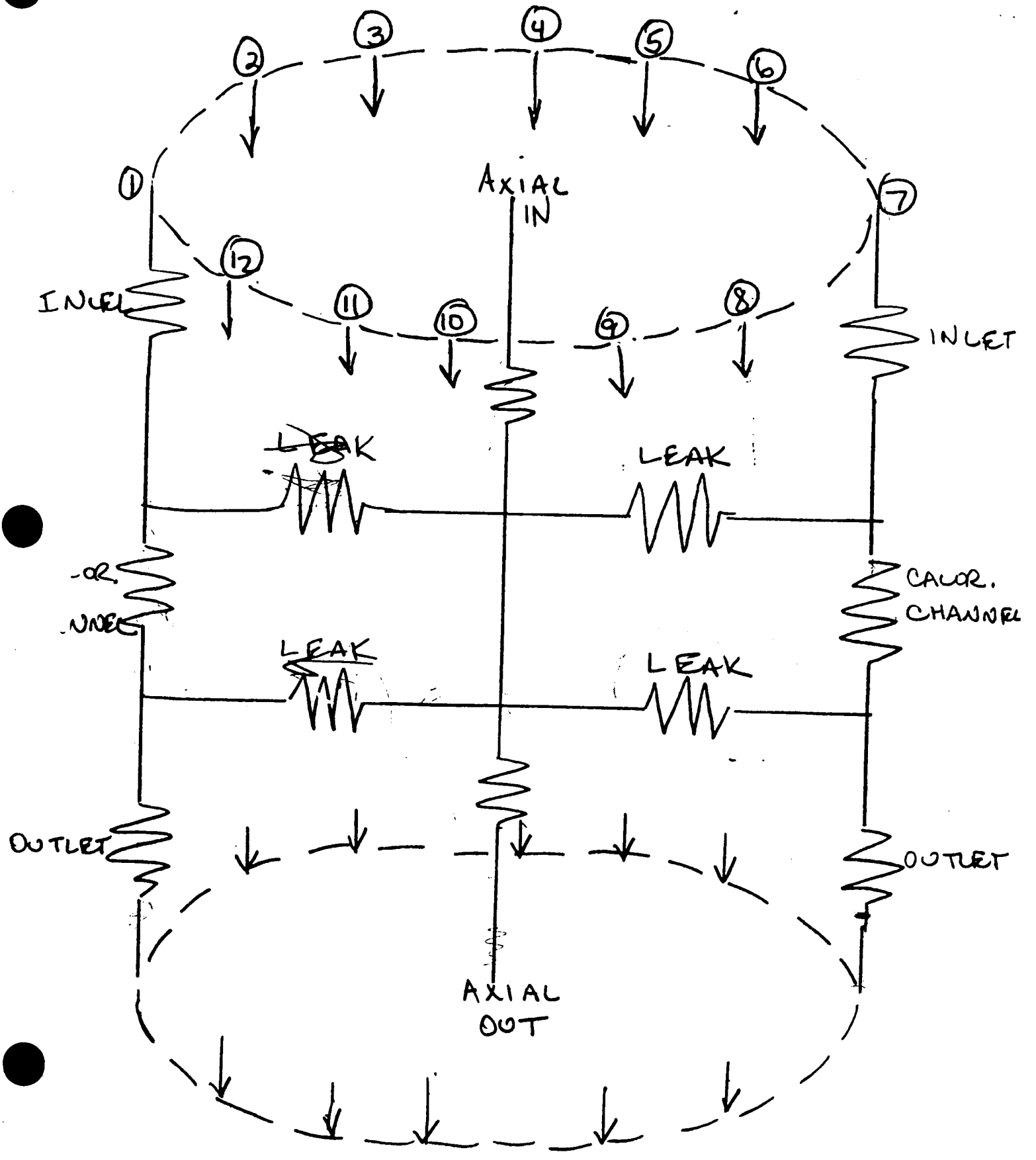
1
2
3
4
5
6
7
8
9
10
11
12
AXIAL IN
INLET
INLET
LEAK
LEAK
-OR-
INLET
CALOR. CHANNEL
LEAK
LEAK
OUTLET
OUTLET
AXIAL OUT

Figure C-3

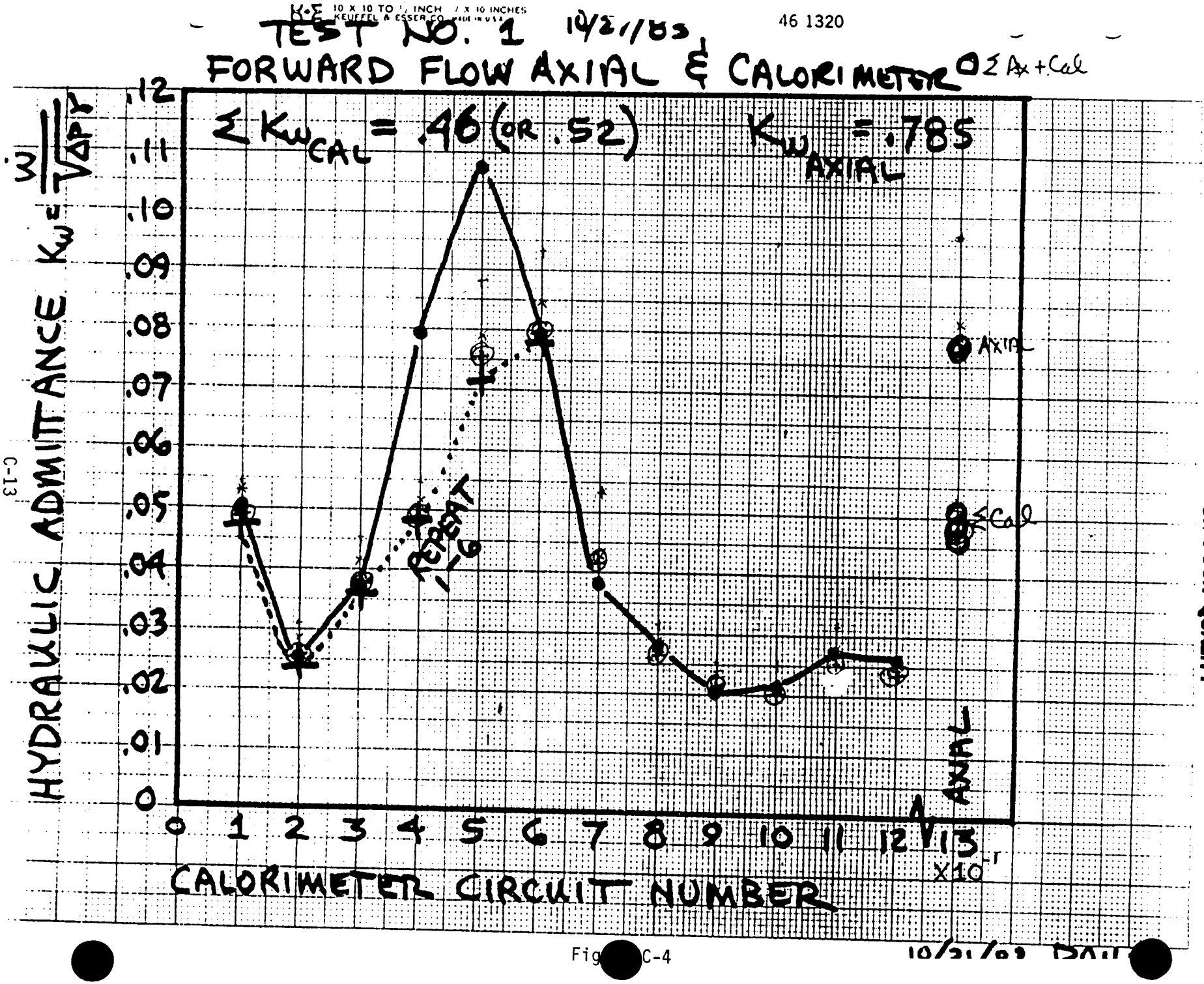

Fig C-4

46 1320

FORWARD FLOW AXIAL TEST NO. 6 10/27/83

CALORIMETER CIRCUIT INLETS CAPPED

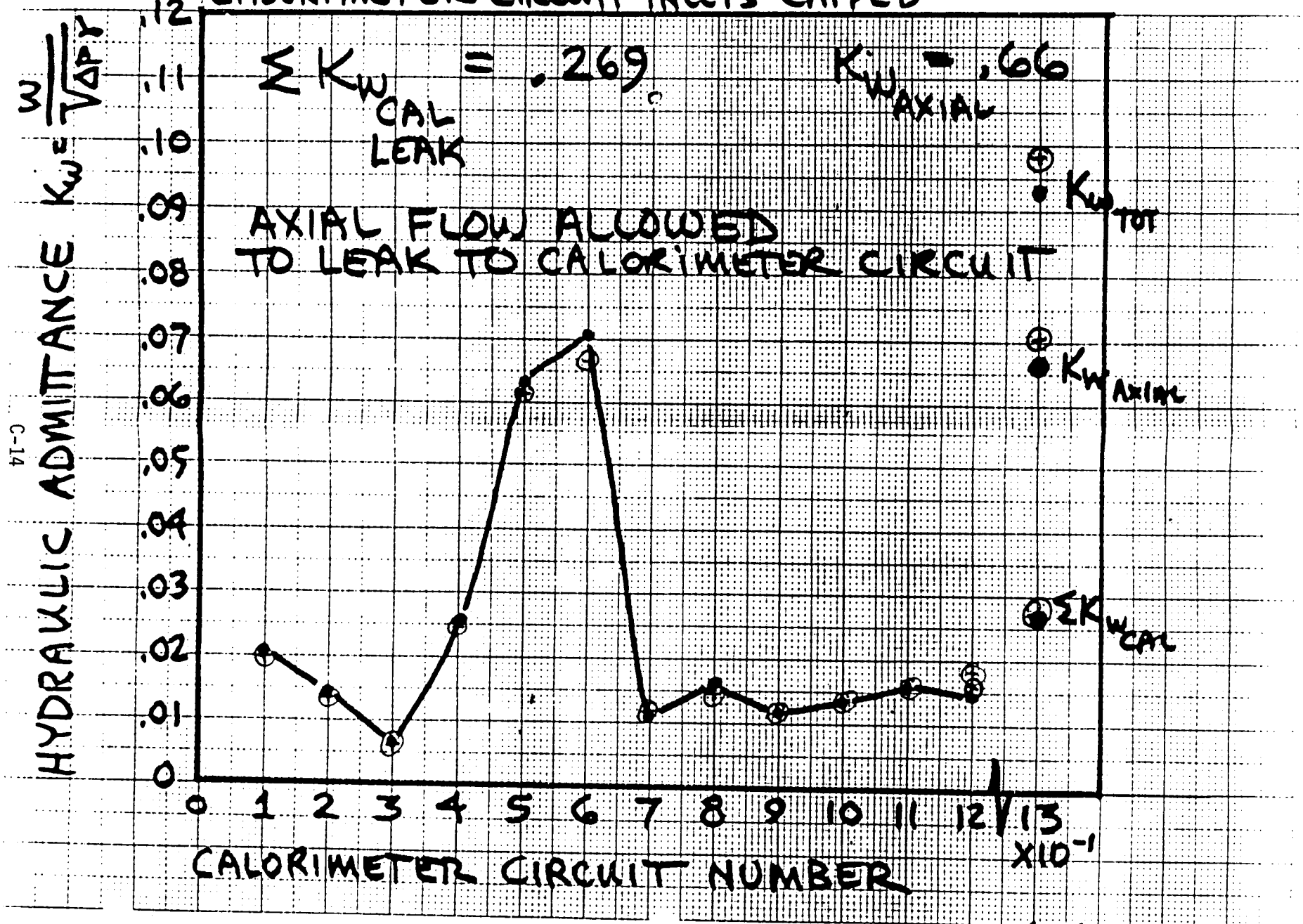

Figure C-5

10/31/83 RA..IT

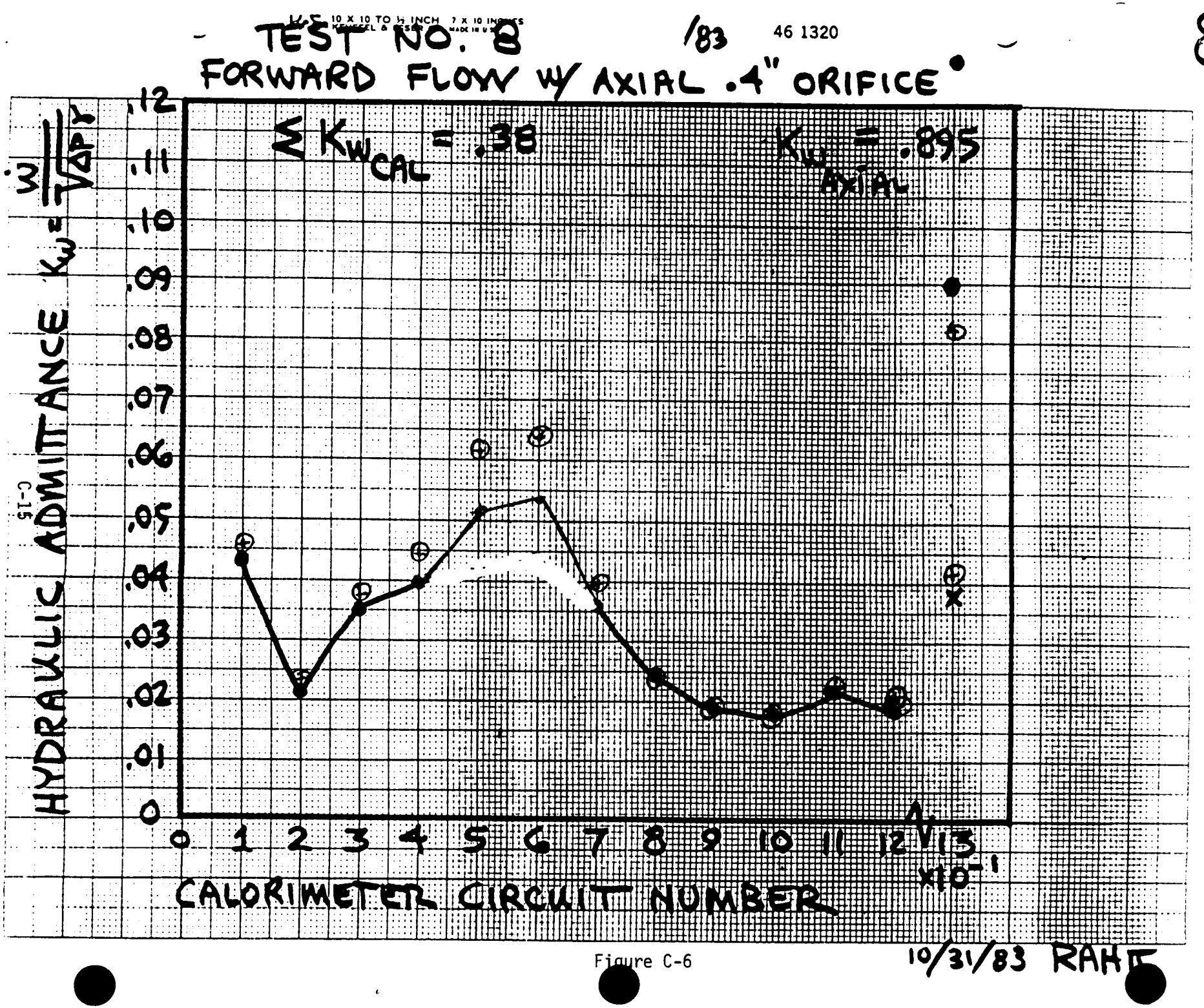

Figure C-6

APPENDIX D

CHAMBER COOLING CIRCUIT DESIGN

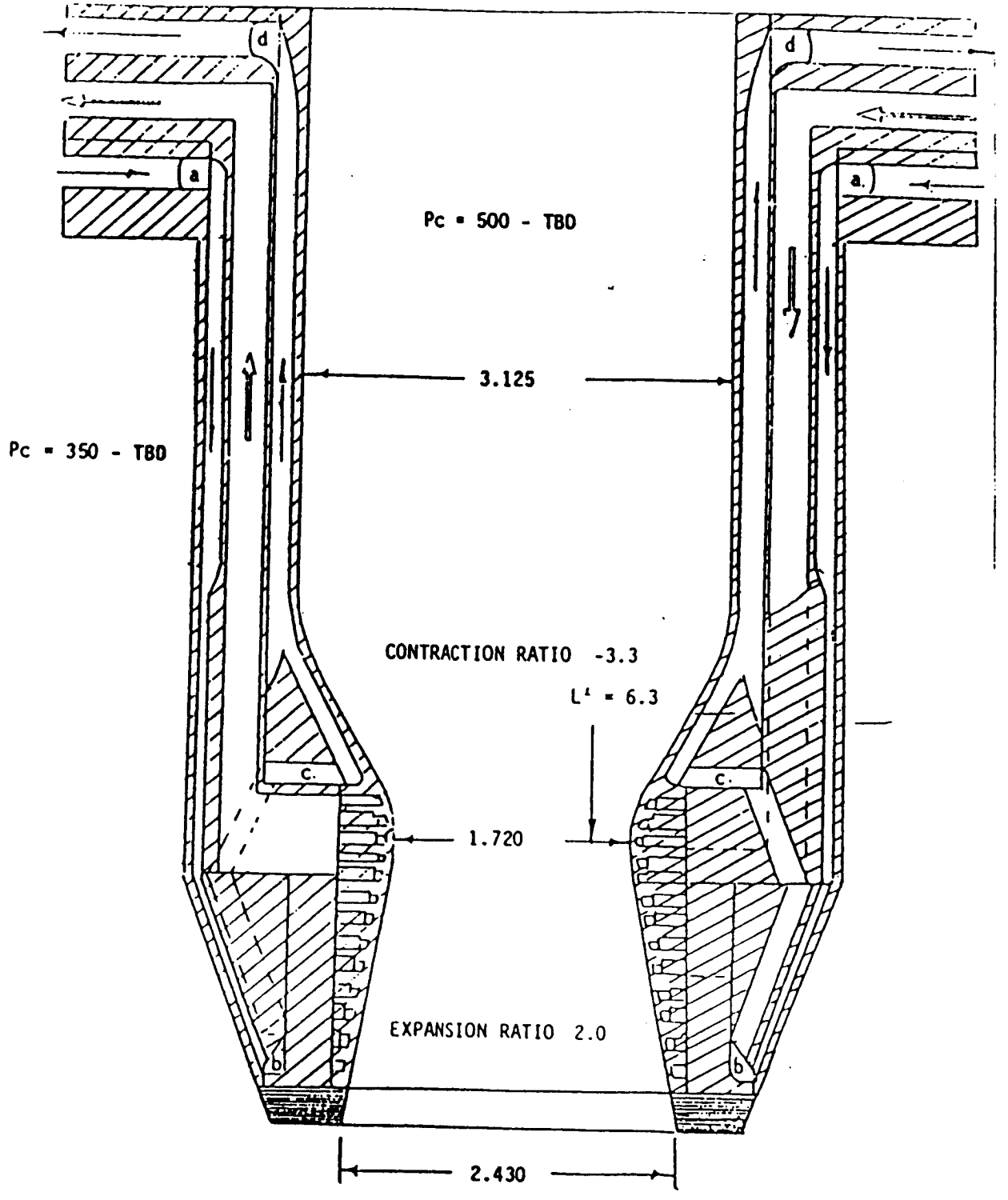

Figure D-1a. Primary Chamber Coolant Circuitry

The chamber cooling system consisted of 27 separate circuits providing 31 heat load measurements as summarized in Table DI. Figures 19 and 23 show the coolant circuits in the primary and secondary chamber, respectively. Twelve calorimetric circuits were provided in the primary chamber: eight in the throat region and nozzle, three at the tip and one on the outer surface just upstream of the tip. The remainder of the primary chamber was cooled with an axial flow circuit consisting of 72 channels on the outer wall in series with 36 channels on the inner wall. Thirteen calorimetric circuits cooled the entire secondary chamber. Five of these circuits, three at the injector and two at the aft end, consisted of two axial segments in series, with coolant bulk temperature measurements in the crossover manifolds between segments to provide two heat load measurements per circuit. A single circuit cooled the secondary spacer used on all but four tests. As shown in Table DII, the cooling circuits were designed to give a maximum wall temperature of 900°F, have a local burnout heat flux equal to twice the predicted maximum coolant heat flux and provide a minimum bulk temperature rise of 50°F in each calorimetric heat load measurement section.

The areas of primary interest for heat flux measurement using calorimetric cooling channels were the primary nozzle and its tip, in order to observe the effects of the flow separation and wake regions associated with Mode 1, and the throat region and nozzle of the secondary chamber due to the primary plume attachment and boundary layer development in Mode II. Providing small measurement spans in the areas of interest dictated the distribution of calorimetric channels within the two chambers.

A. PRIMARY CHAMBER

A complex axial circuit cools much of the primary chamber design as shown in Figure 19. Four distinct regions are cooled in series by this circuit:

TABLE DI. COOLING SYSTEM SUMMARY

	No. of Circuits	No. of Channels	No. of Heat Load Measurements	Maximum Flow Rate lb/sec
Primary - Axial	1	36/72	-	26.7
Primary - Calorimeter	12	18	12	10.7
Secondary Chamber	13	40	18	35.4
Secondary Spaces	1	2	1	3.9
	27		31	76.7

TABLE DII.

CIRCUIT/CHANNEL DESIGN CRITERIA

1. Coolant bulk temperature rise $\geq$ 50°F for accurate heat load measurement in each calorimeter section*

2. Wall temperature $\leq$ 900°F

3. Burnout safety factor $\geq$ 2.01

   2.01 = 1.25 (burnout heat flux correlation scatter)

   x 1.15 (Operating point and dimensional tolerances except for channel width and depth)

   x 1.40 (gas-side heat transfer coefficient uncertainty)

4. Coolant static pressure $\geq$ 1000 psia*

5. Maximum coolant static pressure satisfies wall strength criterion:

   $$P_{max} \leq 2 F_{ty} (t_{w,\,min} / \omega_{max})^2$$

   F_{ty} = yield strength for coarse grain OFHC

   t_w = wall thickness ω = channel width

*Design point only

A, Primary Chamber (cont.)

(1) An outer cylindrical section consisting of 72 machined channels with steel lands,

(2) An outer convergent section, made entirely of OFHC except for a steel end wall, cooled by 72 round EDM holes,

(3) An inner OFHC convergent section cooled by 36 tapered EDM channels and

(4) An inner cylindrical section consisting of 36 machined channels with copper lands but a steel closure.

Channel dimensions for this circuit are included in Table DIII.

Two types of calorimetric circuits cool the remainder of the primary chamber. Seven circuits, each consisting of two channels in parallel except for a single-channel circuit at the throat, cool the throat region and most of the nozzle; these are machined channels closed out by stainless steel rings or a steel sleeve (circuit no. 7). Five single-channel circuits etched in an OFHC platelet stack cool the tip of the primary nozzle. Channel dimensions, coolant flow rates and circuit bulk temperature rises for the calorimetric circuits are given in Table DIV. Note that the two channels of circuit 7 are not the same. Channel 7A was designed to be narrower and deeper than 7B in order to eliminate the need for a very thin closeout ring on the former. Nominal gas-side wall thicknesses at the axial locations of minimum thickness are 0.050 in. for all calorimetric circuits. Operating characteristics for each circuit at the design point are summarized in Table DV. Primary chamber operating limits are shown in Figure D-1; note the very limited operating region for a nozzle spacing of 1.5 in.

TABLE D III

PRIMARY CHAMBER AXIAL CIRCUIT

	Inside		Outside	
	Barrel	EDM	Barrel	O EDM
No. Channels	36	36	72	72
Wall thickness, in.	.055	.050	.080	.075
Channel width, in.	.0938	.077	.125	.100 Dia
Land width, in.	.189	.101	.072	.051
Channel depth, in.	.170	.134	.081	-
Min. velocity, ft/sec	101	155	78	99
Wall Temperature, °F	705	915	769	722
ΔT_b, °F	24	11	17	11
Heat Flux, Btu/in^2 sec				
gas-side	16.2	32.2	12.4	17.0
coolant-side	18.1	32.0	17.6	14.7
BOSF	2.23	2.05	2.04	2.95

TABLE DIV

PRIMARY CHAMBER CALORIMETER CIRCUIT CHANNEL LAYOUT

Circuit	Channel Width in.	Land Width in.	Channel Dept (Avg) in.	Coolat Flow lb/sec	ΔT_b °F	Axial Span in.
		.090				
1	.0625 ± .003	.078	.047 ± .005	1.13	50	.287
	.0625 ± .003	.078				
2	.0625 ± .003		.046	0.55	50	.1405
	.0625 ± .003	.078			50	
3	.0625 ± .003	.078	.048	1.13	50	.286
	.0625 ± .003	.088			50	
4	.0625 ± .003	.098	.055	1.26	50	.321
	.0625 ± .003	.108			50	
5	.0625 ± .003	.118	.060	1.35	50	.356
	.0625 ± .003	.118			50	
6	.0625 ± .003	.118	.065	1.35	50	.3645
7A	.052	.125	.087	1.38	49	.3805
7B	.080	.126	.053			
		.120				
8	.080		.053 ± .003	0.58	54	.180
		.080				
9	.040		.077	0.63	61	.130
		.098				
10	.040		.077	0.30	89	-
		.098				
11	.040		.077	0.59	73	.130
		.080				
12	.080		.053	0.45	82	.180
		.120				

TABLE DV.

PRIMARY CHAMBER CHANNEL DESIGN SUMMARY

Channel	Heat Flux Gas-side Btu/in^{2}sec	Heat Flux Coolant-side Btu/in^{2}sec	Wall Temp. °F	Minimum Velocity ft/sec	BOSF
1A	32.3	37.6	882	192	1.99
1B, 2, 3A	34.5	36.7	886	191	2.02
4B	32.5	36.4	897	187	1.99
5A	31.1	35.8	892	184	2.00
6A	28.5	33.5	861	171	1.99
7B	25.5	31.5	818	165	2.00
8	24.5	27.7	767	151	2.13
9	22.0	42.6	913	230	2.01
10	18.5	19.4	658	108	2.06
11	18.4	38.9	832	213	2.02
12	17.5	22.0	780	118	2.01

B. SECONDARY CHAMBER

The layout of the secondary chamber channels and coolant flow circuits is shown in Figure 23; channel and land widths are given in Table DV1. Forty channels are arranged to provide 13 calorimetric circuits. Five of these circuits, 3 at the injector end and two at the aft end, consist of two heat load measurement segments in series. Therefore, a total of 18 heat load measurements is provided. Circuits 1 and 2 have three channels flowing in parallel for each segment, while all other circuits or measurement segments have two channels in parallel. In addition, circuit 1 has wider channels and circuits 1, 2 and 10-13 have wider lands. This channel layout, which provides the heat load measurement spans given in Table DV11, is consistent with the objective of providing more detailed data in the Mode II plume attachment region, less detail downstream and only gross data in the upstream recirculation region.

A gas-side wall thickness of 0.060 in. was found to be consistent with the wall temperature and wall strength criteria in the throat region and was used for most of the chamber as noted in Table DV1. Wall thicknesses were increased to 0.075 in. for Circuit 1 in order to provide comparable wall strengths with the wider channels of that circuit. Following definition of channel depth requirements to satisfy the burnout safety factor criterion, wall thicknesses were adjusted in several locations in order to match channel outside diameters and thus minimize the number of closeout rings required. These special wall thicknesses are given at the bottom of Table DV1. Wall thicknesses for channels 1-3 were increased to provide O.D. matching with channel 4; the channel 3 wall is thicker because of the gas-side contour. Wall thicknesses for channels 29 and 30 were increased to 0.062 in. to provide O.D. matching between channels 19 and 30. Similarly, the walls for channels 39 and 40 were increased to 0.0655 in. to provide O.D. matching between channels 13 and 40. As can be seen in Figure 23, closeout rings are not required for channels 1-4, 10, 13, 19, 30 and 40.

TABLE DVI

SECONDARY CHAMBER CHANNEL LAYOUT

Channel Numbers	Wall Thickness in.	Channel Width in.	Land Width in.
			.180 max
1-5	.075*	.125 ± .003	.180
			.170
6	.075	.125	-
			.150
7 - 12	.060	.09375	.150
			.070
13 - 32	.060*	.09375	.070
33 - 40	.060*	.09375	.133
			.153
			.200 max
Spacer	.075	.125 (2)	.350
			.200 max

*Special Wall Thicknesses:

Channel Number	Wall Thickness in.
1,2	.0865
3	.093
29,30	.062
39,40	.0655

TABLE DVII

SECONDARY, CHAMBER COOLING CIRCUIT DESIGN

Channels in Parallel	Circuit	Coolant Flow lb/sec	ΔT_b °F	Smaller Channel Depth in.	Axial Span in.
-	Spacer	3.91	75	.150 ± .005	1.0
1-3	1A	5.19	57	.150	1.005
4-6	1B		50	.189	.890
7-9	2B	4.58	50	.203, .188 (2)	.731
10-12	2A		52	.172	.691
13-14	3B	2.41	50	.095	.3275
15-16	3A		52	.105	.3275
17-18	4	2.66	50	.090	.3275
19-20	5	2.64	50	.073, .088	.3275
21-22	6	2.43	50	.077	.3275
23-24	7	2.26	50	.085	.3275
25-26	8	2.18	50	.087, .074	.3275
27-28	9	2.15	50	.080	.3275
29-30	10	2.05	50	.090	.3275
31-32	11	2.15	50	.090	.359
33-34	12A	2.43	53	.121	.4535
35-36	12B		50	.106	.4535
37-38	13B	2.29	50	.112	.4535
39-40	13A		56	.092	.540

B, Secondary Chamber (cont.)

Maximum wall temperatures and other design point operting parameters are summarized in Table DVIII. Wall temperatures approach the design criterion of 900°F only at the maximum flux location and on the heavier end walls, i.e., the spacers and channel 1. Circuit coolant flows and bulk temperature rises for the design operating point are given in Table DVII. All flows, except for the spacer, were selected to provide a 50°F bulk temperature rise in the single-segment circuits and in the lower heat load segment of the double-segment circuits. Bulk temperature rises in the other segments of the latter are 2-7°F higher. Circuits 2, 3 and 12 have the coolant flow through the higher heat flux segment first to take advantage of the greater coolant subcooling. In Circuits 1 and 13 the segments with the end walls are cooled first, since the coolant heat flux is higher in these segments even though the gas-side flux is lower. The spacers were designed for a 75°F bulk temperature rise in order to maintain measurement accuracy if actual heat fluxes near the secondary injector are less than the design value. Such a design also provides a channel O.D. close to that of chamber channels 1-4.

Channel depths required to meet the burnout safety factor criterion are included in Table DVII. These depths are at the maximum channel I.D., i.e., the smallest nominal depth for each channel. Table DVII gives two channel depths for Circuits 2B, 5 and 8 since the channel angle changes within these segments.

A machining error on channel 18 resulted in a wall thickness 0.005 in. less than nominal and a channel which was 0.013 in. too deep. As a result an inlet orifice was used in circuit 4 to limit coolant pressures and maintain wall strength, and the nominal coolant flow rate was increased to maintain the design burnout safety margin.

TABLE DVIII

SECONDARY CHAMBER CHANNEL DESIGN SUMMARY

Channel	Heat Flux Gas-side Btu/in^{2}sec	Heat Flux Coolant-side Btu/in^{2}sec	Wall Temp. °F	Minimum Velocity ft/sec	BOSF
Spacer	13.2	21.8	892	115	2.01
1	13.1	19.8	872	101	2.02
6	13.7	14.2	707	76	2.01
9	15.3	15.6	676	84	2.01
12	18.7	18.3	770	89	2.01
14	21.2	20.0	717	116	2.01
16	23.8	21.0	755	105	2.01
18	27.3	25.8	836	127	2.01
20	30.7	29.8	888	149	2.01
21	30.8	29.9	896	154	2.01
23	30.6	29.6	883	152	2.01
25	29.4	28.3	867	143	2.01
27	27.5	26.1	837	132	2.02
29	25.0	23.0	814	112	2.01
32	22.2	23.0	765	119	2.07
33	20.9	20.7	743	105	2.04
35	19.0	20.8	719	114	2.01
37	17.3	17.9	655	106	2.11
40	14.9	22.7	795	125	2.11

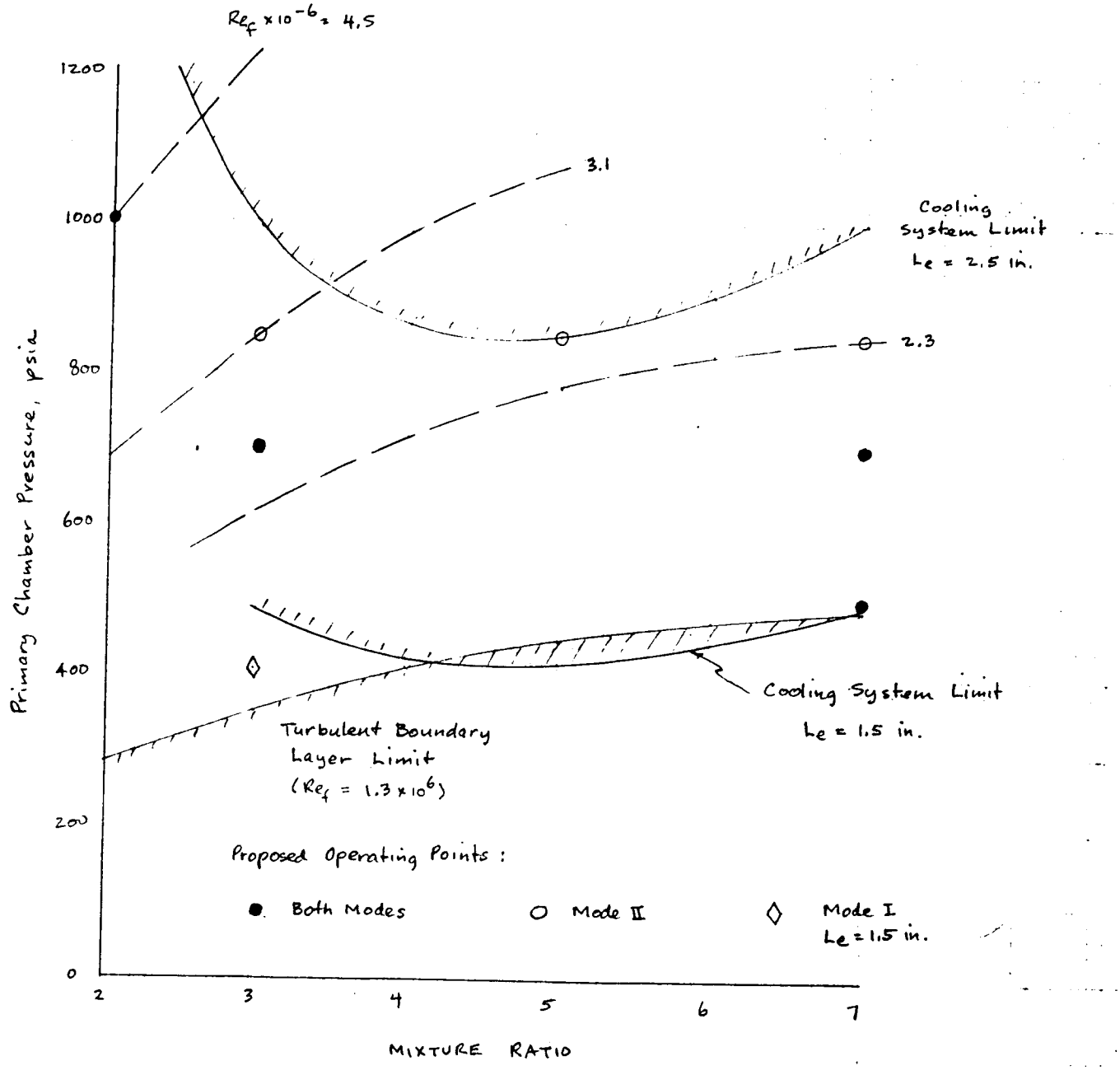

Figure D-1. Primary Chamber Operating Limits

ORIGINAL PAGE IS
OF POOR QUALITY

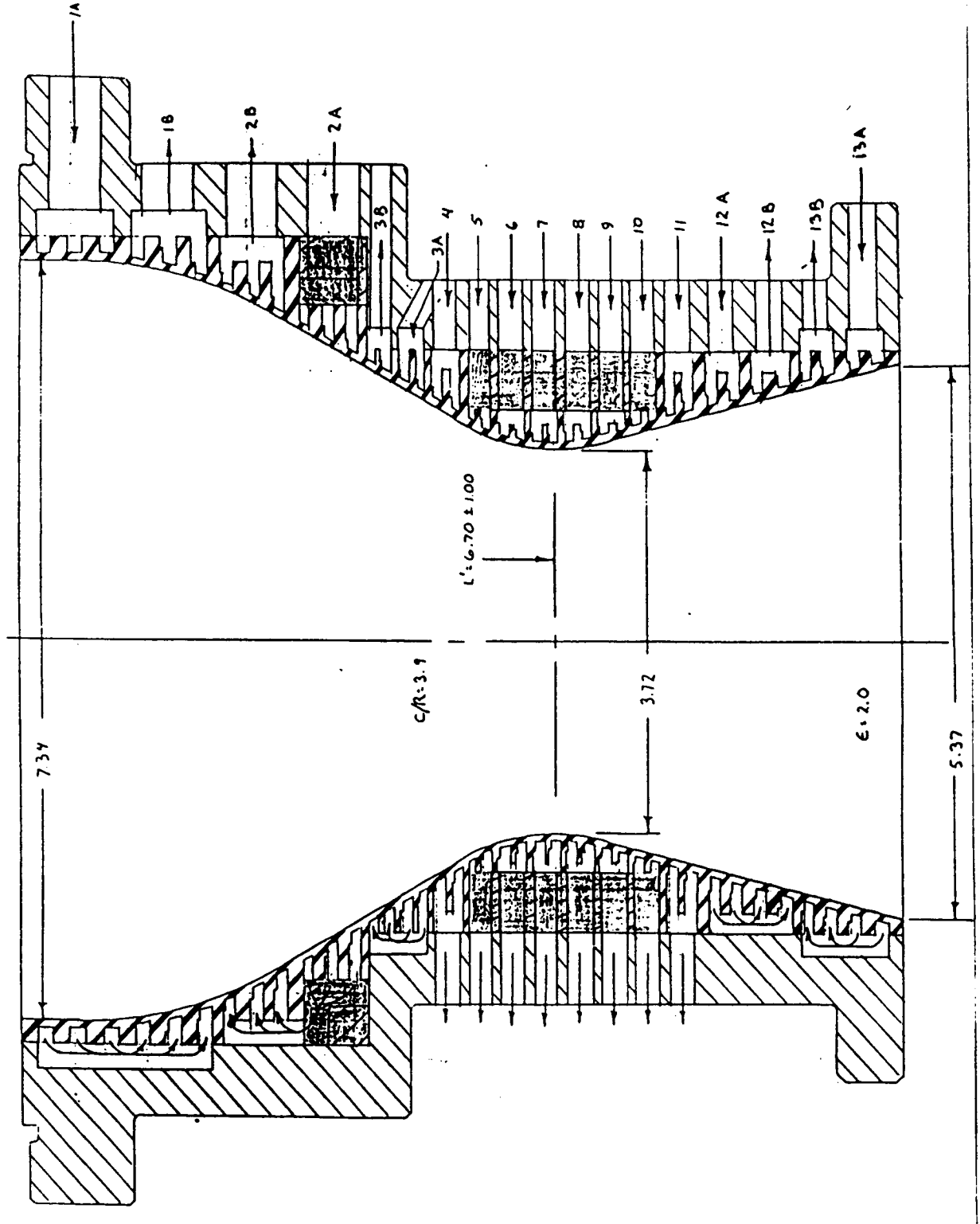

Figure D-2. Secondary Chamber Coolant Circuitry

APPENDIX E

HARDWARE DRAWINGS

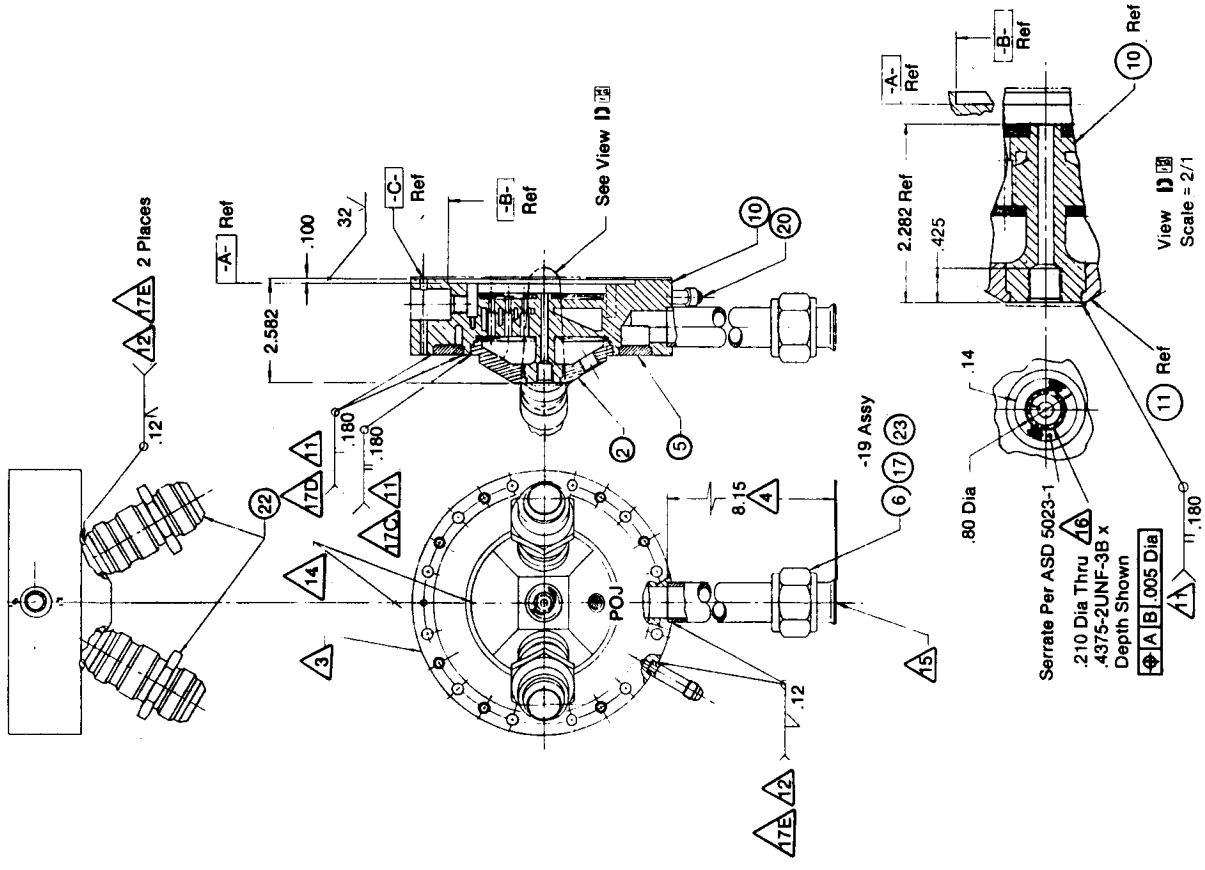

Figure E-1. Dual Throat Thruster Primary Injector Assembly

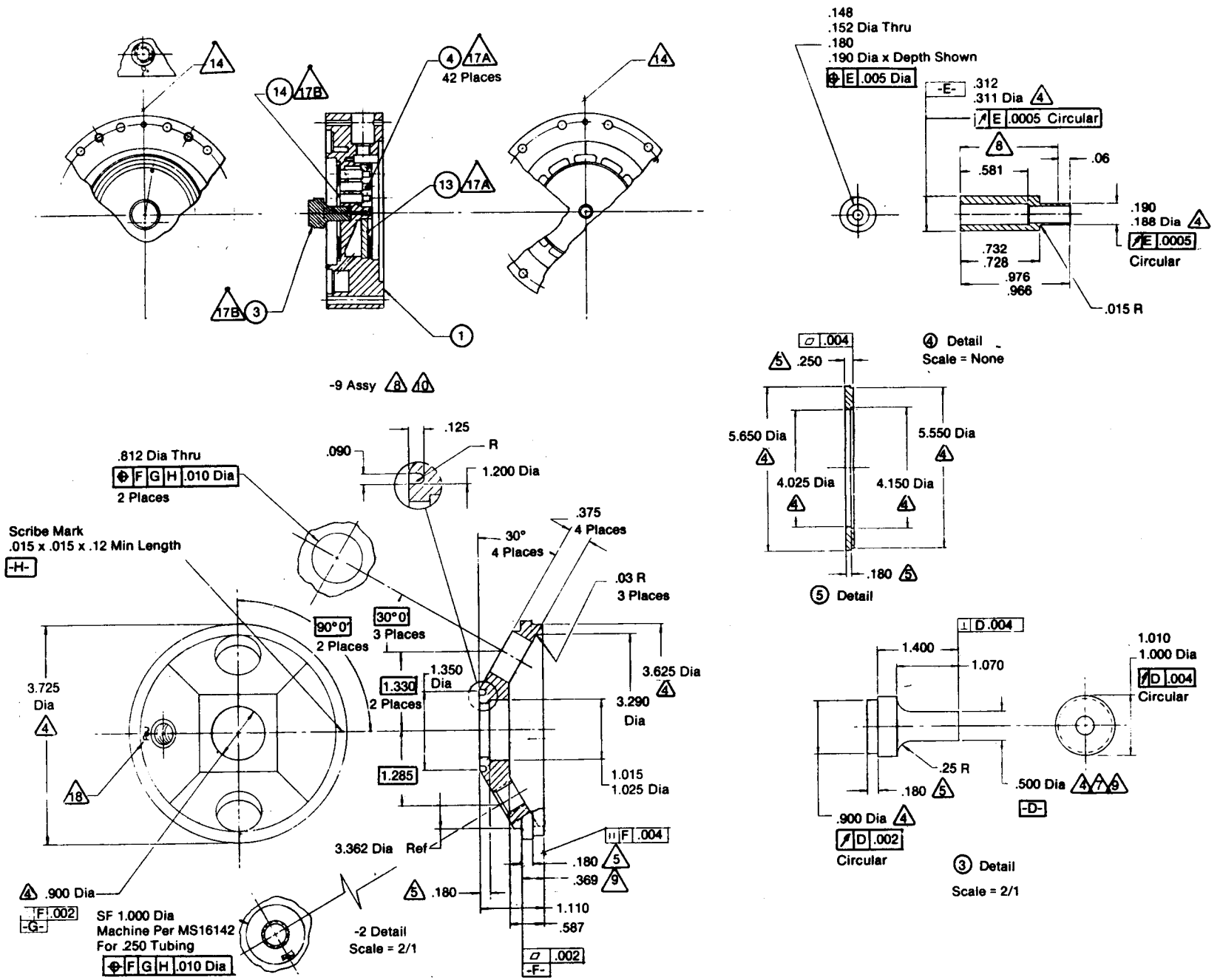

Figure E-2. Dual Throat Thruster Primary Injector Assembly

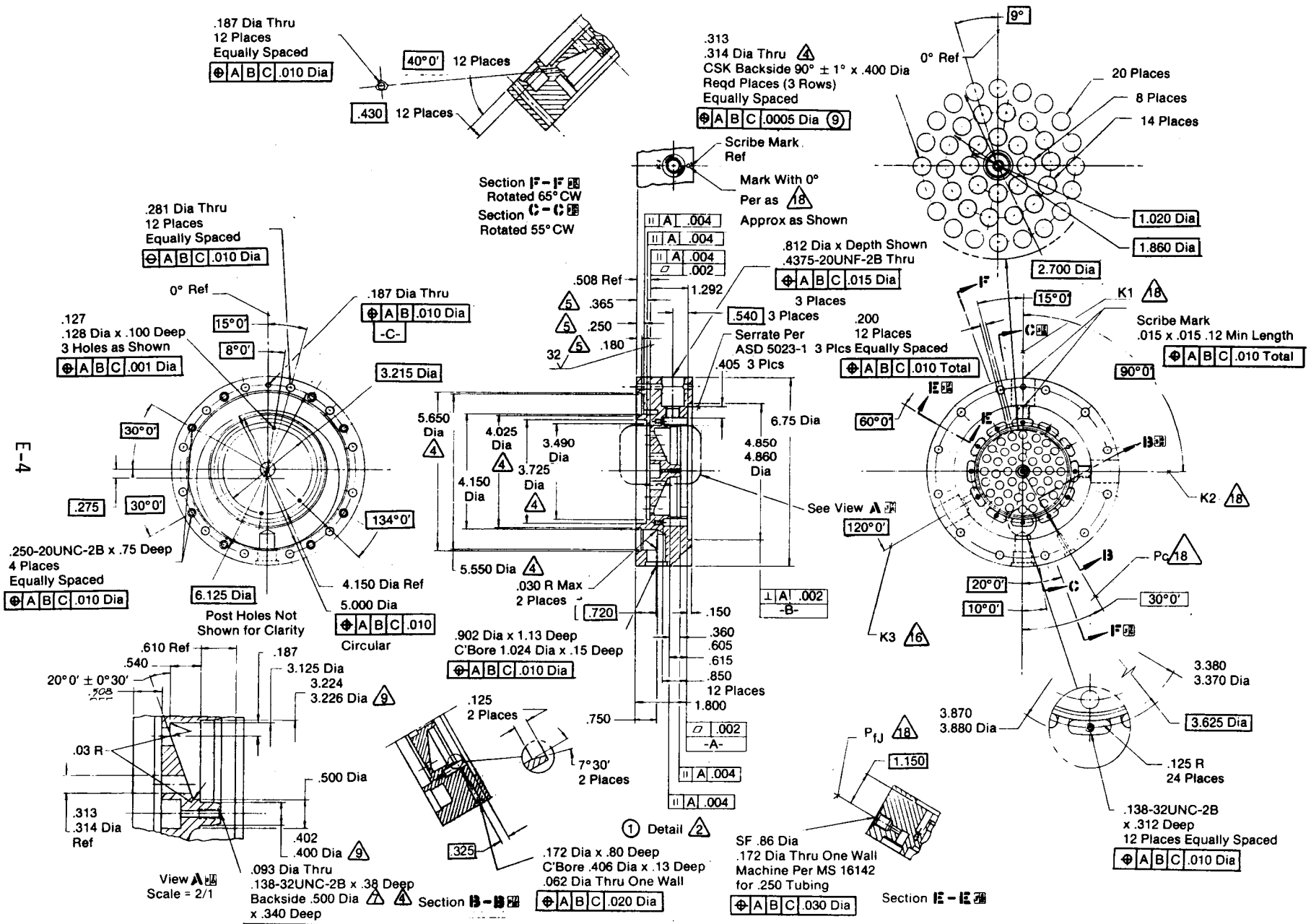

Figure E-3. Dual Throat Thruster Primary Injector Assembly

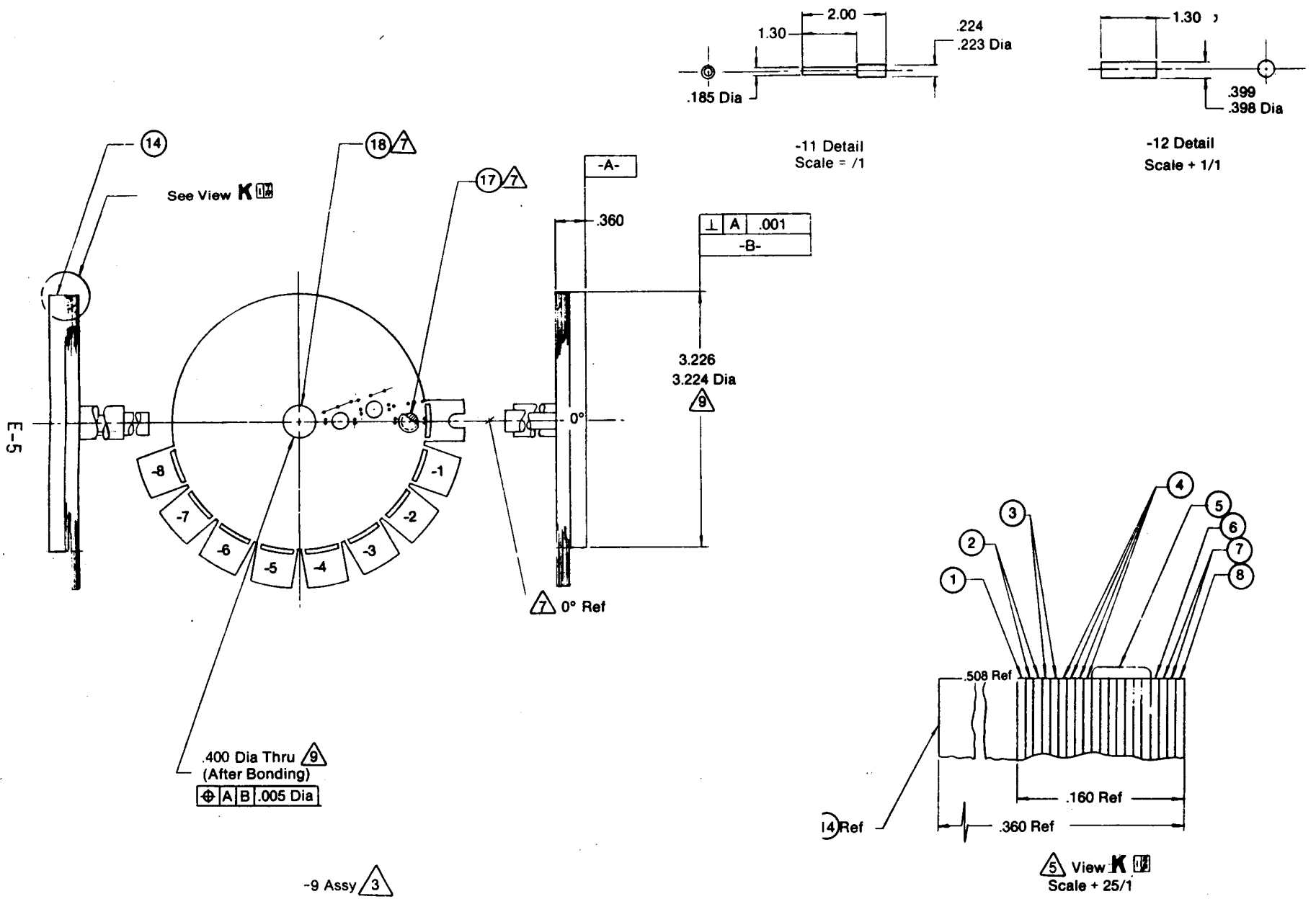

Figure E-4. Primary Injector Fuel Platelet Assembly

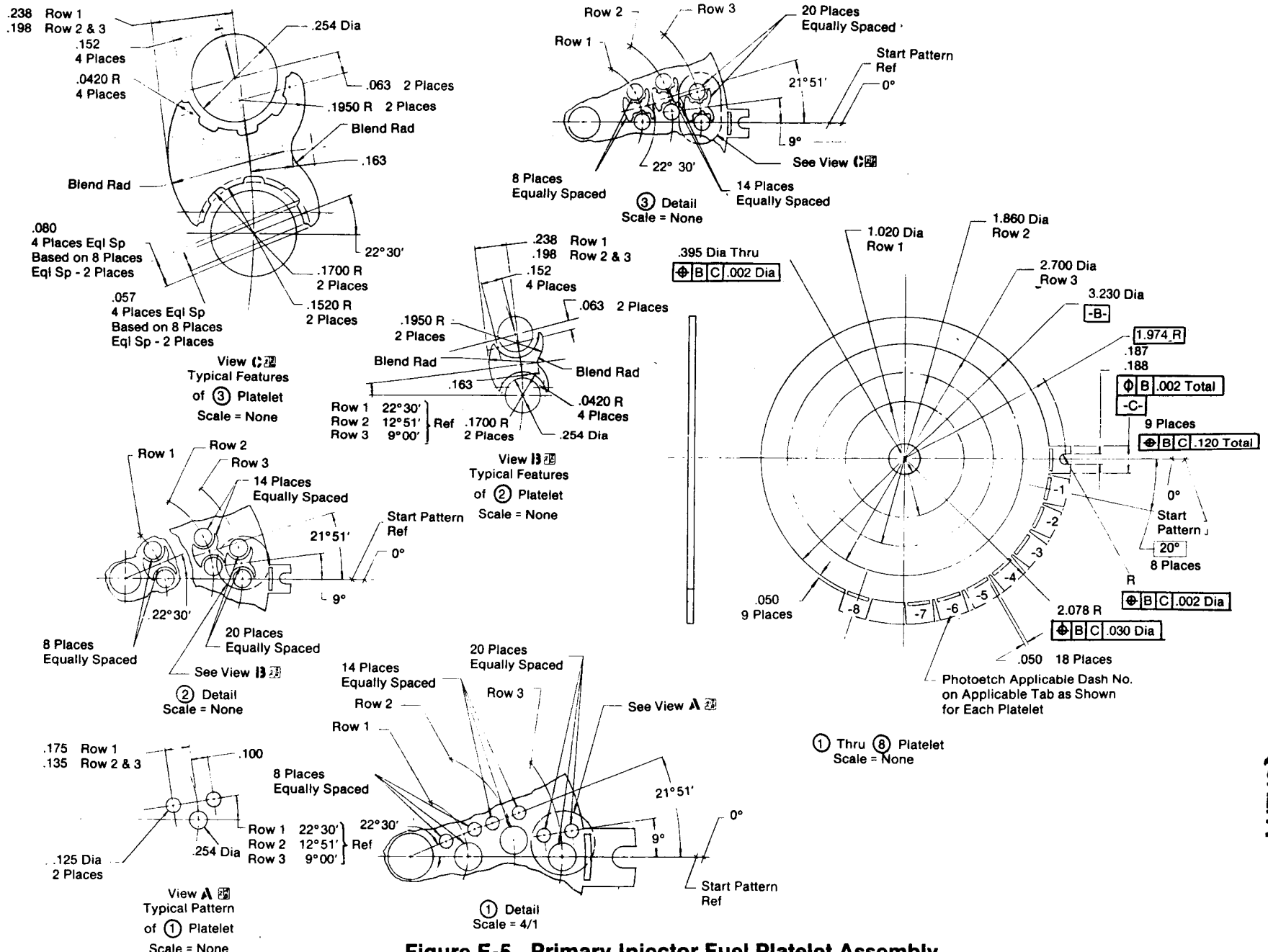

Figure E-5. Primary Injector Fuel Platelet Assembly

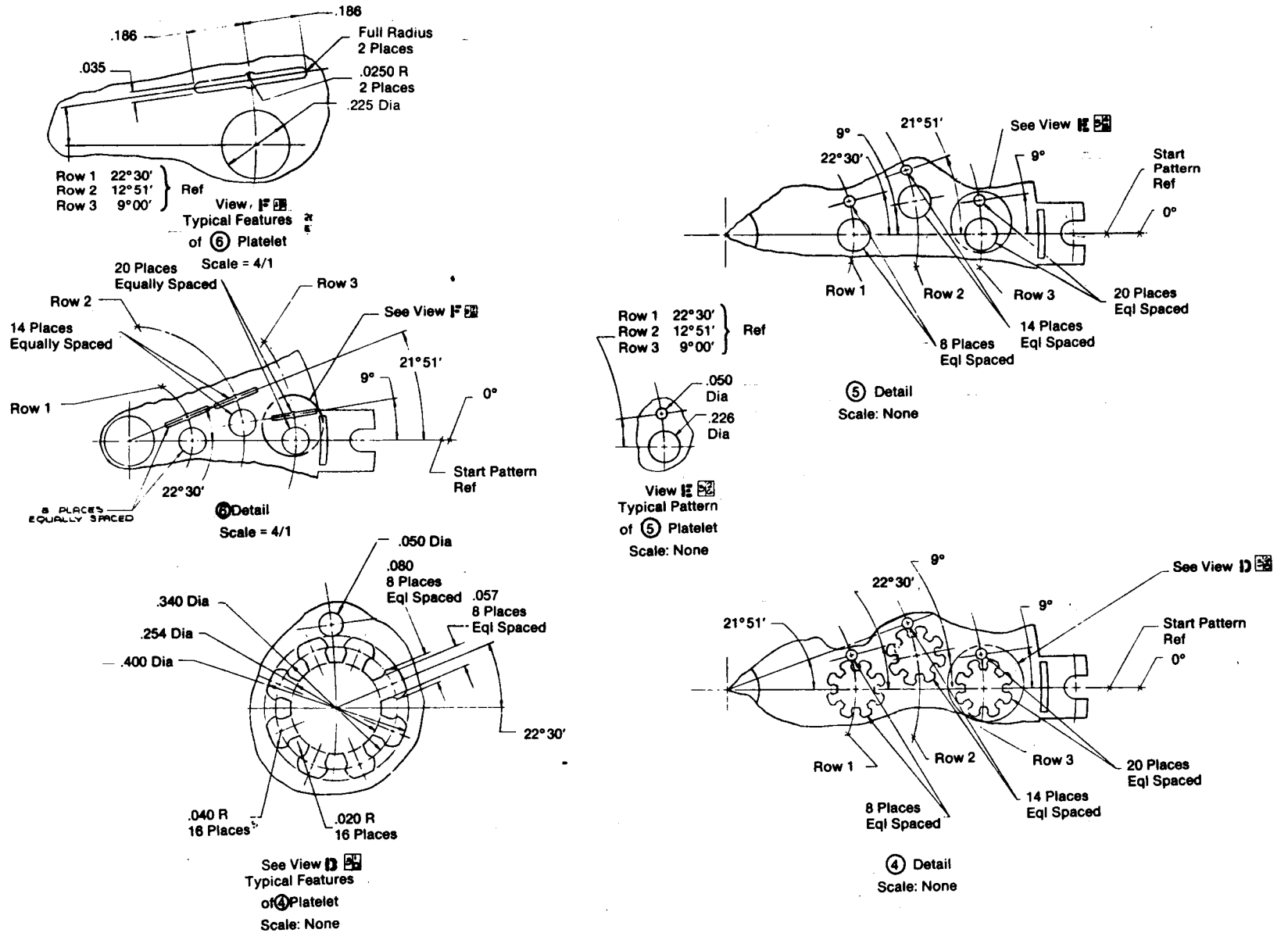

Figure E-6. Primary Injector Fuel Platelet Assembly

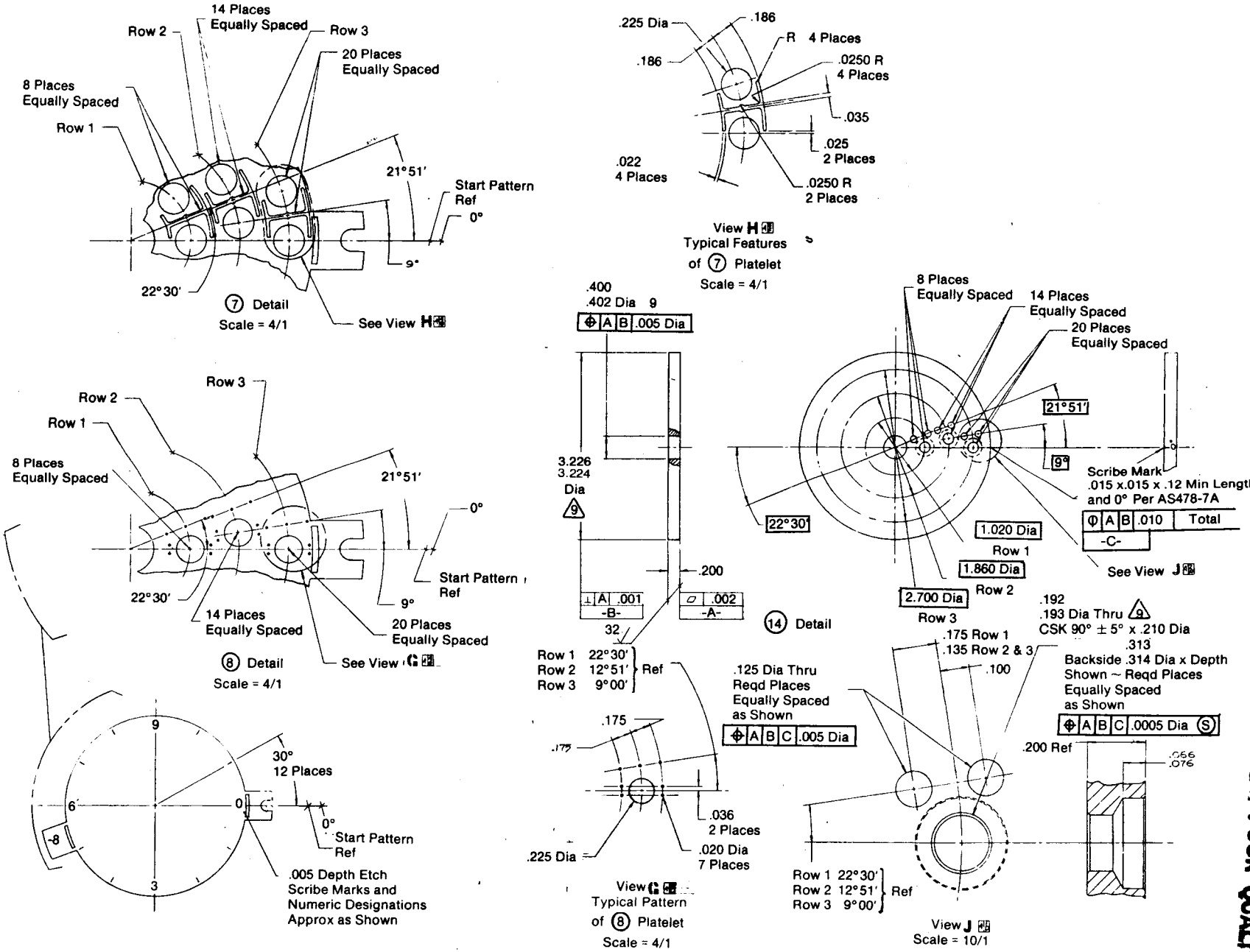

Figure E-7. Primary Injector Fuel Platelet Assembly

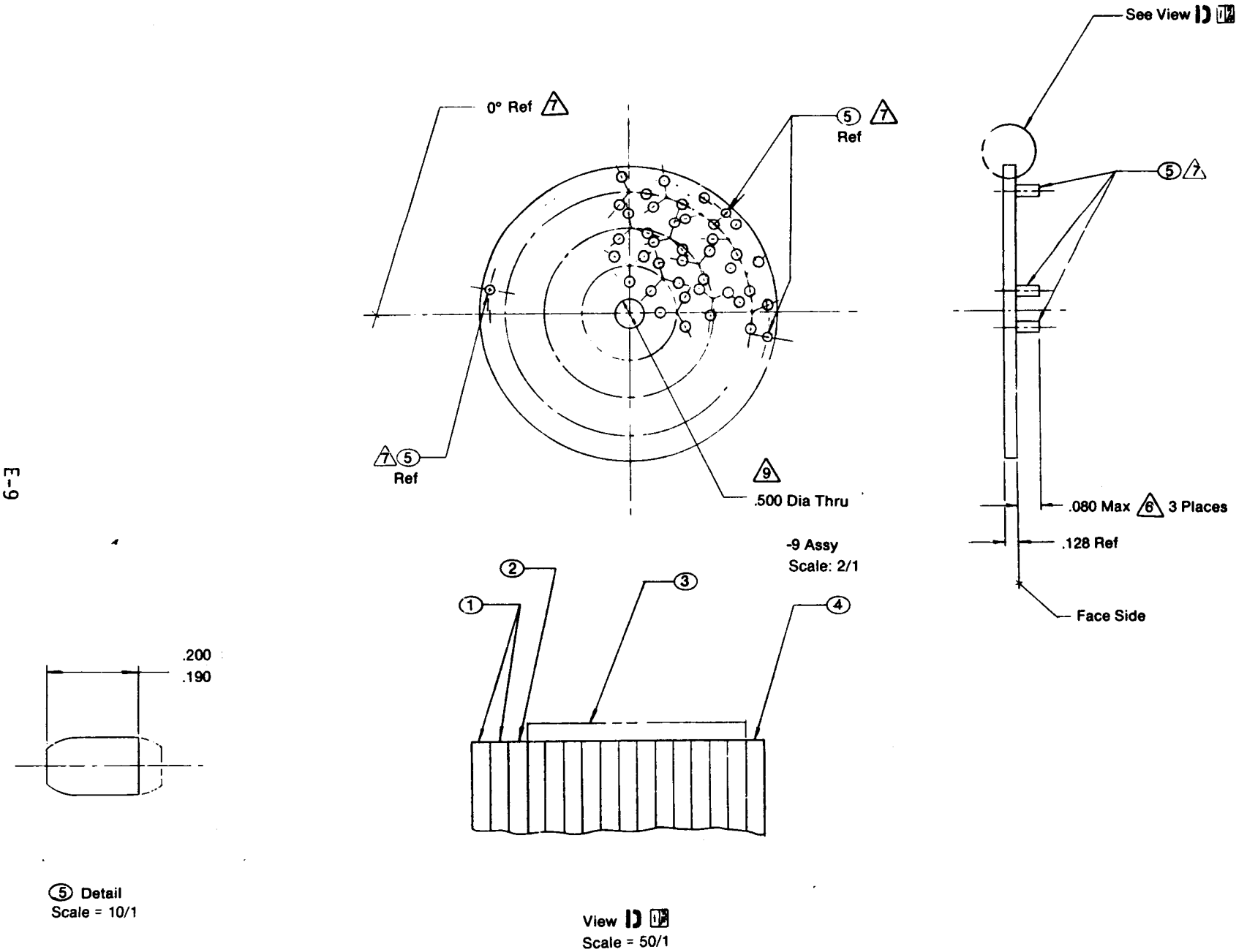

Figure E-8. Primary Injector Oxidizer Platelet Assembly

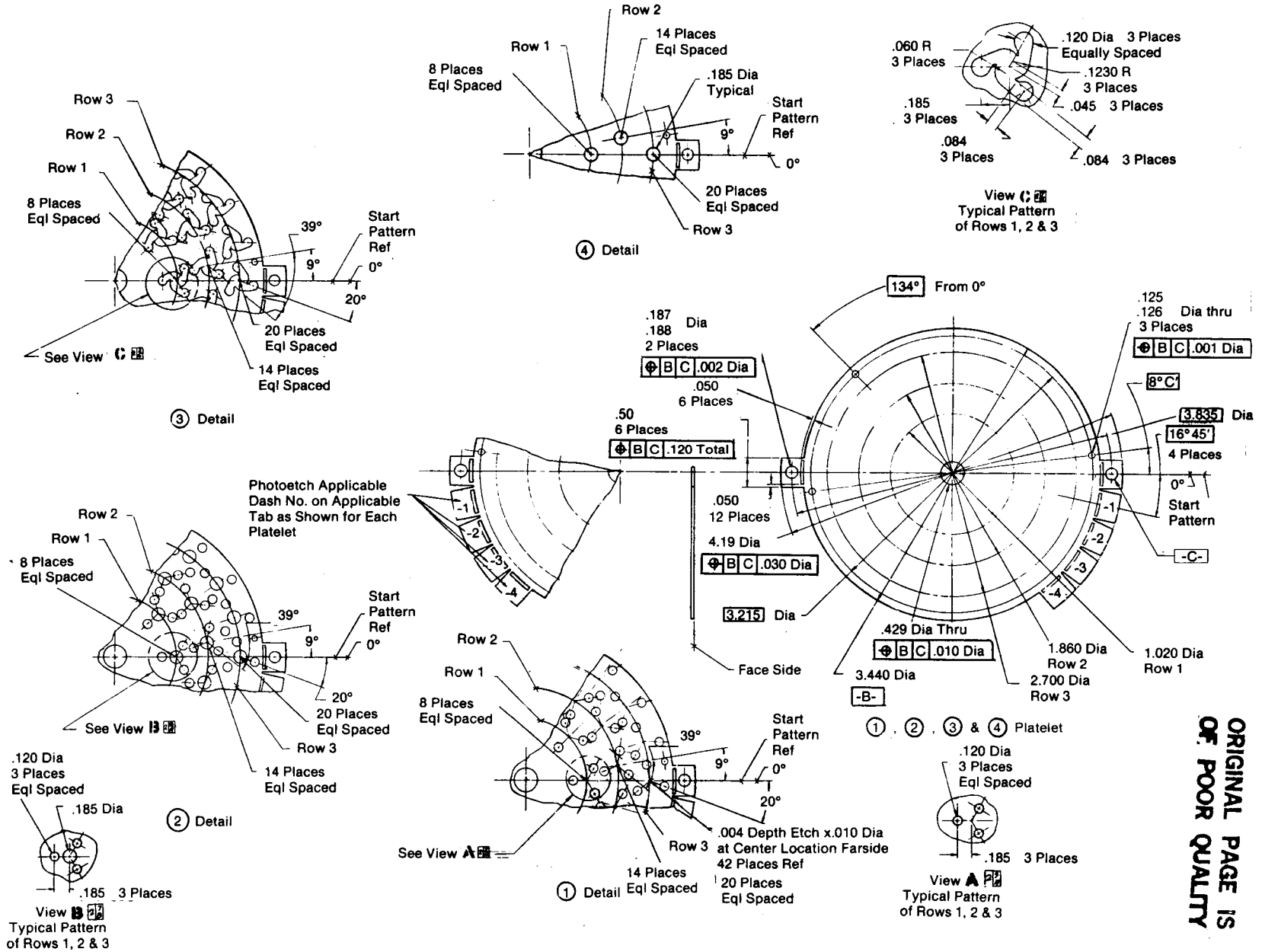

Figure E-9 . Primary Injector Oxidizer Platelet Assembly

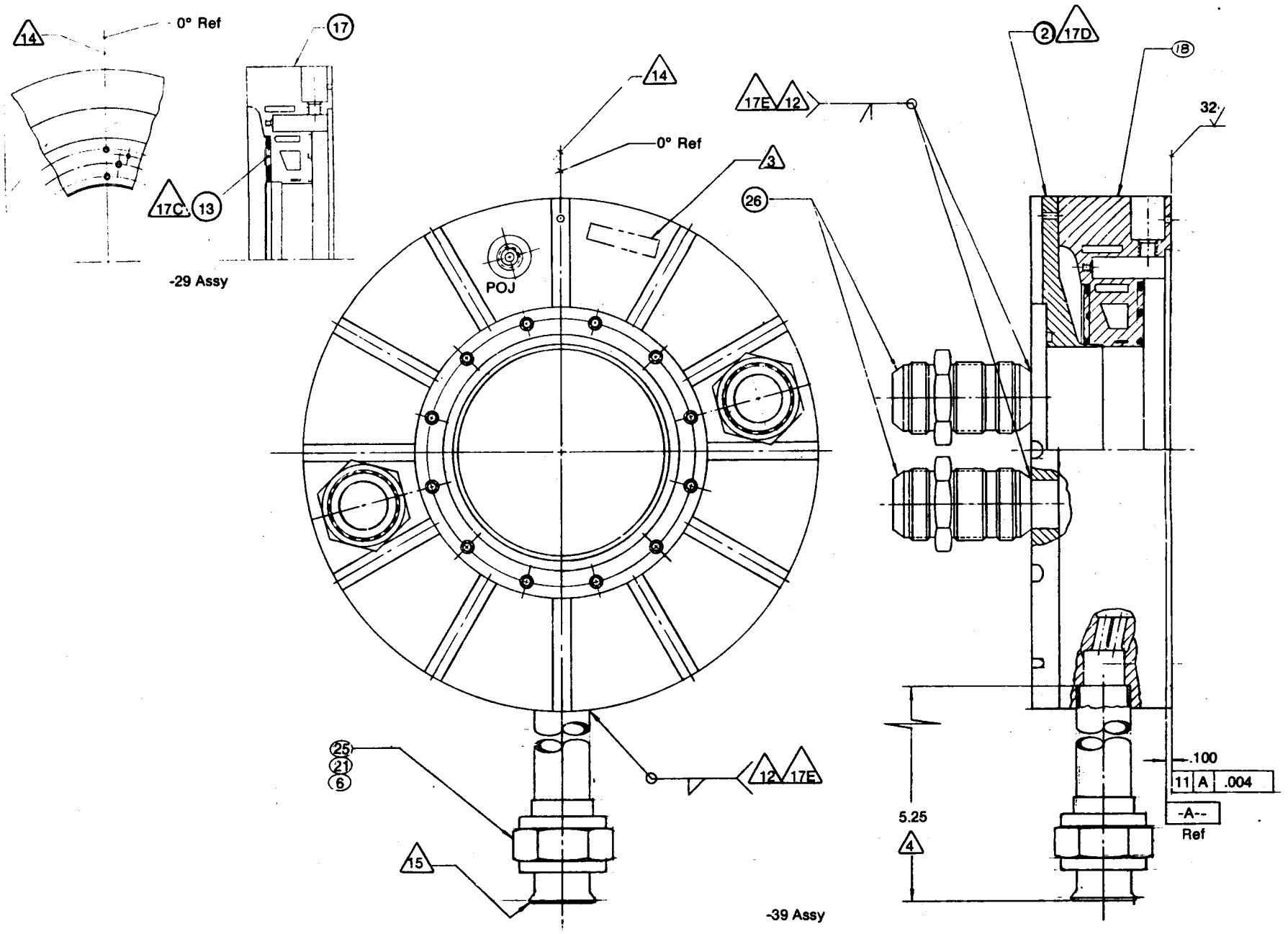

Figure E-10. Dual Throat Thruster Secondary Injector Assembly

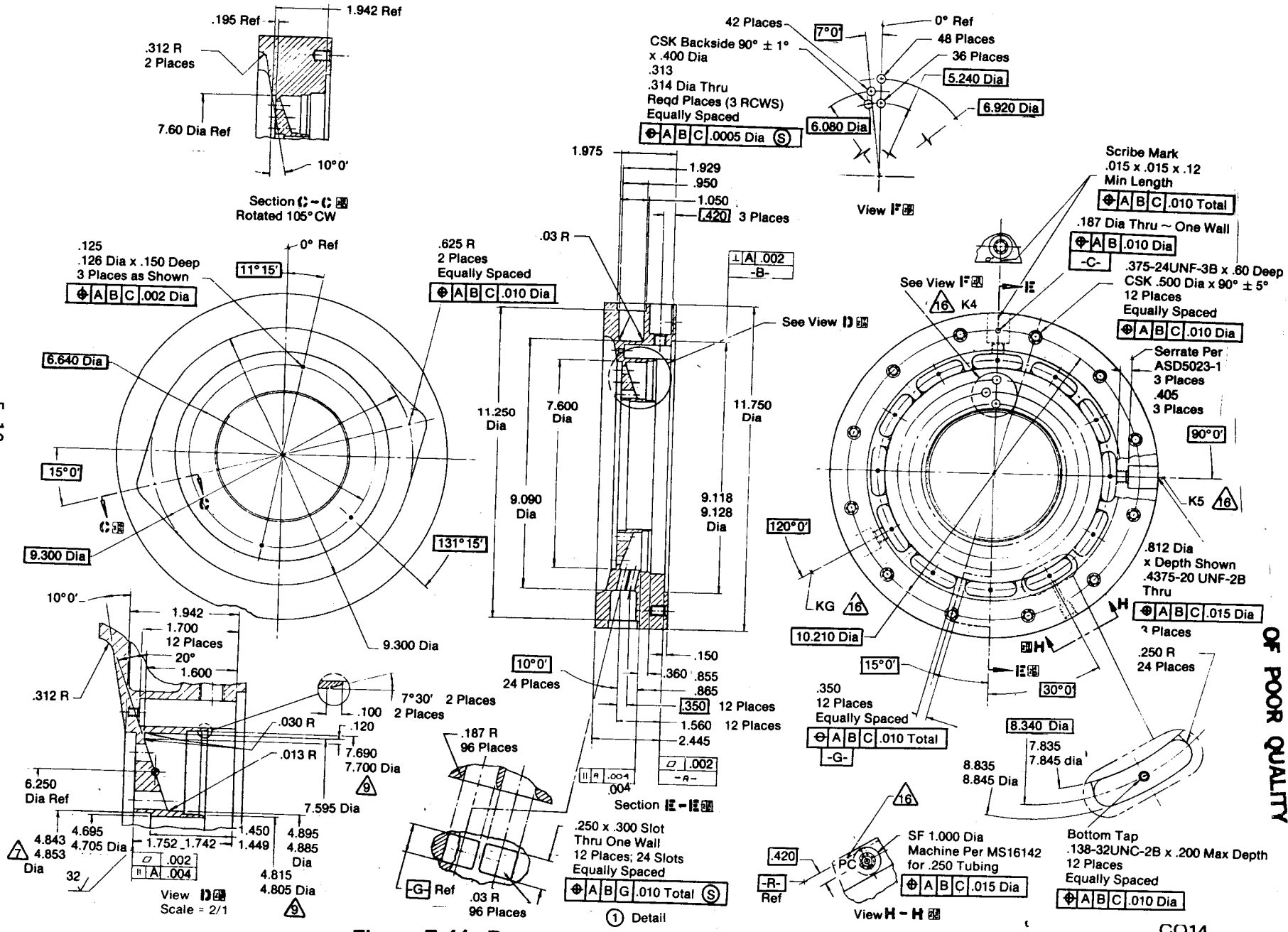

Figure E-11. Dual Throat Thruster Secondary Injector Assembly

CO14

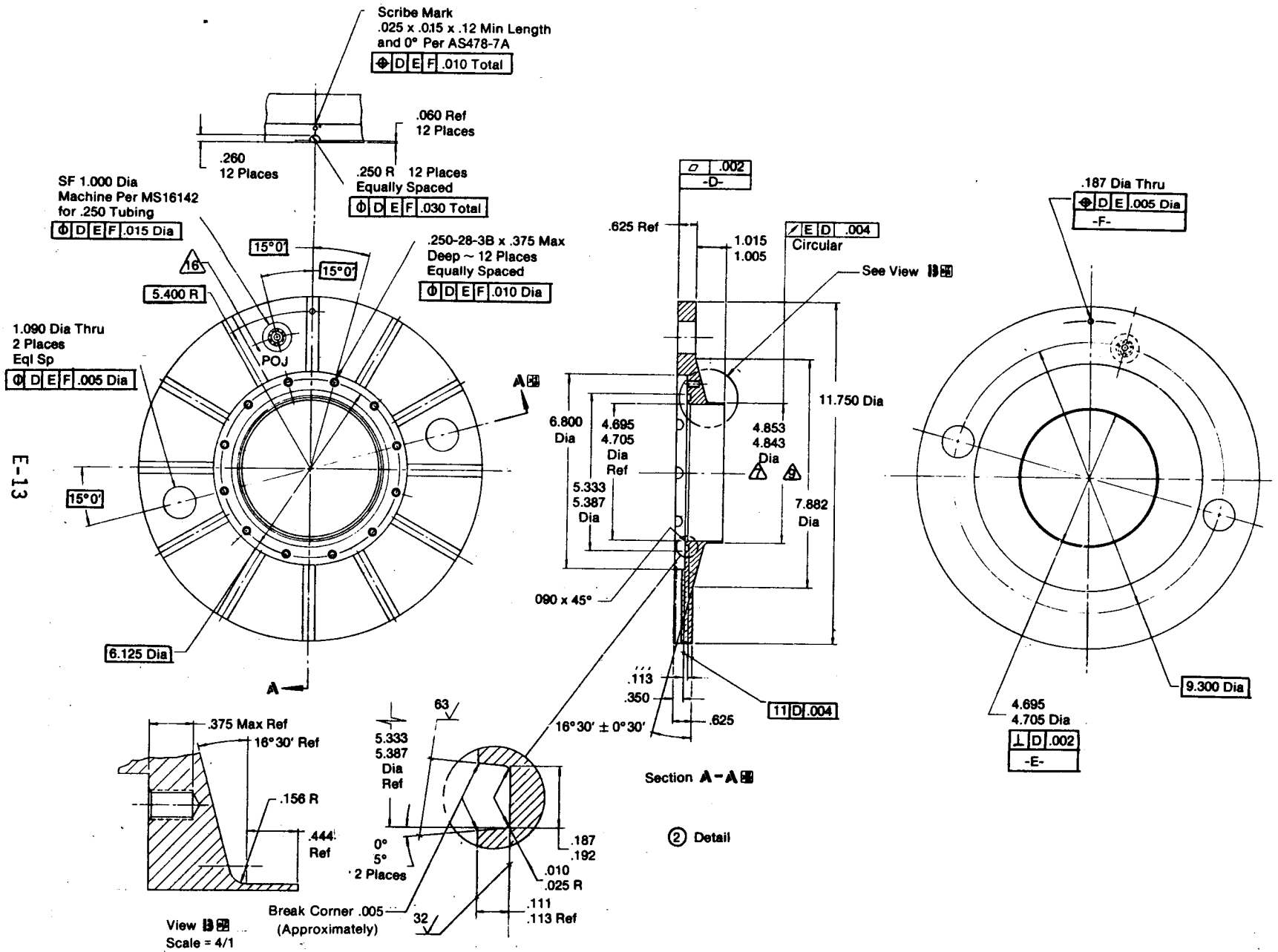

Figure E-12. Dual Throat Thruster Secondary Injector Assembly

ORIGINAL PAGE IS
OF POOR QUALITY

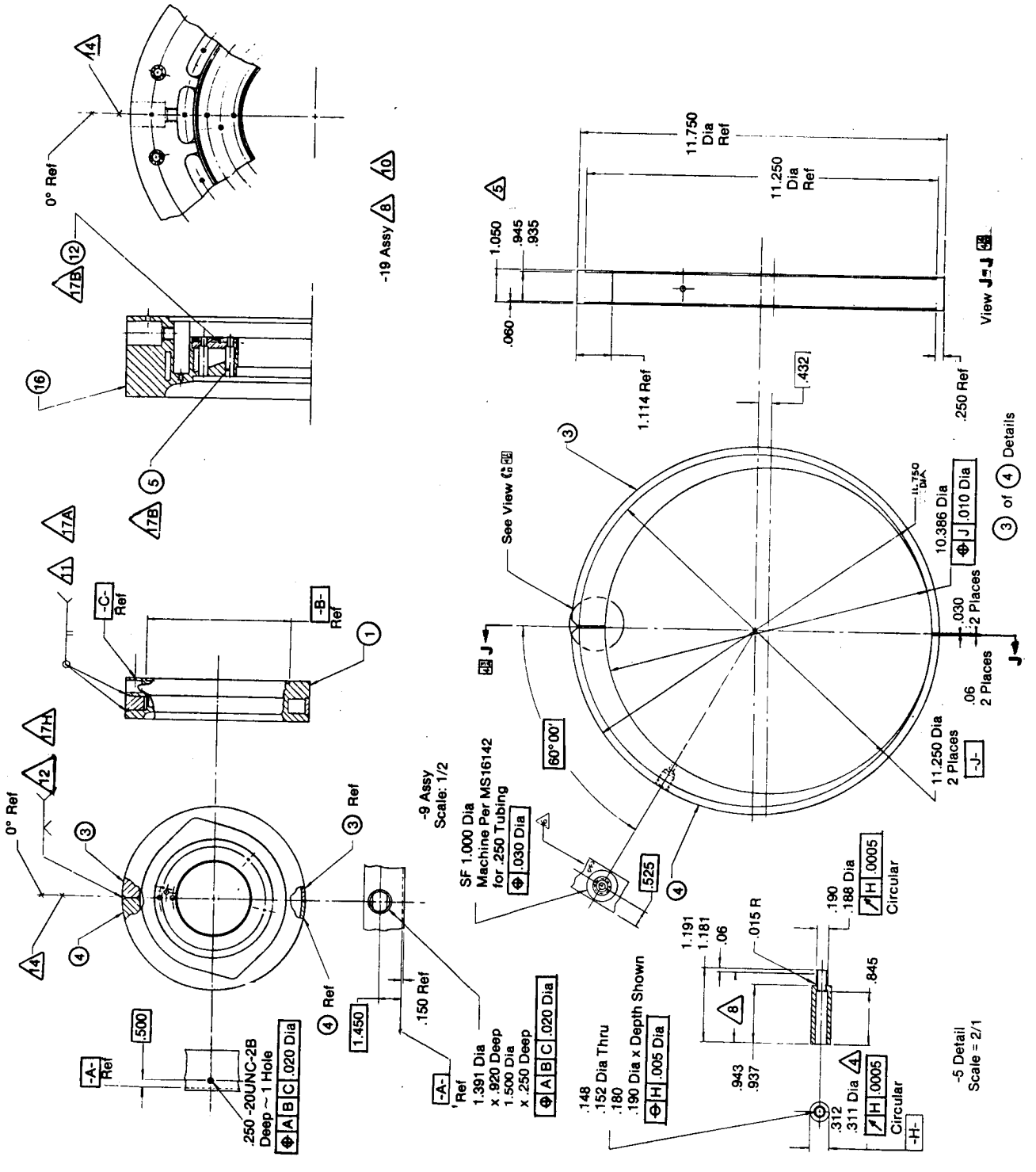

Figure E-13. Dual Throat Thruster Secondary Injector Assembly

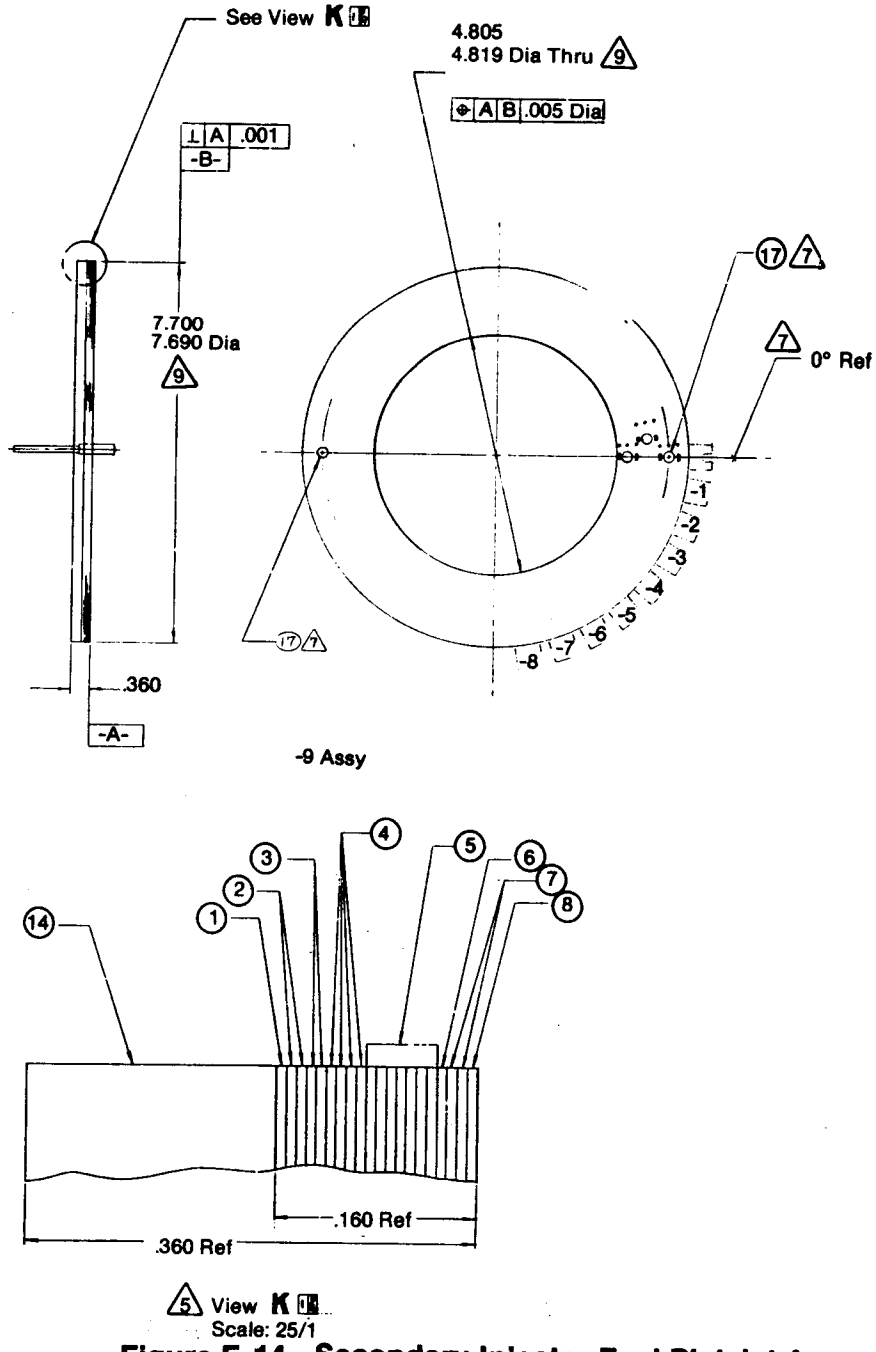

Figure E-14. Secondary Injector Fuel Platelet Assembly

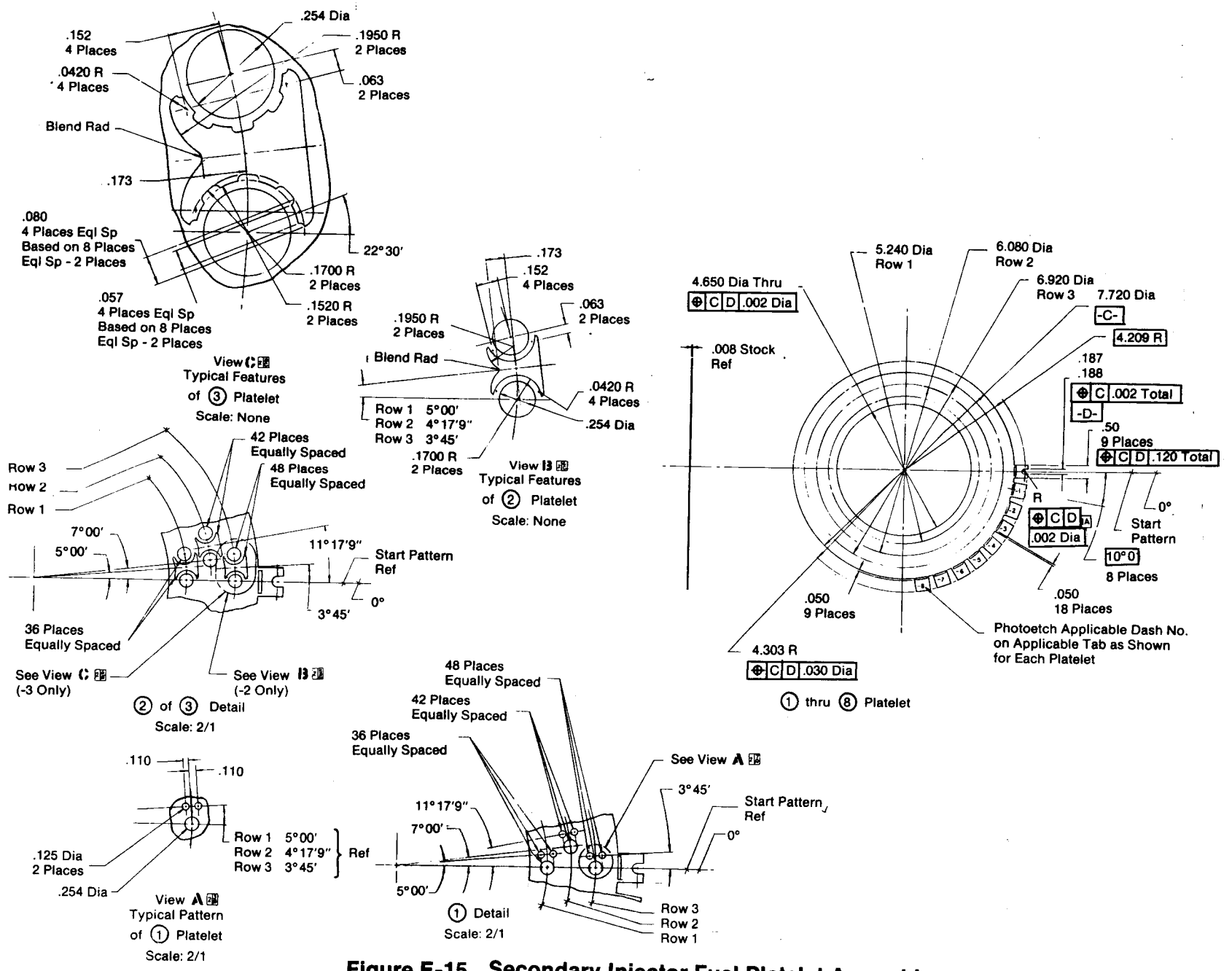

Figure E-15. Secondary Injector Fuel Platelet Assembly

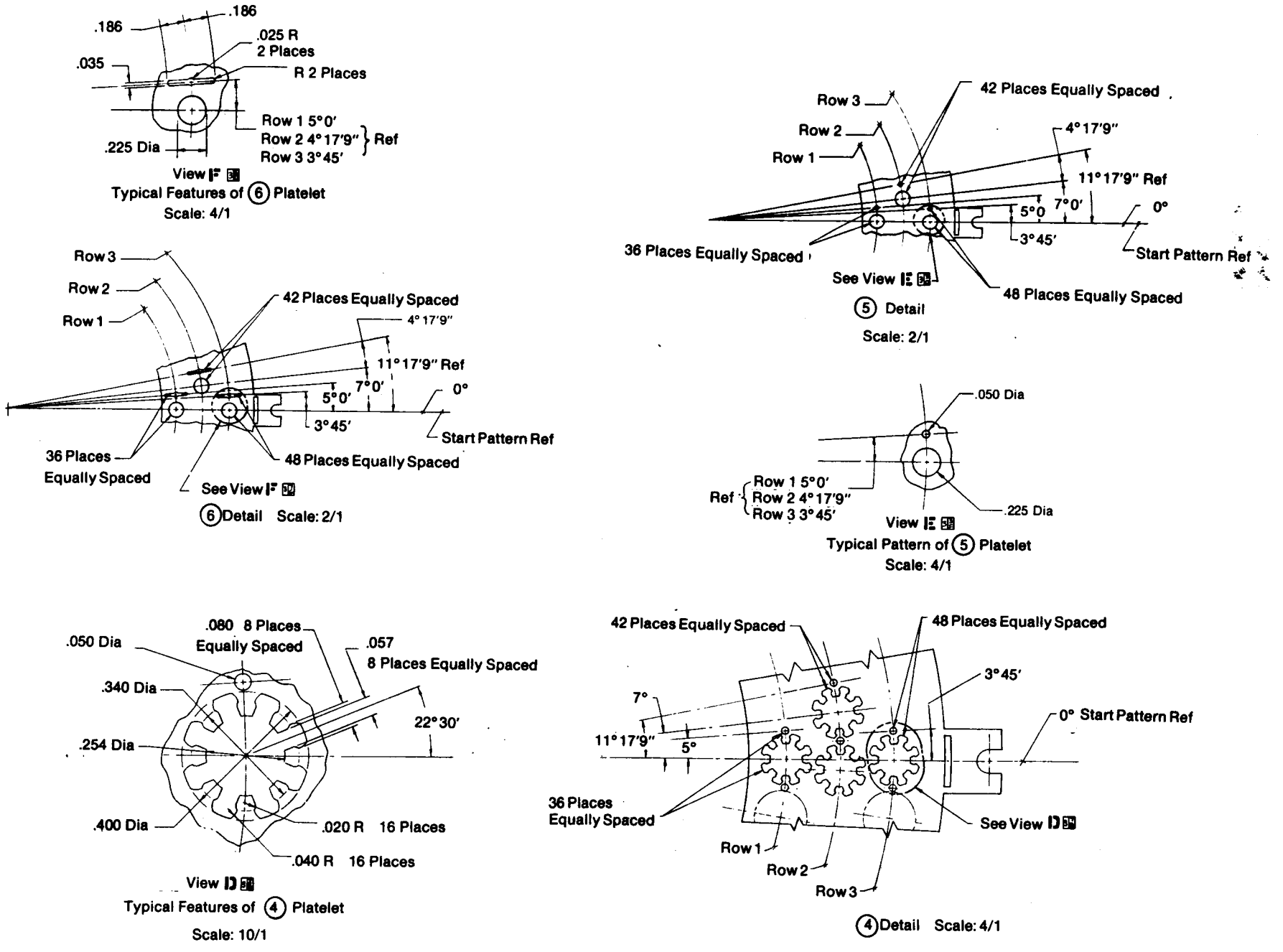

Figure E-16. Secondary Injector Fuel Platelet Assembly

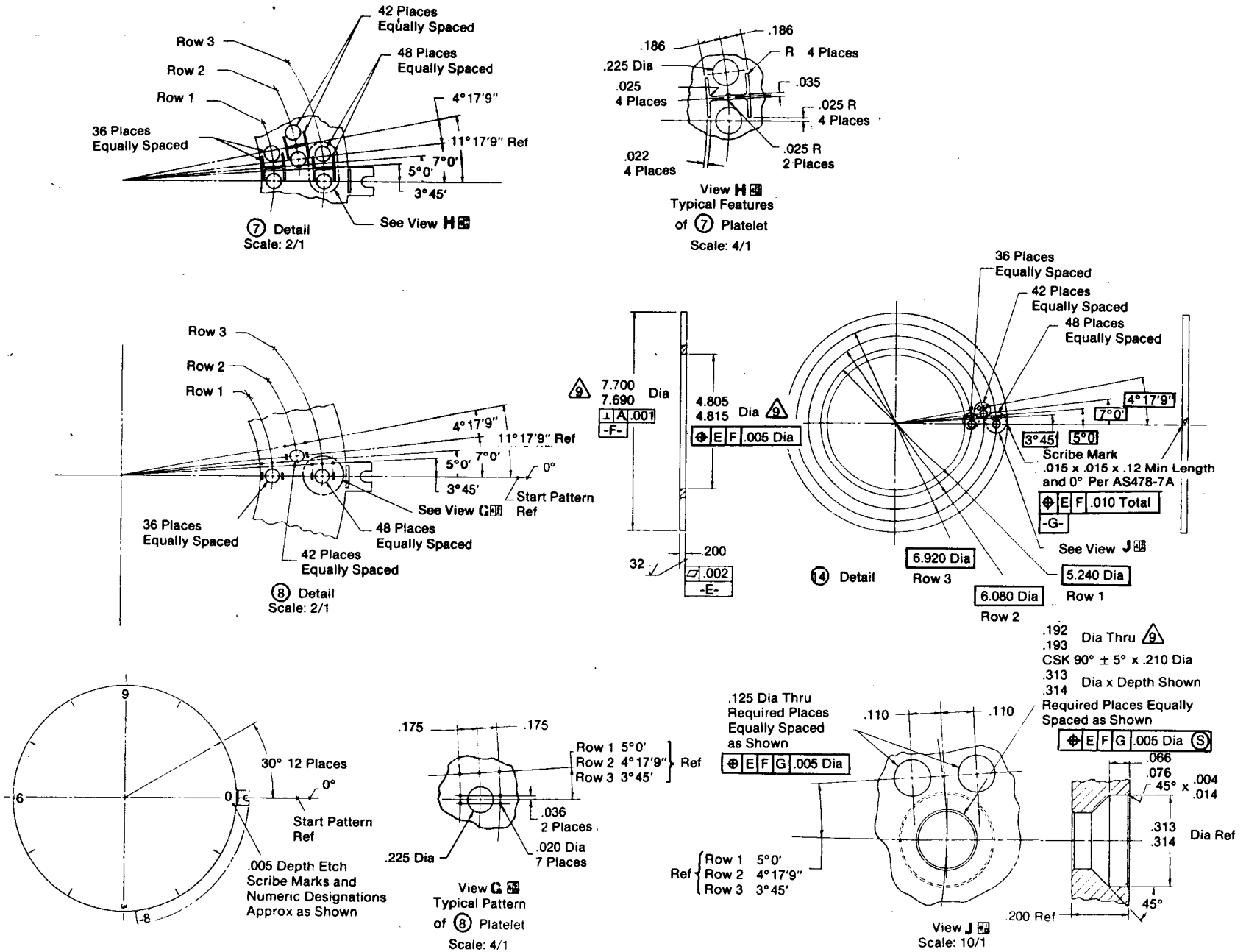

Figure E-17. Secondary Injector Fuel Platelet Assembly

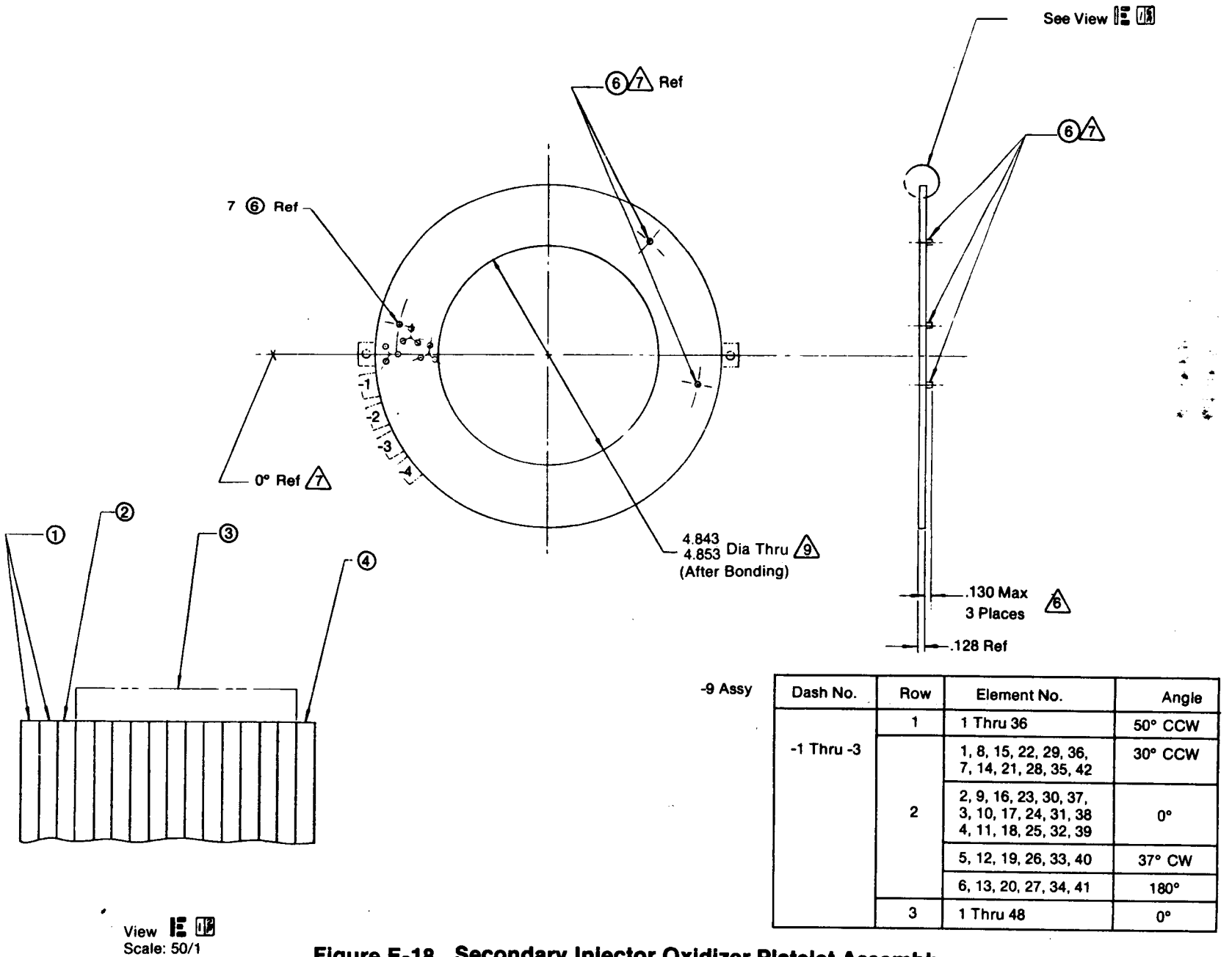

-9 Assy

Dash No.	Row	Element No.	Angle
-1 Thru -3	1	1 Thru 36	50° CCW
	2	1, 8, 15, 22, 29, 36, 7, 14, 21, 28, 35, 42	30° CCW
		2, 9, 16, 23, 30, 37, 3, 10, 17, 24, 31, 38 4, 11, 18, 25, 32, 39	0°
		5, 12, 19, 26, 33, 40	37° CW
		6, 13, 20, 27, 34, 41	180°
	3	1 Thru 48	0°

Figure E-18. Secondary Injector Oxidizer Platelet Assembly

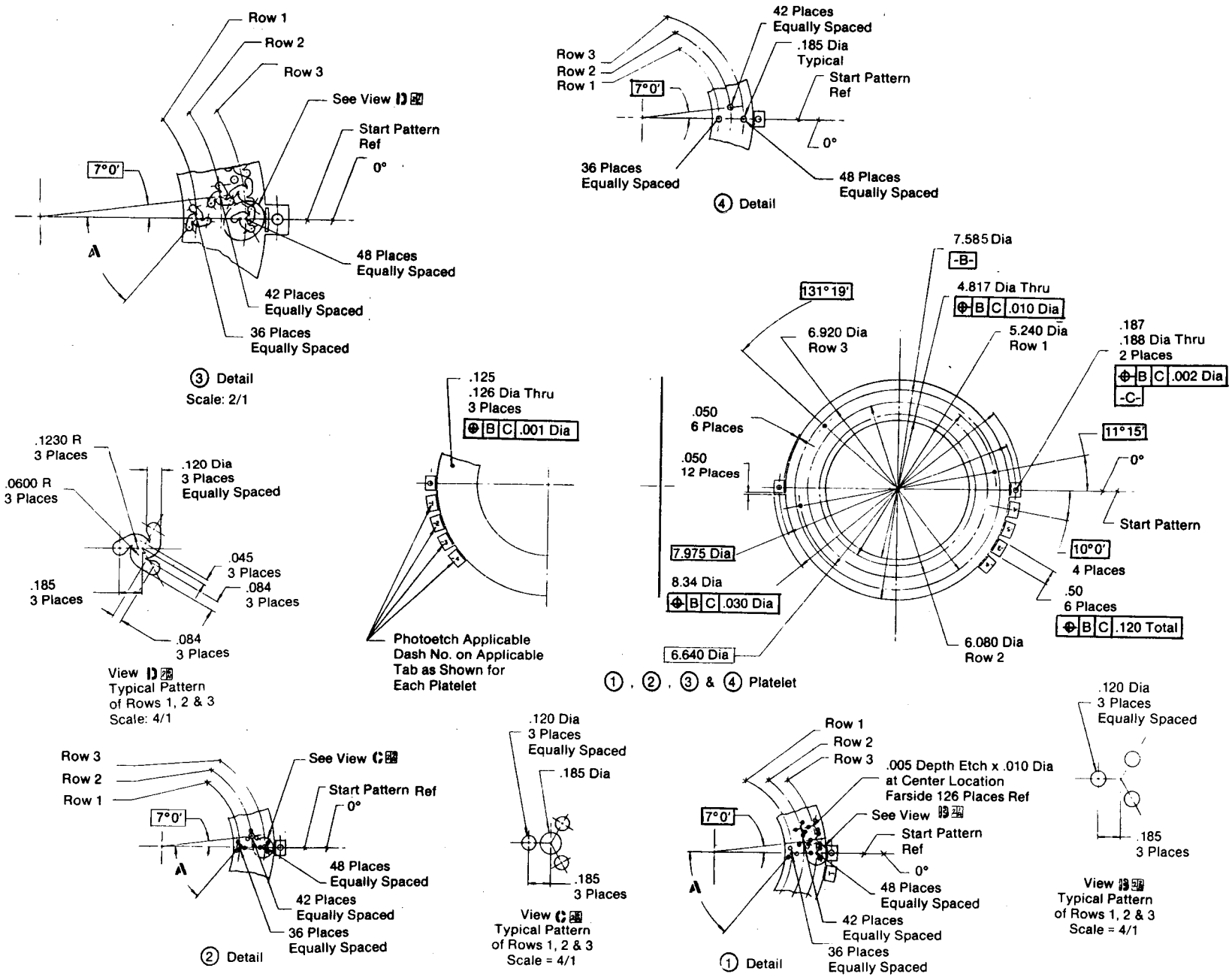

Figure E-19. Secondary Injector Oxidizer Platelet Assembly

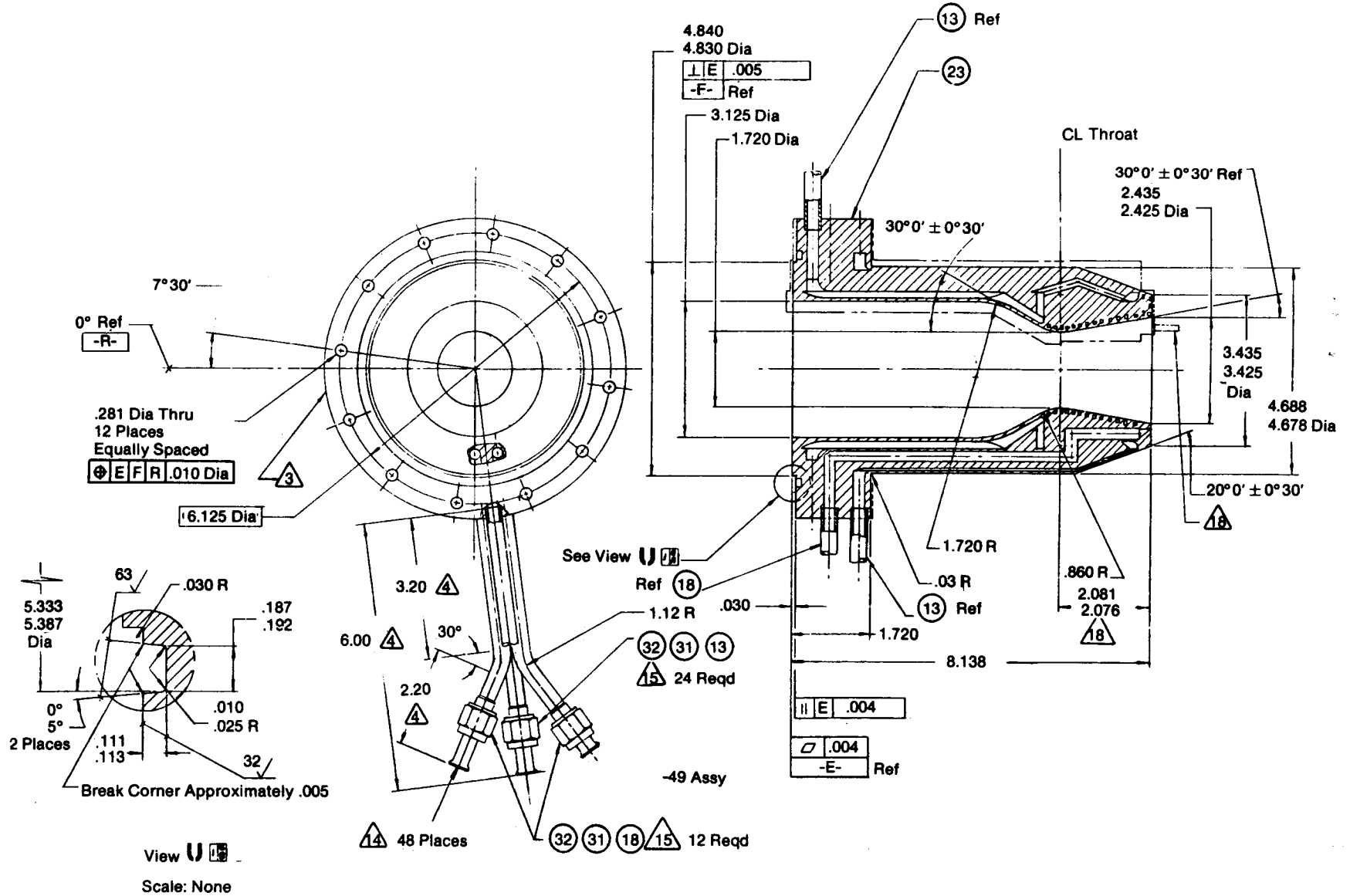

Figure E-20. Primary Chamber Assembly

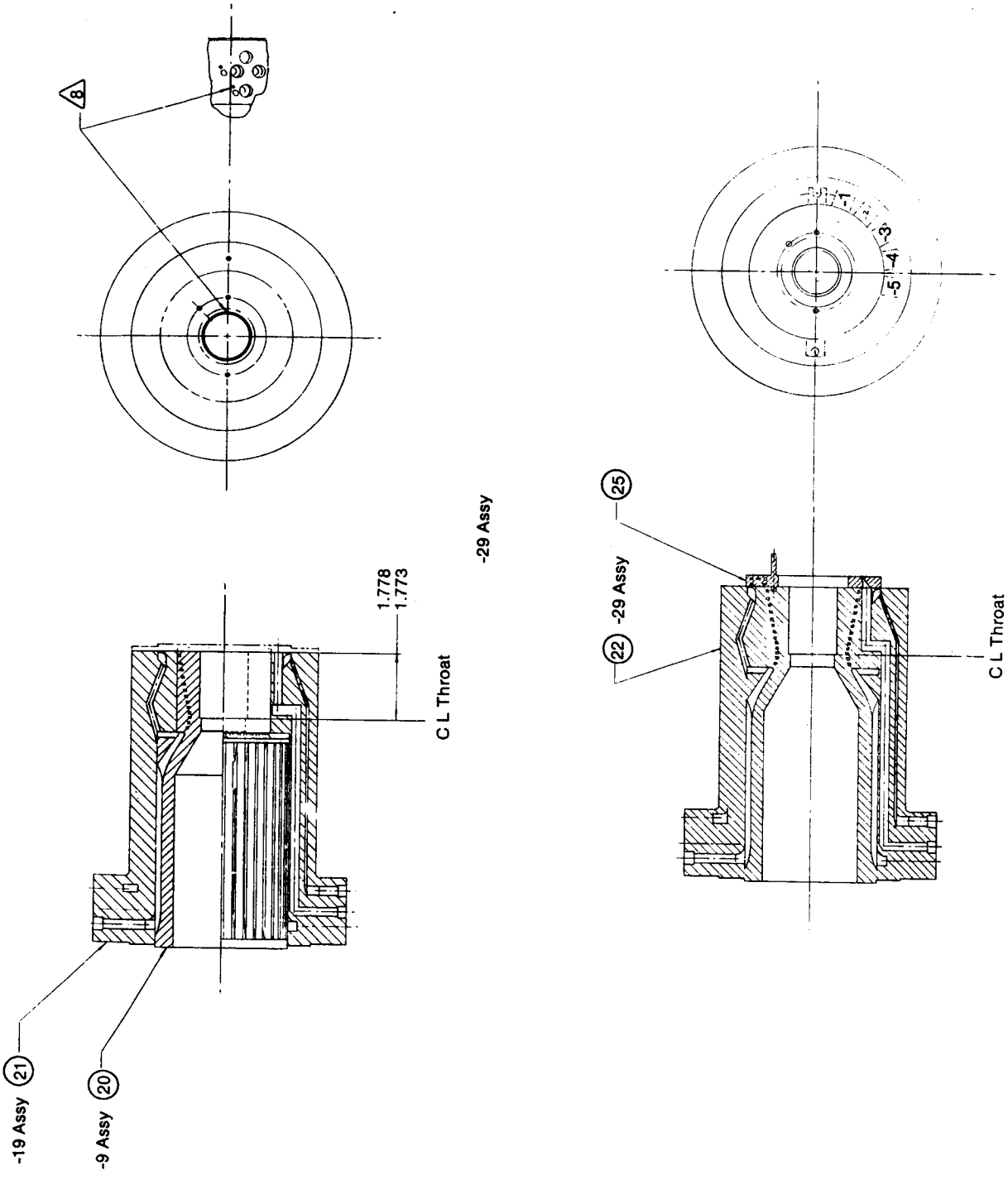

Figure E-21. Primary Chamber Assembly

Channel No.	1A	1B	2	3A	3B	4A	4B	5A	5B	6A	6B	7A	7B
A Dia ± .002	1.943	1.868	1.820	1.834	1.882	1.935	1.991	2.051	2.115	2.179	2.242	2.329	2.388
B Dim ± .005	.098	.230	.371	.512	.652	.882	.963	1.193	1.314	1.494	1.673	1.862	2.040
C Angle ± 0°30'				10°	10°	10°	10°	10°	10°	10°	10°	10°	10°
D Angle ± 0°30'	15°	15°											
E Dia ± .002	2.020	1.945	1.912	1.941	1.989	2.056	2.112	2.182	2.246	2.320	2.385		
Dash No.	-1	-2	-3	-4	-5	-6	-7	-8	-10	-11	-12		
F Dia. ± .002	2.020	1.945	1.912	1.939	1.989	2.056	2.112	2.182	2.246	2.320	2.383		
G Angle ± 0°30' CCW From 0°	165°	165°	105°	45°	45°	15°	15°	75°	75°	135°	135°		
W Ref	.0385	.0385	.0460	.0535	.0535	.0605	.0605	.0655	.0655	.0705	.0705	.1115	.0800

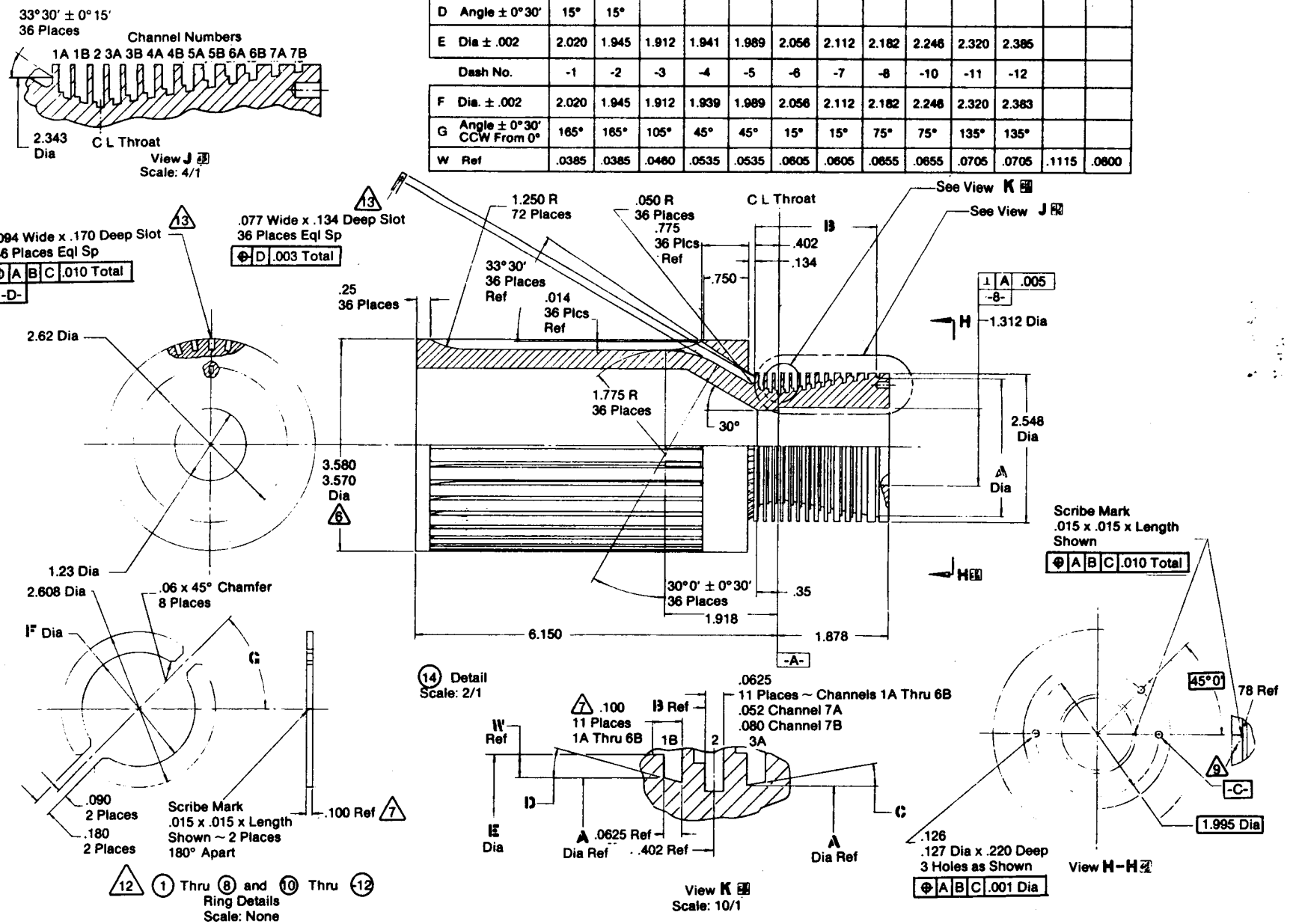

Figure E-22. Primary Chamber Inner Copper Liner

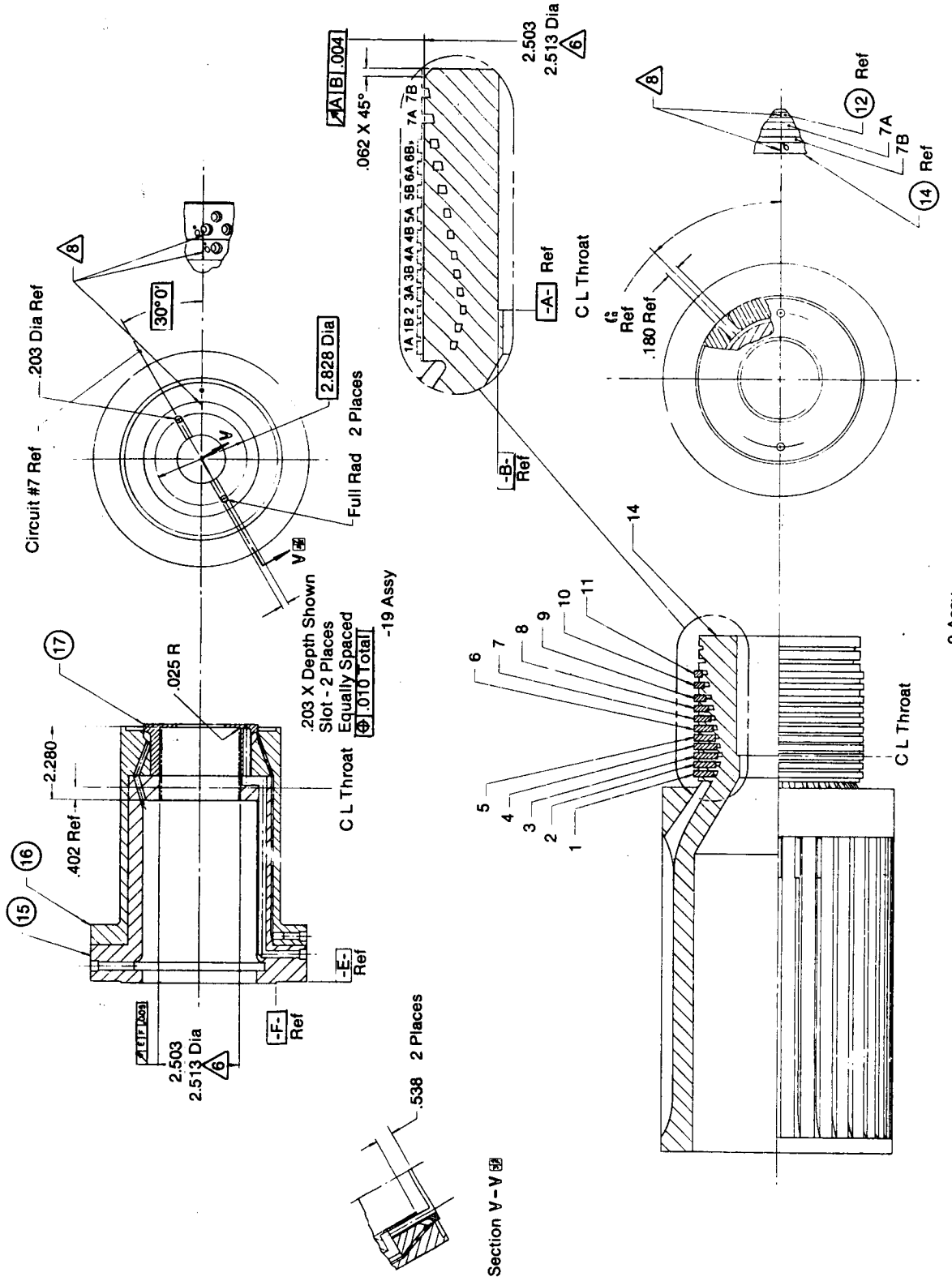

Figure E-23. Primary Chamber Inner Copper Liner

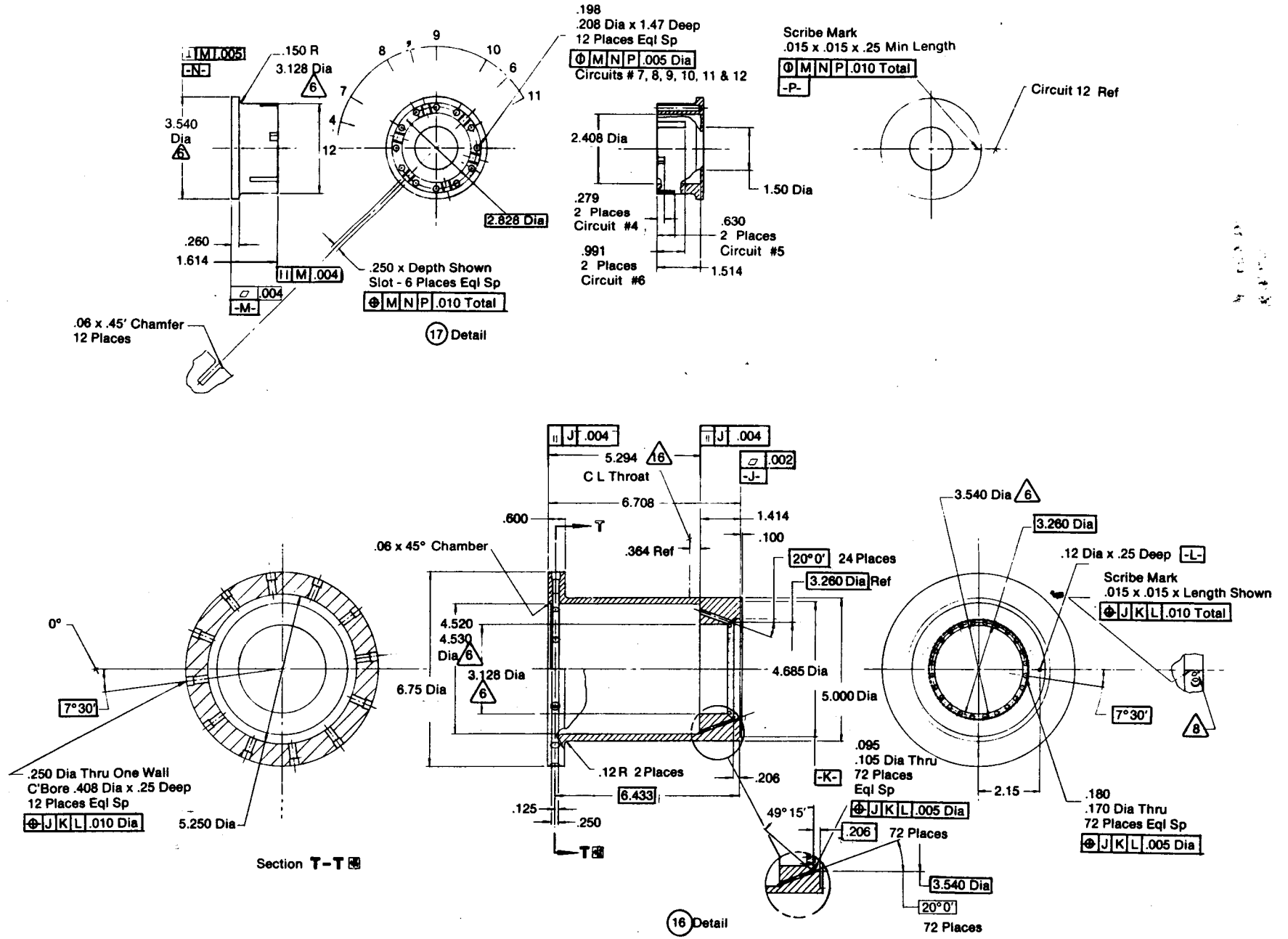

Figure E-24. Primary Chamber Outer Copper Liner

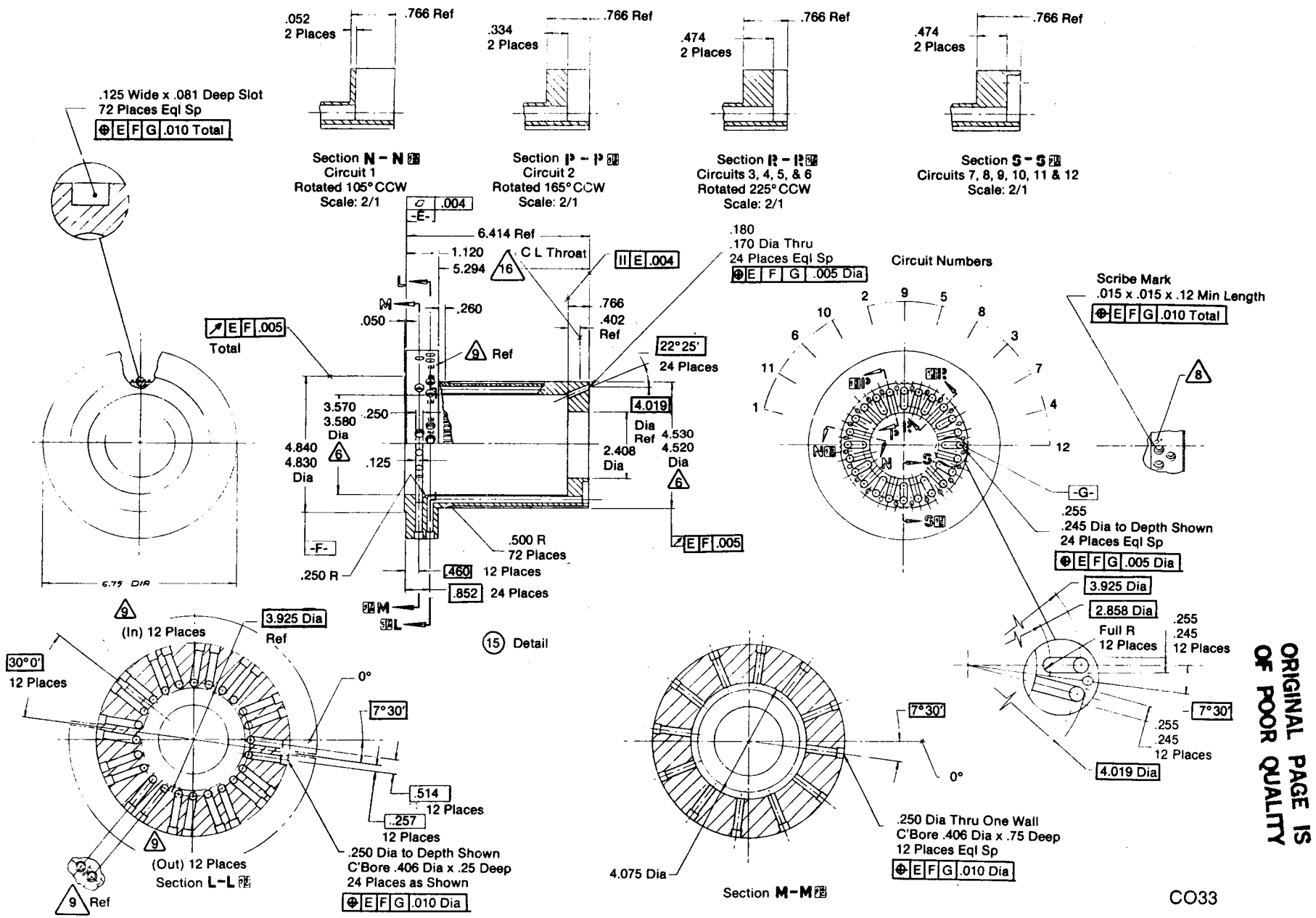

Figure E-25. Primary Chamber Forward Steel Core

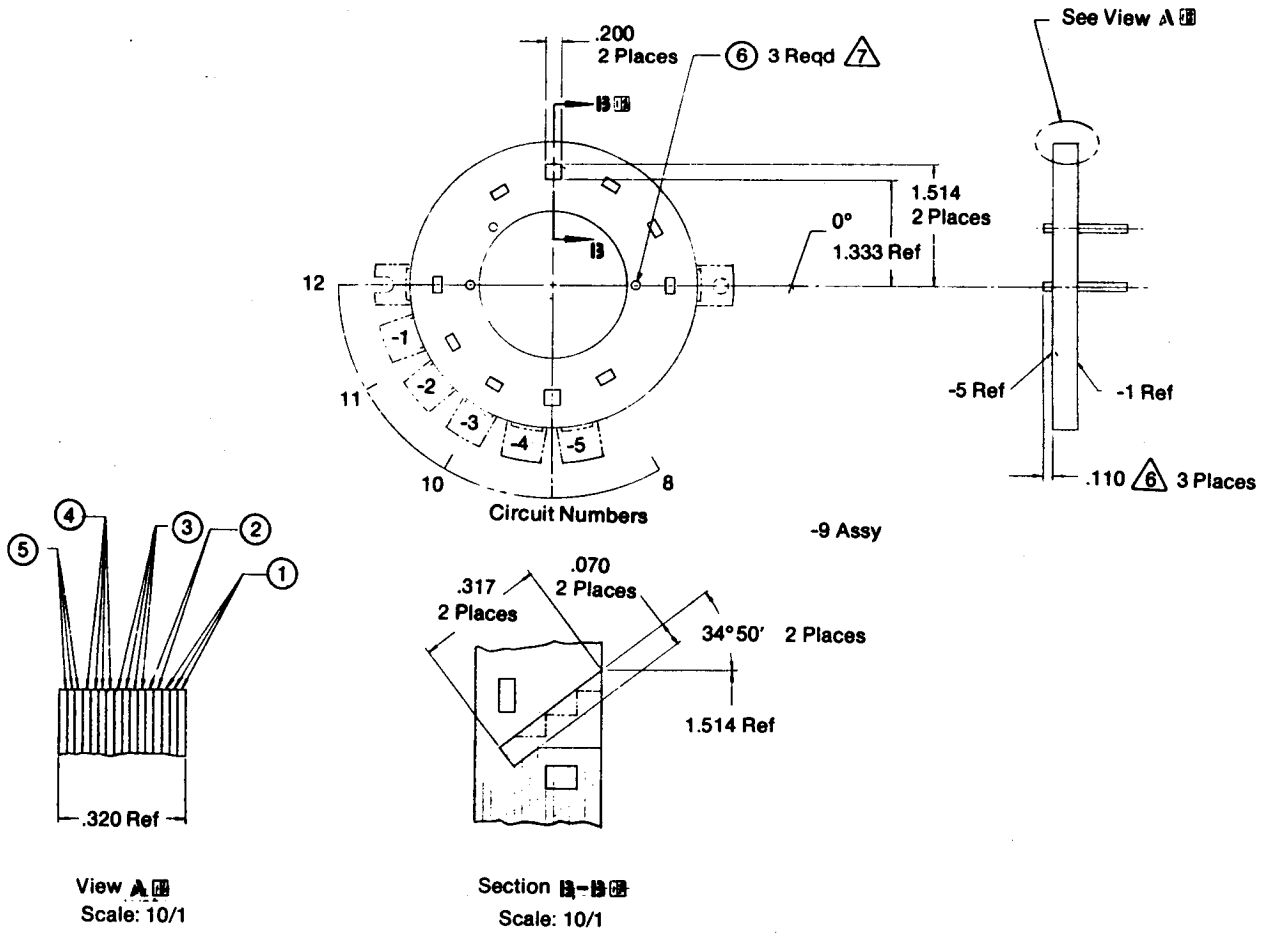

Figure E-26. Platelet Cooling Assembly - Primary Chamber

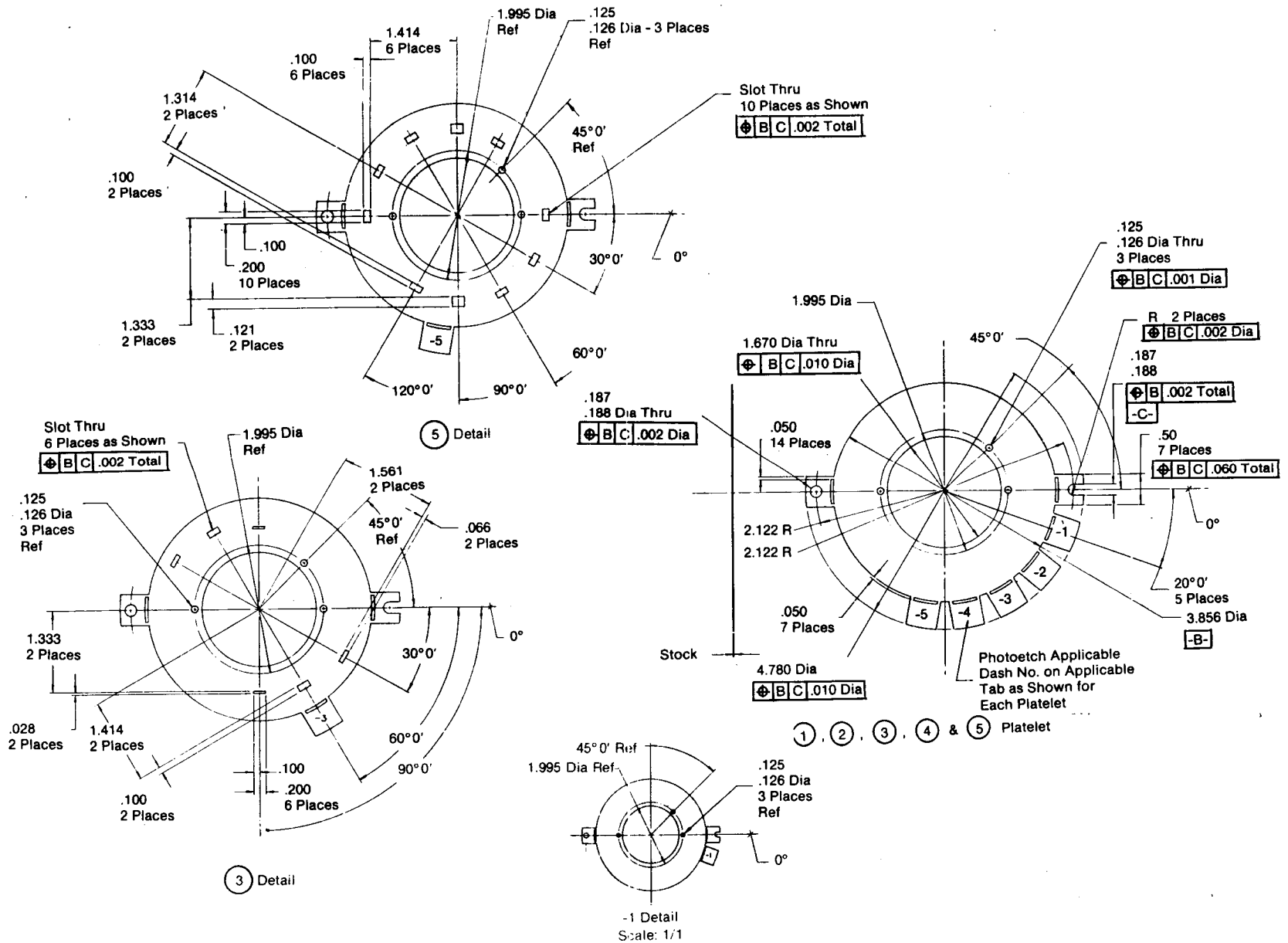

Figure E-27. Platelet Cooling Assembly - Primary Chamber

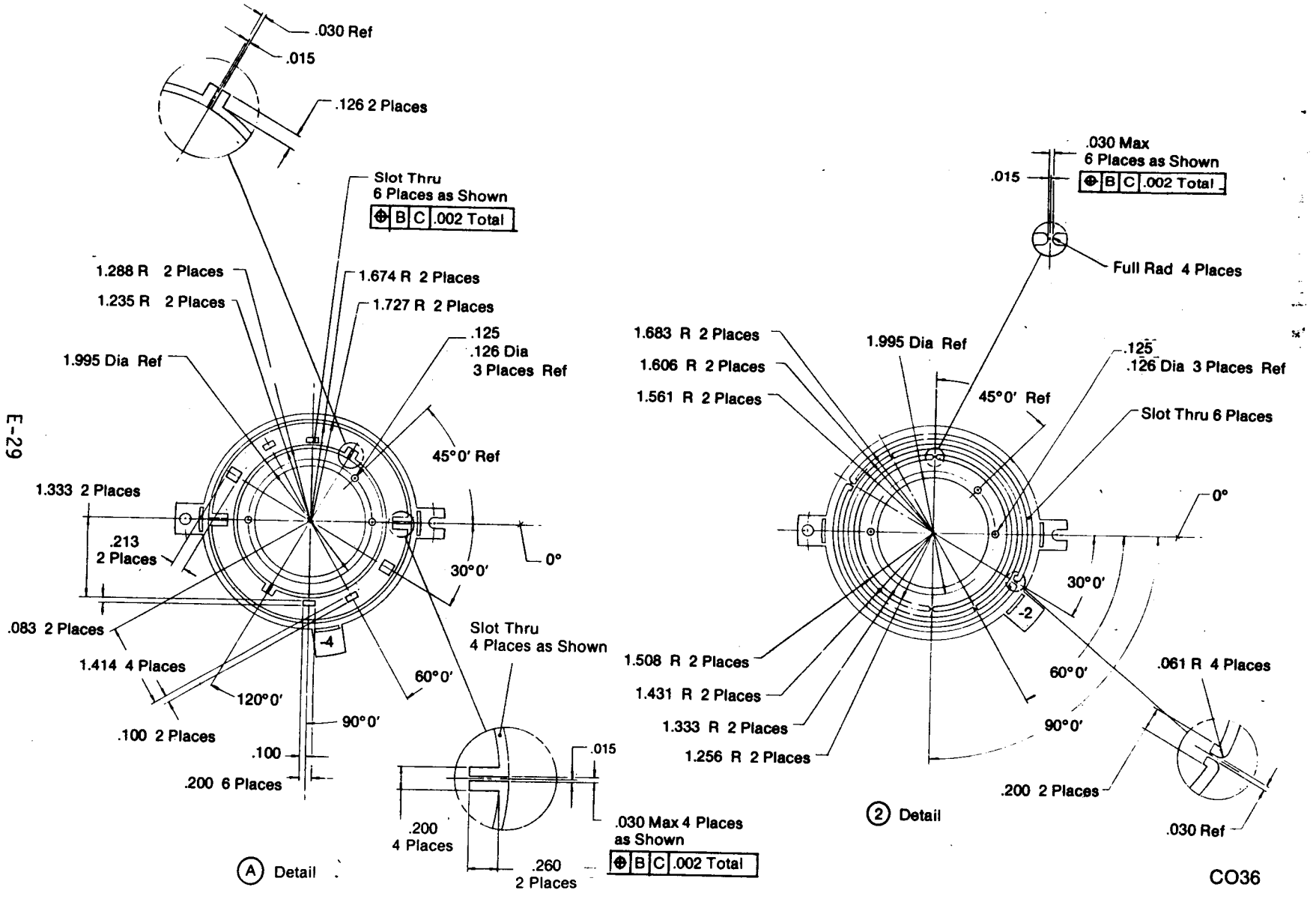

Figure E-28. Platelet Cooling Assembly - Primary Chamber

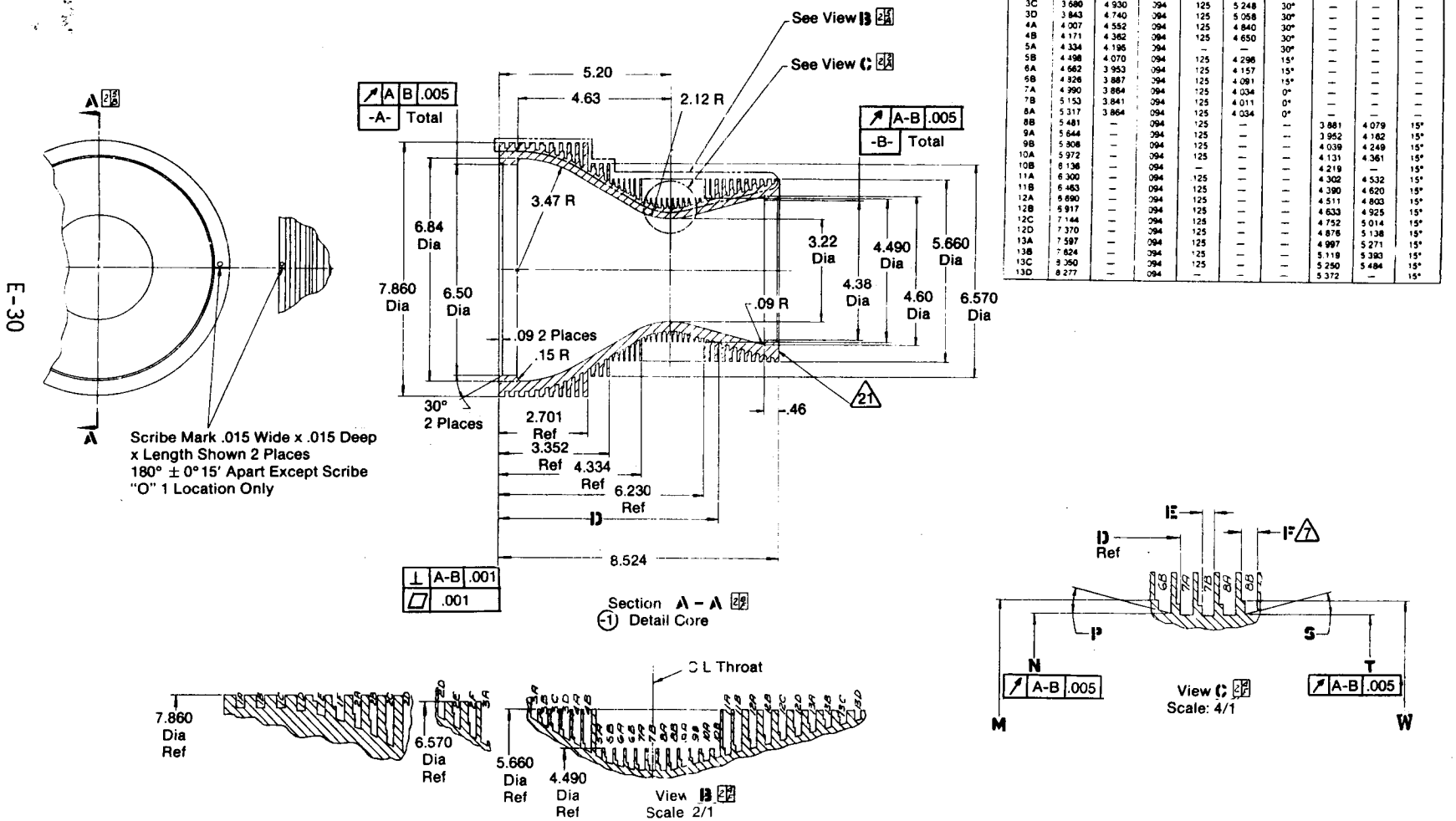

Channel Design Ref	D Dim ±.005	N Dia ±.002	E Dim ±.005	F Dim △	M Dia ±.002	P Angle ±0°30'	T Dia ±.002	W Dia ±.002	S Angle ±0°30'
1A	.180	7.513	.125	—	—	0°	—	—	—
1B	.485	7.513	.125	—	—	0°	—	—	—
1C	.790	7.513	.125	—	—	0°	—	—	—
1D	1.095	7.448	.125	—	—	0°	—	—	—
1E	1.400	7.245	.125	.188	7.690	15°	—	—	—
1F	1.695	7.080	.125	.188	7.525	15°	—	—	—
2A	1.970	6.866	.094	.125	7.322	15°	—	—	—
2B	2.214	6.616	.094	.125	7.100	30°	—	—	—
2C	2.458	6.340	.094	.125	6.843	30°	—	—	—
2D	2.701	6.059	.094	—	—	30°	—	—	—
2E	2.945	5.778	.094	.125	6.230	30°	—	—	—
2F	3.189	5.496	.094	.125	5.948	30°	—	—	—
3A	3.352	5.308	.094	—	—	30°	—	—	—
3B	3.516	5.116	.094	.125	5.414	30°	—	—	—
3C	3.680	4.930	.094	.125	5.248	30°	—	—	—
3D	3.843	4.740	.094	.125	5.058	30°	—	—	—
4A	4.007	4.552	.094	.125	4.840	30°	—	—	—
4B	4.171	4.362	.094	.125	4.650	30°	—	—	—
5A	4.334	4.196	.094	—	—	30°	—	—	—
5B	4.498	4.070	.094	.125	4.296	15°	—	—	—
6A	4.662	3.953	.094	.125	4.157	15°	—	—	—
6B	4.826	3.887	.094	.125	4.091	15°	—	—	—
7A	4.990	3.864	.094	.125	4.034	0°	—	—	—
7B	5.153	3.841	.094	.125	4.011	0°	—	—	—
8A	5.317	3.864	.094	.125	4.034	0°	—	—	—
8B	5.481	—	.094	.125	—	—	3.881	4.079	15°
9A	5.644	—	.094	.125	—	—	3.952	4.162	15°
9B	5.808	—	.094	.125	—	—	4.039	4.249	15°
10A	5.972	—	.094	.125	—	—	4.131	4.361	15°
10B	6.136	—	.094	—	—	—	4.219	—	15°
11A	6.300	—	.094	.125	—	—	4.302	4.532	15°
11B	6.463	—	.094	.125	—	—	4.390	4.620	15°
12A	6.690	—	.094	.125	—	—	4.511	4.803	15°
12B	6.917	—	.094	.125	—	—	4.633	4.925	15°
12C	7.144	—	.094	.125	—	—	4.752	5.014	15°
12D	7.370	—	.094	.125	—	—	4.876	5.138	15°
13A	7.597	—	.094	.125	—	—	4.997	5.271	15°
13B	7.824	—	.094	.125	—	—	5.119	5.393	15°
13C	8.050	—	.094	.125	—	—	5.250	5.484	15°
13D	8.277	—	.094	—	—	—	5.372	—	15°

Figure E-29. Secondary Chamber Assembly

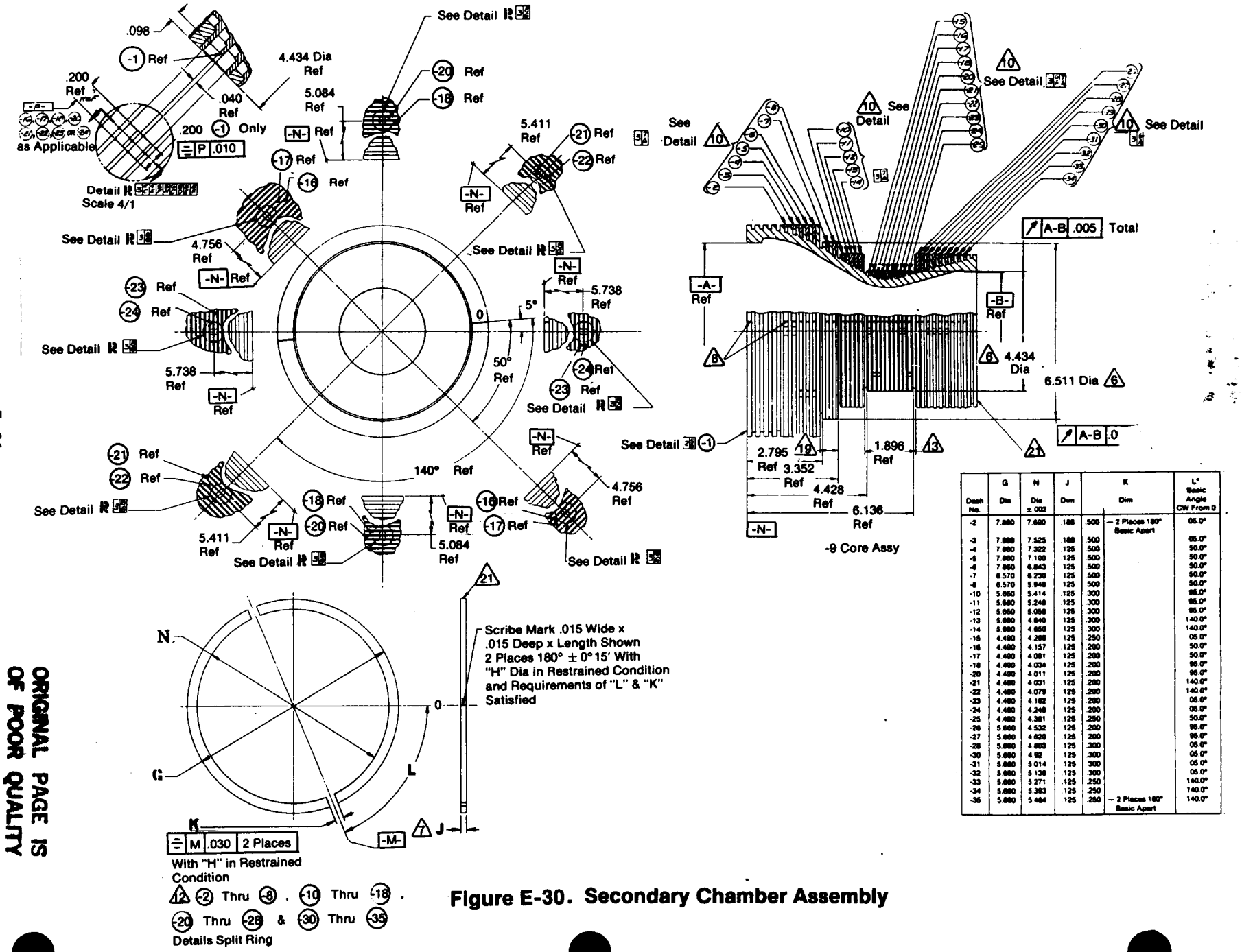

Dash No.	G Dia	N Dia ± .002	J Dim	K Dim	L° Basic Angle CW From 0
-2	7.880	7.680	188	.500 — 2 Places 180° Basic Apart	05.0°
-3	7.880	7.525	188	.500	05.0°
-4	7.880	7.322	.125	.500	50.0°
-6	7.880	7.100	.125	.500	50.0°
-8	7.880	6.843	.125	.500	50.0°
-7	8.570	8.230	.125	.500	50.0°
-8	8.570	5.848	.125	.500	50.0°
-10	5.880	5.414	.125	.300	95.0°
-11	5.880	5.248	.125	.300	95.0°
-12	5.880	5.058	.125	.300	85.0°
-13	5.880	4.840	.125	.300	140.0°
-14	5.880	4.650	.125	.300	140.0°
-15	4.480	4.288	.125	.250	05.0°
-16	4.480	4.157	.125	.200	50.0°
-17	4.480	4.081	.125	.200	50.0°
-18	4.480	4.034	.125	.200	95.0°
-20	4.480	4.011	.125	.200	95.0°
-21	4.480	4.031	.125	.200	140.0°
-22	4.480	4.079	.125	.200	140.0°
-23	4.480	4.162	.125	.200	05.0°
-24	4.480	4.248	.125	.200	05.0°
-25	4.480	4.381	.125	.250	50.0°
-26	5.880	4.532	.125	.200	95.0°
-27	5.880	4.620	.125	.200	95.0°
-28	5.880	4.809	.125	.300	05.0°
-30	5.880	4.92	.125	.300	05.0°
-31	5.880	5.014	.125	.300	05.0°
-32	5.880	5.136	.125	.300	05.0°
-33	5.880	5.271	.125	.250	140.0°
-34	5.880	5.393	.125	.250	140.0°
-35	5.880	5.484	.125	.250 — 2 Places 180° Basic Apart	140.0°

Figure E-30. Secondary Chamber Assembly

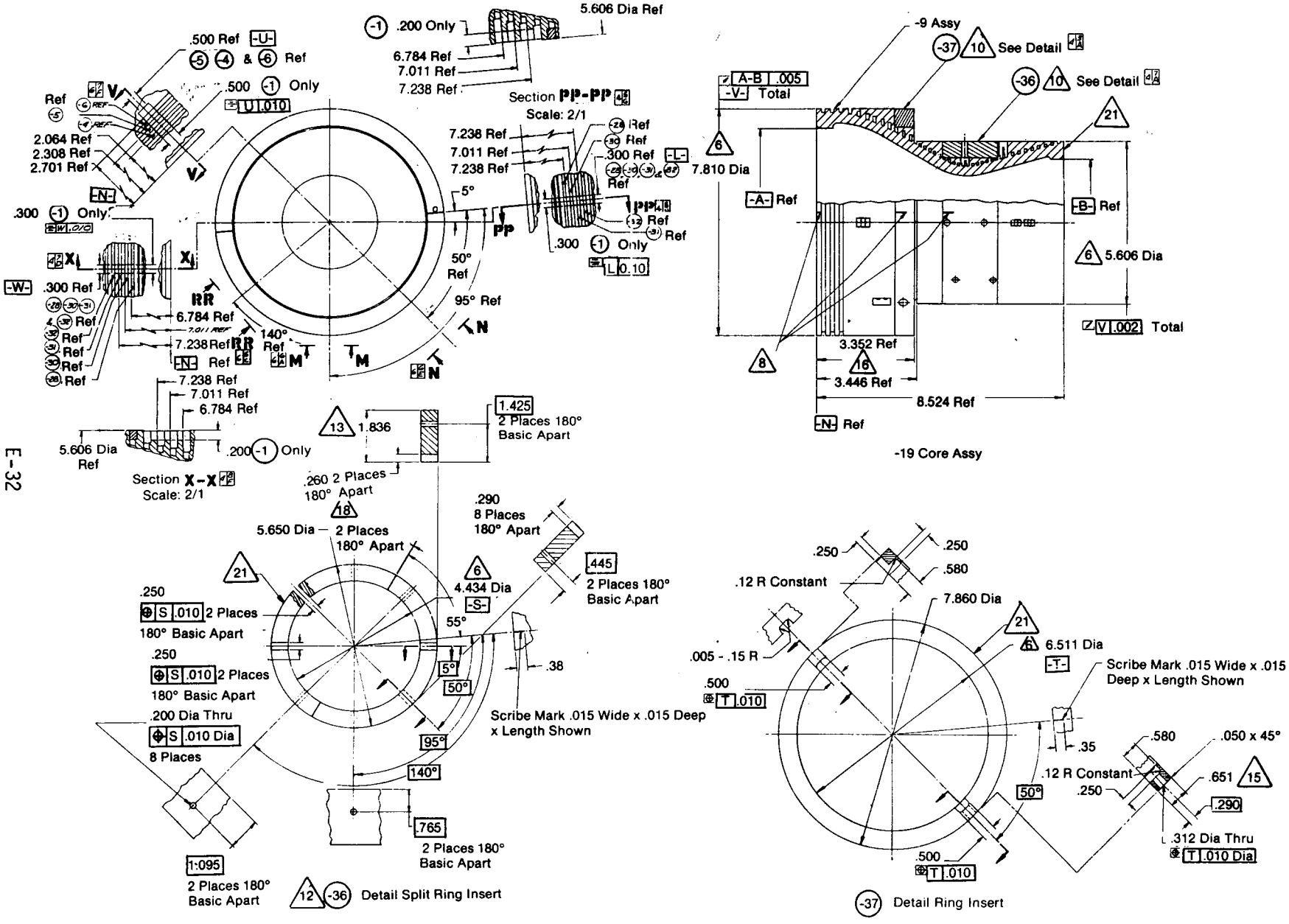

Figure E-31. Secondary Chamber Assembly

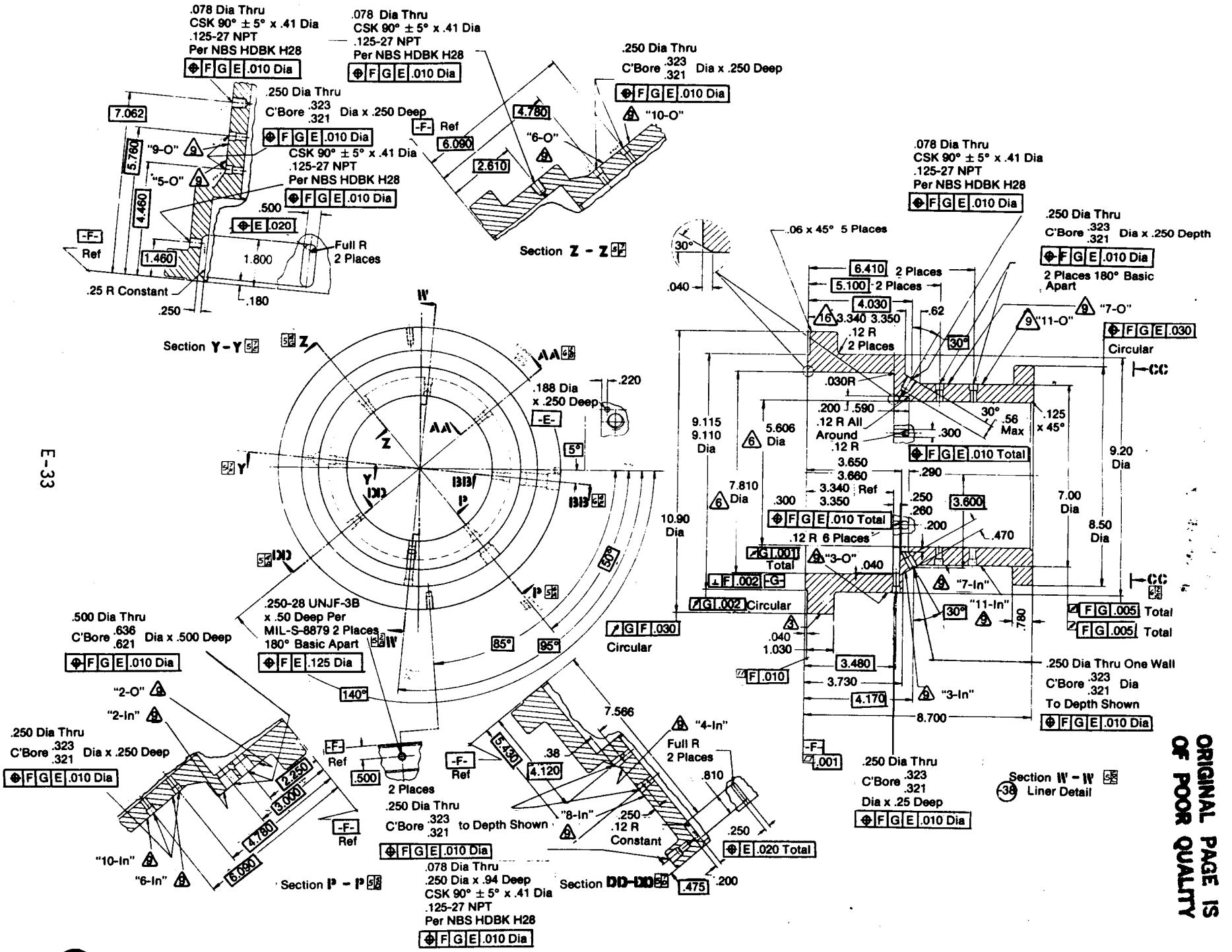

E-33

Figure E[redacted] Secondary Chamber Assembly

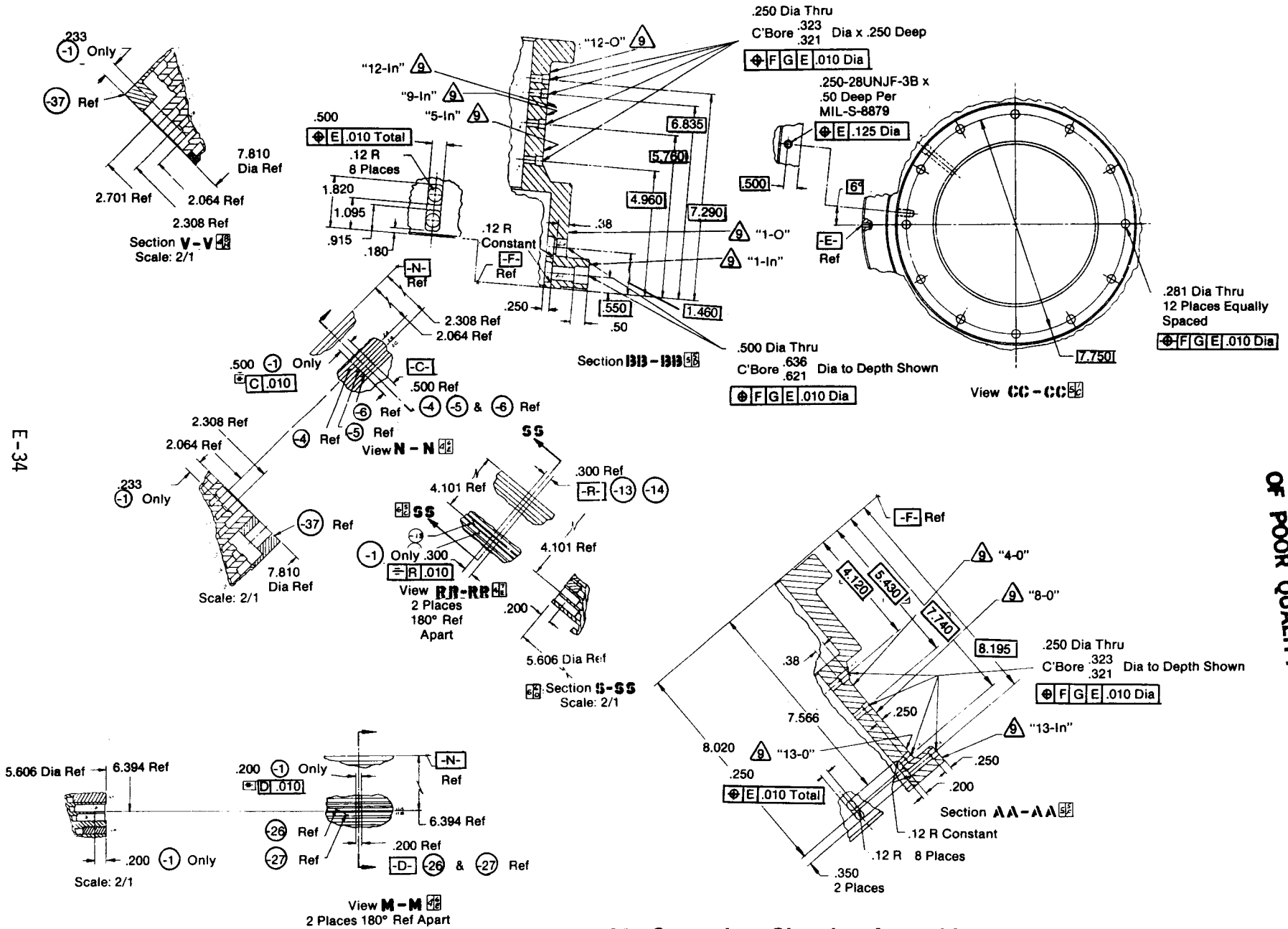

Figure E-33. Secondary Chamber Assembly

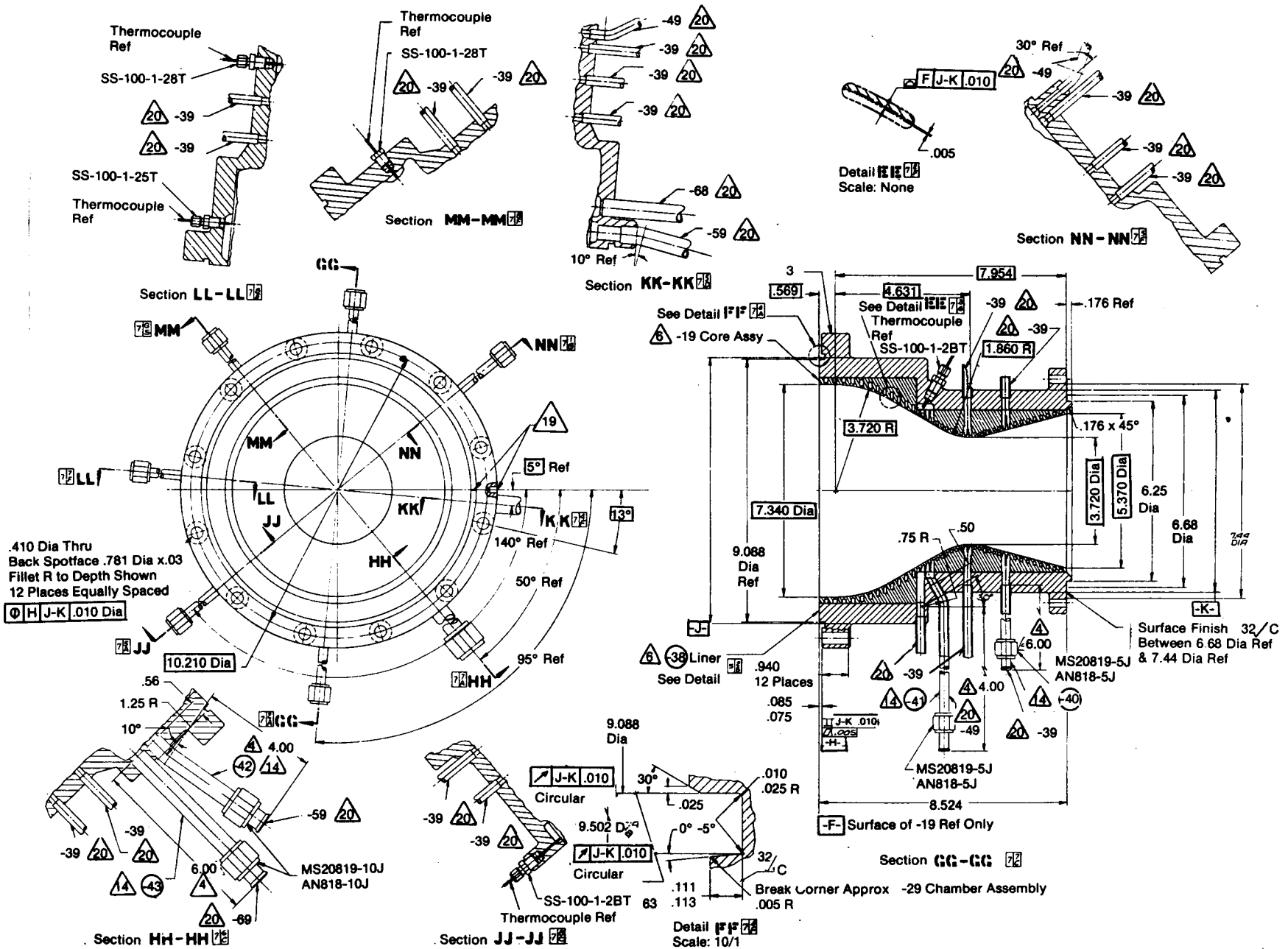

Figure E-34. Secondary Chamber Assembly

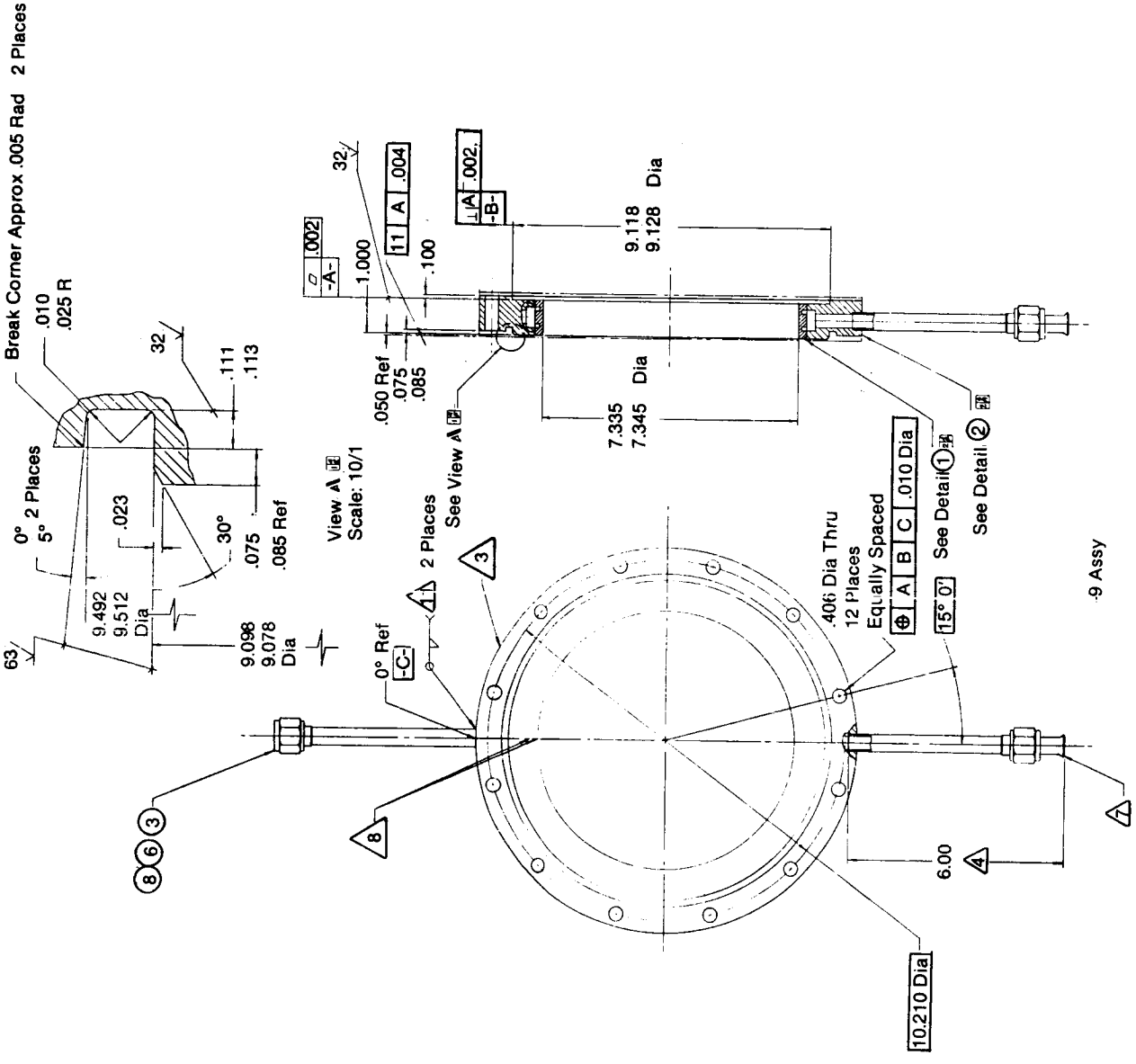

Figure E-35 . L' Spacer

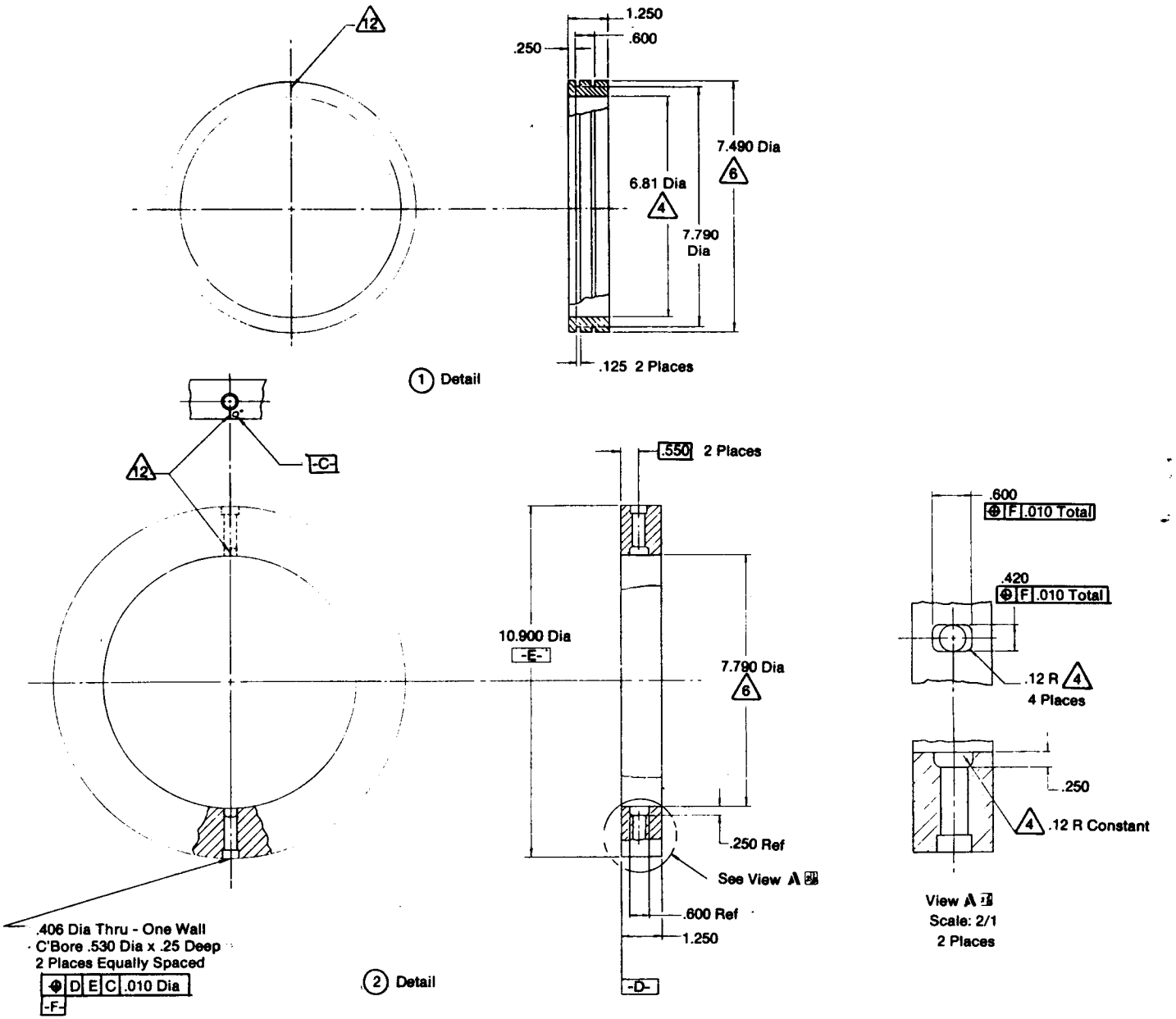

Figure E-36. L' Spacer